SEAFLOOR MAPPING OF LONG ISLAND SOUND -

FINAL REPORT: PHASE II PROJECT

SUBMITTED TO:

THE LONG ISLAND SOUND CABLE FUND STEERING COMMITTEE

STATE OF CONNECTICUT, DEPARTMENT OF ENERGY AND ENVIRONMENTAL PROTECTION, LAND AND WATER RESOURCES DIVISION;

NEW YORK, STATE DEPARTMENT OF ENVIRONMENTAL CONSERVATION, DIVISION OF MARINE RESOURCES;

NEW YORK, DEPARTMENT OF STATE, OFFICE OF PLANNING AND DEVELOPMENT;

CONNECTICUT SEA GRANT;

NEW YORK SEA GRANT;

AND

U.S. ENVIRONMENTAL PROTECTION AGENCY, REGIONS 1 AND 2

BY:

LAMONT – DOHERTY EARTH OBSERVATORY COLLABORATIVE
LONG ISLAND SOUND MAPPING AND RESEARCH COLLABORATIVE
NOAA'S OCEAN SERVICE COLLABORATIVE

JANUARY 2023

This page intentionally left blank.

Executive Summary

This report compiles the efforts of the Collaborative Project Teams conducted from 2017 to 2022 in the Phase II project area of eastern Long Island Sound (LIS). Funded by the Long Island Sound Cable Fund (LISCF) and administered by the Cable Fund Steering Committee, this project is the second of three phases of the LIS Seafloor Habitat Mapping Initiative, focusing on specific regions of LIS identified by managers, scientists, and stakeholders as high priority areas for habitat mapping. Maps depicting the seafloor landscape provide vital information about seafloor habitat structure and the ecological characteristics associated with those habitats. Benthic habitat mapping in LIS has long been identified as a priority need and is essential to improving science-based environmental management and mitigation decisions.

As LIS is diverse in its topography, which in turn supports a diversity of life and natural resources, the comprehensive information needed to manage the Sound and its resources must be gathered at a range of scales. The Collaborative Project Teams, therefore, have used a variety of technologies and methodologies to provide data on a range of scales, from big picture acoustic maps of the features of the underwater landscape to the fine scale distribution of organisms living on and in the seafloor. Similar to the Phase I Pilot project, the Collaborative Teams have delivered data and associated derived products focused on the following thematic areas: 1) Seafloor Topography and Acoustic Intensity; 2) Sediment Texture and Grain Size Distribution; 3) Sedimentary Environments; 4) Benthic Habitat and Ecological Processes; 5) Physical and Chemical Environments; and 6) a Data Management component.

Seafloor Topography and Acoustic Intensity

- Acoustic survey systems measure the sound intensity reflected off the seafloor to present a depiction of the seafloor's features. High-resolution acoustic bathymetry and backscatter data give an indication of the seafloor's composition and types of benthic habitats. The bathymetry conveys detailed information on the seafloor topography while also relaying quantitative data that can be used to develop a number of derived products depicting important features, relief, and seafloor changes. The backscatter data relays geophysical information where softer sediments absorb much more of the sound from the sonar signal, while harder substrates give a stronger acoustic return from the seafloor. These imaging maps serve as the precursor for all subsequent habitat mapping elements.

- The acoustic data collection for this project included the evaluation and compilation of existing and newly acquired acoustic survey data in data gap areas within the Phase II Area of Interest. This evaluation included a quality analysis of the existing surveys and quality assurance metrics to ensure the data collections could be integrated into existing phases of the LIS Seafloor Habitat Mapping Initiative. This data was compiled into high-resolution bathymetric and backscatter images integrated from the newly acquired and existing acoustic datasets. The final geospatial products serve as base layers for habitat mapping for this region of LIS.

- Full coverage topography (bathymetry) and acoustic intensity (backscatter) images are fundamental for predicting sediment classes and habitat types.

- The acoustic data collection achieved in Phase II emphasizes the significance of partner collaboration. The structured coordination between partners for communicating and sharing data has augmented the data collection coverage while also ensuring reliable acoustic data

quality. This collaboration manifested in a division of labor between Stony Brook University (SBU) from the Lamont-Doherty Earth Observatory (LDEO) consortium and the University of Connecticut (UConn) from the Long Island Sound Mapping and Research Collaborative (LISMaRC) to collect new acoustic data in the data gap areas (Survey Blocks) identified by NOAA for new data acquisition and including an acoustic resurvey effort by NOAA conducted in 2015.

- The total area of new bathymetry and backscatter data collected for the Phase II study was 247.3 square kilometers (95.5 square miles). While the prior NOAA mapping in LIS provided details about the morphology and character of the seafloor sediments for large parts of the Phase II area, the new acoustic data acquired within the Phase II area added new details in many mostly nearshore areas where detailed mapping did not exist. The geophysical information contained in the Phase II acoustic products conveys important details describing the shape, extent, and composition of surficial features used to extract detailed information about benthic habitats, sediment texture, grain size, and sedimentary environments.

Sediment Texture and Grain Size Distribution

- Characterizing sediment texture, which includes describing the shape, size, and three-dimensional arrangement of sediment particles, is a critical component of habitat classification.

- Total organic content distribution is also valuable for benthic habitat classification since it can be an indicator of biological activity.

- Abundant old grain size data is available; however, the seafloor environment is highly variable in places, so decades-old data might not reflect the current conditions.

- Acoustic data can provide broad-scale information on the range of grain size composition of the seafloor, but such information is insufficient to discern all the differences in grain size that might be relevant to benthic habitats. Therefore, sediment grain size distribution requires analysis of actual samples.

- In the Phase II study, changes in the backscatter variation were more useful for identifying boundaries between different sediment classes and to a lesser degree for determining the class itself due to several potential factors influencing the backscatter returns, including different mixtures of fine and coarse material and vegetation or shellfish covering the seabed, which reinforced the necessity of sediment sample analysis to accurately determine grain size distribution.

- LISMaRC collected seafloor images and videos at 210 sampling sites and collected and processed surficial sediment samples at 179 of these sites within the Phase II AOI. LDEO acquired and processed for 281 sediment samples for grain size analysis and combined these results with the surficial sediment results provided by LISMaRC. The results of the sediment grain size analyses from both LISMaRC and LDEO revealed the preponderance of sand as the primary seafloor constituent in the Phase II AOI. The data show that sand is the dominating grain size in the Phase II study area and lies generally between 50% and 100%.

- Although strong correlations for the presence of zinc and lead were not observed, both elements show clear but different distribution patterns showing increased concentrations

along the Connecticut coastline. Likely sources include fluvial material originating from rivers along the CT coast and industrial activities.

- The Sediment Texture and Grain Size Distribution element provided a comprehensive dataset to assist with several other elements of the overall Phase II mapping initiative. These include: 1) acoustic backscatter ground-truth data; 2) sedimentary environments; 3) both infaunal and epifaunal ecological characterization; and 4) additional ground-truth data to assist with the physical oceanography component of the initiative.

Sedimentary Environments

- While sediment texture describes the grain size composition at the time of sediment collection, the sedimentary environment describes the processes dominating/controlling a certain location such as deposition or erosion over time.

- Detailed information about the sedimentary environment is an essential part of determining the physical processes of the benthic environment that strongly influence the related habitats.

- Understanding the sediment environment characteristics provides insights into the physical processes of the benthic environment, its stability, and evolution.

- In addition to providing detailed depositional records, sediment cores are useful for distinguishing depositional from erosional/non−depositional areas or identifying a thin layer of sediments covering bedrock outcrop. They are also useful for revealing areas that have been disturbed by isolated or frequent events in the past as well as those where the depositional environment has shifted from one regime to another.

- The cores recovered from the rivers, except for Mystic River, exhibit similar grain size muddy sand and sandy mud, texture, and sedimentation patterns. The nearshore cores are coarser grained and contain marine shells and fragments with thicker beds and intervals of bioturbation.

- The Phase II study area is dominated by erosional/non-depositional and dynamic environments. These are all high energy environments. Lower energy environments are found in some of the embayments along the Connecticut shoreline and on the north side of Fishers Island; although, beaches and actual shores are subject to higher wave energy.

- Similar to the grain size/sediment texture interpretation, the overall trends are the same in both interpretations. The two interpretations differ in some detailed extent of the different classes. This is likely due to the difference in detail in the available data.

Benthic Habitat and Ecological Processes

Seafloor and Habitat Characterization

- The benthic habitats and ecological processes components of the Phase II project incorporates the methodologies developed in the Phase I Pilot project to best identify and characterize the variety of benthic habitats that comprise the study area, identify and characterize infaunal and epifaunal communities relative to the seafloor habitats at multiple spatial scales, and map their spatial distributions relative these habitats.

- Previous studies show the Phase II study area is highly dynamic in terms of sedimentary processes, has a complex geomorphology in some areas, and is dominated by primarily sandy

- and coarser grained sediments, which is supported by the seafloor characterization in the current study.

- For the Phase II project several types of data representing different seafloor characteristics were used to classify and subsequently characterize the seafloor in the study area. These included a multibeam backscatter mosaic, bathymetry, seafloor rugosity as measured by the Terrain Roughness Index (TRI), maximum physical bottom stress, and sediment grain-size composition.

- The existing backscatter data was used as the baseline to develop the habitat characterization as the newly acquired backscatter data was not processed and integrated with the existing data in time to expand the footprint of this important baseline mosaic.

- The term acoustic patch type is used to underscore that the different types of seafloor patches classified through the segmentation process are based on acoustic imagery. Acoustic patches are seafloor areas that have certain image characteristics (i.e., a specific range of pixel intensities) based on acoustic backscatter data that are related to seafloor properties, such as sediment type and geomorphology, which have been defined through a supervised image classification process.

- Acoustic patch types represent general habitat areas that have certain environmental characteristics with regard to sediment grain size composition, topographic roughness, and maximum hydrodynamic stresses on the seafloor. These characteristics are potential determinants of the kinds of infaunal and epifaunal communities that may be found within the acoustic patch types. The acoustic patch types can be designated as habitat types, and their mapped distribution forms the basis of an overall habitat map for the Phase II study area. This also forms the framework for subsequent research and surveys that can assess the accuracy of the characteristics of these habitat types as determined in this study as well as the extent of the distribution of seafloor habitats in this portion of LIS.

- The dominance of sands and coarser sediments in the Phase II study area is evident in the backscatter mosaic that was used for the characterization of seafloor habitat structure. Much of the mosaic has a complex pattern of image characteristics that are primarily associated with sandy/harder sediments than that of muddy/finer sediments. This is in contrast to the Pilot project area where there are large areas of muddy sediments that were distinct features in the backscatter mosaic. Seafloor characterization, which can be used as a basis for habitat mapping, can be difficult in an area such as ELIS.

- Although sandy and gravelly sediments dominate 4 of the 5 acoustic patch types identified, there are distinct differences in the fine-scale composition of sediments in each acoustic patch type, representing a gradient from fine sands and silts to sand to sand/gravel.

- The seafloor environment in the Phase II study area is spatially complex, reflecting the mix of large-scale hydrodynamic and geomorphological features that influence its features. However, some broader trends do emerge that are similar to previous mappings of sediment distributions in this portion of LIS. For example, both the sediment texture map (Figure 5.1-2) and the acoustic patch type map (Figure 5.1-6) indicate finer sediments along the Connecticut shore, as well as closer inshore to Fishers Island, and to the north of Plum and Great Gull Islands. Both characterizations also indicate a large area of gravelly sand in the central portion Phase II study area, extending from south of the Connecticut River to roughly

South of Goshen Point, as well as in the central portions of Fishers Island Sound. Likewise, both characterizations indicate a complex spatial distribution of patch types running north to south from the Connecticut shore to the area of the Race.

- There are also a number of relatively large sand wave fields in the Phase II area, particularly in the western portion. These sand wave fields increase TRI significantly in these areas and are primarily associated with sand and gravelly sand, particularly the large field located along the southwest edge of the Phase II study area, which is almost entirely characterized as sand.

- The spatial density, and as such resolution, of the sampling used to develop the initial sedimentary characterizations of the Phase II study area was low and, thus, provided a spatially coarse understanding of seafloor environments (habitats) in this portion of LIS.

- The most extensive sediment class, which is gravelly sand, is found throughout the Phase II area, particularly in the central portion where there is a large continuous section of seafloor of this type. There are 411 patches of gravelly sand, accounting for 45.1% of the study area.

Ecological Characterization

- As in the Phase I Pilot project, the Ecological Characterization of the Phase II area comprised a comprehensive approach built upon multiple scale technologies and methods required to assess the spatial complexity of the seafloor habitats in the area.

Infaunal Ecological Characterization

- Infaunal grab samples (160) were collected for infaunal analyses using the USGS SEABOSS system during the fall, 2017 and spring, 2018 field campaigns. In the lab, samples were sorted under a dissecting microscope and individuals were identified to the lowest possible taxon.

- Several sets of statistical and GIS-based analyses were conducted to assess the characteristics of infaunal communities (total abundance [total number of identified organisms per sample], taxonomic/species richness [species richness and taxonomic richness are used interchangeably here and represent the number of taxa that were differentiated to the lowest possible taxonomic level], taxonomic/species diversity [as Shannon Diversity Index, a measure that accounts for both total number of taxa/species and relative proportion/evenness], community composition and related metrics [multivariate analyses measuring similarities and trends within and among samples]) among and within the large-scale acoustic patches that were identified, and to map the spatial trends in community structure and biodiversity relative to seafloor habitat structure.

- A total of 289 infaunal taxa were identified in all the samples collected in the LIS Phase II area, and 85% of these were identified to the species level.

- Two sets of analyses were conducted to assess the general infaunal community characteristics (taxonomic richness, total abundance and diversity): one using the entire data set from both sampling periods and also for each sampling period separately to assess potential seasonal differences among the large-scale patch types. Infaunal mean total abundances in the patch types generally ranged from ~ 175 to 225 individuals per 0.1 m². Mean taxonomic richness ranged between 20 and 30 taxa per 0.1 m² using data from both sampling periods.

- The overall range was quite large, with some sites having upwards of 40 to 50 taxa, whereas others had as few as 4 to 5 taxa. Mean taxonomic diversity, which takes into account both the

number of taxa and their proportional abundance and measured by Shannon diversity index H′, ranged from approximately 0.6 to 1.0, although at some sites it was higher approaching approximately 1.4.

- Infaunal community structure is spatially heterogeneous in the Phase II Area and was variable within each of the patch types.

- Classification (cluster) analyses identified 13 community types, some of which were relatively distinct from the others, and others that were more similar.

- Total abundance, taxonomic richness and diversity were highest in the central and eastern portions of the Phase II study area.

- High abundances were found in the central portion of Fishers Island Sound and also within a large, deeper water area of the central portion of the study area. High taxonomic richness was found in the western portion of Fishers Island Sound, south of the Thames River, and in central portion of the study area. High taxonomic diversity followed a similar pattern as taxonomic richness; although, they were not spatially congruent.

- The infaunal community patterns in the Phase II study area exhibit a number of similarities to those found in previous studies.

- Infaunal community characteristics vary across the Phase II study area, but there are some general trends, notably higher total abundance and taxonomic richness from west to east.

- There are several areas of relatively high diversity throughout the study area. Infaunal community composition for each acoustic patch type, is relatively distinct, but variable within acoustic patch types, predominantly due to changes in taxonomic dominance.

- Analysis of community structure without grouping by acoustic patch type revealed that differences were most notable between the south/central, and north coastal portions of the Phase II area. The eastern central portion of the study area is comprised of a variable mix of community types but their similarity is relatively high.

- In addition to clearly defined communities and dominant species, rare infauna (i.e., infaunal organisms present in low numbers) fill important ecological roles in benthic habitats. The presence of these rare organisms, including ophiuroids, deep burrowing shrimp, sand dollars, and large polychaetes, also indicate less disturbed seafloor areas.

Epifaunal Ecological Characterization

- This element of the project develops spatially comprehensive seafloor habitat maps and interpretive products for the Phase II study area that include emergent and epifaunal elements of seafloor habitats.

- There are inherent difficulties sampling hard substratum habitats upon which epifaunal organisms depend, as well as the fragility of those emergent taxa and biogenic structures that occur on the surface of both hard substratum and fine-grained sediments. Specialized sampling tools and approaches for imaging and collection of physical samples (e.g., integrated cameras/grabs, remotely operated vehicles, divers with quadrat cameras and airlift samplers) were used to address these issues.

- A total of 119 taxa were identified to the lowest possible taxonomic unit and an additional 33 biogenic features, structures formed by organisms (e.g., shell, tubes, and burrows) and used as habitat by vagile fauna were observed in the study region.

- Multivariate analyses were implemented to test for differences in the composition of taxa and biogenic features based on eCognition patch assignments for image samples. The eCognition patches exhibit significant differences in both taxa and biogenic features such that each class has distinct characteristics useful to differentiate and map elements of habitats.

- The communities of attached and emergent taxa associated with each acoustic patch type were distinct principally based on changes in dominance and not wholesale differences in composition. As with infaunal community characteristics linked to sediment size fractions, epi- and emergent taxa were associated with multiple grain-sizes differentially represented within each acoustic patch type.

- The distribution and abundance of taxa and features did not follow uniform geographic trends, reflecting the varied seafloor habitats characterized by eCognition patches; although, a number of spatial patterns were identified that provide important insights on this region of LIS.

- Multiple taxa and biogenic habitat features were identified that represent larger gradients and general relationships with physical characteristics of seafloor environments, as well as ecological responses to on-going changes in local and regional environmental conditions. Some of these taxa are worthy of specific consideration due to their role as an ecosystem engineer or biogenic habitat, or their vulnerability, conservation status, or dominance in the community. These taxa are: hydrozoan and bryozoan turfs, ghost anemone *Diadumene leucolena*, macroalgal taxa aggregated as Laminariaceae and Rhodopyhta, and the solitary hydroid *Corymorpha pendula*. These are identified in the analyses and GIS datasets as "Select Taxa."

- A series of maps and brief descriptions were developed that illustrate the distribution and abundance of epifaunal and emergent taxa with diverse life histories as well as biogenic features that fill important functional roles as seafloor habitat. Most of these taxa are structure forming, serving an "ecosystem engineering" role, while the biogenic features are themselves structure. These maps and descriptions also describe many unique ecological relationships and trends occurring in this part of the Sound.

- This component of the study also identified multiple sites with notable biological and geological features that were described and included associated imagery to visualize local conditions. These include Ellis Reef, Ram Island Reef, Black Ledge, Varved Lake Clays and Deltaic Deposits, Deep Boulder Morraines and south of the Race and Fishers Island.

Integrated Ecological Characterization

- The ecosystem dynamics of the seafloor and bottom waters are shaped by both the infaunal and epifaunal communities that are found in any particular habitat/bottom type. Both sets of organisms are critical in seafloor and demersal food webs, are often key ecosystem engineers generating a variety of habitats, both when live and dead (e.g.. shell hash from bivalves), and are critical to different life stages of the full biotic diversity of the seafloor.

- Thus, being able to determine patterns of joint infaunal and epifaunal community structure can provide insights into ecosystem function and also assessments for conservation and

management.

- In order to show the joint trends in several community characteristics for both infauna and epifauna in the Phase II study area, mean taxonomic richness and mean diversity were calculated at the sampling block (SB) and single sample site (NB) levels and plotted together in GIS.

- An integrated habitat map links acoustic patch types to the defining ecological and generalized physical characteristics of biogenic features, infauna, and epi- and emergent fauna. It is notable that patterns of faunal composition and abundance (cover) follow the general grain size composition that is evident in the acoustic patch types (i.e., finer to coarser sediments) along with the concomitant physical attributes.

- The ecological pattern in this area comports with the similarity of sediment composition (a gradient of sand-gravel) such that patterns of diversity and dominance shift across patches but are drawn from a similar species pool. Depth, tidal stress, and related measures are also correlated with these changes in species patterns.

Seafloor/Habitat Classification

- In 2012, the Coastal and Marine Ecological Classification Standard (CMECS) was adopted by the Federal Geographic Data Committee. Sub-components and modifiers included in the CMECS documentation do not necessarily apply in all seafloor environments, which was recognized by its developers, so the approach was to adhere to the extent possible to CMECS modifiers but also to define our own as necessary to accurately describe biotic components specific to the Phase II area. The selections of sub-components and modifiers for the classification are based on the in-depth analyses conducted of the infaunal and epifaunal communities, as well as the analyses of the sediment and environmental data associated with characterization of the seafloor patch structure.

- CMECS classifications were developed at two levels of resolution, at the sample level and at the acoustic patch level. At the sample level, this included a CMECS classification for each sediment sample grab used for infaunal analyses and for those digital images used for epifaunal analyses. Having classifications at two levels of detail provides for more specific information at the scale of a sample site/image location. The CMECS classifications of the acoustic patch types summarize the results from the analyses of both the infaunal and epifaunal communities and associated environmental characteristics, such as surficial features that are ecologically relevant. Several classification levels were added to provide details about the habitat and ecological characteristics in the acoustic patch types.

- The CMECS classification for the acoustic patch types attempts to capture their general attributes across the Phase II study area. As such, it should be used as a starting point for a more detailed consideration of ecological characteristics in any specific portion of the area using the more in-depth analyses presented in the Infaunal and Epifaunal Characterizations and their associated GIS databases.

Physical Oceanography

- The distribution and variability of salinity, temperature, dissolved oxygen, currents, and

bottom stresses created by the complex interaction of geometry and forcing affects the biological communities on the seafloor.

- While the seasonal variations in salinity and temperature are well characterized along the axis of LIS, the north-south structure and variability within the Phase II study area were much less resolved and are much better defined as a result of this effort that identified the north-south, as well as east-west, patterns in salinity and temperature in the generated map products.

- Bottom stress, wave field, and circulation measurements from different wind and river flow conditions in eastern LIS are necessary to adequately evaluate model predictions so they can be reliably used in site assessment applications.

- Springtime and wintertime deployments of bottom tripods with an array of instruments measuring temperature, salinity, currents, and stresses were executed, and two ship surveys were executed, in which salinity, temperature, density structure and current patterns were measured.

- An implementation of the Finite Volume Coastal Ocean Model (FVCOM) was developed and designed to use the results of the operational northwest Atlantic regional model to provide ocean boundary conditions.

- The LIS FVCOM uses a 'nesting' approach that is computationally efficient since it allows the effect of the larger-scale processes to be simulated at coarse resolution and allows computing resources to focus on the smaller-scale structures in LIS and Block Island Sound (BIS).

- A limited measurement program was executed to acquire salinity, temperature, and current distributions so that the performance of the model in describing the small-scale spatial variations and the seasonal scale evolution of the variables could be critically assessed.

- The model output was used to create monthly maps of near-bottom salinity and temperature within the study area as well as maps of both mean and maximum bottom-stresses. The model was also used to produce estimates of along-track mean sea level (MSL) and water heights to support the acoustic surveys, as well as provide further validation of the model results.

- That the spatial and temporal structures of the temperature, salinity, and velocity fields captured by the model show excellent agreement with the field studies clearly supports the model's use as a tool to interpolate spatially between the observations for the purpose of making maps of the ecologically important characteristics of the bottom environment.

Data Management

- The data management efforts of the Phase II Project are intended to (1) ensure that the collaborative partners have access to data during the project to facilitate the creation of final data products, (2) ensure long-term preservation and open access to data generated during the Phase I Pilot project, and (3) establish and refine procedures and protocols for documenting, sharing and archiving data that may be acquired during subsequent efforts.

- To meet the specific needs of the Phase II Project the 2016 Scope of Work (SOW) defined data system design requirements to ensure well-coordinated data management throughout

the full life cycle of the project.

- The long-term plan for archiving project data ensures that data are sufficiently documented to enable scientific discovery and facilitate management of natural resources within LIS well beyond the completion of the project.

- In order to meet the needs of all partners with respect to access to data, the LIS Data Portal at the LDEO Marine Geoscience Data System (MGDS) was utilized to provide a comprehensive metadata catalog and long-term data stewardship solution focused on open access and preservation of all data products (raw and derived) and metadata. The LIS Data Portal ensures compliance with metadata standards and includes links to related content in distributed data systems.

- The LIS Data Portal leverages the technical infrastructure of the MGDS, which is supported primarily by the National Science Foundation (NSF). MGDS is a trusted data repository that provides free public access to a curated collection of marine geophysical data products and complementary data that support the needs of a diverse community of marine scientists, policy makers, educators, and the general public.

- Dedicated hardware for hosting LIS content has been fully integrated into the MGDS infrastructure to accommodate data submissions.

Long Island Sound Cable Fund Steering Committee Organizations and Members

US Environmental Protection Agency, Long Island Sound Study
888 Washington Blvd, Stamford, CT 06901 (203) 977-1541
- Mark Tedesco

State of Connecticut Department of Energy and Environmental Protection, Land and Water Resources Division
79 Elm St., Hartford CT 06106
(860) 424-3034
- Brian Thompson
- Kevin O'Brien
- DeAva Lambert

New York State Department of Environmental Conservation, Division of Marine Resources
205 North Belle Mead Road, Suite 1, East Setauket, New York 11733 (631) 444-0430
- Julia Socrates
- Victoria O'Neill
- Cassandra Bauer

New York Department of State, Office of Planning, Development & Community Infrastructure
One Commerce Plaza Suite 1010, 99 Washington Ave., Albany, NY 12231-0001
(518) 474-6000
- Jeff Herter

Connecticut Sea Grant, University of Connecticut - Avery Point Marine Science Building 1080 Shennecossett Rd, Groton, Connecticut 06340-6048 (860) 405-9128
- Sylvain DeGuise, Ph.D.

New York Sea Grant
121 Discovery Hall, Stony Brook University, Stony Brook, NY 11794-5001
(631) 632-6905
- Rebecca L. Shuford, Ph.D.

Collaborative Project Teams and Members

Lamont-Doherty Earth Observatory of Columbia University Collaborative:

Lamont-Doherty Earth Observatory of Columbia University
61 Route 9W, Palisades, NY 10964
(845) 359-2900
- Frank O. Nitsche, Research Scientist, Ph.D.
- Timothy Kenna, Research Scientist, Ph.D.
- Vicki L. Ferrini, Research Scientist, Ph.D.

Queens College, City University of New York
65-30 Kissena Blvd., Flushing, NY 11367
(718) 997-5000
- Cecilia McHugh, Distinguished Professor

Stony Brook University
School of Marine and Atmospheric Sciences
Stony Brook, NY 11794
(631) 632-6000
- Roger Flood, Research Professor

Long Island Sound Mapping and Research Collaborative:

University of Connecticut Avery Point, Marine Sciences Department
1080 Shennecossett Rd, Groton, Connecticut 06340-6048
(860) 405-9128
- Ivar G. Babb, Research Scientist
- Dennis Arbige
- Peter J. Auster, Ph.D.
- Todd Fake
- Kay Howard-Strobel
- Grant McCardell, Ph.D.
- Jim O'Donnell, Ph.D.

University of New Haven
300 Boston Post Rd, West Haven, CT 06516
(203) 932-7000
- Roman Zajac, Ph.D.
- Chris W. Conroy, Ph.D.
- Nicole Govert
- Courtney Schneeburger
- Olivia Walton

US Geological Survey
384 Woods Hole Rd., Woods Hole, MA 02543-1598
(508) 547-2227
- Seth Ackerman
- Dann Blackwood

National Oceanic and Atmospheric Administration (NOAA) Ocean Service Collaborative:

National Centers for Coastal and Ocean Science (NCCOS):
1305 East West Highway, Silver Spring, MD 20910
(301) 713-3028
- Timothy Battista, Chief Scientist
- Will Sautter

Marine Operations Center – Atlantic:
439 W. York St, Norfolk, VA 23510-1114
(757) 441-6778
- LT Lyndsey Davis

Acknowledgements

Citations

The recommended citations for the overall work and appendices are:

Long Island Sound Cable Fund Steering Committee, eds. (2023). "Seafloor Mapping of Long Island Sound – Final Report: Phase II Project." (Unpublished project report). U.S. Environmental Protection Agency Long Island Sound Study, Stamford, CT.

Long Island Sound Cable Fund Steering Committee, eds. (2023). "Seafloor Mapping of Long Island Sound – Final Report: Phase II Project Appendices." (Unpublished project report). U.S. Environmental Protection Agency Long Island Sound Study, Stamford, CT.

The recommended citations for individual subsections are provided at the beginning of each section.

List of Abbreviations

ACORN	Advanced Continuously Operating Reference Network
ADCP	Acoustic Doppler Current Profiler
AIC	Akaike Information Criteria
ANOSIM	Analysis of similarities
ANOVA	Analysis of variance
ASCII	American Standard Code for Information Interchange
BAG	Bathymetric Attributed Grid
BIS	Block Island Sound
CAP	Canonical analysis of principal coordinates
CARIS	Computer Aided Resource Information System
CMECS	Coastal and Marine Ecological Classification Standard
CO-OPS	Center for Operational Oceanographic Products and Services (NOAA)
CSV	Comma Separated Values
CTD	Conductivity, temperature, depth
CT DEEP	Connecticut Department of Energy and Environmental Protection
CUBE	Combined Uncertainty Bathymetric Estimator (CARIS)
DTM	Digital Terrain Model
ELIS	Eastern Long Island Sound
EMAP	Environmental Monitoring and Assessment Program (EPA)
ENVI	Environment for Visualizing Images (image processing software)
EPA	Environmental Protection Agency (Federal)
ESRI	Environmental Systems Research Institute, Inc.
FGDC	Federal Geographic Data Committee
FIS	Fishers Island Sound
FVCOM	Finite Volume Coastal Ocean Model
FMGT	Fledermaus Geocoder Toolbox
GeoTIFF	Georeferenced and geocoded Tagged Image File Format
GIS	Geographic Information System
GLMM	Generalized linear mixed effects models
GNSS	Global navigation satellite system
GOTM	General Ocean Turbulence Model
GPS	Global Positioning System
GSF	Generic Sensor Format (bathymetry file format)
HDCS	Hydrographic Data Cleaning System
HIPS	Hydrographic Information Processing System (CARIS)
HSSD	Hydrographic Surveys Specifications and Deliverables (NOAA)
HSTP	Hydrographic Systems Technology Program (NOAA)
IHO	International Hydrographic Organization
IOCM	Integrated Ocean and Coastal Mapping (NOAA)
LDEO	Lamont-Doherty Earth Observatory of Columbia University Collaborative
LIS	Long Island Sound
LISCF	Long Island Sound Cable Fund
LISMaRC	Long Island Sound Mapping and Research Collaborative
LMM	Linear mixed effects models
LRT	Likelihood ratio tests

MBES	Multibeam echosounder
MDS	Multidimensional scaling
mMDS	metric-MDS, also known as Principal Coordinate Analysis
MGDS	Marine Geoscience Data System (LDEO)
MLLW	Mean Lower Low Water
MODIS	Moderate Resolution Imaging Spectroradiometer (NASA)
MOU	Memorandum of Understanding
MSL	Mean sea level
NAD 83	North American Datum of 1983
NASA	National Aeronautics and Space Administration
NAVD 88	North American Vertical Datum of 1988
NCA	National Coastal Assessment (EPA)
NCCOS	National Centers for Coastal and Ocean Science (NOAA)
NCLEI	National Centers for Environmental Information (NOAA)
NECOFS	Northeast Coastal Forecast System
nMDS	Non-metric multidimensional scaling
NOAA	National Oceanic and Atmospheric Administration
NOS	National Ocean Service (NOAA)
NRT-5	Navigational Response Team 5 (OCS)
NSF	National Science Foundation
OGC	Open Geospatial Consortium
OCS	Office of Coast Survey (NOAA)
PCA	Principal Components Analysis
PERMANOVA	Permutational analysis of variance
PDBS	Phase Differencing Bathymetric Sonars
PDF	Portable document format
PRIMER	Plymouth Routines in Multivariate Ecological Research
PSD	Power spectral density
QA	Quality Assurance
QC	Quality Control
RTK	Real-Time Kinematic (for GNSS)
R/V	Research Vessel
SBET	Smoothed best estimate of trajectory
SEABOSS	SEABed Observation and Sampling System
SIMPER	Similarity percentage analysis
SIMPROF	Similarity profile routine analysis
SIPS	Sonar Information Processing System (CARIS)
SoMAS	School of Marine and Atmospheric Sciences at Stony Brook University
SOW	Scope of Work
SSH	Sea-surface height
SSS	Sidescan sonar
SST	Sea surface temperature
TRI	Terrain Roughness Index
UConn	University of Connecticut
UMass	University of Massachusetts
USGS	United States Geological Survey

UTC	Coordinated Universal Time
UTM	Universal Transverse Mercator
WAAS	Wide Area Augmentation System
WBD	Wet bulk density
WGS 84	World Geodetic System of 1984
WRF	Weather Research and Forecasting model
WWTP	Wastewater treatment plant
XRF	X-ray fluorescence

Table of Contents

List of Tables

List of Figures

1   Introduction

The LIS Seafloor Habitat Mapping Initiative is supported by the Long Island Sound Research and Restoration Fund, which was instituted in 2004 by a Memorandum of Understanding (MOU) among the members of the Policy Committee of the Long Island Sound Management Conference. The fund stemmed from a six-million-dollar enforcement settlement agreement between Connecticut and New York with the Cross Sound Cable Company, Northeast Utilities, and the Long Island Power Authority. Based upon the conclusion of a 2002 Connecticut legislative study, which found a substantial deficiency in the available scientific data on LIS seafloor habitats, the Policy Committee MOU established this fund would support projects emphasizing benthic mapping of LIS as a priority need to improve management decisions by enhancing the scientific understanding of potential energy infrastructure effects and mitigation of their impacts and to improve Long Island Sound (LIS). The fund is administered by the Long Island Sound Cable Fund (LISCF) Steering Committee, consisting of representatives from DEEP, US EPA Regions 1 & 2, New York Department of Environmental Conservation, New York Department of State, and the SeaGrant offices of Connecticut and New York.

After several years of work to identify specific management needs and outline a benthic mapping program for LIS, the Steering Committee selected a collaborative partnership combining national and local expertise and resources to implement the mapping initiative, which includes the National Oceanic and Atmospheric Administration Biogeography Branch and two regional academic consortiums led by the University of Connecticut and Columbia University's Lamont Doherty Earth Observatory. The Steering Committee and partners then identified three high priority mapping areas based on issues including ecological value, multiple use conflicts, compliance, resource management and potential for further development (Figure 1.1-1). The Steering Committee and partners anticipated that mapping these geographic areas individually would increase the success of completing the entire area while allowing for evaluation and refinement of processes at each phase to improve outcomes.
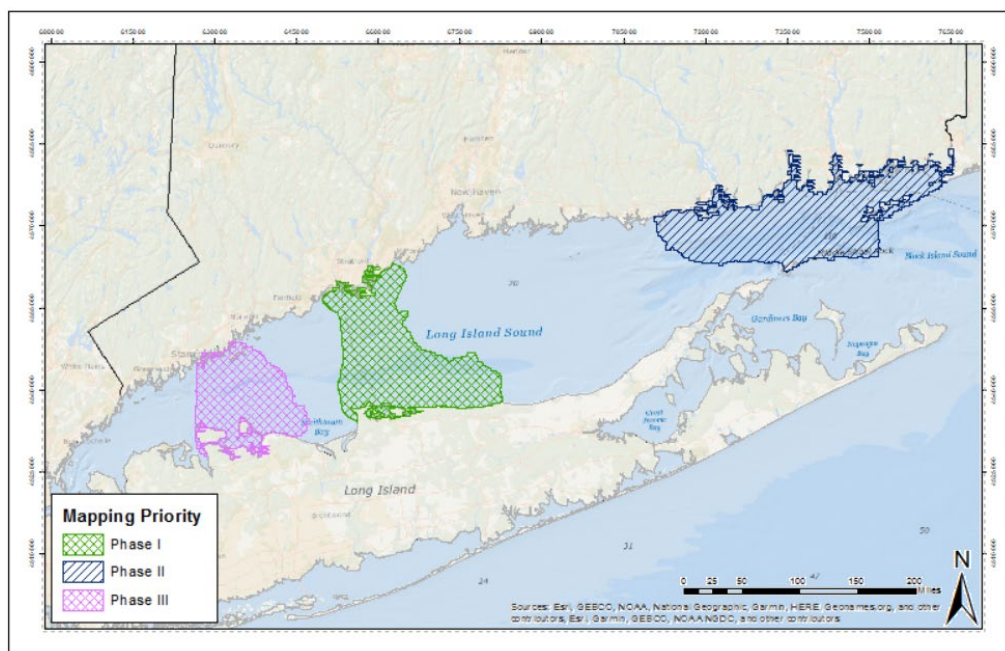
Figure 1.1-1 High Priority Mapping Areas

The Phase I Pilot project was conducted between 2012 and 2014. In 2015 the Steering Committee assessed the final products and reports, including examining the processes implemented. Their assessment affirmed that the inclusive efficacy of partnership & coordination, data collection and analysis, and product delivery in the Pilot project validated pursuing the additional phases of the mapping initiative as well as potential expansion into the additional areas of the Sound.

Several recommendations from the Steering Committee's assessment of Phase I were incorporated into the Phase II scope of work (SOW). Subsequent efforts during the development of the SOW refined the Phase II Area of Interest (AOI), essentially limiting the amount of riverine and nearshore embayments to approximate the following region (Figure 1.1-2):
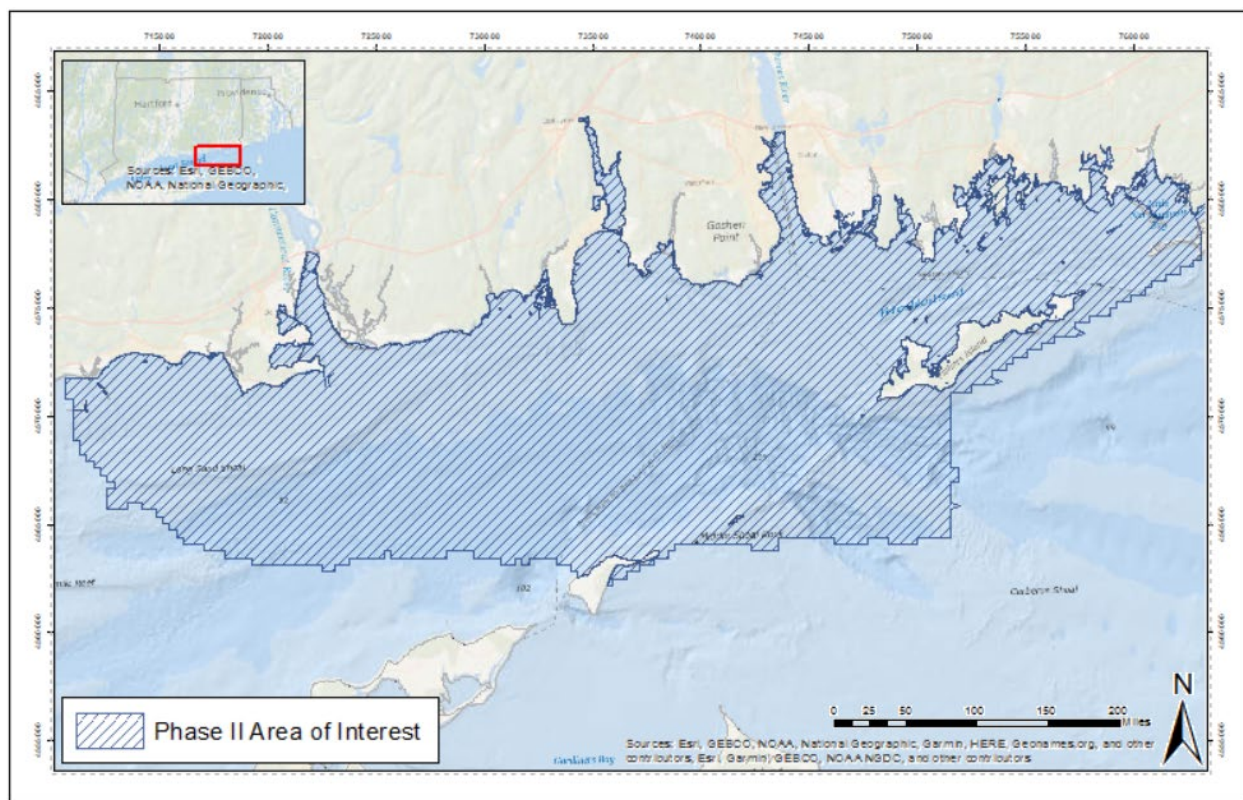
Figure 1.1-2. Phase II Study Area

The goal of the Phase II project has been to provide environmental data and information to help better understand and manage the benthic resources of eastern Long Island Sound (ELIS) by continuing in and improving on the efforts conducted during Phase I. This goal required the following areas of emphasis:

- Data collection and processing by project partners conducted using the same and/or comparable standards to ensure the ability to easily and effectively share information and integrate data into synthesized products.
- Product deliverables designed at spatial scales to include appropriate information to support regulatory and planning uses aimed primarily at site screening and assessment level efforts.
- Improved project management between project partners and the steering committee.

The objectives to achieve this goal included tasks designed to:

- Investigate and evaluate existing data and products that could be incorporated into data products;
- Define the data acquisition approaches and standards for the key data (bathymetry, backscatter, biological/ecological and physical observations) and acquire additional data to fill existing gaps;
- Utilize tested technologies and approaches for shallow water mapping;
- Develop, assess, and refine data products with a focus on the key derived products (geology, benthic habitat characterization, and topography);
- Implement the LIS habitat classification scheme developed by Auster et al. (2009), and;
- Implement and refine the data management strategy from the Pilot project for internal and external dissemination and archival of data.

The contents of this document provide a report on the processes and outcomes of the above objectives. The material presented in this report will be reviewed by the LIS Cable Fund Steering Committee to provide guidance for future mapping efforts.

2 Seafloor Topography and Acoustic Intensity

Recommended Citations:

Battista, T. (2023). Objective. Section 2.1, p. 4-5 in: "Seafloor Mapping of Long Island Sound – Final Report: Phase II Project." (Unpublished project report). U. S. Environmental Protection Agency, Long Island Sound Study, Stamford, CT.

Battista, T., Flood, R., Babb, I., & Arbige, D. (2023). Historical Context. Section 2.2, p. 5-9 in: "Seafloor Mapping of Long Island Sound – Final Report: Phase II Project." (Unpublished project report). U. S. Environmental Protection Agency, Long Island Sound Study, Stamford, CT.

Battista, T., Flood, R., Babb, I., & Arbige, D. (2023). New Data Acquisition. Section 2.3, p. 9-28 in: "Seafloor Mapping of Long Island Sound – Final Report: Phase II Project." (Unpublished project report). U. S. Environmental Protection Agency, Long Island Sound Study, Stamford, CT.

Battista, T. (2023). Integrated Products. Section 2.4, p. 28-33 in: "Seafloor Mapping of Long Island Sound – Final Report: Phase II Project." (Unpublished project report). U. S. Environmental Protection Agency, Long Island Sound Study, Stamford, CT.

Battista, T. & Flood, R. (2023). Discussion. Section 2.5, p. 33-40 in: "Seafloor Mapping of Long Island Sound – Final Report: Phase II Project." (Unpublished project report). U. S. Environmental Protection Agency, Long Island Sound Study, Stamford, CT.

Battista, T., Flood, R., Babb, I., & Arbige, D. (2023). Summary/Conclusions. Section 2.6, p. 41-42 in: "Seafloor Mapping of Long Island Sound – Final Report: Phase II Project." (Unpublished project report). U. S. Environmental Protection Agency, Long Island Sound Study, Stamford, CT.

2.1 Objective

Benthic habitat mapping in LIS has long been identified as a priority need and is essential to improving science-based environmental management and mitigation decisions. Seafloor landscape maps depicting habitat structure and the ecological characteristics associated with those habitats are critical pieces of information, which typically integrate information from a variety of sources including acoustic bathymetry and backscatter, sedimentary, geochemical, physical, and biological data. An important step in benthic habitat mapping has been the collection and analysis of high-resolution acoustic bathymetric and backscatter data that show seabed features, sedimentary processes, and sediment distribution patterns. This chapter describes activities undertaken to plan for, collect, and process data within the Phase II project area of LIS for two product types – Seafloor Topography and Acoustic Intensity.

Acoustic systems project single beam and/or multibeam sonars, which actively ensonify the seafloor to acquire synoptic, continuous data over a survey area. Acoustic sonars provide highly resolved, accurate measurements of absolute water depth (i.e., bathymetry), but the data collected can also be used to depict changes in the seafloor shape (i.e., topography) to highlight seascape changes at a range of spatial scales. Seafloor topography products showing bathymetry and terrain relief are able to depict important features, relief, and seafloor changes to better explain physical, geological, and ecological processes. Full coverage topography (bathymetry) and acoustic intensity (backscatter) images are fundamental for predicting sediment classes and habitat types (Samsudin & Hasan, 2017).

Acoustics sonars are also able to measure the intensity of sound reflected off the seafloor to give a better understanding of the composition and types of benthic habitats. Backscatter and sidescan sonar data represent the acoustic intensity of the echosounder. The amount of sound reflected or absorbed by the seafloor is also used to interpret the hardness, roughness, grain size, or biological composition of bottom features. Therefore, acoustic intensity products provide a valuable means of synoptically measuring and depicting the composition, roughness, and texture of the seafloor to map and identify the distribution of benthic habitats.

Higher frequency systems are able to detect maximum water depths and provide the highest resolution of data needed to discern fine-scale topography and feature types, so they are optimal for surveying shallow estuaries like LIS. A multibeam bathymetric system collects depths across a swath of the seafloor that is perpendicular to the vessel track by sending out an acoustic ping and then recording the sound returns at different angles. The travel time and angle information is processed to determine the water depth across the swath. The strength of the returned echo (the acoustic backscatter) is also recorded. The strength of the backscatter can often be related to the nature of the seabed material. Multibeam echosounder (MBES) systems are capable of collecting very dense, highly accurate bathymetry and backscatter data; thus, they are the most prevalent sonar system used for hydrographic and seafloor mapping efforts. 100% multibeam coverage is also the most desirable for benthic habitat studies. However, the beam swath projected by a MBES is a function of water depth, so as water depth decreases, the efficiency is substantially reduced.

Alternatively, sidescan sonar (SSS) and Phase Differencing Bathymetric Sonars (PDBS) broadcast sound at low grazing angles from each side of the sonar, providing much broader bottom coverage. SSS operates like a MBES in that the sound returned from a ping is recorded (the acoustic backscatter) across a swath. SSS provides very dense backscatter/intensity measurements of the

seafloor but no bathymetry. The angle of the returned sound for a SSS is not generally known, so no depth can be determined. However, since the spatial resolution of a sidescan sonar record is often higher than that of a multibeam system, the sidescan can show more detail about the seabed than a MBES. PDBS is a variant of SSS, which is also capable of inferencing bathymetry. However, PDBS depth calculations are generally less accurate further from the sonar, effectively negating the benefit of broad swaths if bathymetric certainty is required. While lower sound frequencies equate to deeper water penetration, conversely, a larger detection footprint equates to lower data resolution.

Given the range of water depth and clarity within the Phase II AOI, ship-mounted MBES and SSS systems were primarily implemented for much of the Phase II acoustic data acquisition. PDBS was also used to collect coincident depth and intensity (e.g., backscatter) measurements in areas of shallower depth. As in the Phase I Pilot project, federal, state, and academic partners worked collaboratively to identify and fill significant data gaps within the Phase II AOI.

2.2 Historical Context

Acoustic bathymetric and backscatter data has been collected over a large portion of LIS as a result of over two decades of charting activities conducted by the National Ocean Survey branch of NOAA. This represents a remarkable achievement by NOAA, which has resulted in accurate and up-to-date charts of LIS, which are helping to make vessel operations within the Sound safer. The acoustic systems used to collect bathymetric and backscatter data has continued to improve and NOAA survey strategies have also evolved as the charting has progressed. As a result, the data collected during earlier NOAA surveys does not have complete coverage or spatial resolution in the bathymetry or the acoustic backscatter that is needed for benthic habitat mapping. Also, complete (100% coverage) multibeam data was not always required in shallower areas for charting purposes.

NOAA's National Centers for Coastal and Ocean Science (NCCOS) compiled an inventory of existing data for the Phase II area through spatial queries of NOAA's National Centers for Environmental Information (NCEI) data archive repository and through close coordination with NOAA's Office of Coast Survey (OCS). NCCOS obtained the data from twelve distinct multibeam bathymetry surveys within the Phase II area dating from 2003 to 2014, most of which contained multibeam backscatter or sidescan images. The Phase II project extent used for the analysis covered a total area over water of 554 km^2 extending from 0 to -117.8 meters in depth (Table 2-1).

OCS conducted ten of the Phase II surveys using the NOAA Ship *Thomas Jefferson* and its launch vessels, and Navigational Response Team 5 (NRT-5) conducted two supplemental surveys. NOAA primarily utilized the Reson 7125 MBES, which has two frequency settings optimal for shallow (0-100 m; 400 kHz) and moderate (0-200 m; 200 kHz) depths, for bathymetry and backscatter data collection. In areas too shallow for the *Thomas Jefferson* to safely navigate, NOAA survey launch vessels 3101 and 3102 were deployed, each outfitted with a Reson 7125 MBES and Klein 5000 SSS towfishes. The launch vessels were used to collect data in the shallow ports of Old Saybrook for survey H12013 (2009), Niantic Bay for survey H11442 (2005), and New London Harbor for survey H11441 (2005), as well as the entire surveys of H12676 (2014) and H12298 (2011) in the shoals of the Fishers Island Sound (FIS). From July 2013 to November of 2014, NRT-5 was also deployed in a similar launch vessel using Reson 7125 MBES and Klein 5000 SSS to survey the

very western shoals of the Phase II area surveys H12508 and H12509. These efforts contributed to extensive coverage within the area (Figure 2.2-1).

Table 2-1. NOAA surveys available within the LIS Phase II area

Survey #	Platform	State	Year	Bathymetry	Intensity Type	Area (km²)
H11250	*Thomas Jefferson*	NY,CT	2003	Multibeam	Backscatter (BS)	91.9
H11361	*Thomas Jefferson*	NY	2004	Multibeam	BS & SS	7.6
H11441	*Thomas Jefferson*	CT	2005	Multibeam	BS & SS	49
H11442	*Thomas Jefferson*	CT	2005	Multibeam	BS & SS	54.6
H11445	*Thomas Jefferson*	NY	2008	Multibeam	BS & SS	6.4
H11997	*Thomas Jefferson*	NY	2008	Multibeam	BS & SS	88.3
H12012	*Thomas Jefferson*	CT	2009	Multibeam	N/A	54
H12013	*Thomas Jefferson*	CT	2009	Multibeam	Sidescan (SS)	27.7
H12298	*Thomas Jefferson*	CT	2011	Multibeam	BS & SS	7.4
H12508	NRT-5	CT	2014	Multibeam	BS & SS	33.2
H12509	NRT-5	CT	2014	Multibeam	BS & SS	28.9
H12676	*Thomas Jefferson*	CT	2014	Multibeam	BS	52.5
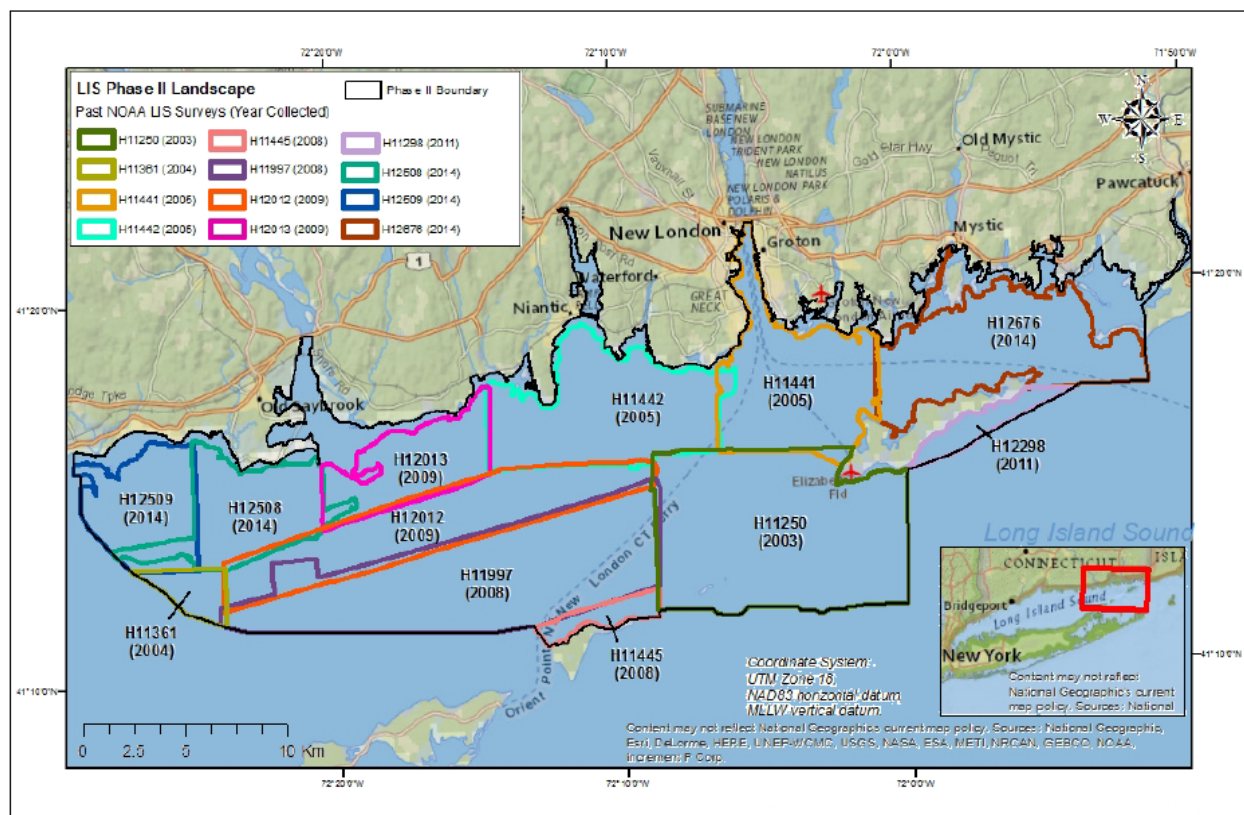
Figure 2.2-1. Phase II map overview of boundary area and landscape of past surveys in the region

The NOAA bathymetry data acquired within the Phase II area were all collected according to NOAA and International Hydrographic Organization (IHO) standards. All of the acquired multibeam data were processed using CARIS HIPS and SIPS software and corrected for tides, sound velocity, vessel motion, and geodetic positioning. An uncertainty surface was also created

using the CARIS Combined Uncertainty Bathymetric Estimator (CUBE) algorithm. Uncertainty contains multiple hypotheses representing potential depth variances on the seafloor. After the bathymetry and uncertainty data were cleaned of artifacts, validated, and accepted, the final data were exported as 32-bit Bathymetric Attributed Grid (BAG) files containing the depth and the uncertainty surfaces projected to the 1983 North American Datum (NAD 83) and set to the Mean Lower Low Water (MLLW) vertical datum. The NCCOS Biogeography Branch requested the datasets from NCEI and downloaded the BAG and raw files. They then exported the bathymetry and uncertainty surfaces from the BAG files into separate products and merged them in ArcMap 10.3 using the Mosaic to New Raster tool. The merged dataset was clipped to the Phase II area extent and finally exported as combined 32-bit, 2-meter resolution GeoTIFFs. The merged bathymetry was also separated into IHO depth thresholds and exported as 32-bit GeoTIFFs to the appropriate standard resolutions (Figure 2.2-2).

Most of the surveys with the Phase II area logged backscatter (excluding H12013 and H12012 in 2009), but this data type was not universally adopted by NOAA until 2012. As a result, many older surveys contained poor quality backscatter that had to be extensively cleaned and reprocessed by the Biogeography Branch. Contractors from NOAA's Biogeography Branch were present onboard the *Thomas Jefferson* during the H12676 survey of 2014 in the Fisher Island Sound, to advise OCS survey technicians regarding new backscatter collection techniques, data quality control, and mosaic processing. The *Thomas Jefferson* has since adopted these new backscatter standard operating procedures developed by the Biogeography Branch and the Integrated Ocean and Coastal Mapping Team (IOCM). These new quality control measures were necessary to optimize the coincidence of sonar intensity measurements between the *Thomas Jefferson* and the two survey launch vessels. The quality control measures also included the use of a newly developed saturation monitoring tool for snippet collection from the University of New Hampshire. In addition, the Biogeography Branch was able to maintain oversight and quality review of NRT-5 collection efforts through frequent remote access to the data. Through NOAA's partnership with the LIS Seafloor Habitat Mapping Initiative, NCCOS was able to make a concerted effort to focus on and ensure the more complete and thorough inclusion of backscatter data in collection efforts.

The Biogeography Branch assessed all of the backscatter from the 2014 *Thomas Jefferson* and NRT-5, and all of the existing backscatter and sidescan data available between 2003 -2011 for the Phase II area available from the NCEI archives. The archived backscatter data was in its raw format and had to be converted to GSF format and cleaned using Fledermaus Geocoder Toolbox 7.4 (FMGT). The original sidescan mosaics were also analyzed for quality and reprocessed using CARIS HIPS and SIPS 9.0. Once all of the intensity data was reprocessed, a new 1 meter resolution mosaic was created and georeferenced using ENVI 5.1 and ArcMap 10.3 GIS software.

NCCOS encountered several issues trying to merge the backscatter data collected during different surveys over a range of years. Inconsistent sonar calibration settings, varying operator settings, and altered bottom conditions during the course of the collection efforts contributed to the difficulties in creating a seamless mosaic. In order to compensate for these problems, each survey from each vessel had to be processed separately with a new beam pattern to adjust for decibel offsets between each sonar system and merged using the FMGT mosaic editor. Many surveys contained artifacts associated with sonar signal to noise issues, insufficient sound velocity corrections, or along-track gain artifacts originating from sonar tuning.

Sonar gain changes are often made by the sonar technician during surveys to optimize bathymetry collection; however, these adjustments can often oversaturate the backscatter data, artificially increasing the decibels of the intensity returns. This can cause the backscatter values to display as almost white (saturated) versus a range of grey scale colors during optimum collection. The Biogeography Branch has developed specialized techniques to minimize these artifacts using the raster segmenting tool in ENVI 5.1, which extracts the areas of tracklines that are oversaturated. Once these areas were extracted, the histograms could be manually rendered to normal values and merged back into the mosaic using ArcMap 10.3. Once each survey was normalized and cleaned, it was imported into the ENVI 5.1 georeferenced mosaic tool to be merged. This tool balances the colors of overlapping pixels from the GeoTIFFs and applies a feathering technique to dissolve the edges for a smoother mosaic. The result is an improved color balanced mosaic.

The final LIS Phase II intensity mosaic is a merger of all the backscatter and sidescan from 2003 to 2014. The image is a rendered 8-bit GeoTIFF in the UTM 18N NAD 1983 projection (Figure 2.2-3). The histogram for the mosaic is valued from 0-255, or respectively low to high intensity. These 0-255 values portray the relative intensity of the decibel values on a stretched greyscale, with the lighter shades representing higher acoustic intensity reflection (i.e., coarser sediment) and darker shades representing lower acoustic intensity reflection (i.e., softer sediments). The reprocessed data from the NOAA bathymetry and sidescan sonar surveys was available to the Phase II project prior to field data collection, and the results were used to help plan ship-based activities for the other elements of the project.
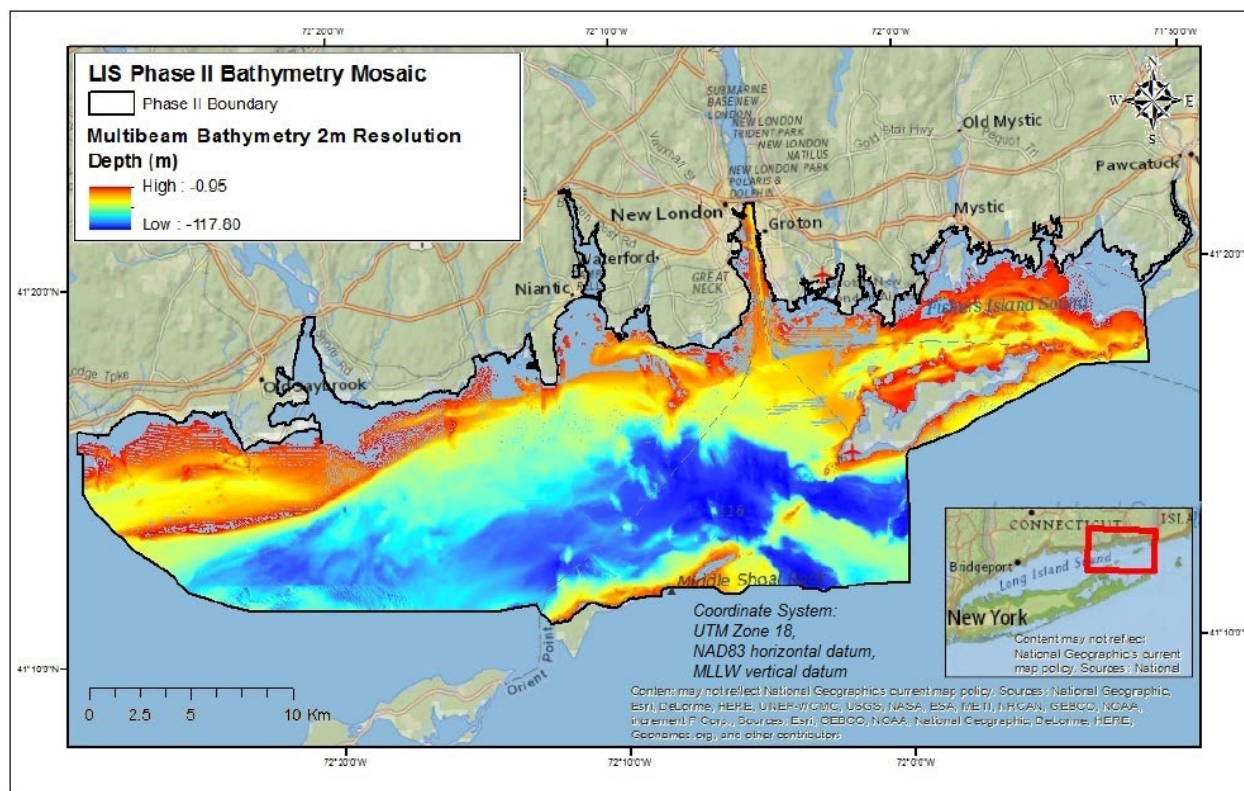
Figure 2.2-2. Unified multibeam bathymetry mosaic for the Phase II area at 2m resolution
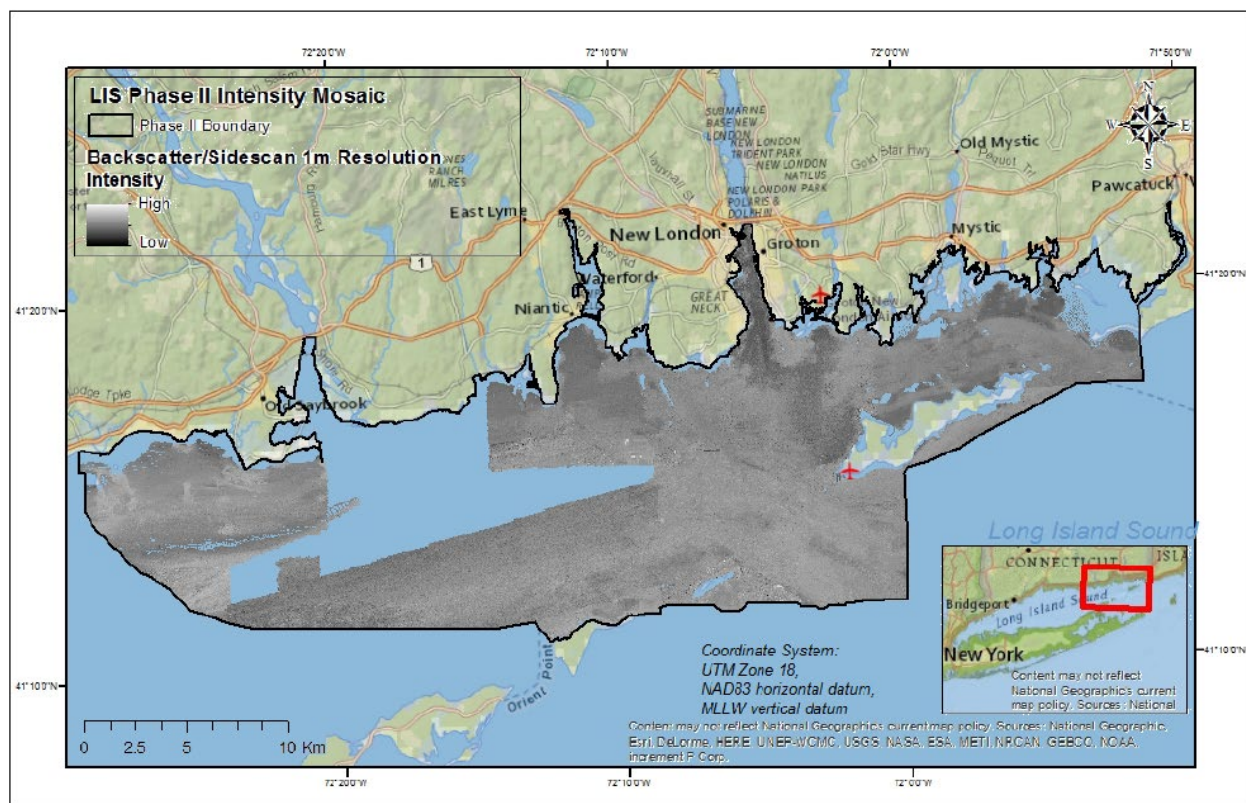
Figure 2.2-3. Unified acoustic intensity mosaic for the Phase II area at 1m resolution

2.3   New Data Acquisition

Within a few areas of the older surveys, the data quality was so poor that the resulting output could not be significantly improved. These areas, along with the H12013 and H12012, which did not contain backscatter or sidescan data at all, required resurvey. The analysis of the existing data also identified data gaps for both bathymetry and backscatter in previously unsurveyed areas within the Phase II AOI. These data gaps were targeted for acoustic data acquisition by the academic collaboratives. The details of both efforts are explained in subsequent sections.

The NCCOS analysis indicated that most of the data gap areas occurred in shallow areas along the Connecticut shoreline or over large shoals. NCCOS provided a prioritization and survey estimates for the data gaps using the Fugro Pelagos, Inc. Survey Estimator Tool for ArcGIS. NCCOS parsed the unmapped areas into two shallow blocks (1-3 fathoms) and thirty deeper blocks (>3 fathoms) (Figure 2.3-1). The decision was made not to attempt surveying the two shallow blocks due primarily to the challenging nature of working in the areas, including the lengthy survey time and shallow vessel draft that would be required. Stony Brook University (SBU) from the Lamont-Doherty Earth Observatory Collaborative (LDEO) and the University of Connecticut (UConn) from the Long Island Sound Mapping and Research Collaborative (LISMaRC) coordinated efforts to map the deeper water priority sites using their respective technologies. Of the thirty deeper blocks, #1-28 were selected for continued study.
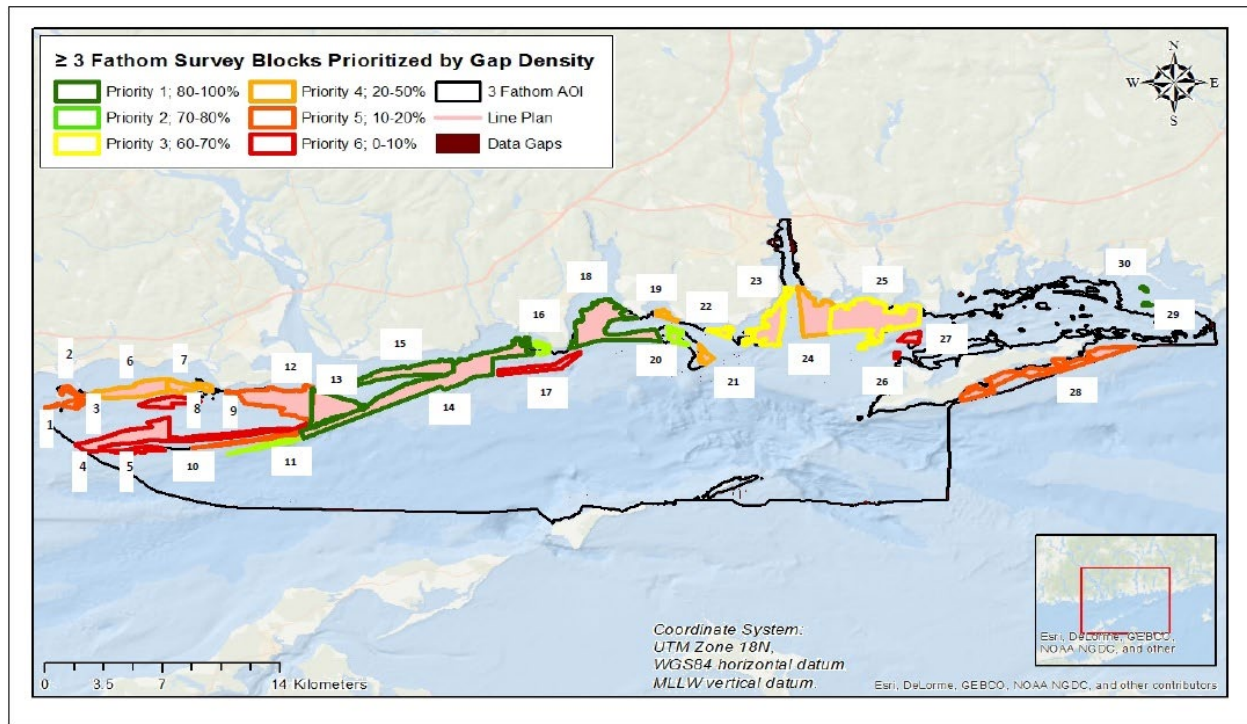
Figure 2.3-1. 30. blocks covering a majority of the ≥ 3 fathom data gaps, prioritized by gap density

2.3.1 NOAA Data Acquisition

The objective of this task was to collect a multibeam bathymetry dataset with 100% seafloor ensonification, along with multibeam backscatter suitable for seafloor characterization in the areas within the Phase II AOI where the existing surveys did not include backscatter or sidescan data and where the existing data quality was insufficient to support habitat mapping. This resurvey was conducted onboard the NOAA Ship *Nancy Foster* in coordination with NCCOS and IOCM between September and October 2015. New acoustic data was acquired over 140.1 square kilometers (54.1 square miles) using Kongsberg Maritime EM 710 and Teledyne RESON SeaBat 7125 SV multibeam sonars.

NCCOS processed the acoustic data using NOAA and hydrographic industry standards to account and correct for vessel motion artifacts. The raw and processed multibeam data was delivered with complete traceability for all positions, soundings, and correctors including sensor offsets, biases, dynamic attitude, navigation, sound velocity, date and time, and vertical datum reducers from acquisition through post-processing. Observed echosounder depths were corrected for all departures from true depths attributable to the method of sounding or to faults in the measuring apparatus. Both the raw digital data files and the final digital corrected files were provided, as well as preliminary geospatial products depicting acoustic intensity and bathymetry derived from the new data (Figure 2.3-2).
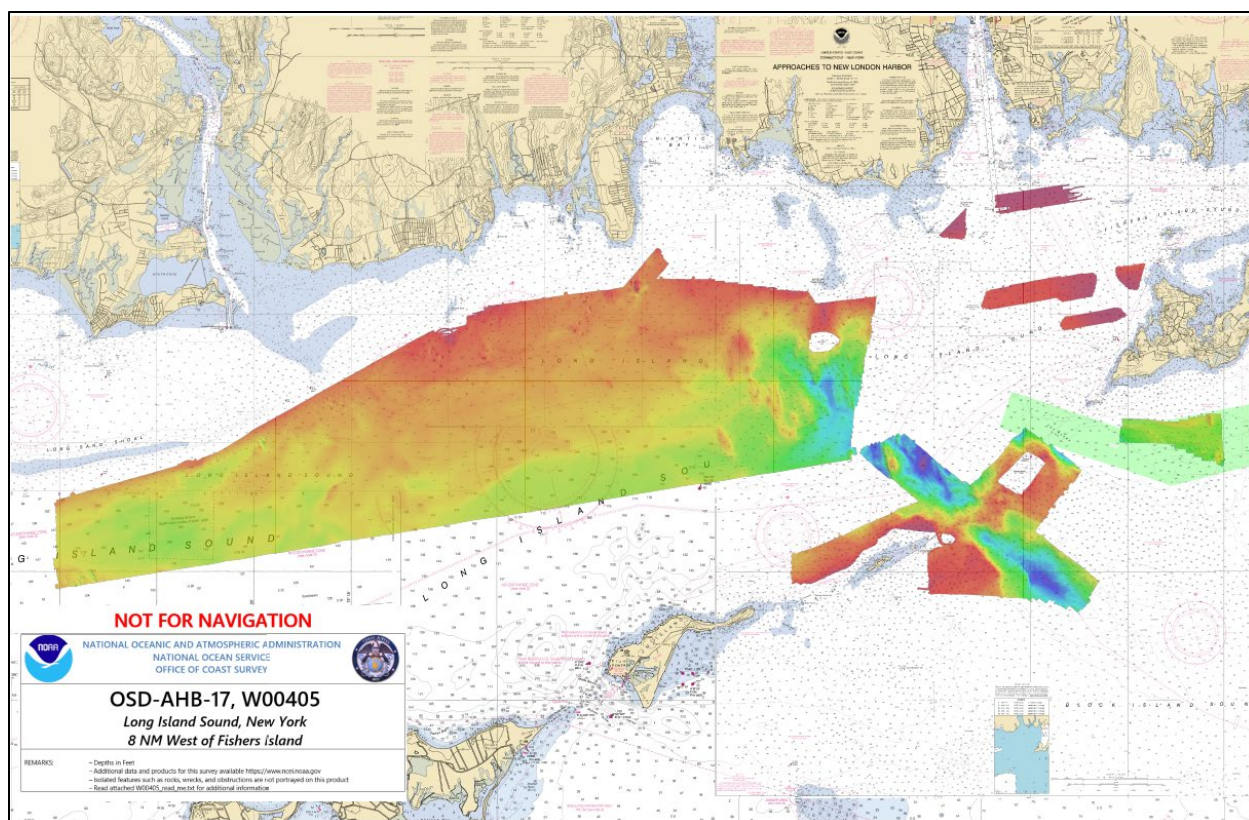
Figure 2.3-2. Bathymetry from the Nancy Foster multibeam survey within the Phase II study area

2.3.2 LDEO Data Acquisition

2.3.2.1 Methodology

Equipment and Survey Parameters

The team from the SBU School of Marine and Atmospheric Sciences (SoMAS) conducted acoustic surveys in twenty-five of the prioritized data gap blocks depicted in Figure 2.3-1 over approximately 91 square kilometers (35 square miles) during two deployments (Table 2-2). The first deployment was from December 2017 through March 2018, and the second deployment was in June and July 2018. NCCOS advised SoMAS on the best practices for data collection and quality control from the NOAA *Hydrographic Surveys Specifications and Deliverables* (HSSD, 2016). This ensured the survey met nautical charting standards for overlap, ping density, and cross line analysis.

During their deployments SoMAS collected data continuously along track; they ran at full speed and did not collect sound velocity profiles. They collected data during transits in order to identify areas where seabed morphology has changed between the prior NOAA surveys and this study. During the block surveys they collected data at normal survey speeds, and tracklines extended far enough beyond the boundaries of each block so that there was significant overlap with data surrounding the block. On several occasions where the blocks were close together, they conducted one survey that included several blocks, or parts of blocks. Due to time constraints not all of the blocks surveyed during the first deployment were completed, so those blocks were completed

during the second deployment. The results of multiple surveys in the same blocks are reported separately. Survey activities in all blocks were completed in 2018.

SoMAS had initially planned to work in the shallowest areas during the first deployment using the 28-foot R/V *Donald W. Pritchard* and then work in the deeper areas using the 80-foot R/V *Seawolf*. However, the R/V *Seawolf* was not available for the second mapping deployment, so the R/V *Pritchard* was also used for the second mapping deployment. During both deployments SoMAS used a Kongsberg multibeam system along with an Applanix motion sensor and GPS system, one or more Trimble RTK-capable GNSS receivers (using networked, land-based satellite corrections provided by the UConn Advanced Continuously Operating Reference Network (ACORN) Real Time Network (RTN)), an AML Oceanographic probe for surface-water sound velocity, and a profiling AML Oceanographic sound-velocity probe for the water-column sound-velocity profile. Other needed survey equipment included a computer system to operate the MBES (including a system to guide the helmsman along the desired survey line) and to log the survey data. The SSS, used during the first deployment to ensure 100% backscatter coverage, had a separate computer to operate the system and log the survey data.

During the first deployment the team used the SoMAS Kongsberg EM 3000D MBES for bathymetry and backscatter and the SoMAS Edgetech 272TD SSS for backscatter at a different frequency. The EM 3000D MBES system uses two transducers mounted so as to create a wider mapping swath (up to 10 times water depth in the shallowest water and decreasing as the water depth increases), which can reduce the surveying effort. The across-track width of the swath is generally a characteristic of the transducer design, and the swath width (line spacing) of a single transducer is often about four or five times the water depth. The 272TD SSS was mounted on a pole rather than towed in the traditional fashion. Mounting the SSS unit on a pole reduces uncertainty in the position of the sonar system and simplifies vessel operations in shallow water settings. However, a pole-mounted SSS has considerably more motion than a towed sonar since the sonar rolls and pitches along with the boat, so the motion of the SSS significantly degraded that data.

The EM 3000D used sound waves of 300 kHz, and the 272TD used sound waves of 100 kHz. The acoustic backscatter depends in part on the wavelength of the sound being used, so mapping at multiple frequencies can provide additional insight into the character of the seabed. Many other factors also affect the recorded backscatter, including sound attenuation in the water column, wind and wave conditions, and the noise of the ship's engine. While the width of the multibeam swath varies with water depth, SSS uses a fixed swath, which SoMAS employed at 150 meters (75 meters/side, 10 pings/second).

Vessel operations in the first deployment from December to mid-March were hindered by wintery conditions and scheduled classes. SoMAS resumed operations during spring break in mid-March and successfully mapped for 21 days. They completed seven of the assigned survey blocks, and collected data in the shallower parts of four other survey blocks.

The EM3000 multibeam system has been used at SoMAS since about 1998, and the system was upgraded to dual-head operation in about 2004. The multibeam system utilizes a SUN Solaris Ultra 2 computer system, which is now obsolete; although, SoMAS has been able to keep their computer systems and Kongsberg hardware and software operating. The license for the Kongsberg software is on a chip in the Ultra 2, which has a built-in battery. That battery had failed on the computer

system being used; although, the computer and software could be started and used by typing in the license code. However, that caused the date being recorded to be consistently incorrect; although, the time of day was correctly set from the GPS system. The multibeam files that were recorded with the wrong dates were renamed and rewritten with the correct file names and dates (except that the names of the sound-velocity profiles incorporated in the .all files were not updated). Only the rewritten files with the corrected dates have been used in processing. The failed chip battery was replaced after the 10th survey day.

SoMAS successfully mapped for 12 days in the second deployment using a leased EM 2040CD MBES. This was the current model of the EM 3000D system, so it had a faster ping rate and could obtain a wider swath than the EM 3000D at the same water depth. NCCOS contractors participated in the installation and patch test of the dual swath EM2040CD to correct for any offsets within the system and ensure that data quality was sufficient for habitat mapping. These improvements somewhat compensated for not using the R/V *Seawolf*, and enabled SoMAS to complete the survey assignment in the second deployment while still meeting the survey requirement of obtaining at least five depth points per grid cell and multibeam backscatter, despite time lost for mechanical issues experienced on the R/V *Pritchard*. The EM 2040CD was operated at 300 kHz, and SSS was not used during the second deployment.

Both multibeam systems recorded raw data in the Kongsberg .all format, which incorporates datagrams from each piece of equipment used during the survey into one large file, including datagrams from the MBES, the motion sensor, GPS navigation systems, and sound velocity data. Navigation data was also recorded independently of the multibeam system to allow for additional filtering. The multibeam survey technique requires that the relative positions and orientations of all of the equipment in use be known and that the times at which the different pieces of equipment made a measurement be known so that the different data streams can be combined. SoMAS used a land surveyor to measure the relative positions of instruments on the R/V *Donald W. Pritchard* when the boat was out of the water, and they performed required calibrations at several times during the survey operations to verify and fine-tune equipment offsets. The survey results using the EM 3000D system were quite good; it successfully collected high-quality bathymetric data even at times when the survey vessel was moving over 1 m vertically with significant roll and pitch. Although, some small motion artifacts were often observed. The survey results with the EM 2040cD system were quite good when vessel motions were small, but the data showed some motion artifacts when significant wave motion was experienced. These motion artifacts in part were caused by a small time offset of about 0.005 seconds between the echosounder (depth) and motion data (roll, pitch, heading, and heave). This offset was apparently not present when using the EM 3000D system on a Sun computer with the Solaris operating system. The EM 2040cD multibeam system is normally used with a Kongsberg motion sensor, but SoMAS used a motion sensor from a different manufacturer. The time offset for the motion sensor is suspected to be somehow related to using the non-Kongsberg motion sensor on the Windows 10 computer. SoMAS was able to substantially correct for a constant timing error, but some residual motion remains in the multibeam depth data.

The data from the pole-mounted Edgetech 272TD SSS was recorded in XTF format on a Windows computer using Triton-Elics software. The XTF files included SSS data and navigation data. The time of the SSS system is synchronized to the time of the MBES system so that data recorded by the MBES (especially water depth, orientation, and filtered navigation) can be applied to the SSS system during data processing.

Table 2-2. Acoustic survey details

SoMAS Acoustic Survey Areas					
Survey Name	Survey Blocks	Survey Area (km²)	Deployment		Blocks Completed?	Rationale
		Total SoMAS Survey Area: 90.96 km²	December, 2017 to March, 2018 (DM)	June-July, 2018 (JJ)	C = Complete P = Partial	
01-02-03_JJ	01, 02, 03	2.29		JJ	C, C, C	Three small, adjacent survey blocks combined into one survey
04-05_JJ	04, 05	1.89		JJ	C, C	Map areas overlap so reported as one survey
06_DM	06	7.34	DM		C	
07_JJ	07	4.15		JJ	C	
08_JJ	08	2.42		JJ	C	
09_JJ	09	2.18		JJ	C	
10_JJ	10	2.14		JJ	C	
11_Cal_JJ	11	0.97		JJ	P	One of several calibration surveys but with a sharp edge and steep slope
11_JJ	11	0.75		JJ	C	
12_JJ	12	1.18		JJ	P	Large survey block off Connecticut River, western portion
13_DM	12, 13	2.70	DM		P	Large block off Connecticut River, eastern portion
13_JJ	12, 13	9.03		JJ	P	Single JJ tracks that overlay with 12_DM survey to evaluate temporal variability
14_JJ	14	5.90		JJ	P	Large survey block, western end
14-16_DM	14, 16	2.84	DM		P, C	Large survey block, eastern end, and nearby small survey block 16
15_DM	15	11.10	DM		C	
17_JJ	17	4.60		JJ	C	
18_DM	18	2.48	DM		P	Large survey block northern portion
18_JJ	18	6.65		JJ	P	Large survey blcck, southern portion
19_DM	19	2.58	DM		C	
20_DM	20	0.47	DM		C	
21_DM	21	1.21	DM		C	
22_DM	22	0.93	DM		C	
24_NL-Light_JJ	24	0.59		JJ	P	Part of survey block 24 near New London Lighthouse that overlaps with LISMarc survey area for comparison purposes
25-26-27_JJ	25, 26, 27	1.86		JJ	P, C, C	Two small, adjacent survey blocks and nearby portion of survey block 25 that overlaps LISMarc survey for comparison purposes
28_JJ	28	5.27		JJ	C	
Barchans_JJ	none	7.45		JJ	C	Barchan dunes observed on earlier NOAA data, resurvey to determine bed form activity and migration rate, map produced at 2 x 2 m grid resolution due to water depth of 50-60 m

2.3.2.2 Data Processing

Multibeam and Backscatter Data

The multibeam depth data was processed using CARIS HIPS and SIPS, version 10.4 and multibeam backscatter data was processed using the QPS FMGT, version 7.9.5. Programs from the University of New Brunswick SwathEd multibeam processing system were also used in evaluating the multibeam depth and backscatter data and for processing the SSS data. The multibeam programs processes the Kongsberg .all files so that data from each ping has the proper orientation, position, and sound-velocity data, taking into account the offsets between instruments. FMGT also corrects the multibeam backscatter data for beam pattern. The software packages can also be used to edit data from individual sensors and calculate the final water depth after integrating water level data and the sound-velocity profile data. The SSS XTF files were processed using SwathEd programs as modified at SoMAS. Vessel motion induced artifacts on sonar soundings were filtered and smoothed using the smoothed best estimate of trajectory (SBET) derived from the Applanix positioning system. Processing steps included reformatting the sonar data, integrating navigation, orientation, and water-depth with data extracted from the multibeam data files, and correcting the SSS data for beam pattern.

Navigation and Water level Data

RTK fixes can have nominal horizontal accuracies of 1 cm and vertical accuracies of 2 cm. Successful RTK fixes require an adequate internet or radio connection to receive correction data from a nearby base station or a correction network. Since the accuracy of the fix degrades with distance, an appropriate satellite geometry and strong satellite signals are needed. Fixes can't be calculated if there are not enough satellites or if they are in a row because the signals can be degraded by solar and weather conditions. When all conditions are met, then the GPS/GNSS receivers can determine a 3D fix (latitude, longitude, and elevation) up to 10 times per second. If all conditions are not met, then the receivers determine a 2D fix (latitude and longitude) using the RTK corrections or possibly Wide Area Augmentation System (WAAS) corrections. The quality and mode of each fix is shown in the navigation telegram. While latitudes and longitudes for 2D fixes are not as accurate as for 3D fixes, 2D fixes can be adequate for determining the position of the survey vessel. The navigation fixes determined using the ACORN RTN are in the NAD83 (2011) coordinate system and elevations are referred to the NAD83 ellipsoidal datum. The navigation fixes were filtered to retain the high quality navigation (latitude, longitude) and elevation (latitude, longitude, and elevation) fixes, and the high quality navigation fixes were merged with the multibeam depth data.

The SoMAS survey results are reported in the NAD83 (2011) horizontal coordinate system and the NAVD 88 vertical datum (North American Vertical Datum of 1988). NAVD 88 is the official vertical datum of the United States and is an approximation of MSL. Water depth on navigation charts is generally referenced to Mean Lower Low Water (MLLW) rather than NAVD 88 because users of those charts want to know about the shallowest likely depth in an area, and that depth occurs at low tide. Users of the data reported here should be aware that water depths reported with respect to NAVD 88 will seem to be deeper than water depths reported with respect to MLLW, and this is one of several reasons why this depth data should not be used for navigation. Depth data can be converted from one vertical datum to another (e.g., from NAVD 88 to MLLW) using NOAA's online and downloadable Vertical Datum's Transformation (VDatum) tool.

Elevations in NAVD 88 can be determined by subtracting the geoidal height from the ellipsoidal height. The ellipsoidal height is reported by the GPS/GNSS fix, and the geoidal height at the navigation point is determined using the NOAA National Geodetic Survey webpage for Computation of GEOID12A Geoid Height. SoMAS verified the elevation measurements in NAVD 88 by comparing elevations they measured while the survey vessel was docked at the Ragged Rock Marina in Old Saybrook, CT to water level measurements at a gauge SoMAS installed at the marina and with the NAVD 88 water level recorded every 5 minutes by USGS at the nearby station at Old Lyme, CT (USGS 01194796).

The precision 1-second latitude, longitude, and elevation fixes were used to determine water level relative to the NAVD 88 datum along the ship track and, thus, to reference the measured seafloor elevation to NAVD 88. The high quality GPS/GNSS elevation fixes were averaged into six-minute intervals to determine the equivalent of a six-minute tidal curve at the position of the vessel during the survey. In the absence of precise elevation data, NOAA generally calculates water level at the vessel location during a survey by scaling water level measurements at a nearby NOAA water level station and applying a time delay. The scaling factor and the time delay are determined based on the NOAA CO-OPS Discrete Tidal Zoning Map. Our GPS/GNSS-based water level record compared favorably to the offset and scaled water level measurements made by NOAA at the New London, CT water level gauge (8461490), and any gaps in the elevation record were filled with values consistent with the offset and scaled NOAA tidal record.

Sound Velocity Profiles

The vertical sound velocity profile in the water column needs to be known to correct for the bending of sound rays (refraction) in the water column, which occurs when sound velocity varies in the water column. Use of an incorrect sound velocity profile can create significant depth errors, especially at the outer edges of the swath. Sound velocity can also vary spatially and temporally because of currents, tidal water movements, flow over topography, varying amounts of fresh water input (especially off rivers), vertical mixing due to winds or waves, and the development of internal waves on density interfaces in the water column.

Much of the survey activity occurred at or near the mouth of the Connecticut River, which is the major source of fresh water to LIS. Freshwater discharge to LIS is largest during ebbing tides when water is drawn from the Connecticut River estuary and river and smallest during flooding tides when LIS water is drawn into the estuary. There is considerable mixing in LIS off the river mouth and in the Connecticut River estuary, which creates significant lateral and temporal local variability in sound velocity values and water column structure. The Connecticut River discharge generally moves eastward in LIS along with the general circulation; although, details of the water motion depend on tidal currents and winds. There are additional complications to the sound velocity structure near the Thames River at New London, but freshwater discharge from the Thames River is significantly smaller than that from the Connecticut River.

Sound velocity casts are taken by lowering a probe through the water column. The profiles are examined immediately after collection and edited if necessary to remove any bad data. Sound velocity profiles with closely-spaced measurements in the vertical need to be subsampled to use with the data acquisition software. The Kongsberg software filters the sound velocity profile but keeps a sufficient number of points to properly calculate ray bending. Standard survey protocol, which was followed, is to collect sound-velocity casts at least every four hours but more often if

anomalies are observed on the bathymetric swath. SoMAS attempted to collect closely-spaced sound-velocity profiles during the first deployment by using a system that can collect a velocity profile while the ship is underway. However, the system proved to be unwieldy on the small survey vessel, so sound velocity profiles could only be collected when the vessel was stopped.

A total of 172 sound velocity profiles were collected during the study – 112 during the first deployment and 60 during the second deployment. CARIS HIPS and SIPS can recalculate water depths based on the sound velocity profiles collected during the survey. However, sound velocity structure in the water column often changes more quickly than can be captured with periodic sound velocity profiles, so some later sound-velocity corrections using tools within CARIS HIPS and SIPS are often required. Internal waves can create small-scale lateral variability in sound velocity structure, which can create depth anomalies, which are most pronounced at the outer portions of the swaths. These kinds of anomalies were generally removed by editing the depth data.

2.3.2.3 Results

Map Creation and Production

CARIS HIPS and SIPS, FMGT, and SwathEd programs were used to create the map products depicted in Figure 2.3-3, Figure 2.3-4 & Figure 2.3-5 using the NAD83 (2011) coordinate system (UTM Zone 18N) and the NAVD 88 vertical datum. Full page versions of these maps in the standard template are provided in Appendix 1 of this report, and the GeoTIFF images are available at the LIS Data Portal.

As noted previously, the defined survey blocks were quite close together in some areas. In some of those cases, data collected during one ship survey included several defined survey blocks; while in other cases, data from adjacent blocks had significant overlap (Table 2-2). Some of the survey blocks were large enough to require data collection during both deployments (i.e., survey blocks 12, 13, 14 and 18), and data collected during different deployments overlapped considerably and were reported separately due to the use of different equipment in the two deployments. The data in survey 13_JJ consists mostly of single tracks that cover the same area mapped in 13_DM in order to evaluate temporal variability. Survey data reported from a portion of block 11 (survey 11_Cal_JJ) is reported separately from the other data in survey 11_JJ. Survey 11_Cal_JJ was one of the calibration areas, so there are many overlapping lines in the survey. This area is of potential interest because it includes a relatively flat 250 m x 500 m area at a depth of 26 m, which has a sharp edge where it intersects a steep slope (with slopes over 30 degrees) that extends to water depths of 50 m over a horizontal distance of about 250 m. This unusual geometry is possibly related to the underlying geological structure at the site.

SoMAS also collected and reported multibeam data in parts of two of the survey blocks mapped by LISMaRC, survey blocks 24 and 25, in order to facilitate the comparison of depth and backscatter data collected by the two sets of surveys. The data collected in block 24 (survey area 24_NL-Light_JJ) was in the vicinity of the New London Ledge Lighthouse, and the data collected in the southernmost portion of survey block 25 is reported in the survey that also covered the small survey blocks 26 and 27 (survey area 25-26-27_JJ, Table 2-2).

A short survey was also conducted at a water depth from about 50 to 60 m where prior NOAA multibeam data showed the existence of barchan sand dunes. This kind of crescentic sand dune,

which opens in the direction of travel is often found in desert areas and underwater where there is some sand over a harder substrate and the unidirectional wind or water flow has swept the sand into one or more barchan dunes. We were interested to learn if currents in the area had been strong enough to cause the barchan sand dunes to move and how far they had moved since the prior NOAA multibeam survey.

Overall, maps were produced for 26 survey areas as GIS-compatible GeoTIFF grids with appropriate metadata using SoMAS data (Table 2-2). Nine survey areas used data collected during the DM deployment and 17 survey areas used data collected during the JJ deployment. Bathymetry maps and hillshade bathymetry maps were created using CARIS HIPS and SIPS. Multibeam backscatter maps were created using QPS FMGT, and SSS backscatter maps were created using SwathEd (DM deployment only). The grid size was 1m x 1m except for the Barchans survey (water depth about 50-60 m) where the depth grid size was 2m x 2m.
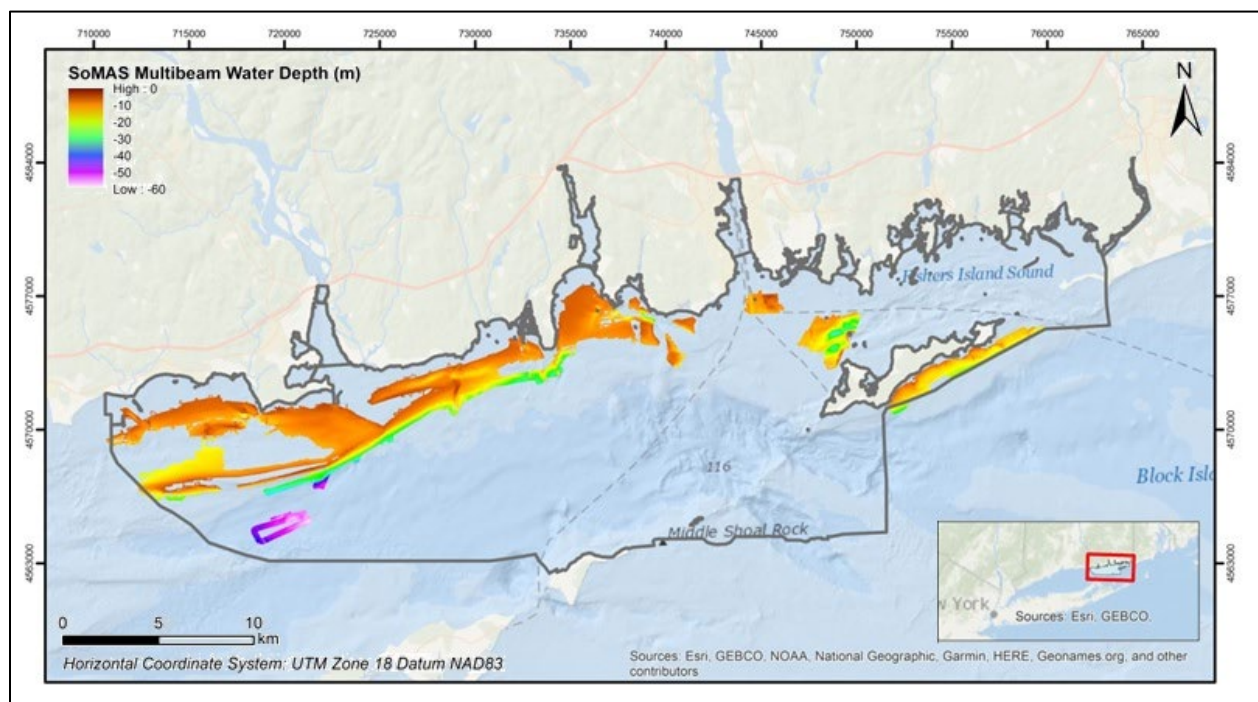
Figure 2.3-3. SoMAS multibeam depth data plotted in the Phase II study area
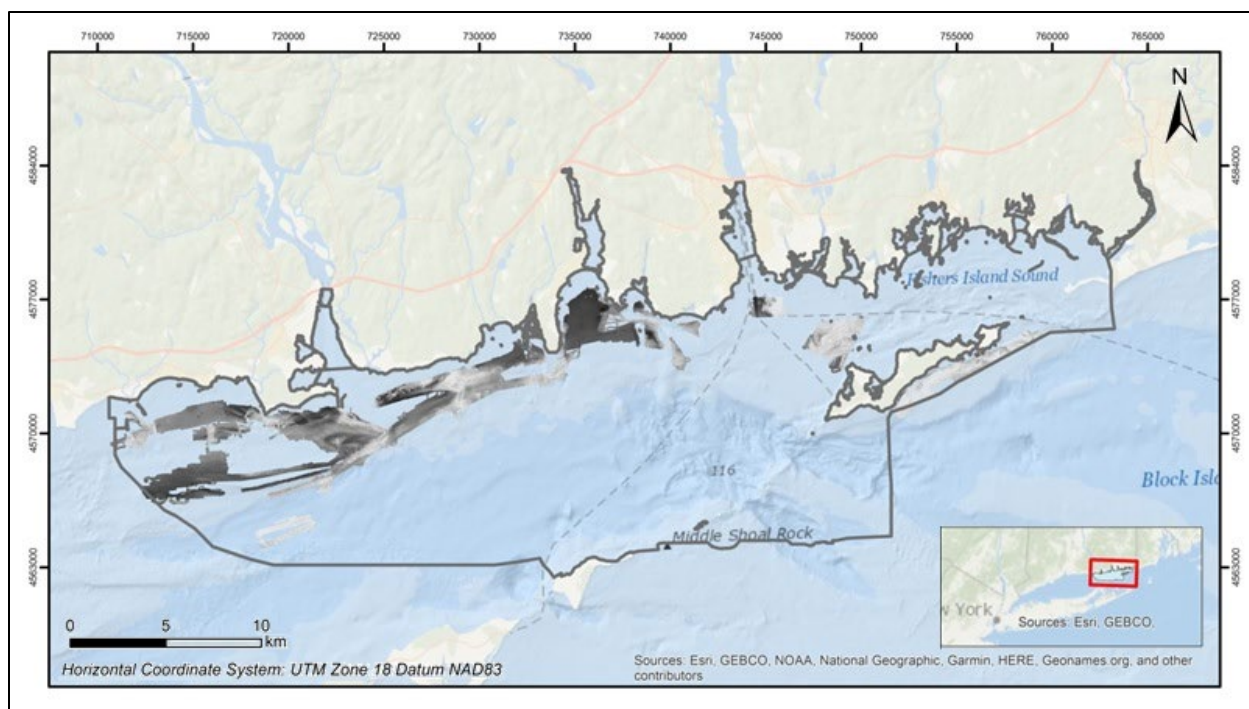
Figure 2.3-4. SoMAS multibeam backscatter data plotted in the Phase II study area
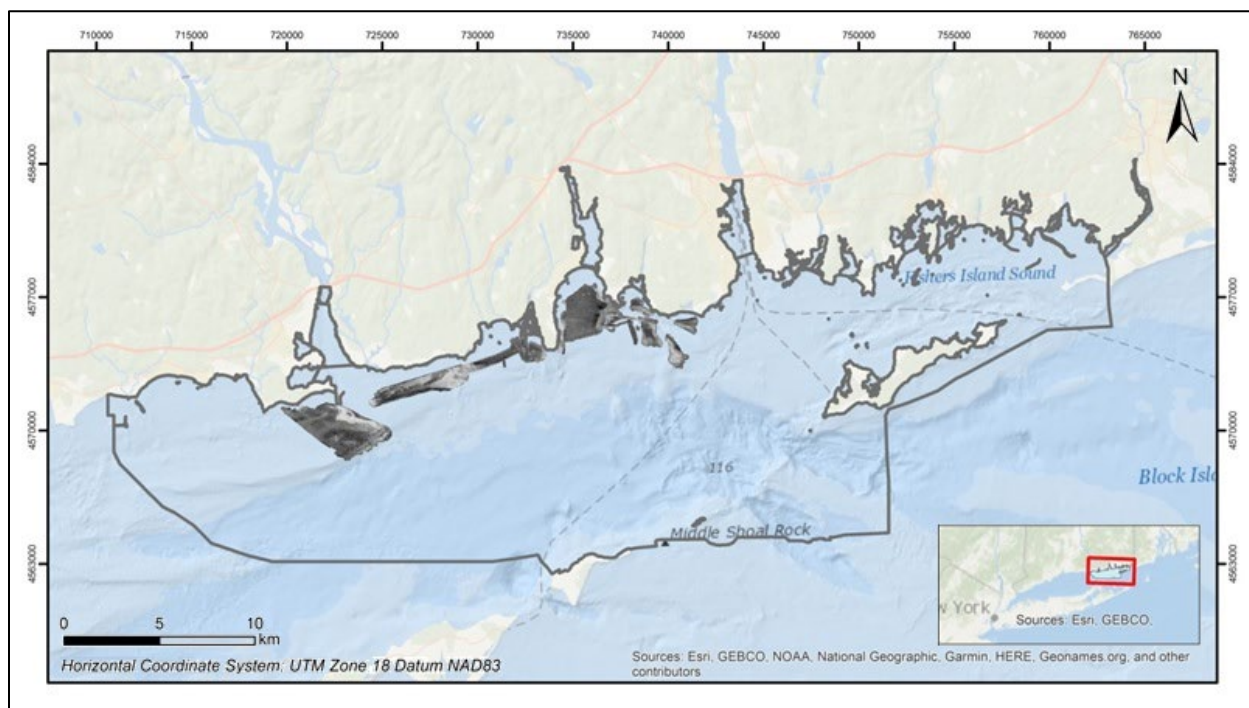
Figure 2.3-5. SoMAS SSS backscatter December-March deployment data plotted in the Phase II study area

2.3.3 LISMaRC Data Acquisition

2.3.3.1 Methodology

Equipment and Survey Parameters

The UConn team conducted a 20-day mapping campaign that included survey blocks 23, 24, and 25 depicted in Figure 2.3-1. This resulted in new data acquisition over 3.49 square kilometers (1.35 square miles) for Block 23 and 12.8 square kilometers (4.95 square miles) for Blocks 24 and 25, for a total of 16.29 square kilometers (6.3 square miles), utilizing its Geoswath PDBS (also called an interferometric system) on the R/V *Weicker*. The Geoswath system was mounted in the moonpool on the R/V *Weicker*, and the acquisition system was located on nearby workbench (Figure 2.3-6). Prior to conducting the acoustic surveys of the selected blocks, LISMaRC consulted with Val Schmidt from the Center for Coastal Ocean Mapping (CCOM) in May 2017 to evaluate the acoustic survey technologies and proposed approach to mapping. His evaluation, which included an on-site review of the Geoswath PDBS sonar installation, system configuration, and data acquisition settings on board the R/V *Weicker*, conveyed insights and recommended strategies for the system's operation. Guidance stressing the importance of keeping the gain, pulse length, and power at same levels throughout the entire survey was most significant.

Figure 2.3-6. Geoswath setup on the R/V Weicker, moonpool cover is in the lower left

The surveys were conducted at a vessel speed between 4-5 knots (10 km/hr) to ensure data density sufficient to meet the NOAA recommendations. Due to the sampling gap at nadir generated by the PDBS, a 100% swath overlap was implemented to provide the recommended 100% coverage of bathymetric and backscatter data. The swath width was also maintained to not exceed the 5 times water depth, which in reality is a conservative approach for an interferometric system (Figure 2.3-

7). A survey line spacing of 25 meters/side was used in shallow areas, while a 30-meter spacing was adopted for deeper areas.
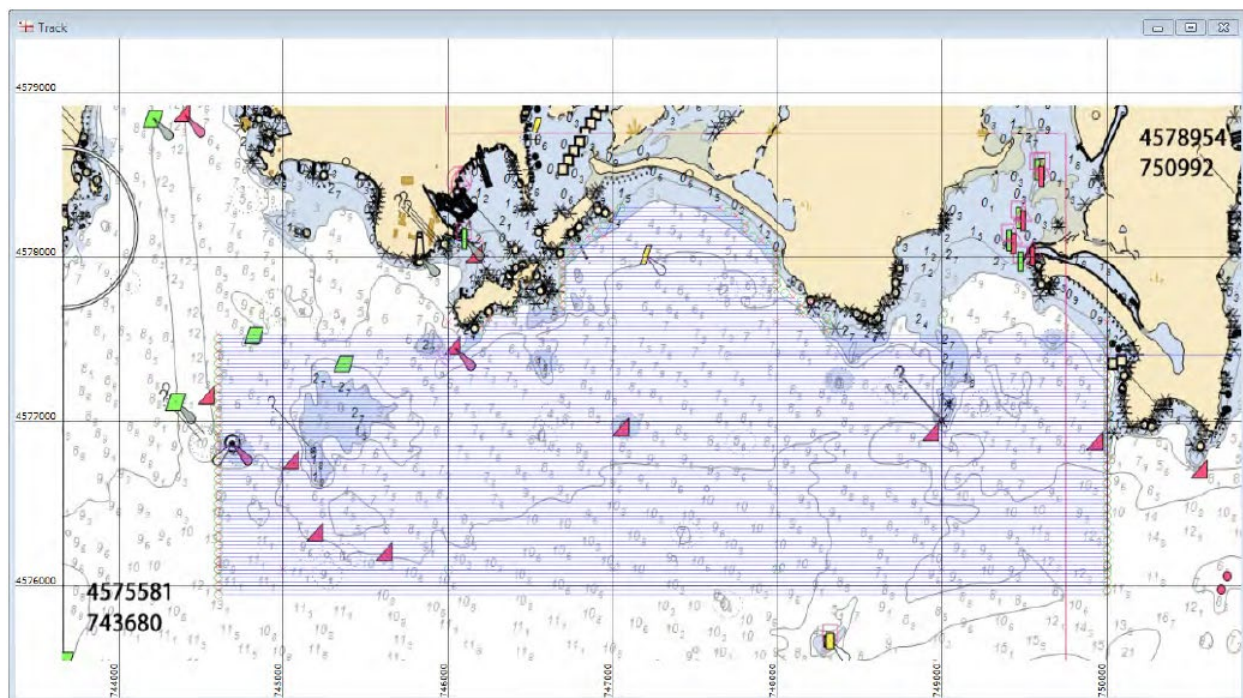
Figure 2.3-7. Screen capture from the R/V Weicker's navigation system illustrating the tight spacing of the survey lines for Survey Blocks 24 and 25

To improve survey accuracy and precision, LISMaRC utilized UConn's ACORN, which is composed of several receivers (GPS) that stream data to on-campus computers. The computers distribute the information to surveyors and mappers to help them in their work. ACORN allows highly accurate positioning in real time. This means that a location anywhere on or above the earth can be pinpointed within the space of a dime. The ACORN maintains nine base stations within Connecticut, including two that provide coverage within the Phase II area. LISMaRC worked with ACORN staff to integrate this RTN into the navigation system on the R/V *Weicker* to provide this much improved accuracy.

Sound velocity profiles (SVP) were conducted every three hours to acquire sound speed data using UConn's Valeport SVP system. Sound velocity data was imported into the processing software for sound speed corrections. Data acquisition was performed using the Geoswath+ acquisition software and saved as .rff files for subsequent post-processing. The system recorded bathymetry and SSS data along with heave, pitch, and roll data from a Seatex MRU-5 mounted on the Geoswath transducer.

The acoustic surveys were conducted over the course of approximately one year from 2017-2018. Seasonal considerations, ship, and crew schedules were the primary drivers for the protracted survey period. Table 2-3 lists the dates and times for the survey legs, showing a total survey investment of about 15 days to map the Survey Blocks 23, 24, and 25. LISMaRC had originally estimated a 20-day mapping period as part of its contribution to the new acoustic data acquisition.

Table 2-3. Survey Log from UConn Geoswath Surveys 2017-2018

Date	Depart (UTC)	Return (UTC)	Hours	Comments
4/31/2017	13:00	18:50	5.833	
5/4/2017	12:00	15:30	3.500	Engine problems
5/8/2017	13:00	17:48	4.800	Rerun lines from 5/4
5/17/2017	13:00	20:05	7.083	
5/18/2017	12:55	19:30	6.583	
6/21/2017	14:57	19:09	4.200	
6/22/2017	13:00	18:38	5.633	
6/23/2017	13:00	17:17	4.283	
Subtotal			41.917	
7/26/2017	15:00	20:31	5.517	
7/27/2017	13:00	19:07	6.117	
7/28/2017	16:00	19:00	3.000	
7/31/2017	16:00	20:06	4.100	
Subtotal			18.733	
8/14/2017	13:00	15:00	2.000	Overheat problems with transmitter
8/15/2017	14:00	17:10	3.167	
8/16/2017	11:30	16:45	5.250	
8/17/2017	12:00	16:50	4.833	
Subtotal			15.250	
6/5/2018	13:30	19:30	6.000	
6/6/2018	13:30	19:30	6.000	
6/7/2018	13:50	20:15	6.417	
6/11/2018	14:00	19:00	5.000	
6/19/2018	14:00	15:00	1.000	Overheat problems with deckbox
6/20/2018	14:20	18:32	4.200	
6/21/2018	14:10	18:55	4.750	
Subtotal			33.367	
7/17/2018	14:30	17:10	2.667	
7/18/2018	14:30	17:20	2.833	Overheat problems with deckbox
7/19/2018	13:00	18:38	5.633	
Subtotal			11.133	
Grand Total Hours			120.400	
Grand Total Days (8 hour days)			15.050	

2.3.3.2 Data Processing

Geoswath

Processing of the acoustic data collected via the Geoswath+ system to develop the data products recommended by NOAA was problematic. Prior to the surveys, UConn had upgraded the software to Geoswath GS4, which generated data in a format that was unreadable by earlier versions of the CARIS software using the CUBE algorithm. According to CCOM, "CUBE, is an error-model based, direct DTM generator that estimates the depth plus a confidence interval directly on each node point of a bathymetric grid. In doing this, the approach provides a mechanism for automatically "processing" most of the data and, most importantly, the technique produces an estimate of uncertainty associated with each grid node." This feature is built into the CARIS software and is recommended by NOAA for acoustic data processing; however, UConn's CARIS license had lapsed at the time of the survey.

Therefore, the bathymetry data were originally processed using the Geoswath GS4 software, while the backscatter data was processed using Kongsberg's Geotexture software. These data products were reviewed by NOAA and were deemed to be very "stripy" and several conversations were had to explore how to address this result. Over the course of several months in 2018-2019, UConn worked with staff from NOAA NCCOS to test several approaches to improve the output. Suggestions were made to export the Geoswath data as GSF files to perhaps allow NOAA technicians to import the data into CARIS, which was done and sent to NOAA in September, 2018. An issue arose from this attempt as all of the necessary survey offsets were removed during the generation of the GSF files, essentially forcing NOAA to work with unfiltered data. Subsequent meetings were held in October, 2018 to discuss other methods to address the issues with the data. Another suggestion was to attempt additional nadir filtering. To that end, a three-meter gap along the nadir was filtered out since there was additional data to fill in the gaps from the adjacent overlapping lines. However, the striping was still just as evident in the final analysis. UConn felt that the major part of the striping was from the density (and noise/scatter) of the data at the edges of the swaths even though the swath width was trimmed very aggressively, essentially using only 4 to 5 times water depth for usable swath width (versus the 10-12 times water depth claimed by Geoswath). The Geoswath SSS backscatter data was also problematic to process, and several attempts to work with NOAA (LTJG Jennifer Kraus) were made, including sending GeoTIFF files for import into CARIS. No improved results were returned.

CARIS

Ultimately, the decision was made to acquire the latest version of the CARIS software to ascertain how well it could address the striping issue, along with its capability to run the CUBE algorithm to address the data uncertainty. The CARIS software was acquired in late 2019, and a second round of data processing was initiated. Several upgrade issues, hardware problems, and operating system incompatibilities had to be addressed before the CARIS software was finally operational on one of UConn's computers.

A schematic of the CARIS processing workflow is illustrated in Figure 2.3-8. The first step is to create a Vessel File (e.g., RV_Weicker.hvf). This vessel file contains all the physical offsets between the various sensors used in the data acquisition (transducers, GPS antennas, gyro, heave sensor, pitch sensor, roll sensor, etc.). It also contains timing delays, and transducer error corrections for pitch, roll, and yaw, which are determined during pre-survey "Patch Tests." The

vessel file also contains the uncertainty values (standard deviation) for the various sensors and measurements which are then used to compute the horizontal and vertical Total Propagated Uncertainty (TPU). Note the creation of a "HIPS file" is also an automatic part of CARIS processing. Figure 2.3-9 is a screen shot of the TPU values that were input into the .hvf file as part of the CARIS processing.
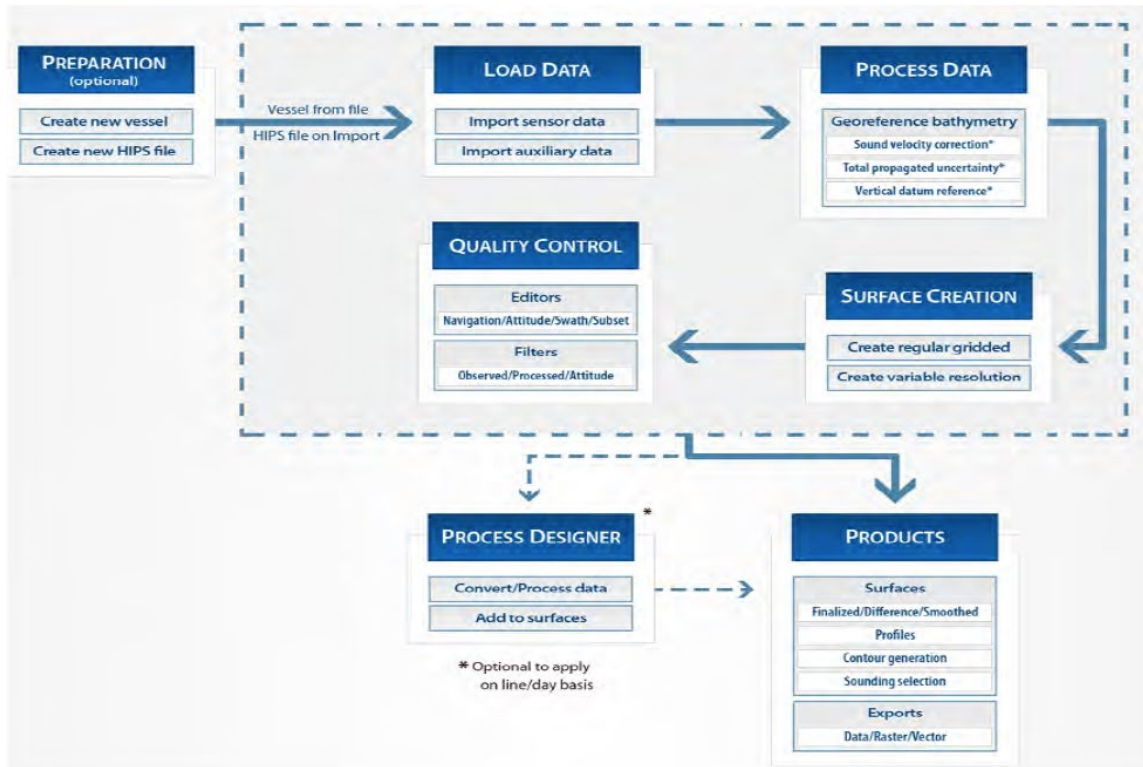
Figure 2.3-8. Schematic of the CARIS data processing workflow (from Teledyne CARIS 2021 Version 11)
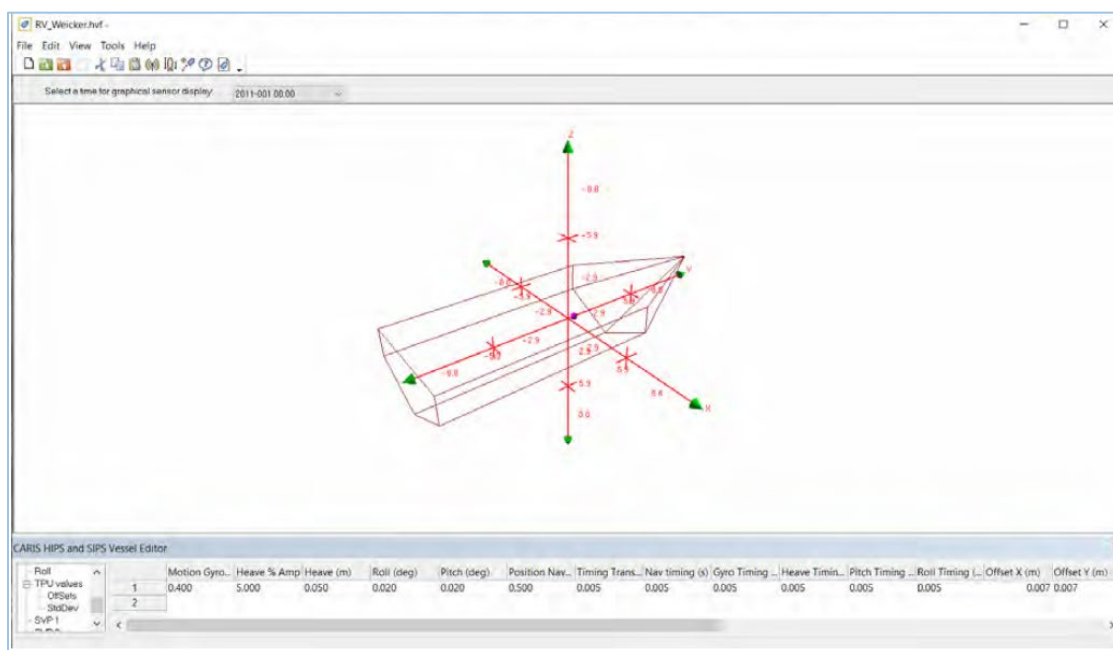
Figure 2.3-9. Screenshot from the CARIS Vessel Editor used to input the uncertainty values for the R/V Weicker

The next processing step was to load the sensor data. The Geoswath acquisition software uses the original "linename" supplied by the operator; it then creates 9 support files using that "linename.xxx" format. Of these files, the .rff file is the raw sensor data that CARIS imports to begin its processing. The tide and sound velocity profile data were then formatted for CARIS and imported as the auxiliary data. These raw data files have been uploaded to the LIS Data Portal.

The next box in the flow diagram is the Process Data. This step is known as "Georeferencing Bathymetry." This process converts the raw data trackline depths into latitude, longitude, and depth by combining the ship navigation with horizontal and vertical offsets from the vessel file. This geographically references the sounding position and depth. Other corrections such as Sound Velocity Correction, TPU, and Vertical Datum Reference are added at this step. The CARIS processing software then allows for the generation of four different types of Regular Gridded Surfaces. These are Swath Angle, Shoalest Depth True Uncertainty, and CUBE. CUBE was selected as the method of choice for generating the gridded surface, as this met the NOAA requirements.

The next step in the process was quality control editing. After creation of a "regular gridded surface", it was necessary to review and edit/clean the raw data before it could be used to create Final Products. This was done with a series of automatic and manual editing tools; including Navigation Editor, Attitude Editor, Swath Editor, and Subset Editor. The final step was to generate the GeoTIFF imagery and PDF standardized map template data products as proposed in the original scope of work.

2.3.3.3 Results

The results below represent the map products generated by the above processing procedures and represent new acquisition of 3.49 km^2 for Block 23 and 12.8 km^2 for Blocks 24 and 25 combined. The map images included below have been reduced significantly; full page versions in the standard map template are provided in Appendix 1 of this report. GeoTIFF images of these map products are also available at the LIS Habitat Mapping and LIS Data Portal websites.

Geoswath

Figure 2.3-10 depicts the mosaic of the bathymetry data from Survey Blocks 23, 24, and 25 generated by the Geoswath GS4 software. The striping of the data generated from the survey lines is evident in this image. The color ramp ranges from orange, representing the shallowest water, to blue, representing the deeper areas. Despite the striping issue, the bathymetry map does provide a very good representation of the seafloor topography of this part of LIS. This Geoswath image has a "shaded relief image" that has slightly exaggerated "z" elevation and "sun lighting," which give it the dramatic shadow effects.
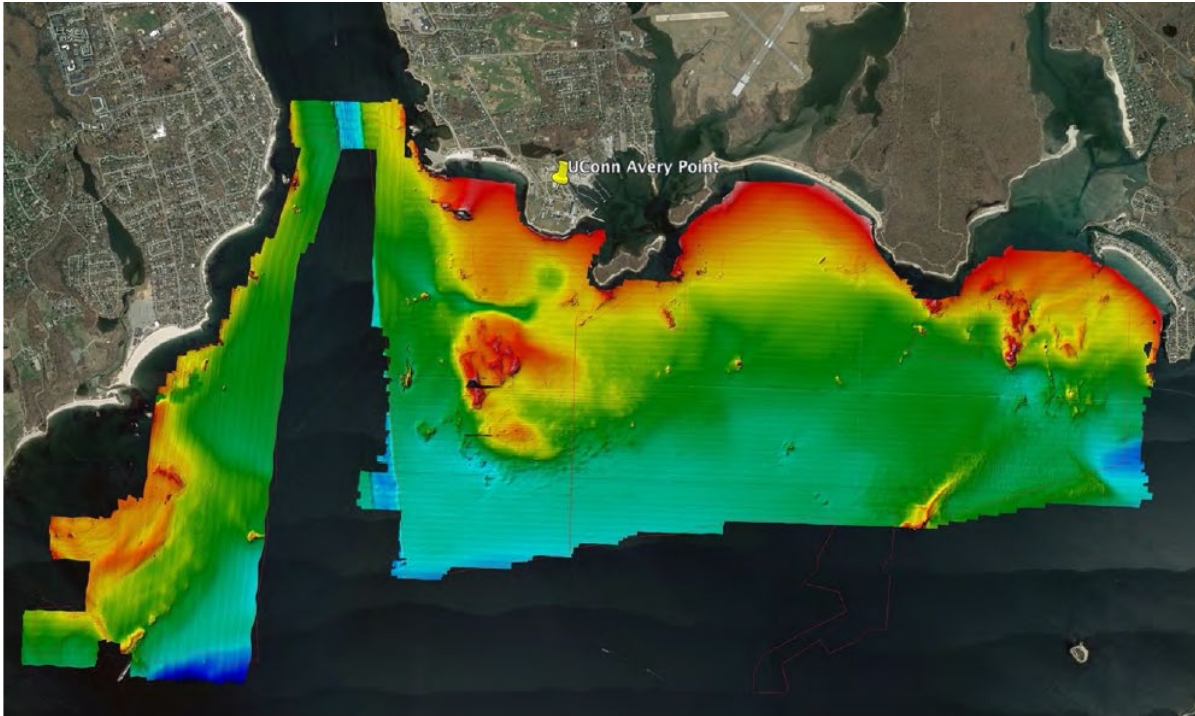
Figure 2.3-10. Mosaic of bathymetry data from Survey Blocks 23, 24 and 25 generated by the Geoswath GS4 processing

As described above, the Geoswath backscatter data was more problematic, and the striping issue is evident in the output shown in Figure 2.3-11. However, the image does provide useful information on the nature of the seafloor in this part of the Sound. The reflectance value was used for these maps, versus absorption, with higher reflectance producing darker color areas to depict harder bottom areas and lighter reflectance in areas with softer substrates.

Figure 2.3-11. Mosaic of backscatter data from Survey Blocks 23, 24, and 25 generated by the Geoswath GS4 processing

Figure 2.3-12 and Figure 2.3-13 represent the results of the CARIS processing for Survey Blocks 23, 24, and 25. The CARIS processed data includes additional data to the south of Survey Blocks 24 and 25, which was acquired after the decision was made to process the acoustic data using CARIS; thus, this area was not included in the Geoswath processed images. The final results in the appropriate CARIS-processed gridded format were not able to be delivered to NOAA to integrate these new data by their recommended deadline of January 31, 2020, due to the delays described in Section 2.3.2.2 in attempting to integrate the results of the data with Geoswath software. These new data were, therefore, not integrated into the final new unified bathymetry and backscatter maps.

As can be seen in Figure 2.3-12, the filtering applied to the surface reduced the striping issue at the expense of topographic resolution. This is particularly evident in the shallower (orange-red) and rougher seafloor areas. This mosaic was generated with only "color shaded" by depth, lacking the sun illumination and hill shading seen the in Geoswath imagery. The mosaic shown in Figure 2.3-13 was generated with a 5x vertical exaggeration, which does provide greater relief but also enhances the striping.
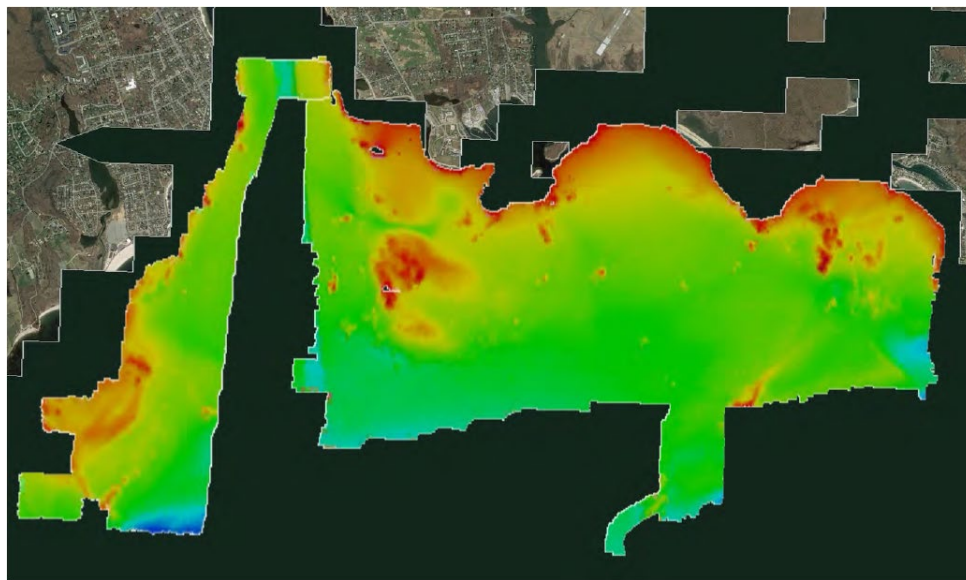
Figure 2.3-12. Mosaic of bathymetry data from Survey Blocks 23, 24, and 25 generated by the CARIS processing
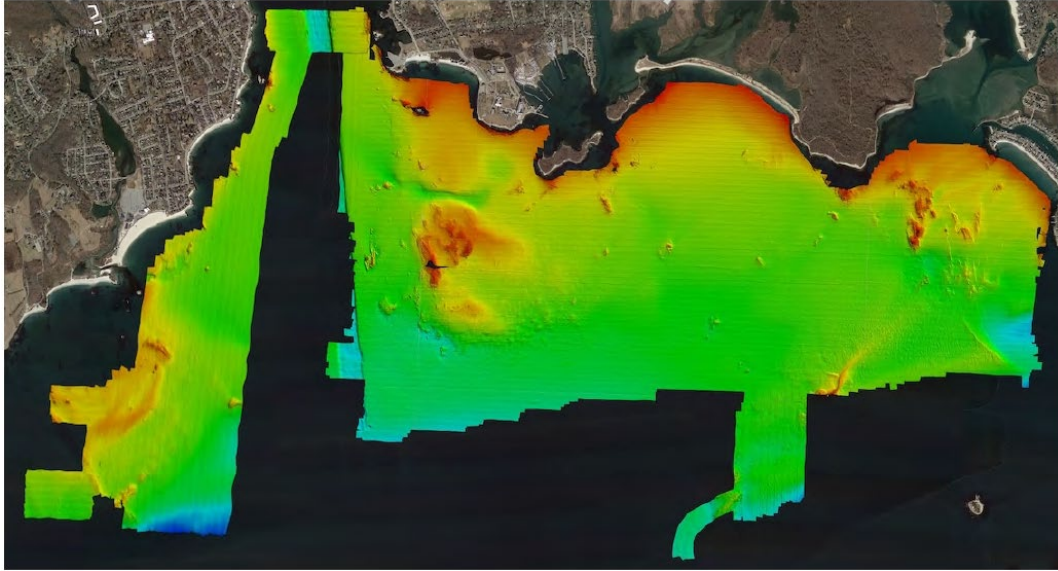
Figure 2.3-13. Mosaic of bathymetry data from Survey Blocks 23, 24, and 25 generated by the CARIS processing with a 5x vertical exaggeration applied

The results of CARIS processing of the backscatter data can be seen in Figure 2.3-14. This image appears to show a bit more striping, particularly in the lighter (lower reflectance) areas.

Figure 2.3-14. Mosaic of backscatter data from Survey Blocks 23, 24, and 25 generated by the CARIS processing

2.4   Integrated Products

The NCCOS Biogeography Branch was tasked with integrating the bathymetric and backscatter images from the OCS surveys by the NOAA Ship *Nancy Foster*, NOAA Ship *Thomas Jefferson*, and NRT-5 with the data collected by LDEO and LISMaRC into a seamlessly unified suite of surfaces.

2.4.1 Data Processing

NCCOS received the SoMAS acoustic data in Kongsberg .all file format containing the raw multibeam bathymetry and beam time series snippets used for creating backscatter mosaics. NCCOS processed the multibeam backscatter data using the FMGT, which corrects for geometric and radiometric distortions by ray-tracing the beam time series snippets to the correct angle and range of the sonar from the seafloor. FMGT paired the final cleaned bathymetric soundings with the snippets to create a final backscatter mosaic. In addition, the following corrections were applied where appropriate and when artifacts were evident: AVG Trend, TX Power and RX Gain, Slant-Range correction, Area Correction, Spreading, and Extracted Beam Pattern. Individual lines were also truncated based on ping number and/or angle of incidence where appropriate. Areas where the survey vessel was logging data while turning produced a "smearing" effect and were trimmed out of the final mosaic. However, most of these sections were outside of the resurvey block polygons and could be clipped out or superseded by the existing good quality backscatter or bathymetry. The final mosaics were exported as GeoTIFFs in NAD 1983 zone 18N on a relative 0-255 linear color scale. The intensity results varied between each vessel as there were no ground validation samples that could be applied to accurately assess and calibrate the beam patterns.

UConn exported their bathymetric and backscatter deliverables for resurvey blocks 23 & 24 to NCCOS in an Esri (.asc) format from the Geoswath software, which were gridded to a GeoTIFF format using ArcGIS software, rather than in the CARIS readable format as NCCOS had recommended. UConn collected the bathymetry surfaces using a PDBS system, which greatly increases the swath width for collecting in nearshore areas but produces inherently noisier data. Additionally, the provided source data and supporting survey information contained significant deficiencies including water column noise, absence of crosslines (for depth verification), and a lack of uncertainty surfaces. The lack of vertical control and uncertainty measurements resulted in a vertical offset greater than 2 meters in some areas, showing a darker color ramp than the surrounding bathymetry (Figure 2.4-1). The data also contained false surfaces from uncleaned noise, uncalibrated vessel offsets, major vessel motion artifacts, and major "striping" across and along track and "stepping" artifacts. Figure 2.4-2 shows raw sonar data and a portion of bathy surface provided by UConn. The left image shows a red colored cluster of noise and false surfaces (circled), and the right shows the major striping artifacts across and along track and a blue profile line from north to south indicating the vertical "stepping" effect. With the lack of supporting survey information and the abundance of processing errors, NCCOS was unable to check and verify the quality of the surfaces, so UConn agreed to reprocess the data to clean the noise and make sure the vessel configuration was properly calibrated.
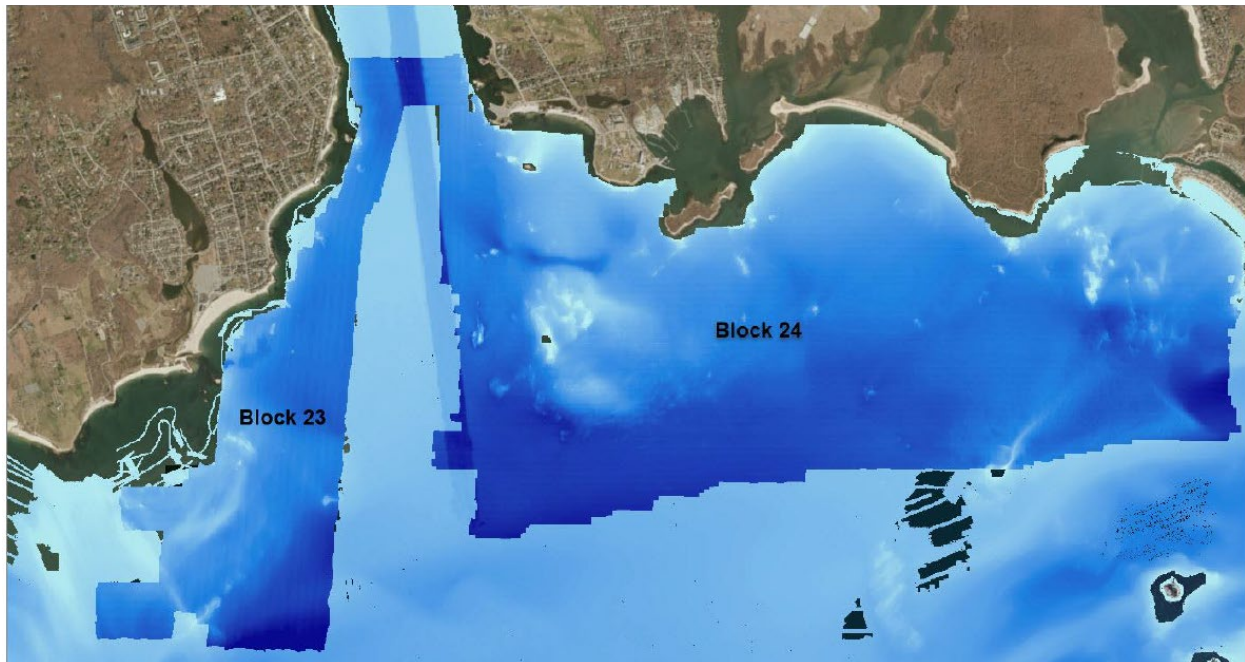
Figure 2.4-1. The bathymetry in Blocks 23 and 24 collected by UConn along the entrance of the Thames River
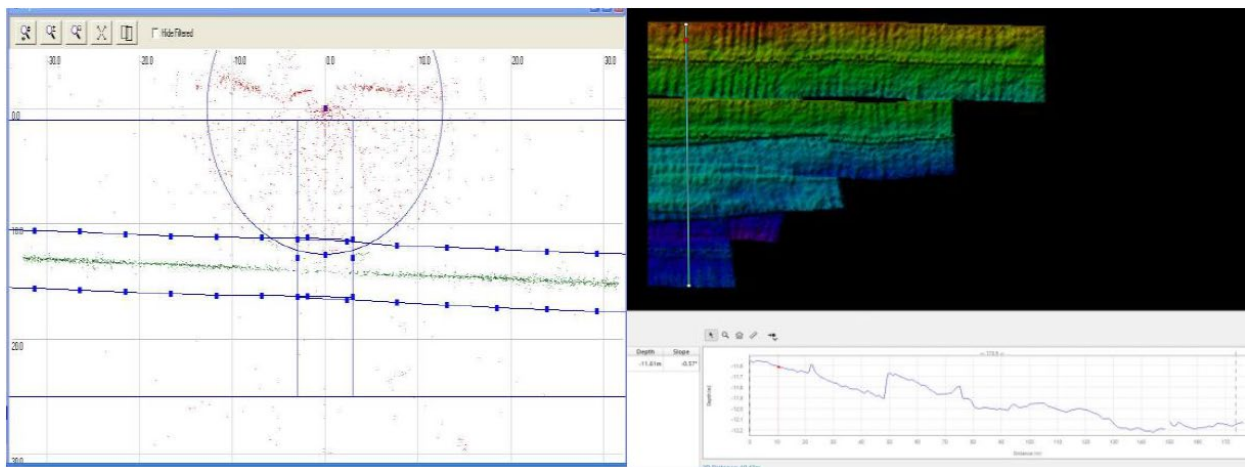
Figure 2.4-2. Data provided by UConn (Left) Profile of a raw sonar soundings subset; (Right) a 3D model of a portion of the bathy surface

UConn had met previously with Val Schmidt, as recommended by NCCOS, to discuss the steps needed to convert the GeoSwath files to a CARIS format. NCCOS also requested that the backscatter data be reprocessed and water column artifacts be corrected. UConn agreed to attempt to reprocess the data to clean the noise, recalibrate the vessel configuration, convert the data to a CARIS format, and deliver the final surfaces to NCCOS before January 31st, 2020. Unfortunately, no usable surfaces were received from UConn by the deadline given; thus, NCCOS used preexisting data for these blocks in the integration.

2.4.2 Data Integration

The initial 2015 compilations of the Phase II LIS bathymetry and backscatter were used as the base layers for the integration of the resurvey blocks collected by SBU using the R/V *Pritchard*. Before the new acquisitions could be merged with the base layers, each individual survey block

went through a rigorous assessment of data quality using the Pydro-QA/QC toolkit developed by NOAA's Hydrographic Systems Technology Program (HSTP). The QA/QC toolkit was used to identify errant pings or false surfaces, areas where sonar ping density did not meet specifications, and areas where there were significant data gaps in sonar coverage. Many of these artifacts were able to be corrected in post-processing, or some instances, were determined to be outside of the survey block areas and therefore could be ignored. NCCOS provided SoMAS with reports detailing the QAQC results that aided in reprocessing the data to meet the HSSD standards. Once all the QA/QC issues were corrected, NCCOS could then begin to integrate them into the Phase II mosaic.

The R/V *Pritchard* bathymetry blocks were exported as 32-bit rasters and converted from the NAVD88 vertical projection to the Mean Low-Low Water tidal datum using VDatum. The vertically corrected bathymetry was then merged with the pre-existing Phase II mosaic using the "Mosaic to New Raster Tool" in ArcGIS 10.7. To blend the edges of the overlapping datasets together, the mean depth of the two layers was used as the output for the final mosaic. These tools allowed the recent collections of multibeam data to become seamlessly mosaicked to OCS surveys from 15 years ago. The final unified bathymetry surface was exported as a 32-bit floating point GeoTIFF in UTM Zone 18N (Figure 2.4-3). The unified bathymetry surface was also exported to individual files according to IHO (2008) standards for depth-to-resolution threshold (Table 2-4). Each of these layers follows the nautical charting standards for the appropriate cell size to depth range, which increases with depth (Figure 2.4-4).
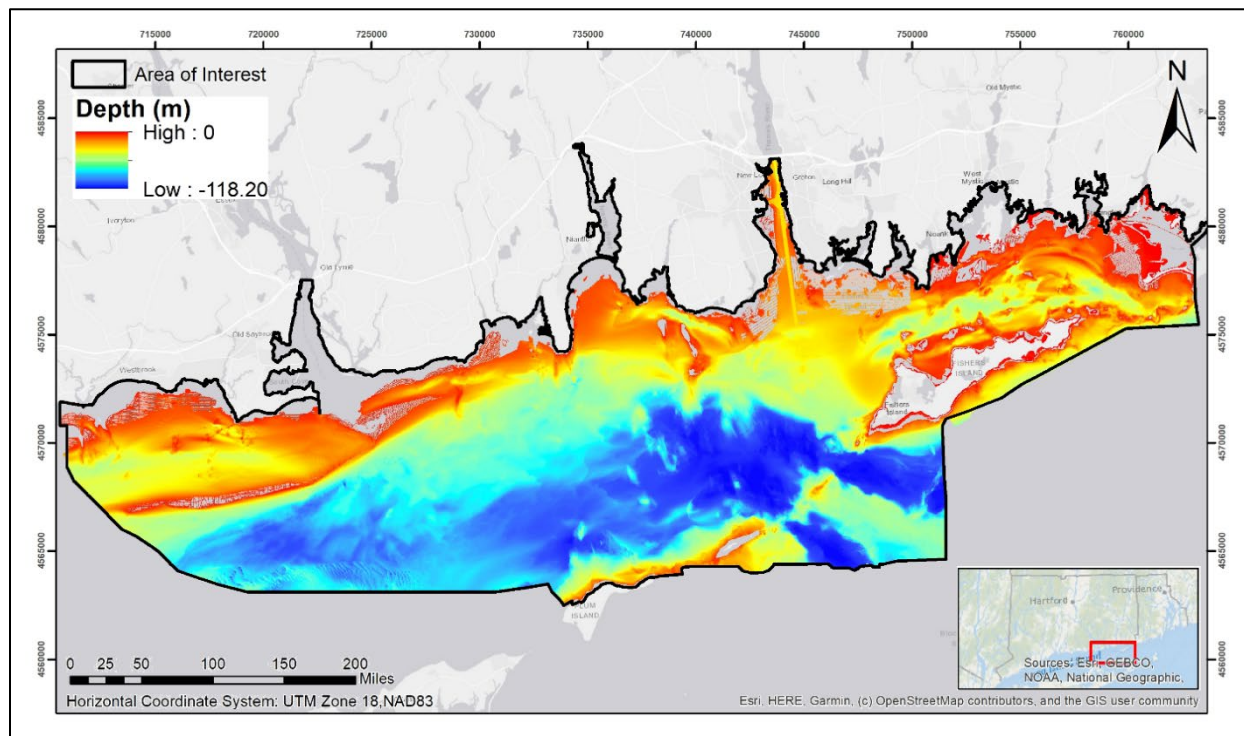
Figure 2.4-3. Bathymetric model of integrated multibeam and LiDAR surveys including the 2018 resurvey blocks from SBU
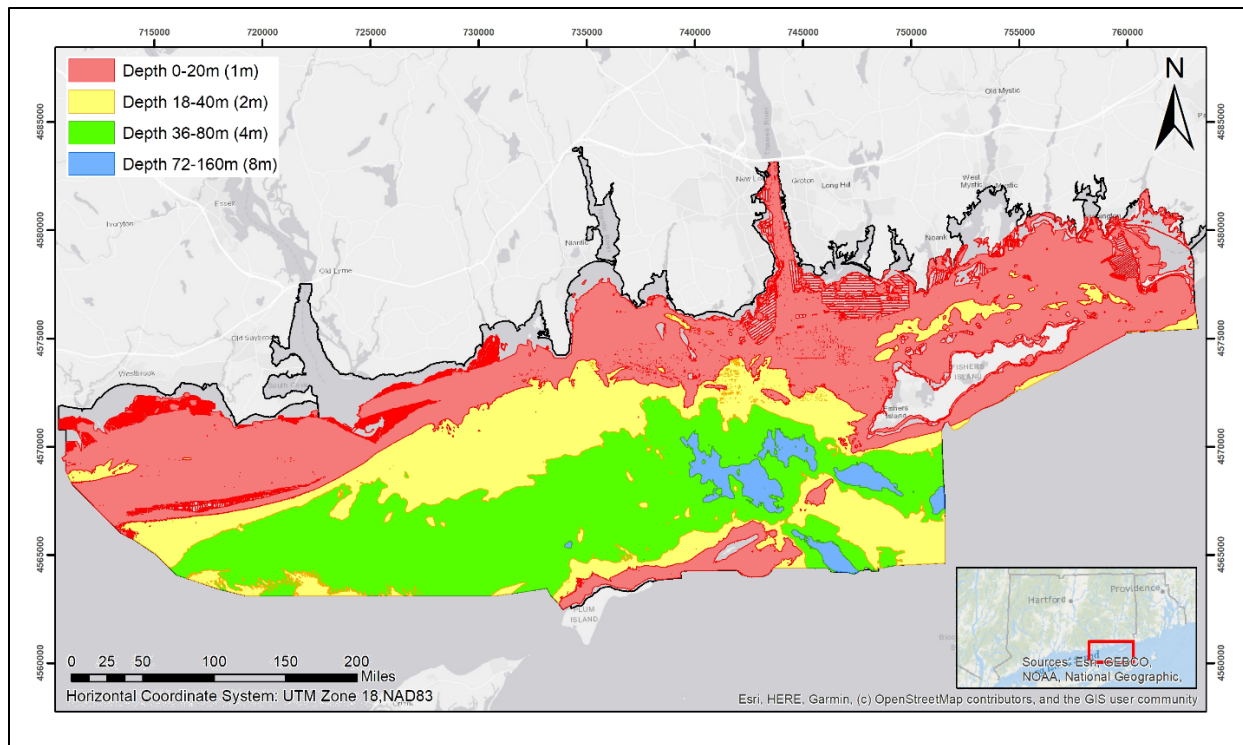
Figure 2.4-4. Depth ranges within the Phase II area of interest defined by the IHO and exported into various resolutions

Table 2-4. IHO depth to resolution specifications for complete coverage survey sheets

Depth Range (m)	Resolution (m)
0 - 20 m	1 m
18 - 40 m	2 m
36 - 80 m	4 m
72 - 160 m	8 m
144 - 320 m	16 m

The newly acquired backscatter data from the R/V *Pritchard* replaced several areas that contained outdated sidescan data. The newly acquired data allowed the habitat mapping team to delineate different bottom types more accurately. However, there were significant differences in the dynamic range and the decibel levels between the SoMAS dual swath EM2040 and the older Reson 7125 and EM3000 backscatter mosaics. To resolve this issue and create a seamless mosaic, NCCOS performed a series of steps. First, NCCOS rendered all of the backscatter mosaics into 8-bit grids to normalize the data to a rendered grayscale image. Next, NCCOS clipped all of the turns and outerbeam data that extended beyond the resurvey block boundaries. Finally, NCCOS used adaptive blending techniques to seamlessly merge the layers together with PCI Geomatica 2018 imagery analysis software (Figure 2.4-5). This produced an 8-bit, 2m GeoTIFF of a smooth and seamless unified backscatter mosaic (Figure 2.4-6). The decibel values of the backscatter mosaic have been rendered to a relative grey scale (0-255).
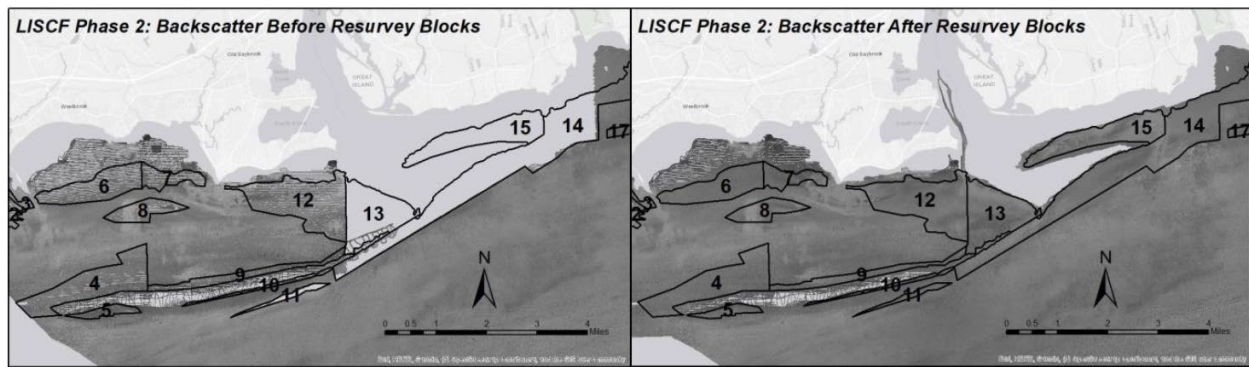
Figure 2.4-5. (Left) Several large blocks within the Phase II AOI with less than 50% coverage or no data; (Right) these blocks resurveyed by SBU.
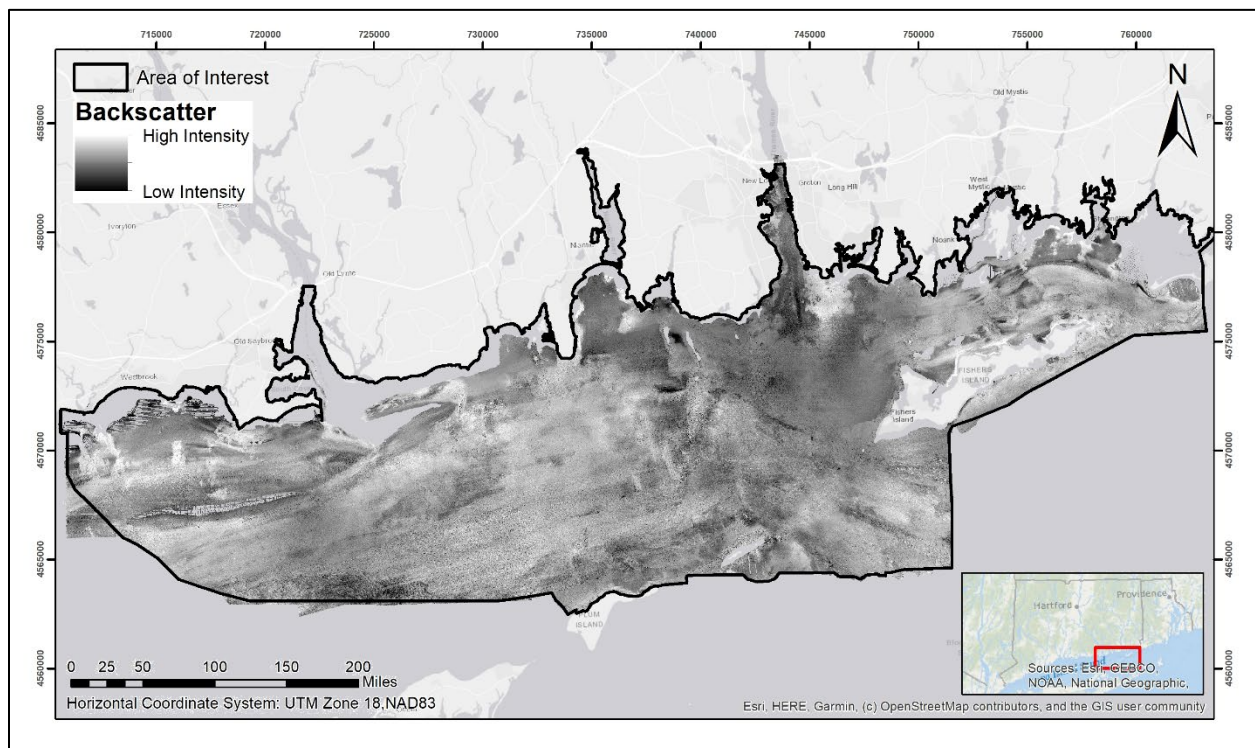
Figure 2.4-6. Intensity model of the integrated multibeam backscatter and sidescan surveys including the 2018 SBU resurvey blocks

2.5 Discussion

Phase II acoustic mapping has provided new details in many mostly nearshore areas where detailed mapping did not exist. The geophysical information contained in the Phase II acoustic products conveys important details describing the shape, extent, and composition of surficial features used to extract detailed information about benthic habitats, sediment texture, grain size, and sedimentary environments. The acoustic products are used to infer and extract seascape features at a range of spatial scales including fine scale biotopes (Auster et al,, 2009) and broader scale geomorphology within LIS.

The final products of the integrated bathymetry and backscatter that NCCOS provided are used for habitat classification only and should not be used for navigation purposes. Ground truthing data is required to confirm hydrographic soundings, as well as determine the bottom type to classify the

habitat. This is especially important for the backscatter imagery, which is a model generated from rendered 8-bit imagery of the intensity and not actually calibrated decibel returns from the sonar. It is also important to recognize that the multibeam data from the collaborators will not be used for nautical charting. The new bathymetric data still conveys important information about the seafloor topography.

2.5.1 Sand waves and Estuarine Flow

Although the Phase II multibeam data will not be used for nautical charting, we expect there to be a basic agreement between the existing nautical chart and the new bathymetric data. The survey area located immediately east of the mouth of the Connecticut River, identified as survey block #15 in Figure 2.3-1 includes a broad, east-west depression that lies between the shoreline and an offshore ridge or bar, which parallels the Connecticut coastline (Figure 2.5-1). According to the navigational charts, the deepest channel of the Connecticut River turns east where it enters LIS and roughly aligns with this depression. On the west side of the Connecticut River, tidal and river flows cross the Saybrook Outer Bar extending southeast from Lynde Point. The Saybrook Outer Bar Channel allows safe navigation between the Connecticut River and LIS. Flow patterns are complex in this area and change with tide, river discharge, weather, and other factors.

The bathymetry from survey block #15 shows the broad depression reaching depths over 14 m and then shoaling eastward to a sedimentary sill at about 10 m deep before deepening eastward into a second depression over 15 m deep (Figure 2.5-2). The hillshade for survey block #15 shows several possible rock outcrops in the trough and apparent erosive lineations on the north flank of the trough east of the sill (Figure 2.5-3). These outcrops seem to be buried in the region of the sill; although, they are present in the shallower waters of the north flank of the trough. Rocks are present again west of the sill; although, the northern end of Hatchett Reef seems to have been buried. Many of the rock outcrops in deeper water (more than maybe 10 m deep) have sediment tails on their west sides suggesting net water flow towards the west.

There are two fields of sand waves along the south flank of the trough visible in Figure 2.5-3. The waves of the eastern wave field have heights of about one meter and wavelengths about 40 m in water depths of about 6 to 8 m. The waves in this field are asymmetric with steep slopes on their western slopes indicating a net water flow towards the west. The waves in the western field are smaller with heights of about 0.25 m and wavelengths about 15 m in water depths of about 5 to 7 m (the shallower limits were not mapped). The waves are slightly asymmetric towards the east suggesting strong tidal flows but a weak net water flow to the east.
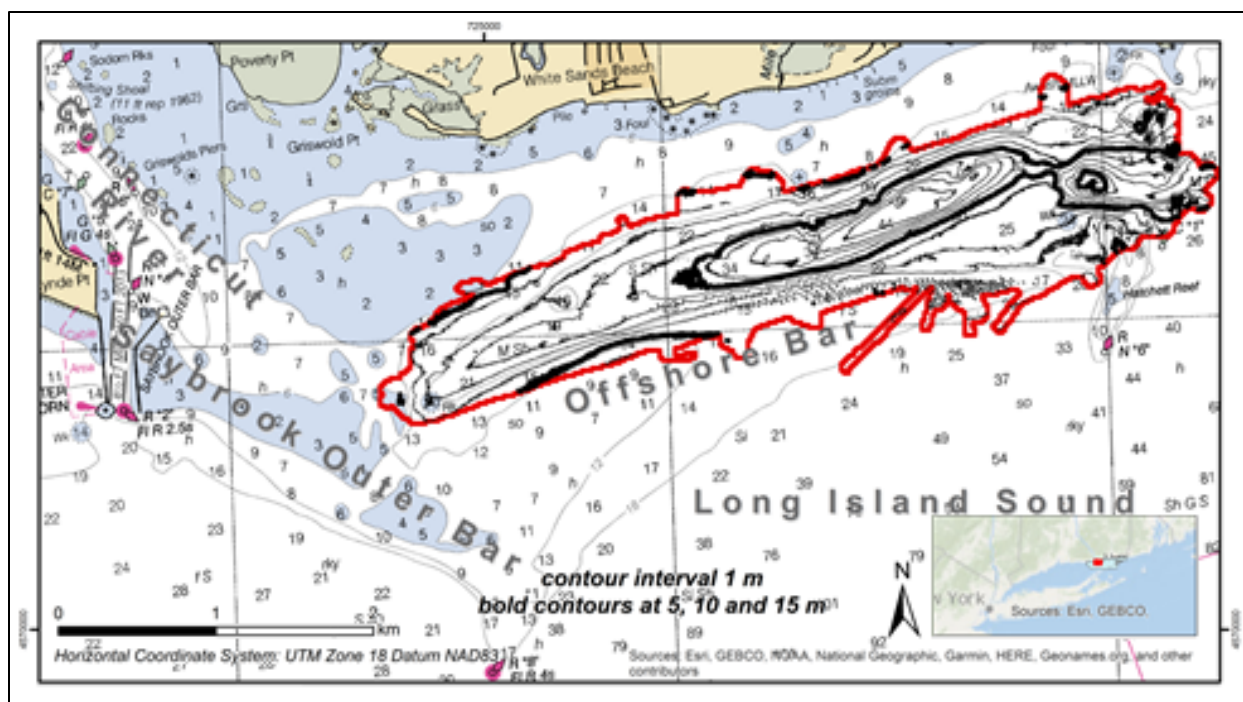
Figure 2.5-1. Block #15 survey area immediately east of the mouth of the Connecticut River
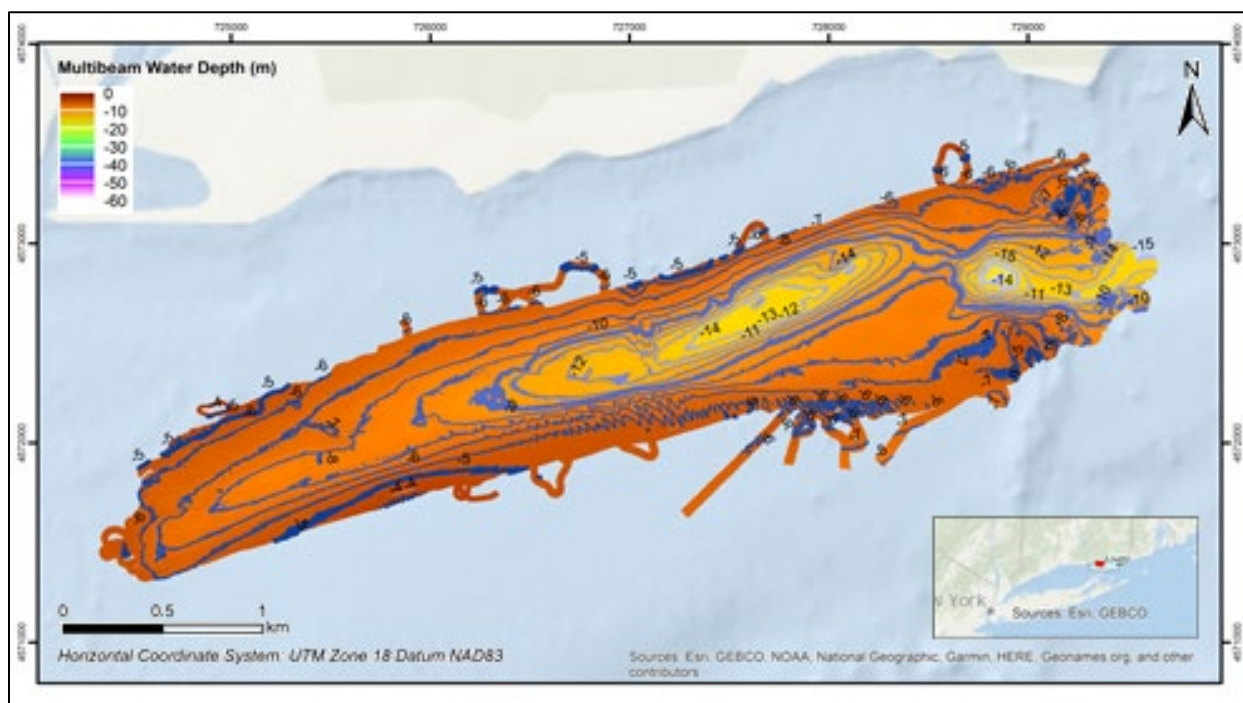
Figure 2.5-2. Multibeam bathymetry for Survey Block #15 showing color-coded depth and 1 m contours
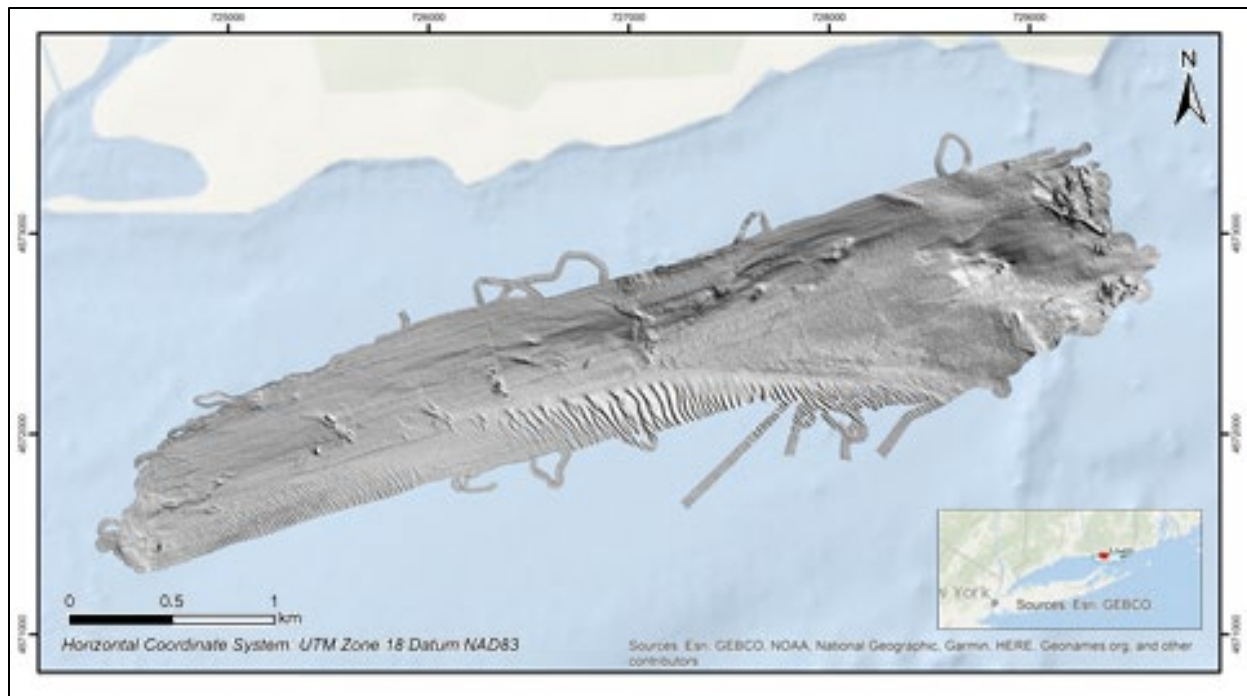
Figure 2.5-3. Hillshade bathymetry of Survey Block #15 shown in smaller-scale relief illuminated from the northwest

The backscatter patterns for the multibeam and sidescan sonar (Figure 2.5-4 & Figure 2.5-5) show lower backscatter (darker color) on the southern flank of the trough consistent with sand waves in the area. Sand can have a low backscatter because there are generally few shells in sandy areas and the sand surface can reflect sound like a mirror, so little sound returns to the sonar instrument. Backscatter is much higher (brighter color) to the east, which may suggest shells on the seabed. Fine-grained sediments with a coarse component can have high backscatter because shells or gravel can reflect sound back towards the transducer while fine-grained sediments with no shell tends to absorb the sound and, thus, can have low backscatter. Samples are required to verify any interpretation of backscatter patterns, but the backscatter data can be used to extend observations at stations to larger areas. Backscatter intensity along the northwest portion of the trough is intermediate, perhaps suggesting some coarser material on the sediment surface in that area, especially since these areas of higher backscatter are sometimes associated with outcrops.
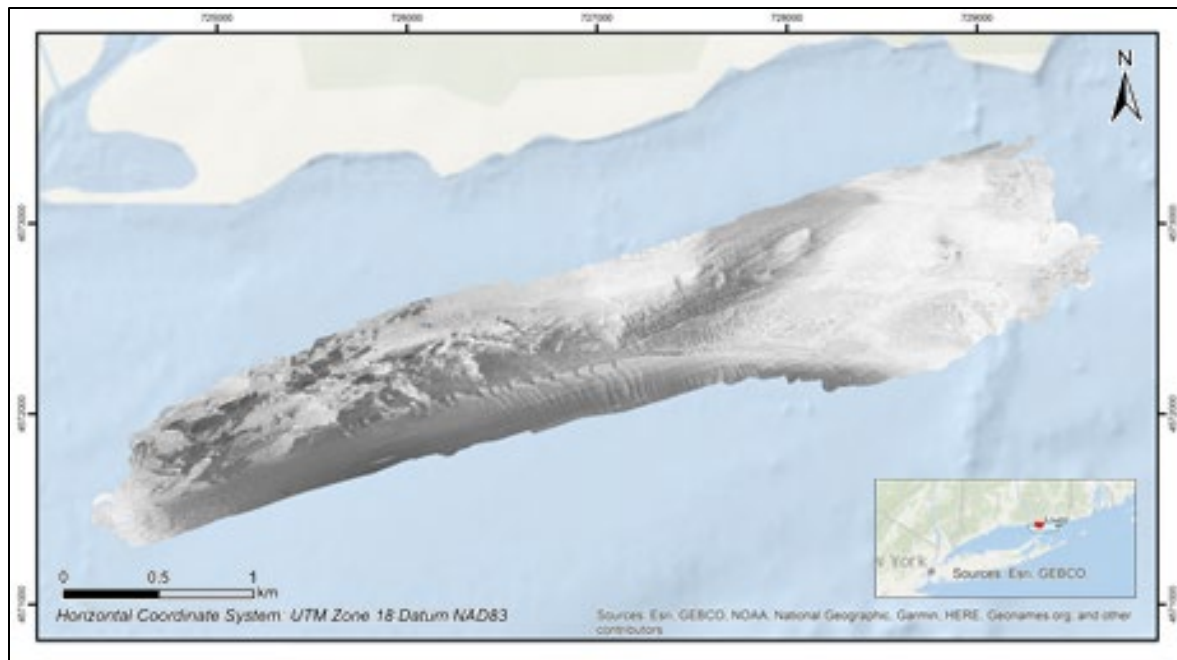
Figure 2.5-4. Multibeam backscatter (300 kHz) of Survey Block #15
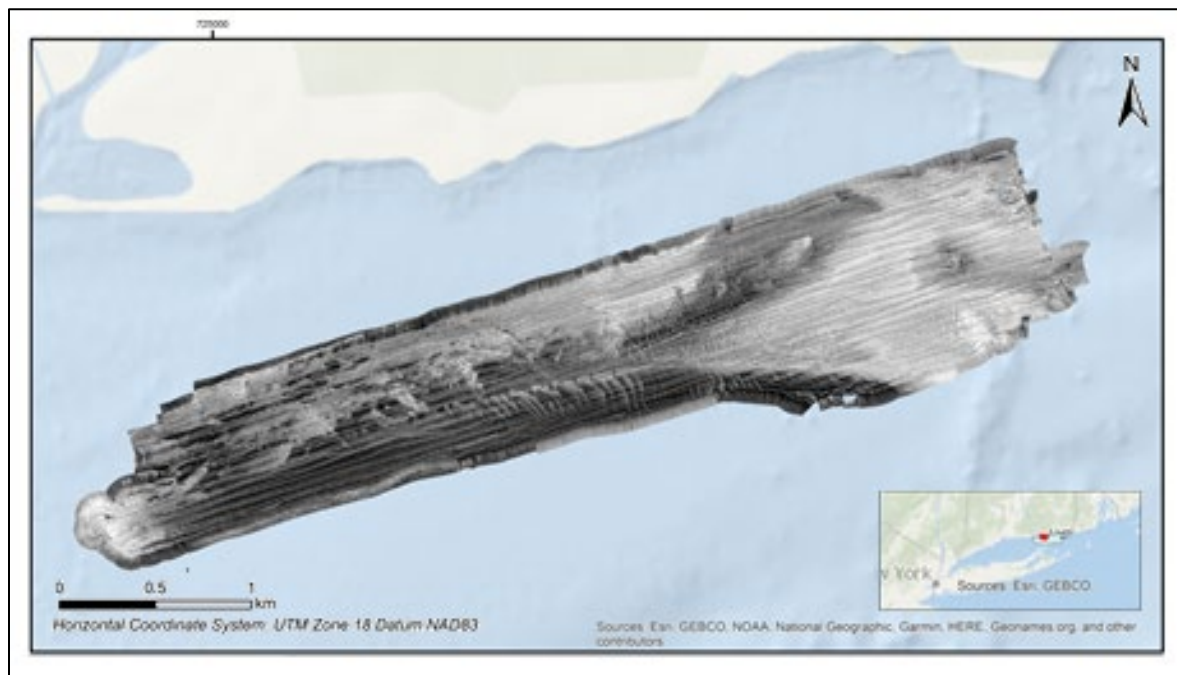
Figure 2.5-5. SSS Backscatter (100 kHz) of Survey Block #15

Sand waves can form when sand-sized sediment is moved by strong currents, and as a result, they are generally a useful indicator of both sandy sediments and strong currents. By their very nature sand waves create an unstable seabed, so a wide variety of bottom-dwelling organisms may not be present in areas of sand waves. Both of the two sand-wave patches described here were also imaged by multibeam tracks run during NOAA survey H12013 in 2009. Comparing profiles over the same waves in 2009 and in 2018 (Figure 2.5-6) shows that sand waves are present in the same areas in both years. However, individual sand waves have moved, so they can't be directly compared. If

currents were only unidirectional, then we'd expect the sand waves to move along the seabed. However, it's likely that the sand waves could stay in the same place if there was a tidal component of the flow. Tidal flows often have a rotary component so that strong flows can flow in a number of directions over a tidal cycle.

The asymmetric larger (eastern) sand waves shown in the upper graph of Figure 2.5-6 suggest a net westward flow consistent a dominant flood current (into the Connecticut River) at about 6 to 8 m water depth; although, there is likely a tidal component to the flow. This net upriver (flood) flow is also consistent with sediment tails behind obstacles in deeper water. The weaker asymmetry of the smaller (western) sand waves shown in the lower graph of Figure 2.5-6 suggests a weak net eastward flow consistent with a dominant ebb current (out of the Connecticut River) at a depth of less than about 7 m. Such a flow pattern (deeper waters having average flow direction into the estuary, and shallow waters having average flow directions out of the estuary) is the expected estuarine circulation pattern.
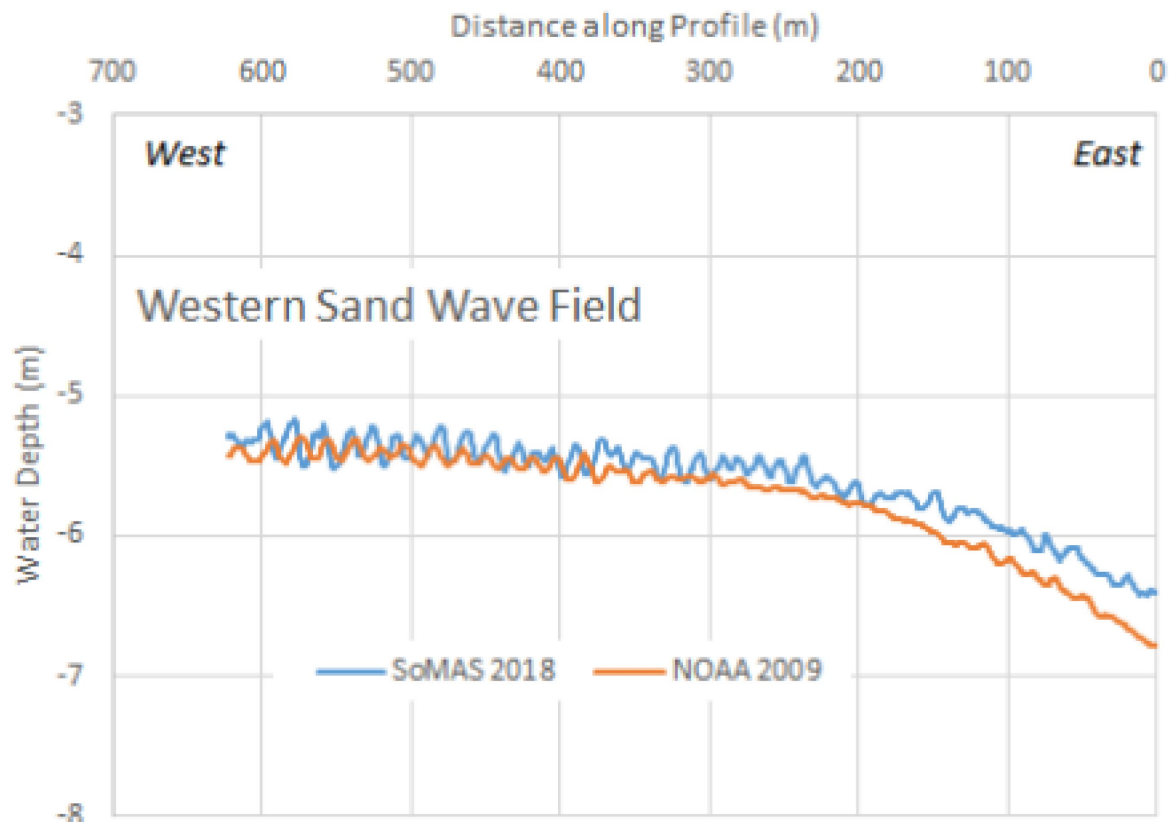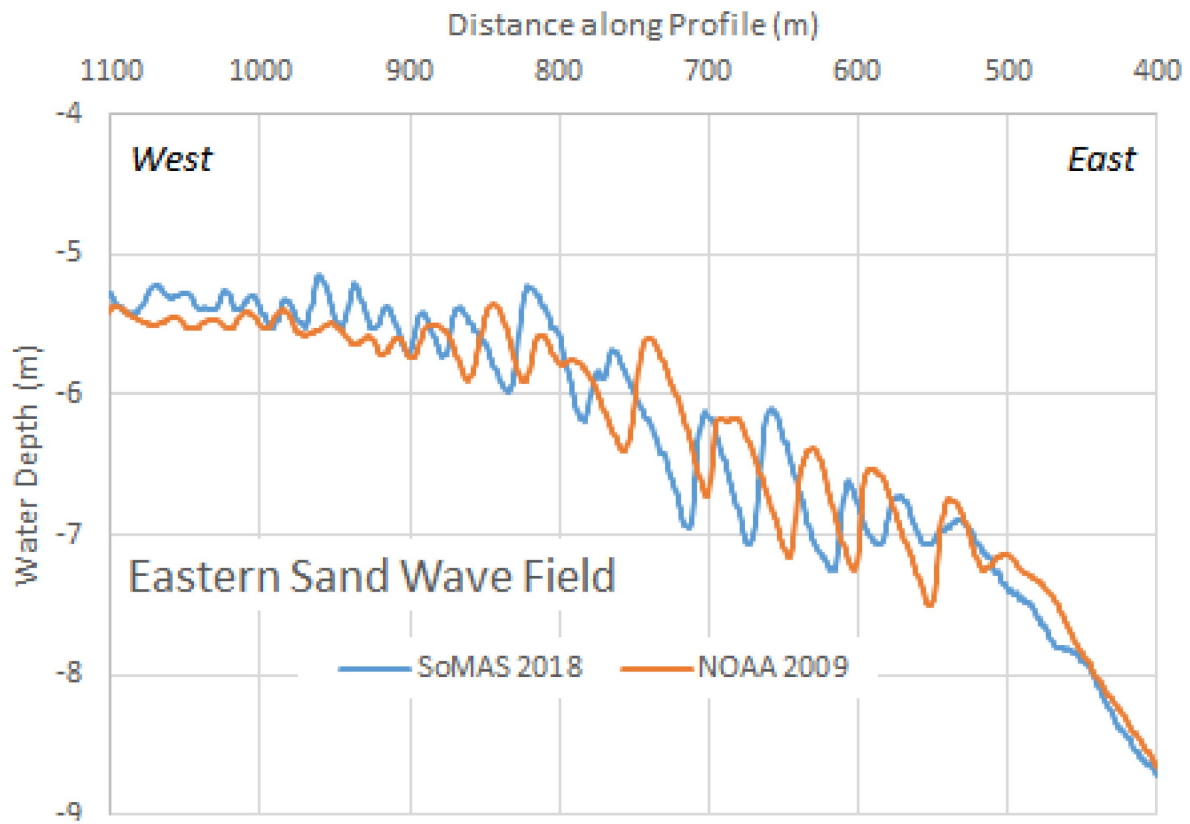
Figure 2.5-6. Profiles across two sand wave fields in survey block #15. The vertical exaggeration of both plots is about 100x.

2.5.2 Barchan Dunes

As noted previously, barchan dunes have been observed on NOAA multibeam data in water depths of 50 to 60 m from a portion of LIS near a dredge disposal site that had been used for clean sediments. A short survey conducted in this area did show barchan dunes, which had heights of about 1.5 to 2 m, widths of about 50 m, and crestal lengths of about 50 to 200 m (Figure 2.5-7). The axes of the dunes are aligned roughly north-south with the horns of the crescents opening towards the west. This orientation is consistent with bedform movement towards the west by a unidirectional current. SoMAS compared the positions of barchan dunes on their data from July 2018 with the positions of the same barchan dunes on the data collected on NOAA survey W00405 from September-October 2015, which revealed the dunes have moved about 50 to 90 m towards the west-southwest at a rate of 19 to 34 m/yr. It is likely that the movement occurs only during a portion of the flood tide when current speeds are high enough to move sand-size sediment but perhaps not during every flood tide. The movement of these sand waves again demonstrates that sand waves indicate the presence of an unstable and mobile sandy seafloor.
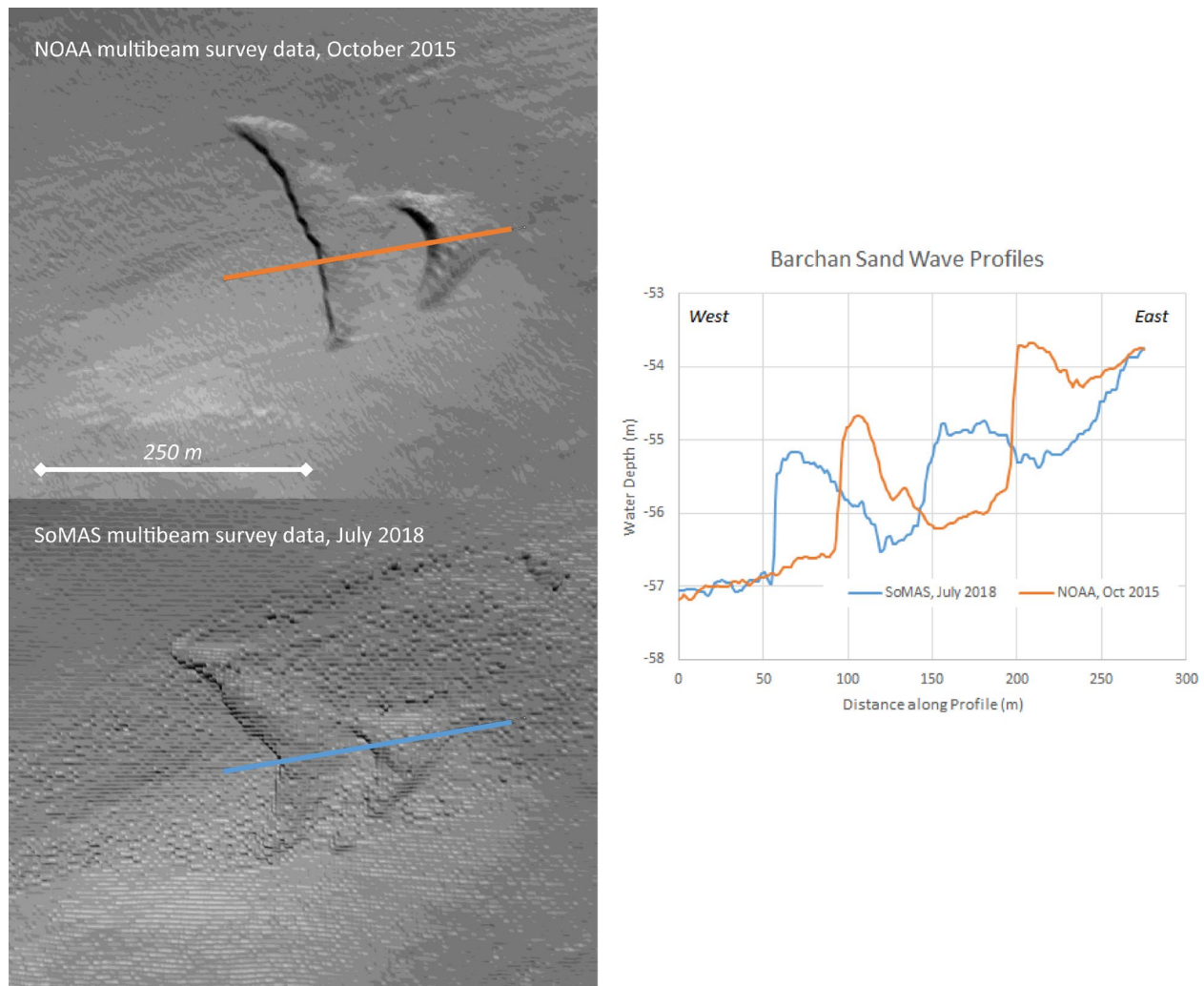
Figure 2.5-7. Left: Hillshade images of barchan sand dunes in survey area Barchans_JJ in October 2015 and July 2018. Right: Bathymetric profiles across the barchan dunes. The vertical exaggeration of the upper and lower plots is about 50x.

2.6   Summary/Conclusions

The compilation and evaluation of existing data prior to the initiation of new collection efforts was very effective for identifying areas for novel acoustic data acquisition, targeting locations that would benefit from more contemporary acoustic data collection, and general project planning. Together the collaborative project teams successfully completed surveys in the areas that required resurvey for improved data quality and in twenty-eight of the blocks identified as needing 100% multibeam coverage. The total area of new bathymetry and backscatter data collected for the Phase II study was 247.3 square kilometers (95.5 square miles). NOAA's recommended data quality standards and technical guidance coupled with the division of labor to conduct the requisite acoustic surveys between all three consortia demonstrated effective collaboration of State, Federal, and academic partners to improve the scientific information on the seafloor topography of ELIS.

Multibeam data was also collected in other areas of interest within the Phase II region in order to study sediment distribution patterns, which supplied some useful information on sedimentary processes and estuarine flow occurring within the region. Sand waves were commonly observed in the previous NOAA acoustic data, as well as in the new data collected within the Phase II area. Sand waves can move across the seabed where there are local sand sources and nearly unidirectional strong flows. Tidal motions tend to create fields of sand waves that are in the same area for long time periods; although, sand is moving across the sand waves on a tidal timescale. High water waves work to re-suspend sediments that can be sculpted by tidal currents, so sand wave fields can be altered during wind events, such as storms, generating high waves. The SoMAS study of sand waves in survey block #15 and barchan dunes in the area of the ELIS dredge disposal site confirmed that bottom currents are at least periodically strong enough to transport sand-size material and, thus, the bed is likely to be unsuitable for benthic organisms that create stable burrows or attach to hard substrates.

The acoustic data generated by the academic partners also emphasized the complexity and constraints of conducting acoustic surveys. SoMAS experienced some equipment challenges during their first deployment, and the resulting acoustic data contained some motion-related artifacts that needed to be filtered and smoothed out in post-processing. UConn experienced challenges in processing their acoustic data to the quality standards established by NOAA, owing primarily to software issues. Although UConn later obtained the appropriate software to complete the requisite processing, their product was not received within the established timeframe to integrate it with the other newly acquired and usable existing acoustic data.

Given the inherent noise generated by the Geoswath PDBS (interferometric) system and the complexities associated with filtering the raw data (both bathymetry and backscatter) through multiple software suites, utilizing this system for additional mapping efforts is not recommended. The challenges met in the acoustic data collection for Phase II validated that future LIS mapping initiatives will benefit from employing a high-resolution, shallow water multibeam system. Ready access to an upgraded MBES that could be interchanged on the research vessels of both SoMAS and UConn would remove the difficulty of synchronizing ship time with equipment availability and allow the survey teams to take advantage of shorter intervals to complete acoustic data collection and provide for more efficient integration of the processed data.

Despite the difficulties the teams confronted in the acoustic data collection and processing, the coordination and methods incorporated in Phase II for the acoustic data acquisition were ultimately

improved over Phase I. The final survey results were largely advantageous for providing valuable information to support the subsequent benthic mapping efforts. While the prior NOAA mapping in LIS provided details about the morphology and character of the seafloor sediments for large parts of the Phase II area, the new acoustic data acquired within the Phase II area added new details in many mostly nearshore areas where detailed mapping did not exist.

The geophysical information contained in the Phase II acoustic products conveys important details describing the shape, composition, extent, and composition of surficial features used to extract detailed information about benthic habitats, sediment texture, grain size, and sedimentary environments. For example, hard bottom areas comprised of boulder/exposed ledge area important habitats for epifauna and many of these were revealed in much greater detail in the bathymetric data. Similarly sand wave features were revealed with much higher resolution and they also represent important habitats, particularly the trough areas. We expect that this new survey data and the improved regional water depth and backscatter compilations that include this data will enhance our overall understanding of the benthic habitat in ELIS and provide an improved basis for the management of submarine cables, pipelines, and other infrastructure in the area.

2.7 References

Auster, P. J., Heinonen, K. B., Witharana, C., & McKee, M. (2009). *A habitat classification for the Long Island Sound region. Long Island Sound Study Technical Report.* Stamford, CT: EPA Long Island Sound Office.

Battista, T., & Husted, R. (2016). *Rough Survey Estimates for Remaining Bathymetry and Intensity Gaps in the ELIS: Seafloor mapping of Long Island Sound.* U.S. Department of Commerce, National Oceanic and Atmospheric Administration, National Ocean Service, National Centers for Coastal Ocean Science, Silver Spring, MD.

Battista, T., & Husted, R. (2016). *Status of Bathymetry and Intensity Coverage in the ELIS: Seafloor mapping of Long Island Sound.* U.S. Department of Commerce, National Oceanic and Atmospheric Administration, National Ocean Service, National Centers for Coastal Ocean Science, Silver Spring, MD.

IHO. (2008). *Standards for Hydrographic Surveys – Special Publication No. 44.* (5th ed.). Monaco: International Hydrographic Organization.

Long Island Sound Cable Fund Steering Committee, eds. (2015). *Seafloor Mapping of Long Island Sound – Final Report: Phase I Pilot project.* U. S. Environmental Protection Agency, Long Island Sound Study. Stamford, CT: (Unpublished project report).

NCCOS. (2015). *Summary Report for Phase 2: Seafloor Mapping of Long Island Sound.* U.S. Department of Commerce, National Oceanic and Atmospheric Administration, National Ocean Service, National Centers for Coastal Ocean Science. Silver Spring, MD: (Unpublished project report).

NOAA & UNH. (2021). *CUBE.* Retrieved from Center for Coastal and Ocean Mapping – Joint Hydrographic Center: http://ccom.unh.edu/theme/data-processing/cube

OCS Hydrographic Surveys Division. (2016). *Hydrographic Surveys Specifications and Deliverables.* Silver Spring, MD: Office of Coast Survey, National Oceanic and Atmospheric Administration.

Samsudin, S. A., & Hasan, R. C. (2017). Assessment of Multibeam Backscatter Texture Analysis for Seafloor Sediment Classification. *International Archives of the Photogrammetry, Remote Sensing & Spatial Information Sciences, 42*.

Teledyne CARIS. (2021). *HIPS and SIPS*. Retrieved from Teledyne CARIS: https://www.teledynecaris.com/en/products/hips-and-sips/

3 Sediment Texture and Grain Size Distribution

Recommended Citations:

Nitsche, F. & Babb, I. (2023). Objective. Section 3.1, p. 43-44 in: "Seafloor Mapping of Long Island Sound – Final Report: Phase II Project." (Unpublished project report). U. S. Environmental Protection Agency, Long Island Sound Study, Stamford, CT.

Babb, I. & Nitsche, F. (2023). Historical Context. Section 3.2, p. 44-45 in: "Seafloor Mapping of Long Island Sound – Final Report: Phase II Project." (Unpublished project report). U. S. Environmental Protection Agency, Long Island Sound Study, Stamford, CT.

Ackerman, S. & Babb, I. (2023). Sediment Sampling and Bottom Photography to Support Ecological Characterization. Section 3.3, p. 46-54 in: "Seafloor Mapping of Long Island Sound – Final Report: Phase II Project." (Unpublished project report). U. S. Environmental Protection Agency, Long Island Sound Study, Stamford, CT.

Nitsche, F., Kenna, T., McHughs, C. (2023). Sediment Grab Collection and Analysis. Section 3.4, p. 54-80 in: "Seafloor Mapping of Long Island Sound – Final Report: Phase II Project." (Unpublished project report). U. S. Environmental Protection Agency, Long Island Sound Study, Stamford, CT.

Babb, I. & Nitsche, F. (2023). Summary/Conclusions. Section 3.5, p. 81 in: "Seafloor Mapping of Long Island Sound – Final Report: Phase II Project." (Unpublished project report). U. S. Environmental Protection Agency, Long Island Sound Study, Stamford, CT.

3.1 Objective

Characterizing sediment texture is a critical component of any habitat classification. Sediment characterization includes describing the shape, size, and spatial arrangement of sediment particles. Sediment grain size directly influences species habitat, so gravel, sand, silt and clay and various mixtures of these major grain size classes are relevant attributes for classifying benthic habitats (Galparsoro et al., 2013; Kenny et al., 2003).

High-resolution acoustic bathymetry and acoustic backscatter are very useful for predicting sediment and habitat types (Samsudin & Hasan, 2017). Acoustic data, especially backscatter or intensity returns can provide broad-scale information on the range of grain size composition of the seafloor, as more reflective coarse sediments typically correspond to high backscatter and less

reflective finer sediments correspond to lower backscatter. This acoustic information on its own, however, is insufficient to discern all the differences in grain size that might be relevant to benthic habitats. In some instances, (e.g., in mud-dominated areas) differences in the backscatter can be caused by fine-scale morphology rather than by differences in grain size content (Ferrini & Flood, 2006; Nitsche et al., 2004). Therefore, determining grain size distribution requires analysis of actual sediment samples.

Total organic content distribution is also valuable for benthic habitat classification since it can be an indicator of biological activity. Basic organic content data is easily extracted from the same sediment samples used for classifying grain size data, so a comparable resolution is desirable. Certain bottom types can also be viewed as valuable provisional resources (e.g., sand). Further, sediment grain size is one of the main factors influencing the distribution of heavy metal contaminant levels (Bastami et al., 2015; McHugh & Kenna, 2015). Thus, surface sediment classification is a key element for managing different marine and coastal resources in LIS.

3.2   Historical Context

Sediment texture has been studied in LIS for many decades because it provides the basis for other studies and management applications. In 2000 USGS compiled existing grain size data and produced a sediment texture map for the entire LIS (Figure 3.2-1). This compilation is based on a large number of grain size data in combination with a limited amount sidescan data where those were available (Poppe et al., 2000).
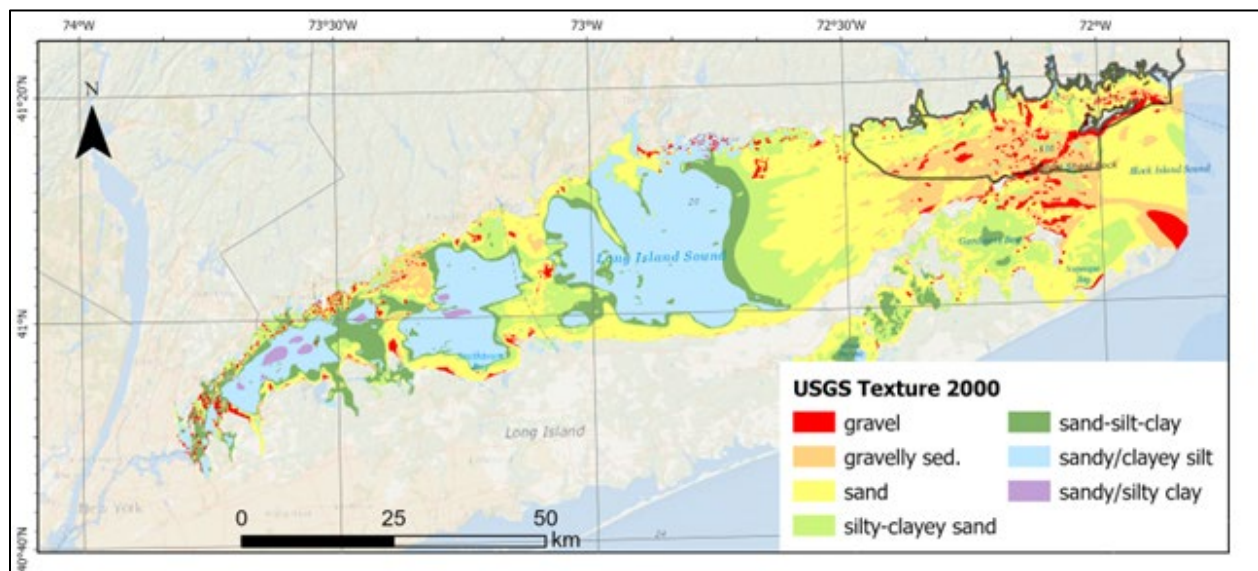
Figure 3.2-1. USGS grain size map of LIS from 2000 (Poppe et al., 2000)

The grain size sample information is compiled in two USGS databases. The LIS Surficial Sediment Sample Database (LISSEDDATA; Poppe et al., 2004) counts >14,000 entries between 1930 and 1998 with a majority ~10,000 from the 1930s (Figure 3.2-2). The second database is the East Coast Sediment Texture Database which contains ~2420 entries for LIS between 1980 and 2010 (McMullen et al., 2014). The vast majority of these data are from sediment grabs; few are from sediment cores and images sources.
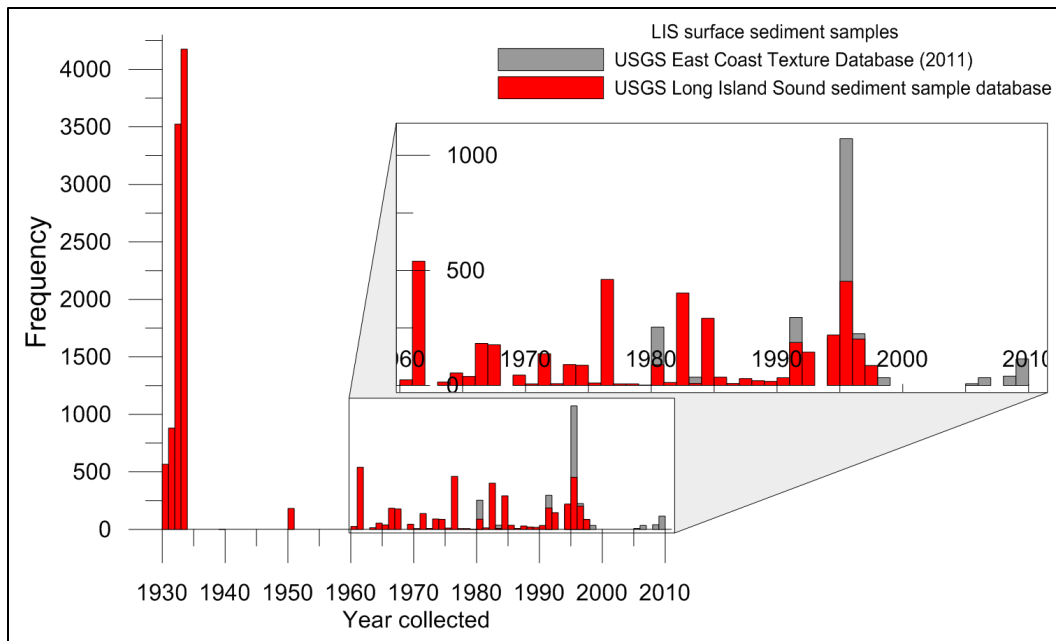
Figure 3.2-2. Existing sediment texture data from the USGS LIS Surficial Sediment Sample Database and the East Coast Sediment Texture Database

While the density of older grain size data is high, the majority of these samples are older than 20 years. It is unclear to what extent older sediment samples from the 1930s reflect the present condition and if their grain size classification follows the present standards for sediment analyses. Samples from the 1930s to 1990s might not represent any changes in the LIS bottom environments during and after this period. Conversely, grain size data from the 1990s and 2000s could still represent current conditions in some areas that have not changed much. However, the characterization of benthic habitats requires an accurate description of the substrate texture, and we cannot be confident that the older sediment data still reflect the present condition. The distribution of these sediment samples from both databases within the Phase II area can be seen in Figure 3.2-3.
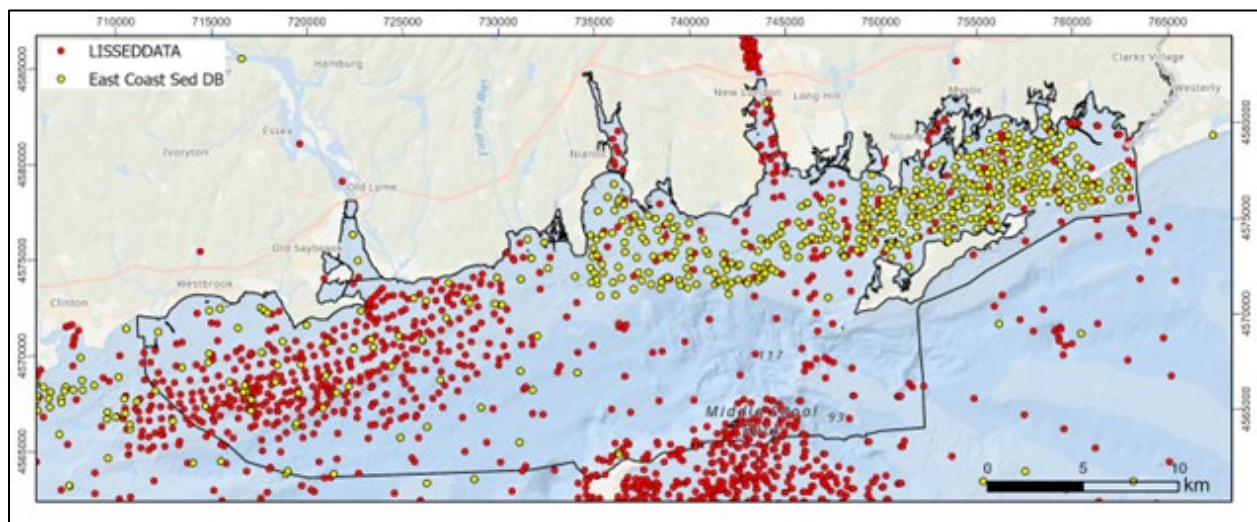
Figure 3.2-3. Map of the Phase II area with locations of the sediment grain size data from the LISSEDDATA database (yellow circles) and the east-coast sediment database (green circles).

3.3 Sediment Sampling and Bottom Photography to Support Ecological Characterization

3.3.1 Overview

Surface sediment characteristics are a primary indicator of the local benthic habitat since benthic organisms typically possess fundamental preferences for specific sediment classes and compositions, which are directly influenced by the energy of the surrounding environment. Photographic data helps to characterize seafloor variability between sampling locations. It is also useful for identifying seafloor characteristics in locations where samples could not be collected (e.g., boulder fields) and for documenting mobile fauna and sedimentary structures, which are indicative of geological and biological processes.

3.3.2 Data Acquisition

The U.S. Geological Survey, University of Connecticut, and University of New Haven through LISMaRC conducted two marine geological surveys within LIS between Connecticut and New York in fall 2017 and spring 2018 (Figure 3.3-1). The SEABed Observation and Sampling System (SEABOSS; Figure 3.3-2) was deployed from the R/V *Connecticut*. Seafloor images and videos were collected at 210 sampling sites within the survey area, and surficial sediment samples were collected at 179 of the sites. The sediment data and the observations from the images and videos were used to identify sediment texture and sea-floor habitats (Ackerman et al., 2020).
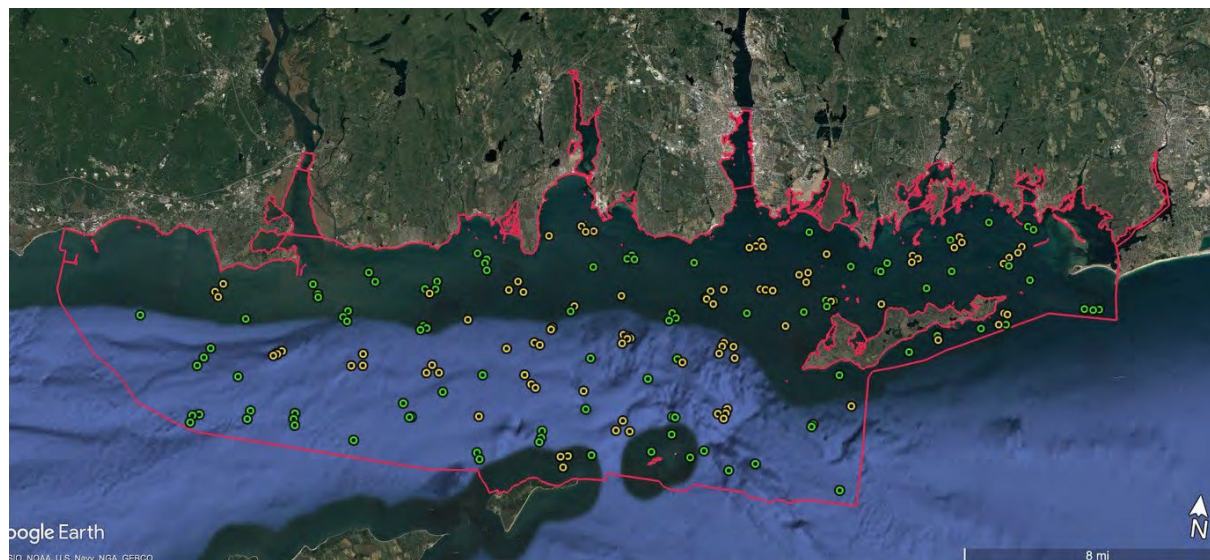
Figure 3.3-1. Map of the Phase II area showing the SEABOSS deployment sites for fall 2017 (yellow circles) and spring 2018 (green circles)

3.3.2.1 Sampling

The R/V *Connecticut* occupied one of the target sites identified by the LISMaRC Ecological Characterization team and the SEABOSS was deployed off the vessel's A-frame on the stern of the ship. The SEABOSS was equipped with a modified Van Veen grab sampler, a Nikon D300 digital still camera with a Photosea strobe, two video cameras (one forward-looking so that a shipboard operator could monitor for proper tow depth and obstacles, and one downward-looking, a Kongsberg Simrad OE1365 in this setup, that overlapped with the field of view of the still camera) with a topside feed, a GoPro HERO4 Black camera recording backup video, and lights to illuminate the seafloor for video and photograph collection (Figure 3.3-2). The elements of this

particular SEABOSS were held within a stainless-steel frame that measured 1.15 x 1.15 meters. The frame had a stabilizer fin that oriented the system as it drifted over the seabed. The winch operator lowered the SEABOSS until the seafloor was observed in the topside live video feed.

For those sites that were primarily targeted for a sediment grab, the vessel and SEABOSS then drifted with wind and current for up to a few minutes to ensure that a decent image with a clear view of the seafloor was acquired. For those sites that were targeted for both a video transect of the seafloor and a sediment grab, the vessel was navigated along a planned transect for up to an hour. A scientist monitored the real-time bottom video and acquired bottom photographs at points of interest by remotely triggering the Nikon camera shutter. Bottom video was also recorded during the drift from the downward-looking video camera. Then, at most sites the winch operator lowered the Van Veen grab sampler until it rested on the seafloor. When the system was raised, the Van Veen grab sampler closed and collected a sample as it was lifted off the seafloor. Times for the sampler retrieval, which would later be used to derive the sample locations, were manually recorded in the survey log when the sampler was lifted off the seabed. The sampler was recovered to the deck of the survey vessel where a subsample was taken for grain-size analysis at the sediment laboratory at the USGS Woods Hole Coastal and Marine Science Center. Sediment samples were only attempted in areas where collecting a sample would not damage the SEABOSS; therefore, no samples were collected in areas with a cobble, boulder, or rocky seabed, as identified in real time using the topside live video feed. Samples were also not attempted if the current was too strong, if the deployment was aborted due to the strobe malfunctioning, or if the grab sampler accidentally tripped earlier in the deployment. A total of 210 sites were occupied aboard the R/V *Connecticut* with the SEABOSS: 93 sites were occupied in fall 2017 during field activity 2017-056-FA, and 117 sites were occupied in spring 2018 during field activity 2018-018-FA. Sediment samples were collected at 179 of the 210 sites. Duplicate sediment samples were collected for collaborators (i.e., Tim Kenna, LDEO) as requested.
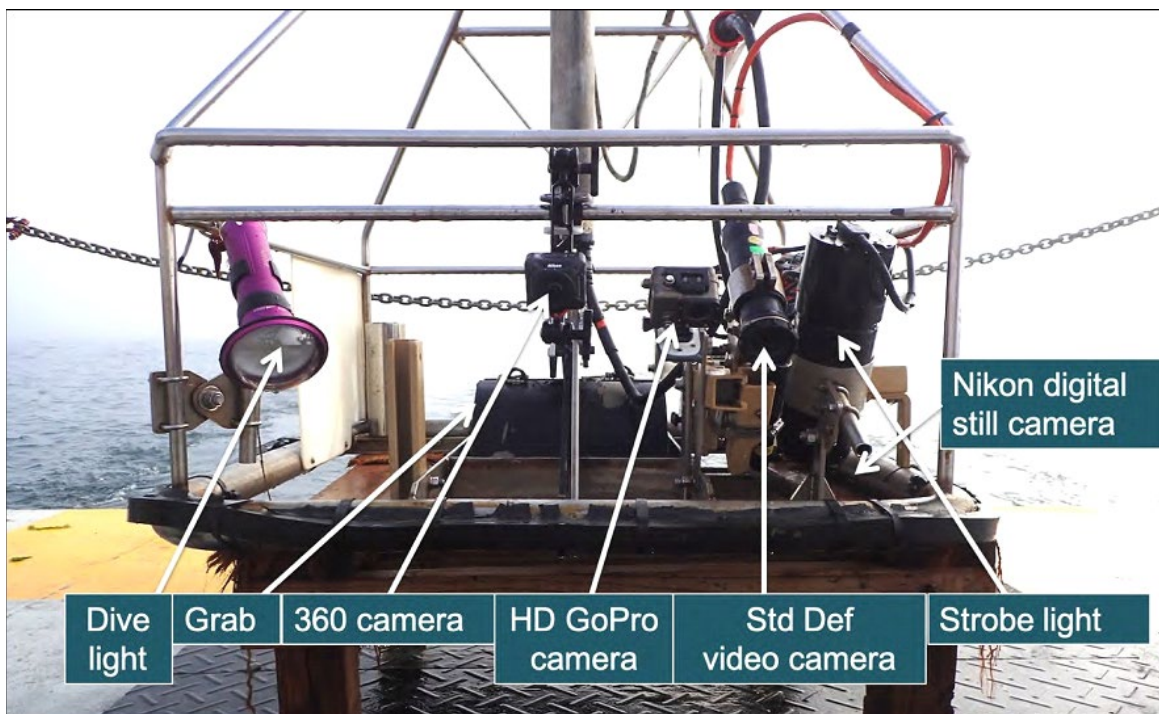
Figure 3.3-2. The USGS SEABOSS illustrating the imaging and sampling systems

3.3.2.2 Navigation Data

During the surveys, WAAS-enabled GPS navigation from a Garmin GPSMAP 76C receiver was logged through a DataBridge data logger and ArcMap GPS. The GPS was set to receive fixes at a 2-second interval in geographic coordinates (WGS 84). Dates and times were recorded in Coordinated Universal Time (UTC). Log files were saved for each Julian day in text format. An AWK script (parsegprmc17056.awk for the fall 2017 log files and parsegprmc18018.awk for the spring 2018 log files) was used to parse the GPRMC navigation string from the log files for each survey and create ASCII Comma Separated Values (CSV) text files. The output files were merged for each survey and then reformatted using an AWK script (navtimereformat.awk), creating a processed navigation CSV text file for each sampling survey.

3.3.2.3 Sample Processing

The sediment sample times (as recorded in the survey logs) were used to parse GPS positions for each sediment sample from the logged GPS data. Approximate depths for each sample were derived from an unpublished composite bathymetry dataset used by LISMaRC. This information was then provided to the sediment laboratory at the USGS Woods Hole Coastal and Marine Science Center with the sample analysis request form for each survey. Duplicate samples were collected for LDEO as requested.

3.3.3 Data Processing

3.3.3.1 Sediment Analysis

The samples from each survey were analyzed in the sediment laboratory at the USGS Woods Hole Coastal and Marine Science Center using two different methods: the Beckman Coulter Multisizer 3 and sieving of the ≥ 4-phi fraction, and the HORIBA LA-960 laser diffraction analyzer and sieving of the ≥ -2-phi fraction. Separate subsamples were taken from each sample submitted to the sediment analysis laboratory for each method.

Beckman Coulter Multisizer 3 Analyses

The subsamples for grain-size analysis using the Beckman Coulter Multisizer 3 and sieving of the ≥ 4-phi fraction were assigned unique analysis identifiers (ANALYSISID), and a macro-enabled Microsoft Excel data entry spreadsheet (GrainSizeWorksheetxxxx.xlsm, where xxxx is the batch number assigned to the sample submission) was created for each survey to record the measurement data. About 50 grams of wet sediment were placed in a pre-weighed beaker, weighed, oven dried at 100°C, and reweighed to correct for salt. The dried sample was wet sieved through a 0.062 mm (No. 230) sieve. The coarse fraction remaining in the sieve was oven dried at 100°C (until completely dried) and weighed. The fine fraction in water was collected in a plastic Nalgene bottle and sealed with a screw lid (stored for no longer than one week). The coarse fraction was dry sieved to determine the individual weights of the 4- to -5-phi fractions, and the weights were recorded in the data entry spreadsheet. The fine fraction was run and combined using the 200-micron and 30-micron Coulter analyses using the Multisizer 3 software to get the fine fraction grain-size distribution for each survey. The fine fraction distribution data were added to the data entry spreadsheet for each survey. The spreadsheet for each survey was used to calculate a continuous phi class distribution from the original fractions.

HORIBA LA-960 Analyses

For the sediments analyzed using the HORIBA LA-960 laser diffraction analyzer and sieving of the ≥ -2-phi fraction, the subsamples for grain-size analysis were assigned unique analysis identifiers (ANALYSISID) and divided into batches of no more than 30 samples.

Each batch was entered into a Microsoft Excel data entry spreadsheet (LD Worksheet Templatexxxx.xlsx, where xxxx is the identifier assigned to the sample submission) to record the initial and dried sample weights, as well as the sieved coarse fraction weights. Each batch was also entered into macro-enabled Microsoft Excel data entry spreadsheets (GrainSizeWorksheetLD1-30xxxx(batchyy).xlsm or GrainSizeWorksheetLD31- 60xxxx(batchyy).xlsm, where xxxx is the identifier assigned to the sample submission, "LD1-30" and "LD31-60" refer to the pre-labeled and weighed glass laser diffraction vials in which the samples will be run, and "batchyy" refers to the sample batch) to record the measurement data coming from the laser diffraction unit and incorporate the initial, dried, and sieved weights. About 10-15 grams of wet sediment were placed in a pre-weighed beaker and the gross weight was recorded. The sample was wet sieved through a 4 mm (No. 5) sieve. If there was any coarse fraction remaining in the sieve, the coarse material was oven dried at 100°C in a pre-weighed beaker and weighed again when dry. This coarse fraction was dry sieved to determine the individual weights of the -2- to -5-phi fractions, and the weights were recorded in the data entry spreadsheet LD Worksheet Templatexxxx.xlsx.

The fine fraction in water was collected in a pre-labeled and weighed glass laser diffraction vial. If there was any coarse fraction remaining in the sieve from wet sieving, this vial was also oven dried at 100°C and weighed when dry. If there was no coarse fraction remaining from wet sieving, the sample can proceed directly to processing for analyses by the HORIBA LA-960 laser diffraction unit. Fine fractions ready for analysis by the HORIBA laser diffraction unit were rehydrated with distilled water if they had been dry. Fifteen (15) ml of pre-mixed 40 g/l sodium hexametaphosphate $[(NaPO_3)_6]$ were added to each sample.

If the height of the fluid in the laser diffraction vial was less than 5 cm, more distilled water was added to raise the level to no more than 8 cm in the vial. The samples were gently stirred, covered, and allowed to soak for at least one hour (for samples that were not dried) or up to 24 hours (for samples that were dried). Soaked vials were placed into an ultrasonic bath and run for 10 minutes at a frequency of 37 Hz with a power level of 100. If the samples appeared to be fully disaggregated, they were placed into pre-determined autosampler locations and were run using the HORIBA LA-960 for Windows software to get the fine fraction grain-size distributions. The fine fraction distribution data were added to the appropriate data entry spreadsheets (GrainSizeWorksheetLD1-30xxxx(batchyy).xlsm or GrainSizeWorksheetLD31- 60xxxx(batchyy).xlsm) for each survey. The spreadsheet for each survey was used to calculate a continuous phi class distribution from the original fractions.

3.3.3.2 Calculated grain-size classification and statistical analyses

Sediment grain size classification was based on a rigorous definition (Shepard, 1954, as modified by Schlee & Webster, 1967; Schlee, 1973; and Poppe et al., 2004). In the definitions below, gravel is defined as particles with nominal diameters greater than 2 mm; sand consists of particles with nominal diameters less than 2 mm, but greater than or equal to 0.0625 mm; silt consists of particles

with nominal diameters less than 0.0625 mm, but greater than or equal to 0.004 mm; and clay consists of particles with nominal diameters less than 0.004 mm.

A continuous phi class distribution from the original fractions was transposed to the "results" tab in the macro-enabled Microsoft Excel data entry workbook (GrainSizeWorksheetLD1-30xxxx(batchyy).xlsm or GrainSizeWorksheetLD31-60xxxx(batchyy).xlsm for the laser diffraction results, where xxxx is the identifier assigned to the sample submission, "LD1-30" and "LD31-60" refer to the pre-labeled and weighed glass laser diffraction vials in which the samples were run, and "batchyy" refers to the sample batch; or GrainSizeWorksheetxxxx.xlsm for the Multisizer results, where xxxx is the identifier assigned to the sample submission) for each survey. Macros in the workbook ("GSMoMArithmatic," "GSstatistics," and "sedimentname" for the laser diffraction results, and "GSstatistics" and "sedimentname" for the Multisizer results) were run to calculate grain-size classification and statistical analyses and to finish processing the data. Sample, navigation, and field identifiers along with continuous phi class distribution data, grain-size classification, and statistical analysis results were copied and pasted into a final Microsoft Excel spreadsheet (xxxxGS-LDresults.xlsx for the laser diffraction results and xxxxGS- MSresults.xlsx for the Multisizer results, where xxxx is the batch number assigned to the sample submission) for each survey. The processed data were quality control checked and assigned a quality grade based on the examination of the analytical data. Processed data were released to the submitter and incorporated into the laboratory's database. All raw analytical data generated by the samples were archived in the sediment analysis laboratory.

3.3.3.3 Final sediment grain-size analysis results CSV files

For the laser diffraction results, the sediment grain-size analysis results spreadsheets for each survey were merged in Microsoft Excel 2016 for Mac and then edited to remove the quality grade and metric distribution fields and to format fields. The Microsoft Excel spreadsheet was then saved as a CSV file (2017-056-FAand2018-018-FAsamplesGS-LD.csv). For the Multisizer results, the sediment grain-size analysis results spreadsheets for each survey were merged in Microsoft Excel 2016 for Mac and then edited to remove some fields, format fields, add site locations for those sites where no sample was successfully collected, and add a no data value (-9999) to empty attributes as needed. The sites with no successful grab were located using the start time of the sampler retrieval from the survey logs; the sampler retrieval position was chosen as the sample location because the video clip is considered the sample in the absence of a physical sample. Some of these site locations from the survey logs did not intersect a bottom video trackline, so they were moved to the last navigation fix along the site's bottom video trackline. Finally, the Microsoft Excel spreadsheet was saved as a CSV file (2017-056-FAand2018-018-FAsamplesGS-MS.csv).

3.3.3.4 Simplified sediment grain-size analysis results shapefile from the Multisizer analysis

The CSV file of the sediment grain-size analysis results from the Multisizer analysis was copied and edited to create a simplified version of the CSV file with fewer attribute fields (specifically, STDEV, SKEWNESS, KURTOSIS, and the individual phi measurements [e.g., PHI11] were removed). A shapefile was created using the simplified version of the CSV file in Esri ArcGIS (version 10.3.1), and XTools Pro (version 12.0) for Esri ArcGIS was used to modify some field parameters in the point shapefile (Table Operations - Table Restructure).

3.3.4 Results

The goal of the Sediment Characterization effort was actually three-fold: 1) provide additional data on the sediment grain size in the Phase II area; 2) provide sediment samples taken by the SEABOSS modified Van Veen grab for subsequent analysis by the LISMaRC Infaunal Ecological Characterization team; and 3) provide digital still images and videos for subsequent analysis by the LISMaRC Epifaunal Ecological Characterization team.

3.3.4.1 Sediment Grain Size

The sediment grain size data were collected to explore the nature of the seafloor and to characterize the seabed by identifying sediment texture. The sediments were analyzed using two different methods: the Beckman Coulter Multisizer 3 and sieving of the ≥ 4-phi fraction as was done in the Phase I Pilot area, and the HORIBA LA-960 laser diffraction analyzer and sieving of the ≥ -2-phi fraction. The HORIBA LA-960 laser diffraction analyzer is a new method for analyzing grain-size distribution at the sediment laboratory at the USGS Woods Hole Coastal and Marine Science Center. This dataset was analyzed using both methods so that the results could be compared, but no comparison was presented in the data release.

The results of the sediment grain size analyses revealed the preponderance of sand as the primary seafloor constituent. Figure 3.3-3 illustrates the percent (by weight) of the major components of each of the samples taken in 2017 and 2018. Figure 3.3-4 presents the results of the sediment classification based on Shepard (1954).
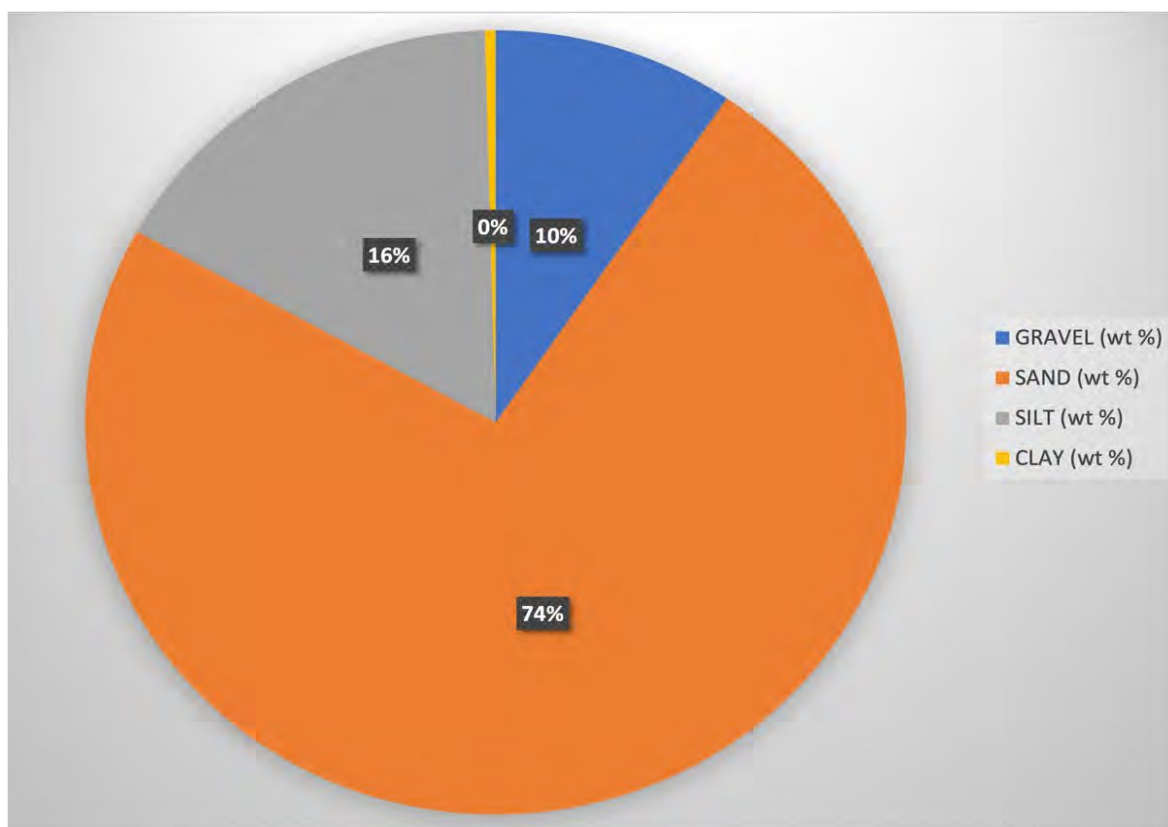
Figure 3.3-3. Percent (by weight) of the main constituents of the sediment samples collected by the USGS SEABOSS in 2017 and 2018
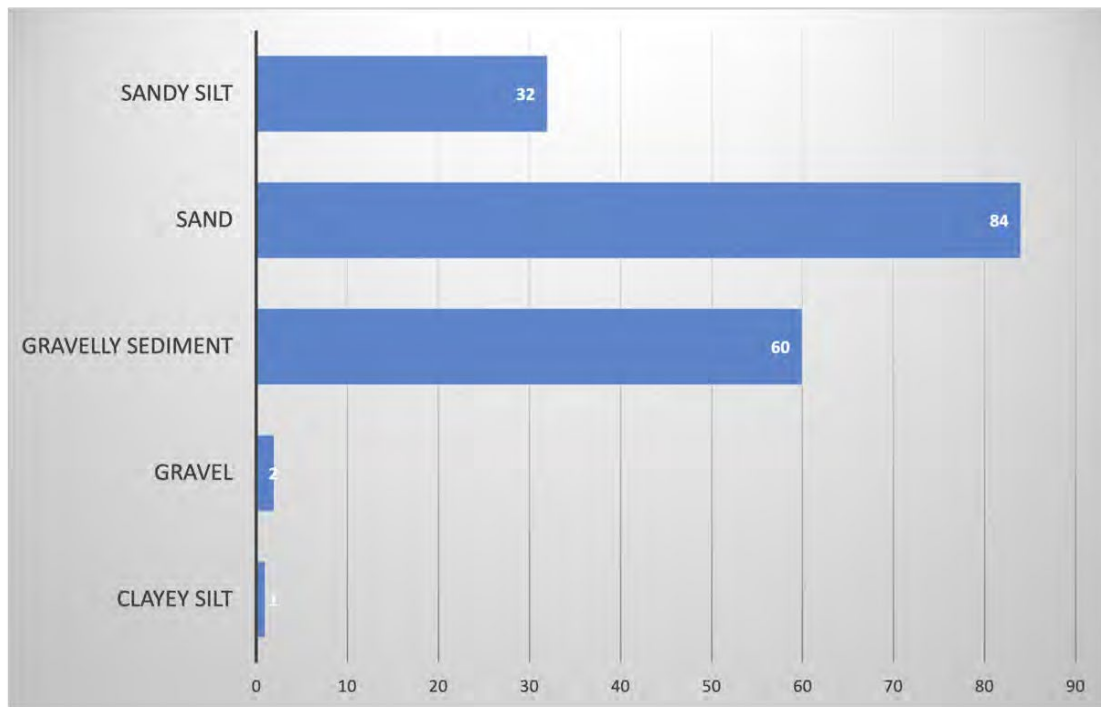
Figure 3.3-4. Sediment classification (Shepard, 1954) of 2017 and 2018 samples

The series of maps below (Figure 3.3-5, Figure 3.3-6 & Figure 3.3-7) illustrate the distribution of the major sediment types in the Phase II area. As can be seen in each map there is a widespread geographic distribution of sand as the major seafloor constituent throughout the Phase II area.
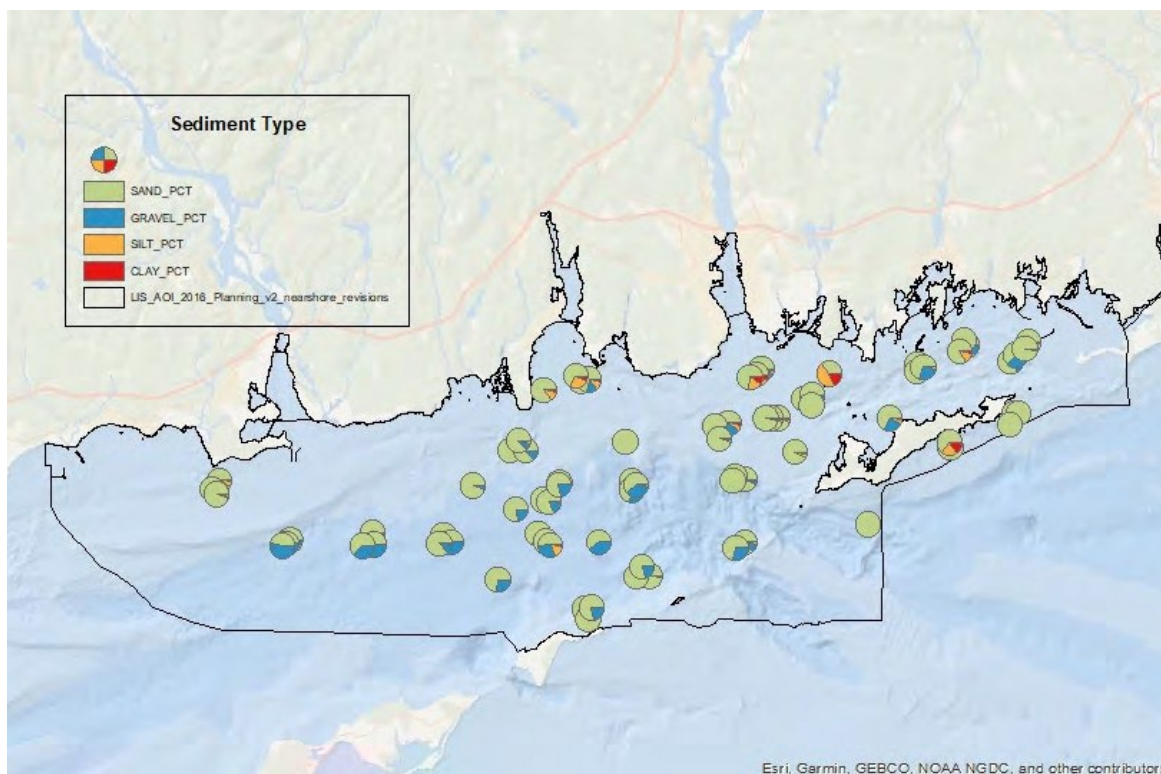
Figure 3.3-5. Map showing the percent (by weight) of the major sediment types in each of the samples collected in the fall 2017
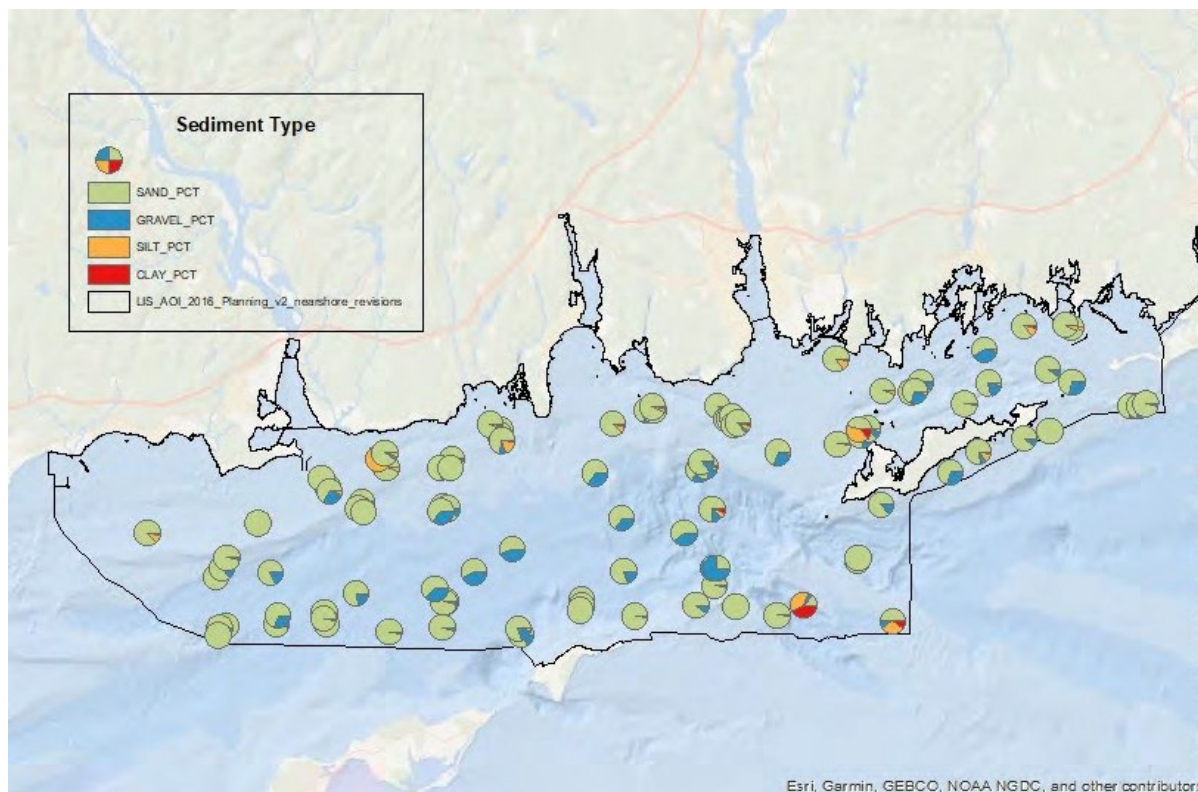
Figure 3.3-6. Map showing the percent (by weight) of the major sediment types in each of the samples collected in the spring 2018
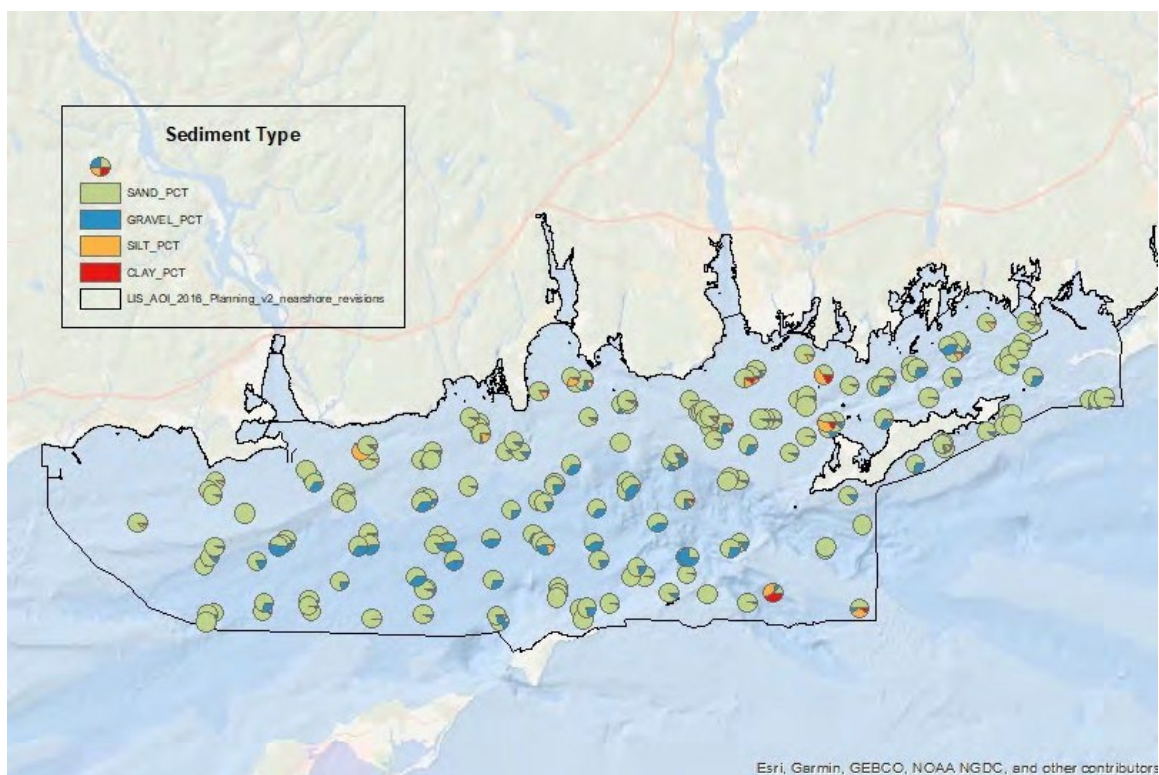
Figure 3.3-7. Map showing the percent (by weight) of the major sediment types in each of the samples collected in both fall 2017 and spring 2018

3.3.4.2 Ecological Characterization – Infauna

Infaunal samples were collected with the 0.1 m^2 modified Van Veen grab on the SEABOSS system. The SEABOSS was lowered to just above the seafloor and then was allowed to drift for several minutes to collect video and still images, after which a grab sample was collected. Of the 179 sediment samples taken, a total of 160 were collected and processed for infauna and results are reported in Section 5.2.

3.3.4.3 Ecological Characterization – Epifauna

The SEABOSS also recorded digital, geotagged sea-floor images and locations of bottom images acquired with a Nikon D300 digital still camera, GoPro HERO4 Black camera, and Kongsberg Simrad OE1365 video camera. A total of 602 images were utilized for epifaunal analyses from the fall 2017 and 595 images from the spring 2018 campaign. These data were collected and analyzed using ImageJ software and the results are reported in Section 5.2.

3.4 Sediment Grab Collection and Analysis

3.4.1 Sediment grab sample collection

LDEO and Queens College selected sampling sites for sediment grabs based on preliminary interpretation of backscatter data from the area. The goal of the site selection was to achieve a dense and well-distributed coverage of the study area that was representative of the range observed backscatter signatures and depositional regimes.

LDEO and Queens College collected all sediment grab samples using a modified van Veen grab. In August 2017 (LIS1701), they targeted 146 locations, acquiring134 samples within the study area onboard the R/V *Pritchard* (Figure 3.4-1). During this field survey LDEO and Queens College also collected bottom videos using a GoPro (Hero 6) system attached to the grab sampler. This was a test of the camera system, so an external light source was not used for this survey. This worked well in shallow water, but in water depth deeper than ~8m the images were often too dark to identify the bottom.

On April 4-5, 2018 (LIS1801), LDEO targeted eight locations, acquiring five samples, within the study area onboard the R/V *Seawolf*. Between June 25 and June 29, 2018 (LIS1802), they targeted 170 locations, acquiring152 samples, within the study area onboard the R/V *Seawolf*. During these surveys bottom videos were again obtained using a GoPro (Hero 6) camera system. They used external light sources and special underwater housing to collect images in water depth up to 100m. In general, locations where material was not recovered were mainly sites with larger size classes such as pebbles, cobbles, and boulders; or in some cases bedrock outcrop, as revealed by the seafloor video images collected from these sites.

Upon recovery of the grab samples, a surface photo was taken and a brief description of the sediment texture and composition was noted in a table. Each sample was characterized for stiffness (very soft, soft, stiff, or very stiff), color (gray-green, gray), and whether the surface was oxidized or not. The grain size (mud, sand, gravel, and pebbles), wood, shell, oyster, mussel, living vegetation, and anthropogenic contents were classified as: absent, rare, common, or abundant. The presence or absence of hydrogen sulfide odor was noted. In the general comments section, additional characteristics particular to each sample were also noted.

After the visual description, the surface sediments (0-2 cm) were sampled directly into pre-weighed and pre-cleaned polystyrene jars, which were then sealed and placed in a cooler on ice until they were placed in cold storage (4°C) at the Lamont-Doherty Core Repository. Sampling tools were cleaned and dried between samples. In addition, LDEO and Queens College recovered push-core subsamples (10cm long and 3.175cm wide) from the grab sampler that preserved the sample stratigraphy. The push cores were capped and sealed with electric tape. These small cores are presently curated in cold storage at the Lamont-Doherty Core Repository.

In addition to the samples collected directly by LDEO, they received 114 sediment grabs collected in December 2017 and in May 2018 from the LISMaRC group, (see Section 3.3).
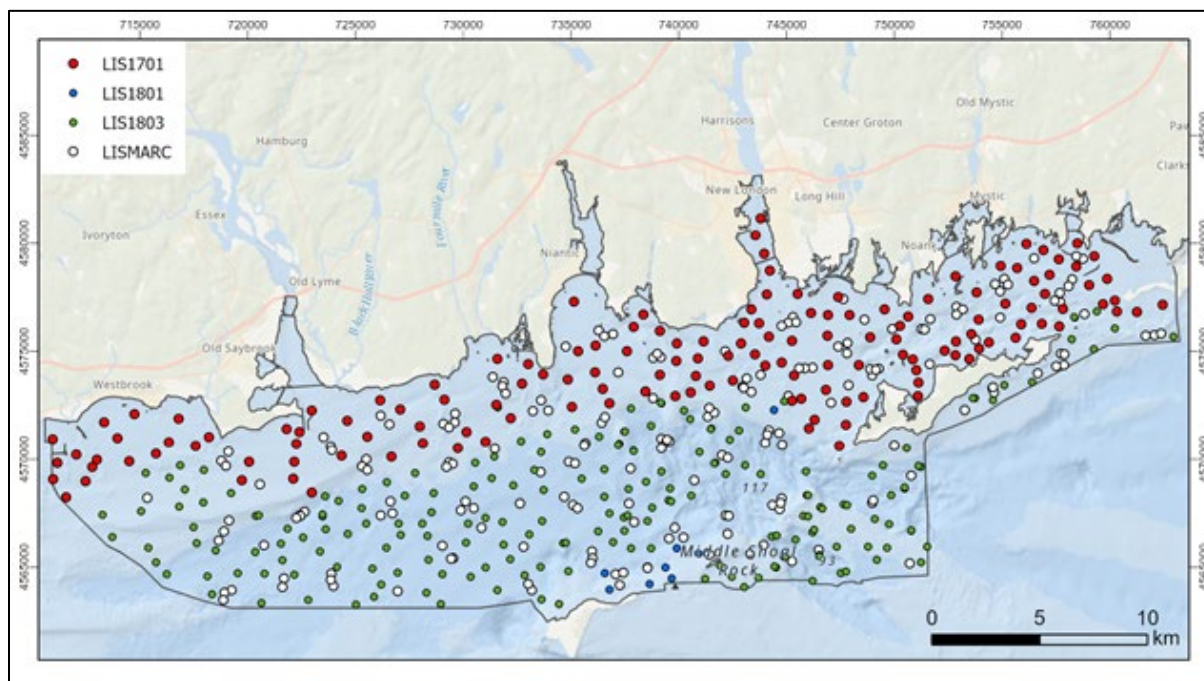
Figure 3.4-1. Location of the collected sediment grabs colored by survey (red, green, blue). White dots are the locations of grab samples acquired and processed by LISMaRC

3.4.2 Sediment grab sample processing

Upon return to the laboratory, push-core samples and one of the 0-2cm sediment sample jars were stored at 4°C, the remaining 0-2cm sediment sample jars were weighed, frozen, and then freeze dried to remove water. Water content was determined by difference in the net sample weight before and after freeze drying. Following this, the dried samples were arranged on a sheet of paper and photographed for reference. The quartering method or 'pie slice' method was used to obtain representative subsamples. For each grab sample, three aliquots were taken: one for grain size analysis, one for the analysis of bulk chemical composition, organic content, and matrix density, and a third in the event duplicate analysis was necessary. Any remaining sample material was archived in its original polystyrene jar. The aliquots designated for grain size and duplicate analyses remained un-ground, while the aliquot collected for bulk chemistry was homogenized using a mortar and pestle to pass through a 500μm sieve. Representative sub-samples of the bulk homogenized material were then taken for X-Ray Fluorescence Spectroscopy (3-5g) and C and N concentration and stable isotopic composition (0.5g). The remaining bulk homogenized material

(10-30g) was stored in a clean 20mL borosilicate glass scintillation vial pending matrix density analysis.

3.4.3 Matrix Density

Sediment matrix densities were determined from dry mass and dry volume measurements of homogenized bulk sediments. Prior to analysis, bulk homogenized samples were heated in an oven at $100° ± 5°C$ for at least 24h and allowed to cool in a desiccator. Sample mass was determined using an analytical balance and sample volumes were determined using a helium-displacement Penta-pycnometer (Quantachrome Instruments, Boynton Beach, FL). Volume measurements were repeated between five and ten times, until the last five measurements exhibited <0.01% standard deviation. A secondary quartz standard was included within each sample set and rotated sequentially among the cells to check for instrument drift and systematic error. Replicate analysis of several samples indicated a precision of <0.01 cm^3.

3.4.4 Grain Size Analysis

3.4.4.1 Peroxide treatment

Prior to determining the grain size distribution, organic matter was removed by treating sediments with 30% hydrogen peroxide (H_2O_2). Grain size aliquots were weighed into beakers with watch glasses (glass/Queens College; Teflon; LDEO) and enough distilled water was added to cover the samples. At this point, 30% H_2O_2 was added in increments of 5mL until no visible reaction occurred up to a total of 25mL, each time allowing the reaction to proceed to completion while covered with a watch glass to prevent loss. After the reaction was complete following the addition of the final 5mL volume of 30% H_2O_2, the watch glass was removed and the sample was allowed to dry on a hot plate at 120°C and cooled in a desiccator (LDEO) or on the deck of the hood at room temperature (Queens College). Once the sample was dried (and cooled), it was weighed again, and the organic content was computed as the difference between sample mass before-and-after the peroxide treatment.

3.4.4.2 Sieving and coarse fraction analysis

After the peroxide treatment, the sample was wet sieved with distilled water through a 63μm sieve. The material retained by the sieve (i.e., the coarse fraction, was air dried and weighed). The dried course fractions were either sieved manually or automatically using a model L3P Sonic-sifter (Advantech Mfg., New Berlin, WI) through 2000μm, 1000μm, 500μm, 250μm, 125μm, and 63μm sieves. When sieving was complete, the mass of material retained by each sieve was measured. Any material that passed through the 63μm sieve was weighed and added to the total fine fraction mass. Because biogenic carbonate shells commonly form in situ but are not hydraulically equivalent to the host sediments, they usually are not considered to be sedimentologically representative of the depositional environment. Therefore, gravel-sized (>2mm) bivalve shells and other biogenic carbonate debris were manually removed and not included in the sediment grain-size data.

3.4.4.3 Fine fraction analysis

During the initial wet sieving, any material passing through the 63μm sieve (i.e., the fine fraction) was collected along with the water in a beaker and allowed to completely settle. Once settled, a majority of the water was carefully removed and discarded. The remaining material was either air

dried or dried under a heat lamp. If the remaining fine-fraction weighed >1.3g, it was selected for Sedigraph analysis and treated as follows at LDEO. Fine fraction samples were soaked in a 60ml solution of 0.2 percent sodium hexametaphosphate. The particle size distribution between 70 and 0.1μm was determined using a Micromeritics Sedigraph 5100; the matrix density used for the Sedigraph analyses was obtained from the pycnometer measurements (see Section 3.4.3). If the remaining fine-fraction weight was below that required for Sedigraph analysis (~1.3 g), an exponential function was used to distribute the fine fraction mass evenly between 5 and 13 Phi. The normalized cumulative frequency data were used in conjunction the GSSTAT program (Poppe et al., 2003) to produce the final size distribution data.

3.4.4.4 Analysis of bottom images

The video footage collected during grab sampling was processed using the open source Shotcut© software (Meltytech, LLC) to crop videos to parts where the bottom is visible, convert them to mp4 format, and to extract still images of the bottom. The still images were inspected manually, and it was determined whether they show large grain size types including gravel, pebbles, or boulders. This additional information was used to guide the sediment texture interpretation.

3.4.4.5 Interpolation and interpretation of results

For the analysis and interpretation of the grain size data, LDEO combined the grain size results from Queens College and LDEO analyses with the results of the LISMaRC samples, analyzed and provided by USGS. The results of the individual samples were integrated to raster for the Phase II study area to better visualize trends and expand the results to a larger area. Using the empirical Bayesian kriging algorithm in ArcGIS Pro (Krivoruchko & Gribov, 2019), they created raster data with 50m cell size of mean phi grain size, percentage silt, clay, sand, and gravel.

In addition to these interpolated distributions, LDEO manually created polygons of likely similar grain size classes based on the grab sample results and taking into account the seafloor morphology and backscatter data as well.

For the analysis and interpretation of the grain size data, LDEO combined the grain size results from their analyses with the results of the LISMaRC samples analyzed and provided by USGS. The results of the individual samples were integrated to raster for the Phase II study area to better visualize trends and expand the results to a larger area. Using the empirical Bayesian kriging algorithm in ArcGIS Pro (Krivoruchko & Gribov, 2019), they created raster data with 50m cell size of mean phi grain size, percentage silt, clay, sand, and gravel.

In addition to these interpolated distributions, LDEO manually created polygons of likely similar grain size classes based on the grab sample results and taking into account the seafloor morphology and backscatter data as well.

For the interpretation and classification, LDEO used a modified version of Shepard's (1954) ternary classification system (Figure 3.4-2) that has been traditionally used in the LIS system (Poppe & Polloni, 2000; Schlee, 1973). This classification scheme provides usable information for determining biological habitat classes and merges with previous interpretations where the dominant grain size classes are sand, silt, clay, and limited amounts of gravel. It should also be noted that although a formal intercalibration for grain size analysis was not conducted between

LDEO/Queens College and USGS laboratories, a measure of confidence is obtained from the observation that data from the different labs fall in the same regions of the Shepard and Schlee ternary diagrams and exhibit similar trends.
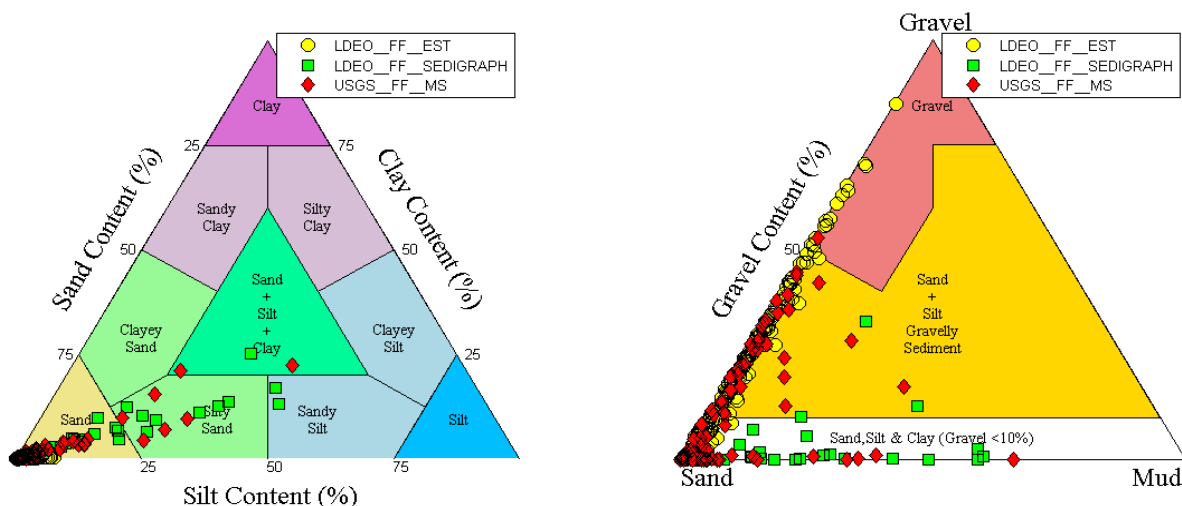
Figure 3.4-2. Shepard and Schlee ternary diagrams for comparison of grain size distribution data LDEO/Queens and USGS Labs. LDEO_FF_EST indicates samples for which the fine fraction mass (<63 um) was below that required for Sedigraph analysis (~1.3g); in these cases, an exponential function was used to distribute the fine fraction mass distribution between 4 and 12 Phi. LDEO_FF_SEDIGRAPH indicates samples for which the fine fraction mass (<63 um) was sufficient for Sedigraph analysis. USGS_FF_MS indicates data for samples collected and analyzed by USGS using a Multisizer III system.

For the sediment texture interpretation of this study, LDEO added a few classes to the traditional Shepard and Schlee grain size classification schema to reflect bottom types with outcropping bedrock and areas where boulders are co-located with sand and gravel. Classifying an area with abounded boulders simply as sand or gravel might not be an adequate description. Since large pebbles or boulders cannot be sampled with the grab system that was used, they relied on bottom images and morphology from bathymetry data for this classification. Figure 3.4-3 shows examples of bottom images for pebbles and boulders. Figure 3.4-4 shows examples where detailed bathymetry indicates the presence of large boulders and bedrock outcrops. The metal rods of the grab system are approximately one centimeter in diameter and used for size reference. The classification was done visually by noting absence, rare, or abundance of large pebbles/cobbles and boulders. Note that these pebbles and cobbles fall into the gravel region in the Schlee classification system.

Figure 3.4-3. Bottom images showing large pebbles (left, LIS1801-G151A) and boulders (right, LIS1802-G221A)
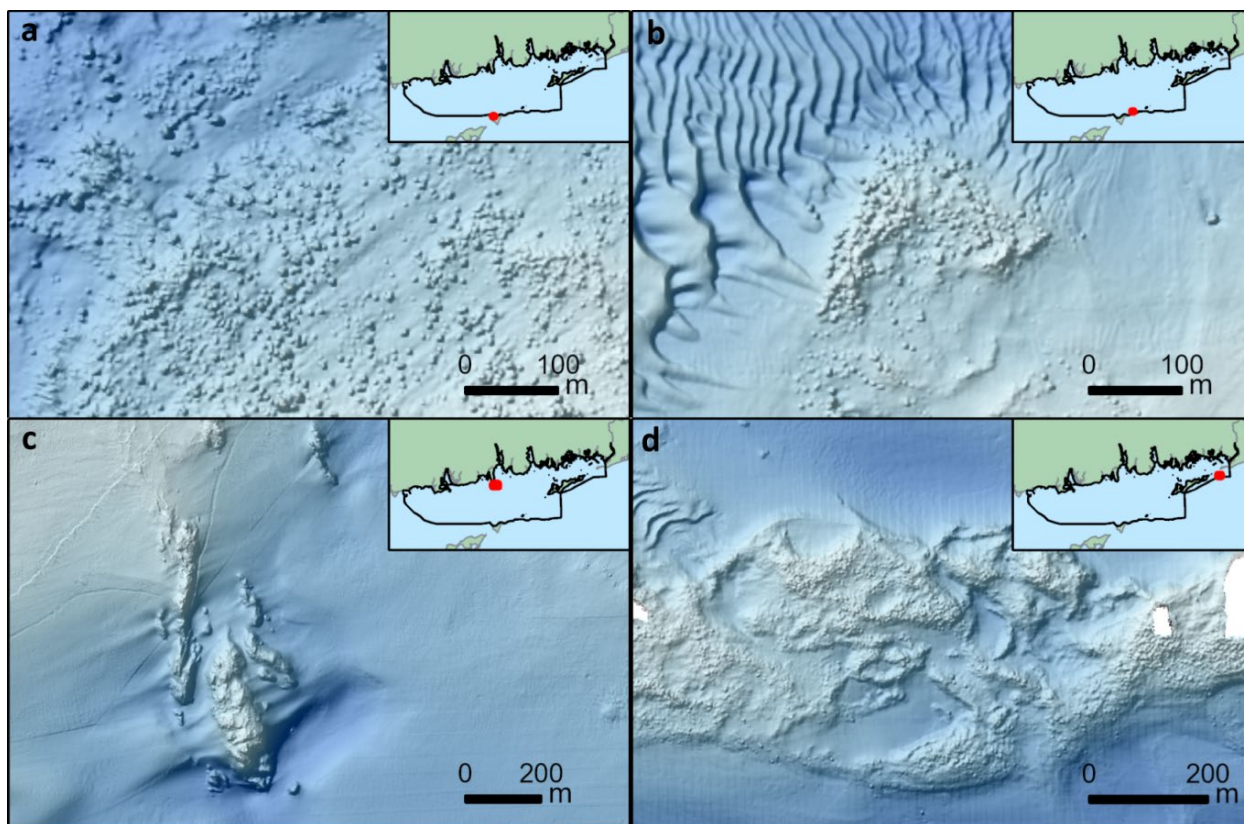
Figure 3.4-4. Detailed views of the bathymetry data showing large boulders (top) and bedrock outcrop (bottom)

If a field of boulders occurs in an area that is clearly dominated by sand otherwise, we assume that the sediment between boulders is mainly sand and the area is classified as *boulders with sand*. If the boulders are surrounded by gravel or gravelly sediment, LDEO classified these areas as *boulders with gravel and sand*.

The sediment texture interpretation for the study area is based on the results from the grain size analysis. The extent of the different sediment classes was manually determined by drawing polygons that generally followed changes in bottom morphology and backscatter based on the assumption that sediments with similar textures will yield similar backscatter signals, which can, in turn, be used to identify similar benthic regimes. The degree to which this assumption holds will be discussed below.

3.4.5 Grain size distribution results

Figure 3.4-5 shows the results of the grain size analysis for 281 samples acquired and processed by LDEO/Queens College in form of pie charts.
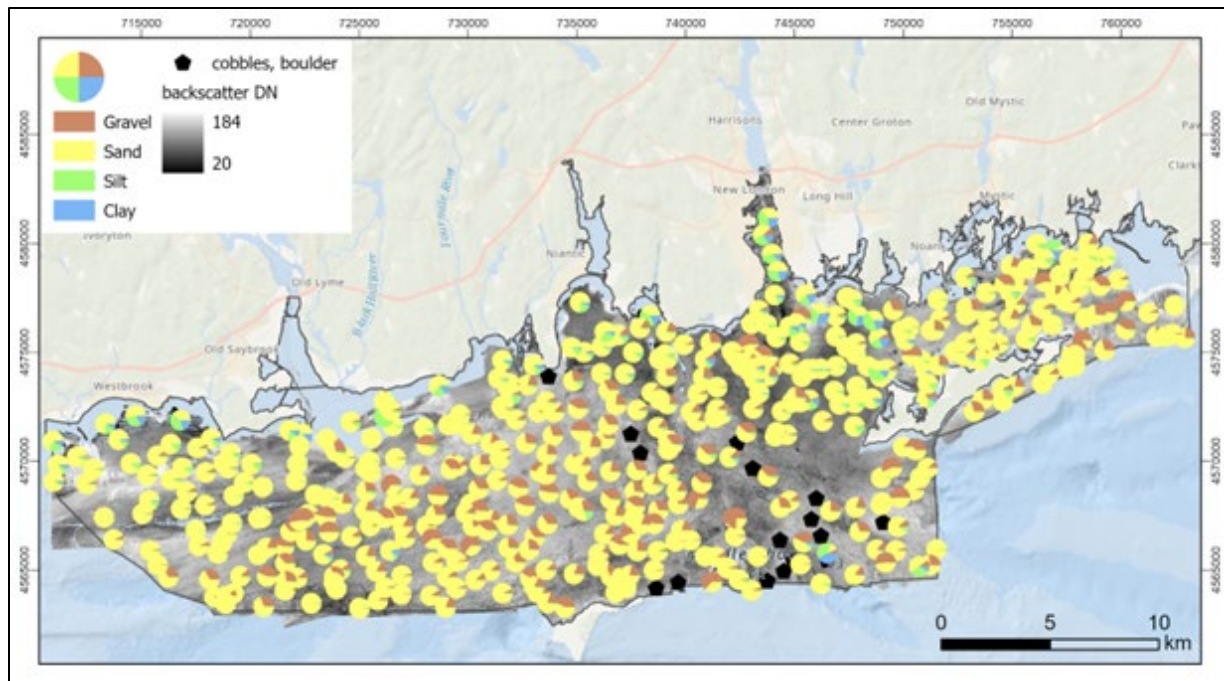
Figure 3.4-5. LDEO grab samples with grain size results displayed as pie charts. Black symbols represent bottom classification based on grab bottom images. The acoustic backscatter mosaic is shown as background

The LDEO results were combined with the 179 results provided by LISMaRC/USGS for further interpretation and descriptions. Based on the combined 460 grain size results from both groups, LDEO created interpolated rasters for the gravel, sand, silt, and clay content, as well as mean grain size shown in Figure 3.4-6, Figure 3.4-8, and Figure 3.4-10. Note that the percentage scale varies between some of the figures; otherwise, some of the variations would not be as visible.
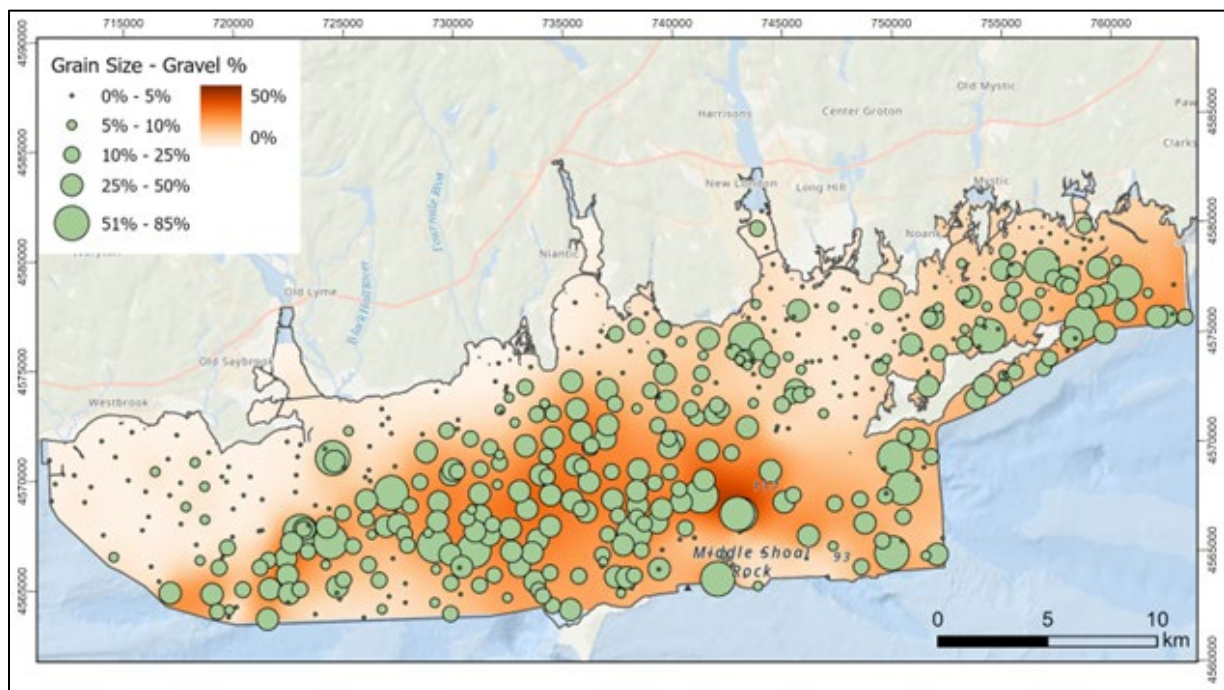
Figure 3.4-6. Map of gravel content (%) in surface sediments based on grab samples (green circles)
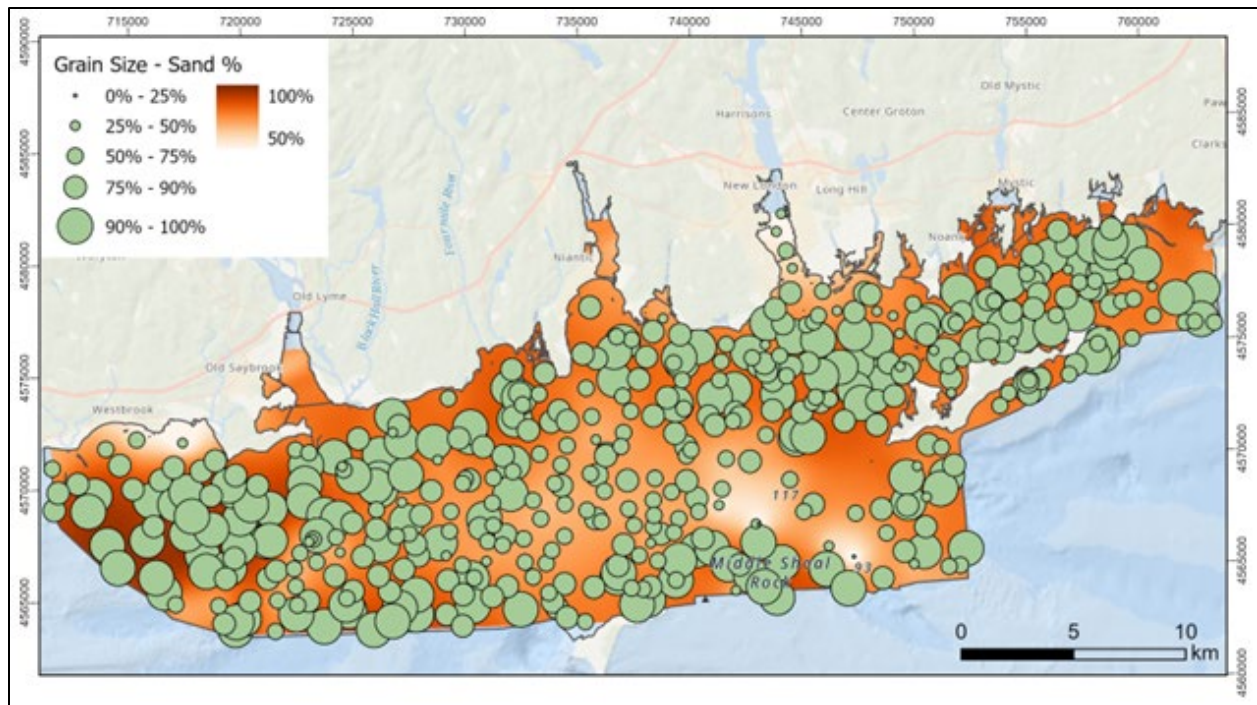
Figure 3.4-7. Map of sand content (%) in surface sediments based on grab samples (green circles). Note that the percentage scale is different from the other maps to highlight variations.
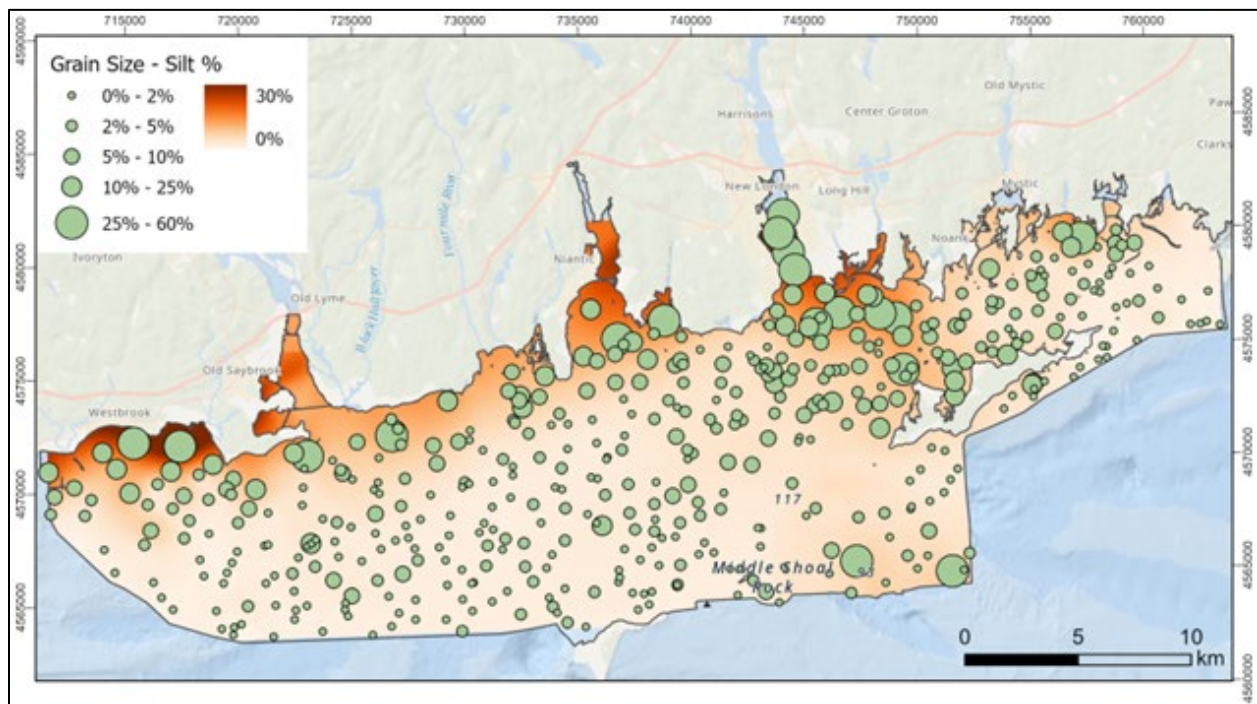
Figure 3.4-8. Map of silt content (%) in surface sediments based on grab samples (green circles)
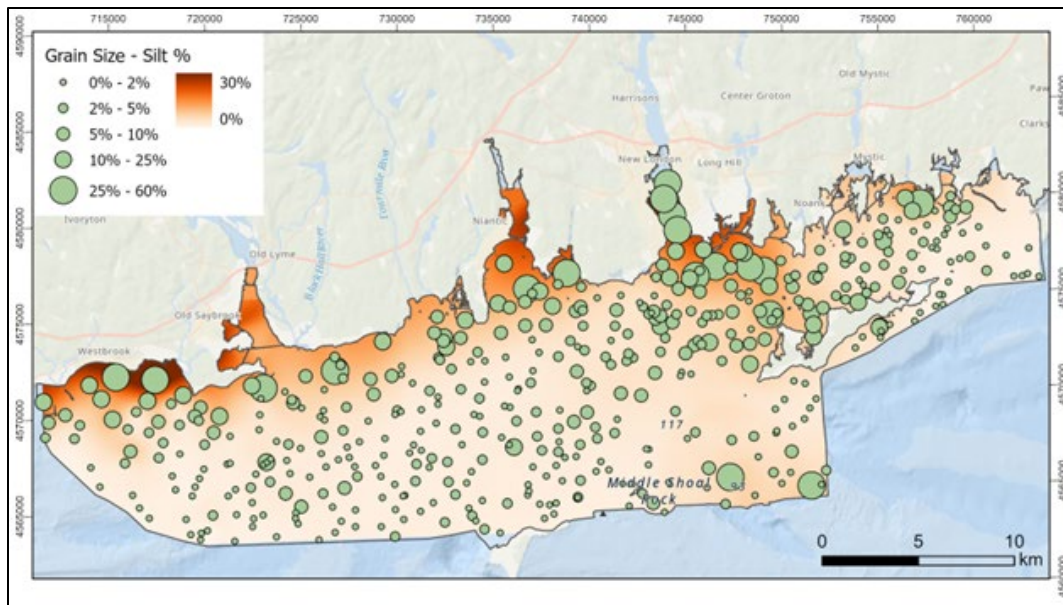
Figure 3.4-9. Map of clay content (%) in surface sediments based on grab samples (green circles). Note that the percentage scale is different from the other maps to highlight variations
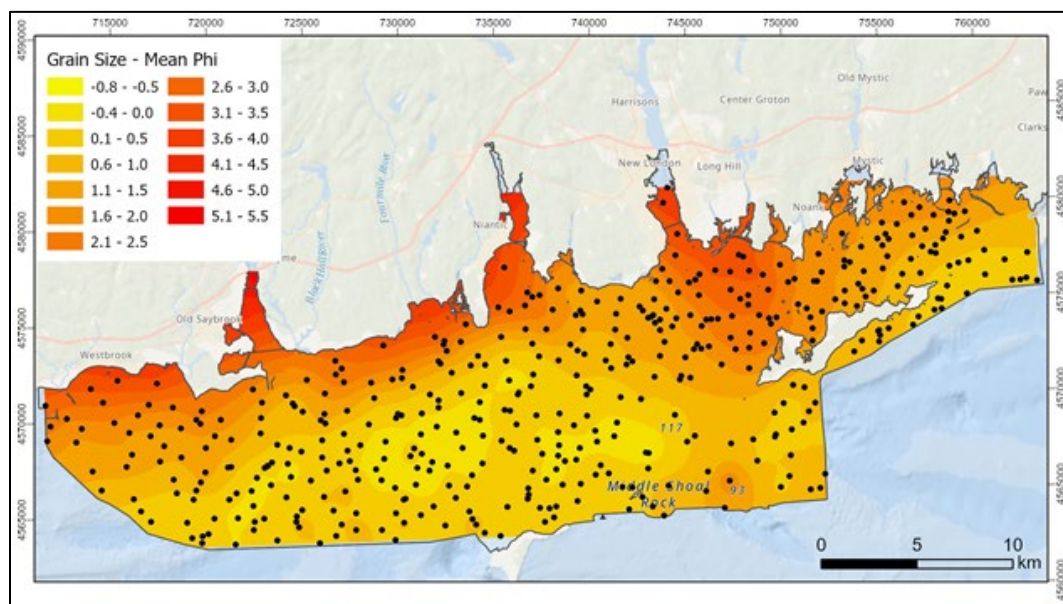
Figure 3.4-10. Map of mean grain size distribution (Phi) of surface sediments based on grab samples (black dots). Red are finer sediments and yellow are coarser sediments (phi < -1: gravel; -1 to 4: sand; 4 – 8: silt).

The data show that sand is the dominating grain size in the Phase II study area and lies generally between 50% and 100%. Lower sand content was measured in the central area and near the race as well as the Thames River. Gravel content is high in Central Basin and the Race areas, especially in areas deeper 20m (see Figure 4.5-1 for location details).

Silt and clay content is low overall with higher values (over 10-20%) near embayments and rivers along the Connecticut shore, especially in the Thames and Connecticut Rivers, especially in the Thames and Connecticut Rivers. The mean phi distribution map (Figure 3.4-10) probably best shows the overall trend of finer grain sizes towards the Connecticut shore.

3.4.5.1 Sediment texture interpretation results

Figure 3.4-11 shows the manually interpreted sediment texture map. As described above, it is mainly based on the modified Shepard's classification with the edition of classes with boulders and outcropping bedrock.
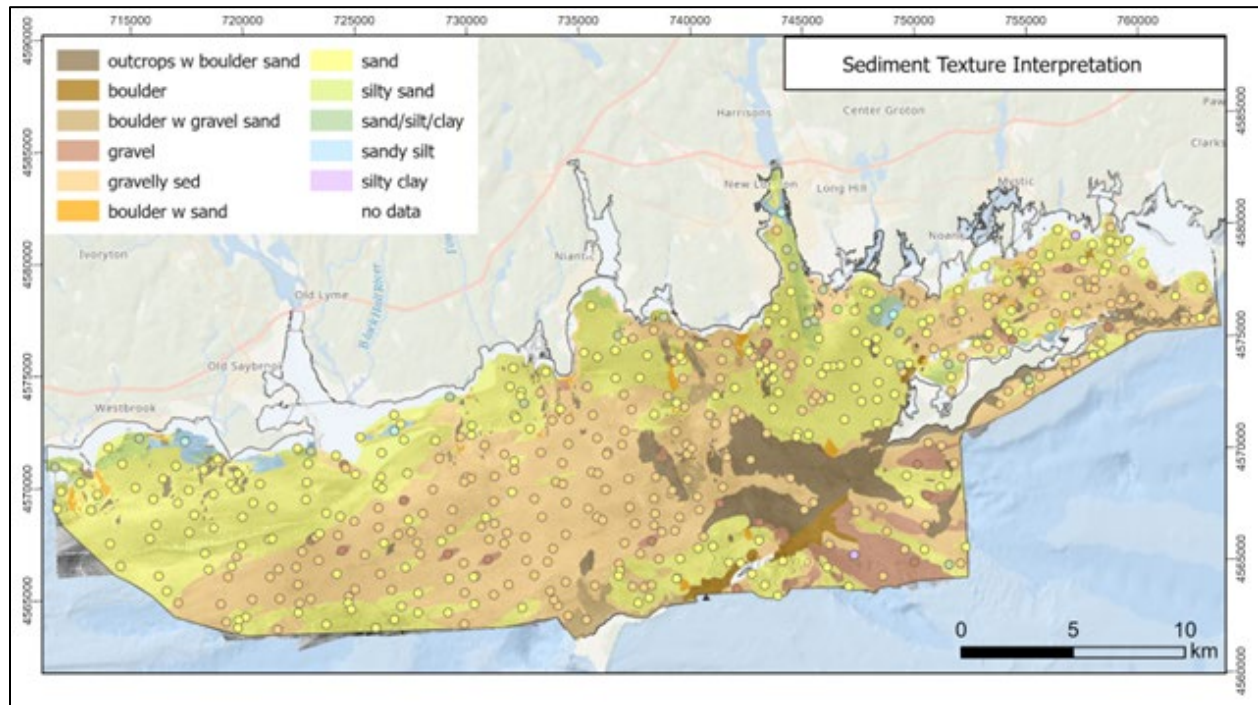
Figure 3.4-11. Map of sediment texture interpretation following the Shepard's classification schema. Colored circles show classification of actual grab samples.

Distinguishing the different sediment texture classes was challenging due to the high variability, especially in areas with outcrop. Acoustic backscatter is often a useful guide when determining sediment texture classes. In this study, however, LDEO found that backscatter was of limited use as general indicator of the grain size classes. In many cases the grain size analysis showed different results for similar backscatter values and a variety of backscatter values for the same grain size/texture class (e.g., Figure 3.4-12). Therefore, they used changes in the backscatter variation more for identifying boundaries between different classes and to a lesser degree for determining the class itself.
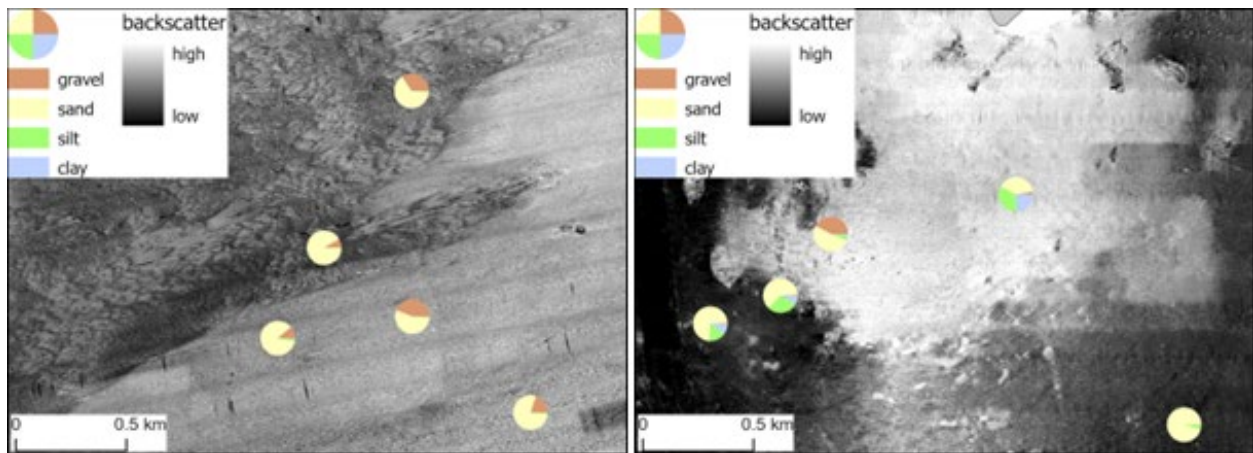
Figure 3.4-12. Two examples of backscatter images with superimposed grain size results. Note that the backscatter scale has not been changed and represents variations in the Phase II area. Darker gray represents lower backscatter, often associated with finer grain size and lighter gray represents higher backscatter, associated with coarser grain, rougher bottom. On the left we see examples where both sandy and gravelly sediments are found in similar backscatter areas. On the right, low backscatter can represent muddy and/or pure sand, and high backscatter has both sandy gravel and sandy mud sediments.

There are several potential reasons for this. A main factor is likely the general coarser nature of the sediment with sand and gravel being dominant. Different amounts of fine and coarse sand, which both are classified as sand, could lead to differences in backscatter.

Another factor that can influence the backscatter response is seabed vegetation. Sandy or gravelly bottom can produce different backscatter depending if they are covered by vegetation or shellfish. Vegetation can reduce the backscatter for gravel bed, while shell beds can result in higher backscatter for fine grain size. The bottom images taken with the grab samples frequently showed different types of bottom vegetation.

Figure 3.4-13 shows examples of backscatter that might relate to seagrass or similar vegetation in the areas. Likewise, shell beds are common in some parts of the study area, making it difficult to determine the underlying sediment texture.
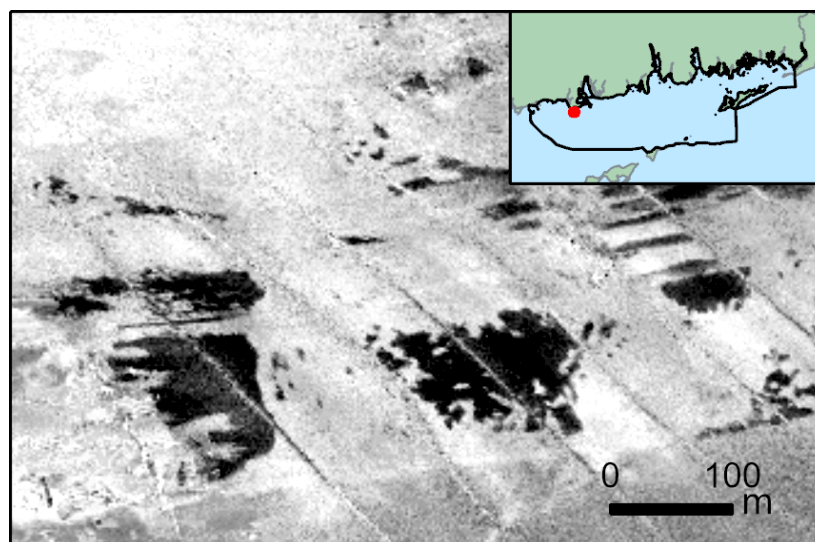
Figure 3.4-13. Backscatter examples whose shape and strong contrast could indicate bottom cover with vegetation (dark gray, low backscatter areas)

The backscatter mosaic is combined from several datasets that have been collected at different times and potentially during different seasons. Some of the seabed vegetation distributions may exhibit a seasonal dependence; making it possible that some of the observed differences in the backscatter mosaic are caused by the presence or absence of vegetation between backscatter acquisition and grab sample collection. As result of the factors mentioned above, some details in the sediment texture map, provided without validation by sediment grain size information, may have a high uncertainty.

Based on available backscatter intensity, grain size distribution data, and bottom images, several major trends and other details in the sediment texture map are clearly visible. It shows that, overall, the study area is dominated by sand, while bays along the northern shore show pockets with more clay and silt. There are larger amounts of gravel in the deeper, central parts of the study area. Some of the distributions reflect the geological history and dynamic nature of this area (see description and interrelation of sediment environments in Section 4 for more details).

3.4.5.2 Comparison with previous work

Prior to this project, the USGS had created a sediment texture map for the entire LIS based on samples in the 1990s (Figure 3.4-14; Poppe et al., 2000).
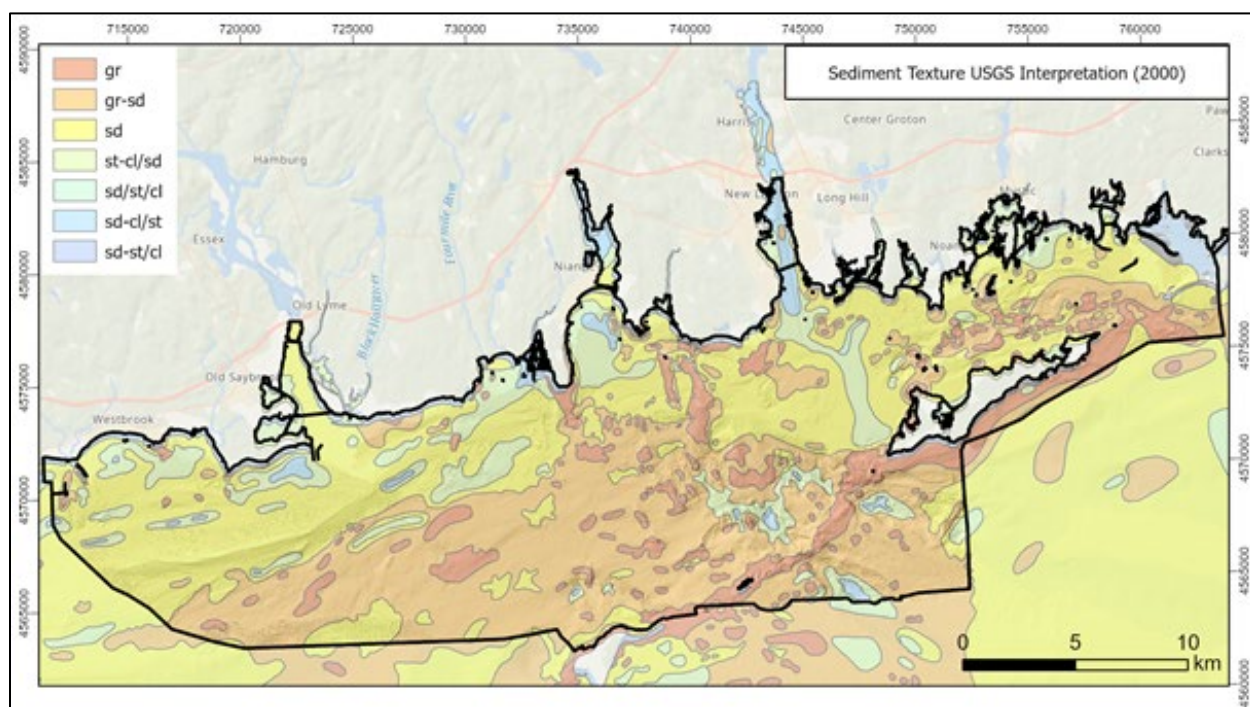
Figure 3.4-14. Map of sediment texture interpretation from Poppe et al. (2000). The black line marks the extent of the Phase II AOI

The overall pattern of the sediment texture distribution of the earlier interpretation by Poppe et al. (2000) is very similar, with dominating sand and gravelly sediment. There are differences in the detailed boundaries of these features and the location of the pockets of fine-grained sediment. Much of the difference can be explained by the availability of the more detailed bathymetry and backscatter data now that were not available for the earlier interpretation. Some of the fine-grained pockets might also have been temporary, and the sediment might have been moved (e.g., by storms).

3.4.6 Sediment surface chemistry and matrix density

3.4.6.1 Sediment surface sample characterization

In addition to grain size distribution, LDEO measured several chemical constituents and matrix density in order to better characterize the surface sedimentary environment within the Phase II study area. This includes evaluating the source of particulate organic matter of surface sediments using organic carbon and nitrogen concentrations and their stable isotope compositions and measuring bulk sediment chemical composition and matrix density.

Generating surface constituent distribution raster datasets

Available surface parameter results were interpolated into continuous raster datasets for the entire study area, making it easier to visualize and identify spatial distribution. In the case of bulk sediment chemical composition, LDEO selected elements with significant concentration values (i.e., the concentrations for some elements were below detection).

The results were imported into ArcGIS Pro and used the "empirical Bayesian kriging" method provided by ArcGIS geostatistical toolbox (Krivoruchko & Gribov, 2019). A raster resolution of 50m was used for the interpolation. The results were clipped to the extent of the Phase II boundaries and exported as a GeoTIFF raster.

3.4.6.2 Analysis of carbon and nitrogen

Sample preparation and analysis

Sub-samples of dried homogenized sediments splits (see Section 3.4.2) were sent to the Cornell Isotope Laboratory (COIL) to be analyzed for carbon and nitrogen concentrations as well as stable isotopic compositions. Total carbon (TC), total nitrogen (TN), and $\delta^{15}N$ were determined on an aliquot of untreated, dried homogenized sediments. In order to accurately determine total organic carbon (TOC) and $\delta^{13}C$, removal of carbonate is necessary (Schlacher & Connolly, 2014). This was affected through sequential treatments of the sediments with dilute hydrochloric acid until no bubbling was observed. The acidified sediments were then rinsed in deionized water and re-dried.

Aliquots of between 10 and 70mg of both untreated and acidified sediments were carefully weighed into separate Costech tin capsules, rolled and shaped into a ball, and then injected into a combustion column on a NC2500 elemental analyzer interfaced with a Thermo Delta V isotope ratio mass spectrometer (IRMS). The carbon and nitrogen concentrations are reported as elemental percentage of these elements based on weight. Carbon and nitrogen isotope compositions are measured as isotope ratios, $^{13}C/^{12}C$ and, $^{15}N/^{14}N$, respectively, which can be determined more precisely than absolute abundances. Results are expressed in per mil deviations from an accepted standard reference material (i.e., delta notation) as follows:

Equation 1

$$\delta^{15}N \, or \, \delta^{13}C \, (\text{‰}) = \frac{R_{sample} - R_{standard}}{R_{standard}} \times 1000$$

Where:
R_{sample} is the measured = $^{13}C/^{12}C$ or $^{15}N/^{14}N$ ratio and $R_{standard}$ is the corresponding ratio measured in the standard NBS 19, which has a certified Vienna Pee Dee Belemnite (VPDB=+1.95‰) and Atmospheric Air (AIR=0.00‰) for carbon and nitrogen isotope ratios, respectively. For additional

details on stable isotope systematics see (Karhu, 1999; Ostrom & Ostrom, 1999; Hoefs, 2004, and references therein).

Total organic carbon and total nitrogen concentrations

In the LIS Phase II study area, the distributions of total organic carbon (TOC) and total nitrogen (TN) are similar (Figure 3.4-15 & Figure 3.4-16, respectively). In general, we observe a pattern of increasing concentration with decreasing proximity to shore, with the highest levels at the mouths of Thames and Connecticut Rivers. Excessive nutrient inputs to estuaries and coastal waters as a result of anthropogenic activities can cause eutrophication. Depending on the severity, hypoxic to anoxic conditions in sediments and bottom waters due to excess organic matter derived from algal blooms can degrade or destroy important benthic habitats. Given that primary productivity in estuaries is nitrogen limited, the levels of organic carbon and nitrogen in surface sediments are both important indicators of benthic habitat quality as well as the effectiveness of mitigation efforts.
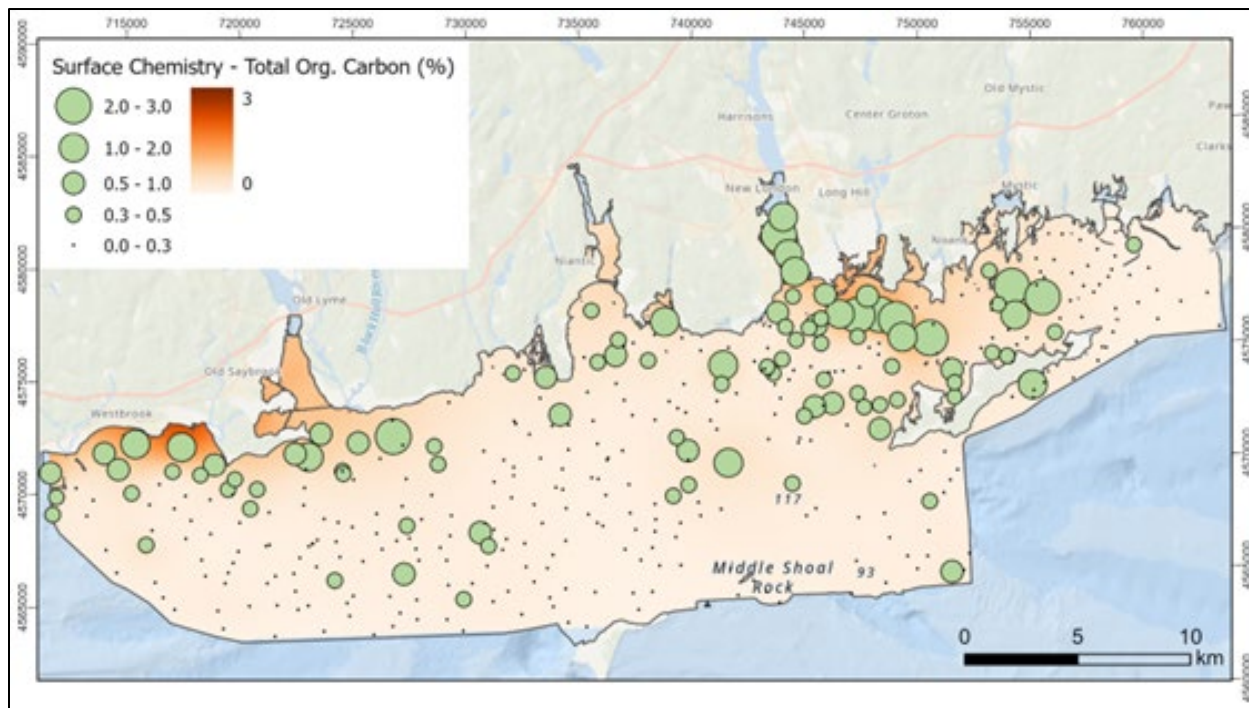
Figure 3.4-15. Map of total organic carbon (TOC) distribution in surface sediments based on surface samples (green circles)
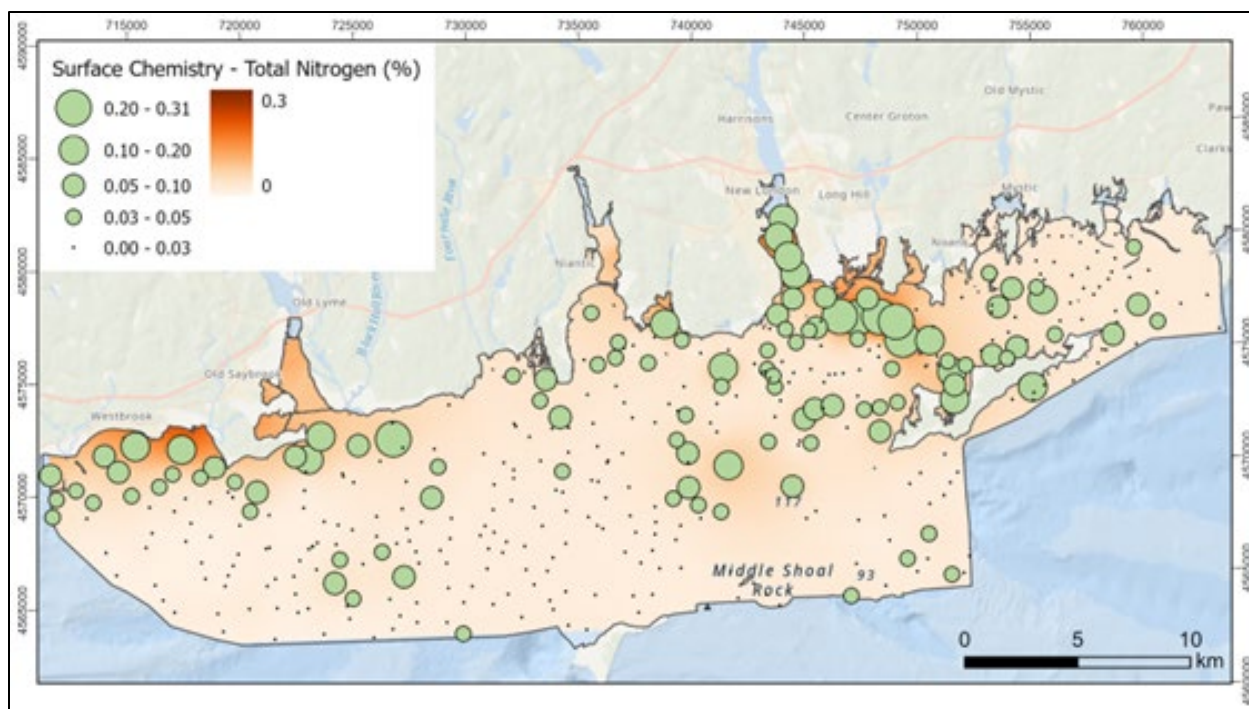
Figure 3.4-16. Map of total nitrogen (TN) distribution in surface sediments based on surface samples (green circles)

Organic carbon and nitrogen isotopic compositions

Due to significant differences between organic matter derived from marine and terrestrial pools, organic carbon and nitrogen stable isotope ratios have seen wide application as tools to study sources, fate, and transport of sedimentary organic matter (Peters et al., 1978; Sweeney et al., 1980; Cifuentes et al., 1988; Meyers, 1994; Thornton & McManus, 1994). The $\delta^{13}C$ and $\delta^{15}N$ results for surface samples are presented in Figure 3.4-17 and Figure 3.4-18, respectively. The $\delta^{13}C$ composition ranges between -28‰ and -16‰, with marine algae as the dominant source (-25‰ to -21‰) and contributions from C3 plants (<-25‰) and to a lesser extent C4 plants (>-21‰). The $\delta^{15}N$ composition ranges between 0‰ and 15‰. Similar to $\delta^{13}C$, we observe marine algae as the dominant source, with contributions of material consistent with terrigenous plants and fertilizers. Additionally, we observe enriched $\delta^{15}N$ values in surface samples, which are indicative sewage input from wastewater treatment facilities and/or denitrification, a microbially-driven process by which, nitrate (NO_3^-) is reduced through a series of nitrogen oxide constituents and ultimately producing molecular nitrogen (N_2).
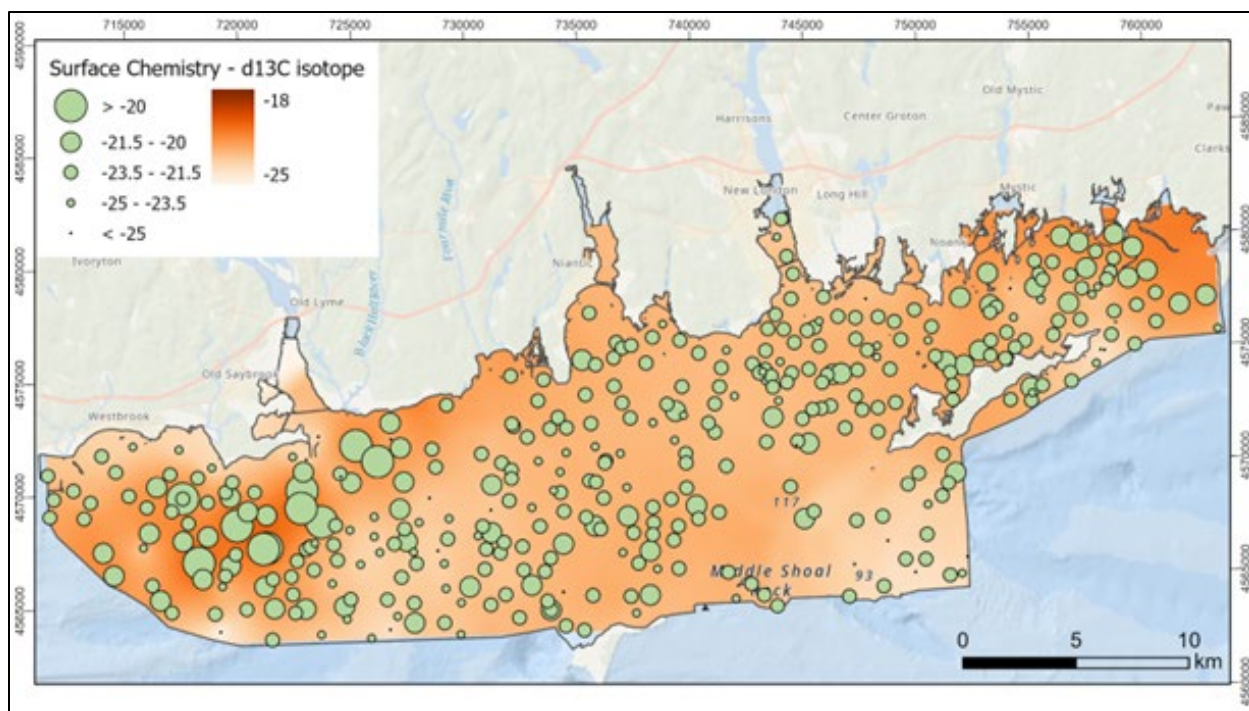
Figure 3.4-17. Map of organic carbon isotope δ¹³C distribution in surface sediments based on surface samples (green circles)
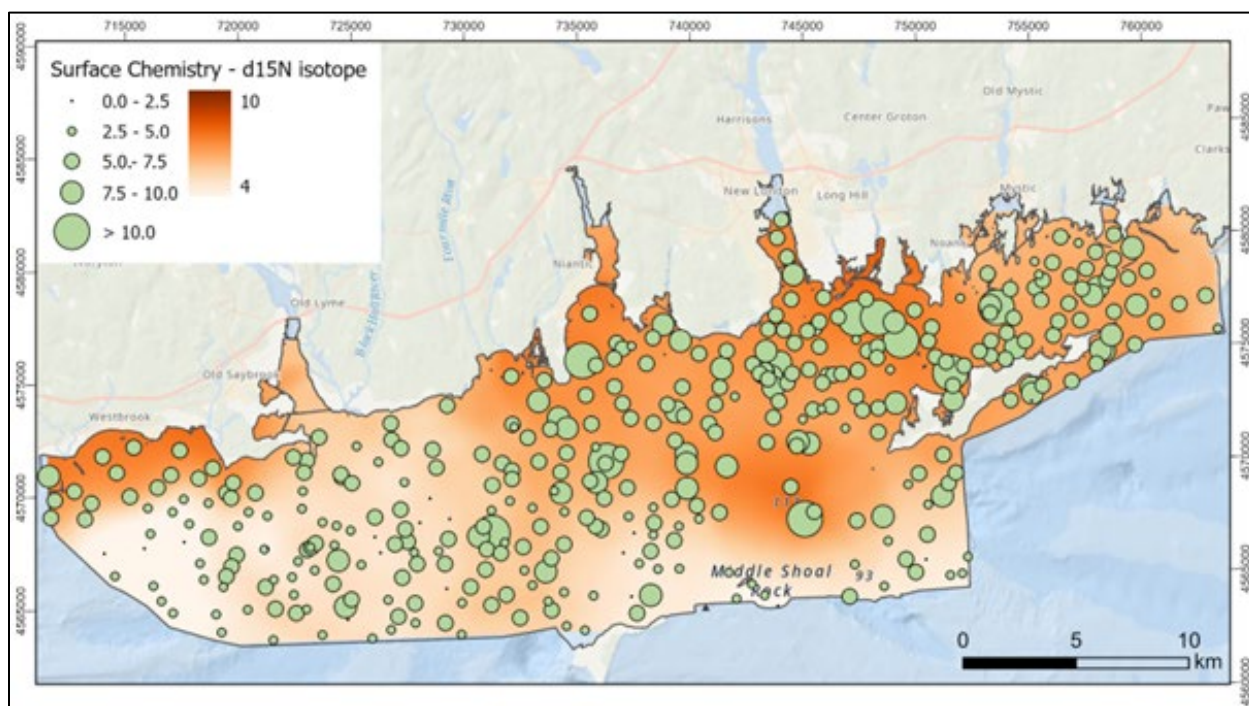
Figure 3.4-18. Map of nitrogen isotope (δ15N‰) distribution in surface sediments based on surface samples (green circles)

A comparison of the C-N isotopic signatures measured in Phase II surface sediment samples along with different sources of organic material and/or the impact of natural processes is shown in Figure 3.4-19. A majority of the data are consistent with being an admixture of organic material derived from terrigenous plants (C3 and C4) and marine algae. However, sediments with δ¹⁵N

values exceeding the typical range of Marine Algae (i.e., $\delta^{15}N$ values greater than ~7‰) require the addition of organic matter that is enriched in $\delta^{15}N$ (e.g., effluent from wastewater treatment plants (WWTPs) and septic systems, and manure) or indicate the occurrence of denitrification, a natural process that can occur under conditions of hypoxic or anoxic conditions (Figure 3.4-20; Joye and Anderson, 2008).
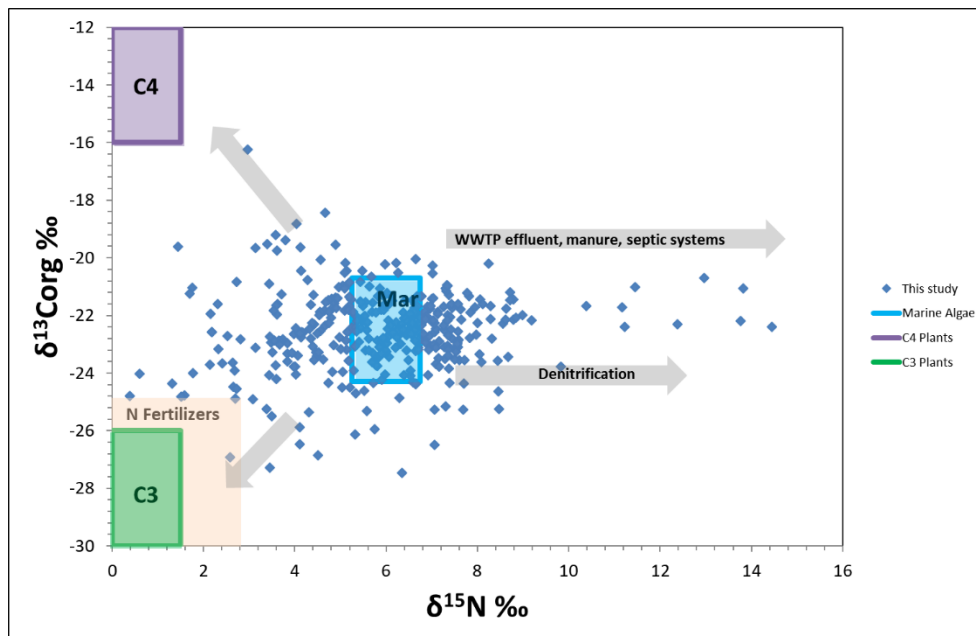
Figure 3.4-19. C-N isotope relations in Phase II surface sediment samples with different sources of organic material and/or the impact of natural processes. While a majority of the data are consistent as an admixture of organic material derived from terrigenous plants (C3 and C4) and marine algae, there is a clear enrichment in ^{15}N in a portion of the data. This is most likely indicative of nitrogen pollution originating from WWTPs and the natural process of denitrification (Varekamp et al., 2010).
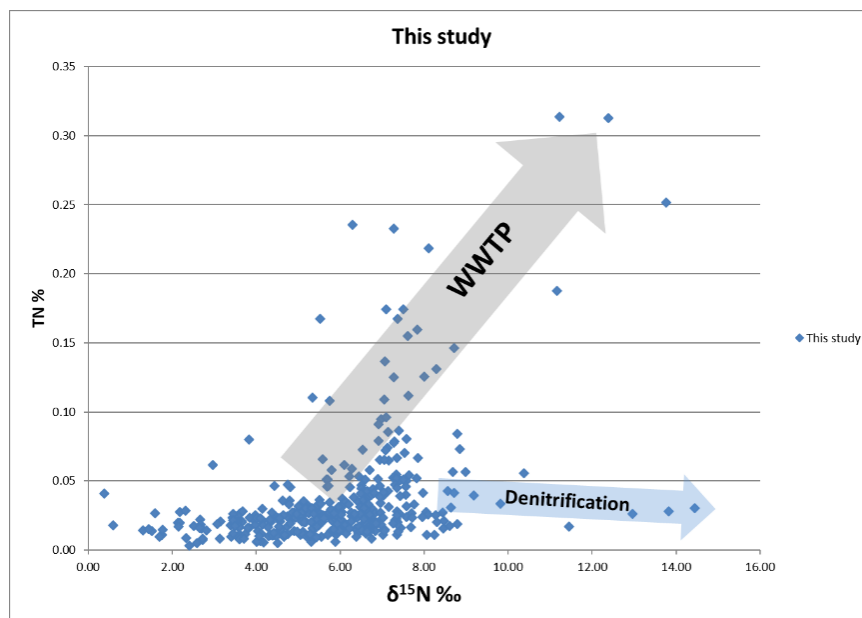
Figure 3.4-20. Nitrogen isotopic composition and total nitrogen concentration in our surface sediment samples. Two distinct trends are visible with respect to increases in $\delta^{15}N$. A majority of the samples that exhibit ^{15}N enrichment also contain higher levels of nitrogen (large gray arrow), suggesting input from WWTPs, while a minority of the samples that exhibit $\delta^{15}N$ enrichment show no apparent increase in nitrogen concentration (small blue arrow), suggesting that denitrification may also be occurring.

If one examines the relationship between the nitrogen isotopic composition and nitrogen concentration in our sediment samples, two distinct trends are visible with respect to increases in $\delta^{15}N$ (Figure 3.4-19). A majority of the samples that exhibit $\delta^{15}N$ enrichment also contain higher levels of nitrogen, suggesting input from WWTPs, while a minority of the samples that exhibit $\delta^{15}N$ enrichment show no apparent increase in nitrogen concentration, suggesting that denitrification may also be occurring. A comparison of the distribution maps for TN and $\delta^{15}N$ (Figure 3.4-16 & Figure 3.4-18) indicates that samples where TN and $\delta^{15}N$ both increases are located primarily at the mouth of the Thames River, while a pattern for samples with enriched $\delta^{15}N$ only is not readily discernable. Although we observe slightly larger $\delta^{15}N$ enrichments, our results are entirely consistent with stable isotope data available for LIS sediments (Altabet & Varekamp, 2004; Varekamp et al., 2006; Altabet & Varekamp, 2007; Varekamp et al., 2010; Varekamp et al., 2014).

3.4.6.3 Analysis of surface element composition (XRF)

Sample measurements

Dried homogenized sediments, SRMs, and blanks consisting of clean SiO_2 powder were analyzed for chemical composition using an Innov-X Alpha series 4000 XRF (Innov-X Systems, Woburn, MA). Approximately 3 g of dried sediments and SRMs selected for dry XRF analysis were packed into sample cups equipped with Mylar polyester supports (Chemplex part Nos. 1330 and 257, respectively). Dry materials were analyzed with the FP-XRF positioned in a sampling test stand supplied by the manufacturer. Analyses and data processing were performed using published protocols which are covered in detail elsewhere (Kenna et al., 2011).

Surface element composition (XRF) results

The XRF analytical protocol included the following elements: P, S, Cl, K, Ca, Ti, V, Cr, Mn, Fe, Co, Ni, Cu, Zn As, Se, Br, Rb, Sr, Zr, Mo, Ag, Cd, Sn, Sb, I, Ba, Hg, Pb, Bi, Th, and U. However, only Cl, K, Ca, Ti, Cr, Mn, Fe, Co, Cu, Zn, As, Br, Rb, Sr, Zr and Pb were consistently present at levels above background detection in surficial sediments collected in the LIS Phase II area. The results are summarized in Table 3-1.

Table 3-1. Summary of XRF results

Element	Min-Max (ppm)	Median (ppm)	MAD (ppm)*
Cl	0 - 37646	14741	4183
K	8550 - 35107	13531	1766
Ca	5275 - 331038	22050	10555
Ti	409 - 18176	2360	933
Cr	B.D. - 290	22	11
Mn	97 - 4849	529	188
Fe	4203 - 82502	15974	4657
Co	B.D. - 31	4	2
Cu	B.D. - 55	7	4
Zn	7 - 289	38	11
As	1 - 12	4	1
Br	B.D. - 227	19	18
Rb	37 - 187	59	10
Sr	121 - 755	195	26
Zr	51 - 1129	154	65
Pb	9 - 63	20	3
MD	2.01 - 5.57	2.73	0.04
*Median Average Deviation			

The pair-wise Pearson linear correlation coefficients were computed for selected elements based on their respective surface distributions for the entire Phase II area, which are presented in Table 3-2 along with the associated p−values.

Table 3-2. Pearson correlation coefficients and associated p−values for element pairs measured in surficial sediments

Constituent	Cl	K	Ca	Ti	Cr	Mn	Fe	Co	Cu	Zn	As	Br	Rb	Sr	Zr	Pb	MD
Cl	1	0.01	0.00	0.00	0.00	0.14	0.01	0.23	0.23	0.00	0.00	0.00	0.09	0.00	0.00	0.37	0.05
K	0.12	1	0.05	0.33	0.00	0.05	0.00	0.00	0.00	0.00	0.63	0.00	0.00	0.00	0.09	0.00	0.00
Ca	0.21	0.10	1	0.01	0.22	0.44	0.21	0.07	0.01	0.28	0.84	0.98	0.15	0.00	0.00	0.71	0.38
Ti	0.15	0.05	-0.14	1	0.00	0.00	0.00	0.00	0.00	0.00	0.00	0.00	0.04	0.01	0.00	0.00	0.15
Cr	0.14	0.23	-0.06	0.64	1	0.00	0.00	0.00	0.00	0.00	0.00	0.00	0.38	0.07	0.00	0.34	0.90
Mn	0.07	-0.10	0.04	0.66	0.58	1	0.00	0.00	0.00	0.00	0.00	0.05	0.00	0.00	0.00	0.00	0.19
Fe	0.13	0.20	-0.06	0.78	0.77	0.81	1	0.00	0.00	0.00	0.00	0.00	0.21	0.00	0.00	0.04	0.05
Co	0.06	0.19	-0.09	0.68	0.68	0.65	0.82	1	0.00	0.00	0.00	0.00	0.53	0.00	0.00	0.02	0.00
Cu	-0.06	0.23	-0.13	0.35	0.42	0.23	0.47	0.50	1	0.00	0.00	0.00	0.00	0.04	0.00	0.00	0.00
Zn	0.25	0.19	-0.05	0.47	0.47	0.29	0.58	0.48	0.53	1	0.00	0.00	0.19	0.61	0.00	0.00	0.63
As	0.20	0.02	-0.01	0.24	0.31	0.25	0.34	0.52	0.37	0.35	1	0.00	0.67	0.35	0.00	0.00	0.00
Br	0.42	0.29	0.00	0.14	0.18	-0.10	0.14	0.20	0.27	0.38	0.32	1	0.00	0.00	0.00	0.00	0.75
Rb	0.08	0.83	-0.07	-0.10	0.04	-0.35	-0.06	0.03	0.23	0.07	0.02	0.30	1	0.00	0.80	0.00	0.10
Sr	0.23	0.30	0.82	-0.14	-0.09	-0.18	-0.16	-0.15	-0.10	-0.03	-0.05	0.15	0.22	1	0.04	0.17	0.04
Zr	0.15	0.09	-0.19	0.78	0.52	0.42	0.56	0.56	0.32	0.38	0.19	0.24	0.01	-0.10	1	0.04	0.26
Pb	-0.04	0.24	-0.02	-0.15	0.05	-0.22	-0.10	0.12	0.35	0.23	0.38	0.23	0.32	0.07	-0.10	1	0.00
MD	-0.10	-0.24	-0.04	-0.07	-0.01	-0.07	-0.10	0.25	0.14	-0.02	0.65	0.02	-0.08	-0.10	-0.06	0.49	1

Pearson correlation coefficients appear in the unshaded cells in the bottom half of the table and the corresponding p−values appear in shaded cells located in the top half of the table. Strong correlations (r >0.75) are identified by bold green text and moderate correlations (0.5< r <0.75) are identified by bold blue text. The corresponding p−values are identified by bold purple text.

An example of how to read the table is given for the K−Rb pair−wise correlation. Starting in the second column (K) and following the blue arrow down to the seventh row (Rb) of the table, the moderately strong correlation for K−Rb of 0.8304 is identified by the red box. Following the purple arrow along the top of the table, the p−value for the K−Rb correlation is found by starting in the second row (K) of the table and proceeding right to the thirteenth column (Rb). The value of 0.00 identified by the yellow box indicates that the correlation is indeed significant (i.e., the probability that the correlation between K and Rb is due to random chance is extremely unlikely.

We observe strong correlations (r >0.75) with significant p−values for the following element pairs: K-Rb, Ca-Sr, Ti-Zr, Fe-Ti, Fe-Cr, Fe-Mn, and Fe-Co. Moderate correlations (0.5< r <0.75) are observed between the following element pairs: Ti-Cr, Ti-Mn, Ti-Co, Cr-Mn, Cr-Co, Cr-Zr, Mn-Co, Fe-Zn, Fe-Zr, Co-As, Co-Zr, Cu-Zn, and As-matrix density (MD). Although potential pollution indicators Zn and Cu exhibit a moderate correlation, Pb does not, correlate strongly with either of these or any other elements. This may be due to a high percentage of the surface sediments having a pre-industrial deposition age and/or significant dilution by sand and larger particles, which typically do not act as transport vectors for industrial pollutants such as Cu, Zn, and Pb. While we do observe numerous weak correlations (r<0.5) with significant p−values, these relationships are difficult to interpret at the current time. It is also likely, that additional significant

relationships would be observed if correlations were examined between Phase II sub-areas, rather than over the entire area. Surface distribution maps of elements with strong and moderate correlations are shown in Figure 3.4-21 to Figure 3.4-34. In nearly all cases, the statistical results are confirmed by visual inspection:

K and Rb − (Figure 3.4-21 & Figure 3.4-22, respectively): these elements show similar distributions with higher concentrations observed in the eastern portions of our study area.

Ca and Sr − although less clear, both Ca and Sr (Figure 3.4-23 & Figure 3.4-24, respectively) show elevated concentrations along the southeastern portion of our study site.

Fe, Mn, Ti, Cr, Co, As, and Zr − the surface distributions for Fe, Mn, Zr, and Ti are shown in Figure 3.4-25, Figure 3.4-26, and Figure 3.4-28. The surface distributions for Fe and Mn are very similar to one another, both showing high concentrations along the southern boundary of our study site. The distributions of Zr and Ti are similar in this respect, but unlike Fe and Mn, they also show increased concentrations along the north central to northwest boundary of our study site.

Zn, Cu, and Pb − the surface distributions of Zn, Cu, and Pb are shown in Figure 3.4-32, Figure 3.4-33, and Figure 3.4-34. Although we do not observe strong correlations for these elements at present, they show clear but different distribution patterns showing increased concentrations along the Connecticut coastline. Likely sources include fluvial material originating from rivers along the CT coast and industrial activities. Areas showing increased concentrations largely track areas with the highest clay and silt concentrations, which is consistent with increased surface area and metal sorption sites associated with fine sediment fractions. The differences between Pb and Zn distributions may be due to different sources/applications of the metals.
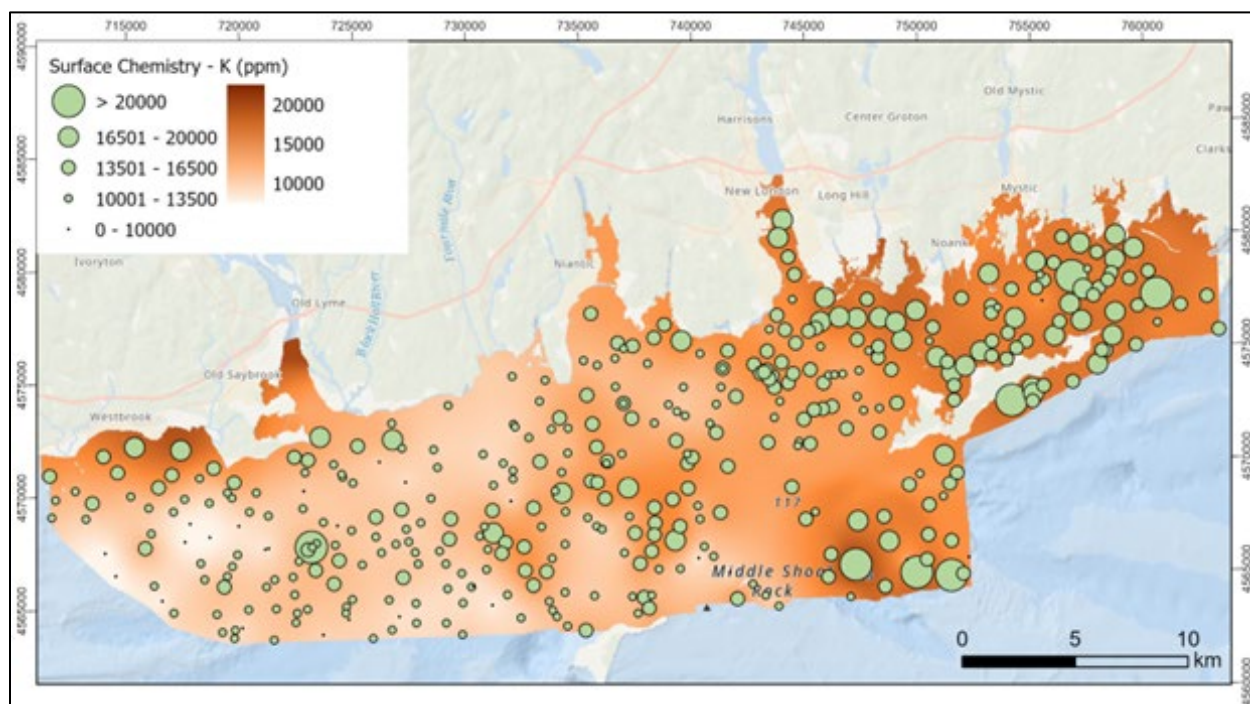
Figure 3.4-21. Map of potassium (K) distribution in surface sediments with the point values shown as graduated circles
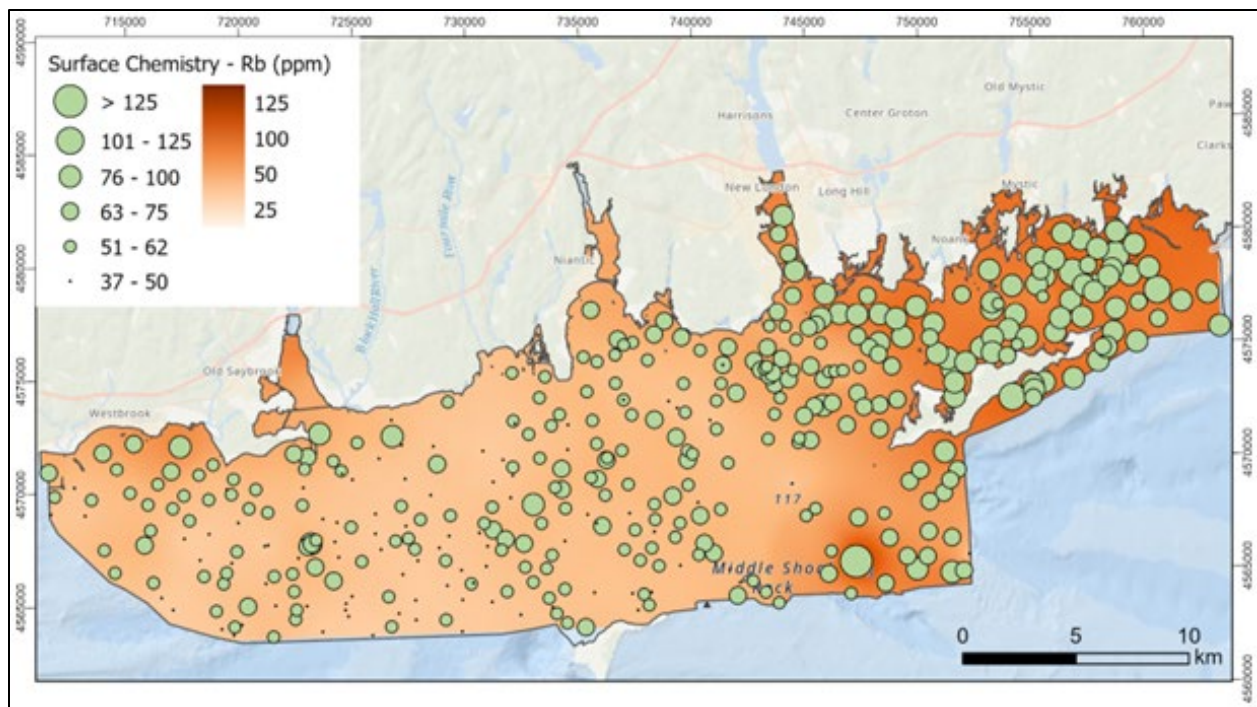
Figure 3.4-22. Map of rubidium (Rb) distribution in surface sediments with the point values shown as graduated circles
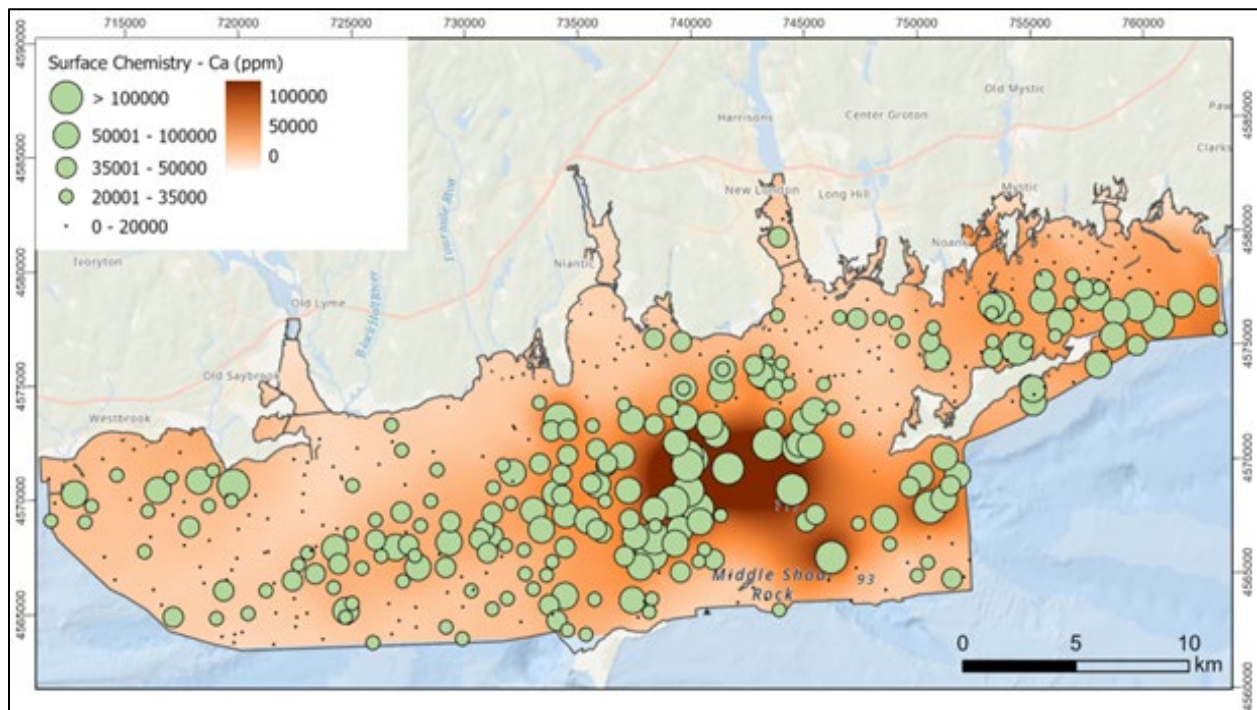
Figure 3.4-23. Map of calcium (Ca) distribution in surface sediments with the point values shown as graduated circles
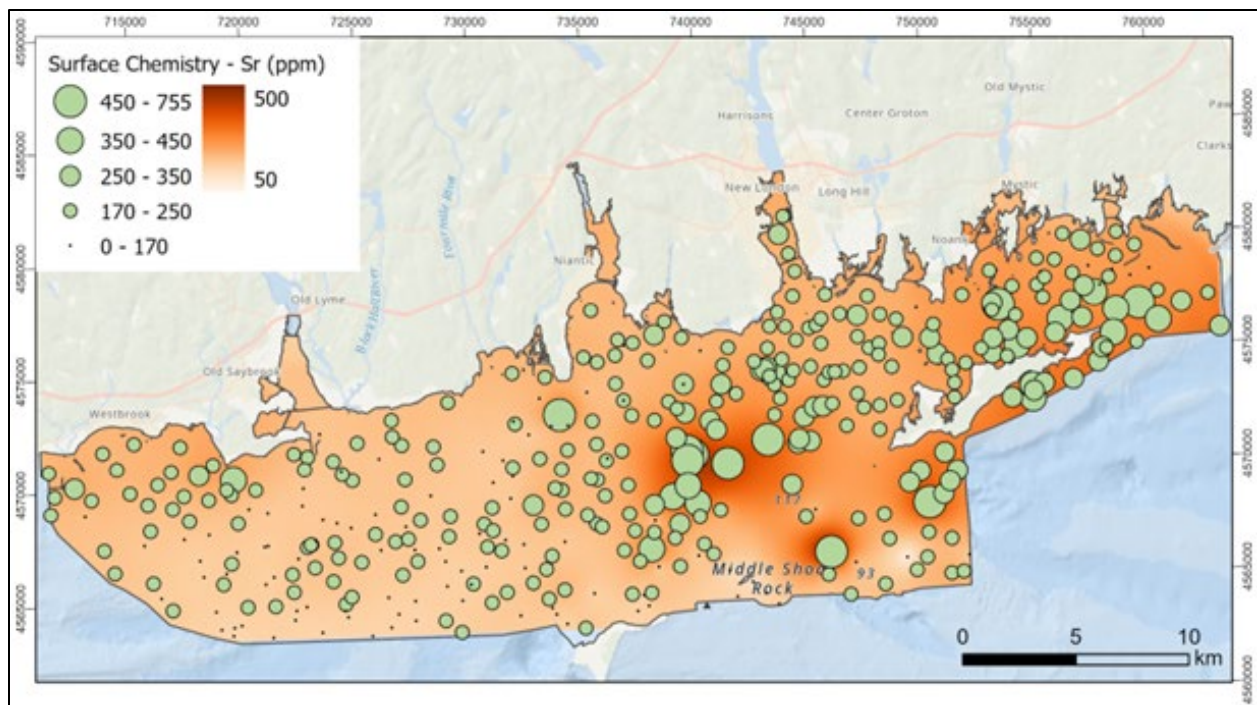
Figure 3.4-24. Map of strontium (Sr) distribution in surface sediments with the point values shown as graduated circles
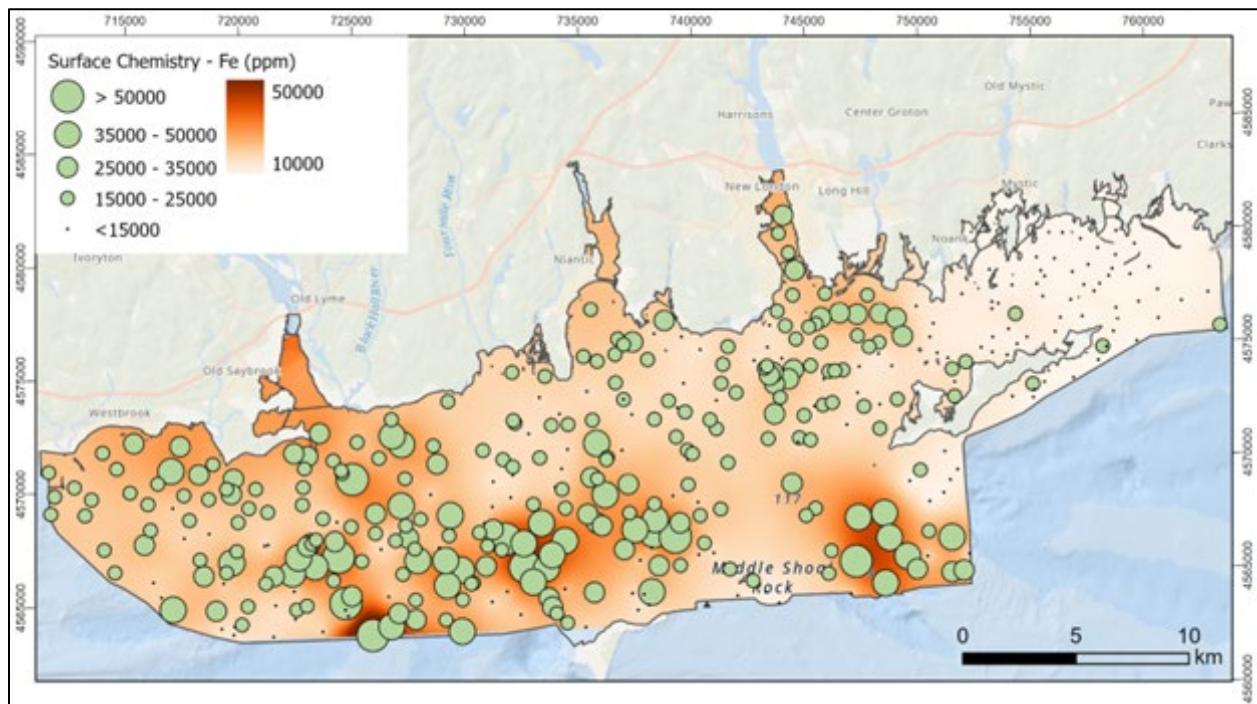
Figure 3.4-25. Map of iron (Fe) distribution in surface sediments with the point values shown as graduated circles
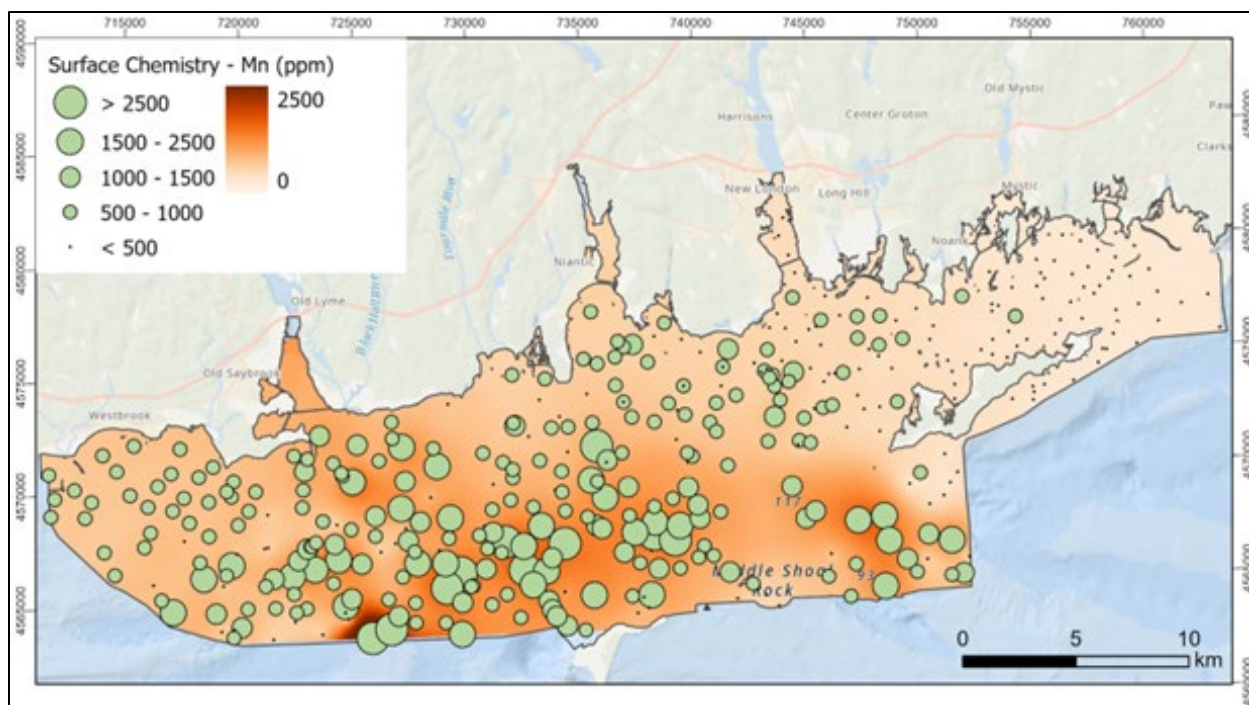
Figure 3.4-26. Map of manganese (Mn) distribution in surface sediments with the point values shown as graduated circles
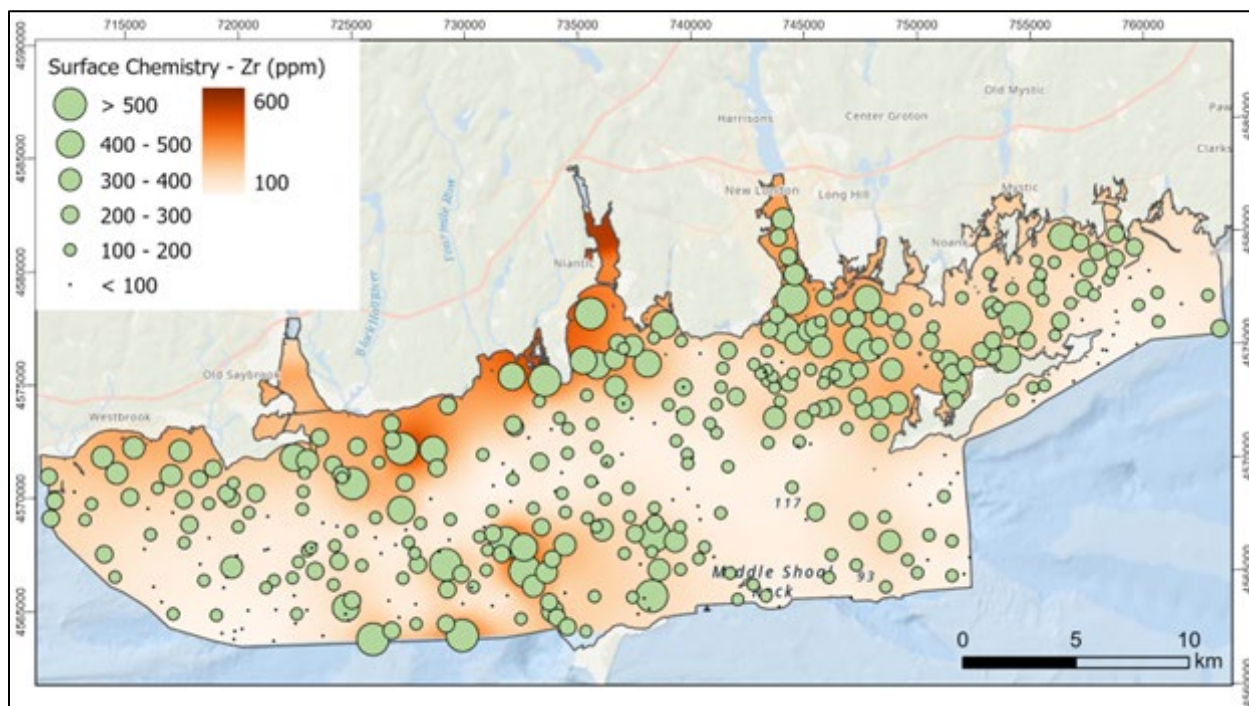
Figure 3.4-27. Map of zircon (Zr) distribution in surface sediments with the point values shown as graduated circles
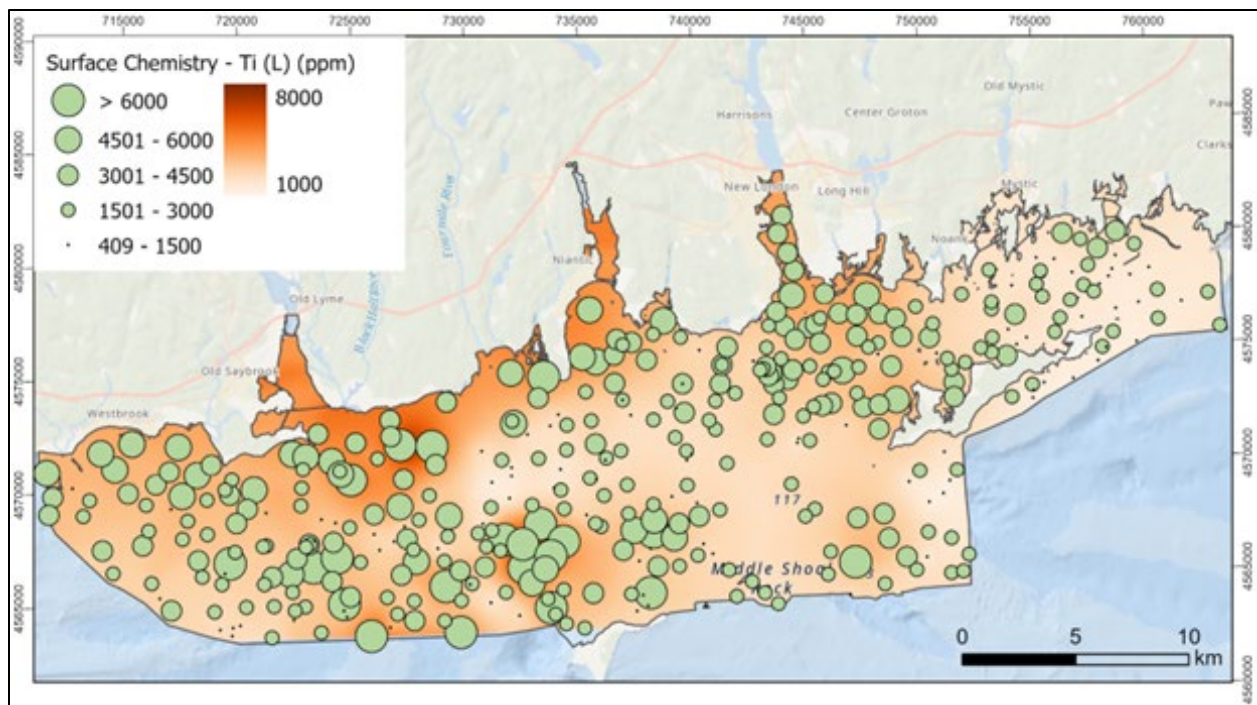
Figure 3.4-28. Map of titanium (Ti) distribution in surface sediments with the point values shown as graduated circles
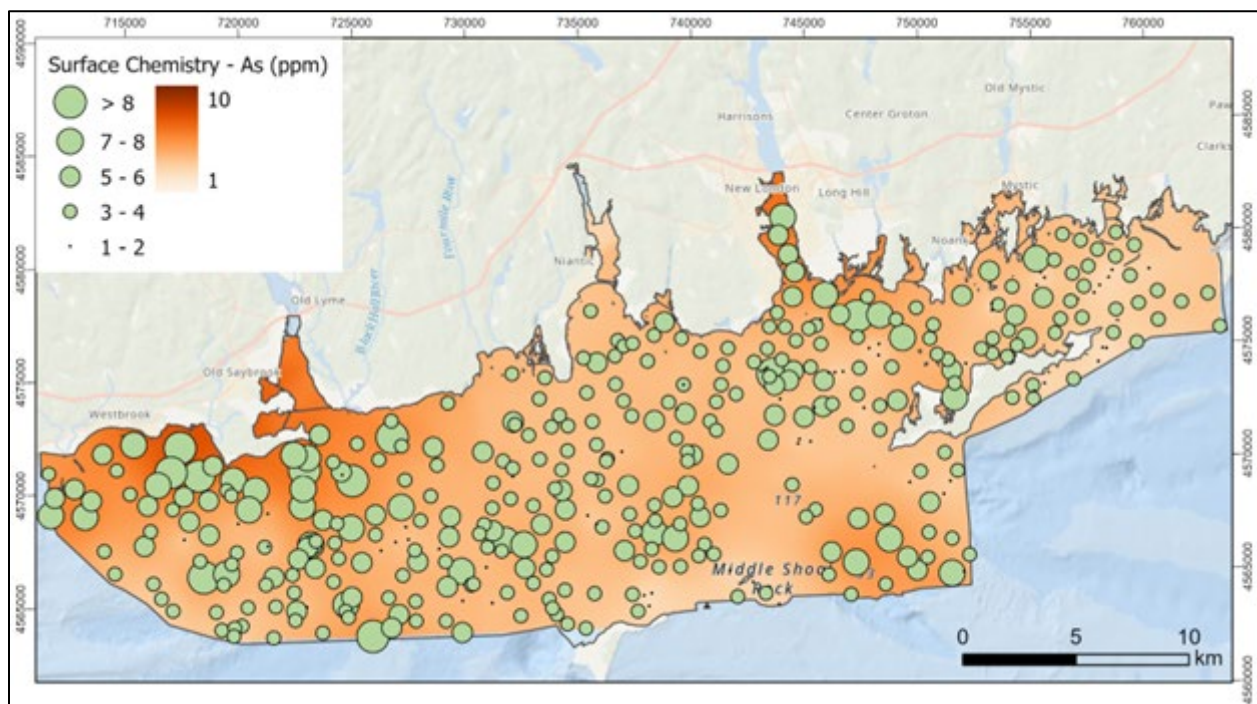
Figure 3.4-29. Map of arsenic (As) distribution in surface sediments with the point values shown as graduated circles
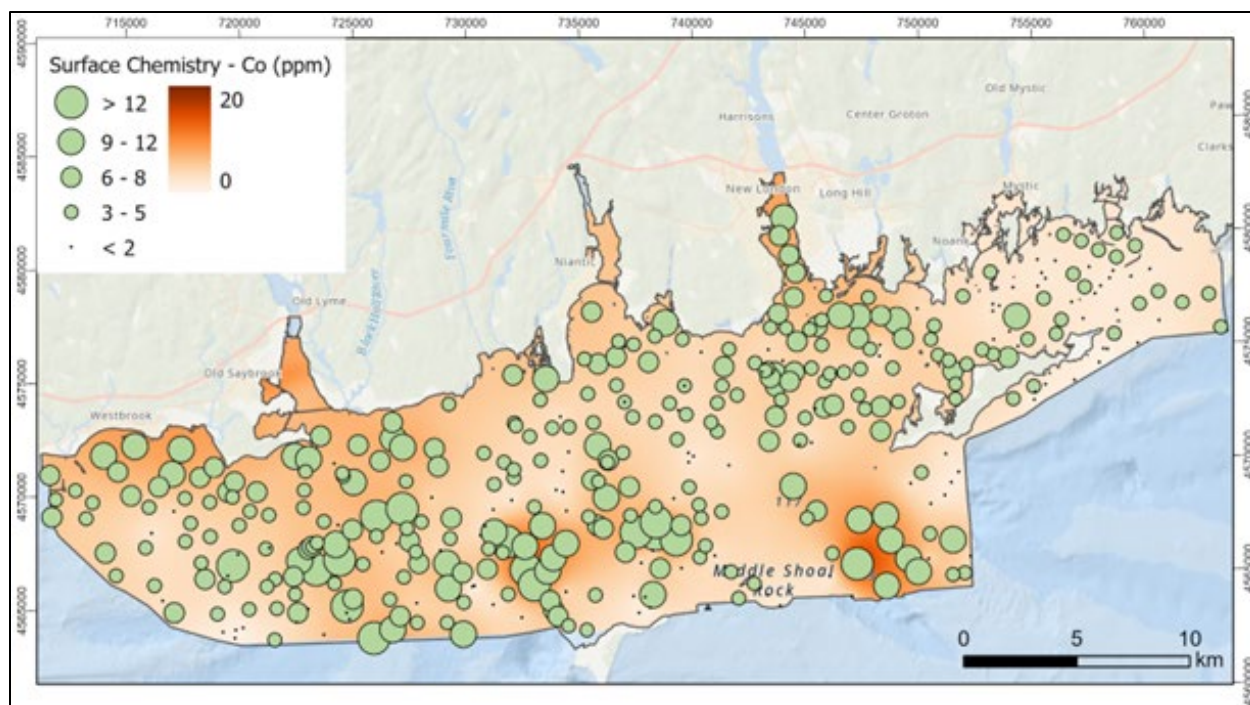
Figure 3.4-30. Map of cobalt (Co) distribution in surface sediments with the point values shown as graduated circles
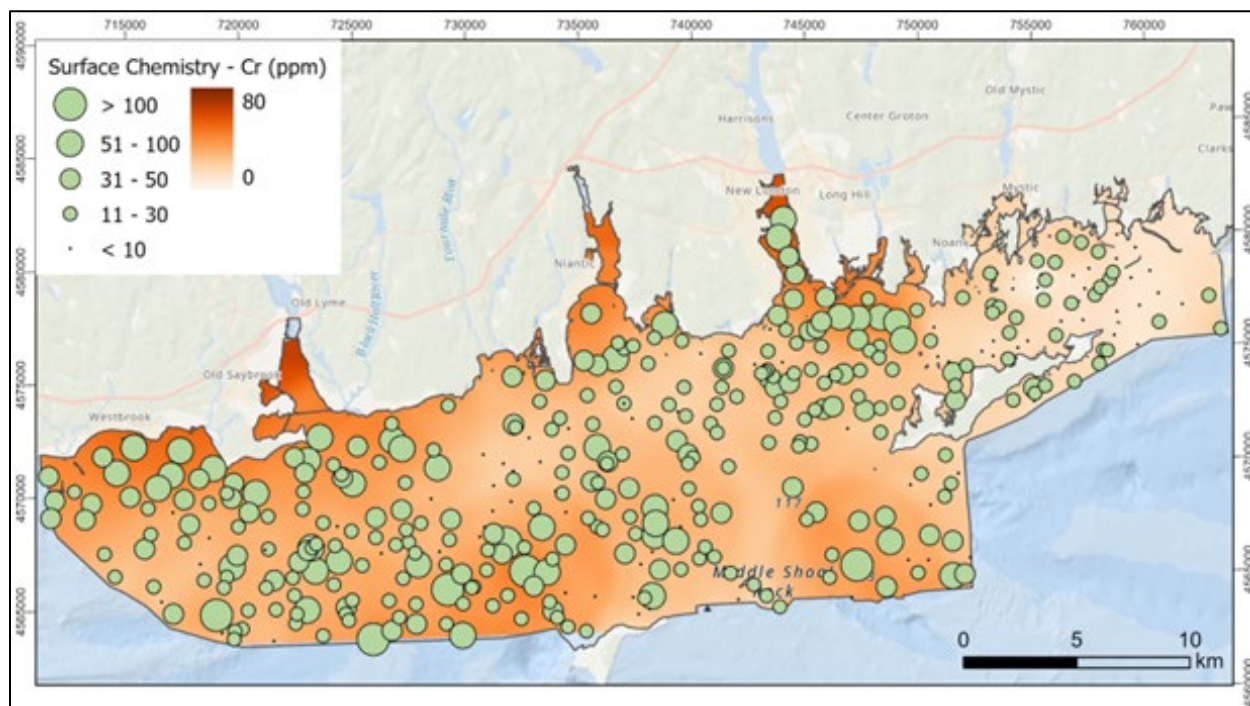
Figure 3.4-31. Map of chromium (Cr) distribution in surface sediments with the point values shown as graduated circles
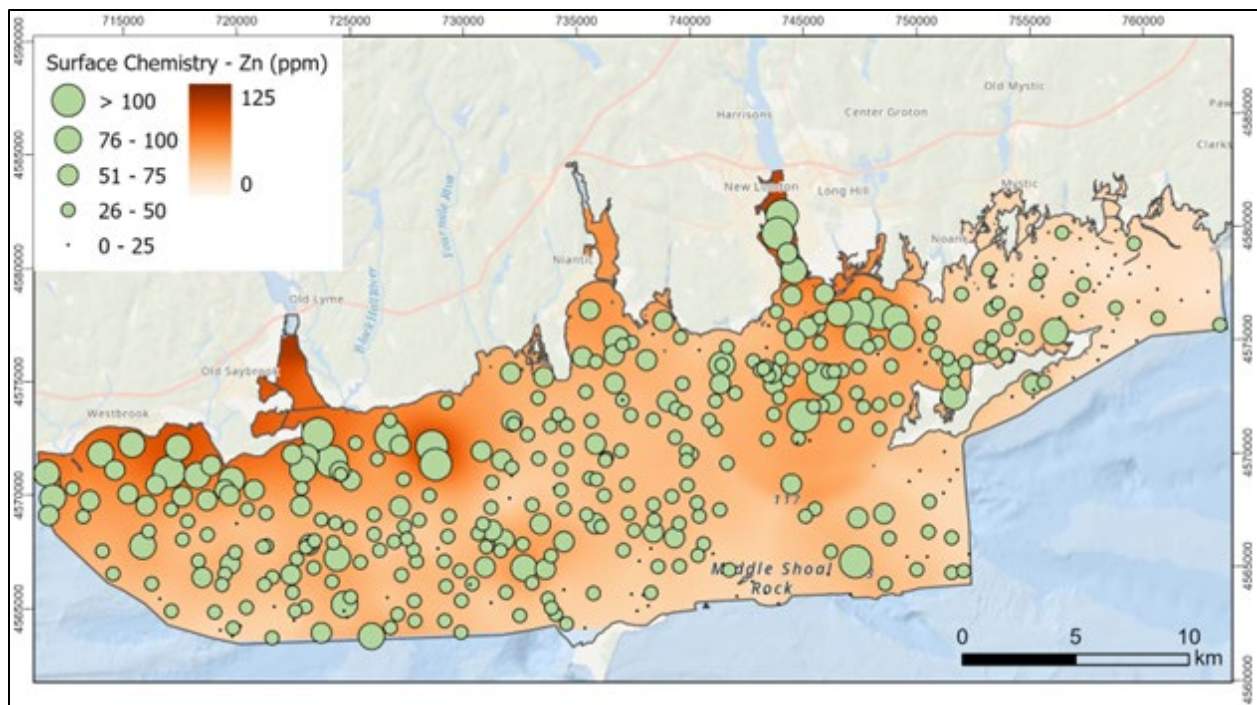
Figure 3.4-32. Map of zinc (Zn) distribution in surface sediments with the point values shown as graduated circles
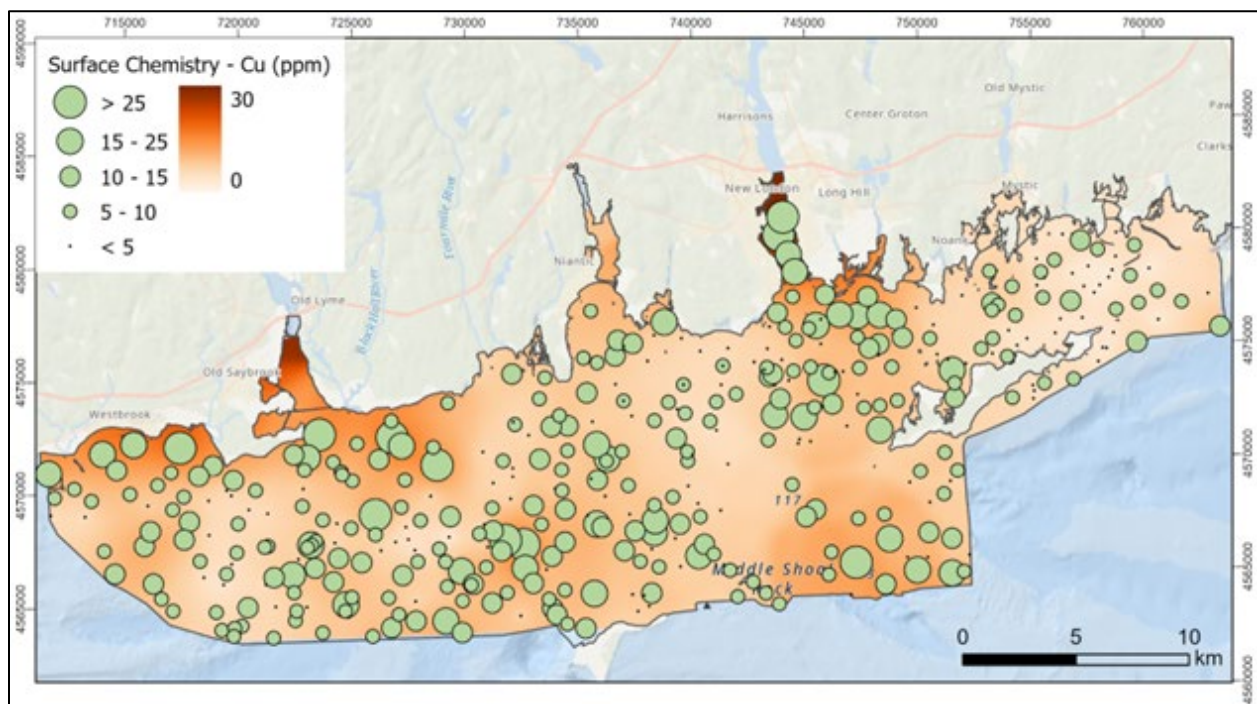
Figure 3.4-33. Map of copper (Cu) distribution in surface sediments with the point values shown as graduated circles
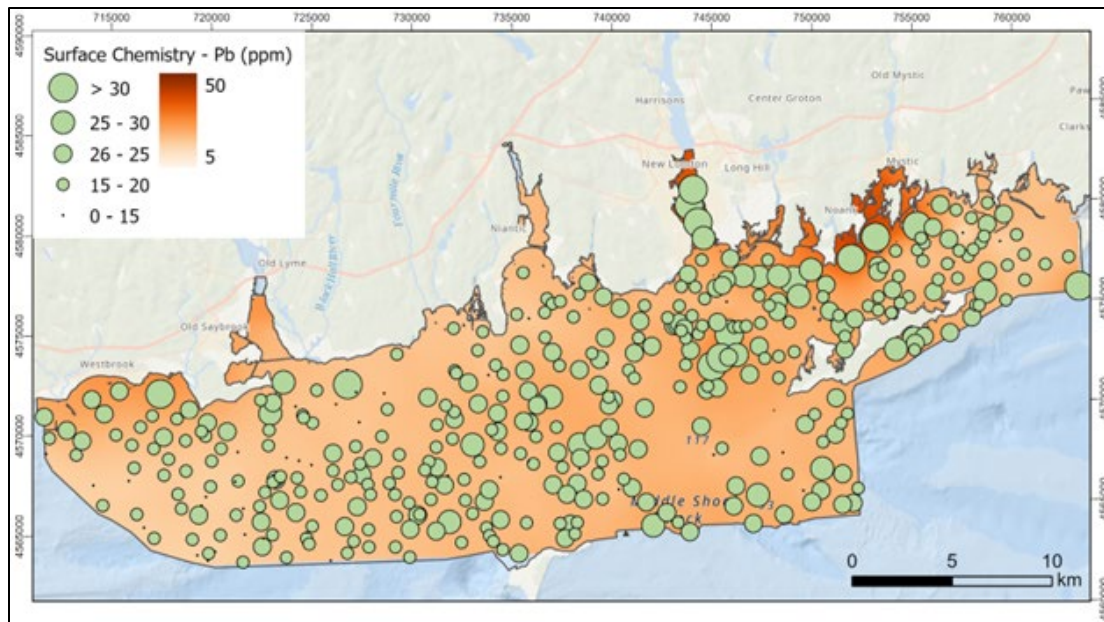
Figure 3.4-34. Map of lead (Pb) distribution in surface sediments with the point values shown as graduated circles

3.4.6.4 Dry matrix density surface distribution

Although it is required as part of the grain size analysis protocol, matrix density of the dry bulk sediment is indicative of mineral composition. Mapping the surface distribution provides additional information with regard to the sediment surface environment. Figure 3.4-35 shows the distribution of matrix density within the study site. We observe fairly uniform values between 2.5 and 3 g/cm^3 along the northern portions, while higher values (>3 g/cm^3) are observed in the southern portions of the study site. This trend is likely due to differences in sediment supply sources and/or deposition age (i.e., the influence of active deposition versus that of erosion and exposure of older material). This parameter may be useful for identification and/or evaluation of different sediment sources in LIS.
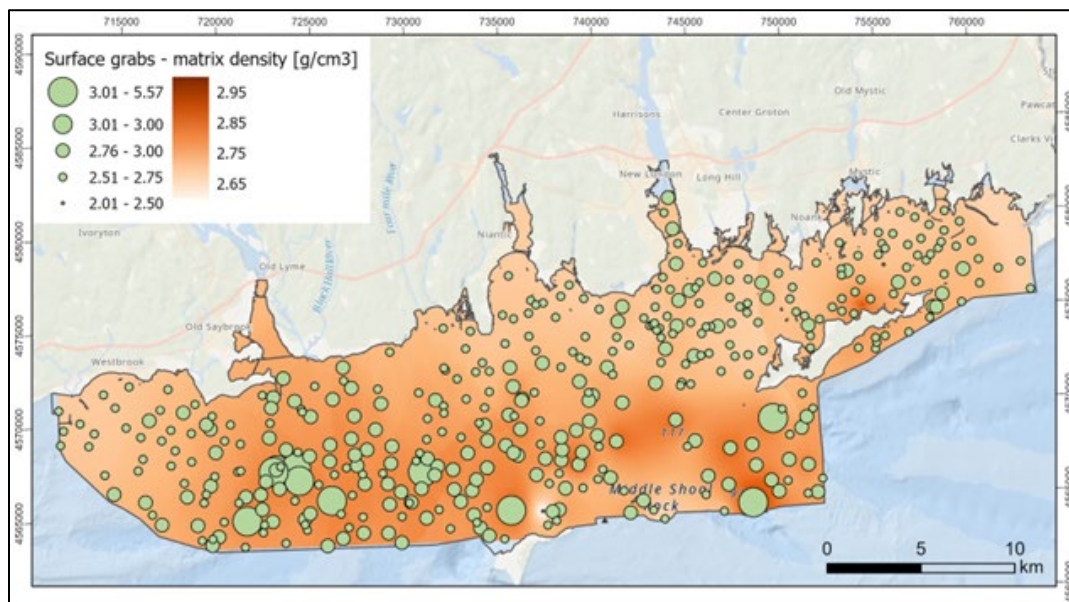
Figure 3.4-35. Map of dry matrix density (g/cm³) of surface sediments based on grab samples (green circles)

3.5   Summary/Conclusions

Sediment texture and chemical information from surface grabs provide important information for understanding habitat and the general nature of sediments in the study area. Sediment texture and grain size also provide a comprehensive dataset to assist with interpretations of several other components of the Phase II mapping initiative. The grain size data are critical for verifying and interpreting the backscatter data. They are also a critical component for infaunal and epifaunal ecological characterization and the determination of sedimentary environments. Moreover, they provide additional ground-truth data to assist with the physical oceanography component of the initiative.

Correlation of backscatter amplitude and grain size is not always unique and can be influenced by other factors. Comprehensive validation using grab samples and discreet grain size measurements should therefore be included in any detailed habitat mapping effort.

The dominant grain size is sand or gravelly sediment with high sand content. Silt and clay size sediment are found in pockets closer the northern shoreline. In several locations, especially in the area of the Race, the bottom is characterized by larger boulders with sand or gravelly sediment in between.

Relative to sub-areas located farther from shore, nitrogen and organic carbon content is higher near the river mouths and are likely indicative of anthropogenic input. In this respect, the carbon and nitrogen stable isotopic compositions are useful for tracking these sources, especially nitrogen pollution.

The chemical composition of sediment samples shows differences between the major rivers and is another indicator of different sediment sources. It usually works best with fine grained (silt, clay) sediments. Some elements are good indicators of fine fraction, while other are useful for identifying sediments influenced by anthropogenic activities.

Understanding distribution of different sediment types is important for management decisions on projects using the benthic resources of Long Island Sound, including cables and pipelines. For example, the grain size results have already been used as part of the data sets assisting the Equinor Corporation with its power cable routing in support of the Beacon Wind offshore windfarm currently under development.

3.6   References

Ackerman, S. D., Huntley, E. C., Blackwood, D. S., Babb, I. G., Zajac, R. N., Conroy, C. W., . . . Walton, O. L. (2020). *Sea-floor sediment and imagery data collected in Long Island Sound, Connecticut and New York, 2017 and 2018*. (U.S. Geological Survey data release) Retrieved from USGS ScienceBase: https://doi.org/10.5066/P9GK29NM

Altabet, M. A., & Varekamp, J. C. (2004, May). Nitrogen isotopic ratio records the eutrophication history of Long Island Sound. *American Geophysical Union*, *Spring Meeting 2004*, pp. GC41B-02.

Altabet, M. A., & Varekamp, J. C. (2007). The nitrogen isotope biogeochemistry of Long Island Sound; insights into mechanism(s) of 15N enrichment in eutrophication-impacted estuaries. *ASLO 2007 Aquatic Sciences Meeting.* Sante Fe, NM.

Bastami, K. D., Neyestani, M. R., Shemirani, F., Soltani, F., Haghparast, S., & Akbari, A. (2015). Heavy metal pollution assessment in relation to sediment properties in the coastal sediments of the southern Caspian Sea. *Marine Pollution Bulletin, 92*(1-2), 237-243. Retrieved from https://doi.org/10.1016/j.marpolbul.2014.12.035

Cifuentes, L. A., Sharp, J. H., & Fogel, M. L. (1988). Stable carbon and nitrogen isotope biogeochemistry in the Delaware estuary. *Limnology and Oceanography, 33*(5), 1102-1115.

Ferrini, V. L., & Flood, R. D. (2006). The effects of fine-scale surface roughness and grain size on 300 kHz multibeam backscatter intensity in sandy marine sedimentary environments. *Marine Geology, 228*(1-4), 153-172.

Galparsoro, I., Borja, Á., Kostylev, V. E., Rodríguez, J. G., Pascual, M., & Muxika, I. (2013). A process-driven sedimentary habitat modelling approach, explaining seafloor integrity and biodiversity assessment within the European Marine Strategy Framework Directive. *Estuarine, Coastal and Shelf Science, 131*, 194-205.

Hoefs, J. (2004). Isotope Fractionation Mechanisms of Selected Elements. In *Stable Isotope Geochemistry.* Berlin, Heidelberg: Springer. Retrieved from https://doi.org/10.1007/978-3-662-05406-2_2

Karhu, J. (1999). Carbon Isotopes. In C. P. Marshall, & R. W. Fairbridge (Eds.), *Encyclopedia of Geochemistry* (pp. 67-73). Dordrecht: Kluwer Academic Publishers.

Kenna, T. C., Nitsche, F. O., Herron, M. M., Mailloux, B. J., Peteet, D., Sritrairat, S., . . . Baumgarten, J. (2011). Evaluation and calibration of a Field Portable X-Ray Fluorescence spectrometer for quantitative analysis of siliciclastic soils and sediments. *Journal of Analytical Atomic Spectrometry, 26*, 395-405. https://doi.org/10.1039/c0ja00133c

Kenny, A. J., Cato, I., Desprez, M., Fader, G., Schu¨ttenhelm, R. E., & Side, J. (2003). An overview of seabed-mapping technologies in the context of marine habitat classification. *ICES Journal of Marine Science, 60*, 411–418.

Knebel, H. J., & Poppe, L. J. (2000). Sea-Floor Environments within Long Island Sound: A Regional Overview. *Journal of Coastal Research, 16*(3), 533-550.

Krivoruchko, K., & Gribov, A. (2019). Evaluation of empirical Bayesian kriging. *Spatial Statistics, 32*, 341-368.

McHugh, C. M., & Kenna, T. C. (2015). Sediment Grab Collection and Analysis. Section 3.4. *Seafloor Mapping of Long Island Sound – Final Report: Phase I Pilot project*, 65-83. U. S. Environmental Protection Agency; Long Island Sound Study, Stamford, CT: (Unpublished project report).

McMullen, K. Y., Paskevich, V. F., & Poppe, L. J. (2014). GIS data catalog (ver. 3.0, November 2014). *USGS east-coast sediment analysis: Procedures, database, and GIS data*. (L. J. Poppe, K. Y. McMullen, S. J. Williams, & V. F. Paskevich, Eds.) Geological Survey Open-File Report 2005-1001. Retrieved from http://pubs.usgs.gov/of/2005/1001/

Meyers, P. A. (1994). Preservation of elemental and isotopic source identification of sedimentary organic matter. *Chemical Geology, 114*(3), 289-302.

Nitsche, F. O., Bell, R., Carbotte, S. M., Ryan, W. F., & Flood, R. D. (2004). Process-related classification of acoustic data from the Hudson River Estuary. *Marine Geology, 209*, 131-145.

NOAA & UNH. (2021). *CUBE*. Retrieved from Center for Coastal and Ocean Mapping – Joint Hydrographic Center: http://ccom.unh.edu/theme/data-processing/cube

Ostrom, N. E., & Ostrom, P. H. (1999). Nitrogen isotopes. In C. P. Marshall, & R. W. Fairbridge (Eds.), *Encyclopedia of Geochemistry* (pp. 431-434). Dordrecht: Kluwer Academic Publishers.

Peters, K. E., Sweeney, R. E., & Kaplan, I. R. (1978). Peters, K. E., Sweeney, R. E., and Kaplan, I.R. (1978). Correlation of carbon and nitrogen stable isotope ratios in sedimentary organic matter. *Limnology and Oceanography, 23*(4), 598-604.

Poppe, L. J., & Polloni, C. F. (2000). *USGS east-coast sediment analysis; Procedures, database, and georeferenced displays (No. 2000-358).* United States Geological Survey, Coastal and Marine Geology Program, Woods Hole Field Center.

Poppe, L. J., Eliason, A. H., & Hastings, M. E. (2003). A Visual Basic program to classify sediments based on gravel-sand-silt-clay ratios. *Computers & Geosciences, 29*(6), 805-809.

Poppe, L. J., Knebel, H. J., Mlodzinska, Z. J., Hastings, M. E., & Seekins, B. A. (2000). Distribution of surficial sediment in Long Island Sound and adjacent waters: texture and total organic carbon. *Journal of Coastal Research*, 567-574.

Poppe, L. J., Paskevich, V. F., Moser, M. S., DiGiacomo-Cohen, M. L., & Christman, E. B. (2004). *Sidescan sonar imagery and surficial geologic interpretation of the seafloor off Branford, Conneticut.* Open-File Report 2004-1003. U.S. Geological Survey.

Samsudin, S. A., & Hasan, R. C. (2017). Assessment of Multibeam Backscatter Texture Analysis for Seafloor Sediment Classification. *International Archives of the Photogrammetry, Remote Sensing & Spatial Information Sciences, 42*.

Schlacher, T. A., & Connolly, R. M. (2014). Effects of acid treatment on carbon and nitrogen stable isotope ratios in ecological samples: a review and synthesis. *Methods in Ecology and Evolution, 5*(6), 541-550.

Schlee, J. (1973). *Atlantic Continental Shelf and Slope of the United States sediment texture of the northeastern part.* U.S. Geological Survey , Professional Paper (No. 529-L).

Schlee, J., & Webster, J. (1967). A Computer Program for Grain Size Data. *Sedimentology, 8*(1), 45-53.

Shepard, F. P. (1954). Nomenclature based on sand-silt-clay ratios. *Journal of Sedimentary Petrology, 24*, 151-158.

Sweeney, R. E., Kalil, E. K., & Kaplan, I. R. (1980). Characterisation of domestic and industrial sewage in Southern California coastal sediments using nitrogen, carbon, sulphur and uranium tracers. *Marine Environmental Research, 3*(3), 225-243.

Teledyne CARIS. (2021). *HIPS and SIPS*. Retrieved from Teledyne CARIS: https://www.teledynecaris.com/en/products/hips-and-sips/

Thornton, S. F., & McManus, J. (1994). Application of Organic Carbon and Nitrogen Stable Isotope and C/N Ratios as Source Indicators of Organic Matter Provenance in Estuarine Systems: Evidence from the Tay Estuary, Scotland. *Estuarine, Coastal and Shelf Science, 38*(3), 219-233.

U.S. Geological Survey East-Coast Sediment Texture Database. (2014, December 30). Retrieved from Woods Hole Coastal and Marine Science Center: http://woodshole.er.usgs.gov/project-pages/sediment/

Varekamp, J. C., McElory, A. E., Mullaney, J. R., & Breslin, V. T. (2014). Metals, Organic Compounds, and Nutrients in Long Island Sound: Sources, Magnitudes, Trends, and Impacts. In J. S. Latimer, M. A. Tedesco, R. L. Swanson, C. Yarish, P. E. Stacey, & C. Garza (Eds.), *Long Island Sound* (pp. 203-283). New York, NY: Springer.

Varekamp, J. C., Thomas, E., Buchholtz ten Brink, M., & Mecray, E. (2006). The Environmental Impact of Early Western Colonization on Long Island Sound: Beavers Meet Climate Change. *Eighth Biennual Long Island Sound Research Conference Proceedings*, (p. 84). New London, CT.

Varekamp, J. C., Thomas, E., Buchholtz ten Brink, M., Altabet, M. A., & Cooper, S. (2010). *Environmental change in Long Island Sound in the recent past: eutrophication and climate change.* Final report Long Island Sound Research Fund grant #CWF 334-R (FRS #525156)., Wesleyan University, Middletown, CT.

4   Sedimentary Environment

Recommended Citations:

Nitsche, F., Kenna, T., McHughs, C. (2023). Objective. Section 4.1, p. 85 in: "Seafloor Mapping of Long Island Sound – Final Report: Phase II Project." (Unpublished project report). U. S. Environmental Protection Agency, Long Island Sound Study, Stamford, CT.

Nitsche, F., Kenna, T., McHughs, C. (2023). Historical Context. Section 4.2, p. 85-86 in: "Seafloor Mapping of Long Island Sound – Final Report: Phase II Project." (Unpublished project report). U. S. Environmental Protection Agency, Long Island Sound Study, Stamford, CT.

Nitsche, F., Kenna, T., McHughs, C. (2023). Subbottom Data Acquisition and Analysis. Section 4.3, p. 86-90 in: "Seafloor Mapping of Long Island Sound – Final Report: Phase II Project." (Unpublished project report). U. S. Environmental Protection Agency, Long Island Sound Study, Stamford, CT.

Nitsche, F., Kenna, T., McHughs, C. (2023). Sediment Cores Collection and Analysis. Section 4.4, p. 90-103 in: "Seafloor Mapping of Long Island Sound – Final Report: Phase II Project." (Unpublished project report). U. S. Environmental Protection Agency, Long Island Sound Study, Stamford, CT.

Nitsche, F., Kenna, T., McHughs, C. (2023). Sediment Environment Characterization. Section 4.5, p. 103-112 in: "Seafloor Mapping of Long Island Sound – Final Report: Phase II Project." (Unpublished project report). U. S. Environmental Protection Agency, Long Island Sound Study, Stamford, CT.

Nitsche, F., Kenna, T., McHughs, C. (2023). Summary and Recommendation. Section 4.5, p. 112-113 in: "Seafloor Mapping of Long Island Sound – Final Report: Phase II Project." (Unpublished project report). U. S. Environmental Protection Agency, Long Island Sound Study, Stamford, CT.

4.1   Objective

While sediment texture describes the grain size composition at the time of sediment collection, the sedimentary environment describes the processes dominating/controlling a certain location such as deposition or erosion over time providing a spatial and temporal understanding of the setting. Characterizing the sedimentary environment is critical for understanding the dynamic character of the seafloor in LIS and for identifying areas that are stable or changing through time. This information is integral for determining the physical processes of the benthic environment that strongly influence the related habitats. These include physical processes such as tidal currents, wind generated waves, storms, and floods and how they have modified the environment. Understanding the physical processes that influence the evolution and stability of the benthic environment can aid in assessing the impacts of projects likely to cause disturbances such as the installation of cables and pipelines, dredging, and other construction activities. Conversely, this information can aid in identifying areas suitable for these types of projects.

4.2   Historical Context

Several previous studies of LIS include evaluation of the sediment environments to provide perspective on the seafloor dynamics (e.g., Knebel and Poppe, 2000; Knebel et al., 1999). The USGS conducted most of these studies, which present an interpretation of sediment environments across LIS (Figure 4.2-1). Like the USGS sediment texture interpretation (Section 3.2), the USGS sediment environment interpretation was based on previously existing sidescan and seismic data as well as bottom samples and photographs. This USGS classification distinguished deposition, erosion, sorting, and transportation environments.
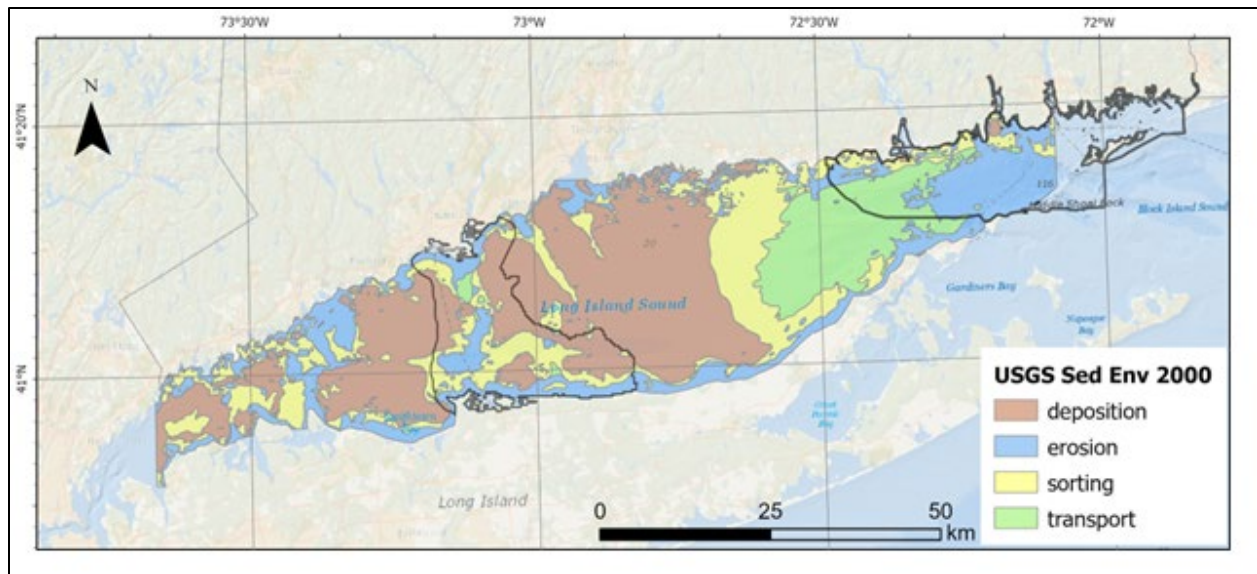
Figure 4.2-1. LIS sediment environment interpretation (Knebel and Poppe, 2000; Knebel et al., 1999)

4.3 Subbottom Data Acquisition and Analysis

4.3.1 Subbottom Data Acquisition

4.3.1.1 Subbottom Principle

Subbottom seismic data provide information on the spatial variation of geological processes, such as deposition and erosion, as well as insights into ongoing processes and the physical evolution of the benthic environment. They are collected as continuous profiles and show the changes of sediments with depth over a distance.

A sound signal (acoustic energy) is sent from a transmitter source Figure 4.3-1). A portion of this signal is reflected at the seafloor, and the remaining signal passes into the seabed. At each subsequent interface where the acoustic parameters are changing, a fraction of the sound energy is reflected back. A towed receiver measures the reflected energy and the time that has passed since the signal was transmitted.
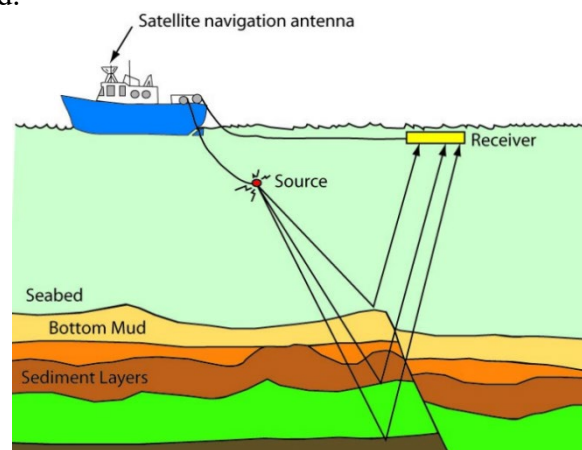
Figure 4.3-1. Subbottom principle

4.3.1.2 Subbottom Profiler Data

The purpose of these subbottom data was to guide subsequent sediment coring to obtain good penetration and recovery of sediments and to place results from the sediment core analysis into a wider spatial and temporal context. Given the dominance of hard bottom types in the Phase II area (e.g., sand, gravel, bedrock), the acoustic penetration and resulting subsurface information was expected to be limited. As a result, we opted not to conduct a comprehensive subbottom survey. Rather, we collected subbottom profiler data only across selected areas where the preliminary backscatter data suggested the presence of softer sediment layers that could be recovered in sediment cores.

The subbottom surveys were conducted using a high-resolution Chirp subbottom profiler system consisting of an EdgeTech 424 tow fish and an EdgeTech P3200 acquisition unit with Discovery software (Figure 4.3-2). The system was operated using an acoustic sweep signal between 4-24 kHz that results in a nominal high vertical resolution of 0.1m. The horizontal resolution depends on the survey speed. The system transmits data at a rate of 4-5 pings/second. At survey speeds of 5-6 knots these transmission rates result in an along track spacing of traces between 0.5 and 1m. Data were recorded in EdgeTech's proprietary JSF format as well as in Standard SEGY format.

Figure 4.3-2. Lamont EdgeTech Chirp 424 subbottom profiler system (left) and EdgeTech Discovery software (right)

The subbottom data are geo-referenced using a differential GPS system mounted on the ship, which provides horizontal accuracy <1m. The offset between the ships DGPS antenna and the actual towed fish location was determined for later correction of the positions.

The actual subbottom survey was performed in two segments in spring 2018 (Figure 4.3-3; Table 4-1). For the first segment we used the R/V *Seawolf* and for the second segment, which included shallower areas, the R/V *Pritchard* was used. In total LDEO collected 69 subbottom lines, which represent ~310 km of subbottom data.
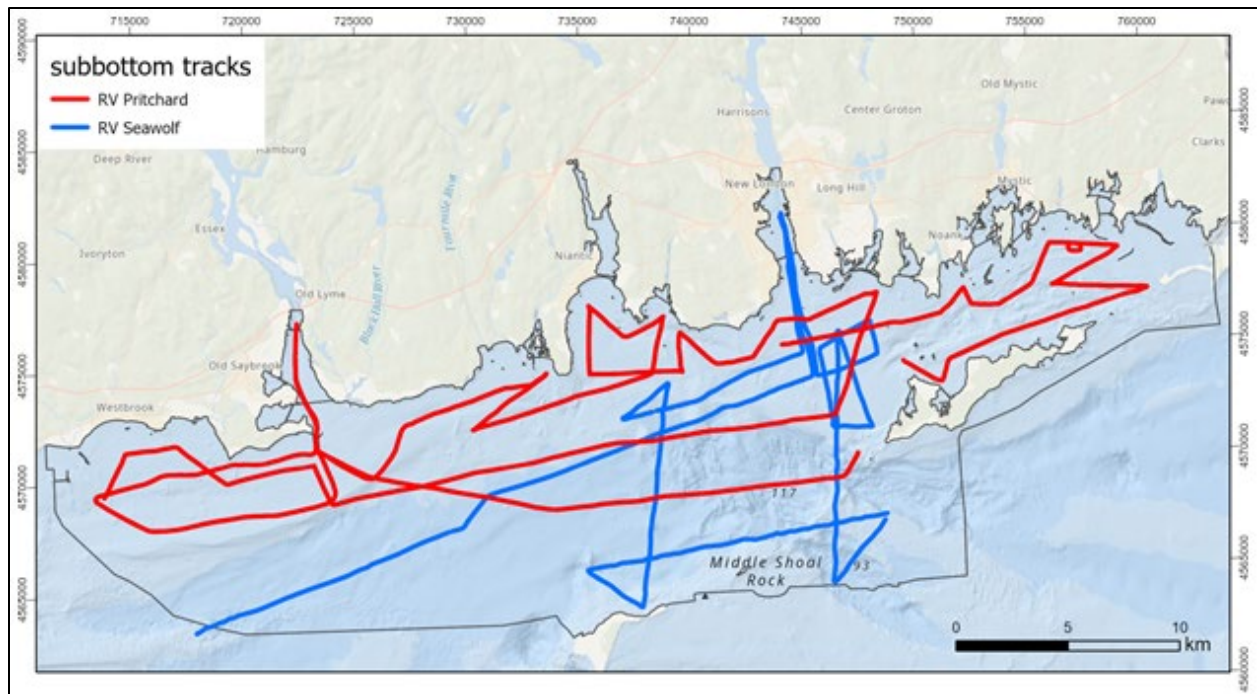
Figure 4.3-3. Map of the new subbottom profiles collected as part of the Phase II project. Red and blue tracks indicate the different surveys with the R/V Pritchard and R/V Seawolf, respectively.

Table 4-1. Subbottom field data collection details

Survey	Survey date	Field days	Vessel	# lines	Length/km
LIS1801	April 2-3, 2018	2	R/V *Seawolf*	25	120
LIS1801B	April 9-11, 2018	3	R/V *Pritchard*	44	190
Total		5		69	310

4.3.2 Subbottom Data Processing and Results

4.3.2.1 Data Processing

Data processing of the subbottom data was performed using a combination of tools including the EdgeTech Discovery software system, the Seismic Unix processing package, Chesapeake SonarWiz, and various in-house scripts. The data were corrected for vertical offset by tides and for horizontal offsets of the tow fish to the GPS antenna (layback correction). For each subbottom file we generated images in JPEG format. For analysis and interpretation of the subbottom data we loaded the processed and corrected SEGY files into the SMT Kingdom Suite software package. The resulting images of all lines together with the SEGY files can be downloaded from the database.

4.3.2.2 Results

The resulting images of all lines together with the SEGY files can be downloaded from the LIS Data Portal. The data show a variety of subbottom environments. Here we show examples of the data that demonstrate the different bottom environments and features observed in the subbottom data.

Large parts of the subbottom data, especially in central and southern part of the study area, showed little to no penetration. These are hard bottom areas, often characterized by sand and gravel. In other parts the subbottom data show that rough outcrops often extend below the surface and are partially covered by softer sediments (Figure 4.3-4).
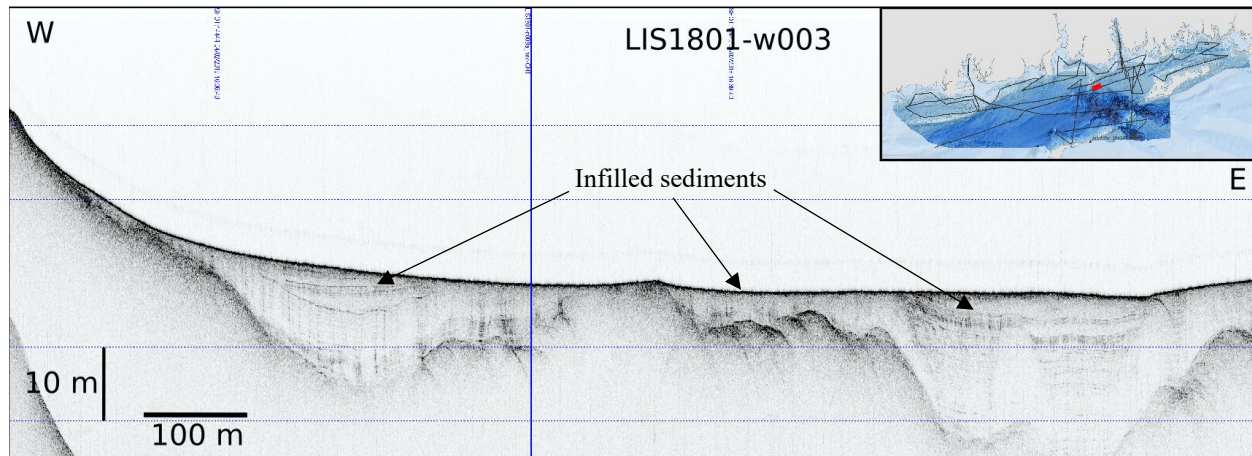
Figure 4.3-4. Example of subbottom image showing harder bedrock features that are filled with sediments

In some places the subbottom signal penetrates the sand-gravel layers to reveal thick (>10m) bands of prallel reflections that are often truncated at the top (Figure 4.3-5). These thick bands are likely glacial clays deposited when present-day LIS was covered by proglacial Lake Connecticut and subsequently eroded during the drainage of the lake and the following fluvial period. The fact that the subbottom system is imaging these layers suggests that the overlying gravel and sand layer identified in the surface grabs is just a surface cover. It might not be more than a meter thick or even less in some places.
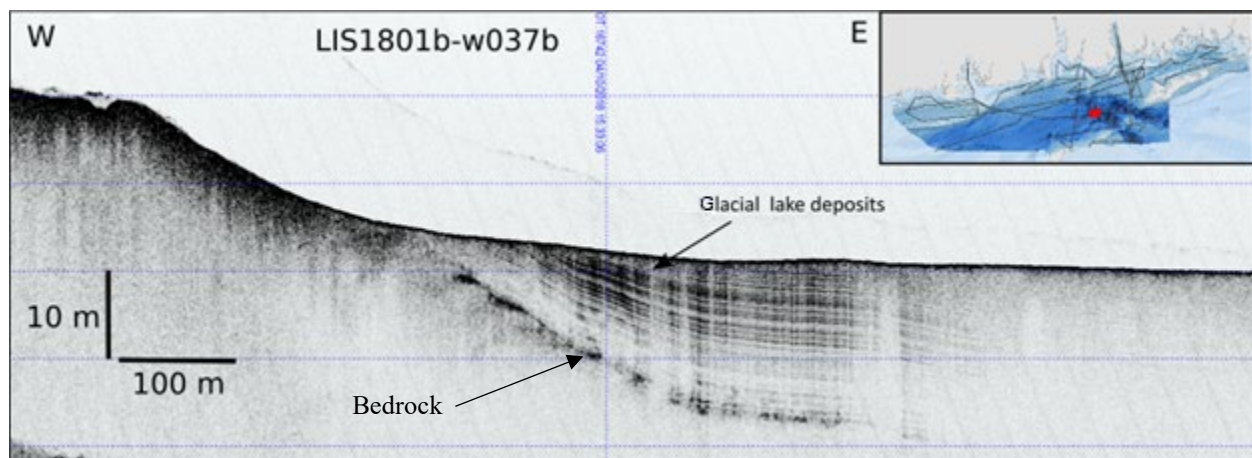
Figure 4.3-5. Example of subbottom image showing what is likely glacial lacustrine clay layers from Lake Connecticut that are eroded at the top and fill underlying bedrock topography that outcrops to the West

In other places the subbottom data also show several meters of depositions (e.g., Figure 4.3-6). The deposition appears to be sometimes bound by bedrock outcrops. In the case of a large dredge disposal site south of the Thames River, the subbottom data cleary show the thickness of this disposed sediments (Figure 4.3-7).
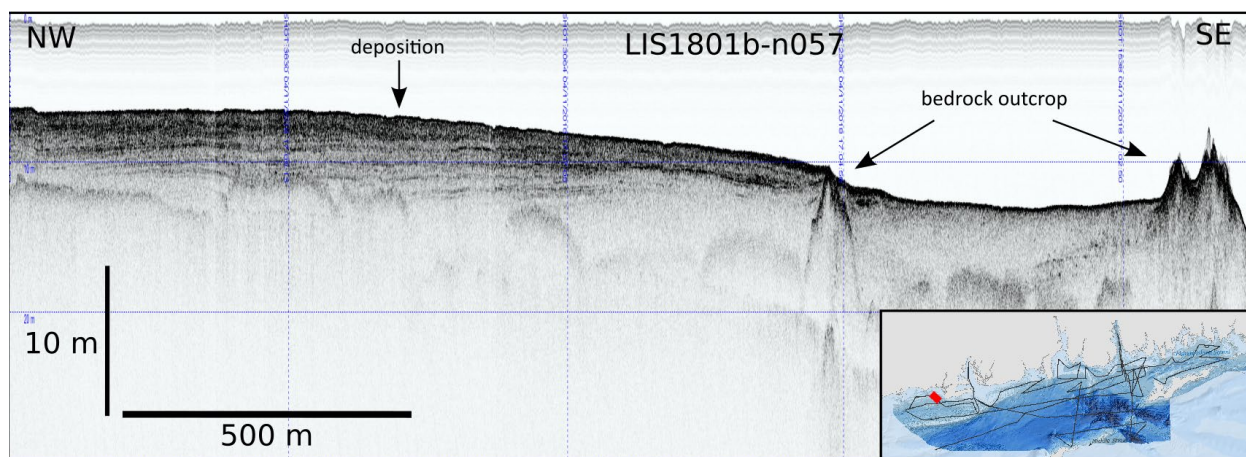
Figure 4.3-6. Example of subbottom image showing several meters of more recent deposition near the northern shore west of the Connecticut River on top of a rougher bedrock that outcrops in a few places
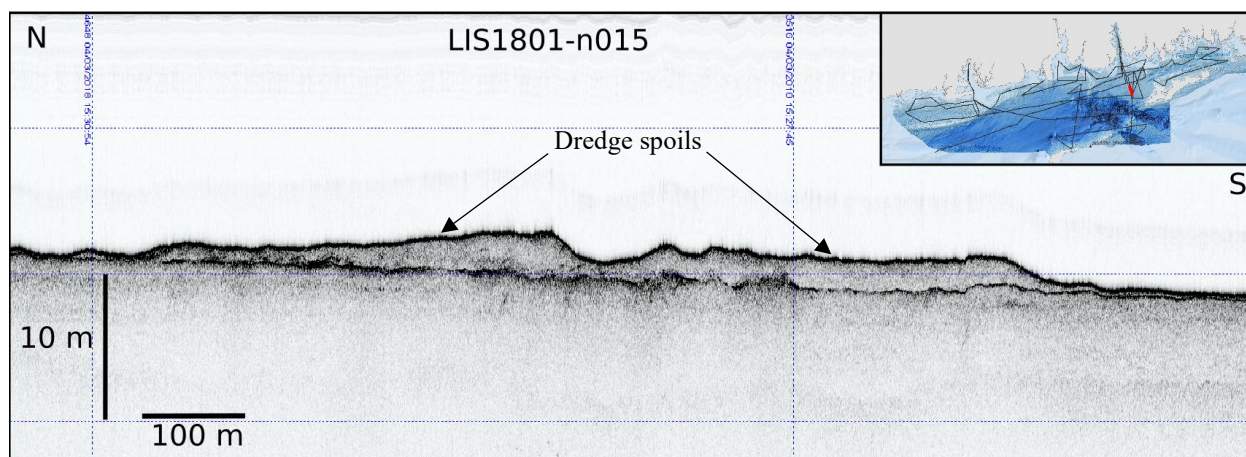
Figure 4.3-7. Example of subbottom profile across the dredge disposal site south of Thames River shows the extent and thickness of the disposed sediment

Despite the fact that much of the LIS Phase II area has hard surface sediments that are difficult to penetrate with the deployed subbottom system, we acquired valuable data in several areas. These data are critical in understanding sediment structures just below the surface and provide valuable context for the interpretation of the grab samples and sediment cores. They have been critical in identifying suitable sediment core locations.

4.4   Sediment Cores Collection and Analysis

4.4.1 Sediment Core Collection

In order to provide detail needed for the interpretation of the acoustic data and constrain the temporal aspects of the various sedimentary environments within the Phase II study area, a series of sediment cores was collected. In addition to providing detailed depositional records, sediment cores are useful for distinguishing depositional from erosional/non−depositional areas or identifying a thin layer of sediments covering bedrock outcrop. They are also useful for revealing areas that have been disturbed by isolated or frequent events in the past, as well as those where the depositional environment has shifted from one regime to another.

Sediment sampling locations were chosen based on available multibeam bathymetry and backscatter data as well as the subbottom profile described above. Sediment cores were collected on two cruises in 2018 onboard the R/V *Seawolf* and the R/V *Donald W. Pritchard* (both of Stony Brook University – see Table 4-2). Sampling sites with significant gravel, sand, or otherwise hard bottoms were not targeted since they suitable for coring; as a result, the locations where core samples were retrieved are concentrated in the northern part of the study area (Figure 4.4-1), which has more fine-grained material, which is generally softer and more easily sampled (see also Section 3.4.3).

Table 4-2. Details of the sediment core collection field efforts

Survey date	Field days	Vessel	Core samples
LIS1801	April 4 2018	*Seawolf*	3
LIS1803	August 21-24, 2018	*Pritchard*	25
Total			28
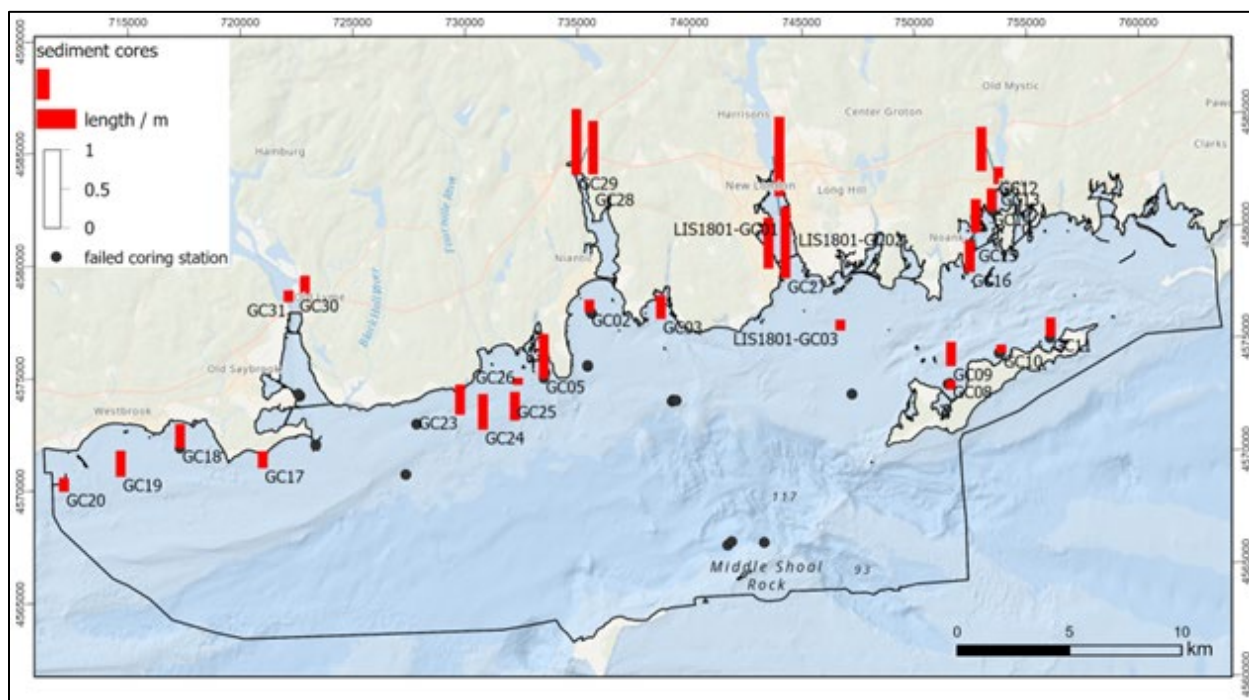
Figure 4.4-1. Location of sediment cores collected in the Phase II AOI. Note that the dark gray dots make locations where coring was tried but failed, most likely due to hard bottom.

Ldeo collected 28 cores in total using their gravity coring system, which consists of a core head weighing ~150 kg with an internal check valve connected via a cam-groove coupling system to clear schedule 40 PVC pipes (2m long x 4" diameter). Clear coring tubes allow us to visually inspect the length and quality of sediment core as they are collected. This was essential for deciding to retry to take another core at a core location and to determine if the surface of the sediment core was intact. Once on deck, sediment cores were capped, sealed with tape, and visually described. The overlying water was retained in the core barrel to reduce disturbance of the sediment during transportation and storage. For additional details, see Table 4-3.

Table 4-3. LIS Phase II Sediment Core Information

Core ID	Latitude	Longitude	Water Depth (m)	Date	Sampling Device	Core Length (cm)
LIS1801-GC01	41.33576	-72.08707	8.3	4/4/2018	Gravity Core	66
LIS1801-GC02	41.34469	72.08672	12.8	4/4/2018	Gravity Core	101.5
LIS1801-GC03	41.296	-72.058	11.8	4/5/2018	Gravity Core	14
LIS1803-GC02	41.31126436	-72.19143178	6.6	8/21/2018	Gravity Core	16
LIS1803-GC03	41.30645803	-72.15372389	7.0	8/21/2018	Gravity Core	32
LIS1803-GC05	41.28596569	-72.21802378	7.2	8/21/2018	Gravity Core	58
LIS1803-GC08	41.27281503	-72.00230578	8.1	8/22/2018	Gravity Core	12.5
LIS1803-GC09	41.2797905	-72.00144028	7.6	8/22/2018	Gravity Core	33
LIS1803-GC10	41.28351836	-71.97431444	9.2	8/22/2018	Gravity Core	10
LIS1803-GC11	41.288568	-71.94755444	6.4	8/22/2018	Gravity Core	26
LIS1803-GC12	41.35288356	-71.97029611	8.9	8/22/2018	Gravity Core	57
LIS1803-GC13	41.34837275	-71.96974308	9.0	8/22/2018	Gravity Core	21
LIS1803-GC14	41.34059372	-71.97484281	6.3	8/22/2018	Gravity Core	32
LIS1803-GC15	41.32654367	-71.98362644	5.1	8/22/2018	Gravity Core	42
LIS1803-GC16	41.31676856	-71.98801083	7.4	8/22/2018	Gravity Core	42
LIS1803-GC17	41.25749855	72.37022057	7.4	8/23/2018	Gravity Core	28
LIS1803-GC18	41.26774375	72.41333279	5.5	8/23/2018	Gravity Core	35
LIS1803-GC19	41.25767251	72.44585818	7.6	8/23/2018	Gravity Core	34
LIS1803-GC20	41.25316955	72.47646286	4.9	8/23/2018	Gravity Core	19
LIS1803-GC23	41.27369994	72.26364407	12.4	8/23/2018	Gravity Core	42
LIS1803-GC24	41.26708269	72.25203495	18.0	8/23/2018	Gravity Core	45
LIS1803-GC25	41.26986872	72.23479327	24.7	8/23/2018	Gravity Core	40
LIS1803-GC26	41.28410254	72.23197325	6.4	8/23/2018	Gravity Core	10
LIS1803-GC27	41.3194253	-72.086106	4.0	8/23/2018	Gravity Core	94
LIS1803-GC28	41.3662994	-72.1932292	2.4	8/24/2018	Gravity Core	27
LIS1803-GC29	41.3663155	-72.1933472	2.6	8/24/2018	Gravity Core	35
LIS1803-GC30	41.3244377	-72.346365	4.0	8/24/2018	Gravity Core	12.5
LIS1803-GC31	41.3232291	-72.3507746	7.3	8/24/2018	Gravity Core	6

4.4.2 Sediment Core Processing

After the cores were collected, they were stored and transported upright in order to preserve sediment stratigraphy and core top integrity. At the end of each survey, cores were transported to LDEO's core facility and stored in a walk-in refrigerator at 4°C before processing. Sediment cores were then carefully dewatered, excess PVC above the sediment water interface was removed, and a foam plug was securely fitted to stabilize sediment surface. Sediment cores were split longitudinally and prepared for long-term cold storage archive, which includes inserting depth markers, and digitally photographing both core halves. Split cores were visually described, logged for physical properties, analyzed by XRF for elemental composition, and x−radiographs and high-resolution images were taken. In between various processing steps and upon completion of analysis, sediment core samples were placed in D-tubes and stored at 4°C.

Working halves of the gravity cores were sampled for additional analyses by carefully removing 1 cm thick sections every 5-10 cm. Prior to further processing, the outer edge of each sample was removed to prevent contamination due to smearing. Wet core subsamples were processed and analyzed following the same protocols that were used for grab samples (see Section 3.4.2).

4.4.2.1 Physical properties

Physical properties were measured at 1mm intervals using a GEOTEK Multi-Sensor Core Logger. Properties measured included density, porosity and magnetic susceptibility. In order to precisely co-register information from the different sensors, each core was run in a custom sample holder equipped with density, height, and distance markers, as well as wet bulk density calibration section. In order to achieve high-resolution density measurements, the window on the NaI detector, used to measure gamma ray attenuation, was modified to a 1mm x 20mm slit using a custom-made lead insert. We further modified the system by reconfiguring the laser displacement sensors to make precise, non-contact core thickness deviation measurements, which are required to estimate wet bulk density from the gamma attenuation signal. Magnetic susceptibility was measured using a Bartington MS2E sensor with a probe diameter of 25mm. An example of the physical property results is shown in Figure 4.4-2. Detailed logs for all cores are presented in Appendix 3.
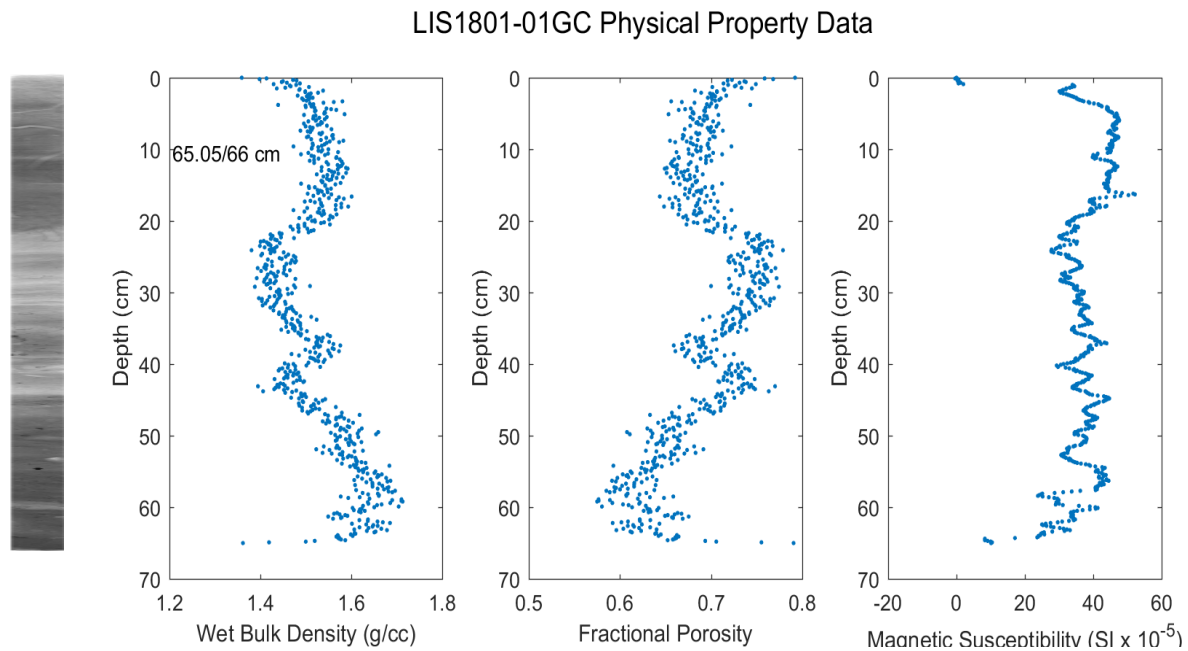
Figure 4.4-2. Physical property results for LIS1801−GC01 along with x−radiograph

4.4.2.2 Estimated water content, wet bulk density, porosity, and dry bulk density

Wet bulk density (WBD) estimates derived from gamma ray attenuation and measured with the GEOTEK logger are used to calculate water content using the following equations:

Equation 2

$$WBD\left(g_{wet}/cc_{wet}\right) = \frac{1}{\left(\dfrac{wc}{\rho_{water}} + \dfrac{(1-wc)}{\rho_{sed}}\right)}$$

Equation 3

$$\text{Water content} = \frac{\left(\dfrac{\rho_{water} \cdot \rho_{sed}}{WBD} - \rho_{water}\right)}{(\rho_{sed} - \rho_{water})}$$

Where: ρ_{water} is the water density and ρ_{sed} is the dry matrix density. In this study, we assumed 1.019g/cm³ for the density of seawater; dry matrix density was based on the average of values measured via gas pycnometry on discrete core subsamples.

The fraction porosity is calculated from the following equation:

Equation 4

$$\text{Fractional porosity} = \frac{(\rho_{sed} - WBD)}{(\rho_{sed} - \rho_{water})}$$

In a similar fashion, dry bulk densities can be calculated using water content and matrix density. For wet sediments, we use estimated water content and matrix density as:

Equation 5

$$\text{DBD}(g_{dry}/cc_{wet}) = \frac{(1 - wc)}{(\frac{wc}{\rho_{water}} + \frac{(1 - wc)}{\rho_{sed}})}$$

4.4.3 X-ray fluorescence spectrometry

Split sediment cores were analyzed using LDEO's ITRAX Core Scanner (Cox Analytical Systems, Mölndal, Sweden), which combines high resolution XRF scanning, X-ray radiographic images, and high-quality optical images. For XRF measurements, an X−ray tube equipped with a molybedenum anode was operated at a voltage of 30kV and a current of 55mA. Each measurement was made for 30s integrated over a depth interval of 0.5cm by 17mm wide. After scanning was complete, any spectra flagged as invalid were removed and all remaining spectra were summed into a single spectrum. A full spectrum fundamental parameter peak fitting program, provided by the manufacturer, was used to calculate individual elemental abundances in terms of element rates (i.e., cps/mA). Variables in the fundamental parameter algorithm were adjusted to minimize the difference between the measured spectra and the model fit. Once the fitting routine was complete, the optimized parameters were used to calculate down-core elemental rates. The analytical uncertainty of the element signals is estimated based on the dead time corrected total counts for each element. Prior to calibration, elemental rates were first normalized to the coherent scattering peak signal to account for matrix variability and then standardized for each core/each element by subtracting the average element rate and dividing by the standard deviation of the element rate.

In order to transform the high-resolution standardized element rates into accurate elemental abundances, discrete sub-samples were collected from each of the cores, which were then processed following the protocol for XRF dry sample analysis (see Section 3.4.6). In order to obtain calibration information for the same elements measured in the wet sediment cores, dried, homogenized core samples were placed in specially designed sample holders and analyzed on ITRAX along with numerous standard reference materials as calibration standards. An example of the calibration results for Fe and the standard reference materials used is shown in Figure 4.4-3. Data processing and analyses were performed using published protocols, which are covered in detail elsewhere (Kenna et al., 2011). For each core, the elemental abundance data obtained from the dry sub-samples, were used to produce calibrated high resolution concentration profiles for the

entire sediment core. For each element, the previously standardized element rates measured in a particular core were unstandardized by multiplying by the standard deviation and adding the mean concentration of the element measured in the calibration set for that core. Examples of calibrated concentration profiles for LIS1803-27GC are shown in Figure 4.4-4, Figure 4.4-6, and Figure 4.4-7.
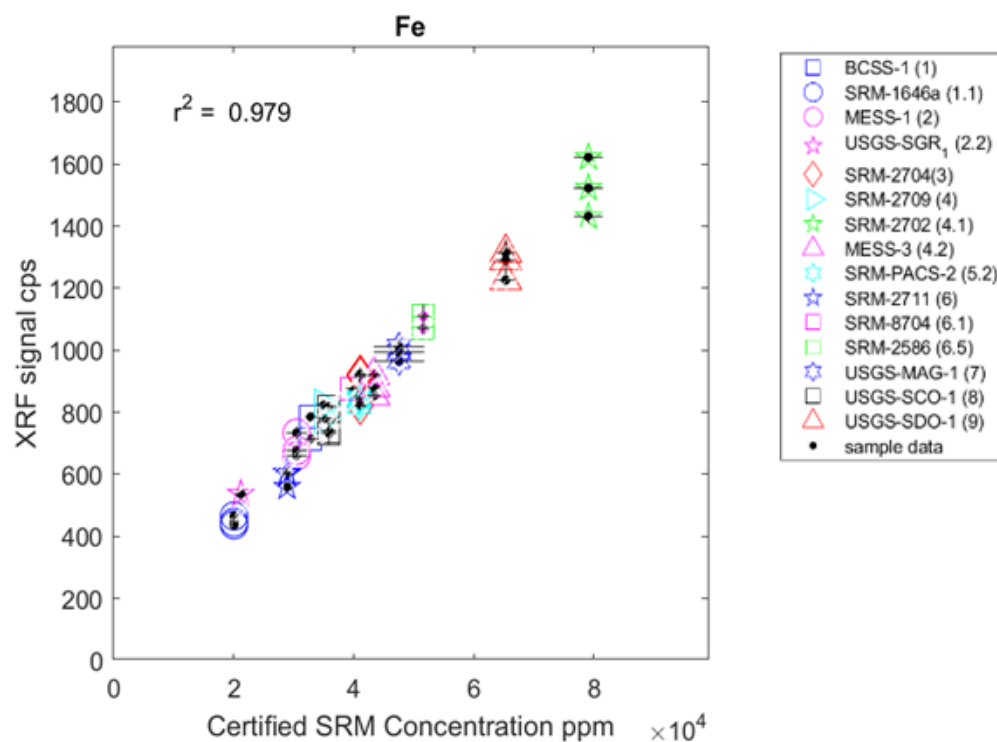
Figure 4.4-3. ITRAX Fe calibration results for selected standard reference materials
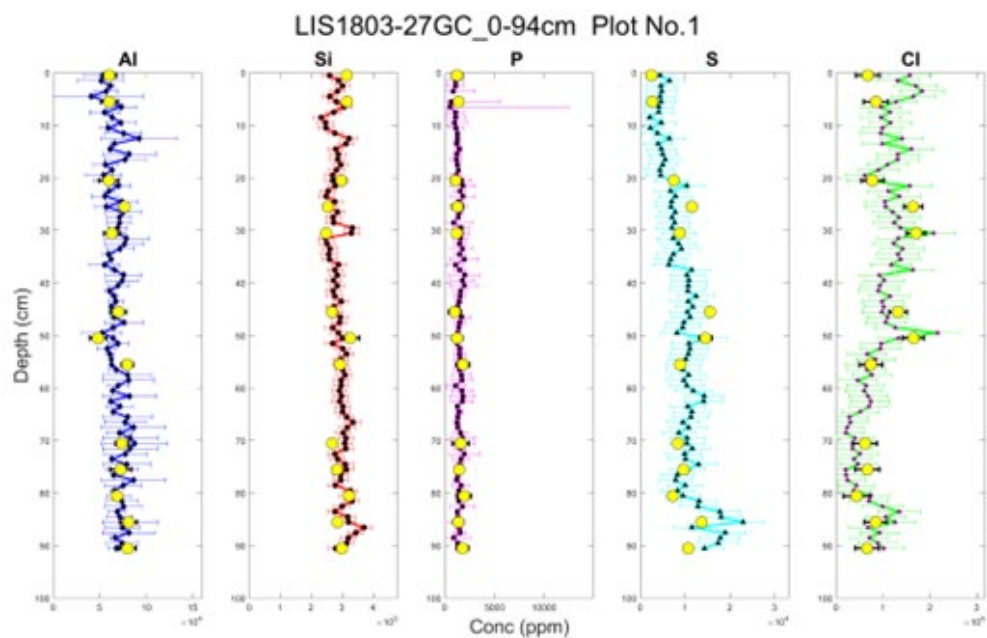
Figure 4.4-4. Al, Si, P, S, and Cl concentration profiles along with calibration samples (yellow dots) for sediment core LIS1803-27GC
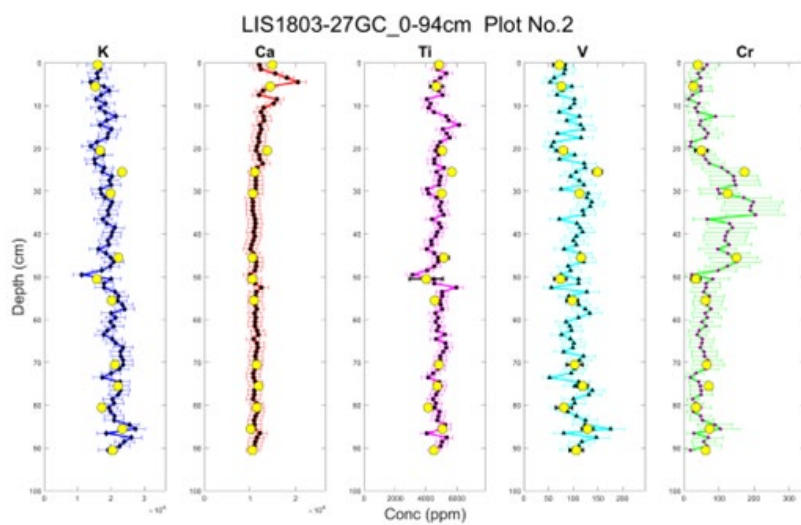
Figure 4.4-5. K, Ca, Ti, V, and Cr concentration profiles along with calibration samples for sediment core LIS1803-27G
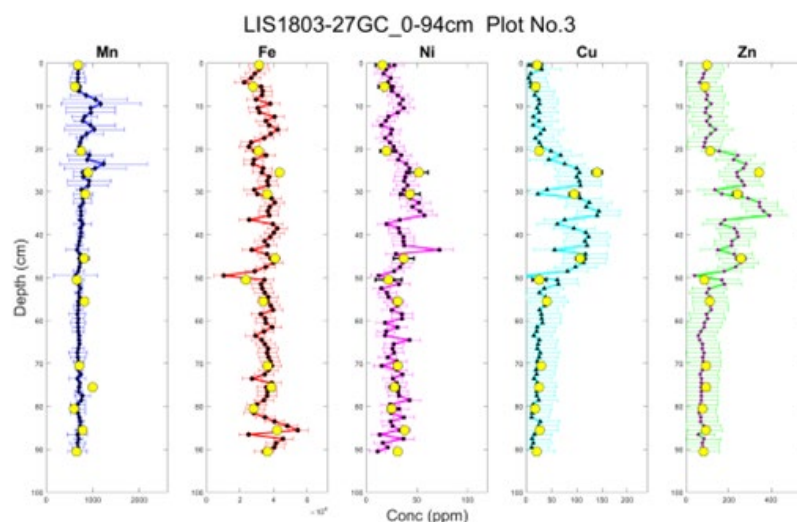
Figure 4.4-6. Mn, Fe, Ni, Cu, and Zn concentration profiles along with calibration samples for sediment core LIS1803-27GC
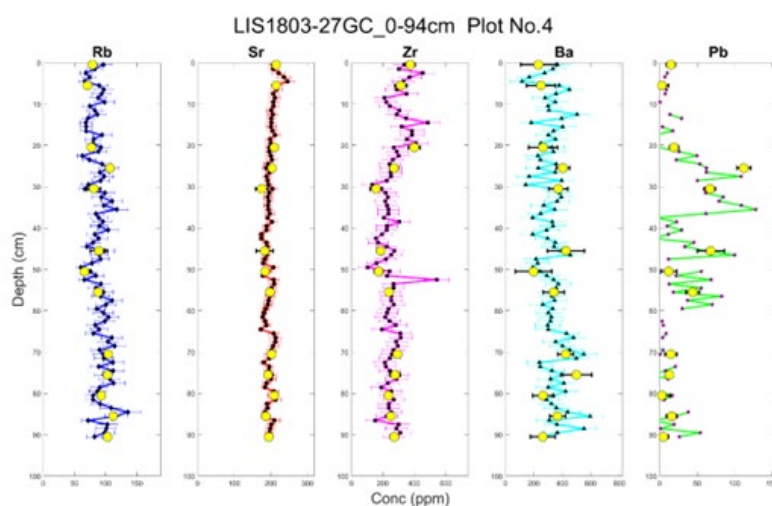
Figure 4.4-7. Rb, Sr, Zr, Ba, and Pb concentration profiles along with calibration samples for sediment core LIS1803-27GC

4.4.4 Radiographic Images

Radiographic images were taken along the centerline of each core with the molybdenum X−ray tube operated at 55kV and 50mA, and exposure time of 1.2s and a down core step-size of 0.2mm by 200mm wide. The resulting images were processed using custom Matlab scripts. Radiographic images were rotated to a vertical orientation, non-core elements were cropped, and the contrast was enhanced by histogram equalization in order optimize the level of detail. As an example, the X−radiograph obtained for LIS1803−05GC is shown in Figure 4.4-8 (left) overlain by the wet bulk density for reference. The core radiographs show changing lithology, the detail of sedimentary structures, bioturbation, and accessories such as shells and clasts. These, together with the visual core descriptions, show the variability of the depositional environment through time.
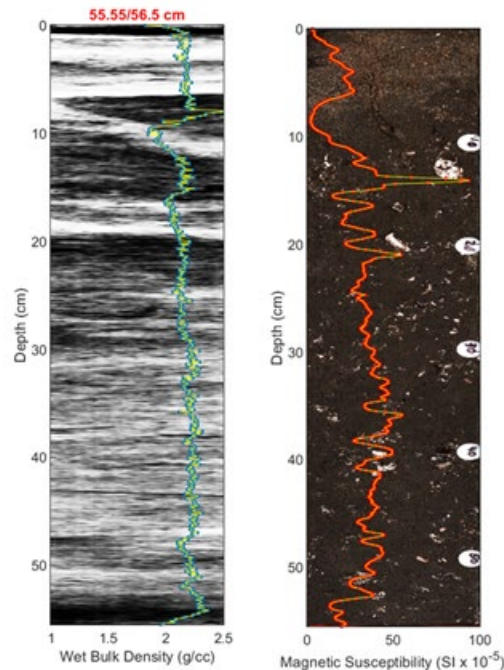
Figure 4.4-8. The left-hand panel shows the processed radiographic image overlain by the wet bulk density; the right-hand panel shows the processed optical image overlain by magnetic susceptibility for sediment core LIS1803-05GC

4.4.5 Optical Images

Optical images were collected using an RGB line camera equipped with crossed polarizing filters. Medium resolution images and high-resolution 16-bit images were routinely collected. After collection, optical images were processed using custom Matlab scripts. Images were rotated to a vertical orientation, non-core elements were cropped, and lightness levels were increased to optimize the level of detail and better show core features. As an example, the optical image obtained for LIS1803−05GC is shown in Figure 4.4-8 (right) overlain by the magnetic susceptibility for reference.

4.4.6 Core Description

The gravity cores were split, photographed, and visually described following the Integrated Ocean Drilling Project protocol (e.g., IODP Expedition 356). The observations were entered in core barrel sheets and then in Adobe Illustrator as drawings (Figure 4.4-9). The core photos obtained by using the new ITRAX core scanner are of very high resolution and allowed for much greater detail of the sedimentary structures, fossil assemblages, and degree of bioturbation to be observed when compared to the core descriptions from the Pilot Phase that were not photographed with the ITRAX system. The main lithology was determined by using a hand lens. The main sedimentary structures include contacts (sharp, gradual, angular), beds (if greater than 1cm thick), laminae (if less than 1cm thick), and lenses (not continuous along the thickness of the core). The color of the lithology was determined using the Munsell color chart. The grain size was classified as gravel, pebble, sand, or mud based on the Wentworth (1922) scale. Bioturbation was characterized as moderate, heavy, very heavy, or non-bioturbated. The main accessories are shells and fragments (identified whenever possible), lithic clasts (identified by their size, mineralogy when possible, and their texture as rounded, sub-rounded and angular), wood, and anthropogenic materials (coal, slag). The

degree of sediment disturbance due to the sampling process was also described. Descriptions of all sediment cores are included in Appendix 3; an example is provided in Figure 4.4-9.
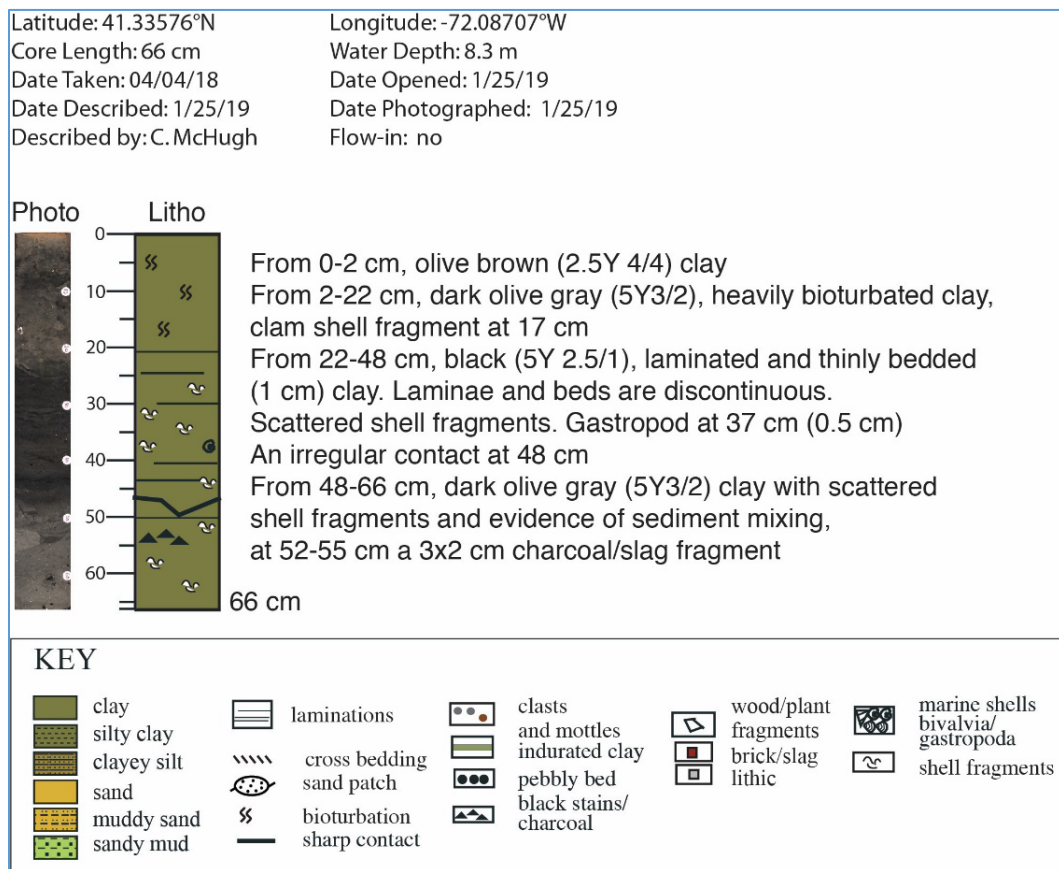
Figure 4.4-9. Example of a detailed core description

4.4.7 Sediment core data integration

The sediment cores were recovered from very distinct depositional settings that highlight spatial and temporal changes in sediment deposition used to characterize sedimentary environments (Figure 4.4-10). Strater plots allow for correlations between the XRF elemental data, the sediment physical properties, core descriptions, photos, and x-rays. All these variables also highlight the changing depositional environments with depth in a core.
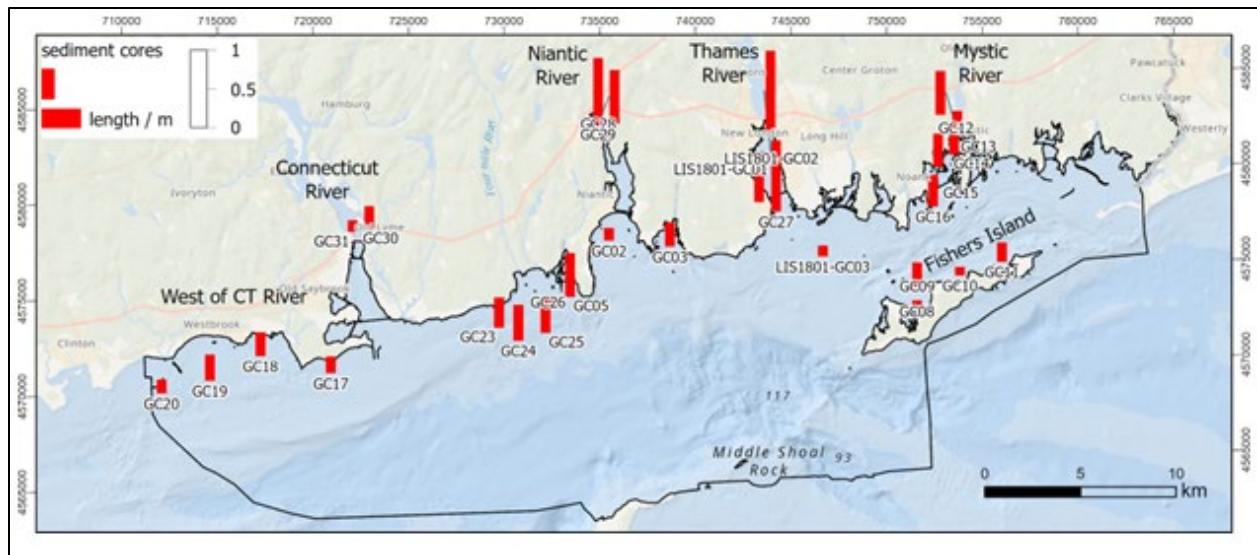
Figure 4.4-10. Core locations as described based on XRF chemistry, physical properties, and lithology

4.4.7.1 Nearshore west of Connecticut River

Sediment cores were recovered along the nearshore west of the Connecticut River in water depths of 5 to 10 m (LIS1803-GC17, GC18. GC19, GC20). The cores recovered ~50 cm thick sections. The sediments are composed of silty clay collected in embayments near the mouth of the river. These sediments coarsen to very fine sand towards the west away from the river mouth. Shells and shell fragments are most abundant towards the west with razor clams being a dominant species. Closer to the river mouth the sediment texture is laminated revealing of episodic pulses of fine-grained sedimentation. The sediments are moderate to heavy bioturbated. The sandier sediments towards the west are also bioturbated but their texture reveals thicker intervals of reworked sediment noted by sharp basal contacts and containing mud clasts and fluid intrusions above. The fluid intrusions in the sediment reveal rapid sediment accumulation on top of water saturated sediments and are noted by changes in color, lithology, and texture. The sediment density correlates with grain size in that it is larger (2 g/cc) in the sand intervals and lower (1.5-1.8 g/cc) in the muddy intervals. Both grain size and shell content influence the magnetic susceptibility that exhibits more variability (increase and decrease) in the signal down core as the lithology changes. The elements Fe, Ti, K, and Ca vary in intensity with changes in sediment texture due to grain size and sediment transport events noted by sharp contacts and/or laminated intervals (Figure 4.4-11).

In summary, there is a gradation in processes from the river mouth towards the west from a more tranquil depositional environment to a dynamic setting. This is manifested in the sediment grain size, shell content, and sedimentary structures. The location from where gravity core GC17 was recovered is more influenced by fluvial processes than the core GC20 to the west, which is influenced by dynamic processes. The gravity core, GC17, recovered from an embayment setting shows episodic sediment deposition events in what is a more tranquil depositional setting. The gravity core, GC20, recovered farther west contains coarser sand and broken shell fragments revealing of a more energetic setting.
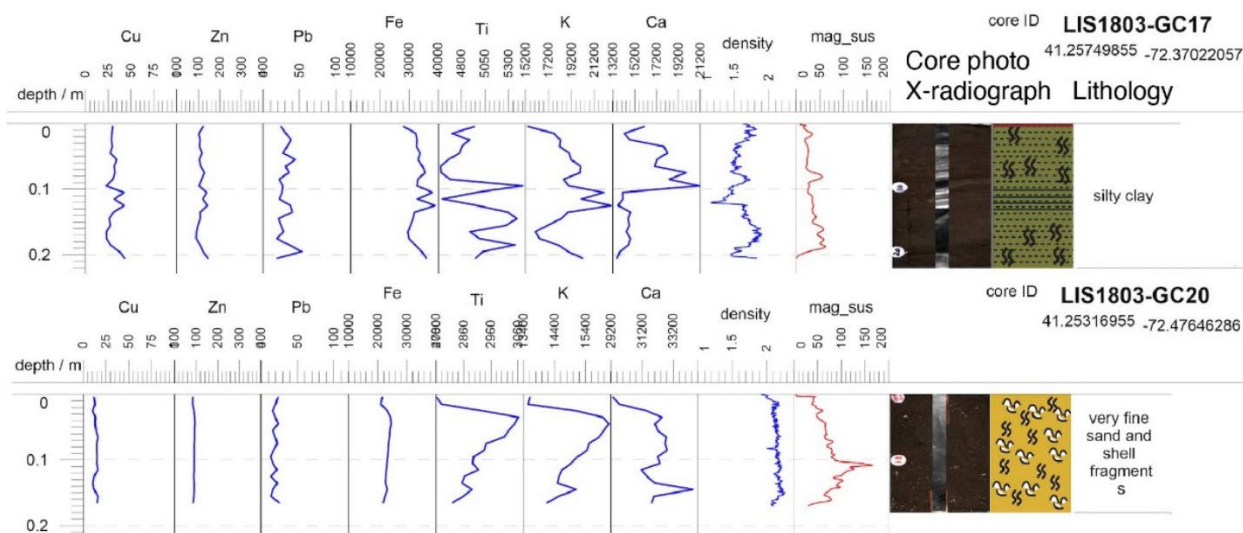
Figure 4.4-11. Illustrating the changing nearshore depositional environments west of the Connecticut River from east (top) to west (bottom). From left to right XRF chemistry, physical properties, core photo, X-ray radiograph, and core lithology.

4.4.7.2 Connecticut River

The two short cores, 15 cm-long LIS1803-GC30 and 30 cm-long GC31, were recovered in water depths of 4-7 m. The sediment is characterized by 1 to 2 cm thick mud and sand beds interpreted as episodic sedimentation likely the result of storms and/or seasonal changes. Coarse, medium sand was in the upper 5cm of both cores and is possibly related to a storm event.

4.4.7.3 Niantic River

Two cores, 69 cm-long LIS1803-GC28 and 85 cm-long GC29, were recovered from the Niantic River in water depths of ~2-4m. The sediments are mainly composed of mud containing evidence of current activity such as laminae and cross-bedding. Intervals of tranquil deposition are evident by bioturbation. Rare shells and plant detritus indicate a fluvial-estuarine setting.

4.4.7.4 Nearshore east and west of Niantic River

Two cores 15 and 30 cm thick (LIS1803-GC02 and GC03, respectively) were recovered at the mouth and east of the Niantic River in water depths of 7 m. The sediments in both cores are composed of muddy, very fine sand containing shell fragments and evidence of bioturbation and mixing.

LDEO recovered 10-60 cm-long cores of sediment (LIS1803-GC05, GC25, GC26, GC24, GC23) to the west in water depths of 6-25 m. The sediments are composed of muddy, fine to coarse sand containing abundant shells and fragments, revealing evidence of reworking and of a higher energy setting than the rivers. This setting is influenced by wave action and by tidal currents.

4.4.7.5 Thames River

The best sediment recovery was obtained from cores in the Thames River in water depths from 8 to 13 m (LIS1801-GC01, GC02, LIS1803-GC27). Sediment thickness ranges from 66 to 101 cm. The sediment is dominantly silty clay with rare intervals of sandy mud. The cores show laminated and bioturbated intervals, scattered mollusk shell fragments, and moderate bioturbation. A 92 cm-

long core, LIS1803-GC27, recovered at the mouth of the Thames River provides a good example of a dynamic reworking setting. The upper ten centimeters are composed of sandy mud that is heavily bioturbated, suggesting a tranquil depositional environment. But, at the 20 to 30 cm depth the sediment is mixed, containing broken shell fragments and clay clasts above a sharp erosional contact suggestive of a sediment transport event. Down core from 30-92 cm, the sediment shows episodic mixing of clayey silt and sand. Bioturbation was not observed in this interval, suggesting that organisms didn't have enough time to establish and mix the sediment. These are three very distinct depositional environments.

The core X-rays highlight this variability as alternating high and low reflectivity bands that correspond with the sandy layers and clayey silt intervals. The density also highlights this variability by increasing to 2.0 g/cc in correspondence with the sand layers and decreases in density corresponding to the silty clay intervals at 1.6 g/cc. The magnetic susceptibility signal also varies with depth but is more reflective of changes in the mineralogy; for example, a correspondence with Fe peaks between 10 and 20 cm depth. Heavy elements such as Cu, Zn, and Pb show increases in their signals that correspond with the finer grained silty clay intervals – for example, between 20 and 50 cm depth (Figure 4.4-12).
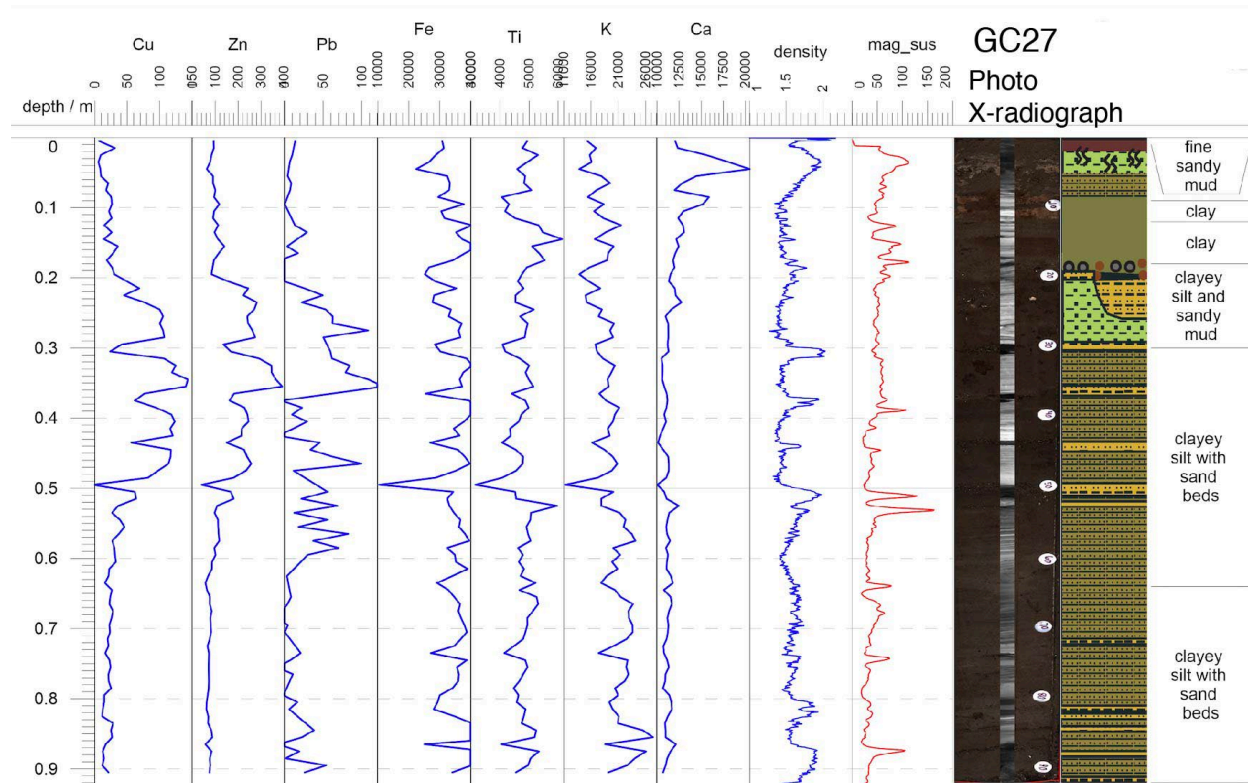
Figure 4.4-12. Gravity core 27 shows a dynamically changing depositional environment with episodes of higher energy containing sandy mud and sharp, erosional basal contacts, and laminated intervals suggestive of more episodic deposition.

4.4.7.6 Mystic River

Five cores (LIS1803-GC12, GC13, GC14, GC15, GC16) were recovered in water depths of 5 to 9 m and sediment thicknesses ranging from 22 to 57 cm. The sediment in this area is mixed and doesn't show a trend of coarsening from the river towards the sound as in the Connecticut and Niantic Rivers. The sediments are dominated by sand ranging in size from coarse with pebbles to

fine. The cores show changing of facies with intervals of sandy mud, muddy sand, and gravelly, coarse sand upriver indicative of a dynamic setting where sediment reworking and deposition are common. Bioturbation is moderate to heavy in the silty clay and clayey silt intervals suggestive of a more tranquil setting. The sediment density varies downcore reflecting the changes in lithology (sand-mud). Where shell fragments, pebbles, and lithic clasts are present, the magnetic susceptibility shows increases and decreases in its signal. The intensity of Fe, Ti, K, and Ca also reflect the lithologic variability and changing depositional environment. In summary this region is characterized by very dynamic and tranquil depositional environments.

4.4.7.7 Fishers Island

LDEO recovered four sediment cores (LIS1803-GC8, GC9, GC10, and GC11) west of Fishers Island in shallow water embayments ranging in depth from 6.4 to 9.2 m. The recovered sediment ranges in thickness from 10 to 30 cm. The lithology is composed of very fine sandy mud and muddy, very fine sand with abundant shell fragments. Mollusks, some live (limpet gastropods), are common. The sediment density of 1.5 to 2 g/cc reflects the mixing of mud and sand. Cores with higher density sediments are dominated by very fine sand. In contrast, muddy sediments have lower density. The occurrence of shells (fragments and complete gastropods) is manifested as increases in the magnetic susceptibility signal, which otherwise shows a homogeneous profile without increases or decreases in its signal. The elements Fe, Ti, Ca, and K vary slightly in their intensity downcore, reflecting changes in the sediment composition and distinct pulses of sediment mixing. All sampled sediments are moderately to heavily bioturbated.

In Summary: the cores recovered from the rivers (except for Mystic River) exhibit similar grain size muddy sand and sandy mud, texture, and sedimentation patterns. Sediment recovered from embayments tends to be finer grained (silty clay and clayey silt) with heavy bioturbation. The nearshore cores are coarser grained and contain marine shells and fragments with thicker beds and intervals of bioturbation. In Fishers Island embayments, the mixing of fine sand, mud and shell fragments, and elemental variability indicate a moderately dynamic setting with overall sediment deposition through time. The variability in the depositional environment with depth in a core is noted by sharp contacts and lithological changes.

4.5 Sediment Environment Characterization

The sedimentary environments are influenced by many factors including tidal currents, storms, wave activity, sediment texture, bioturbation, sediment input, the geological history, and related pre-existing substrate. We use the combined information of the seafloor morphology, the surface grab sample analysis, the subbottom data, and the sediment core analysis results to differentiate different sediment environments and determine dominant processed in the study area.

4.5.1 Geological Background

Much of seabed environment in the study area is controlled by the underlying geology and has been shaped by the last glaciation and deglaciation events. Lewis (2014) provides a comprehensive summary. Key points from this summary that provide a framework for the description and interpretation of different sediment environments are the following: Around 22 ka ago the ice front of the last glaciation reached to the northern shore of Long Island and the moraine followed the North Fork, Plum Island, and Fisher Island line. When retreating, the glacier created another moraine (Old Saybrook Moraine) in the LIS during a temporally still stand around 17ka running

approximately along the Long Shoal, northern Central Basin and the southern edge of Thames River area. During the glacial retreat the LIS Basin turned into a glacial lake, Lake Connecticut. The spillway for Lake Connecticut was across the moraine between Orient Point, Long Island, and Fishers Island, New York, at The Race where it breached and eroded the moraine. Around 18.7 ka, Lake Connecticut had drained completely, and stream channels eroded into the glacial lake sediments. Global sea level was still significantly lower than today. The streams brought additional sand and gravel along their path. As sea level rose, ocean waters transgressed into LIS and turned it into an estuary, causing the rivers flowing into LIS to form deltas where they entered the estuary. Sedimentation rates and accommodation space resulting from this geological history are key factors in what is preserved in the record.

The Mattituck Sill forms the western edge of the Phase II study area and is underlain by Glacial Lake Connecticut deposits. Although it is not a sill in the sense of a structural high, it does mark the transition from the highly eroded eastern Sound to the depositional environments occurring west of this study area.

4.5.2 Sediment Environment Interpretation and Description

As described in the sediment texture Section 3.4.5, the seabed of the study area varies significantly, often over short distances. To achieve a quick overview, we distinguish several major groups of sediment environments as described in Table 4-4.

Table 4-4. Sediment Environment classes and their definitions

Classification	Description / Definition
Deposition	Presence of higher metal levels; homogeneous layers, and/or preservation of sedimentary structures in sediment cores and clear layers in the sub bottom; can have bioturbation.
Deposition – dredge disposal site	This is an area where a large amount of sediment is deposited by mechanical dredge disposal.
Dynamic – sediment waves	Areas that are dominated by sediment waves as seen in the bathymetry and backscatter. Generally sand rich.
Dynamic - reworking	Areas with no signs of long-term deposition (e.g., layers), mostly sandy, finer materials are not settling here and/or have been removed.
Non-deposition / erosion	Areas where outcrops, boulders, and gravel indicate that no significant deposition has occurred since glacial time and where sediments are likely being eroded, although amount of erosion is not clear.
No data	Parts of the study areas where we don't have enough data to assign a category. These are mainly very shallow areas near the shore.

4.5.2.1 Sedimentary Energy Levels

The combination of the different data sets provide insight into the dominant energy levels of the different areas. High, moderate, or low energy regimes can be caused by tidal currents, other

currents, and wave action. They increase mixing and result in sorting, transport, and windowing of finer sediments (Table 4-5).

Table 4-5. Interpreted energy regimes of different sediment environments and their definitions

Classification	Description / Definition
High energy	Strong signs of current- or wave-related mixing in sediment core, areas of erosion or non-deposition likely to be subject to strong currents.
Moderate/ high energy	Signs of mixing by currents and waves; mix of sand and mud; shell fragments (likely transported).
Moderate energy	Signs of current activity; mix of mud and sand, shells, and fragments; some biology; some signs of mixing.
Low / moderate energy	Few signs of current activity; mainly fine-grained material, biological activity, layers in sediments and subbottom data. Few sandy layers.
Low energy	No signs of current activity; mainly fine-grained material, biological activity, undisturbed layers in sediments and subbottom data.
Unsurveyed	Parts of the study areas where we don't have enough data to assign a category. These are mainly very shallow areas near the shore.

4.5.3 Detailed description of different sub-regions

For a more detailed discussion of key environmental processes, the Phase II area was divided in several sub-regions with similar characteristics, for example similar morphology and dominant processes (Figure 4.5-1). The details of the sediment environments of each sub-region follows. A map of the sediment environments describing the different dynamics of these sub-regions is shown in Figure 4.5-2.
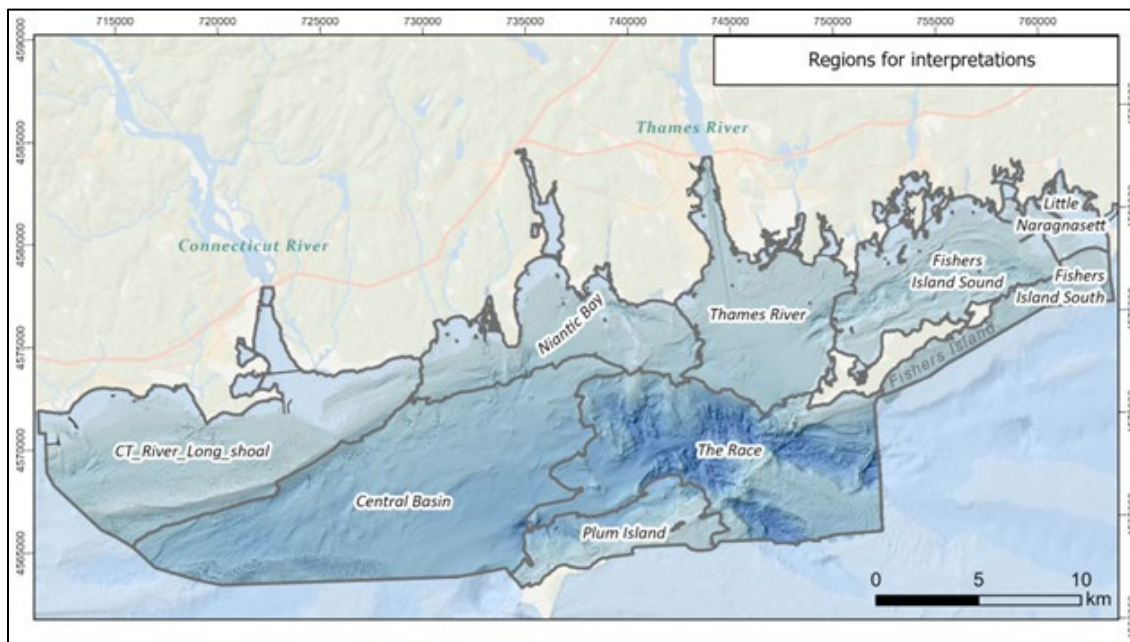
Figure 4.5-1. Main sub-regions of the Phase II AOI used for detailed description of different sedimentary environments and processes
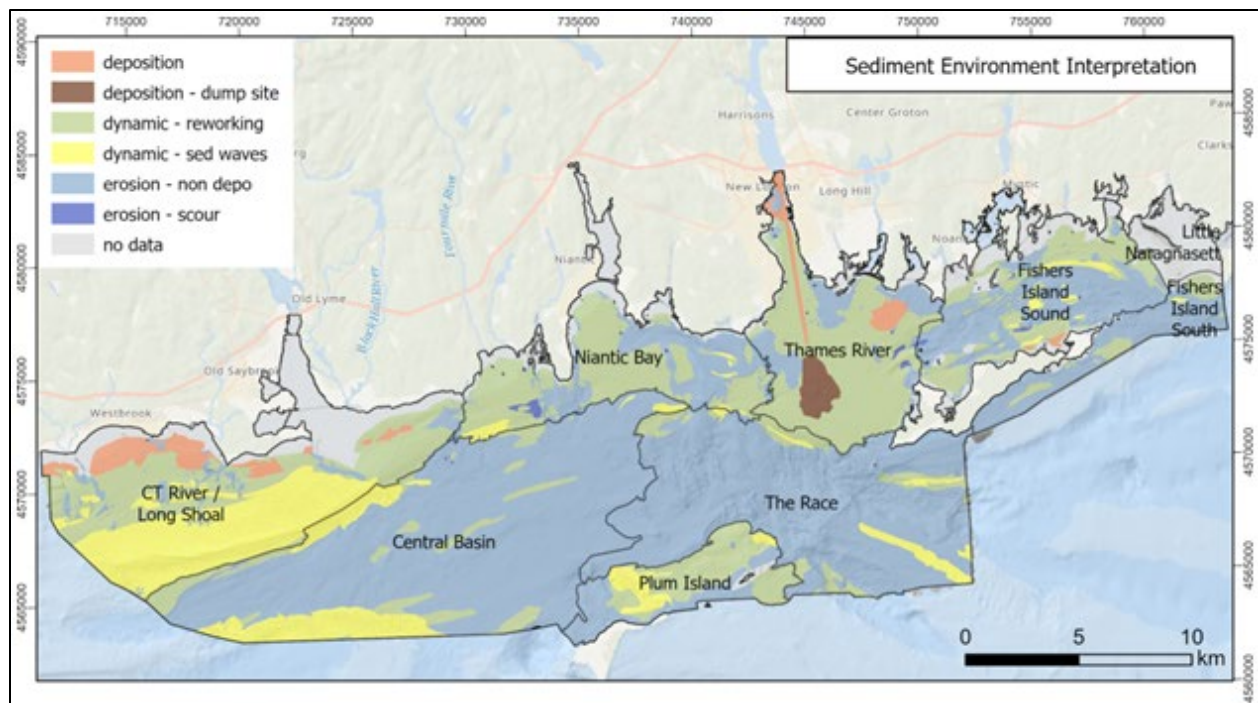
Figure 4.5-2. Map of sediment environments describing the different dynamics of the study area

4.5.3.1 Central Basin

The Central Basin is the largest region in the study area. It forms the deeper part of the LIS between the shallower areas near the Connecticut shore and the Long Island north fork and Plum Island to the south. The western edge is formed by the Mattituck Sill, which is not a sill in the sense of a structural high (it is underlain by Glacial Lake Connecticut deposits), but mark the transition from the highly eroded eastern Sound to the depositional environments to the west of this study area (Lewis, 2014). Its morphology is the result of erosion and transport of fine-grained Lake Connecticut deposits out of the east and to the west, and over time the "sill" is moving westward driven by strong bottom currents. Today, strong bottom currents prevent finer materials from settling here.

As a result, the Central Basin is dominated by gravelly sediment and sand with few outcrops. Small pockets of deposition might occur where outcrops protect sediment from strong currents. We characterize most of the region as erosional or non-depositional. Some of the gravel layers might be armoring underlying sediment from erosion. With the data we have we cannot determine if, and how much actual erosion might be occurring at present. In a few places the subbottom signal penetrates the coarser sediments on the surface, revealing glacial lake sediments directly underneath, strongly suggesting that no deposition has happened since the glaciation.

A bottom current model by Signell et al. (2000) for LIS predicts strong sediment transport including sand for this area. Extended sediment wave fields found at the northern and southern end of the central basin indicate sediment transport of sandy material across the area (Figure 4.5-3).
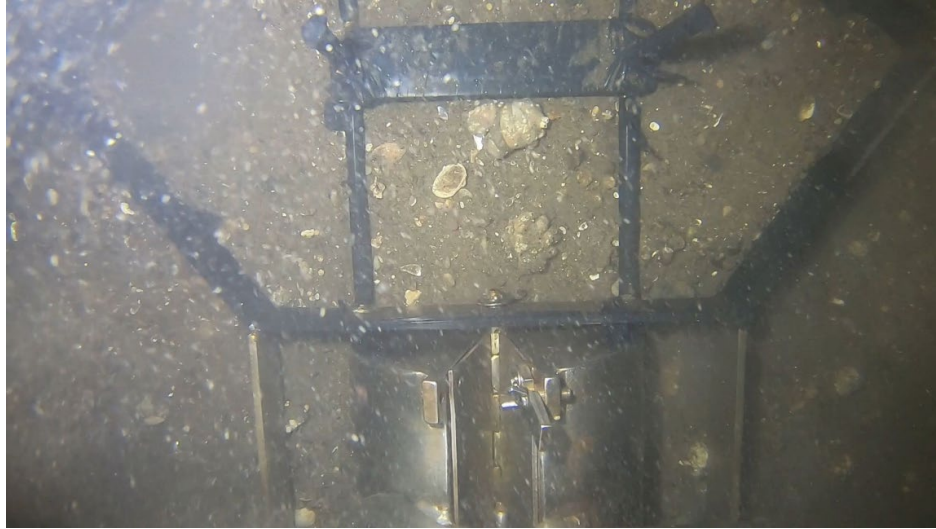
Figure 4.5-3. Example GoPro image of sediment grab station LIS1802-G311 in the Central Basin showing coarser sediments and shell fragments indicating stronger currents

4.5.3.2 The Race

The Race between Plum and Fisher Island is the deepest part of LIS (> 100m) and the main connection between LIS and the Atlantic Ocean. This area has been described in detail by Poppe, DiGiacomo-Cohen et al. (2006). A SW-NE trending ridge between Plum Island and Fishers Island is at the center of the Race area. The ridge is part of the former terminal moraine of the last glaciation, which was breached around ~12ky (Lewis, 2014). The out flow of the glacial lake and later river systems through this gap was probably the main cause for the deep scour on either side of the ridge. The bottom current data provided by the LISMaRC group show some of the strongest currents for this area. These strong currents continue to erode this basin or at least prevent deposition, where the bottom is armored by pebbles and boulders.

North of the ridge, there are several smaller ridges trending N-S and NNW to SSE. These are bedrock features, sculpted by overflowing ice during the glaciation. The orientation of these ridges could represent the direction of ice flow, as it is commonly seen in other previously glaciated areas. These smaller ridges might also reflect differences in underlying bedrock type. While these bedrock features were probably covered by glacial clay during the glacial lake stage, they were later exposed by the erosion during time of glacial lake and river outflow. The strong prevailing currents in this area prevented any subsequent deposition, and present-day currents continue to keep these bedrock features exposed. A bottom current model by Signell et al. (2000) for the LIS predicts transport of materials as large as sand for this area.

The seabed in this area has abundant boulders and gravel of a wide range of sizes (Figure 4.5-4). These boulders, cobbles, and pebbles found in the area are likely remnants of the glacial deposits under the ice and from the moraine. Some of this material was distributed around the reach by breeching of and outflow through the moraine. While the strong current removed unprotected finer sediment, most of the coarser material, especially the large boulders, remained in place.

Figure 4.5-4. Example GoPro image of sediment grab station LIS1802-G206A in the Race showing pebbles and boulders

Again, subbottom data show that glacial lacustrine clay is still underlying some of the sand and gravel in this area. Thin cover of glacial clay layers is further evidence that no significant deposition is occurring. Although most the area is characterized as erosion/ non-deposition, one grab sample (USGS sample NB50-T) recovered finer materials, indicating that locally, in protected areas some finer material can accumulate or at least reside temporarily. Due to the hard bottom, we were not able to recover any sediment cores in this area.

4.5.3.3 Plum Island

The area north of Plum Island and south of the Central Basin and The Race areas shows slightly shallower water depths. Plum Island is a remnant of the former terminal moraine. Much of the area surrounding the Island is covered with boulders, gravel, and sand (Figure 4.5-5). Boulders are likely remnants from the moraine and glacial deposits. As a result, we do not have cores from this area.

In addition to the Race, there is a narrower connection between the open ocean and the Sound on the west side of Plum Island. Thus, the area is dominated by strong currents and no deposition occurs.
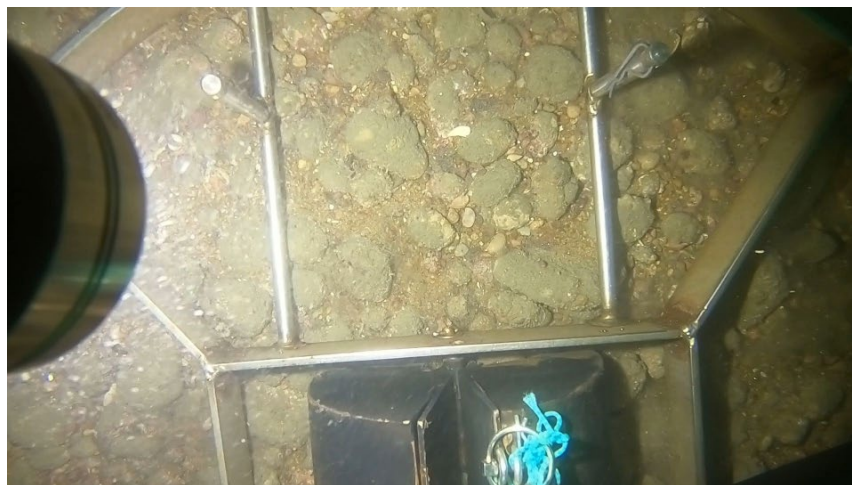
Figure 4.5-5. Example GoPro image of sediment grab station LIS1801-G152 near Plum Island showing rounded pebbles and sand

4.5.3.4 Fishers Island South

The south side of Fishers Island is exposed to wave action and storms that prevent finer sediments from depositing (Figure 4.5-6). There is likely some amount of along shore transport happening. Several outcrops and boulders are remnants of the former moraine, which formed Fishers Island.
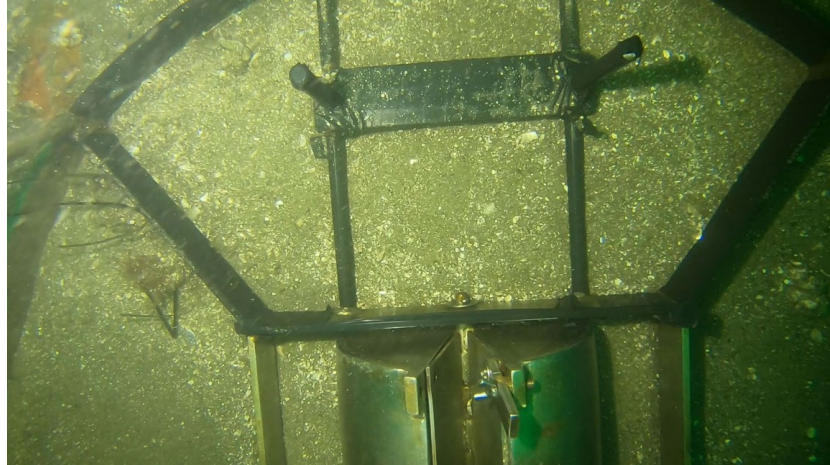
Figure 4.5-6. Example GoPro image of sediment grab station LIS1802-G240 south of Fishers Island showing well sorted sand and shell fragments indicating currents or wave activities

4.5.3.5 Fishers Island Sound

This area between Fishers Island and the Connecticut shoreline can be subdivided into several subareas: there are smaller bays on the northern shore of Fishers Island; larger, shallow (<2m) bays and rivers on the Connecticut shore; and a deeper (>5m) area in between.

Sediment cores form the Fishers Island bays show heavily bioturbated but overall finer sediments in the sheltered parts of these bays. The bays on the Connecticut shoreline, as far as we were able to access those, are dominated by sand and gravelly sediments with little indication of continuous deposition, which is likely prevented by storms and wave action. Strong tidal currents prevent deposition and potentially cause scour and erosion in the central area, which is characterized by coarse sediment and the presence of sediment waves.

There are many outcrops and remains of underlying bedrock geology in the area, which leads to a rough and variable bottom morphology. It is possible that locally, small pockets of deposition might exist in areas protected by bedrock outcrops.

4.5.3.6 Thames River area

This area includes the Thames River and the area directly south of it. Much of this area has been built up as fluvial delta after the glaciation with material from the river. In the center of the area is a large dredge disposal site of mixed materials (Figure 4.5-2) that is classified here as deposition, but we cannot determine if this site is accumulating any new material or if all the accumulation is from disposal of dredged sediments. It is possible that disposed material is actually dispersing.

The mouth of the Thames River has a dredged channel, in which material is depositing. There are signs of material depositing on either side of the dredged channel (Figure 4.5-7), but there is a high variability of sediment texture. The sediment cores located on the sides contain interbedded coarser

materials. This could indicate that this area locally experiences periods of deposition, switching with periods of increased waves or currents (e.g., during storms, rework, or moved sediment). For example, core LIS1802-27 shows several events.
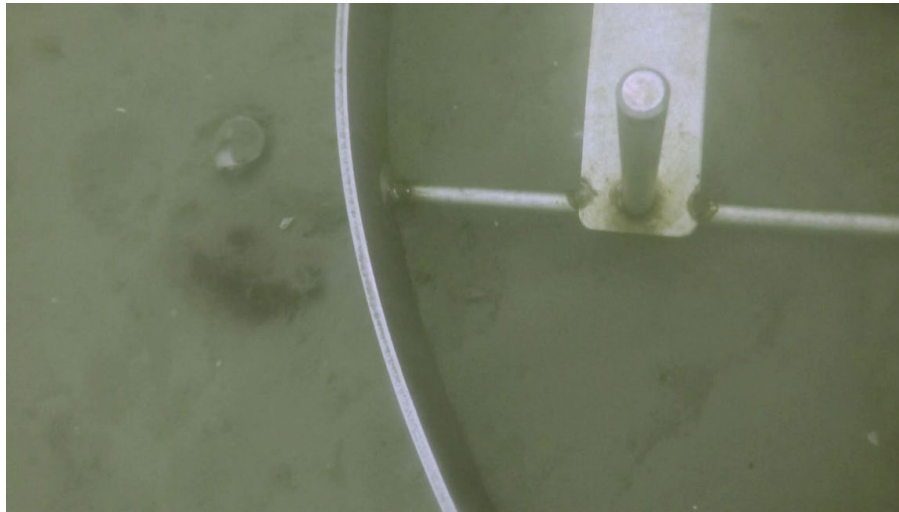
Figure 4.5-7. Example GoPro image of sediment grab station LIS1701-G097 near the mouth of the Thames River showing soft mud indicating a depositional environment

4.5.3.7 Long Sand Shoal / Connecticut River

This area south and west of the mouth of the Connecticut River has a mix of depositional and dynamic areas. Sediment is delivered from the Connecticut River, which has built up a shallow (<3m deep) delta at its mouth. A dredged and protected channel at the western side provides access to the river. Fine grain sediment is likely derived from the river and dispersed mostly to the west and occasionally to the east of the river's mouth. The shallow (<3m) sand bar (Long Sand Shoal) protects the mouth somewhat. This shoal might be a remnant from an older temporary moraine (Old Saybrook Moraine). The long shoal is also likely directing the current flow in this area and created a large sediment wave field (Figure 4.5-8). Wind and wave energy keep sediments from depositing on outcrops. Deposition in some of the embayments might be encouraged by protection due to outcrops.

Figure 4.5-8. Example GoPro image of sediment grab station LIS1802-G299 from sand waves in the Long Shoal area showing fine sands and turbid waters

4.5.3.8 Niantic Bay and River

This area is series of shallower (<10m) embayments along the Connecticut shoreline that are separated by North-South trending outcrops that represent exposed bedrock, probably sculpted by glacial flow and that have not been covered by sediments since (or previous sediments on top of these outcrops have been eroded. Most of these embayments are subject to waves and tidal currents and probably reworked. Some deposition is occurring in the more protected parts inside these embayments. Sediment might come from the Niantic River.

4.5.3.9 Little Narragansett Bay

Shallow embayment at the very eastern edge. Due to the shallow depth, this area was not surveyed for this study.

4.5.3.10 Sediment Energy Environment

The study area is dominated by erosional/non-depositional and dynamic environments. These are all high and moderate/high energy environments. Low/moderate energy environments are found in some of the embayments along the Connecticut shoreline and on the north side of Fishers Island; although, beaches and actual shores are subject to higher wave energy (Figure 4.5-9).
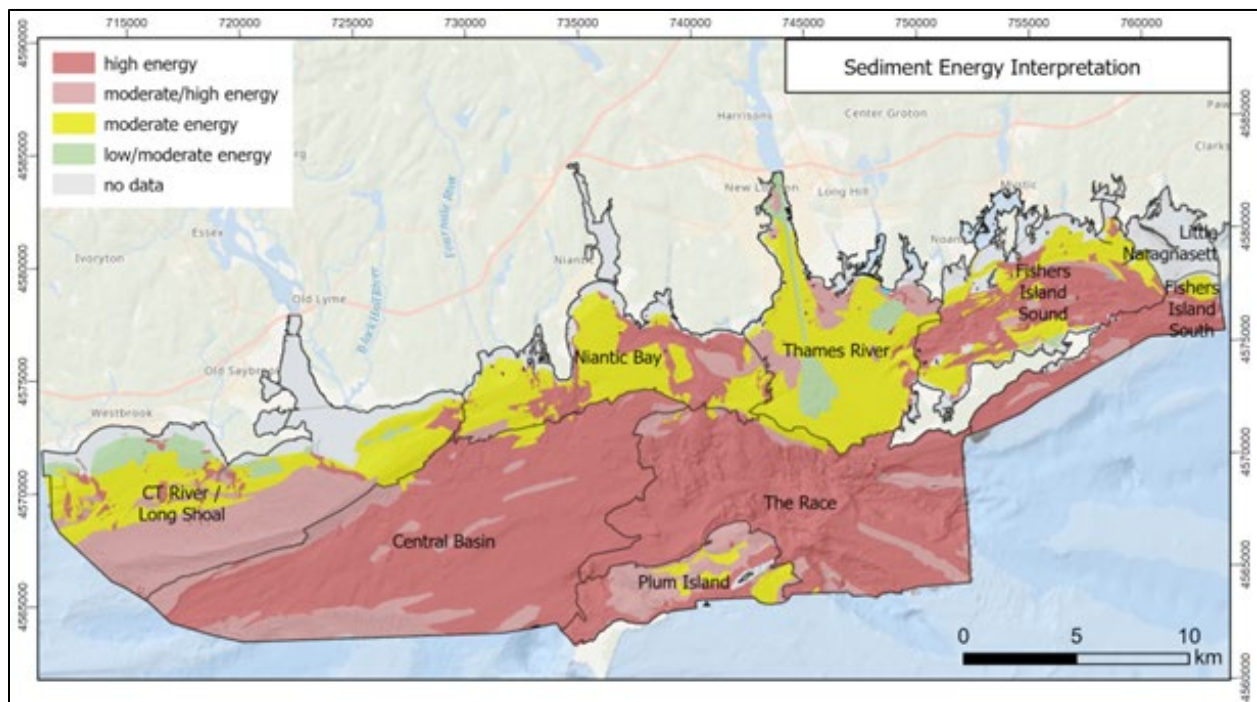
Figure 4.5-9. Map of sediment energy interpretation of the Phase II study area

4.5.4 Comparison with previous sediment environment interpretation

Figure 4.5-10 shows a previous interpretation of sediment environments described in Knebel & Poppe (2000). This description was based on data collected and available in the 1990s, which were less detailed than the data acquired and combined for the Phase II mapping project.

The earlier interpretation only reaches up to the Thames River and did not include the eastern most end of the study area.

Similar to the grain size/sediment texture interpretation, the overall trends are the same in both interpretations. The two interpretations differ in some detailed extent of the different classes. This is likely due to the difference in detail in the available data.
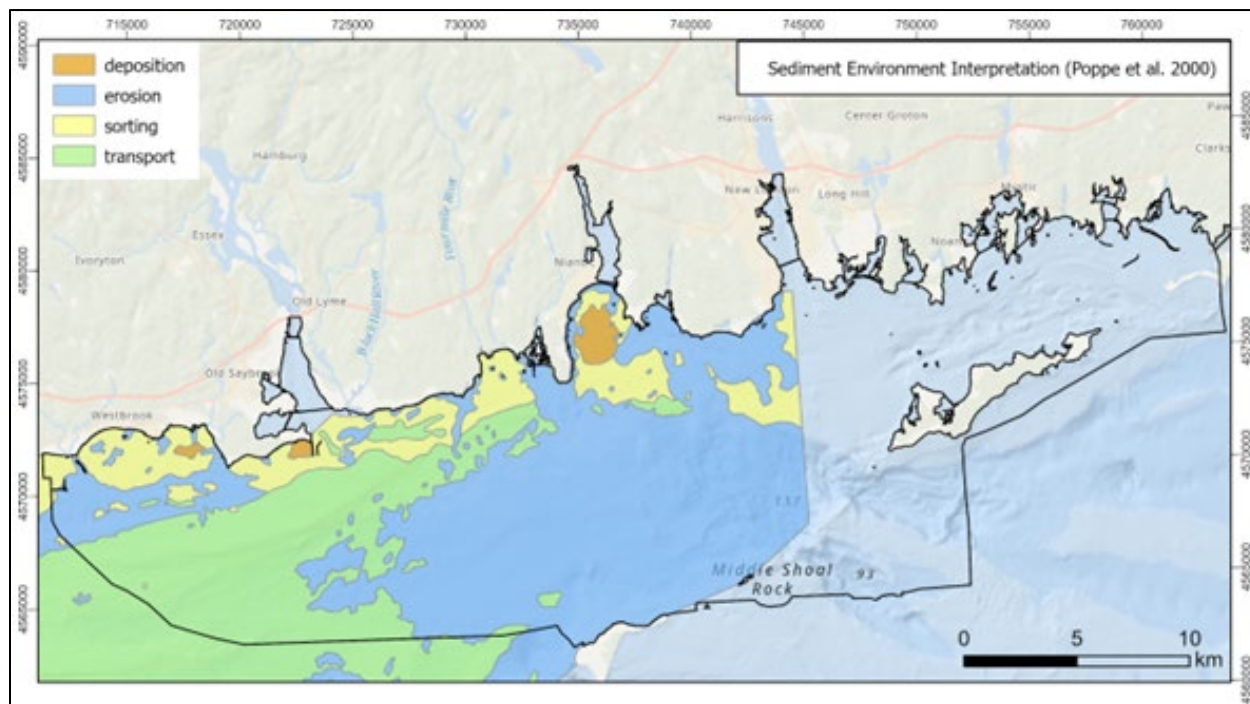
Figure 4.5-10. Map of sediment environment characterization for a portion of the Phase II study area from Knebel and Poppe et al. (2000). The blue-gray background is the hill-shaded bathymetry dataset.

4.6 Summary and Recommendation

Detailed descriptions of the different sediment environments provide insights into dynamic processes that have changed in the past or might impact the area in the future that go beyond the snapshot description of the current surface sediments. A comprehensive interpretation of the sediment environment requires integration of all different available information including detailed bathymetry, backscatter, subbottom, sediment cores, and bottom images. Of these, sediment cores and subbottom data provide this critical direct information of past changes and sub-surface morphology, which otherwise can only be inferred from the surface morphology and texture. Most of the study area is highly dynamic, with large parts subject to strong currents that prevent deposition or cause erosion. The sub-surface morphology and core data (chemistry, physical properties, and sedimentology), document how these environments have changed in the past providing insights into the future. Closer to the northern shore the environments are more variable, where, in addition to currents, sediment delivered from the rivers, the existence of protective bays, and the influence of sediment waves control sediment deposition and movement.

Hard bottom areas, dominated by sand and gravel prevented the acquisition of sediment cores and subbottom data in parts of the Phase II area. However, the sub-surface and sediment core information worked well in other areas with softer sediments near the Connecticut coast where they provided valuable information. For future work planned in the central and western LIS, which is dominated by finer sediment, we expect longer core recovery and deeper subbottom penetration.

This should lead to an improvement in our ability to better characterize the depositional settings through time.

Detailed subbottom information including sediment changes with depth is also critical for future development projects that require accurate subsurface information (e.g., pipelines or cables connecting to offshore windfarms). Subbottom data from the Phase II area have already been shared with the Equinor Corporation for its power cable routing study in support of the Beacon Wind offshore windfarm currently under development. The subbottom and core information is also useful for environmental remediation by providing information about the pollution history.

4.7 References

Knebel, H. J., Signell, R. P., Rendigs, R. R., Poppe, L. J., & List, J. H. (1999). Seafloor environments in the Long Island Sound estuarine system. *Marine Geology, 155*(3-4), 277-318. Retrieved from https://doi.org/10.1016/S0025-3227(98)00129-7

Knebel, H. J., & Poppe, L. J. (2000). Sea-Floor Environments within Long Island Sound: A Regional Overview. *Journal of Coastal Research, 16*(3), 533-550.

Lewis, R. (2014). The Geology of Long Island Sound. In J. S. Latimer, M. A. Tedesco, R. L. Swanson, C. Yarish, P. E. Stacey, & C. Garza (Eds.), *Long Island Sound* (pp. 47-77). New York, NY: Springer.

Poppe, L. J., DiGiacomo-Cohen, M. L., Smith, S. M., Stewart, H. F., & Forfinski, N. A. (2006). Seafloor character and sedimentary processes in eastern Long Island Sound and western Block Island Sound. *Geo-Marine Letters, 26*, 59. Retrieved from https://doi.org/10.1007/s00367-006-0016-4

Poppe, L. J., Knebel, H. J., Mlodzinska, Z. J., Hastings, M. E., & Seekins, B. A. (2000). Distribution of Surficial Sediment in Long Island Sound and Adjacent Waters: Texture and Total Organic Carbon. *Journal of Coastal Research, 16*(3), 567-574.

Signell, R. P., List, J. H., & Farris, A. S. (2000). Bottom Currents and Sediment Transport in Long Island Sound: A Modeling Study. *Journal of Coastal Research, 16*(3), 551-566.

U.S. Geological Survey East-Coast Sediment Texture Database. (2014, December 30). Retrieved from Woods Hole Coastal and Marine Science Center: http://woodshole.er.usgs.gov/project-pages/sediment/

Wentworth, C. K. (1922). A scale of grade and class terms for clastic sediments. *The journal of geology, 30*(5), 377-392.

5 Benthic Habitats and Ecological Processes

Recommended Citations:

Schneeburger, C. & Zajac, R.N. (2023). Seafloor and Habitat Characterization. Section 5.1, p. 114-130 in: "Seafloor Mapping of Long Island Sound – Final Report: Phase II Project."

(Unpublished project report). U. S. Environmental Protection Agency, Long Island Sound Study, Stamford, CT.

Zajac, R.N., Auster, P.J., Conroy, C.N., Walton, O., Schneeberger, C., & Govert, N.M. (2023). Ecological Characterization. Section 5.2, p. 131-293 in: "Seafloor Mapping of Long Island Sound – Final Report: Phase II Project." (Unpublished project report). U. S. Environmental Protection Agency, Long Island Sound Study, Stamford, CT.

5.1 Seafloor and Habitat Characterization

5.1.1 Historical Context

Studies characterizing the geomorphology and sedimentary environments of the seafloor in LIS, as well as benthic ecological studies, have a history going back to the mid-1950s (Zajac, 1998). However, collectively the studies are spatially and temporally disjointed to various degrees, including the area encompassed by the Phase II study area. Early studies of sediment composition indicated that the Phase II study area was primarily comprised of sandy to coarse grained sediments with various mixtures of gravel, and in some shallow depths, small areas that also had sandy silts and clays (Figure 5.1-1). The spatial density, and as such resolution, of the sampling used to develop these initial sedimentary characterizations was low and, thus, provided a spatially coarse understanding of seafloor environments (habitats) in this portion of LIS.

Poppe et al. (2000) compiled data sets from a variety of studies conducted between the 1970s and 1990s and generated a more comprehensive characterization of the sediment distribution in LIS, including the whole of the Phase II study area (Figure 5.1-2). Their surficial sediment texture map revealed a spatially complex distribution of sedimentary patches of varying sizes comprised of primarily sand, gravelly sand, gravel/bedrock and to a lesser extent silty sand. A few patches of sand-silt-clay and sandy silt were identified in some shallow water areas along coasts and in harbors and bays. Poppe et al.'s (2000) map provides a large-scale depiction of the spatial distribution of general sediment /habitat types in the Phase II area. A related study by Knebel & Poppe (2000) showed that the sedimentary environment in the Phase II area is dominated by large areas of erosion or nondeposition and coarse-grained bedload transport (Figure 5.1-3), as well as geomorphological features such as sand wave and boulder fields.
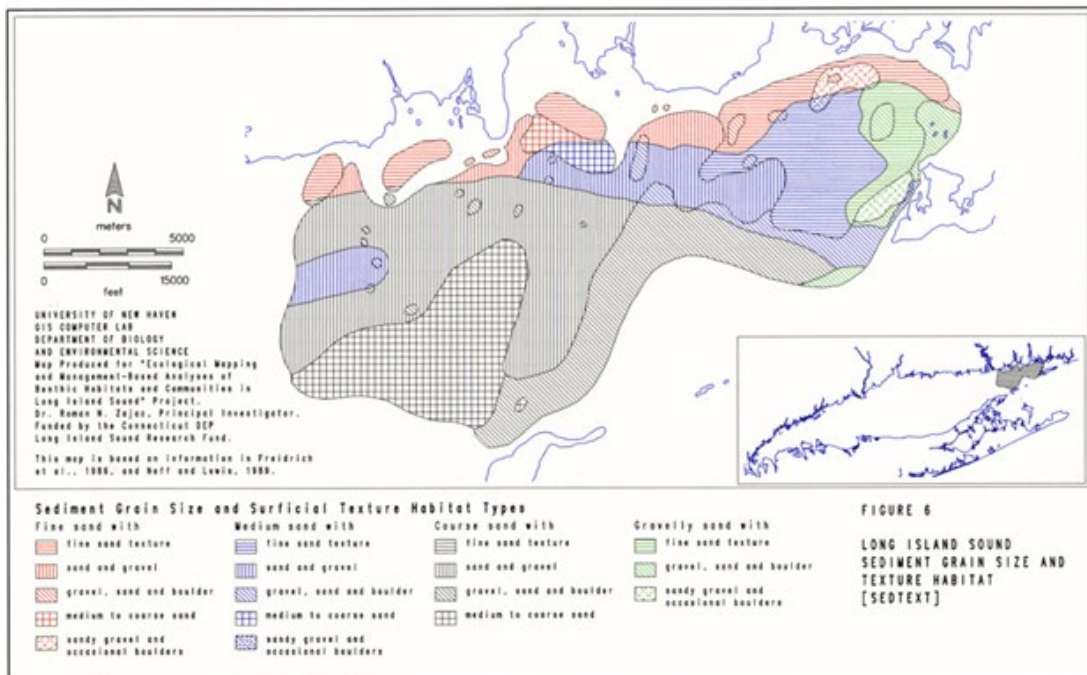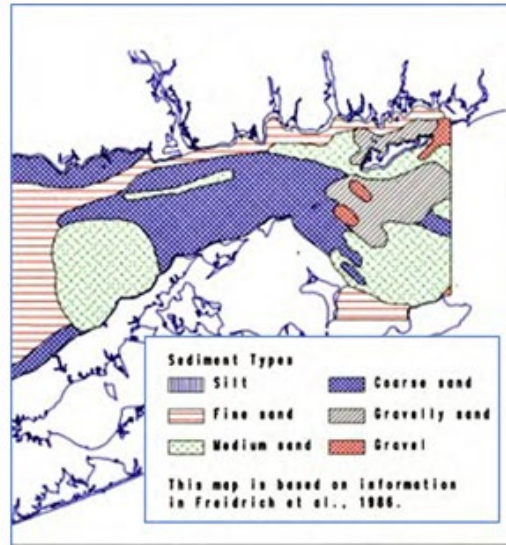
Figure 5.1-1. Examples of early sediment/habitat maps of the Phase II study area. Top: section of map from Freidrich et al. (1986), which reviewed and incorporated information from previous studies to develop a sediment grain-size distribution map. Bottom: Map developed by Zajac (1998) by combining information in Freidrich et al. (1986) and Neff et al. (1988) to delineate sedimentary habitats in ELIS.
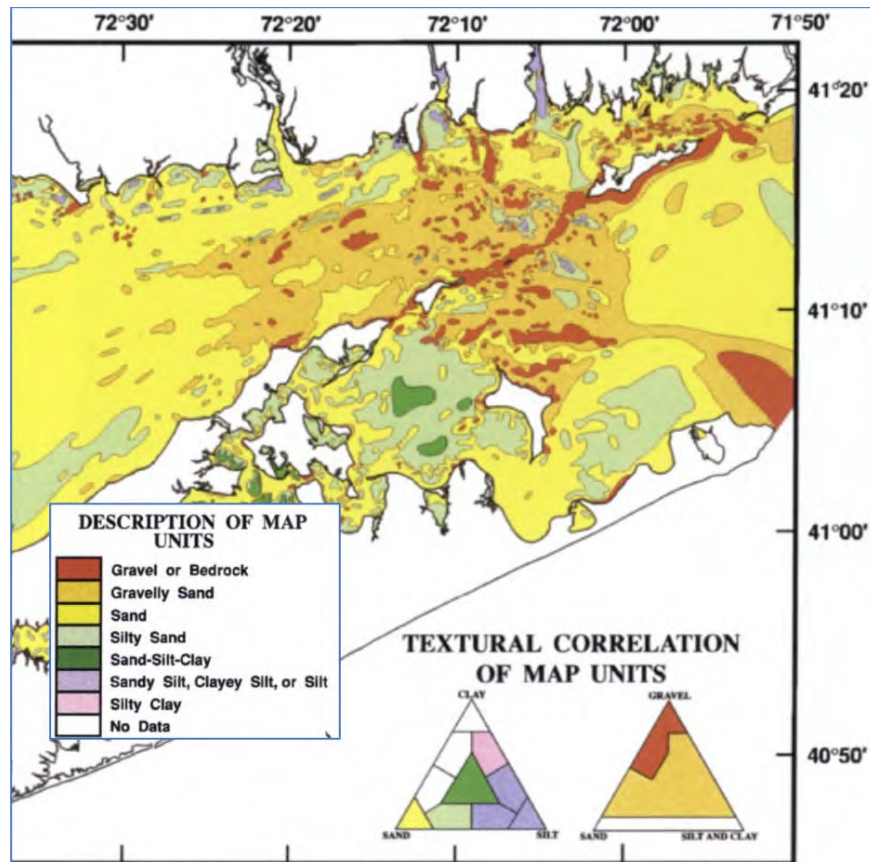
Figure 5.1-2. Portion of sedimentary texture map developed by Poppe et al. (2000) for LIS showing large-scale distribution of sediment types in the Phase II study area
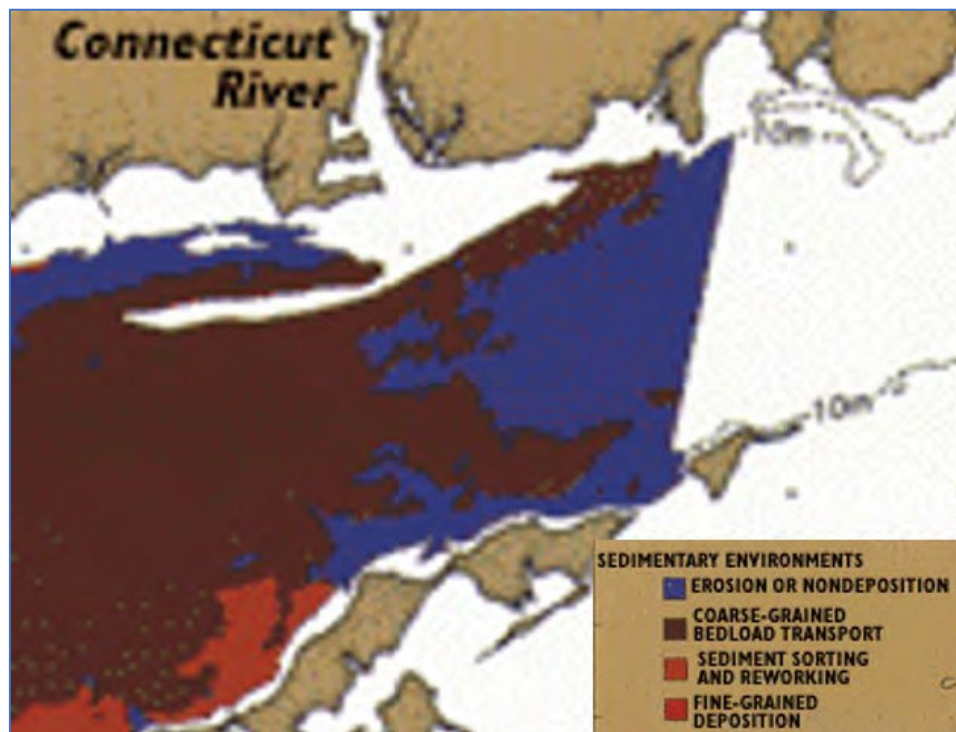
Figure 5.1-3. Sedimentary environments from Knebel & Poppe (2000) in a portion of the Phase II study area

More spatially detailed studies of specific locations in the Phase II area revealed significant complexity to the seafloor landscape (or benthoscape) at smaller scales. For example, Zajac et al. (2000, 2003) studied a 19.4 km^2 area of the seafloor off the mouth of the Thames River and found that within large-scale, general sediment-type patches interpreted from a side scan mosaic image (i.e., acoustic patches) there was significant variation in sediment grain-size composition and biogenic and geomorphologic structural features. There have been several other studies of the seafloor in this region (see for example: https://coastalmap.marine.usgs.gov/regional/contusa/eastcoast/midatl/lis/data.html).   Acoustic patches are seafloor areas that have certain image characteristics (i.e., a specific range of pixel intensities) based on acoustic backscatter data that are related to seafloor properties, such as sediment type and geomorphology, which have been defined through a supervised image classification process.

Based on these previous studies, the Phase II study area is highly dynamic in terms of sedimentary processes, has a complex geomorphology in some areas, and is dominated by primarily sandy and coarser grained sediments. Specific sediment composition and geomorphological characteristics can vary within patches of general sediment types (e.g., those indicated in Figure 5.1-2) and particularly across the many transition zones (e.g., Zajac et al., 2003) from one general sediment type to another that are present in the Phase II area as local physical conditions vary across the region.

5.1.2 Methods

5.1.2.1 Data Sources Used for Seafloor Characterization

Several types of data representing different seafloor characteristics were used to classify and subsequently characterize the seafloor in the study area. These included a multibeam backscatter mosaic (Figure 5.1-4), bathymetry, seafloor rugosity as measured by the Terrain Roughness Index (TRI), maximum physical bottom stress, and sediment grain-size composition. The backscatter and bathymetric data and subsequent mosaic images created from the backscatter were collected by NOAA (Batista et al., 2017). The existing backscatter data was used as the baseline to develop the habitat characterization as the newly acquired backscatter data was not processed and integrated with the existing data in time to expand the footprint of this important baseline mosaic. The spatial resolution of the backscatter was 2 m per pixel. The TRI for the study area was calculated by Conroy (2021 – this report) and the maximum bottom shear stress projections were developed by O'Donnell et al. (2015; see Section 6). Sediment data at each bottom sampling site was obtained and processed by the USGS (Ackerman et al., 2020).

Figure 5.1-4. Acoustic backscatter mosaic of the Phase II study area that was used for seafloor characterization. Darker shades generally represent finer sediments; lighter shades generally represent coarser sediments.

5.1.2.2 Object-oriented Classification

The integrated backscatter mosaic of the seafloor of the Phase II area was analyzed using eCognition Developer 9.4.0 (Trimble, 2019). This software segments the mosaic into meaningful objects (image-objects) of various sizes based on spectral and spatial characteristics (Lucieer, 2008) to perform a multi-segmentation classification to find regions with similar pixel values based on mean pixel brightness. The resulting multiresolution segmentation classification is referred to as acoustic patch types. The multiresolution segmentation criteria for this study were modeled based on previous studies on object-based seafloor image classification conducted by Lucieer (2008). Based on eCognition terminology, the mean brightness is equivalent to the mean intensity value of the backscatter pixels. The algorithm for multiresolution segmentation works by producing image objects based on pixel intensity to produce discrete objects that are homogeneous with respect to spectral characteristics (Drăguţ et al., 2010).The multiresolution segmentation was performed several times with different scale parameter segmentations to produce image objects that best represented the backscatter tones. A scale parameter value restricts the objects from becoming too heterogeneous (Trimble, 2019). A low parameter (near 0) would allow for higher heterogeneity and as the scale parameter increases, heterogeneity decreases. It was determined that a scale parameter of 100 worked best for the backscatter image of the Phase II study area used in this analysis. A homogeneity criterion determines how spatially close the segments will be to one another and is comprised of shape and compactness. Several trials indicated that setting shape/smoothness to 0.9 and compactness to 0.6 were most effective for the backscatter image. The segmentation procedure resulted in an image that differentiated areas with similar pixel properties (Figure 5.1-5).
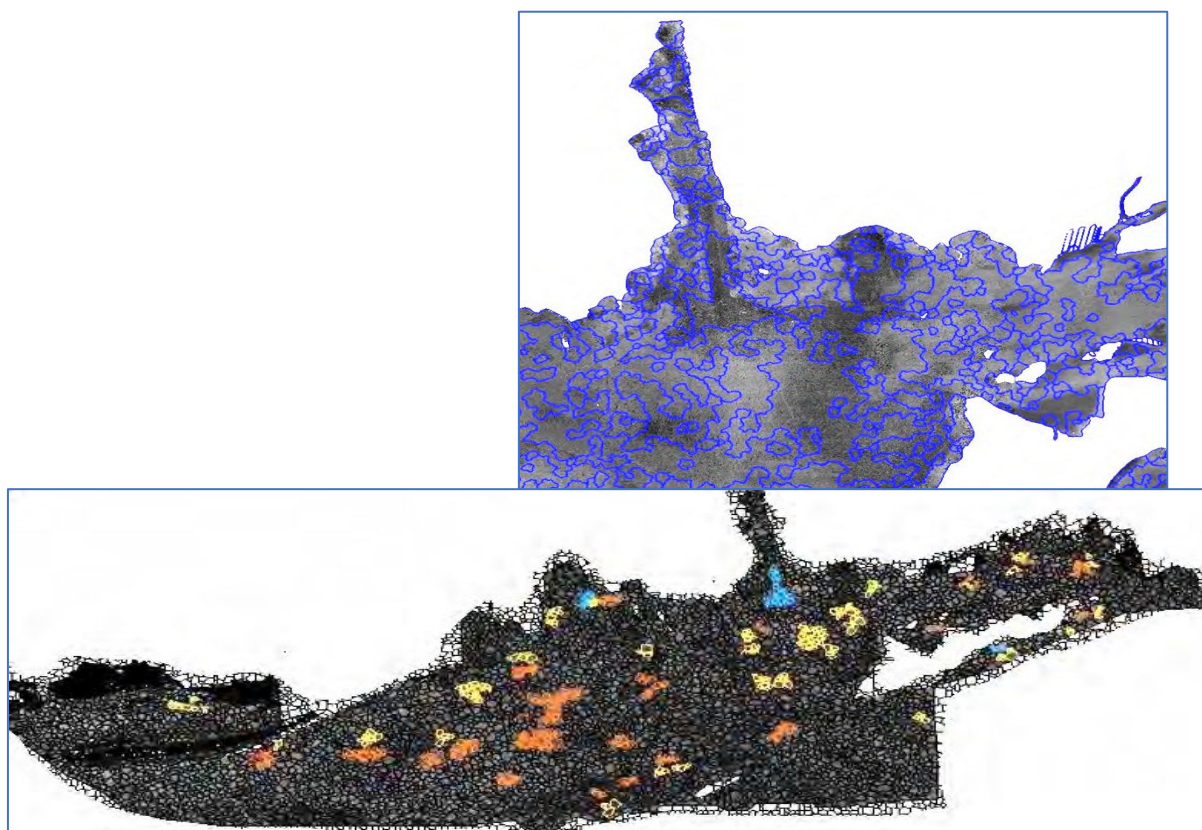
Figure 5.1-5. Examples of image segmentation and class sampling. Top: Results of image segmentation zoomed in around the mouth of the Thames River. Bottom: Sampling different segments to develop classification.

An unsupervised classification was then performed using eCognition by comparing the image objects with the underlying boundaries of pixel tone across the image. Five classes were designated based on general sedimentary groups (gravel, gravelly sediment, sand, silty sand, and sandy silt) used by the USGS for analysis of sediment samples obtained at the Phase II sampling sites (Ackerman et al., 2020). These classes were assigned initial image properties (mean and standard deviation of pixel intensities) by "sampling" visually distinct areas in the segmented backscatter mosaic (Figure 5.1-4). These properties were then adjusted as needed as well as setting nearest neighbor parameters that set how adjacent segments are merged into a specific class based on local homogeneity among neighboring segments and their image properties or identified as being in different classes. The merging procedure produced 2,425 patches based on the image properties of the backscatter mosaic, which are referred to acoustic patches and assigned to the five, initial, sediment-based classes used in the classification/merging procedure. These acoustic patch types were then analyzed to assess their environmental characteristics and used as the basis for habitat identification and ecological characterization.

After the completion of object-oriented classification, the classified image was exported so that it could be integrated into GIS for further analyses. Using GIS, the classified image was imported as a shapefile and the classes assigned by eCognition were symbolized as separate acoustic patch types. The term acoustic patch type is used to underscore that the different types of seafloor patches classified through the segmentation process are based on acoustic imagery. This acoustic patch type data layer was then spatially joined with a file containing the sample points from the 2017 and 2018 surveys and the sediment data from the USGS. Patch analyst (REF) was used to run

spatial statistics and derive acoustic patch metrics (e.g., size and area). Sample points were joined with environmental data layers to extract data for bathymetry, TRI, and bottom shear stress. All GIS analyses were conducted using ArcGIS 10.5.1. The data base was exported form GIS and used for univariate and multivariate statistical analyses using NCSS 11 (NCSS, LLC, 2016) and PRIMER7 (Clarke & Gorley, 2015).

5.1.3 Results

The identified acoustic patches were distributed throughout the Phase II study area (Figure 5.1-6); although, there are some generally geographical trends. The most extensive class is patch Type D, which was designated as gravelly sand (Table 5-1). It is found throughout the study project area, particularly in the central portion where there is a large continuous section of seafloor of this type. There are 411 patches of Type D, accounting for 45.1% of the study area. The second most extensive class is Type C, designated as sand. The largest areas of this patch type are found along the Connecticut coast, south of the Thames River, and along the southern boarders of the project area. Acoustic patch Type C is comprised of 479 patches and makes up 41% of the study area. The three other classes A, B, and E cover smaller portions of the project area making up 0.86%, 11.3%, and 1.7% of the study area, respectively. Types A and E occur as small patches. Type A is classified as sandy silt and found scattered along the northern boundaries and in central areas of the study area. Type B is designated as silty sand and found in the western section of the project study area and primarily along the coasts of Connecticut, Fishers Island, and Long Island. Type E is classified as sandy gravel, and patches are primarily found in the west central portion of the Phase II study area.
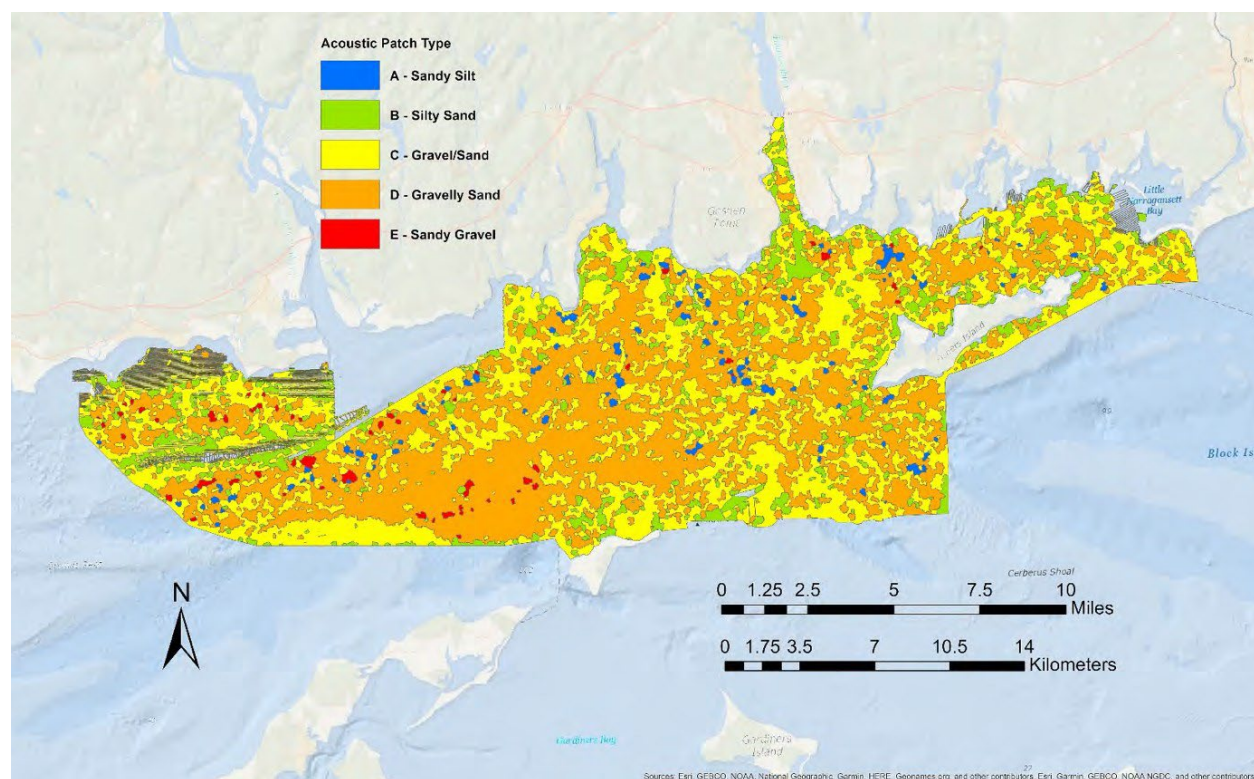
Figure 5.1-6. Acoustic patch types in the Phase II study area

Table 5-1. General characteristics of acoustic patch types identified in the Phase II study area. The number of samples from which sediment data is available is given as well as general sediment composition (% by weight) as determined by Ackerman et al. (2020); G = gravel, S= sand, Si = silt, C = clay. Ranges of depth, maximum tidal stress and TRI based on data extracted from these data layers in GIS at the point locations of sediment samples and photographic images.

	Patch Type A	Patch Type B	Patch Type C	Patch Type D	Patch Type E
Total Area (ha) (% of total area)	780 (1.7%)	5,160.3 (11.3%)	18,650.1 (41%)	20,527 (45.1%)	391.7 (0.86%)
# Sediment Samples	1	15	71	81	1
Sediment class composition Mean % ± 1SE	G: 0.0 S: 35.3 Si: 45.5 C: 19.1	G: 6.6 ± 3.0 S: 82.3 ± 3.6 Si: 8.5 ± 2.5 C: 2.7 ± 0.8	G: 6.4 ± 1.4 S: 88.7 ± 1.6 Si: 3.5 ± 0.7 C: 1.3 ± 0.3	G: 19.9 ± 1.6 S: 75.4 ± 1.8 Si: 3.2 ± 0.7 C: 1.6 ± 0.6	G: 38.4 S: 61.1 Si: 0.4 C: 0.1
Depth Range (m)	8.9 - 9.1	4.95 - 86.8	5.39 - 95.01	6.0 - 89.48	30.54 - 48.0
Tidal Max Stress (Pascal) Range	0.451-0.461	0.191-2.685	0.221-2.052	0.214 - 1.864	0.938 - 0.997
TRI	0.013 -0.141	0.002 – 1.867	0.191 - 2.685	0.003 - 1.662	0.024 - 0.093

Although there were some broad geographical differences in spatial distribution of the acoustic patch types, the fact that each of the types were generally found in all areas of the Phase II study area suggest that the environmental factors that determine their specific characteristics are complex and interrelated. Over 85% of the Phase II study area is comprised of sandy sediment, and each acoustic patch type, except Type A, is characterized by over 65% sands by weight (Figure 5.1-7). Using a finer delineation of sediment grain- sizes based on a Phi scale, the acoustic patch types have different sediment compositions (Figure 5.1-8). Acoustic patch type A has the highest fraction of smaller grain sizes, dominated by silts and clays. Acoustic patch types B, C, D, and E were dominated by sands, but have increasingly greater proportions of coarser grained sands and gravelly sediments, respectively. Patch types B, C, and D had small amounts of silts and clays, whereas acoustic patch type E had almost no fine-grained sediments, but had the most gravel. Based on the sediment grain-size composition, the ND samples (which were not within the backscatter mosaic image area) are likely intermediate between patch type A and B, which is in line with these patch types being generally located in shallower waters (Figure 5.1-6 & Figure 5.1-9).

Patch types C, D, and E were found in increasingly deeper waters, although there was great variation in depth for these patch types. Terrain roughness was relatively low for patch types A, E, and the ND sample sites, and higher for types B, C, and D (Figure 5.1-10). Most notable, was the high variation in TRI for patch Types B, C, and D, indicating that for each of these patch types there are areas that have relatively large variations in local geomorphology, such as sand waves of different sizes and/or boulder fields. Maximum seabed stress increased in patch types A to C, respectively, and is highest in patch types D and E (Figure 5.1-11). As with TRI, bed stress is highly variable in patch types B, C, and D.
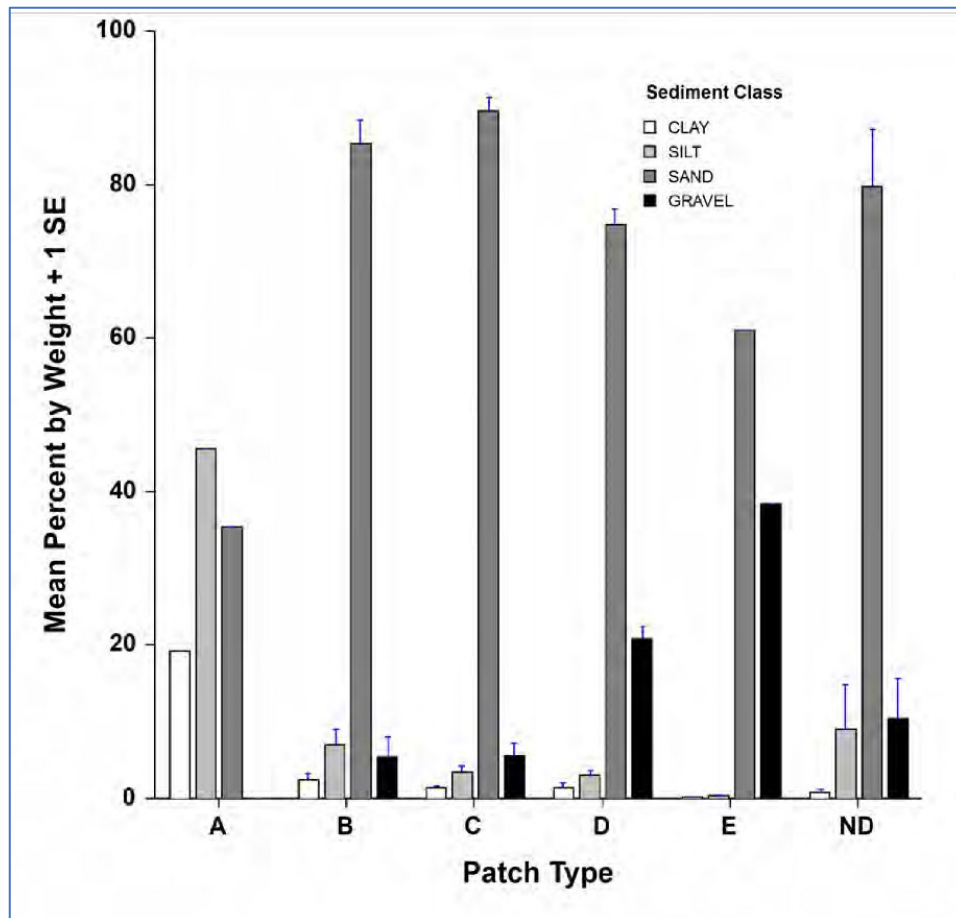
Figure 5.1-7. Mean percent composition (+1 standard error) of different sediment grain-size classes based on USGS classification (see Section 3.2)
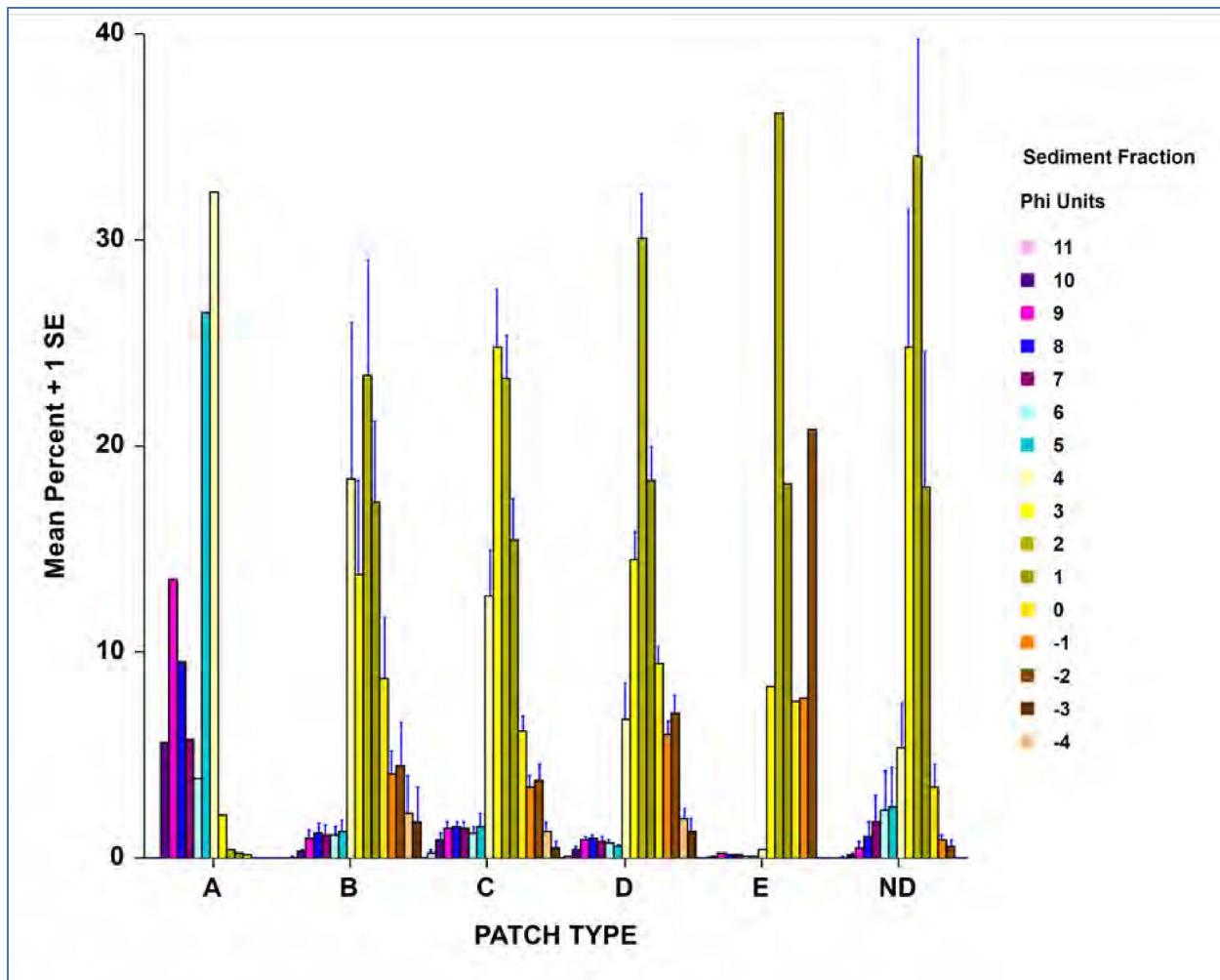
Figure 5.1-8. Sediment grain-size composition in the Acoustic Patch Types identified in the Phase II study area. ND = Not Determined (i.e., sites that were not in the backscatter mosaic image used to classify the patch types). Phi units range: clays, 11 to 8; silts, 8 to 4; sands, 4 to -1; gravels, -1 to -4. Lower phi values in each group indicate coarser sediments in that group. Sediment data was provided by the USGS (Section 3.2).
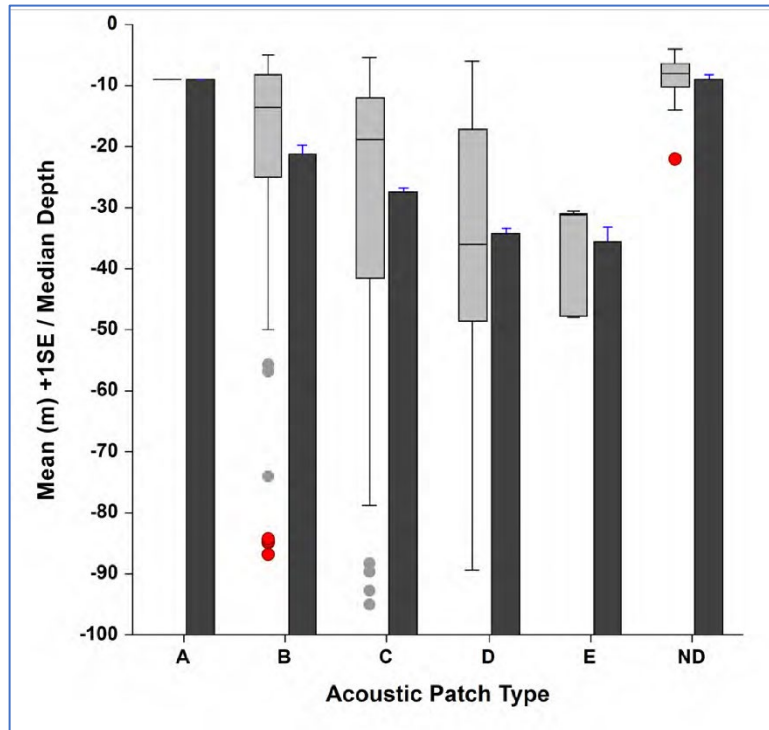
Figure 5.1-9. Depth characteristics of the acoustic patch types identified in the Phase II study area. ND = Not Determined (i.e., sites that were not in the backscatter mosaic image used to classify the patch types). Shown are the mean depth (+1 standard error, SE) and box plots showing the median (median ± 1.57 × (IQR) / √n), the inter-quartile range (IRQ) defined by the upper (75th percentile) and lower 25th percentile ends of the box, whiskers extending to 1.5 * IRQ. Outliers are shown as dots.
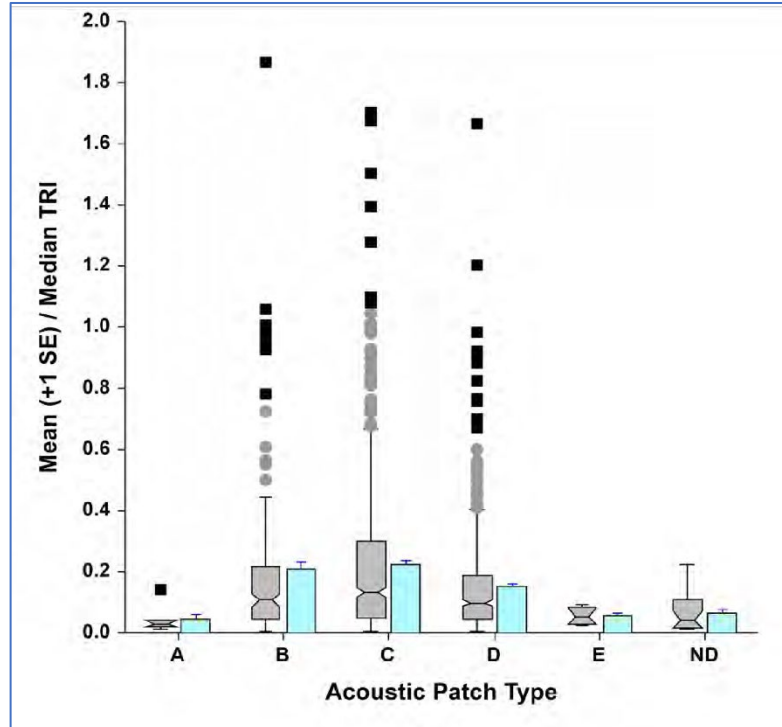
Figure 5.1-10. TRI characteristics of the acoustic patch types identified in the Phase II study area. ND = Not Determined (i.e., sites that were not in the backscatter mosaic image used to classify the patch types). Shown are the mean depth (+1 standard error, SE) and box plots showing the notched median (median ± 1.57 × (IQR) / √n), the interquartile range (IRQ) defined by the upper (75th percentile) and lower 25th percentile ends of the box, whiskers extending to 1.5 * IRQ. Outliers are shown as dots.
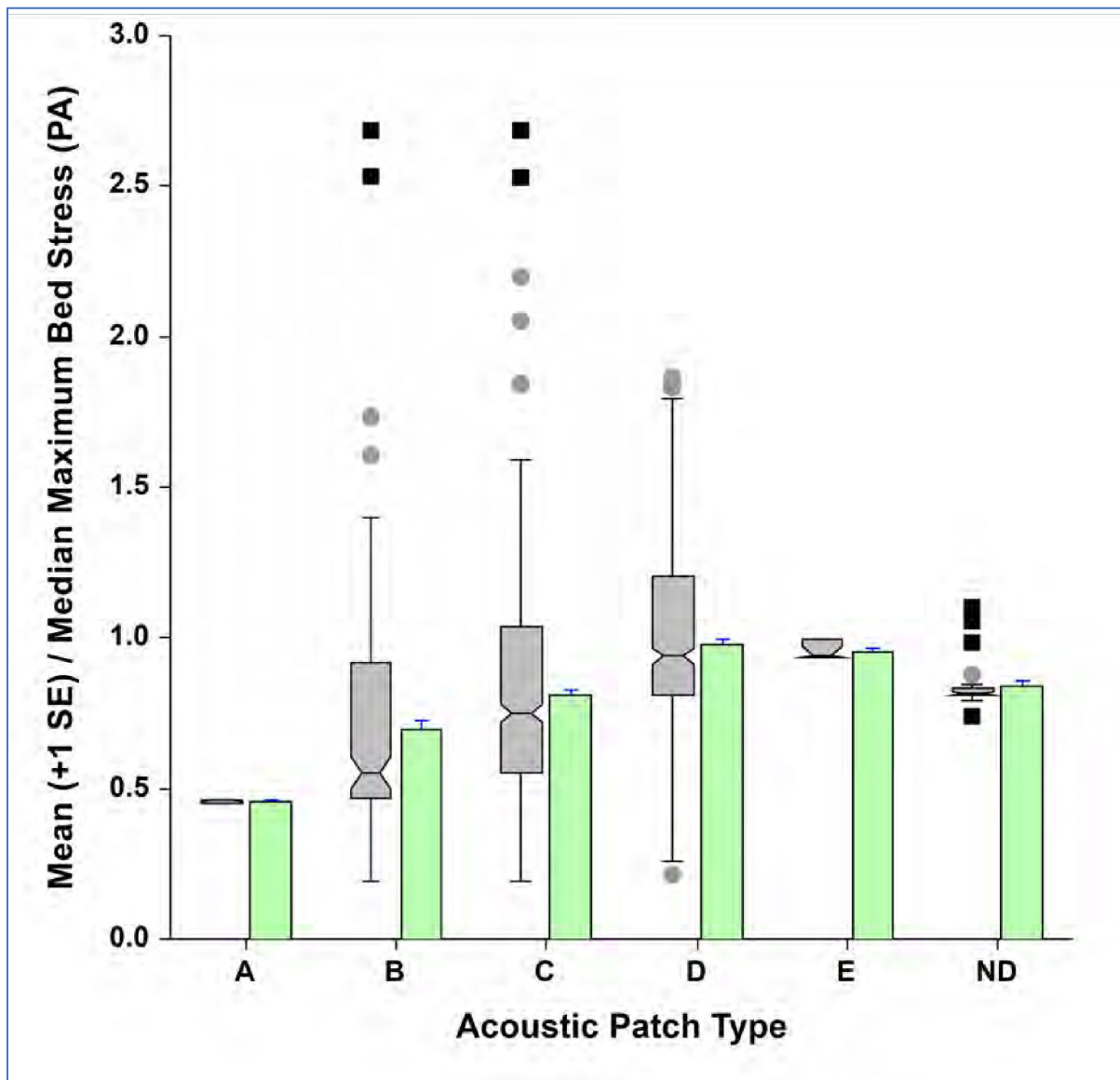
*Figure 5.1-11. Maximum bed stress (PA=Pascals) characteristics of the acoustic patch types identified in the Phase II study area. ND = Not Determined (i.e., sites that were not in the backscatter mosaic image used to classify the patch types). Shown are the mean depth (+1 standard error, SE) and box plots showing the notched median (median ± 1.57 × (IQR) / √n), the interquartile range (IRQ) defined by the upper (75th percentile) and lower 25th percentile ends of the box, whiskers extending to 1.5 * IRQ. Outliers are shown as dots.*

Although the acoustic patch types are similar in that they are dominated by sandy sediments, multivariate analyses indicate that based on all the environmental variables considered jointly there are statistically significant differences with respect to their overall characteristics (Table 5-2). Pair-wise comparisons indicate that differences among patch Types A and B were marginally significant, and significant differences exist among patch Types C and D, C and A, D and ND, and D and A. Principal Components Analysis (PCA) ordination indicated that there was relatively high variability (dispersion) within patch Types B and C and that most patch Type D samples were located closer together in the ordination space (Figure 5.1-12). Many of the Type C samples were

separated from the other patch types due to being located in shallower depths and also containing higher proportions of sediments in the Phi 3 and 4 size-classes.

Most of the patch type D sites were separated due to being in deeper waters and having coarser grain sizes and increasing maximum seabed stress. The gradient in sedimentary differences and in the other environmental factors can be seen in the results of a Canonical analysis of principal coordinates (CAP) analysis (Figure 5.1-13). The ND and C patch types give way to patch Type D along the CAP2 axis, along a gradient from shallower depths and finer grain sizes to coarser grain sizes and to some extent increases in seabed stress and TRI.

Table 5-2. Results of PERMANOVA analysis of differences among acoustic patch types relative to environmental factors (depth, TRI, maximum tidal stress, and sedimentary phi classes). Data were normalized prior to generating a resemblance matrix using Euclidian distance. The analysis used a Type III (partial) sums of squares; fixed effects summed to zero for mixed terms; and 999 permutations of raw data.

PERMANOVA Results:

Source	df	SS	MS	Unique Pseudo-F	P(perm)
Patch Type	5	236.18	47.236	2.7603	0.003
Res	153	2618.2	17.113		
Total	158	2854.4			

Pair-wise tests (significant pairs are highlighted):

Groups	t	P(perm)
B, C	0.744	0.815
B, D	1.241	0.127
B, ND	1.072	0.290
B, E	0.664	0.745
B, A	1.958	0.062
C, D	1.931	0.001
C, ND	1.221	0.169
C, E	0.794	0.617
C, A	2.405	0.034
D, ND	1.930	0.004
D, E	0.652	0.738
D, A	2.971	0.018
ND, E	0.887	0.192
ND, A	2.241	0.190
E, A	No test	
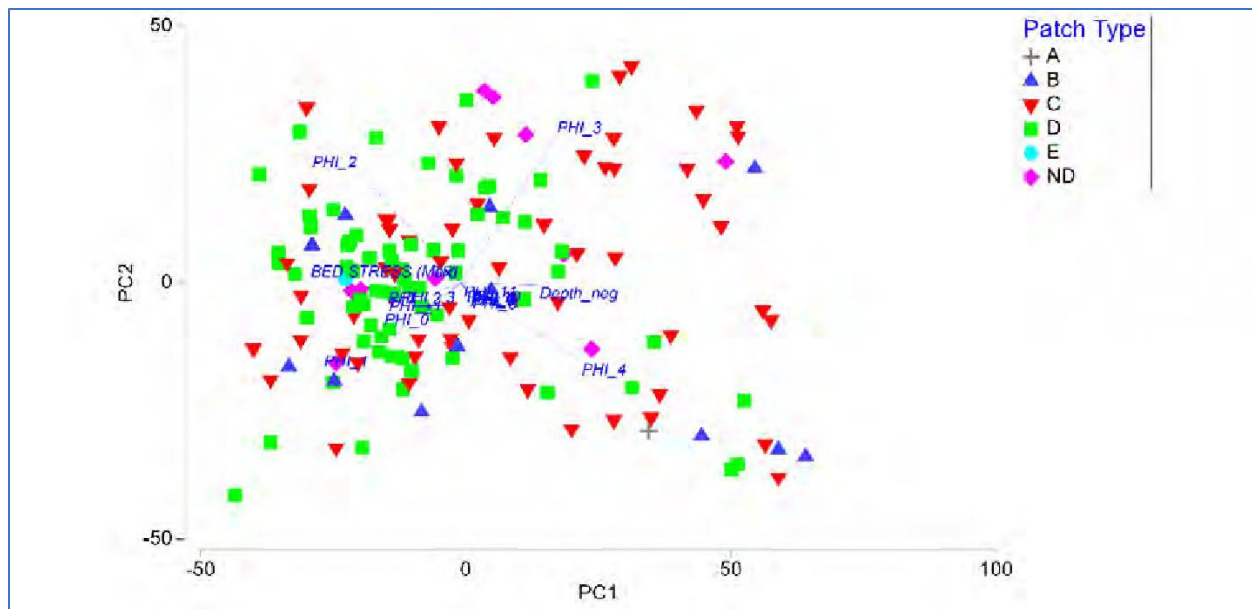
Figure 5.1-12. PCA of sample sites in different acoustic patch types using sediment phi sizes, depth, maximum bed stress, and TRI as variables. Vectors indicate the direction of separation of the sample sites due to the variables. Principal component axes 1 (PC1) and 2 (PC2) account 59.4 % of the total variation in the data.
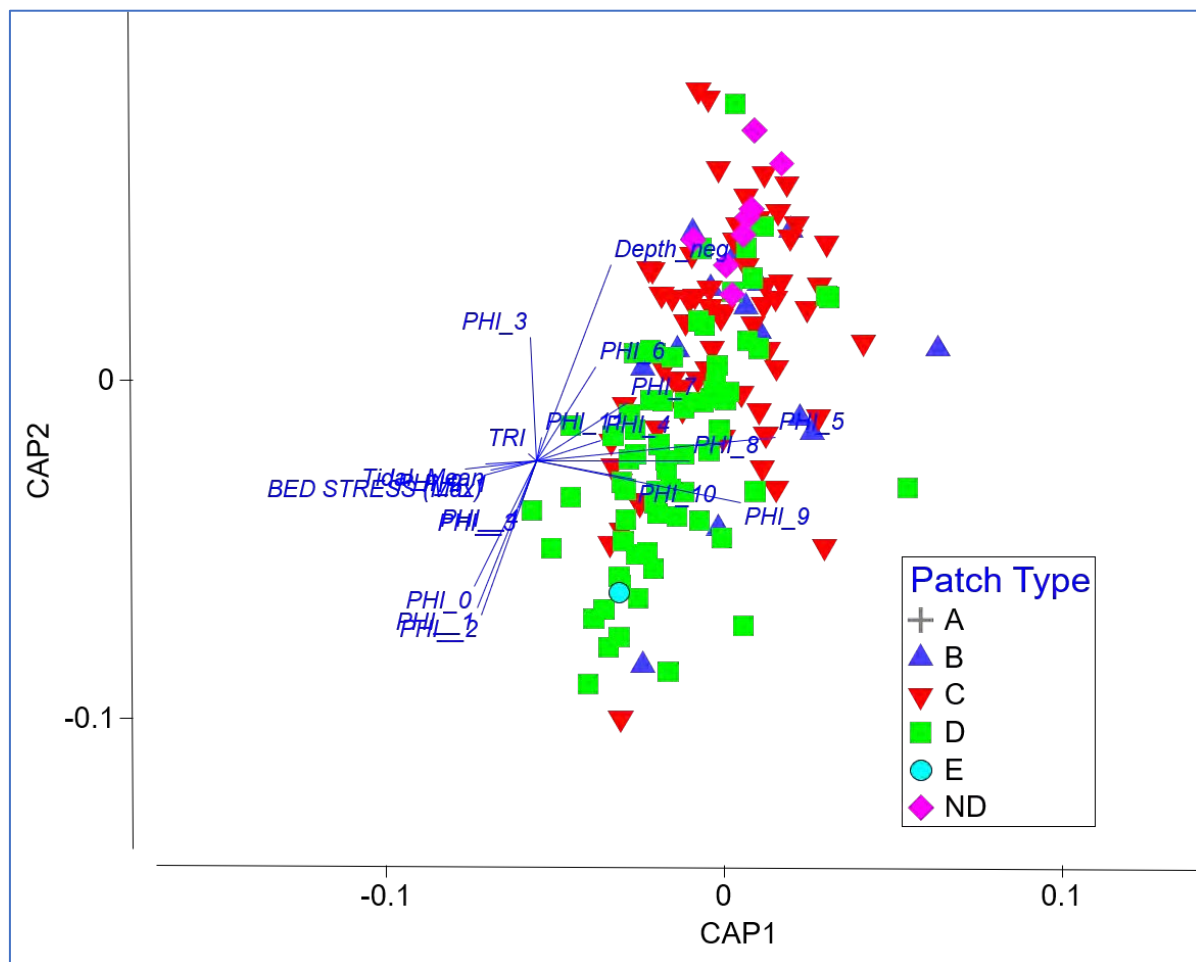
Figure 5.1-13. CAP Results to discriminate among acoustic patch types

5.1.4   Discussion

Although sandy and gravelly sediments dominate 4 of the 5 acoustic patch types, there are distinct differences in the fine-scale composition of sediments in each acoustic patch type, representing a gradient from fine sands and silts to sand to sand/gravel from acoustic patch type A to E, respectively. The distribution of the patch types is spatially complex throughout most of the Phase II study area; however, some broader trends do emerge that are similar to previous mappings of sediment distributions in this portion of LIS. Both the sediment texture map (Figure 5.1-2) and the acoustic patch type map (Figure 5.1-6) indicate finer sediments along the Connecticut shore, as well as closer inshore to Fishers Island, and to the north of Plum and Great Gull Islands. Both characterizations indicate a large area of gravelly sand in the central portion Phase II study area, extending from south of the Connecticut River to roughly South of Goshen Point, as well as in the central portions of FIS. Likewise, both characterizations indicate a complex spatial distribution of patch types running north to south from the Connecticut shore to the area of the Race.

Likewise, both characterizations indicate a complex spatial distribution of patch types running north to south from the Connecticut shore to the area of the Race. One noticeable difference is that the sediment texture map (Figure 5.1-2) indicates a large band of bedrock/gravel extending from Plum Island to all along the southern shore of Fishers Island. The acoustic patch type characterization (Figure 5.1-6) identifies these areas primarily as gravelly sand and a mix of gravel/sand and silty sand, particularly up against the Fishers Island south shore. This difference is likely due to extrapolations that were done for the sediment texture map and also the inability to collect samples in boulder areas using the sampling equipment for this project. There are boulder areas at a few of our sampling locations but these were not considered within the overall characterization, which was based solely on sediment composition, depth, maximum seabed stress, and topographic roughness. Increasing topographic roughness in patch types C, D and E indicate the presence of larger geomorphological features such as bedrock and boulder fields, as well as sand waves, in these patch types. For example, there are a number of relatively large sand wave fields in the Phase II area, particularly in the western portion (Figure 5.1-14). These sand wave fields increase TRI significantly in these areas and are primarily associated with acoustic patch types C and D, particularly the large field located along the southwest edge of the Phase II study area, which is almost entirely patch Type C.

The seafloor of the Phase II study area as represented by the acoustic patch types provides a framework for identifying benthic habitats and their spatial variation in this portion of LIS. The acoustic patches were identified using the image information in the acoustic backscatter data collected during multibeam surveys, and how that image data was compiled into the overall mosaic (Figure 5.1-4). The initial classification of bottom types was based on tonal differences in the backscatter mosaic. There are tonal differences across the mosaic that are not related to specific bottom type (e.g., in general, darker tones being finer sediments and letter tones being coarser sediments) due to striping where individual data segments were combined, shadowing, and also differences based on when the data was collected. In the segmentation process, differences in image tone across the mosaic may lead potential misclassification of certain areas in terms of one acoustic patch type or another. However, given the fact that much of the area is dominated by sandy sediments, the segmentation and delineation of acoustic patch types did differentiate among areas that had differing compositions of sand and gravel grain sizes. Additional analyses (not provided in this report) indicate that the sediment grain-size composition of each acoustic patch

type was fairly consistent from east to west in the study area. The acoustic patch types thus represent general habitat areas that have certain environmental characteristics with regard to sediment grain size composition, topographic roughness, and maximum hydrodynamic stresses on the seafloor. These characteristics are potential determinants of the kinds of infaunal and epifaunal communities that may be found within the acoustic patch types. However, other environmental and ecological factors can shape the ecological communities that may be present in the acoustic patch types. A more specific discussion of the link between the acoustic patch types and their ecological characteristics is provided in Section 5.2.6.
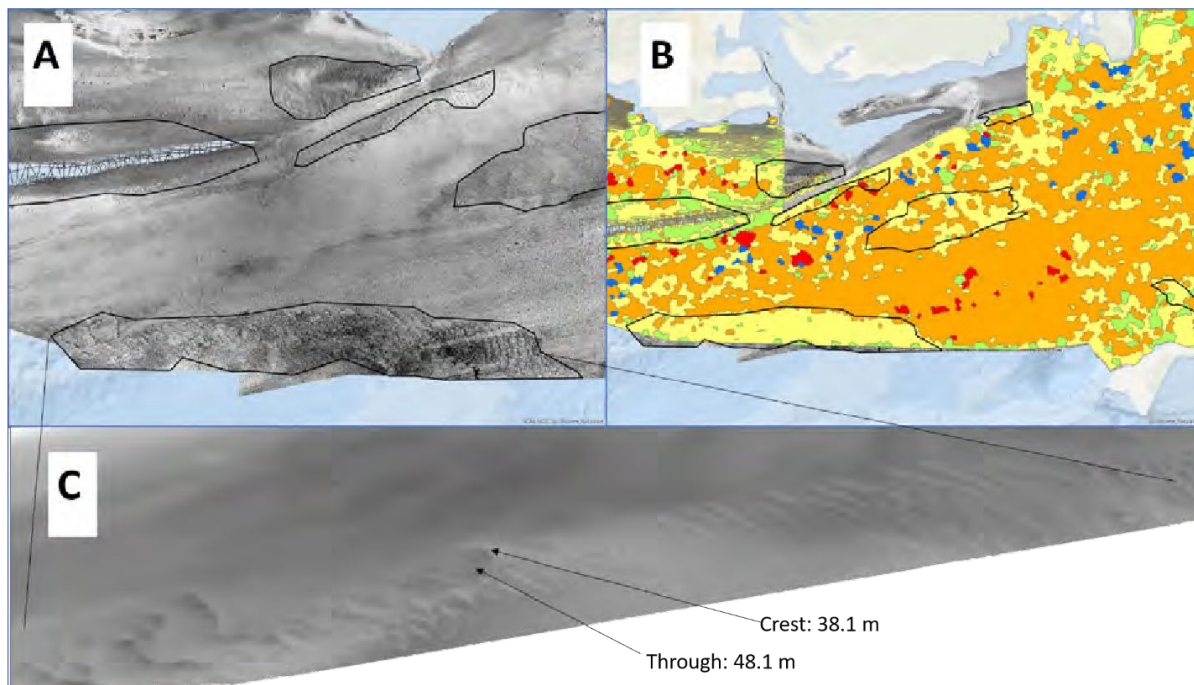
Figure 5.1-14. A: Location of several sand wave fields in the western portion of the Phase II study area. B: Areas of sand wave fields superimposed over acoustic patch types distribution (see Figure 5.1-6 for key for patch types. C: 3-D close-up of sand wave along the south-western edge of the Phase II study area; values represent depths at a representative crest and through within the sand wave field.

5.1.5 References

Ackerman, S. D., Huntley, E. C., Blackwood, D. S., Babb, I. G., Zajac, R. N., Conroy, C. W., . . . Walton, O. L. (2020). *Sea-floor sediment and imagery data collected in Long Island Sound, Connecticut and New York, 2017 and 2018.* (U.S. Geological Survey data release) Retrieved from USGS ScienceBase: https://doi.org/10.5066/P9GK29NM

Battista, T. W., Sautter, W., & Husted, R. (2017). *Bathymetry, acoustic backscatter, and LiDAR data collected in Long Island Sound for the Phase II Long Island Sound Seafloor Mapping Project (NCEI Accession 0167531).* NOAA, National Centers for Environmental Information: http://www.ncei.noaa.gov/access/metadata/landing-page/bin/iso?id=gov.noaa.nodc%3A167531

Clarke, K. R., & Gorley, R. N. (2015). PRIMER v7: User Manual/Tutorial. Plymouth: PRIMER-E.

Drăguţ, L., Tiede, D., & Levick, S. (2010). ESP: a tool to estimate scale parameter for multiresolution image segmentation of remotely sensed data. *International Journal of Geographical Information Science, 24*(6), 859-871.

Freidrich, N. E., McMaster, R. L., Thomas, H. F., & Lewis, R. S. (1986). *Non-energy Resources: Connecticut and Rhode Island Coastal Waters.* U.S. Deptartment of Interior, Minerals Management Service Cooperative Agreement No. 14-12-0001-30115. Final Report FY 1984.

Knebel, H. J., & Poppe, L. J. (2000). Sea-Floor Environments within Long Island Sound: A Regional Overview. *Journal of Coastal Research, 16*(3), 533-550.

Lucieer, V. L. (2008). Object-oriented classification of sidescan sonar data for mapping benthic marine habitats. *International Journal of Remote Sensing, 29*(3), 905-921.

NCSS, LLC. (2016). NCSS 11 Statistical Software. Kaysville, UT, USA. Retrieved from https://ncss.com/software/ncss

Neff, N. F., McMaster, R. L., Lewis, R. S., & Thomas, H. F. (1988). *Non-energy resources: Connecticut and Rhode Island coastal waters.* U.S. Department of Interior, Minerals Management Service Cooperative Agreement No. 14-12-0001-30316. Final Report FY 1986.

Poppe, L. J., Knebel, H. J., Mlodzinska, Z. J., Hastings, M. E., & Seekins, B. A. (2000). Distribution of surficial sediment in Long Island Sound and adjacent waters: texture and total organic carbon. *Journal of Coastal Research*, 567-574.

Trimble. (2019). eCognition Developer 9.4.0. https://geospatial.trimble.com/products-and-solutions/ecognition

Zajac, R. N. (1998). A review of research on benthic communities conducted in Long Island Sound and an assessment of structure and dynamics. In L. J. Poppe, & C. Polloni (Eds.), *Long Island Sound Environmental Studies.*
Retrieved from https://pubs.usgs.gov/of/1998/of98-502/chapt4/rz1cont.htm

Zajac, R. N., Lewis, R. S., Poppe, L. J., Twichell, D. C., Vozarik, J., & DiGiacomo-Cohen, M. L. (2000). Relationships among sea-floor structure and benthic communities in Long Island Sound at regional and benthoscape scales. *Journal of Coastal Research*, 627-640.

Zajac, R. N., Lewis, R. S., Poppe, L. J., Twichell, D. C., Vozarik, J., & DiGiacomo-Cohen, M. L. (2003). Responses of infaunal populations to benthoscape structure and the potential importance of transition zones. *Limnology and Oceanography, 48*, 829-842.

5.2   Ecological Characterization

5.2.1 Objectives and Historical Context

The main focus of this portion of the Phase II LIS mapping project was to identify, characterize, and map the benthic habitats that comprise the study area and the infaunal and epifaunal communities found in these seafloor habitats at multiple spatial scales. Based on these efforts, information on ecologically significant locations in the Phase II study area can be identified, and the information can be used for a variety of marine spatial management efforts, as well as for assessing how the ecological communities and habitats might be affected by future impacts.

Maps depicting seafloor habitats and their ecological communities are critical for many environmental management, conservation, and research activities, and for the growing focus on coastal and marine spatial planning. Such maps depict either separately or in combination the spatial distribution and extent of benthic habitats classified based on physical, geological, geomorphological, and biological attributes and the benthic communities that reside in the mapped habitats. Additionally, maps can be produced that depict ecological processes across the seafloor. These results and products add to the overall LIS Cable Fund Seafloor Habitat Mapping project and continue to increase our understanding of LIS and FIS in a geospatial context.

5.2.1.1 Infaunal Communities

Studies of the benthic infaunal ecology in the Phase II area have included both Sound-wide surveys that extended into portions of ELIS and FIS, and studies within specific locations. One-time surveys in the mid and late 1970s provided data that helped establish trends in general community composition, diversity and relationships to habitat features (sediment type, depth, see Zajac, 1998, Zajac et al., 2000). In some cases, the spatial resolution was relatively coarse; in another survey (Pellegrino & Hubbard, 1983) the spatial resolution was high but only CT waters were sampled. In the early 1990s and then in the early 2000s a series of benthic samples were taken in LIS in support of the EPA Environmental Monitoring and Assessment Program (EMAP) and National Coastal Assessment (NCA) programs, respectively. A few of the sample sites were located in the Phase II study area. Some of the general trends that emerge from these studies is that infaunal taxonomic richness generally increases from west to east in the area, ranging from 21 to 60 taxa 0.25 m^{-2}, and that community structure changes as well in the same direction (Figure 5.2-1 & Table 5-3). Relatively distinct communities were located just south of the Connecticut River, in deeper waters between the Connecticut River and the mouth of the Thames River, at the mouth of the Thames River, and in FIS. Zajac et al. (2003) found smaller scale variation in community types within specific patches of different sediment types and that taxonomic richness could be elevated across transition zones among different sediment types/habitat types. Specific comparisons of taxonomic and community composition between these previous studies and the results from this Phase II project are represented in the discussion of the infaunal community characterization section of this report (Section 5.2.2).
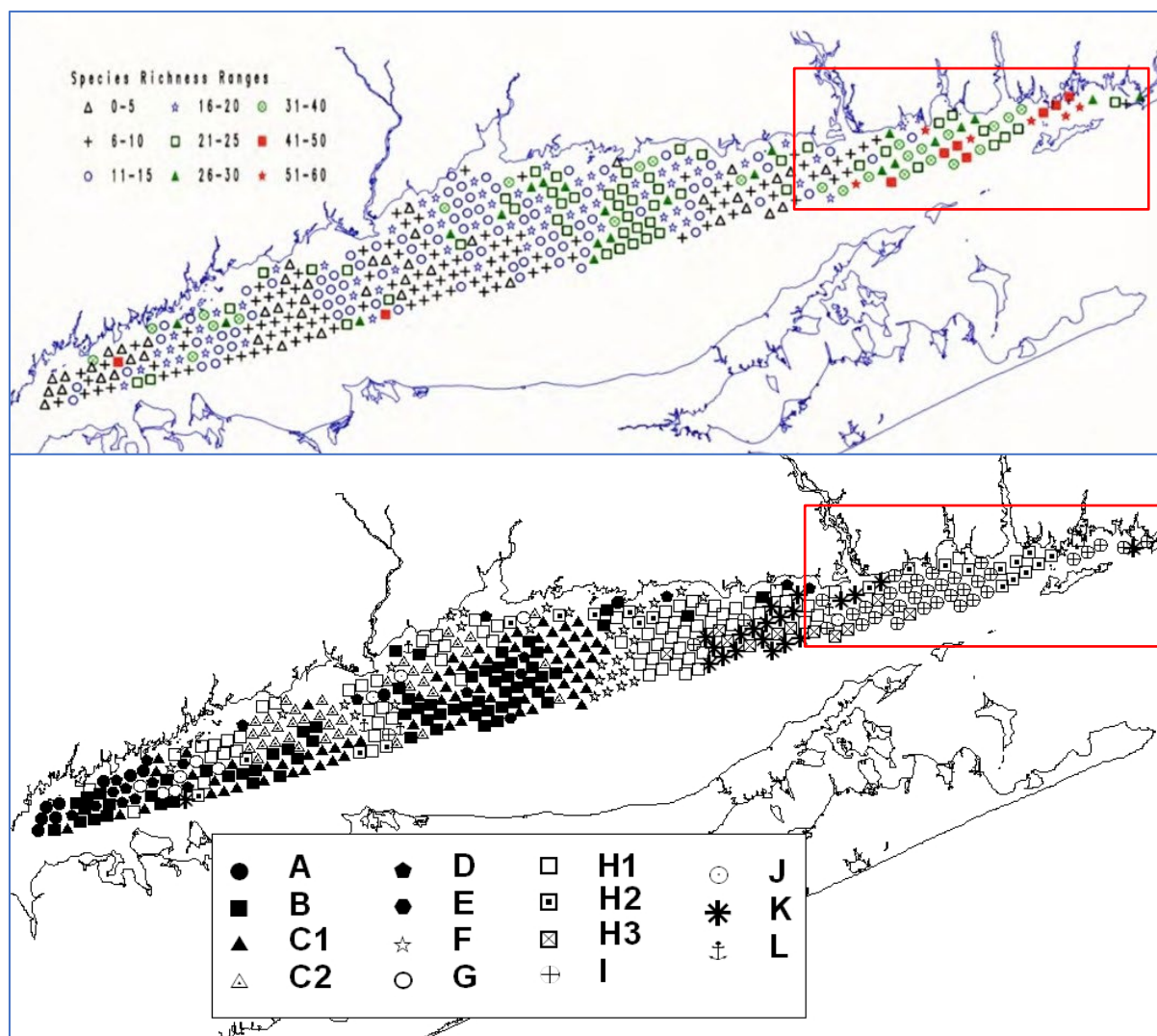
Figure 5.2-1. Distribution of species richness (Top) and infaunal community types (Bottom) based on analyses by Zajac et al. (2000) from data provided in Pellegrino & Hubbard (1983). Approximate location of the Phase II study area delineated by the red box. Descriptions of the community types are given in Table 5-3.

Table 5-3. Abundances (mean +/- 1SE) per 0.04 m² of dominant species in each of the community types found in LIS based on analyses by Zajac et al. (2000) of the data provided in Pellegrino & Hubbard (1983). The community structure analyses were based on the 35 most abundant species found by Pellegrino & Hubbard (1983) throughout LIS. Community types (A, B, C1, etc.) are given along the top row. P (polychaetes), B (bivalves) and A (arthropods) indicate the beginning of each taxonomic group.

SPECIES	A	B	C1	C2	D	E	F	G	H1	H2	H3	I	J	K
Pectinaria gouldii P	0.3 +/-0.2	0.9 +/-0.3	4.7 +/-1.7	0.0 +/-0.0	40.9 +/-11.7	0.4 +/-0.2	10.2 +/-6.5	10.2 +/-2.8	0.5 +/-0.4	0.4 +/-0.4			0.3 +/-0.3	0.0 +/-0.0
Nephtys incisa	0.5 +/-0.3	5.4 +/-0.4	6.4 +/-0.6	6.5 +/-0.6	2.5 +/-0.9	0.8 +/-0.4	11.2 +/-5.2	1.5 +/-0.7	0.6 +/-0.3	1.0 +/-0.6				
Mediomastus ambiseta		1.6 +/-0.4	2.0 +/-0.7	2.6 +/-0.9	4.1 +/-1.8	0.2 +/-0.2	53.3 +/-17.7		1.7 +/-0.6	4.7 +/-3.2				
Polydora websteri		0.0 +/-0.0	0.2 +/-0.2	0.8 +/-0.8	1.9 +/-1.1		0.7 +/-0.7		3.5 +/-1.4	0.2 +/-0.2		2.5 +/-1.5	1.0 +/-0.7	
Aricidea jeffersyii					1.3 +/-1.0		2.4 +/-2.0	1.7 +/-1.2	3.4 +/-0.9	0.0 +/-0.0	2.8 +/-1.1	8.3 +/-4.0		
Prionospio heterobranchia		0.0 +/-0.0			0.6 +/-0.4		0.3 +/-0.3		0.8 +/-0.4	4.5 +/-2.7		14.5 +/-5.7		0.4 +/-0.3
Paraonis fulgens	0.1 +/-0.1	0.4 +/-0.2	0.1 +/-0.1	0.1 +/-0.0		0.6 +/-0.6			0.0 +/-0.0	1.0 +/-0.7	0.2 +/-0.2			
Asabellides oculata		0.1 +/-0.1	0.6 +/-0.4	0.0 +/-0.0	0.3 +/-0.3	0.4 +/-0.2	4.3 +/-1.6	2.7 +/-2.0	12.3 +/-2.1	0.3 +/-0.3			1.0 +/-0.7	
Clymenella zonalis		0.3 +/-0.2	0.7 +/-0.3		0.9 +/-0.7		190.7 +/-45.2	3.5 +/-3.3	5.6 +/-1.6	1.7 +/-0.9	0.4 +/-0.3	2.8 +/-1.7		0.2 +/-0.2
Spiophanes bombyx							0.4 +/-0.4		7.4 +/-1.8	6.4 +/-3.7	0.6 +/-0.4	0.5 +/-0.4	0.5 +/-0.3	1.0 +/-1.0
Cirratulus grandis		0.0 +/-0.0		0.1 +/-0.1	0.3 +/-0.3		0.4 +/-0.4		0.0 +/-0.0	2.5 +/-1.8		35.3 +/-14.6		
Cirratulus cirratus		0.0 +/-0.0							0.2 +/-0.2			8.9 +/-4.6		0.0 +/-0.0
Lepidontus squamotus									0.6 +/-0.4		0.3 +/-0.3	2.4 +/-1.0		0.3 +/-0.2
Steblospio benedicti		0.0 +/-0.0			3.4 +/-2.4		9.7 +/-6.4		0.2 +/-0.1	1.7 +/-1.7				0.1 +/-0.1
Owenia fusiformis					0.3 +/-0.3		1.6 +/-1.1		2.0 +/-1.1					
Nephtys picta					0.3 +/-0.3				3.6 +/-1.2	2.1 +/-2.0				0.3 +/-0.3
Capitella capitata										2.1 +/-1.7		2.8 +/-1.8		
Ampharete arctica									0.1 +/-0.1	0.6 +/-0.4	1.3 +/-0.9	6.5 +/-2.2		
Prionospio tenuis									0.4 +/-0.4	0.7 +/-0.7		9.9 +/-3.8		
Ampelisca abdita A		0.7 +/-0.3	2.2 +/-1.0	0.6 +/-0.5	0.8 +/-0.5		3.1 +/-1.5	1.2 +/-1.2	1.7 +/-0.5	124.2 +/-37.6	0.4 +/-0.4	0.5 +/-0.4		
Unciola irrorata		0.3 +/-0.3	0.1 +/-0.1						1.4 +/-0.4	8.7 +/-4.0	6.0 +/-1.9	1.0 +/-0.4		0.2 +/-0.1
Leptocheirus pinguis									0.2 +/-0.2	9.6 +/-6.3			0.5 +/-0.5	
Ampelisca vadorum		0.0 +/-0.0	0.3 +/-0.3					0.8 +/-0.8	0.1 +/-0.1	21.3 +/-10.4		0.1 +/-0.1	0.3 +/-0.3	
Protohaustorus wagleyi									0.1 +/-0.1		0.3 +/-0.2			24.7 +/-8.1
Ancanthohaustorius miltsi										2.0 +/-2.0	0.3 +/-0.3			3.1 +/-1.3
Aeginina longicornis										0.3 +/-0.3	1.1 +/-1.1	11.4 +/-3.5		
Corophium acheruscum					17.4 +/-17.4		3.0 +/-3.0		0.2 +/-0.2	18.5 +/-18.0	0.2 +/-0.2	4.0 +/-1.3		1.0 +/-1.0
Mulinia lateralis B	5.3 +/-0.9	11.4 +/-1.2	41.9 +/-5.7	118.2 +/-10.5	15.9 +/-6.0	0.4 +/-0.2	299.6 +/-59.2	0.9 +/-0.4	1.5 +/-1.0					1.0 +/-1.0
Nucula annulata	0.1 +/-0.1	8.6 +/-0.9	125.8 +/-13.9	11.3 +/-2.1	15.3 +/-5.0	3.4 +/-0.9	21.0 +/-7.8	0.7 +/-0.7	0.4 +/-0.3	2.8 +/-1.6		0.3 +/-0.3		
Pitar morrhuana		3.3 +/-0.8	5.2 +/-0.9	5.1 +/-1.3	4.9 +/-2.3		3.3 +/-1.5	3.0 +/-1.4	0.1 +/-0.0	2.8 +/-1.6				
Tellina agilis	0.1 +/-0.1	0.4 +/-0.2	0.7 +/-0.3	0.4 +/-0.3	6.4 +/-4.6		12.8 +/-3.8		8.4 +/-1.1	2.0 +/-1.1		0.3 +/-0.3		0.6 +/-0.3
Yoldia lamatula		0.8 +/-0.2	2.3 +/-0.7	1.6 +/-0.4	0.6 +/-0.5	0.6 +/-0.4	1.2 +/-0.7		0.4 +/-0.4					
Pandora goultdina		0.1 +/-0.1	2.0 +/-1.4	0.3 +/-0.3	0.6 +/-0.6		0.2 +/-0.2		0.1 +/-0.0	0.4 +/-0.4		1.7 +/-1.4		0.2 +/-0.1
Ensis directus		1.0 +/-0.4	0.6 +/-0.3		18.0 +/-9.9	0.2 +/-0.2	0.3 +/-0.3		0.9 +/-0.5	0.6 +/-0.6		0.3 +/-0.3		
Mytilus edulis		0.1 +/-0.1	0.0 +/-0.0	0.1 +/-0.1			0.1 +/-0.1					38.6 +/-36.6		0.0 +/-0.0

5.2.1.2 Epifaunal Communities

That there are no historic, spatially comprehensive, studies focused on epifaunal communities in the Phase II study region is noteworthy, despite the ecosystem engineering functions played by structure forming fauna dominant in such communities and their contribution to the biological diversity of the region (i.e., epifaunal species and associates). This is in large part due to the difficulty of directly sampling such communities on hard substratum, in often precipitous topographies, requiring either imaging or some form of hand manipulated sampling gear (e.g., airlift) to collect samples. Pelligrino & Hubbard (1983) did include some characteristic emergent and attached fauna (on small diameter gravels) in grab samples, but they did not sample substrates that were not amenable to the sampling gear. Seafloor imaging as a component of sidescan and multibeam mapping has been used to qualitatively characterize epifaunal communities and their habitat role in ELIS and FIS (e.g., Poppe et al., 2004; Poppe et al., 2013; Langton et al., 1995).

There have been multiple studies that focus on select sites within the Phase II area. Welsh & Stewart (1984) characterized benthic macrophyte communities and associated fauna in the Thames River estuary (south to Ledge Light and Black Ledge), using direct quadrat sampling and seafloor imagery, established a baseline for comparison to address changes in human uses of the region. Macrophytes were found to increase habitat complexity with diverse and abundant fauna and utilized year around. Epifauna and associated vagile species were important prey for economically important species. Macrophytes also served as nursery habitats for juveniles of multiple species. In shallow waters, there is a time series from aerial surveys for seagrass habitats, addressing the changing distribution and status of *Zostera marina* and associated submerged aquatic vegetation (Tiner et al., 2003).

Moving offshore, monitoring of the New London dredge material disposal site had included time series from visual diver transects of seafloor habitat conditions and associated fauna, principally on soft sediments, with a focus on emergent fauna and ecosystem engineering species (e.g., crustacea, burrowing fishes) that modify the seafloor landscape (e.g., Stewart, 1980; Parker & Revelas, 1989). More recent monitoring (AECOM, 2009) has included sediment profiling and plain view imaging to assess, among diverse metrics, surface boundary roughness and conditions that address effects of physical sedimentary transport processes (e.g., producing ripples, sand wave features) and biogenic elements of habitat (e.g., shell, habitat forming species).

Fisheries resource monitoring, linked to seafloor characteristics, have a detailed time series in the LIS region but bounded by the east of LIS, excluding FIS (e.g., Gottschall et al., 2000; Howell et al., 2016). Localized citizen science studies around the Thames River region (Snyder et al., 2019) also provide direct and inferential measures of habitat conditions and change over time. Multiple autecological studies at select sites also provide snapshots of local conditions during earlier periods. For example, Lund et al. (1971) describe seafloor habitat conditions at Ram Island Reef from a study of American lobster ecology. Parry (1981) describes the sponge fauna at select sites in FIS.

The results from Phase II studies of the distribution of emergent and epifaunal communities, with component species, is the first spatially comprehensive assessment for this region and can provide a foundation for linking use of such habitats to diverse human uses of the region today.

5.2.1.3 Overview of Previous Studies

While certain geologic and ecological characteristics have been mapped in ELIS, there remained data gaps that limited the ability to produce contemporary and spatially more comprehensive benthic habitat and ecological maps in the Phase II area. These data gaps are spatial, thematic and temporal in nature, and limited the utility of existing products for resource management applications. Spatial data gaps existed because historical information was generally analyzed at coarse spatial scales, limiting its use for the breadth of management applications, particularly those focused on specific areas. In addition to spatial gaps, there were also thematic and temporal data gaps.

Existing maps of the seafloor are primarily geology based (surficial sediment types and sedimentary environments), and do not incorporate geomorphological, bathymetric, and, perhaps most critically, ecological components of habitat, and particularly epifaunal communities and habitats, and habitat forming species (e.g., mussel beds, oyster reefs, sponge communities, tube mats). There were also no maps that show the distribution and variation of both epibenthic and benthic infaunal communities within defined seafloor patches/habitats, except in some areas based on smaller scale studies (see above). In terms of temporal data gaps, many of the data collected that were used to produce geologically themed seafloor maps currently available, were collected over a time span approaching 80 -100 years in the case of the surficial texture sediment map, and close to 20 years for spatially-coarse side scan data that was used in part to produce the sedimentary environment map. Likewise, no significant ecological sampling of the benthos across the full extent of LIS, either the epifaunal or infaunal components, nor in shallow or deep waters, over a large spatial scale has been done since the mid-1970s to early 1980s, and no comprehensive sampling in the Phase II study area since 1998. Habitat maps produced using contemporary, and generally more accurate data, are more likely to be utilized for many different management

applications because they contain added information that may be relevant and scalable t a wider array of issues in the marine environment. Furthermore, new management problems cannot always be anticipated (e.g., with respect to climate change), making extracting the maximum amount of information from acoustic imagery potentially important for being prepared to meet the future needs of the coastal and marine management community.

5.2.2   Infaunal Ecological Characterization

5.2.2.1   Objectives

The main focus of this portion of the study was to characterize the infaunal communities across the different seafloor environments found in the Phase II project study area, to assess differences in infaunal community structure among the large-scale acoustic patch types identified through our analyses of the backscatter data (see Section 3.1), and also ecological variability within these patch types. Infaunal communities comprise those organisms that live in seafloor sediments and/ or just at the sediment-water interface. The acoustic patch types can be viewed as large-scale (on the order of 10s-100s of km^2) and general habitat types that have been identified based on reflectance information in the backscatter mosaic image and then characterized based on their sediment composition and associated physical dynamics.

These characteristics vary on a relative basis within each acoustic patch type, creating smaller scale habitats with specific sets of characteristics that may support different sets of ecological communities. Based on these efforts, information on ecologically significant locations in the Phase II study area can be identified, as well as how the infaunal community characteristics and habitat distributions might shape future impact assessments and management efforts.

5.2.2.2   Methods

Field Data Acquisition

Samples for ecological characterization were collected during two sampling periods between November 28 and December 3, 2017, and May 8 and 15, 2018. The sampling design comprised a series of sampling blocks (SB) and sampling sites (NB) that were distributed across the Phase II study area based on acoustic backscatter and bathymetric data that was available prior to the November - December sampling period (See Section 5.1.1, Figure 5.1-4 & Figure 5.2-27). The spatial distribution and locations of the sampling locations were selected with the overall objective to sample as many of the different seafloor habitats that were evident in the side scan mosaic that had been previously developed for the study area. These included both areas that were within large-scale seafloor features (acoustic patches) and areas where there are transitions among large scale features. Initial identification of seafloor features was based on previous work conducted in this portion of LIS (Poppe et al., 2000; Zajac et al., 2000, 2003), visual interpretations of the available side scan mosaic, and general information from the literature on seafloor mapping and ecological characterization using acoustic data for habitat identification characterization (e.g. Brown et al., 2012; Kostylev et al., 2001). This planning phase resulted in the selection of 160 sampling locations. Infaunal grab samples were not obtained at several locations due bottom hazards for the sampling equipment and or high currents.

Infaunal grab samples were collected using the USGS SEABOSS system (See Section 3.3.2.1 for details).

The sampling design included taking three randomly located grab samples (generated using ArcGIS) in each SB and one sample at each NB location. Infaunal samples were collected with a 0.1 m^2 modified Van Veen grab. The SEABOSS was lowered to just above the seafloor and then was allowed to drift for several minutes to collect video and still images, after which a grab sample was collected.

Infaunal Sample Processing and General Analytical Approaches

In the field, the entire contents of a grab sample obtained at each sampling site was washed on a 1 mm sieve using filtered seawater, after a small portion of surficial sediment, approximately 25 cm^2 by 2 cm deep, was removed for sediment analyses. At several locations a 500 μm was used to process the samples to check for mesh size effects. The sieved sample was preserved with 70% ethanol and stained with Rose Bengal. In the lab, samples were sorted under a dissecting microscope and individuals were identified to the lowest possible taxon. A total of 160 samples were processed.

After the data sets were assembled, several sets of statistical and GIS-based analyses were conducted to assess the characteristics of infaunal communities (total abundance [total number of identified organisms per sample], taxonomic/species richness [species richness and taxonomic richness are used interchangeably here and represent the number of taxa that were differentiated to the lowest possible taxonomic level], taxonomic/species diversity [as Shannon Diversity Index, a measure that accounts for both total number of taxa/species and relative proportion/evenness], community composition and related metrics [multivariate analyses measuring similarities and trends within and among samples]) among and within the large-scale acoustic patches that were identified, and to map the spatial trends in community structure and biodiversity relative to seafloor habitat structure.

Community composition and related metrics were analyzed using multivariate analyses, including classification analysis (clustering), non-metric multidimensional scaling (MDS), and CAP. These analyses determined community similarities and trends among and within among large-scale acoustic patches. Species contributions to community similarities within acoustic patches and dissimilarities among patches were assessed using similarity percentage analysis (SIMPER). Statistical differences in community structure were assessed using an analysis of similarities (ANOSIM) and permutational analysis of variance (PERMANOVA) procedures. All multivariate procedures were carried out using PRIMER+ PERMOVA software (Clarke & Gorley, 2006). Calculation of several diversity indices were also carried out in PRIMER. Shannon diversity was calculated as:

Equation 6

$$H' = - \sum_{i=0}^{S} (pi \; x \; log10pi)$$

Where *S* is the total number of species/taxa, and *pi* is the proportion of individuals belonging to the ith species. Higher values of *H'* indicate greater species diversity.

Differences in total abundance, taxonomic richness, and Shannon diversity among acoustic patch types were tested using analysis of variance (ANOVA) in the NCSS statistical software package

(NCSS, LLC, 2012). The results of the statistical analyses were used to develop GIS data layers that depicted the spatial distribution of community types and biodiversity across the Phase II study area. Details of analytical steps and conditions are provided below as needed.

5.2.2.3 Results

General infaunal community characteristics

A total of 289 infaunal taxa were identified in all the samples collected in the LIS Phase II area. 85% of these were identified to the species level. Two sets of analyses were conducted to assess the general infaunal community characteristics (taxonomic richness, total abundance and diversity): one using the entire data set from both sampling periods and also for each sampling period separately to assess potential seasonal differences among the large-scale patch types. Only one sample was taken in Patch Types A and E; as such, they were excluded from several of statistical tests of general community characteristics among patch types. Tests among samples processed using a 1 mm versus a 500 μm sieve indicated no statistical differences for total abundance, taxonomic richness and diversity, and as such all the samples were combined for subsequent analyses.

Infaunal mean total abundances in the patch types generally ranged from ~ 175 to 225 individuals 0.1 m^{-2} (Figure 5.2-2). The abundance in the one sample taken in Patch Type A was very high, primarily due to a very high number of the slipper shell *Crepidula fornicate* (440) and oligochaetes (72) in the sample. The total abundance in the one sample taken in Patch Type E was lower than the mean values in the other patch types. There were some samples in each of the other patch types that had relatively high total abundances as well, as revealed by the boxplots (Figure 5.2-2). In one case, a sample taken in Patch Type D had close to 1,000 individuals per 0.1 m^2.
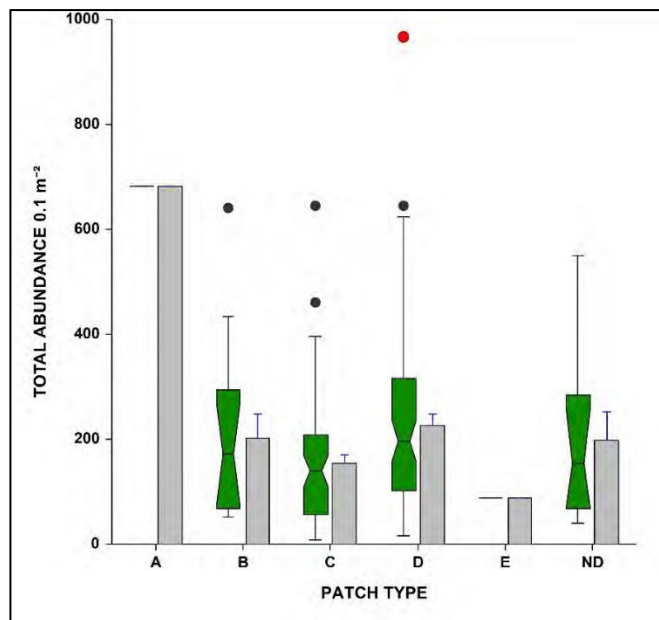
*Figure 5.2-2. Total abundance in the Patch Types in the LIS Phase II Study area. Shown are the mean total abundances (+1 standard error, SE) and box plots showing the notched median (median ± 1.57 × (IQR) / √n), the inter-quartile range (IRQ) defined by the upper (75th percentile) and lower 25th percentile ends of the box, whiskers extending to 1.5 * IRQ. Outliers are shown as dots.*

One-way ANOVA indicated that there was a marginally significant difference in mean total abundance among patch types, with a post hoc test indicating that abundances in Patch Type D were greater than in Patch Type C (Table 5-4). In general, mean abundances were higher in the November/December samples than in the May samples, particularly in Patch Type B (Figure 5.2-3). Two-way ANOVA indicated that there was a significant difference in mean total abundance among seasons, as well as a significant difference between Patch Types B, C, and D (Table 5-4). Individual sample abundance exhibited large spatial variation across the study area (Figure 5.2-4 & Figure 5.2-5). Relatively low abundances were found at most sample sites along the southern boundary of the Phase II study area, as well as in an area to the southeast of the mouth of the Connecticut River. Moderate to high abundances were found throughout the central portion of the study area and in portions of FIS. Sample sites with locally high abundances were scattered throughout the Phase II area.

Table 5-4. Results of statistical analyses of differences in general community characteristics among patch types in the LIS Phase II study area. Patch types differences tested with one- way ANOVA: patch type and season differences tested with two-way ANOVA.

Total Abundance – Patch types only

Term	DF	Sum of Squares	Mean Square	F-Ratio	Prob Level
Patch Type	3	1.112615	0.3708718	2.5795	0.05567
Within (Error)	154	22.14193	0.1437788		
Adjusted Total	157	23.25455			
Total	158				

Bonferroni (All-Pairwise) Multiple Comparison Test

Group	Count	Mean	Different from Groups
B	14	2.174418	
C	63	2.045596	D
D	71	2.226692	C
ND	10	2.165776	

Total Abundance – Patch types and Season

Term	DF	Sum of Squares	Mean Square	F-Ratio	Prob Level	Power (Alpha=0.05)
Patch Type	2	1.516051	0.7580255	5.61	0.004517*	0.852134
Season	1	1.617094	1.617094	11.97	0.000714*	0.930052
Patch x Season	2	0.3752294	0.1876147	1.39	0.252778	0.294603
S	142	19.18506	0.1351061			
Total (Adjusted)	147	22.04943				
Total	148					

Taxonomic Richness – Patch types only

Model Term	DF	Sum of Squares	Mean Square	F-Ratio	Prob Level
Patch Type	3	0.4506538	0.1502179	3.0061	0.03218
Within (Error)	154	7.69563	0.04997163		

Adjusted Total   157   8.146284
Total   158

Bonferroni (All-Pairwise) Multiple Comparison Test

Group	Count	Mean	Different from Groups
B	14	1.340354	
C	63	1.292122	D
D	71	1.40567	C
ND	10	1.306752	

Taxonomic Richness – Patch types and Season

Source Term	DF	Sum of Squares	Mean Square	F-Ratio	Prob Level	Power (Alpha=0.05)
Patch Type	2	13.22823	6.614113	5.22	0.006519*	0.823943
Season	1	12.8402	12.8402	10.13	0.001796*	0.885030
Patch x Season	2	1.396607	0.6983033	0.55	0.577789	0.139724
S	142	180.0695	1.268095			
Total (Adjusted)	147	208.1521				
Total	148					

Diversity (H′): Patch types only

Model Term	DF	Sum of Squares	Mean Square	F-Ratio	Prob Level
Patch Type	3	0.1785805	0.05952685	0.8080	0.49122
Within (Error)	154	11.34503	0.07366905		
Adjusted Total	157	11.52361			
Total	158				

Diversity (H′): Patch types and Season

Source Term	DF	Sum of Squares	Mean Square	F-Ratio	Prob Level	Power (Alpha=0.05)
A: Patch Type	2	0.2395536	0.1197768	1.75	0.176769	0.362893
B: Season	1	0.06691325	0.06691325	0.98	0.323882	0.165983
AB	2	0.1897867	0.09489333	1.39	0.252494	0.294819
S	142	9.695569	0.06827866			
Total (Adjusted)	147	10.51536				
Total	148					
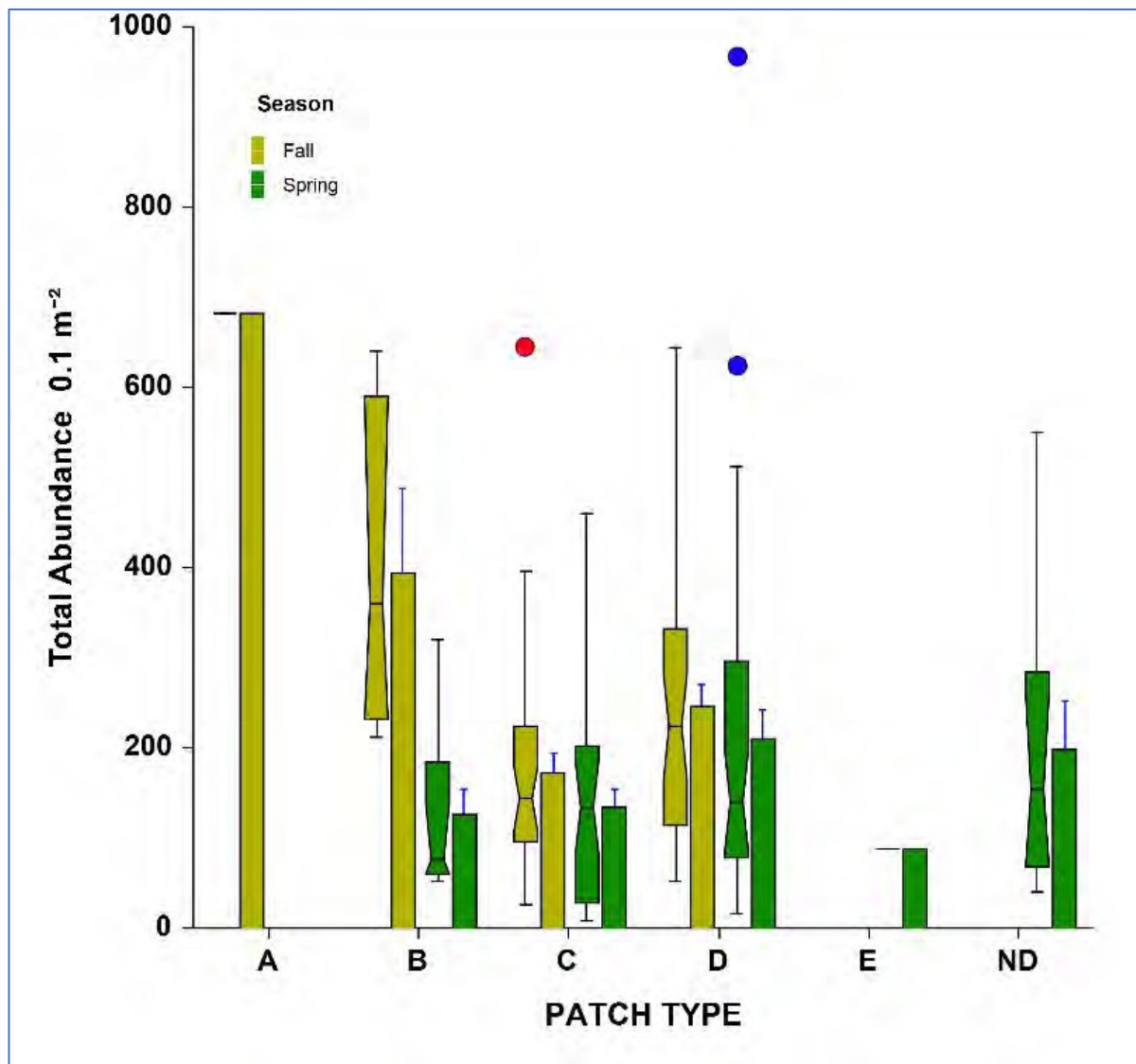
Figure 5.2-3. Seasonal differences in total abundance in the Patch Types in The LIS Phase II Area. Plot explanation as in Figure 5.2-2.
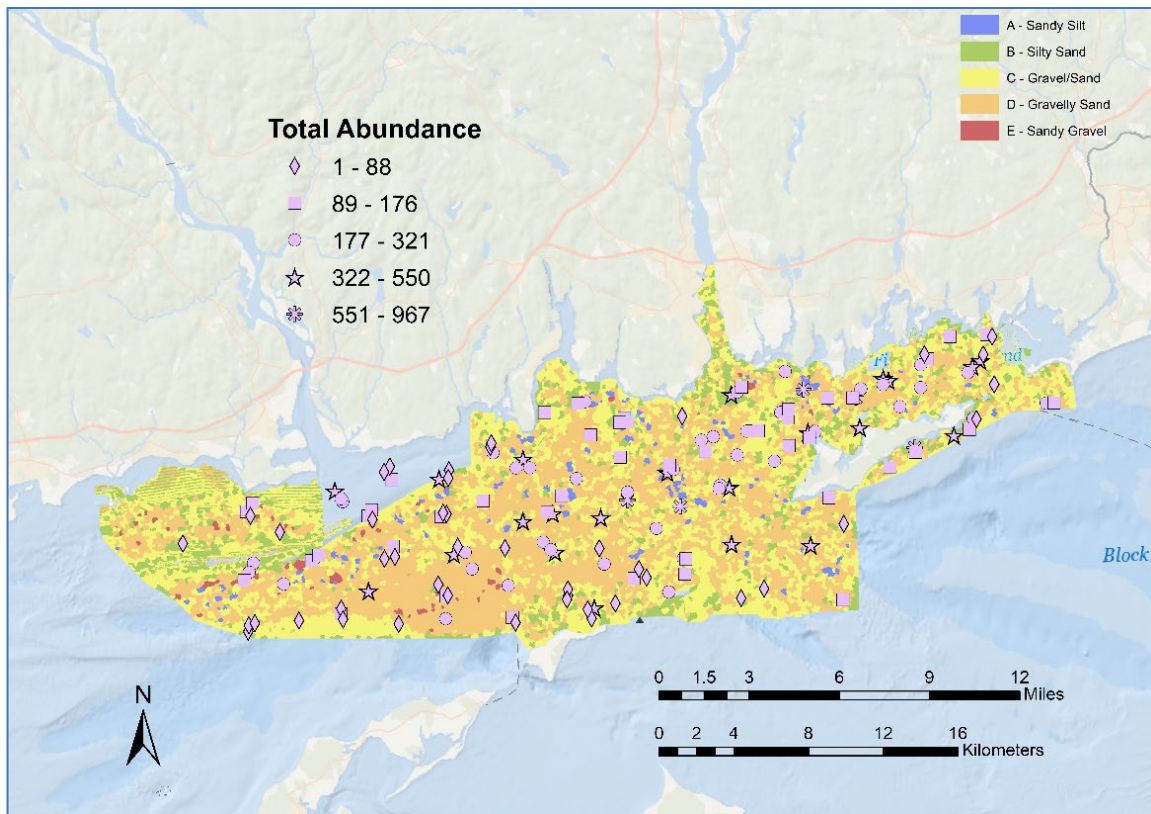
Figure 5.2-4. Spatial distribution of total abundance of infauna among the sample locations in the LIS Phase II study Area
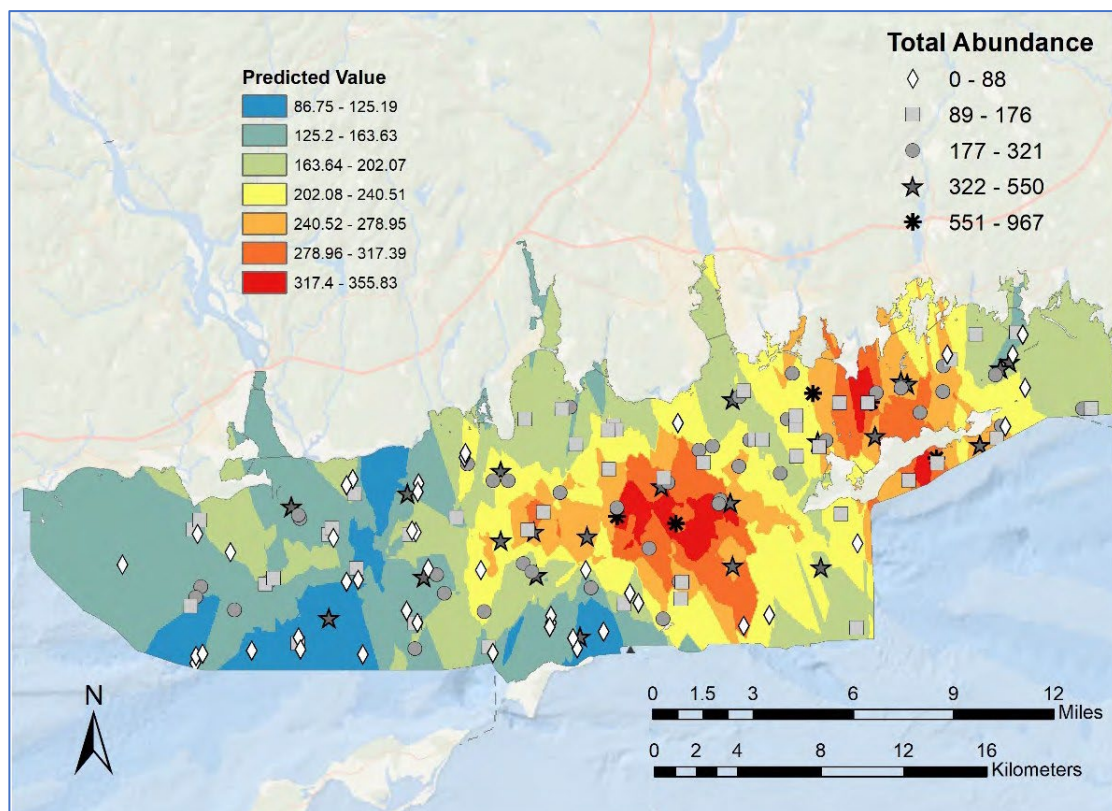
Figure 5.2-5. Interpolation (using kriging) of total abundance across the LIS Phase II Study Area

Mean taxonomic richness ranged between 20 and 30 taxa 0.1m^{-2} using data from both sampling periods (Figure 5.2-6). The overall range was quite large, with some sites having upwards of 40 to 50 taxa, whereas others had as few as 4 to 5 taxa. There was a statistical difference in taxonomic richness among the acoustic patch types (Table 5-4), with post hoc test indicating that richness in Patch Type D was statistically greater than in Patch Type C. More taxa were generally found in samples taken in November – December (fall) than in the May (spring) sampling periods (Figure 5.2-6). Taxonomic richness was higher in fall than in spring for the patch types that were sampled at both times (B, C, and D). In general, the range of the number of taxa found among sampling sites was large and acoustic patch types C and D in both seasons; however, the variation in taxonomic richness among sample sites in Patch Type B was much lower (Figure 5.2-7). Two-way ANOVA indicated significant differences among patch types and seasons but not a significant interaction (Table 5-4). Similar to total sample abundance, taxonomic richness was relatively low at sites along the southern portion of the Phase II area (Figure 5.2-8 & Figure 5.2-9). Higher richness was found at sites through the central portion of the area, and also at sites in FIS.
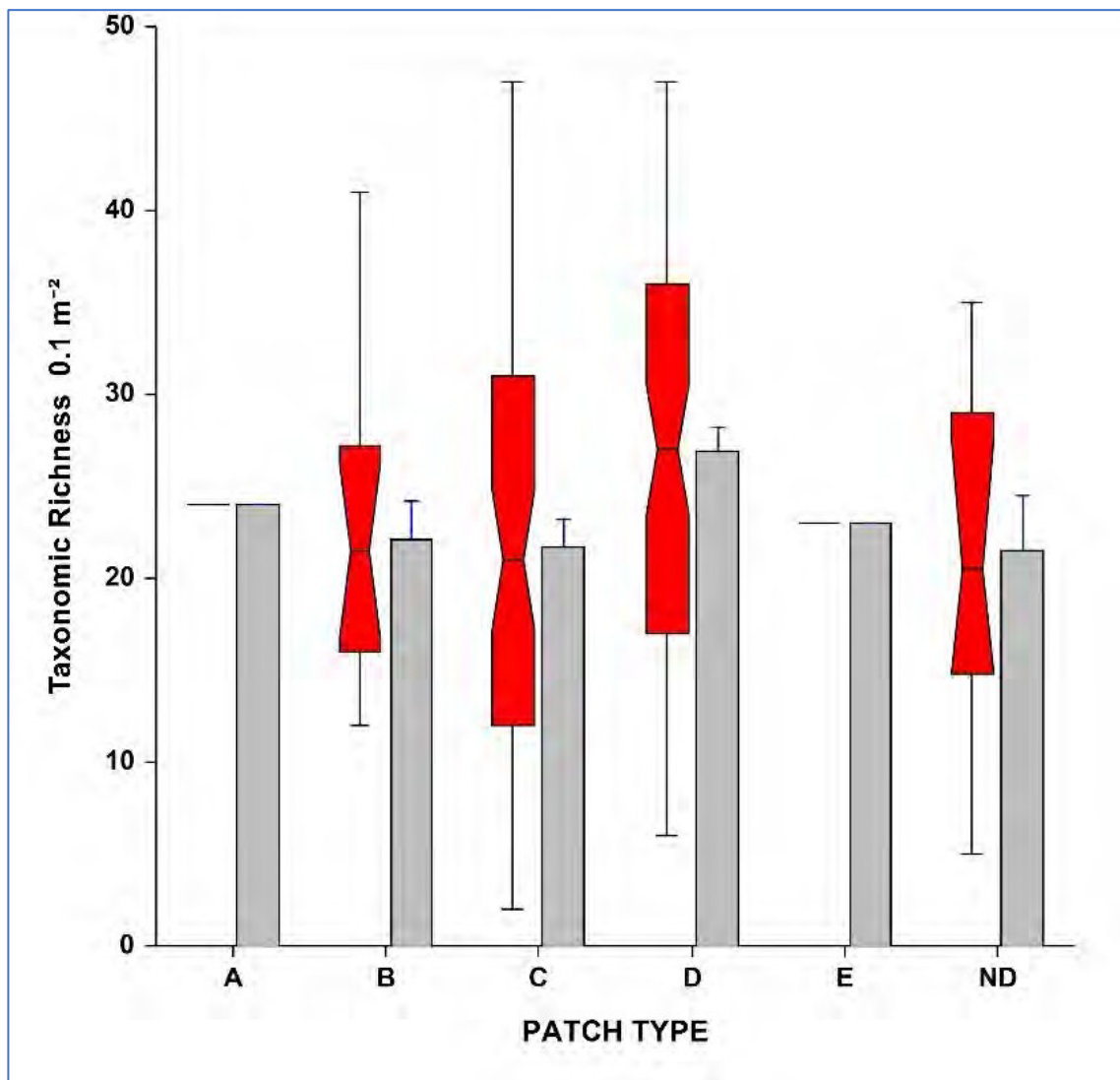
Figure 5.2-6. Taxonomic richness in the Patch Types in the LIS Phase II Study area. Plot explanation as in Figure 5.2-2
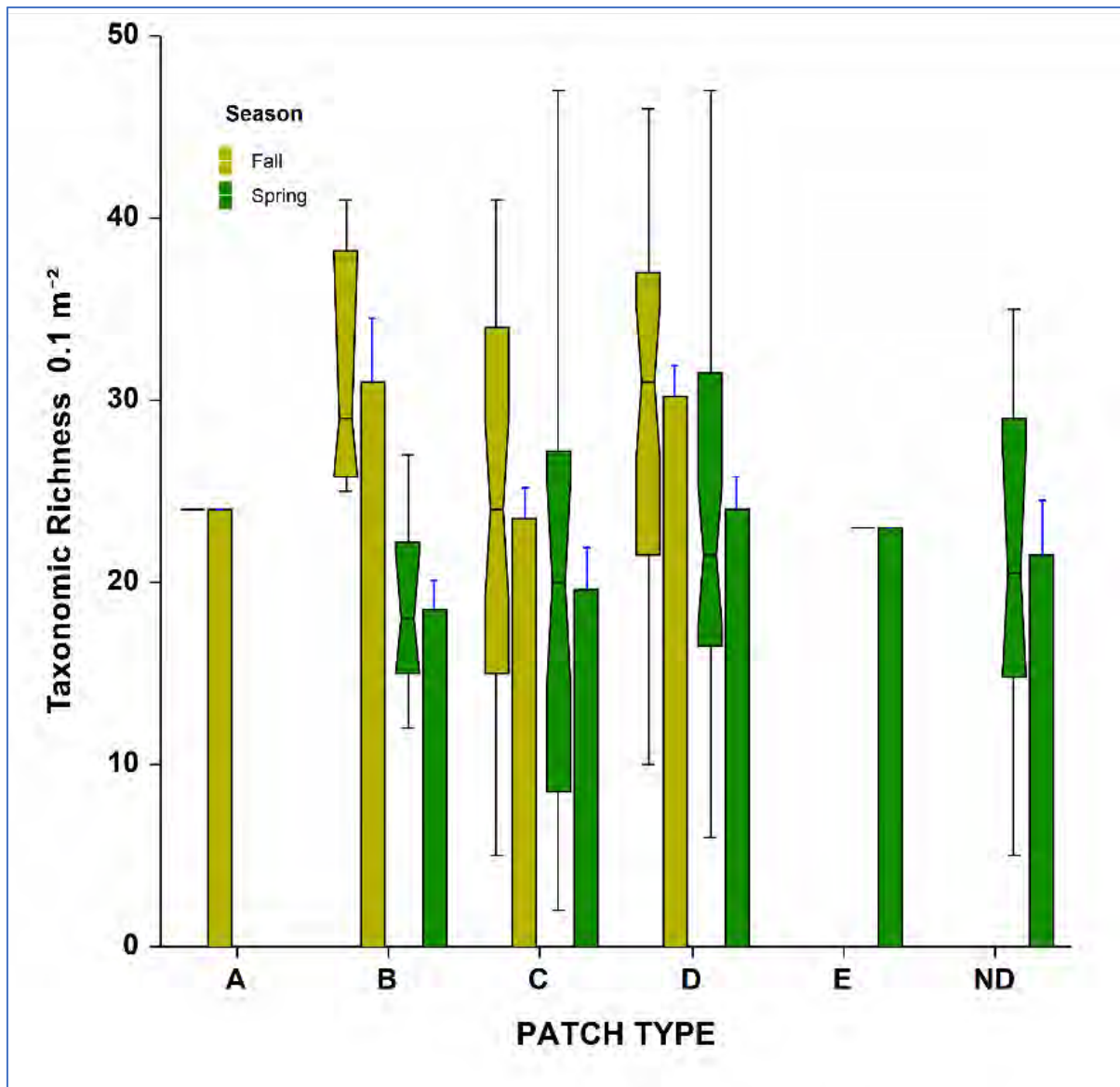
Figure 5.2-7. Seasonal differences in taxonomic richness in the Patch Types in the LIS Phase II Study area. Plot explanation as in Figure 5.2-2.
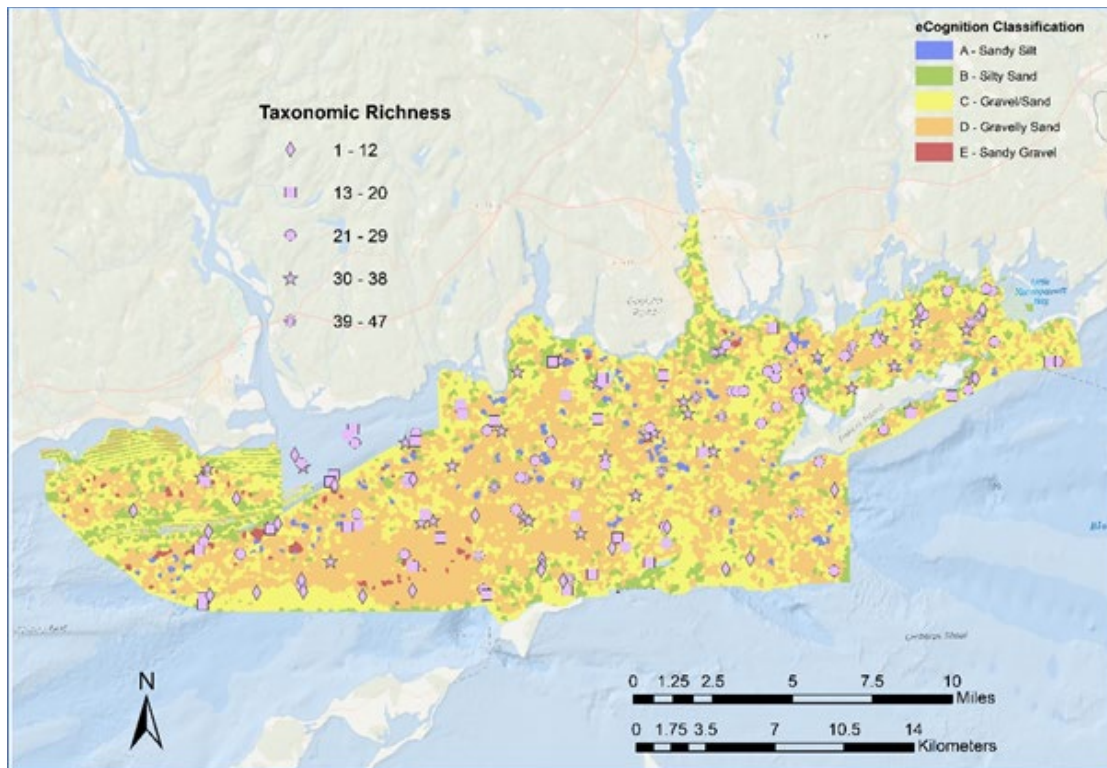
Figure 5.2-8 Spatial distribution of taxonomic richness of infauna among the sample locations in the LIS Phase II study Area
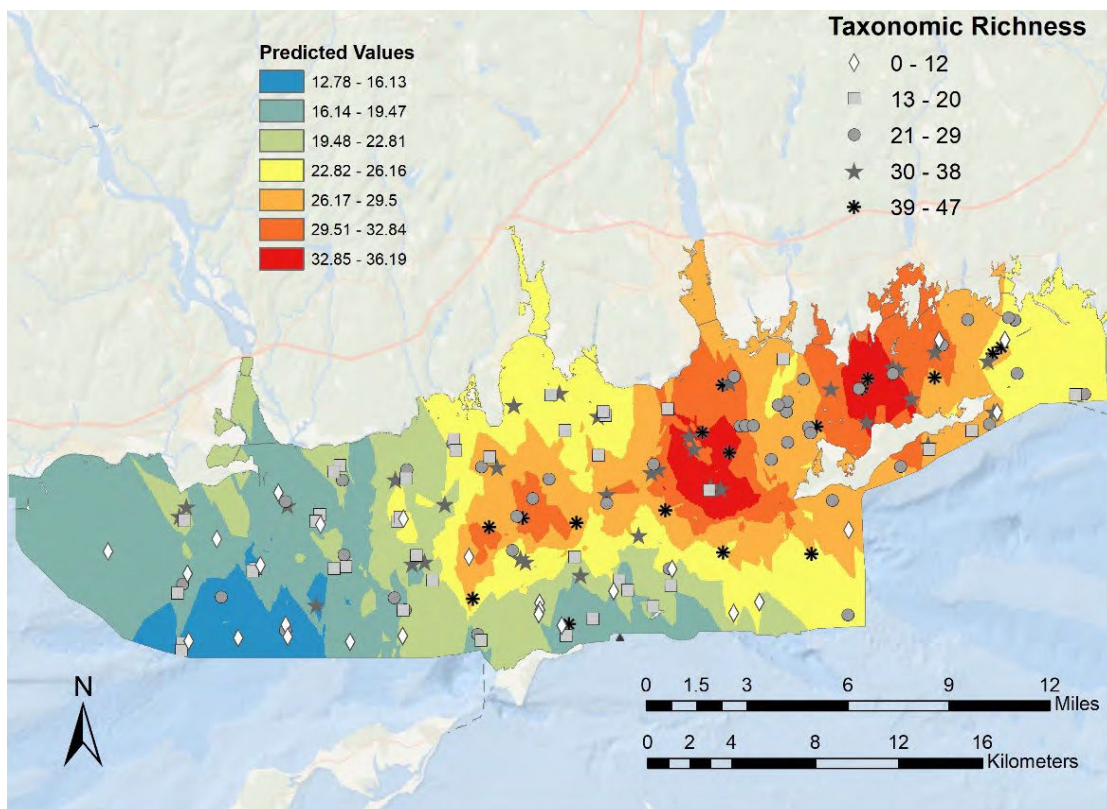
Figure 5.2-9. Interpolation (using kriging) of taxonomic richness across the LIS Phase II Study Area

Mean taxonomic diversity, which takes into account both the number of taxa and their proportional abundance and measured by Shannon diversity index H′, ranged from approximately 0.6 to 1.0; although, at some sites it was higher approaching approximately 1.4 (Figure 5.2-10). One-way ANOVA indicated there were no significant differences among patch types in mean Shannon diversity (Table 5-4). However, diversity increased in patch types with increasing proportions of coarser sediments (i.e., in the gradient from patch type A to patch type E). This trend has been previously reported when comparing benthic species richness across the whole of LIS (Zajac, 1998) and agrees with previous studies and hypotheses that indicate increasing diversity with increasing sediment grain-size/variability (e.g., Whitlatch, 1981; Etter and Grassle, 1992; Gray, 2002; Thrush et al., 2003). This trend was evident over the small and meso-scale spatial patterns of sediment variation within and among the large-scale acoustic patch types. There were no statistically significant differences among sampling periods (seasons) nor among the acoustic patch types in which seasonal samples were taken (Table 5-4). Diversity was somewhat higher in patch types C and D in the fall versus the spring but higher in the spring and patch type B (Figure 5.2-11). Shannon diversity exhibited a somewhat different spatial pattern than taxonomic richness with more spatially constrained areas of high and low diversity (Figure 5.2-12 & Figure 5.2-13). For example, there was relatively high diversity in the areas southeast of the mouth of the Connecticut River and also in the central portion of the Phase II area. There was a particularly large cluster of high diversity in samples taken south of the mouth of the Thames River and into FIS.
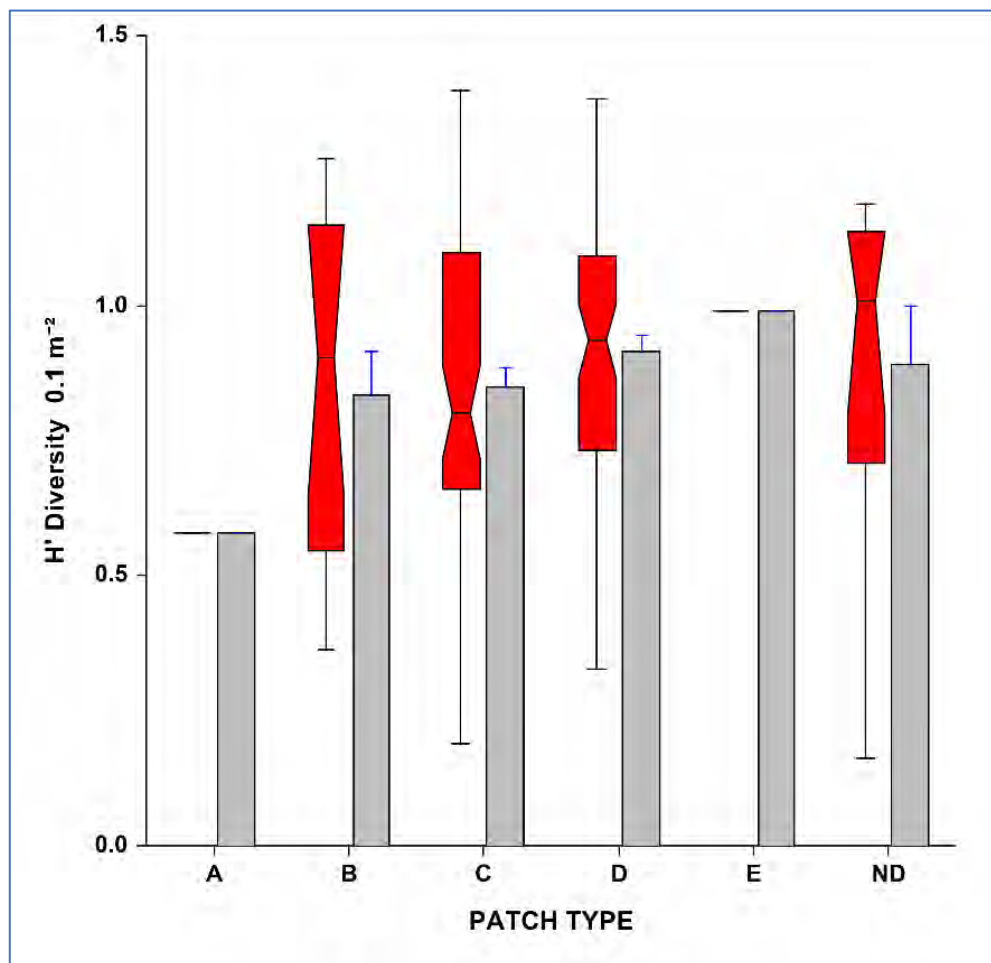
Figure 5.2-10. Taxonomic diversity in the Patch Types in the LIS Phase II Study area. Plot explanation as in Figure 5.2-2.
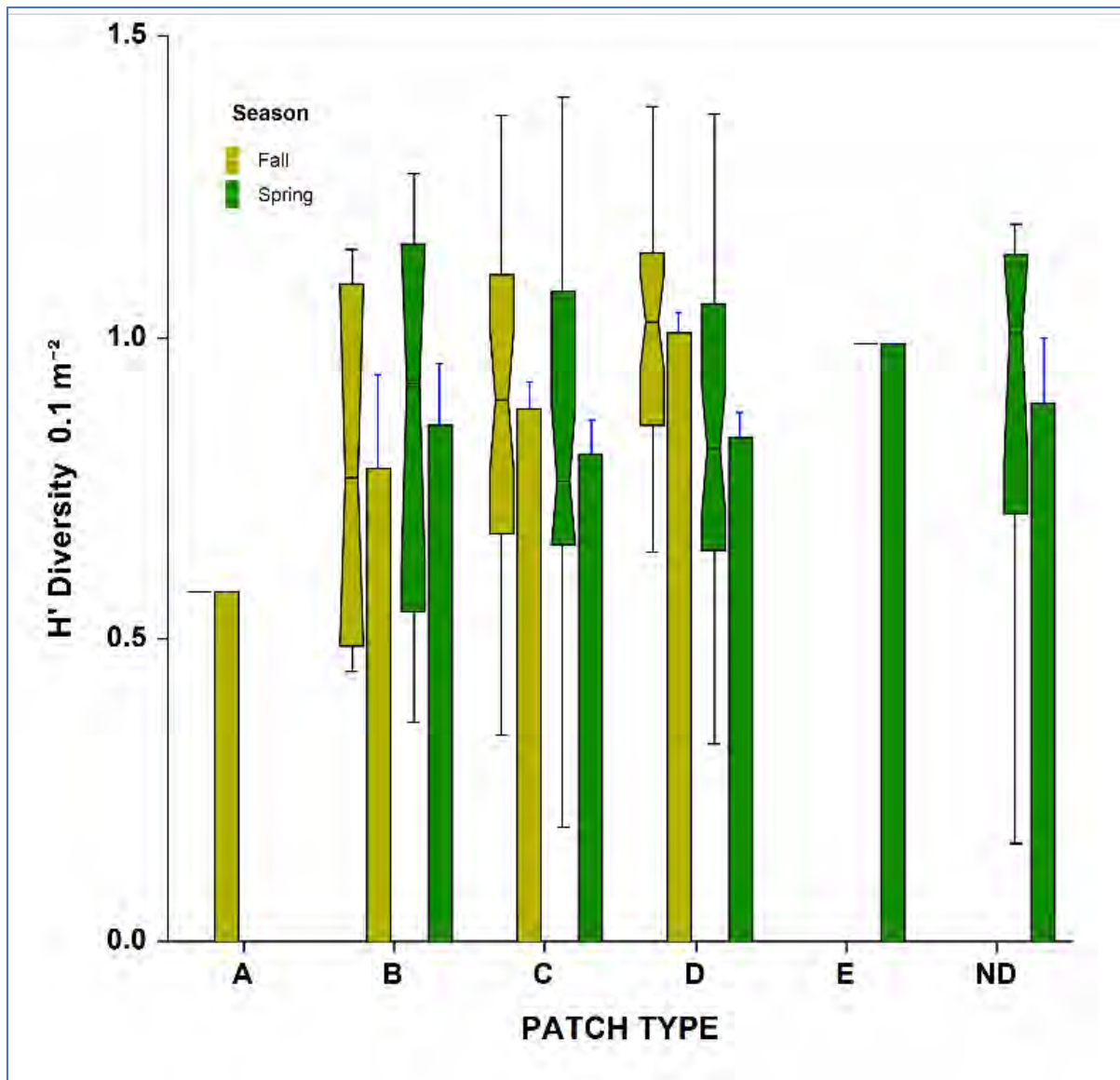
Figure 5.2-11. Seasonal differences in taxonomic diversity in the Patch Types in the LIS Phase II Study area. Plot explanation as in Figure 5.2-2.
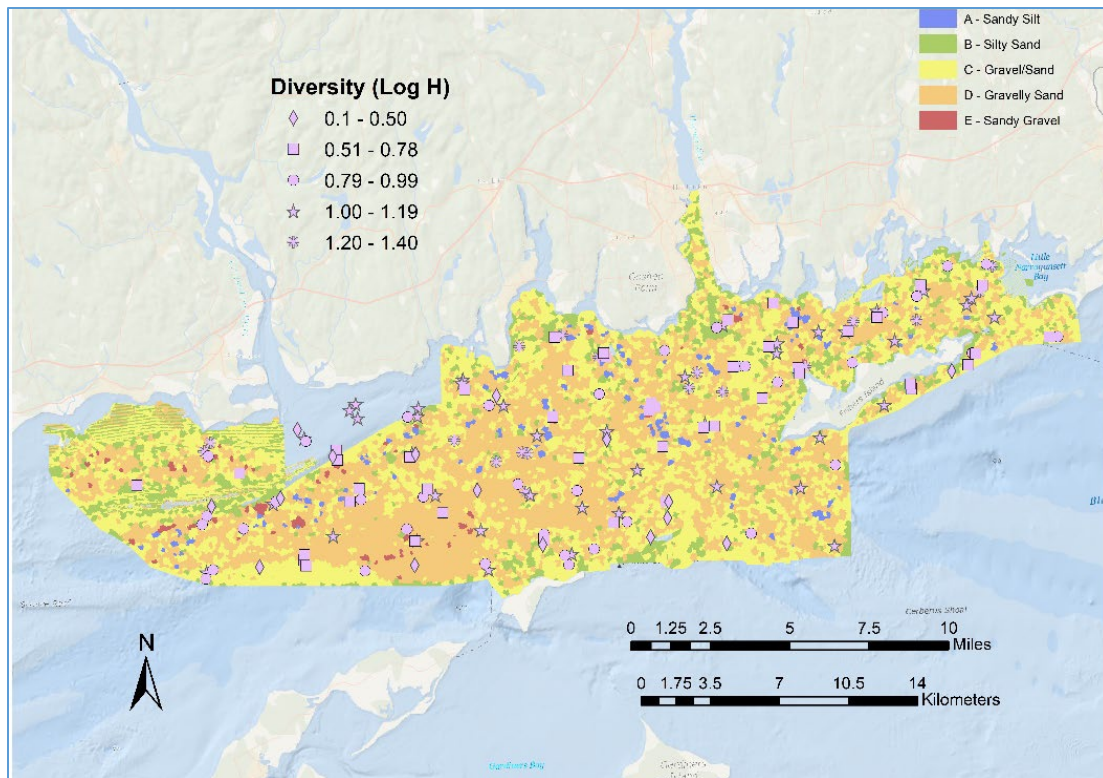
Figure 5.2-12. Spatial distribution of taxonomic diversity of infauna among the sample locations in the LIS Phase II Study Area
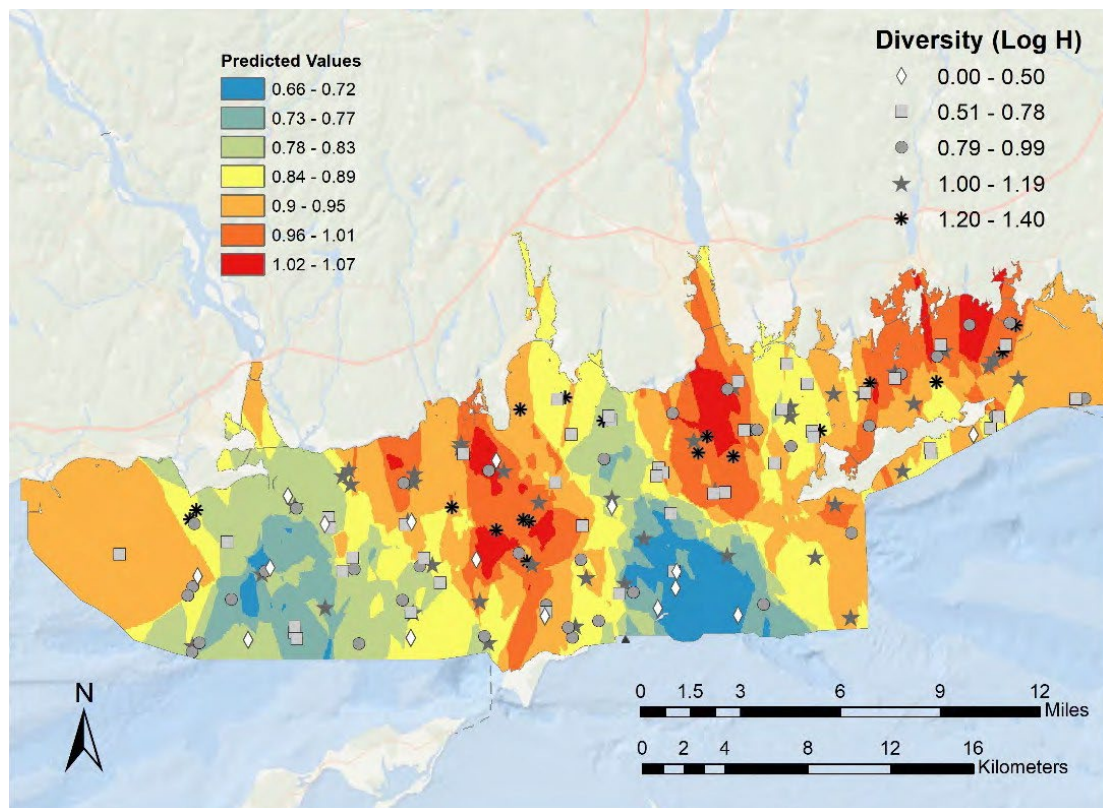
Figure 5.2-13. Interpolation (using kriging) of taxonomic diversity across the LIS Phase II Study Area

Patterns in infaunal community structure within acoustic patch types

Infaunal community structure is spatially heterogeneous in the Phase II Area. Although there were no sharply distinct community types associated with each of the acoustic patch types identified through the eCognition analysis, there were some notable differences among them (Figure 5.2-14). Community structure was variable within each of the patch types, but there were a set of samples in Patch Type D, which had very similar communities as indicated by their tight clustering in the center of the ordination space. ND samples (collected in shallower water areas along the CT coast where there was no backscatter data) also had relatively similar community structure. Communities in Patch Type C were highly variable, being spread across the entire ordination space; however, there appear to be two subcommunities in this patch type, given the separation of the two clouds of points at either side of the ordination space. Communities in Patch Type B were also variable but were not as varying as those in Patch Type C (Figure 5.2-14). A multivariate index of dispersion analysis indicated that samples in Patch Types D and ND had communities that were relatively more similar as compared to those in patch types B and C (Table 5-5). An analogous test of the homogeneity of multivariate dispersions indicated that there were significant differences in within-patch type community variation among patch types, with differences among specific pairs of patch types being mostly significant or marginally significant (Table 5-5). An ANOSIM test indicated that overall, there were significant differences in community structure among the different patch types, primarily among Patch Types B, D, C, and ND (Table 5-5). A PERMANOVA test to assess differences in community structure among patch types and seasons indicated that both factors had a significant effect on community structure, but that their interaction was not significant (Table 5-5). Both patch type and season accounted for about the same level of variation in the data set. These results suggest that community differences among patch types were relatively consistent among the two sampling periods. Pairwise comparisons based on the PERMANOVA test were consistent with the other multivariate analyses, indicating significant differences among patch types B and D, C and D, C and ND, and among D and ND.
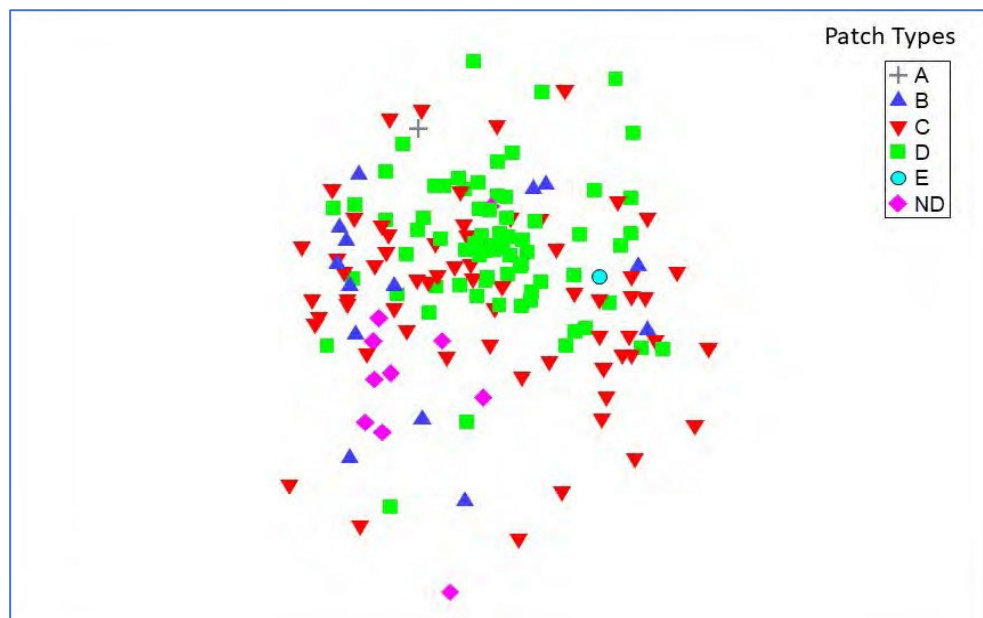
Figure 5.2-14. nMDS ordination of sample site infaunal communities grouped by their location in the large-scale Patch Types identified in the LIS Phase II study area. (Stress = 0.24, 4th root transformed abundances, Hellinger Distance Similarity Function)

Index of Multivariate Dispersion (IMD) for Patch Types

Global Analysis

Factor value	Dispersion
D	0.825
ND	0.887
C	1.214
B	1.261

Pairwise Comparisons

Factor values	IMD
B, C	0.06
B, D	0.427
B, ND	0.386
C, D	0.389
C, ND	0.348
D, ND	-0.079

Distance-based Test for Homogeneity of Multivariate Dispersions among Patch Types
Deviations from Centroid
F: 55.528 df1: 5 df2: 154
P(perm): 0.001

Pairwise Comparisons

Groups	t	P(perm)
(B,C)	1.0239	0.613
(B,D)	1.5249	0.338
(B,ND)	2.2048	0.069
(B,E)	12.366	0.067
(B,A)	12.366	0.056
(C,D)	4.2815	0.001
(C,ND)	3.5428	0.021
(C,E)	12.967	0.017
(C,A)	12.967	0.016
(D,ND)	0.89129	0.674
(D,E)	9.8446	0.018
(D,A)	9.8446	0.009
(ND,E)	11.739	0.098
(ND,A)	11.739	0.072
(E,A)	No test	

ANOSIM Test for Differences Among Patch Types

Global Test
Sample statistic (R): 0.139

Significance level of sample statistic: 0.001%

Pairwise Tests

Groups	R	Significance
B, C	0.034	0.314
B, D	0.33	0.001
B, ND	0.052	0.221
B, E	0.055	0.400
B, A	0.031	0.467
C, D	0.072	0.001
C, ND	0.145	0.052
C, E	-0.084	0.641
C, A	0.201	0.203
D, ND	0.41	0.001
D, E	0.078	0.361
D, A	0.334	0.181
ND, E	0.467	0.182
ND, A	0.527	0.182

PERMANOVA of Differences in Community Structure among Patch Types and Seasons

Source	DF	Sum of Squares	Mean Square	Pseudo-F	P-value
Patch	5	5.4063	1.0813	1.5679	0.001
Season	1	2.0354	2.0354	2.9514	0.001
P x S	2	1.4404	0.72022	1.0443	0.334
Res	151	104.14	0.68964		
Total	159	114.51			

Estimates of components of variation

Source	Estimate	Square root
Patch	0.020293	0.14245
Season	0.035206	0.18763
P x S	0.0014922	0.038629
V(Res)	0.68964	0.83044

PERMANOVA Pair-wise Tests for Patch Type

Groups	t	Significance Level
B, C	1.042	0.269
B, D	1.3341	0.004
B, ND	1.0688	0.212
B, E	1.0293	0.399
B, A	0.9824	0.512
C, D	1.4508	0.002
C, ND	1.4103	0.002
C, E	0.95219	0.686
C, A	1.0654	0.173
D, ND	1.7336	0.001

D, E	0.99741	0.456
D, A	1.114	0.148
ND, E	1.1017	0.195
ND, A	No test	df = 0
E, A	No test	df = 0

Several additional analyses were done to assess differences and relative variabilities of infaunal community structure among the patch types. A CAP was performed to ordinate the samples based on which specific patch type they were taken. The analysis indicates that while there is substantive overlap for some samples, most samples taken in patch types C, D, and ND had relatively more distinct infaunal communities than Patch Type B (Figure 5.2-15). An overlay of environmental factors associated with the samples indicates that increasing depth and coarser sediments grain sizes ($\Phi < 1$) correlated to the separation of patch type D samples from patch type C, which also was correlated with finer sediments. Infaunal communities at the ND sites were quite variable but distinct from the other patch types. They were correlated with somewhat higher latitudes (closer to the CT Shore) and a variable mix of sediment grain sizes. An analysis of rank correlations among communities in the patch types and environmental factors indicated the factors that were most highly correlated with trends community structure among the patch types included longitude, latitude, depth maximum bed stress, terrain roughness, and the $\Phi 1$ sediment grain-size fraction (Table 5-6).
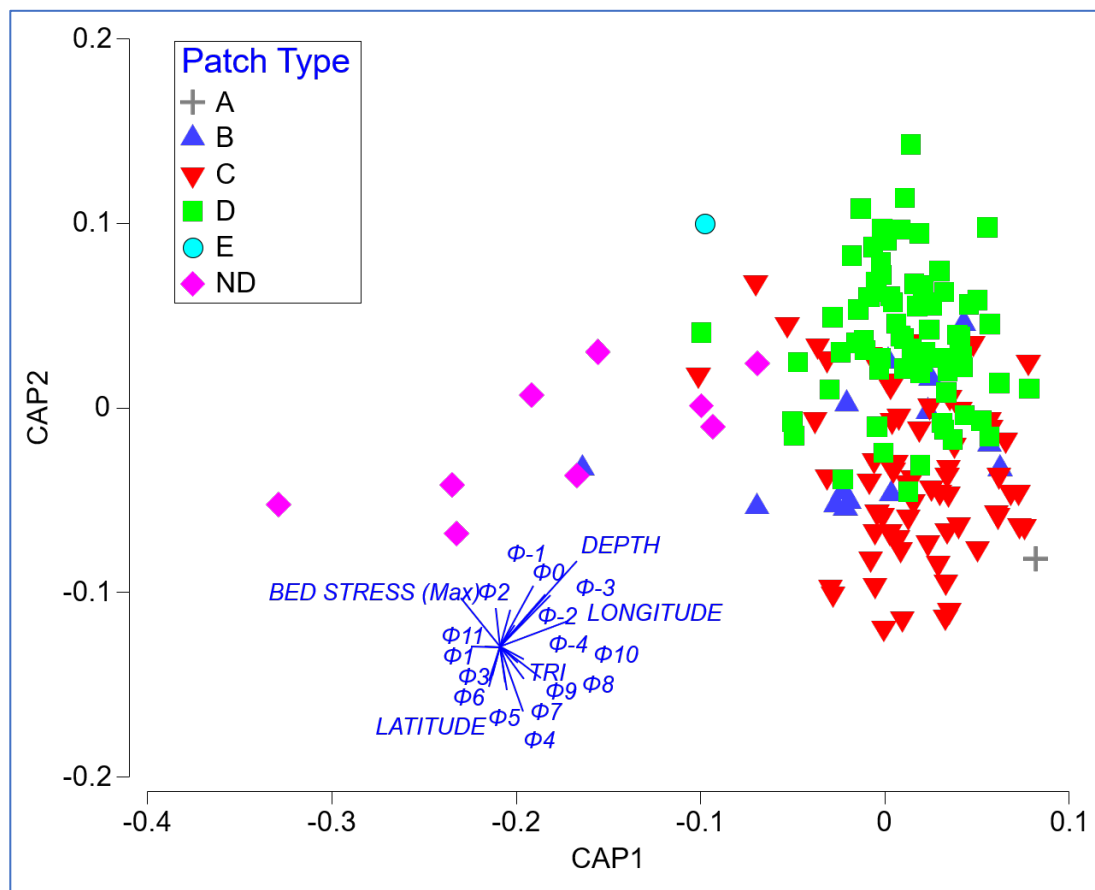
Figure 5.2-15. CAP analysis to discriminate community structure among a priori groups, in this case Patch Types. Also shown are vectors of correlation to environmental factors and geographic location

Table 5-6. Results of BVStep stepwise analysis of rank correlations among infaunal communities in different patch types and measured environmental variables. The Best results indicate the environmental variables that resulted in the highest correlation with the infaunal data within the different patch types.

Parameters
Correlation method: Spearman rank Method:
BVSTEP

Global Test
Sample statistic (Average Rho): 0.39
Significance level of sample statistic: 0.1% (p < 0.001)

Best results

No.Vars	Correlation	Variables Selected
6	0.390	Longitude, Latitude, Depth, Max Bed Stress, TRI Roughness, $\Phi1$*

* $\Phi1$: 0.5 mm sediment grain size fraction

The relative distinctness of infaunal communities was also borne out in an analysis of mean dispersion among patch types by randomizing (bootstrapping) calculation of centroids in ordination space. As indicted by the results presented above, communities in patch types C and D were relatively more similar than in patch type B in the ND samples which exhibit a much broader 95% envelope (Figure 5.2-16). Also, communities in patch types B and C were more similar relative to that in other patch types.
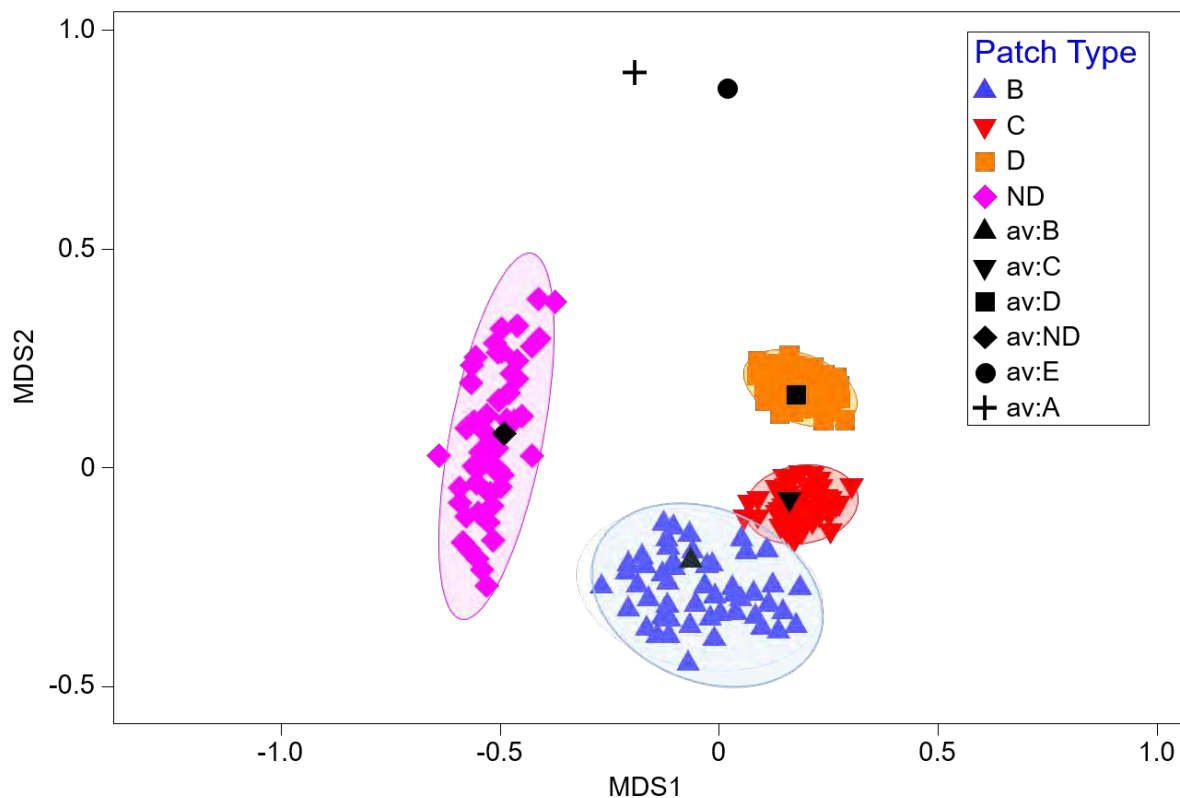
Figure 5.2-16. Results of bootstrap averages analysis for community structure among patch types in the LIS Phase II study area. This analysis calculates and plots bootstrap averages and confidence regions by bootstrapping centroids of resemblance matrix groups (in this case Patch Types). Shown are the bootstrap centroids and mean (average) centroid and 95% envelopes. Patch Types A and E only had one sample.

The abundances and species composition of the communities that were found in samples among the different patch types was fairly variable (Table 5-7). Only one sample was taken in patch type A and it was dominated by a very high abundance of the slipper shell *Crepidula fornicata,* as well as the polychaete *Cirratulus cirratus*, oligochaetes, and corophiid amphipods. In Patch Type B, the dominants were several crustacean taxa including corophiid amphipods, *Ampelisca vadorum*, the hermit crab *Pagurus longicarpus*, and several polychaetes including *Neptys picta* and *Praxillella praetermissa.* Infaunal communities in Patch Type C were dominated by the small bivalve *Astarte* spp, and several polychaete species including *Glycera capitata*, *Spiophanes bombyx* and *Mediomastus ambiseta*. *Pagurus longicarpus* and *Ampelisca vadorum* were also found in relatively high abundances in Patch Type C. The dominant taxa in Patch Type D were *Astarte* spp., corophiid amphipods, *Glycera capitata*, *Spiophanes bombyx* and *Mediomastus ambiseta*, similar to Patch Type C. Only one sample was taken in Patch Type E, and it was dominated by *Astarte* spp., the mussel *Mytilus edulis*, the sand dollar *Echinarachnius parma*, as well as *Crepidula fornicate* and the polychaete *Tharyx acutus.* The ND samples were dominated by several polychaete taxa including *Marenzallaria viridis, Mediomastus ambiseta, Spiophanes bombyx,* and *Nephtys picta* as well as corophiid amphipods. There were also notable differences in the taxonomic composition of less abundant species among the different patch types (Table 5-7).

Table 5-7. Results of SIMPER analysis of species contributions to the similarity of community structure within acoustic patch types

Patch Type A
No analysis - Less than 2 samples in group; given are top 10 species based on abundance in the one sample taken in patch type A

Crepidula fornicata	440
Cirratulus cirratus	92
Oligochaeta	72
Corophium spp.	18
Harmothoe imbricata	9
Anadara transversa	7
Dyspanopeus sayi	7
Idunella clymenellae	6
Crepidula plana	5
Glycera dibranchiata	5

Patch Type B
Average similarity: 20.48

Species	**Av.Abund**	**Av.Sim**	**Sim/SD**	**Contrib%**	**Cum.%**
Corophium spp.	0.90	1.74	0.93	8.50	8.50
Mediomastus ambiseta	0.93	1.70	0.77	8.28	16.78
Ampelisca vadorum	1.43	1.50	0.52	7.31	24.09
Pagurus longicarpus	0.73	1.05	0.51	5.14	29.23
Nephtys picta	0.61	0.90	0.42	4.41	33.64
Praxillella praetermissa	0.78	0.84	0.53	4.09	37.72
Spiophanes bombyx	0.69	0.82	0.53	3.98	41.71
Paraonis fulgens	0.63	0.78	0.42	3.83	45.54
Spiochaetopterus costarum oculatus	0.68	0.78	0.54	3.82	49.36

Species	Av.Abund	Av.Sim	Sim/SD	Contrib%	Cum.%
Arabella iricolor	0.66	0.72	0.53	3.52	52.88
Glycera capitata	0.56	0.57	0.40	2.76	55.65
Ilyanassa trivittata	0.45	0.55	0.35	2.69	58.33
Scalibregma inflatum	0.48	0.54	0.44	2.63	60.97
Cirratulus cirratus	0.36	0.54	0.35	2.62	63.59
Tanaid spp.	0.38	0.44	0.34	2.16	65.75
Astarte spp.	0.79	0.42	0.24	2.07	67.82
Nicomache lumbricalis	0.53	0.42	0.34	2.05	69.87
Magelona papilliformis	0.63	0.41	0.21	2.00	71.87

Patch Type C
Average similarity: 20.38

Species	Av.Abund	Av.Sim	Sim/SD	Contrib%	Cum.%
Astarte spp.	1.36	2.56	0.73	12.54	12.54
Glycera capitata	0.79	1.69	0.58	8.30	20.84
Spiophanes bombyx	0.86	1.23	0.68	6.05	26.89
Pagurus longicarpus	0.73	1.13	0.65	5.53	32.42
Mediomastus ambiseta	0.69	0.96	0.53	4.70	37.12
Ampelisca vadorum	0.96	0.93	0.42	4.56	41.69
Corophium spp.	0.77	0.89	0.56	4.36	46.05
Paraonis fulgens	0.54	0.79	0.35	3.85	49.90
Praxillella praetermissa	0.64	0.77	0.50	3.76	53.67
Echinarachnius parma	0.46	0.64	0.29	3.13	56.80
Spiochaetopterus costarum oculatus	0.49	0.47	0.41	2.30	59.10
Nicomache lumbricalis	0.49	0.46	0.39	2.26	61.36
Scalibregma inflatum	0.44	0.44	0.39	2.16	63.52
Syllidae	0.43	0.41	0.36	2.03	65.55
Cirratulus cirratus	0.43	0.40	0.33	1.97	67.52
Tharyx acutus	0.48	0.37	0.36	1.83	69.35
Spisula solidissima	0.39	0.35	0.32	1.71	71.06

Patch Type D
Average similarity: 28.27

Species	Av.Abund	Av.Sim	Sim/SD	Contrib%	Cum.%
Astarte spp.	2.34	4.69	1.41	16.61	16.61
Corophium spp.	1.29	2.04	1.06	7.23	23.83
Glycera capitata	1.05	1.89	0.94	6.69	30.52
Spiophanes bombyx	0.90	1.29	0.77	4.56	35.08
Mediomastus ambiseta	0.91	1.26	0.73	4.46	39.55
Paraonis fulgens	0.77	0.94	0.62	3.32	42.87
Pagurus longicarpus	0.72	0.92	0.63	3.24	46.11
Praxillella praetermissa	0.75	0.83	0.60	2.94	49.05
Nicomache lumbricalis	0.72	0.81	0.60	2.88	51.93
Ampelisca vadorum	0.89	0.73	0.45	2.59	54.53
Crepidula fornicata	0.86	0.73	0.44	2.59	57.12

Astyris lunata	0.70	0.71	0.52	2.50	59.62
Cirratulus cirratus	0.60	0.65	0.49	2.31	61.93
Anadara transversa	0.71	0.63	0.48	2.22	64.15
Syllidae	0.62	0.61	0.51	2.17	66.32
Scalibregma inflatum	0.56	0.60	0.50	2.12	68.44
Crenella	0.49	0.49	0.42	1.75	70.19

Patch Type E: No analysis - Less than 2 samples in group; given are top 10 species based on abundance in the one sample taken in patch type E

Astarte spp.	32
Mytilus edulis	16
Echinarachnius parma	8
Crepidula fornicata	4
Tharyx acutus	4
Glycera capitata	4
Unciola spp.	3
Mediomastus ambiseta	2
Harmothoe imbricata	1
Crepidula plana	1

ND (Patch type not determined)
Average similarity: 25.96

Species	Av.Abund	Av.Sim	Sim/SD	Contrib%	Cum.%
Marenzallaria viridis	1.96	4.82	1.29	18.56	18.56
Mediomastus ambiseta	1.11	2.35	1.16	9.06	27.62
Corophium spp.	1.09	1.84	0.89	7.07	34.69
Spiophanes bombyx	1.03	1.80	0.87	6.93	41.62
Nephtys picta	0.93	1.76	0.89	6.79	48.41
Pagurus longicarpus	0.94	1.15	0.68	4.43	52.84
Praxillella praetermissa	0.73	0.92	0.52	3.53	56.37
Lepidonotus squamatus	0.58	0.76	0.52	2.94	59.30
Ilyanassa trivittata	0.57	0.69	0.51	2.67	61.97
Paraonis fulgens	0.57	0.66	0.51	2.55	64.53
Ampharete arctica	0.52	0.66	0.51	2.54	67.06
Tellina agilis	0.53	0.59	0.37	2.29	69.35
Protohaustorius wigleyi	0.75	0.57	0.25	2.20	71.55

Patterns in community structure across acoustic patch types

Although infaunal communities differed among the large-scale patch types, there was a high degree of variability within patch types and, concurrently, similarity among some samples taken in different patch types (e.g., Figure 5.2-14). Classification (cluster) analysis coupled with a SIMPROF test was used to assess patterns in infaunal community structure across all samples, and identify groupings of samples with similar community structure irrespective of patch type, in order to better understand the distribution and composition of infaunal communities across the Phase II study area (Figure 5.2-17). This resulted in the identification of 13 community types, some of

which were relatively distinct from the others, and others that were more similar. Applying the community groupings to the nMDS ordination of the samples reveals that there were six relatively distinct communities (types b, c, d, g, l, and m), whereas the others (a, e, f, h, i, j, and k) exhibited a high degree of overlap (Figure 5.2-18). When three ordination axes are considered, there is greater separation among types j and k. A CAP ordination supports the results from the nMDS analysis, indicating that when the ordination is constrained by community type there are distinct differences in community structure among the types (Figure 5.2-19). Community types c, d, l and m, were most separated from the other types, but exhibited relatively more within community type variation. This assessment is also supported by a bootstrap averages analysis in which the 95% envelopes for the group centroid calculations are broader for these community types (Figure 5.2-20). It is interesting to note that for community type b the 95% envelope was quite large, indicating much more variable community structure within that community type.
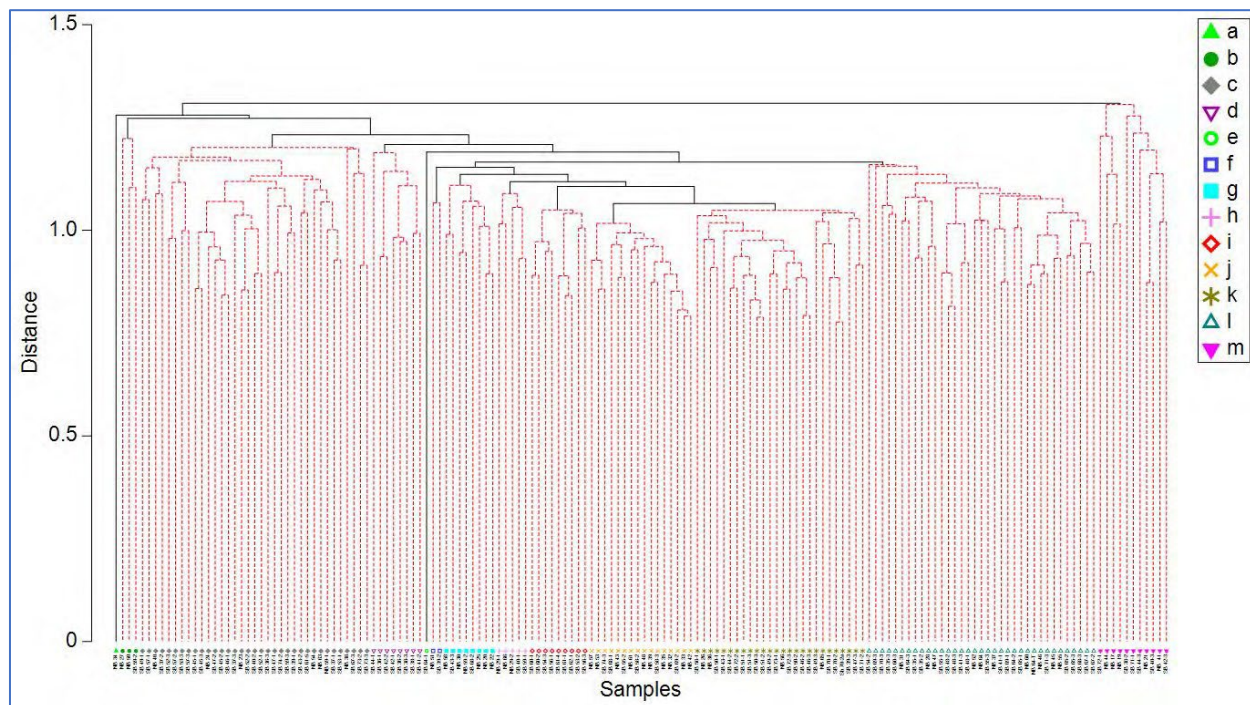
Figure 5.2-17. Classification dendrogram of infaunal samples in the Phase II study area. Data were 4th root transformed and similarity calculated using Hellinger distance resemblance function. A SIMPROF test was run to identify groups that are significantly different at p < 0.005.
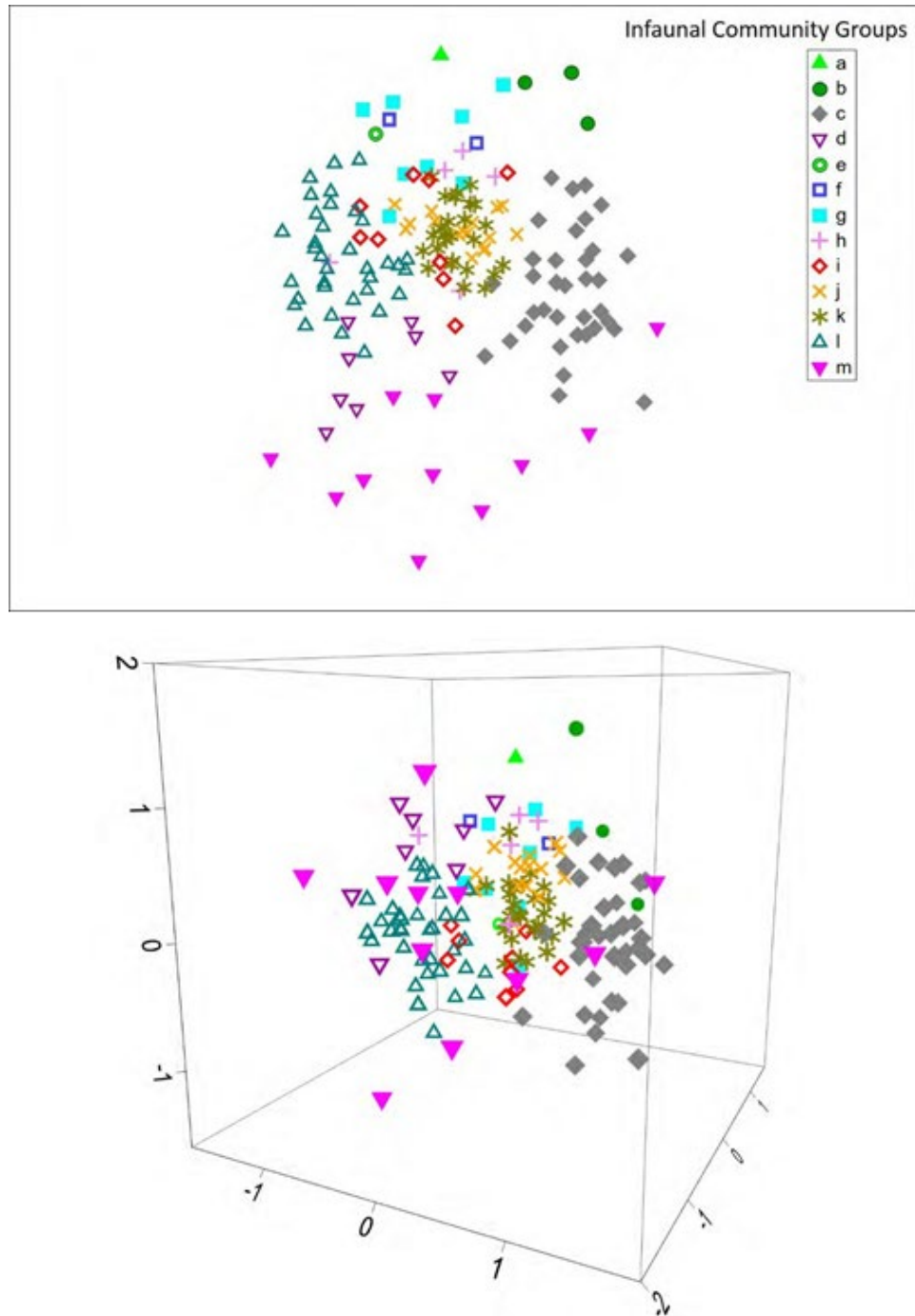
Figure 5.2-18. TOP: nMDS ordination of sample site infaunal communities grouped by community types as determined by classification and SIMPROF (see Figure 5.2-17) test in the LIS Phase II study area. Stress = 0.24, 4th root transformed abundances, Hellinger Distance Similarity Function. BOTTOM: Same nMDS ordination but showing group separation along 3 axes. Stress = 0.19.
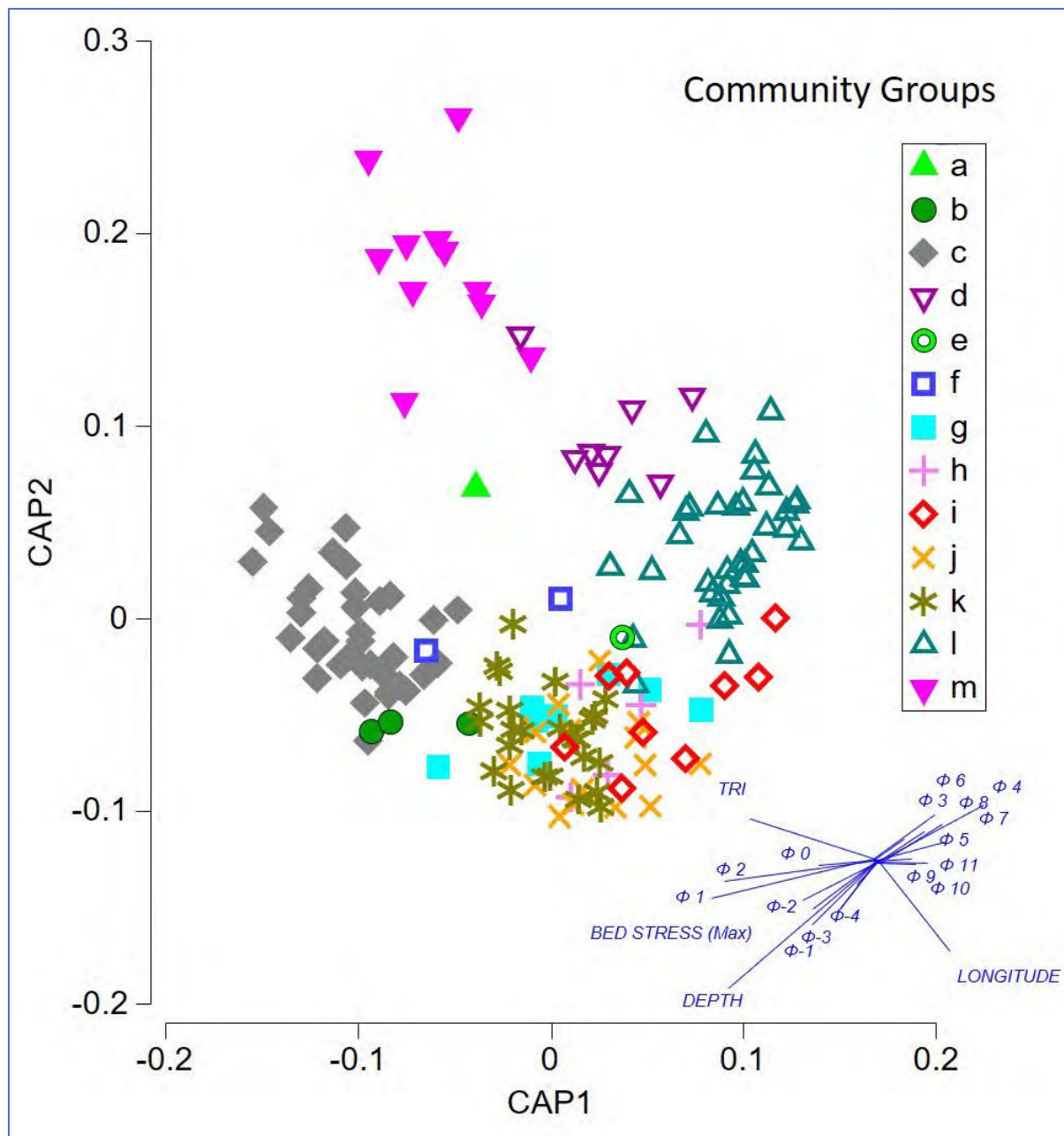
Figure 5.2-19. CAP analysis to discriminate community structure among a priori groups, in this case Community Types identified by a SIMPROF analysis (see Figure 5.2-17). Also shown are vectors of correlation to environmental factors and geographic location.
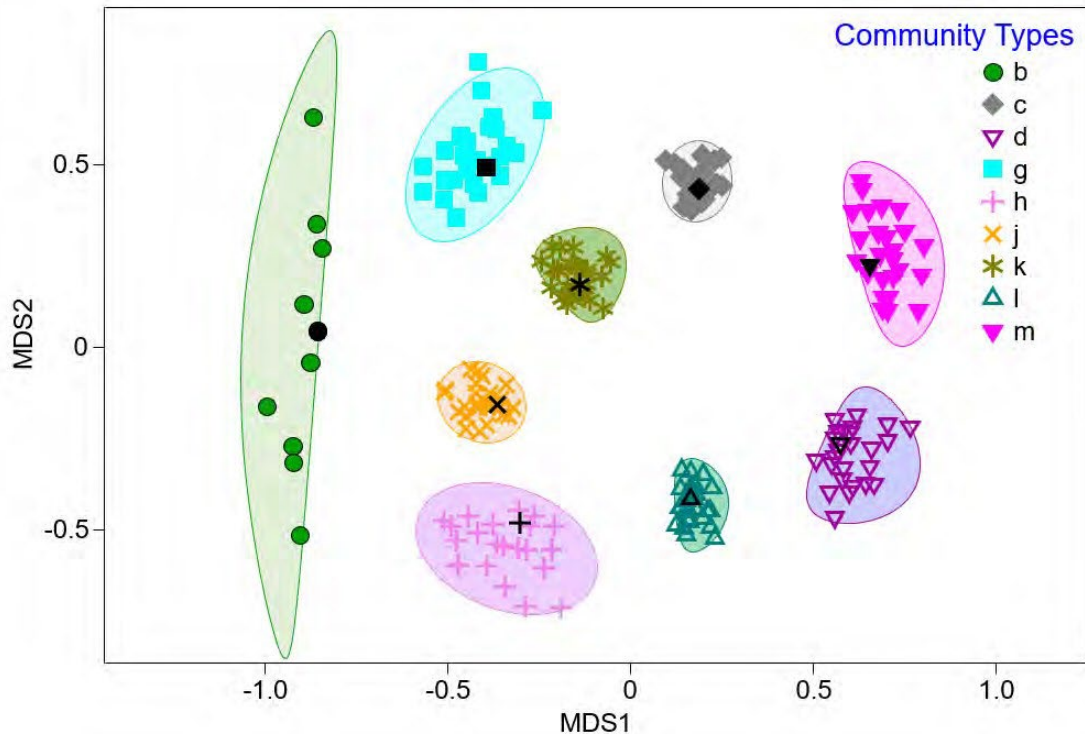
Figure 5.2-20. Results of bootstrap averages analysis of centroid location within community types in the LIS Phase II study area. This analysis calculates and plots bootstrap averages and confidence regions by bootstrapping centroids of resemblance matrix groups (in this case Community Types). Shown are the bootstrap centroids and mean (average) centroid (black symbol) and 95% envelopes. Community types with less than 4 samples were excluded from the analysis.

Both ANOSIM and PERMANOVA analyses indicated that there were significant differences among community types (Table 5-8) and that most pairwise comparisons of the community types were significantly different. SIMPER analysis indicted that some community types were dominated by just a few taxa, whereas others were relatively more diverse in terms of how many taxa contributed to similarity within the community (Table 5-9). Community Type b was dominated by just two taxa (the bivalves *Astarte* spp. and *Anadara transversa*), and type c by five taxa (notably also *Astarte* spp., but also several polychaete species and the sand dollar *Echinarachnius parma*). Community type d was dominated by polychaete taxa but also the crustacea *Corophium* spp. *Protohaustorius wigleyi* and *Chiridotea tuftsii*. Community types f and g were dominated by the slipper shell *Crepidula fornicata*; type f also had nigh abundances of *Corophium* spp. and the polychaete *Cirratulis cirratus*; type h also had relatively high abundances of *Corophium* spp but otherwise was dominated by bivalve and crustacean taxa (Table 5-9). Community type i had 20 taxa contributing to within-type similarity, with a diverse mix of crustacea, polychaetes and bivalves but also ophiuroids. Community type j also had a relatively large number of taxa contributing to within -type similarity in this community, dominated by *Astarte* spp. and the polychaetes *Ampharete arctica* and *Harmothoe imbricata*. Community type k was similar to type j but had a different mix of polychaete taxa at higher abundances than found in community type j. Community type l was dominated by the amphipod *Ampelisca vadorum* and the maldanid polychaete *Praxillella praetermissa*; there are also relatively high abundances of the hermit crab *Pagurus longicarpus*. Community type m also did not have many taxa contributing to overall community similarity, and was dominated by the Haustoriid amphipod *Phoxocephalus holbolli*, and the polychaete *Nephtys picta*.

Table 5-8. Results of multivariate statistical tests of differences among community types in the Phase II study area.

ANOSIM Test Global Test
Sample statistic (R): 0.576
Significance level of sample statistic: 0.1% (p<0.001)

Pairwise tests –community types pairs that are not significantly different (p < 0.05); are shaded in red; x – not test was performed.

	a	b	c	d	e	f	g	h	i	j	k	l	m
a													
b	0.25												
c	0.028	0.002											
d	0.111	0.006	0.001										
e	x	0.25	0.028	0.111									
f	0.333	0.1	0.002	0.022	0.333								
g	0.111	0.006	0.001	0.001	0.111	0.022							
h	0.167	0.018	0.001	0.001	0.167	0.048	0.002						
i	0.1	0.005	0.001	0.001	0.1	0.018	0.001	0.002					
j	0.059	0.001	0.001	0.001	0.059	0.007	0.001	0.001	0.001				
k	0.037	0.004	0.001	0.001	0.037	0.003	0.001	0.001	0.001	0.001			
l	0.028	0.001	0.001	0.001	0.028	0.002	0.001	0.001	0.001	0.001	0.001		
m	0.083	0.003	0.001	0.005	0.083	0.013	0.001	0.001	0.001	0.001	0.001	0.001	

PERMANOVA results of differences in Community Types

Source	df	SS	MS	Pseudo-F	P(perm)
Co	12	26.645	2.2204	3.7149	0.001
Res	147	87.863	0.5977		
Total	159	114.51			

Estimates of components of variation

Source	Estimate	Square root
S(Co)	0.1426	0.37763
V(Res)	0.5977	0.77311

Table 5-9. SIMPER results for community types found in the Phase II study area

Group a
Less than 2 samples in group

Group b
Average similarity: 21.93

Species	**Av.Abund**	**Av.Sim**	**Sim/SD**	**Contrib%**	**Cum.%**
Astarte spp.	1.64	12.02	3.91	54.82	54.82
Anadara transversa	0.86	3.46	0.58	15.76	70.58

Group c
Average similarity: 28.21

Species	Av.Abund	Av.Sim	Sim/SD	Contrib%	Cum.%
Astarte spp.	2.35	9.62	3.18	34.11	34.11
Glycera capitata	1.18	4.76	1.32	16.86	50.98
Echinarachnius parma	0.84	2.22	0.57	7.88	58.85
Paraonis fulgens	0.75	1.79	0.60	6.35	65.20
Astarte castaneum	0.70	1.56	0.56	5.51	70.72

Group d
Average similarity: 30.81

Species	Av.Abund	Av.Sim	Sim/SD	Contrib%	Cum.%
Marenzallaria viridis	2.16	6.32	2.82	20.51	20.51
Nephtys picta	1.04	2.81	1.55	9.13	29.64
Corophium spp.	1.32	2.33	1.01	7.56	37.20
Spiophanes bombyx	1.06	2.22	1.01	7.20	44.40
Mediomastus ambiseta	1.07	2.02	1.00	6.57	50.97
Protohaustorius wigleyi	0.99	1.30	0.34	4.23	55.20
Praxillella praetermissa	0.85	1.22	0.71	3.97	59.17
Sabellaria vulgaris	1.17	1.14	0.46	3.71	62.88
Magelona papilliformis	0.85	0.94	0.50	3.04	65.91
Tellina agilis	0.60	0.91	0.50	2.95	68.86
Chiridotea tuftsii	0.58	0.83	0.50	2.70	71.57

Group e
Less than 2 samples in group

Group f
Average similarity: 33.20

Species	Av.Abund	Av.Sim	Sim/SD	Contrib%	Cum.%
Corophium spp.	2.26	6.18	SD=0!	18.62	18.62
Crepidula fornicata	3.10	4.88	SD=0!	14.70	33.32
Nicomache lumbricalis	1.56	3.57	SD=0!	10.75	44.06
Praxillella praetermissa	1.54	3.57	SD=0!	10.75	54.81
Ceriantheopsis americanus	1.09	3.00	SD=0!	9.04	63.85
Cirratulus cirratus	2.05	3.00	SD=0!	9.04	72.89

Group g
Average similarity: 35.68

Species	Av.Abund	Av.Sim	Sim/SD	Contrib%	Cum.%
Crepidula fornicata	3.10	6.01	2.38	16.85	16.85
Astyris lunata	1.60	3.67	4.30	10.30	27.15
Crepidula plana	1.61	2.90	1.51	8.13	35.28
Corophium spp.	1.54	2.52	1.47	7.06	42.33
Anadara transversa	1.52	2.51	1.56	7.04	49.37
Astarte spp.	1.59	2.50	0.89	7.01	56.38
Pyramidellidae Family	1.48	2.38	1.04	6.66	63.04
Lepidonotus squamatus	1.05	1.50	1.01	4.20	67.24

| *Pagurus longicarpus* | 0.99 | 1.40 | 1.02 | 3.92 | 71.16 |

Group h
Average similarity: 38.90

Species	Av.Abund	Av.Sim	Sim/SD	Contrib%	Cum.%
Astarte spp.	1.71	5.22	6.68	13.41	13.41
Corophium spp.	1.49	4.61	5.03	11.85	25.26
Mytilus edulis	1.32	3.90	5.74	10.02	35.27
Praxillella praetermissa	1.21	3.73	13.32	9.59	44.86
Spiophanes bombyx	1.00	2.37	1.13	6.10	50.97
Ampharete arctica	1.10	2.17	1.15	5.57	56.54
Pagurus longicarpus	0.80	2.09	1.15	5.38	61.92
Lepidonotus squamatus	0.85	1.49	0.62	3.82	65.74
Nicomache lumbricalis	0.74	1.37	0.62	3.52	69.26
Glycera capitata	0.86	1.23	0.60	3.16	72.42

Group i
Average similarity: 41.52

Species	Av.Abund	Av.Sim	Sim/SD	Contrib%	Cum.%
Corophium spp.	1.70	2.95	7.21	7.10	7.10
Astarte spp.	2.46	2.92	0.98	7.04	14.14
Mediomastus ambiseta	1.79	2.60	1.64	6.25	20.40
Pagurus longicarpus	1.28	1.79	1.69	4.31	24.71
Arabella iricolor	1.15	1.77	1.66	4.27	28.99
Tharyx acutus	1.20	1.73	1.61	4.16	33.15
Lyonsia hyalina	1.10	1.66	1.64	4.00	37.15
Nucula spp.	1.18	1.36	1.07	3.28	40.43
Scalibregma inflatum	1.15	1.33	1.13	3.21	43.64
Anadara transversa	0.85	1.17	1.15	2.81	46.45
Asychis elongatus	1.07	1.15	0.77	2.76	49.21
Spiochaetopterus costarum oculatus	0.89	1.14	1.15	2.74	51.95
Nephtys picta	0.85	1.10	1.16	2.65	54.60
Astarte undata	1.07	1.10	0.81	2.64	57.24
Amphipholis squamata	0.87	1.06	0.83	2.54	59.78
Nicomache lumbricalis	1.01	0.99	0.81	2.38	62.17
Spiophanes bombyx	1.00	0.97	0.80	2.34	64.51
Syllidae	0.84	0.96	0.82	2.30	66.81
Amphipholis abditis	0.85	0.91	0.80	2.19	69.00
Paraprionospio tenuis	0.92	0.79	0.57	1.91	70.91

Group j
Average similarity: 44.84

Species	Av.Abund	Av.Sim	Sim/SD	Contrib%	Cum.%
Astarte spp.	3.00	4.98	3.47	11.10	11.10
Ampharete arctica	1.78	2.78	2.28	6.21	17.31
Harmothoe imbricata	1.34	2.29	2.25	5.11	22.43

Species	Av.Abund	Av.Sim	Sim/SD	Contrib%	Cum.%
Corophium spp.	1.53	2.10	1.59	4.67	27.10
Glycera capitata	1.29	2.03	1.47	4.54	31.64
Spiophanes bombyx	1.18	1.76	1.27	3.93	35.56
Pagurus longicarpus	1.08	1.60	1.06	3.57	39.14
Anadara transversa	1.04	1.55	1.31	3.46	42.60
Nicomache lumbricalis	1.10	1.55	1.28	3.46	46.06
Mediomastus ambiseta	1.02	1.46	1.30	3.25	49.30
Cirratulus cirratus	1.08	1.36	1.03	3.04	52.35
Marenzallaria viridis	0.96	1.27	1.03	2.83	55.17
Marphysa sanguinea	0.78	1.04	0.89	2.32	57.49
Praxillella praetermissa	0.82	1.01	0.89	2.24	59.73
Paraonis fulgens	0.90	0.98	0.74	2.19	61.92
Glycera dibranchiata	0.70	0.97	0.88	2.16	64.08
Mytilus edulis	0.86	0.96	0.69	2.15	66.23
Mulinia lateralis	0.86	0.94	0.74	2.09	68.32
Astarte undata	0.75	0.89	0.75	1.99	70.31

Group k
Average similarity: 41.31

Species	Av.Abund	Av.Sim	Sim/SD	Contrib%	Cum.%
Astarte spp.	2.74	5.59	3.82	13.54	13.54
Corophium spp.	1.64	3.19	2.59	7.73	21.27
Glycera capitata	1.37	2.83	2.42	6.86	28.13
Mediomastus ambiseta	1.37	2.45	1.59	5.94	34.07
Spiophanes bombyx	1.28	2.26	1.51	5.48	39.55
Paraonis fulgens	1.07	1.67	1.12	4.04	43.59
Tharyx acutus	1.11	1.60	1.10	3.88	47.47
Anadara transversa	1.18	1.58	0.97	3.82	51.29
Syllidae	1.04	1.49	1.12	3.60	54.89
Astyris lunata	1.07	1.33	0.87	3.22	58.10
Cirratulus cirratus	0.90	1.30	0.92	3.14	61.24
Praxillella praetermissa	0.98	1.22	0.82	2.95	64.19
Crepidula fornicata	1.25	1.08	0.60	2.62	66.81
Ampelisca vadorum	0.96	1.08	0.72	2.61	69.42
Pagurus longicarpus	0.84	1.05	0.80	2.55	71.97

Group l
Average similarity: 34.00

Species	Av.Abund	Av.Sim	Sim/SD	Contrib%	Cum.%
Ampelisca vadorum	2.40	5.44	1.54	16.01	16.01
Praxillella praetermissa	1.31	3.17	1.60	9.31	25.32
Spiophanes bombyx	1.26	2.72	1.48	8.01	33.33
Pagurus longicarpus	1.00	1.97	1.02	5.78	39.12
Corophium spp.	0.99	1.72	0.95	5.05	44.17
Arabella iricolor	0.87	1.65	0.97	4.85	49.02

Species	Av.Abund	Av.Sim	Sim/SD	Contrib%	Cum.%
Spiochaetopterus costarum oculatus	0.90	1.54	0.89	4.53	53.56
Nephtys incisa	0.87	1.27	0.70	3.74	57.30
Nicomache lumbricalis	0.78	1.11	0.66	3.27	60.57
Mediomastus ambiseta	0.77	1.10	0.66	3.23	63.79
Scalibregma inflatum	0.68	1.08	0.72	3.17	66.96
Clymenella torquata	0.79	0.91	0.55	2.67	69.64
Nephtys picta	0.69	0.86	0.52	2.53	72.17

Group m
Average similarity: 17.68

Species	Av.Abund	Av.Sim	Sim/SD	Contrib%	Cum.%
Phoxocephalus holbolli	1.06	3.35	0.57	18.94	18.94
Nephtys picta	0.72	2.32	0.57	13.10	32.04
Pagurus longicarpus	0.52	1.73	0.45	9.80	41.84
Tellina agilis	0.49	1.58	0.45	8.93	50.78
Paraonis fulgens	0.54	1.55	0.32	8.76	59.54
Glycera capitata	0.53	1.50	0.32	8.49	68.02
Ilyanassa trivittata	0.53	1.39	0.44	7.87	75.89

Several community types were generally found in each of the patch types (Figure 5.2-21, Table 5-10). However, there were differences within the community types based on patch type. For example, community type c was found in patch types B, C, D and E, whereas community type k was only found in patch types C, D and ND. Although several community types were found in each patch type, they were primarily comprised by predominantly one community type (Table 5-10). In Patch Type B, 50% of the sites were comprised of community type l, in Patch Type C, 60% of the sample sites were comprised of community types c and l, in Patch Type D, 63% of the sites were comprised of community types c, j and k, and in the ND group, 60% of the sites were comprised of community typed. Patch Types C and D had had the most community types across sites that were in those patch types, 10 and 12, respectively. Community types c, l, and m were each found in four patch types.
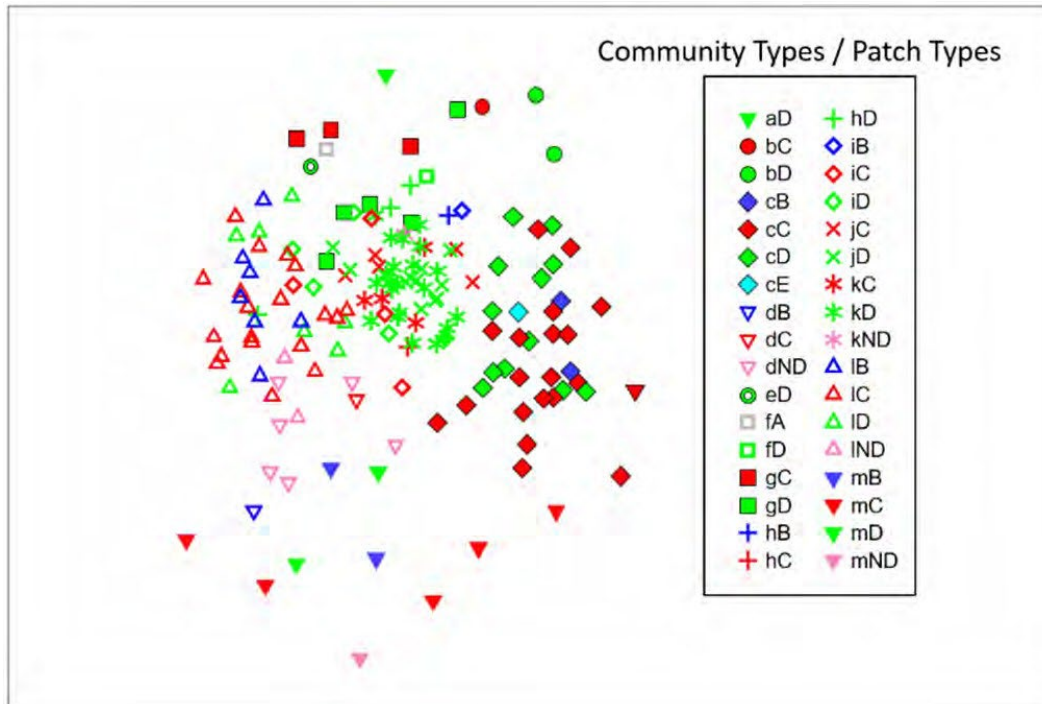
Figure 5.2-21. nMDS ordination of sample site infaunal communities grouped by community types and patch types in the LIS Phase II study area. (Stress = 0.24, 4th root transformed abundances, Hellinger Distance Similarity Function)

Table 5-10. Frequency of community types in each patch type

	PATCH TYPES							
COMMUNITY TYPE	A	B	C	D	E	ND	Total Patch Types	Total Sites
a	0	0	0	1	0	0	1	1
b	0	0	1	2	0	0	2	3
c	0	2	19	13	1	0	4	35
d	0	1	1	0	0	6	3	8
e	0	0	0	1	0	0	1	1
f	1	0	0	1	0	0	2	2
g	0	0	3	5	0	0	2	8
h	0	1	1	3	0	0	3	5
i	0	1	4	4	0	0	3	9
j	0	0	5	11	0	0	2	16
k	0	0	4	21	0	1	3	26
l	0	7	19	7	0	2	4	35
m	0	2	6	2	0	1	4	11
Total community types	1	6	10	12	1	4		
Total Sites	1	14	63	71	1	10		160

In general, infaunal community types showed a variety of spatial distributions across the Phase II area (Figure 5.2-22). The most prevalent community types c, j, k, l and m, were found primarily in specific areas of the Phase II area. Community type c was primarily distributed along the southern margins of the Phase II area, and also through the west central area. In relation to environmental conditions, these communities appear to be associated with higher seafloor rugosity (as measured by TRI), sand size-fractions in the range of ~ 1 to 0.25 mm (Φ 0 to1) and for some locations increasing depth (Figure 5.2-19). Community types j and k, which were relatively similar (Figure 5.2-19), were mostly distributed thorough the central portions of the Phase II area, with some j and k communities also found in FIS (Figure 5.2-22). These communities were found at greater depths within the Phase II area and had greater proportions of coarser sediment grain-sizes (~ 2 to 15 mm; Φ -1 to -4). Community type l was found primarily along the northern boundary of the Phase II area, in relatively shallower depths along the Connecticut shore, and were characterized by greater proportions of fine-grained sediments < 1 mm (Φ 3 to 8) (Figure 5.2-19 & Figure 5.2-22). Community type m was primarily found in the western portion of the Phase II area, south of the mouth of the Connecticut River, although there were a few sites with this community type in the eastern portions of the area (Figure 5.2-22). This community type was associated with high seafloor rugosity and mixed sediment grain sizes (Figure 5.2-19). Community type d was distributed primarily thought this area as well. Community types j and k were found in the central portion of, and across the north to south breadth, of the Phase II area. The other community types were somewhat more scattered throughout the Phase II area. The relative similarities amongst the sample sites and their community types were significantly correlated with the geographic distances among the sites (RELATE procedure, average ρ= 0.186, p = 0.009), consistent with the result that most sites within a specific community type were geographically closer to each other relative to sites in the other community types.
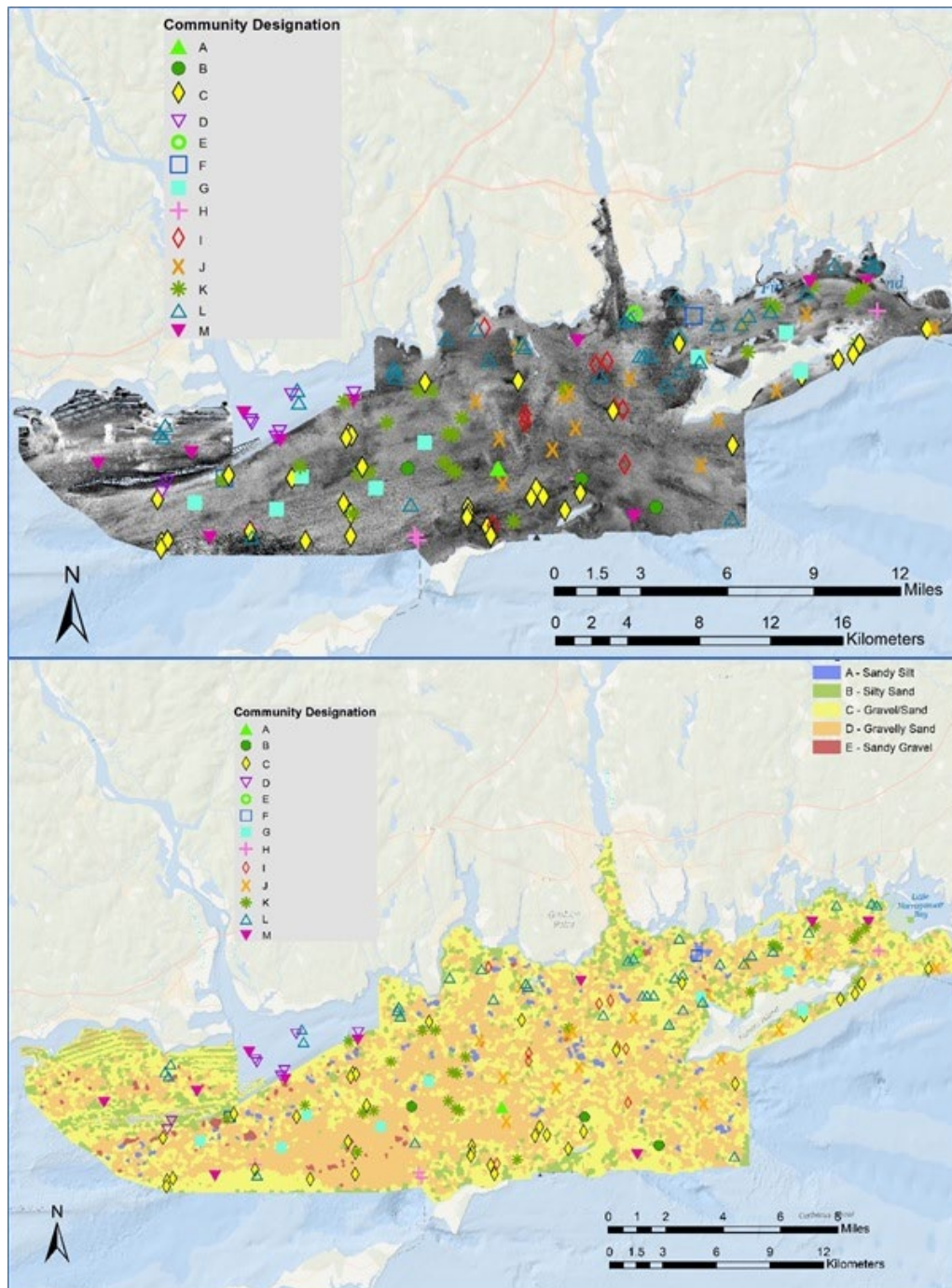
Figure 5.2-22. Spatial distribution of community types as shown on backscatter mosaic (top) and Patch Types (bottom)

The distributions of the ten most abundant taxa were also spatially variable (Figure 5.2-23 – Figure 5.2-26). Three taxa, the amphipod *Ameplisca vadorum*, the maldanid polychaete *Praxiella praetermissa*, and the spionid polychaete *Marenzellaria viridis*, were most abundant along the northern sections of the Phase II area (Figure 5.2-23). *Ameplisca vadorum* and *Praxiella praetermissa* were also found in relatively high abundances in some of the deeper water sections of the central portion of the Phase II area. *Marenzellaria viridis* was most abundant southeast of the mouth of the CT River, and in FIS.
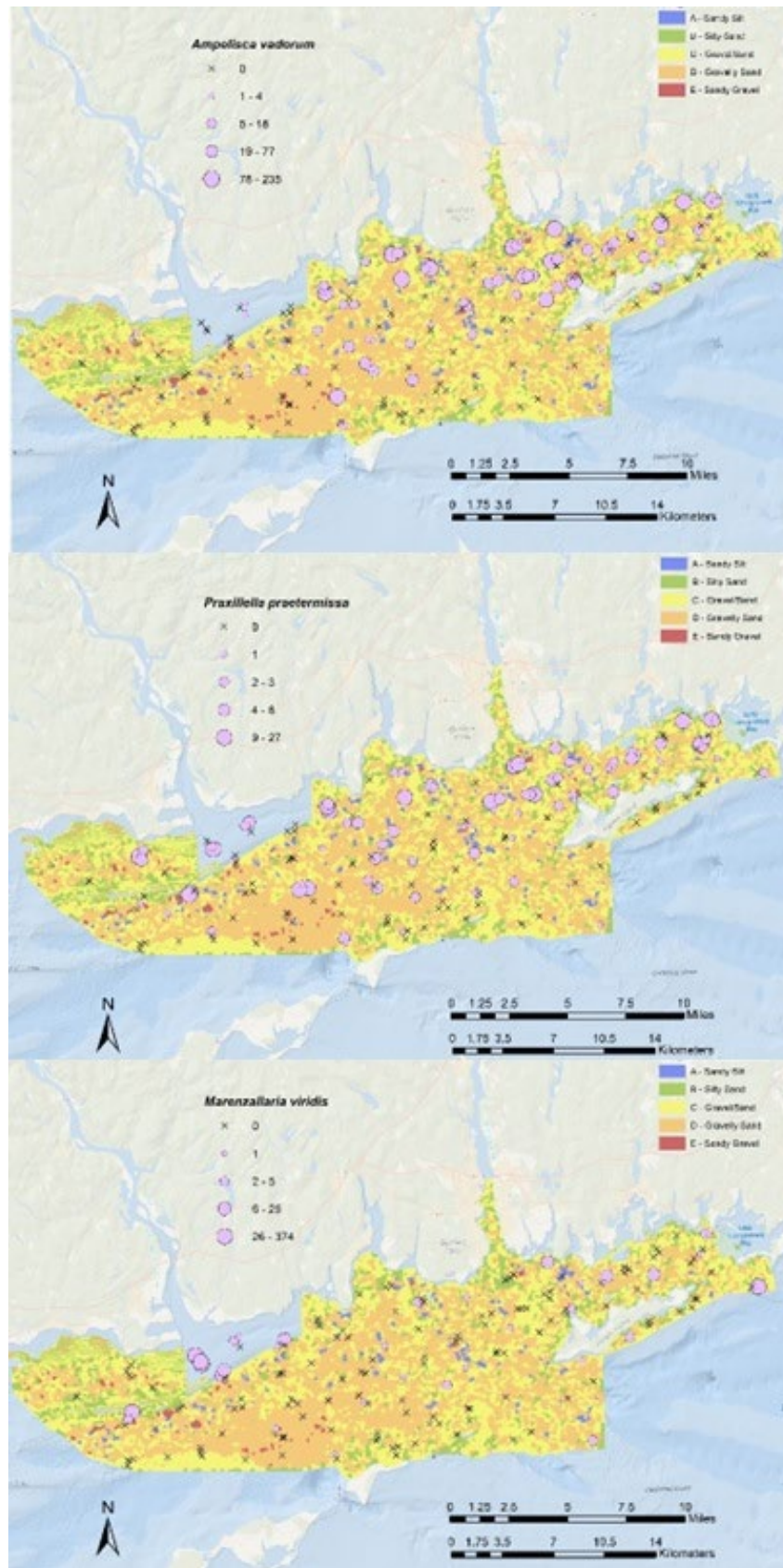
Figure 5.2-23. Spatial distribution of several dominant infaunal taxa in the Phase II study area
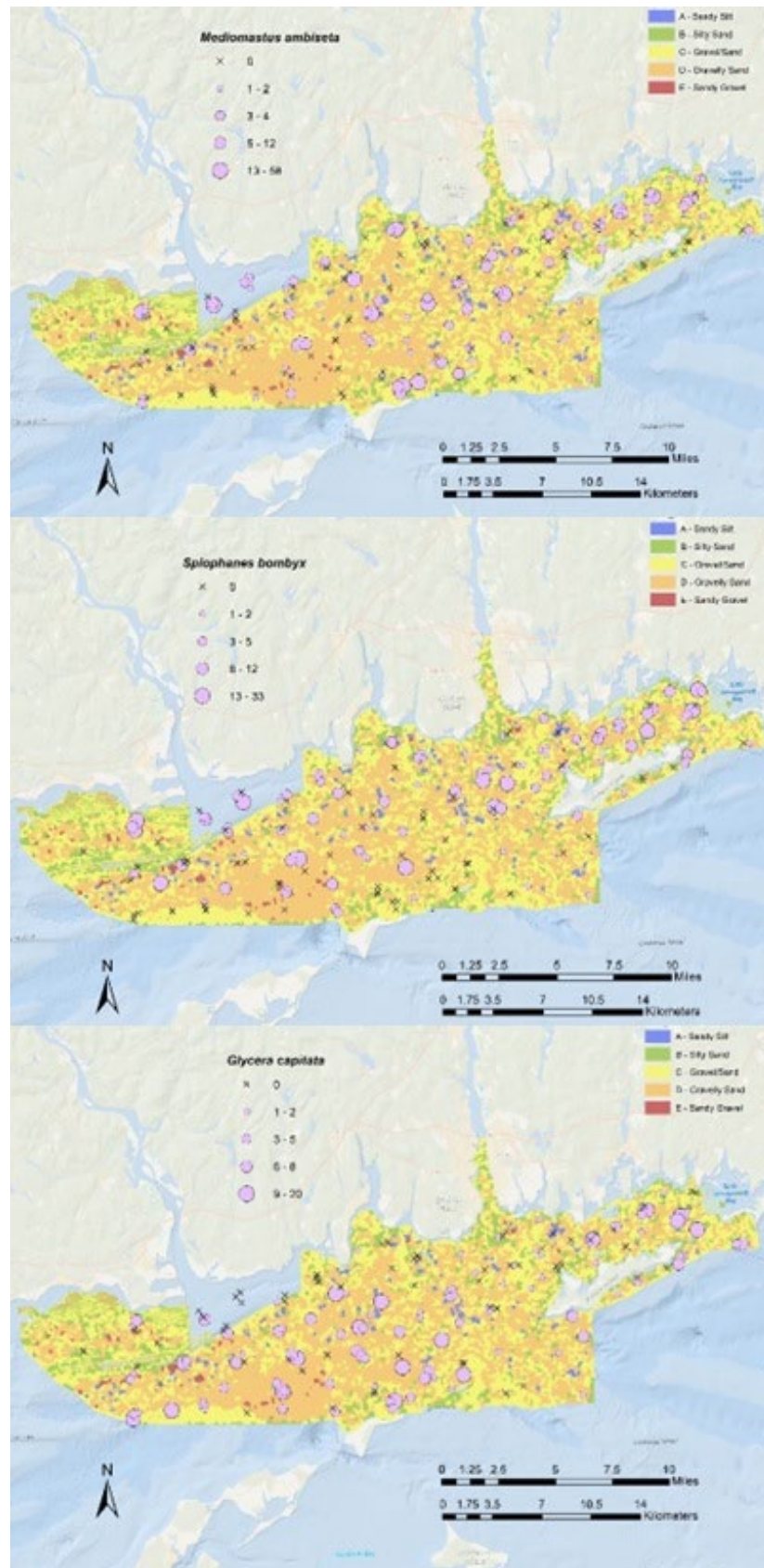
Figure 5.2-24. Spatial distribution of several dominant infaunal taxa in the Phase II study area
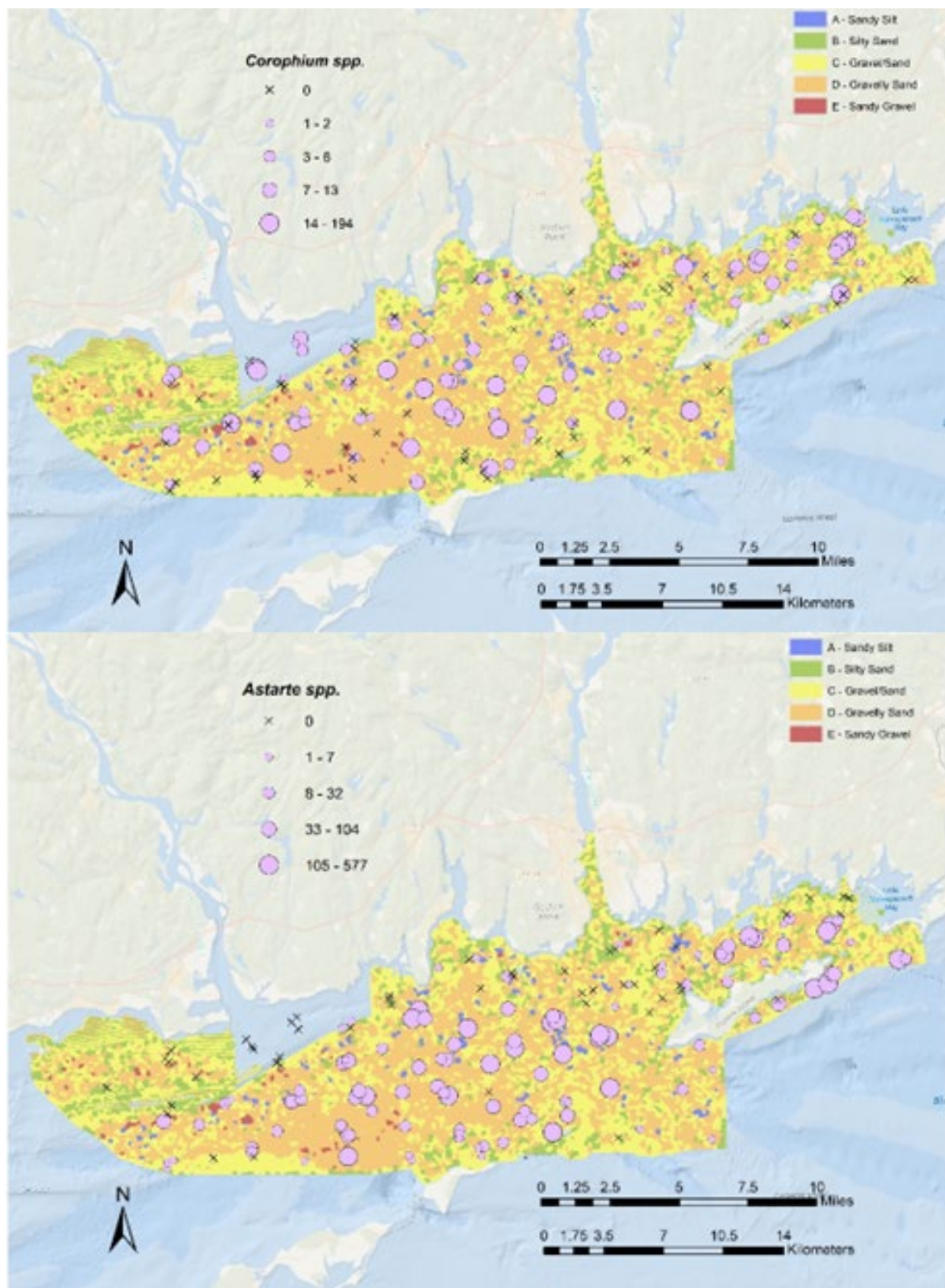
Figure 5.2-25. Spatial distribution of several dominant infaunal taxa in the Phase II study area
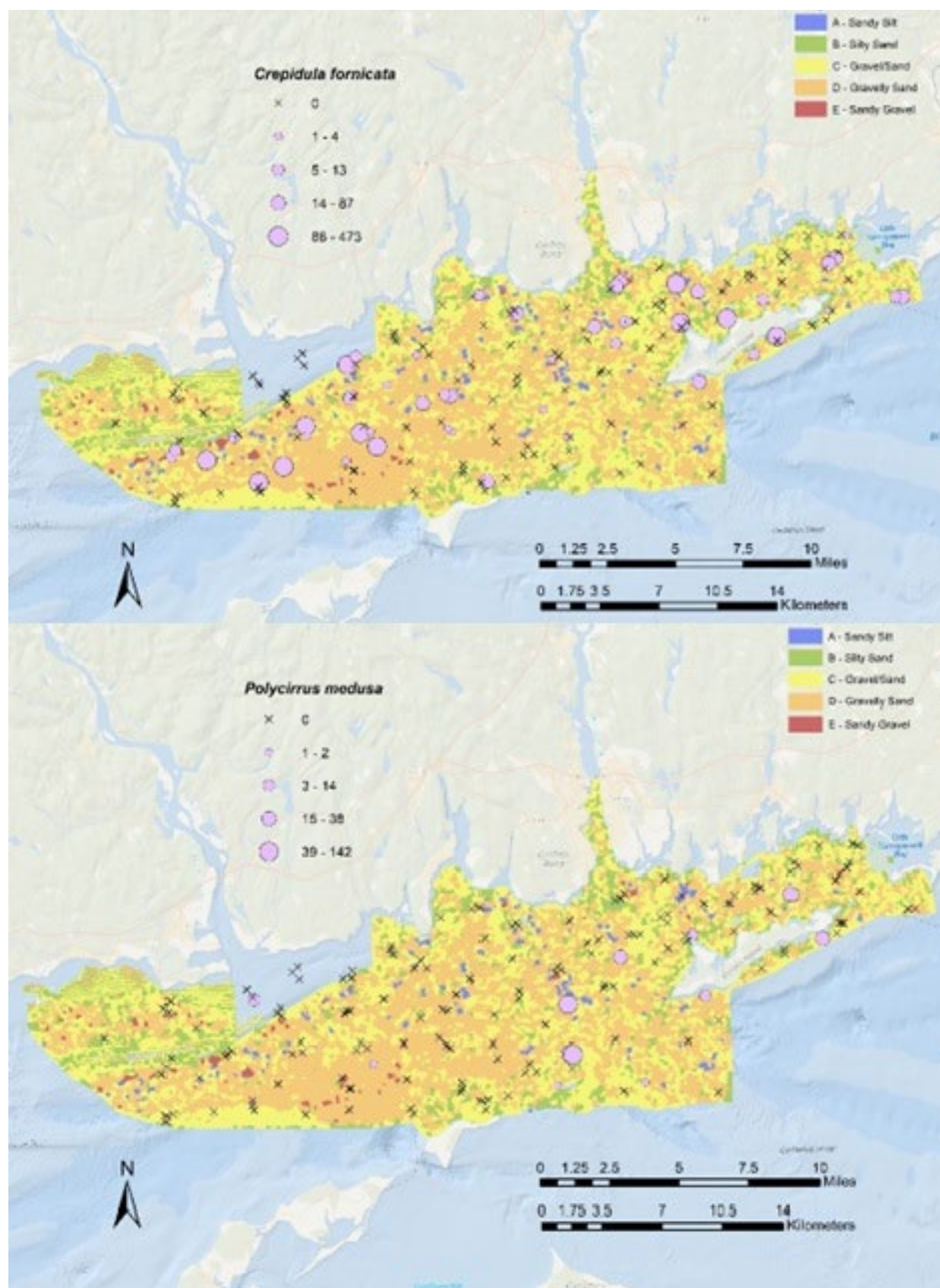
Figure 5.2-26. Spatial distribution of several dominant infaunal taxa in the Phase II study area

Five taxa were abundant throughout the deeper sections, as well as in some other locations, of the Phase II area (Figure 5.2-24 & Figure 5.2-25). The capitellid polychaete *Mediomastis ambiseta* was most abundant through the center of the area, along the southern border northwest of Plum Island, and in FIS. Relatively high abundances were also found south of the mouth of the Connecticut River and Niantic Bay. *Spiophanes bombyx*, a small, tube building polychaete, was found in high abundances in the western half of the Phase II area, in a cluster south of the mouth of the Thames River, and in FIS. A small predatory polychaete, *Glycera capitata*, had a similar spatial distribution (Figure 5.2-24). A group of corophiid amphipods, *Corophium* spp., were distributed in high abundance through the central portion of the Phase II area, extending into the area of the Race southwest of Fishers Island and also in FIS. A group of small bivalves within the genus *Astarte*, (designated as *Astarte* spp. as these may be juveniles of several other *Astarte* species that were found; alternatively, these may be *Astarte subaequilatera*) were found in very high abundances throughout the central portion of the Phase II area and also in FIS and south of Fishers Island (Figure 5.2-25).

Two of the dominant taxa found during the study had somewhat more limited spatial distributions. The slipper shell *Crepidula fornicata* was found in high abundance in the western portion of the Phase II area and also in FIS and south of Fishers Island (Figure 5.2-26). No individuals were found in deeper waters of the central portion of the area and southeast towards the Race. The terebellid polychaete *Polycirrus medusa* was found in high densities at several sites in the eastern most portion of the study area in deeper water, as well around the nearshore areas of Fishers Island (Figure 5.2-26).

5.2.2.4 Discussion

Infaunal community composition and structure varied across the Phase II study area. This variation can likely be attributed, in part, to the environmental differences found among the acoustic patch types and environmental variability within each acoustic patch type relative to the large-scale environmental gradients across this portion of LIS. The ecological characteristics and dynamics of the infauna that are found in this area will also contribute to variations in community structure. These include such factors as life history, seasonality of reproduction and recruitment, differences in local species pools, functional characteristics (e.g., feeding type, motility, etc.), and habitat requirements. However, there are some general trends that can be identified. Total abundance, taxonomic richness, and diversity were highest in the central and eastern portions of the Phase II study area (Figure 5.2-4, Figure 5.2-8 & Figure 5.2-12). High abundances were found in the central portion of FIS and also within a large, deeper water area of the central portion of the study area. High taxonomic richness was found in the western portion of FIS, south of the Thames River, and in central portion of the study area. High taxonomic diversity followed a similar pattern as taxonomic richness although they were not spatially congruent. For example, an area of high diversity south of the Thames River was spatially broader than that of taxonomic richness, whereas diversity extended further to the east in FIS, then taxonomic richness.

These community characteristics were found at relatively low levels in the western portion of the Phase II area. This area is highly dynamic due to the influence of freshwater discharge from the Connecticut River, and hydrodynamic conditions which generate sand wave fields with varying geomorphologies (Bokuniewicz et al., 1977; Fenster et al., 1990)). Although the sand waves are

relatively stable over the large-scale (Fenster et al., 1990), they are locally dynamic in terms of sediment flux. These overall conditions in this portion of the Phase II area may reduce habitat suitability for certain infauna. Higher taxonomic richness and diversity in the central and eastern portions of the study area may reflect the number of environmental and ecological conditions. From the central to eastern portions of the area, there is a greater spatial heterogeneity of acoustic patch types, and related small-scale diversity in patch types. Taxonomic richness and diversity in this area may be due in part to increased habitat diversity. These areas are also closer to BIS and areas of tidal change through The Race and eastern FIS, and are thus more likely to have a larger species pool to draw on. High total abundance in many of the samples was due to the presence of a small bivalve, *Astarte* spp., particularly in the general high abundance areas outlined in Figure 5.2-22.

Community structure was assessed both with respect to acoustic patch types and in general across the Phase II area. Based on latter assessment, there were three prevalent community types distributed across this portion of LIS. Community type c was found mostly across the western portion of the Phase II study area, along its southern border, north of Plum and Gull islands, and south of Fishers Island (Figure 5.2-22). Taxa with highest average abundance in this community type included the small bivalve *Astarte* spp. (likely *Astarte subaequilatera*, the lentil Astarte), a predatory polychaete annelid (bloodworm) *Glycera capitata,* the sand dollar *Echinarachnius parma,* and the burrowing polychaete *Paraonis fulgens.* Each of these taxa are known to prefer sandy sediments, such as found through much of the western and southern portions of the study area, where acoustic patch types C and D dominated much of the seafloor. With several patches of type E. Community Type c was similar to the composition of numerically dominant taxa identified for acoustic patch types C and D, and to a lesser extent type E. Community Type k was most common across the west-central portion of the Phase II area and also in the eastern-most portions of FIS (Figure 5.2-22). Dominant taxa included *Astarte* spp.*,* the amphipods *Corophium* spp. and *Glycera capitata,* and the tubiculous polychaete annelids *Mediomastus ambiseta* and *Spiophanes bombyx.* This community had same dominance structure as that identified for acoustic patch type D and was found mostly in this acoustic patch type. Community type l was primarily found in shallower waters along the Connecticut coast both in LIS and through FIS (Figure 5.2-22). It was dominated by the tube building amphipods *Ampelisca vadorum* and *Corophium* spp., the tube building polychaete annelids *Praxillella praetermissa* (a species of bamboo worms) and *Spiophanes bombyx,* and the hermit crab *Pagurus longicarpus.* This set of dominants is very similar to that found for acoustic patch type B and reflects a preference for shallower habitats comprised of finer sediments where many of the Type B patches are located.

The infaunal community patterns discussed above exhibit a number of similarities to those found in previous studies. Data from Pellegrino and Hubbard (1983) indicated a gradient of increasing species richness from the area of the Connecticut River east to FIS (Figure 5.2-1) with an area of elevated species richness in the central portion of the area south of Niantic Bay. These patterns agree with those found in this study for taxonomic richness (Figure 5.2-8). Analysis of community structure using the Pellegrino and Hubbard (1983) by Zajac (1998) resulted in recognizing several community groupings (or types) in ELIS spanning the Phase II area (Figure 5.2-1). The most prevalent was a community designated as Group I (Table 5-11), which was found primarily in the west-central portion of the Phase II area but also in FIS. A community group designated as H2 was distributed primarily south of the Thames River and also in some areas westward along the Connecticut coast to the Connecticut River. Just south of the Connecticut River there was a mixture of community groups H2, I, and K. The most prevalent community types in the area surveyed by

Pellegrino and Hubbard (1983) that were designated in this study included community types l and k (Table 5-12). The taxonomic compositions of the community types designated in both studies were very similar. There was a similar set of tube-building polychaetes among the communities, including *Spiophanes, Prionospio, Ampharete,* and *Clymenella*; although, there was a greater variety of bamboo worms (e.g., *Praxillella,* in the communities designated in this study). There is also a similar set of burrowing polychaetes including *Paraonis, Cirratulis, Nephtys*, and *Mediomastus/Capitella*. However, there is also a greater diversity of these kinds of annelids in the communities designated in this study. The composition of crustaceans was dominated by *Ampelisca* and *Corophium* taxa, and other amphipods. The biggest differences were in the composition of mollusk taxa. *Nucula* and/or *Mulinia* were found in all of the community types; community types l and k designated in the study were dominated by a small clam, *Astarte* spp., and also had locally high abundances of the slipper shell *Crepidula* (Table 5-12). Ophiuroids were also common in the community types designated in this study. Differences in the specific overall composition of dominant taxa among the two studies may be due to the seasonality of sampling and differences in the collection and processing of samples. However, generally there are similarities in the overall suites of species with similar life habits and functional characteristics (see also Table 5-13). For example, tube-building spionids were prevalent component of all communities, as well as bamboo worms which construct tubes deeper into the sediments. Another significant component in all communities were several different taxa of tube-building amphipods. In terms of burrowing infauna, although, communities were dominated by Cirratulid and Paraonid polychaetes and the carnivorous/omnivorous nephtyid polychaetes.

Table 5-11. Results of PERMANOVA test of differences in community structure

Factors

Name	Abbrev.	Type	Levels
Patch Type	Pa	Fixed	6
Community BC 4th root	Co	Fixed	13

PERMANOVA table of results

Source	df	SS	MS	Pseudo-F	P(perm)	Unique perms
Pa	5	3.1814	0.63628	1.0763	0.22	996
Co	12	17.905	1.4921	2.524	0.001	993
PaxCo**	16	10.303	0.64394	1.0893	0.046	995
Res	126	74.485	0.59115			
Total	159	114.51				

** Term has one or more empty cells

Details of the expected mean squares (EMS) for the model

Source	EMS
Pa	1*V(Res) + 9.6265*S(Pa)
Co	1*V(Res) + 6.4768*S(Co)
PaxCo	1*V(Res) + 3.8772*S(PaxCo)
Res	1*V(Res)

Construction of Pseudo-F ratio(s) from mean squares

Source	Numerator	Denominator	Num.df	Den.df

Pa	1*Pa	1*Res	5	126
Co	1*Co	1*Res	12	126
PaxCo	1*PaxCo	1*Res	16	126

Estimates of components of variation

Source	Estimate	Sq.root
S(Pa)	0.0046882	0.068471
S(Co)	0.1391	0.37296
S(PaxCo)	0.013615	0.11668
V(Res)	0.59115	0.76886

Table 5-12. Comparison of composition of dominant taxa in the Phase II study area among communities identified by Zajac (1998) and Zajac et al. (2000) based on data in Pellegrino and Hubbard (1983) and this study. See Figure 5.2-1 and Figure 5.2-22 for locations.

Zajac 1998 Type I	Zajac 1998 Type H2	This Study Type L	This Study Type K
Polychaetes			
Prionospio heterobranchia	*Prionospio heterobranchia*	*Prionospio steenstrupi*	
Spiophanes bombyx	*Spiophanes bombyx*	*Spiophanes bombyx*	*Spiophanes bombyx*
Prionospio tenuis	*Steblospio benedicti*	*Marenzallaria viridis*	*Sabellaria vulgaris*
Polydora websteri		*Spiochaetopterus c. oculatus*	*Spiochaetopterus c. oculatus*
Ampharete arctica		*Ampharete arctica*	*Ampharete acutifrons*
Clymenella zonalis	*Clymenella zonalis*	*Clymenella torquata*	*Asychis elongatus*
		Praxillella praetermissa	*Praxillella praetermissa*
		Nicomache lumbricalis	*Nicomache lumbricalis*
	Paraonis fulgens	*Paraonis fulgens*	*Paraonis fulgens*
Cirratulus cirratus		*Magelona papilliformis*	*Cirratulus cirratus*
Cirratulus grandis	*Cirratulus grandis*	*Tharyx acutus*	*Tharyx acutus*
Aricidea jeffersyii	*Mediomastus ambiseta*	*Mediomastus ambiseta*	*Mediomastus ambiseta*
Capitella capitata	*Nephtys incisa*	*Nephtys incisa*	*Glycera capitata*
Nephtys picta	*Nephtys picta*	*Nephtys picta*	*Syllidae*
		Scalibregma inflatum	*Scalibregma inflatum*
		Arabella iricolor	*Arabella iricolor*
			Polygordius spp
			Nereis grayi
Crustaceans			
Ampelisca vadorum	*Ampelisca vadorum*	*Ampelisca vadorum*	*Ampelisca vadorum*
Ampelisca abdita	*Ampelisca abdita*	*Ampelisca verrrilli*	*Corophium* spp.
Corophium acheruscum	*Corophium acheruscum*	*Corophium* spp.	*Pagurus longicarpus*
Lepidontus squamotus	*Leptocheirus pinquis*	*Pagurus longicarpus*	*Lepidonotus squamatus*
Unciola irrorata	*Unciola irrorata*	*Pinnixulala retinens*	*Caprella penantis*
Aeginina longicornis	*Ancanthohaustorius millsi*	*Pinnixa sayana*	*Lysianopsis alba*
			Idunella clymenellae
			Americamysis bigelowi
Mollusks			
Pandora gouldina	*Nucula annulata*	*Astarte* spp.	*Astarte* spp.
Ensis directus	*Pitar morrhuana*	*Mulinia lateralis*	*Mulinia lateralis*

Nucula annulata	*Mulinia lateralis*	*Crepidula fornicata*	*Crepidula fornicata & C. plana*
Tellina agilis	*Tellina agilis*	*Spisula solidissima*	*Anadara transversa*
Mytilus edulis		*Bittiolum alternatum*	*Bittiolum alternatum*
			Nucula proxima
			Pyramidellidae Family
			Astyris lunata
Ophiuroids			
			Amphipholis squamata

Table 5-13. Dominant taxa found within a 19.4 km² area just south of mouth of the Thames River that was surveyed using habitat mapping and ecological characterization approaches similar to those used for this study (Zajac et al., 2000 2003).

	Feeding	**Motility, Sediment Modification**
Polychaetes		
Prionospio steenstrupi	Surface deposit-feeding, Filter feeding	Discretely motile, Tubiculous
Kirkegaardia dorsobranchialis	Surface deposit-feeding	Discretely motile/motile, Sediment bioturbating?
Chaetozone spp.	Surface deposit feeder	Discretely motile
Aricidea catherinae	Herbivore, Surface deposit feeder	Motile, Burrower
Polycirrus exumis	Surface deposit feeder	Discretely motile
Nephtys spp.	Carnivorous, Burrowing deposit feeder	Motile
Clymenella torquata	Subsurface deposit feeder	Sessile, Tubiculous, Bioturbation, Oxygenation
Mediomastus ambiseta	Burrowing deposit feeder	Motile, Pelletization
Amphipods		
Ampelisca vadorum	Surface deposit/ suspension feeder	Tubiculous
Unicola irrorata	Surface deposit/ suspension feeder	Tubiculous
Microduetopus gryllotalpa	Surface deposit/ suspension feeder	Tubiculous
Phoxocephalus holboli	Surface deposit/ suspension feeder	Tubiculous
Exogenes hebes	Herbivore, Surface deposit feeder, Carnivore	Motile, Burrower, Nontubiculous
Bivalve		
Nucula annulata	Subsurface deposit feeder	Discretely motile
Other		
Nemertean	Carnivore	Burrowing
Oligochaete spp.	Burrowing deposit feeder	Motile

A more recent study by Zajac et al. (2003), that used similar seafloor mapping and ecological characterization approaches in a small area south of the mouth of the Thames River found a suite of dominant species similar (Table 5-13) to those designated in this study and by Zajac (1998) in that general location.

5.2.3 Epifaunal Ecological Characterization

5.2.3.1 Background and Objectives

This element of the project is an extension of studies to develop spatially comprehensive seafloor habitat maps and interpretive products for Phase II study area inclusive of emergent- and epi-faunal elements of seafloor habitats (Zajac et al., 2020). There are inherent difficulties sampling hard substratum habitats upon which epifaunal organisms depend, as well as the fragility of those emergent taxa and biogenic structures that occur on the surface of both hard substratum and fine-grained sediments. Variable life histories make optimal timing for sampling problematic for diverse, short-lived, but ecologically important taxa (Cau et al., 2020). Further, sampling for these taxa is difficult with standard sample gears such as grabs and dredges. For example, the jaws of grab samplers don't close on pebbles and cobbles or are ineffective on boulders and outcrops, while some abundant taxa with weak attachment to the seafloor can be dispersed by the pressure wave in front of sampling gear deployed rapidly from the surface. Specialized sampling tools and approaches for imaging and collection of physical samples (e.g., integrated cameras/grabs, remotely operated vehicles, divers with quadrat cameras, and airlift samplers) can solve some of these issues or at least provide samples to contrast and evaluate those that are more widely applied.

Hard substratum habitats are spatially rare in LIS, especially in deep waters (>10 m) of the central and western basins (Knebel & Poppe, 2000; Poppe et al., 2000), but are more spatially extensive in the eastern part of the region (Poppe et al., 1998, 2006; Langton et al., 1995). Associated structure-forming seafloor communities contribute uniquely to the rich biological diversity of LIS, functioning as physical habitat features and prey for a wide range of vagile species including fish, crustaceans, mollusks, and echinoderms of ecological and economic importance (e.g., Auster et al., 1995, 1997, 1998; Langton et al., 1995; Malatesta & Auster, 1999; Stefaniak et al., 2014; Lindholm et al., 1999; Cau et al., 2020). Further, a number of these species or species groups can serve as sentinels for assessing direct and indirect effects of natural and human-caused events due to their structural fragility or environmental thresholds linked to growth, reproduction, and survival (e.g., turbidity, temperature, salinity, wave energy, trophic interactions). For example, invertebrates with morphologies based on calcium carbonate can exhibit deleterious responses to ocean acidification (e.g., Holcomb et al., 2012 for *Astrangia poculata*), shifts in size and composition of planktonic food resources for filter feeders can shift signs and direction of competitive dominance hierarchies due to the effects of warming (e.g., Thieltges, 2005), and changes in time of reproduction due to warming can influence dispersal patterns based on seasonal changes in oceanographic drivers (Fuchs, et al., 2020). The map products presented here provide a foundation for marine spatial planning and a snapshot in time against which change can be measured. Most importantly, this can serve as a baseline to measure change over time with sufficient temporal resolution in monitoring (e.g., Stefaniak et al., 2014).

The objectives of this project component were to produce: (1) maps of emergent- and epi- faunal community types based on multivariate analyses of faunal data related to physiographic features, (2) maps of faunal and biogenic features richness and diversity, (3) maps of selected species and biogenic habitat features, (4) and in collaboration with other project elements, an integrated habitat map combining infaunal and epifaunal/emergent species diversity.

5.2.3.2 Image Acquisition and Methods

Sample Site Selection and General Cruise Details

Sample locations were selected through a multi-step process. First, sampling effort was spread throughout the geographic extent of the study area across 90 sampling blocks (SB) or sites (NB; Figure 5.2-27). The spatial distribution and locations of the sample areas were selected with the overall objective to sample as many of the different seafloor habitats as possible based on examination of existing seafloor bathymetry and backscatter data to be inclusive of depth and grain size gradients, the presence of transition zones between distinct seafloor features, and efforts to distribute sampling throughout the longitudinal range of the study area. The original plan for the sampling effort was to implement three grab samples and three image transects in blocks and one each at sample sites.

Figure 5.2-27. Map of the Phase II area, showing the sample blocks (squares) and sample sites (ovals)

The majority of the samples for ecological characterization were collected during 2 sampling periods, between November 28 and December 3, 2017, and May 8 and 15, 2018, using the USGS SEABOSS (Valentine et al., 2000; Figure 5.2-28) for both infaunal grab and epifauna video/photographic samples. Additional sampling details for the SEABOSS cruises are provided in (Ackerman et al., 2020). The R/V *Connecticut* was used to support both cruises.
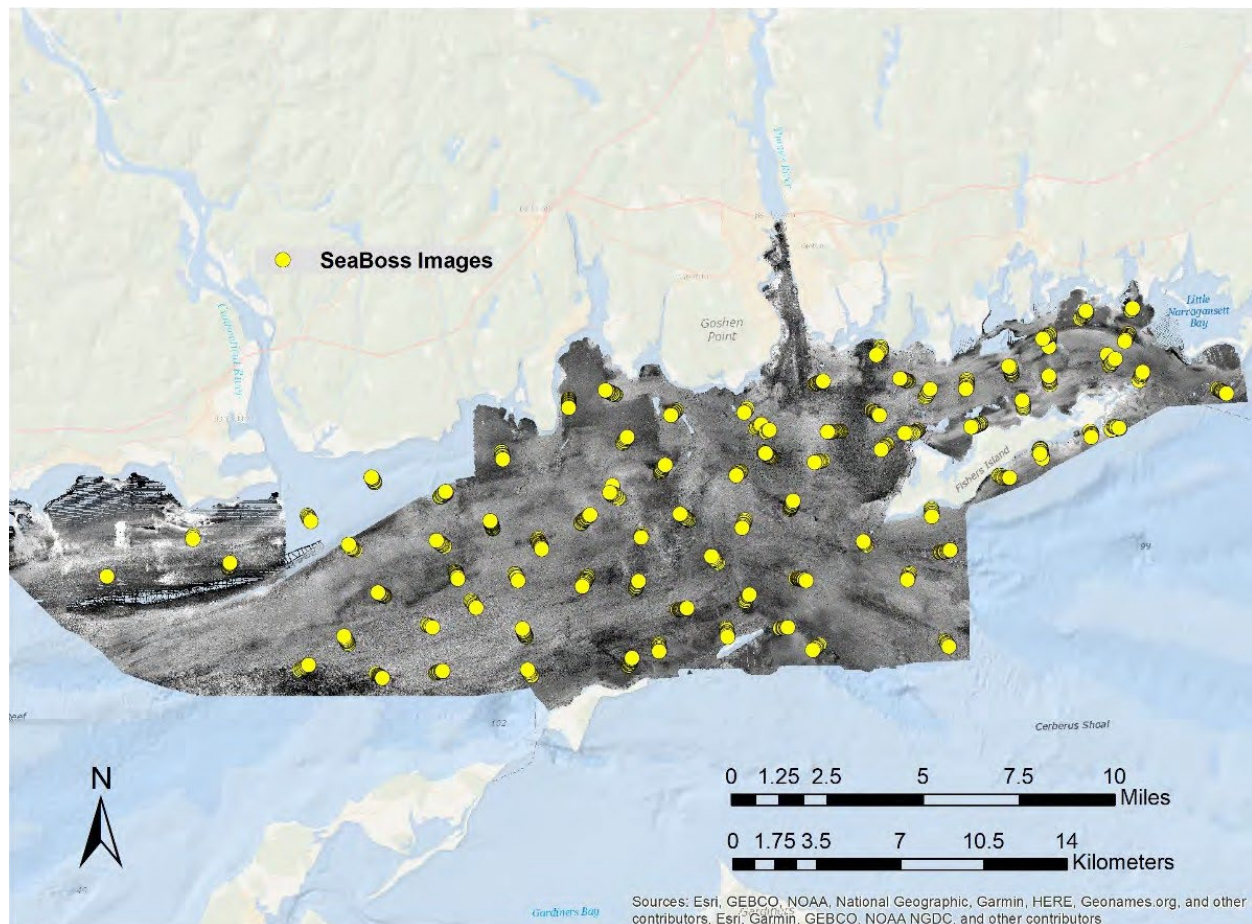
Figure 5.2-28. Map illustrating the locations of images acquired by the SEABOSS platform

Locations with high rugosity and complex topographies were sampled via still and video imagery with the Kraken2 ROV during 1 cruise conducted during May 2018, again using the R/V *Connecticut* (Figure 5.2-29). Scuba was employed to collect quadrat camera still images and associated suction samples to assess and contrast patterns of diversity using visual versus direct sample approaches. This wet-diving component of the project was conducted between August 2017 and August 2018 (Figure 5.2-30).
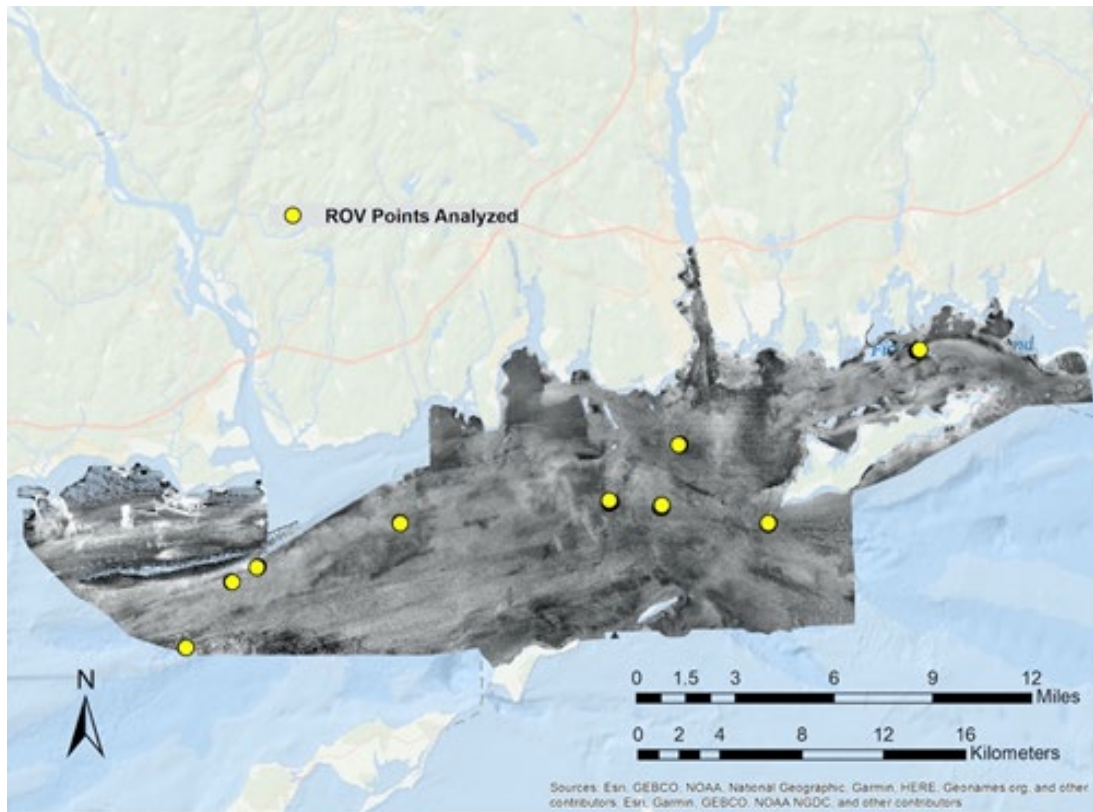
Figure 5.2-29. Map illustrating the locations of images acquired by the Kraken2 ROV platform
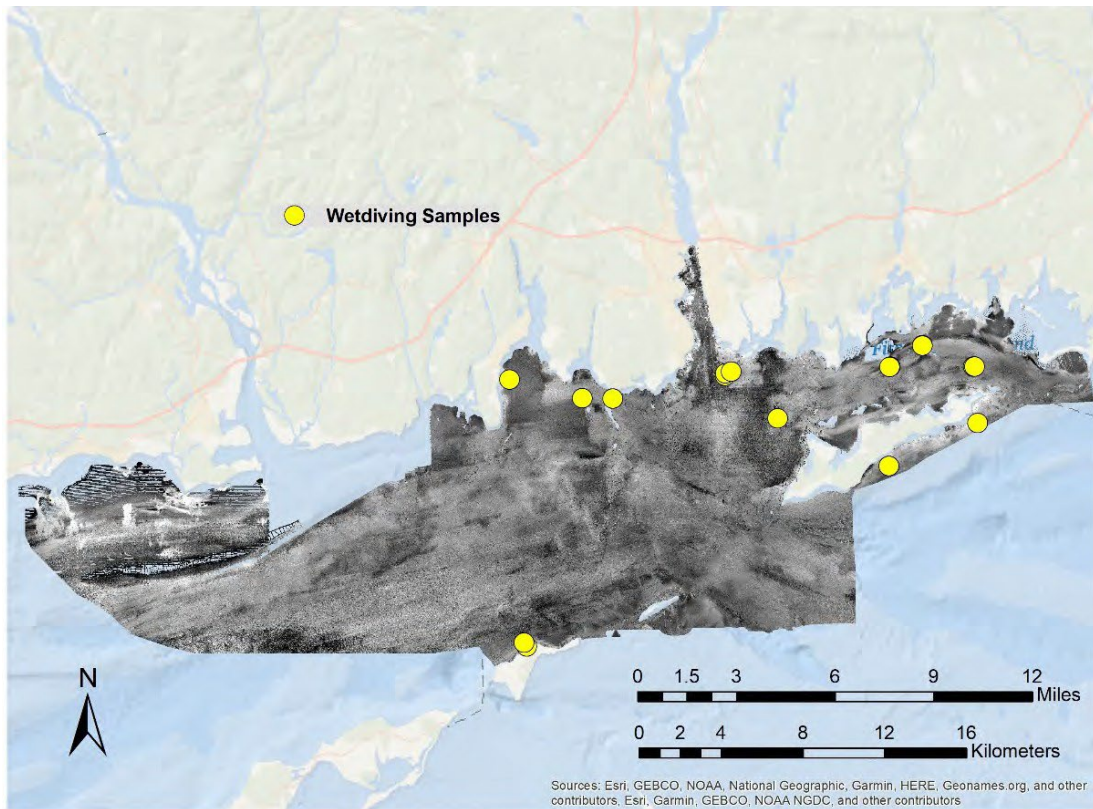
Figure 5.2-30. Map illustrating the locations of images and suction samples acquired by wet- diving

5.2.3.3 Epifaunal Sample Design

Epifaunal and emergent seafloor organisms and associated biogenic features were characterized using seafloor imagery and suction sampling by divers. Images were collected during SEABOSS and ROV transects (n = 602 SEABOSS images fall 2017, n = 595 SEABOSS images spring 2018, n = 110 ROV images spring 2018, n = 87 wet-diving images 2017-18). Sampling efforts depended on seafloor characteristics. While most effort was concentrated in the SEABOSS cruises referenced above, select areas with precipitous topographies were sampled via still and video imagery via wet-diving or with the ROV.

Within both sampling blocks and sites, sampling location selection differed based on the sampling method and platform. Trajectories for SEABOSS transects were selected algorithmically. Large numbers of potential transects (n = 1000) with randomized start and end points were randomly generated for each sampling block and site. Transect locations were constrained by simple rules; transects could not be generated within 6.1 m lateral distance (i.e., the beam of the R/V *Connecticut*) of 5 m depth contour or identified obstructions. Bathymetry and backscatter profiles of each randomly generated transect were extracted from acoustic data sets. These profiles were ordered based on the variance and range of bathymetry and backscatter profile data such that transects with the greatest range and highest variance were highest ranked. The highest ranked transects were retained and implemented based on logistic constraints (e.g., ship handling due to wind and wave direction, safety regarding depth and fixed gear such as navigation aids, trap buoys).

This approach was taken since changes in bathymetry and backscatter are key indicators of transition zones (Zajac et al., 2003 & 2020) and sampling transition zones was central to characterizing variation in communities. This algorithmic process was the principle means of efficiently sampling seafloor habitats within blocks and sites across the study region (Figure 5.2-31). This transect selection approach resulted in an overall reduction in the number of transects sampled per sample block (originally planned as n=3, reduced to n=1) and increased the number of sample blocks that were actually sampled during research cruises. Wet-diving locations were determined based on visual assessment of fine scale bathymetric data and were limited to shallow areas <22 m in depth. Trajectories for image and video sampling via ROV were selected using bathymetric data and navigation data from topographically challenging areas identified during SEABOSS transects. Using 3 distinct sampling approaches was necessary to characterize epi- and emergent fauna across available habitats and depths within Phase II area.
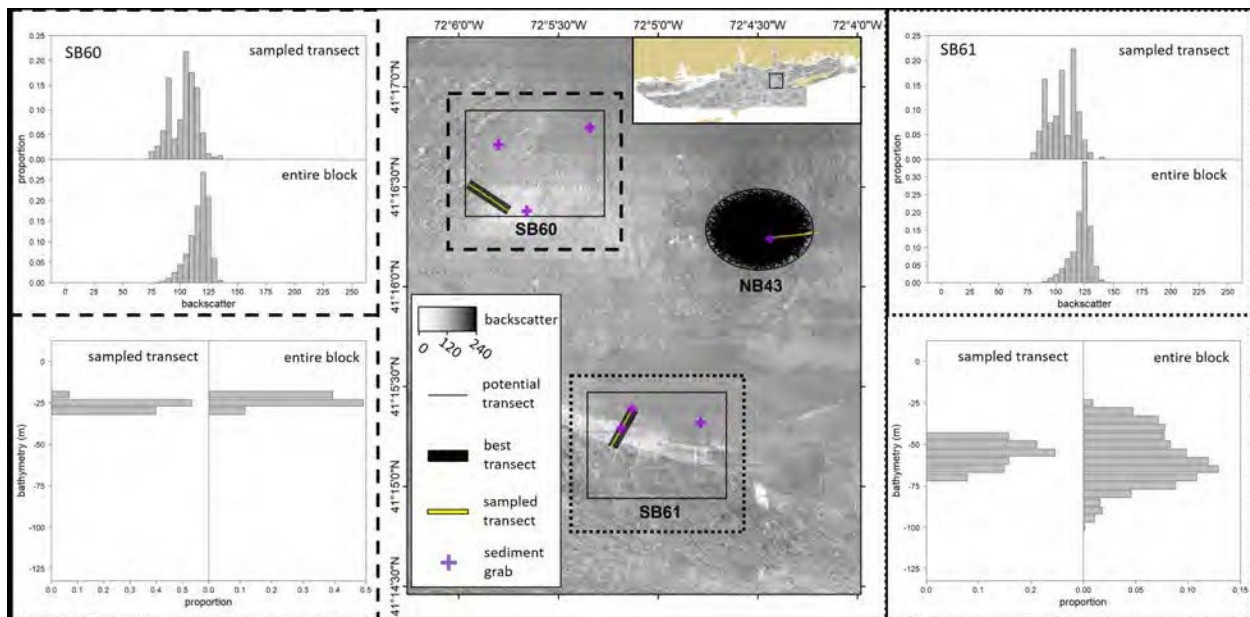
Figure 5.2-31. Example of approach for selecting transect location. Map depicting sampling blocks SB60 and SB61 and site NB43 (center) with acoustic backscatter base layer. In each sample block and site, yellow line depicts the sampled transects and purple crosses sediment grab locations during fall 2017 (SB60 and SB61) or spring 2018 SEABOSS sampling.

Sampled transects were selected a priori from 2000 randomly generated potential transects (depicted as thin black lines at site NB43) as best representing the physical seafloor habitats available in a specific block or site. The range of physical seafloor habitats available in blocks SB60 (left) and SB61 (right) are represented by histograms of backscatter and bathymetry along sampled transects and within entire sample blocks. Note that the distributions of backscatter and bathymetry in the sampled transects largely matches those of the entire sample blocks.

SEABOSS sampling consisted of imaging, video, and sediment grab sampling. Still images were taken using a Nikon D300 camera and Photosea electronic flash set-up for orthogonal imagery (Figure 3.3-2). Video imagery was collected using a GoPro Hero4 for oblique forward-facing field-of-view and a SIMRAD SD video camera mounted for an orthogonal field-of-view. All bottom videos were acquired using a Kongsberg Simrad OE1365 video camera on the SEABOSS. A scientist monitored the real-time bottom video and acquired bottom photographs at approximately 25 s intervals (when the camera was at approximately 1 m off the seafloor) by remotely triggering the Nikon camera shutter. Bottom video was also recorded during the drift from the downward-looking Kongsberg video camera directly to hard drives using an Odyssey7 video recorder. Bottom videos were recorded in MP4 format and a trackline shapefile of the location of the ship for the duration of the video collected during the fall 2017and spring 2018 field activities. A total of 210 sites were occupied within the study area, and bottom videos were acquired at all 210 sites resulting in 218 videos with a total duration of 48 hours 30 minutes and 218 video tracklines with a total length of 41.4 kilometers (Ackerman et al., 2020).

Wet-diving sampling, limited to depths <22 m, consisted of seafloor imaging and suction sampling. Images were taken using either a Sony NEX-5 or Sea & Sea DX-1200HD digital camera with two Sola Video lights mounted on a camera quadropod, set-up for orthogonal imagery (Figure 5.2-32). Images captured $0.5m^2$ square area of seafloor. Seafloor samples were collected via suction sampling (Figure 5.2-32). Suction sampling consisted of collecting epifauna within a $0.5m^2$ quadrat area using a compressed air suction sampler. Samples were collected in sealable 0.5mm mesh bags connected to the suction sampler then transferred to storage containers and preserved in 70% ethanol for later processing. Specific suction sample locations were imaged prior to and following

suction samples.

Figure 5.2-32. Diver conducting quadrat photo transect (left) and suction sampling (right)

The Kraken2 ROV (Figure 5.2-33) was utilized to acquire imagery in topographically complex and spatially constrained habitats where maneuverability of the camera platform is required to collect adequate image samples. Such areas were difficult to access using SEABOSS.

| HMI light | Strobe light | Digital still camera | Hi def camera | Digital still camera | Scanning sonar |
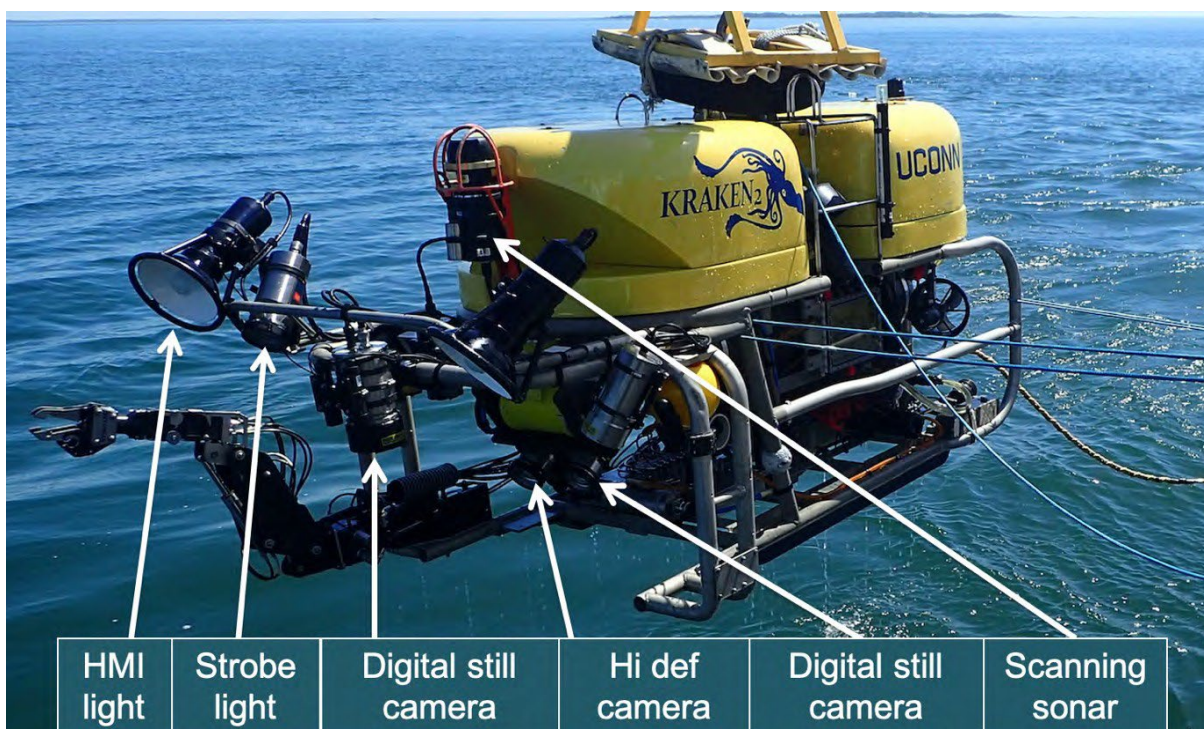
Figure 5.2-33. The Kraken2 ROV illustrating its still and video imaging and sonar capabilities

ROV sampling consisted of still and video imagery. Still images were recorded using a Nikon E995 digital camera and electronic flash set-up for orthogonal imagery. A Canon PowerShot G11 and electronic flash were also installed for mobile pan-tilt imagery.

All images were taken using artificial lighting (electronic flash or daylight color temperature

lighting using HMI or LED sources) to enhance color saturation, edge sharpness, and depth of field. Paired parallel lasers were mounted adjacent to cameras and projected points into each image at 20 cm spacing to facilitate image calibration. All imagery was batch processed using the automated color correction routine in Irfanview software (version 4.50) in order to enhance color saturation and delineate color boundaries to facilitate identification of taxa.

Each image was subsequently examined for clarity and focus. Images with water turbidity that obscured the seafloor or that were out of focus such that identification of all organisms or biogenic features was impeded were rejected. Transects were divided into 50 m segments and images subsampled randomly from each segment, ensuring epifauna along the entire length of each transect would be characterized. Images selected for analysis were approximately 2m apart to preclude analyzing the same areas of the seafloor multiple times. This step produced a total of 1307 processed images for analysis.

Each color corrected image was analyzed for percent cover of all living seafloor species (excluding fish) and biogenic features (e.g., shell, mud tubes, burrows) using ImageJ software (version 1.45s; Abramoff et al., 2004). Percent cover was quantified using a grid of square cells overlaid on each image. The grid featured 280 cells filling the entire image space, but the cells lining the image edge were ignored due to reduced lighting and potential optical distortion caused by the flat port and open aperture of the underwater camera, resulting in a usable grid of 216 cells (Figure 5.2-34).
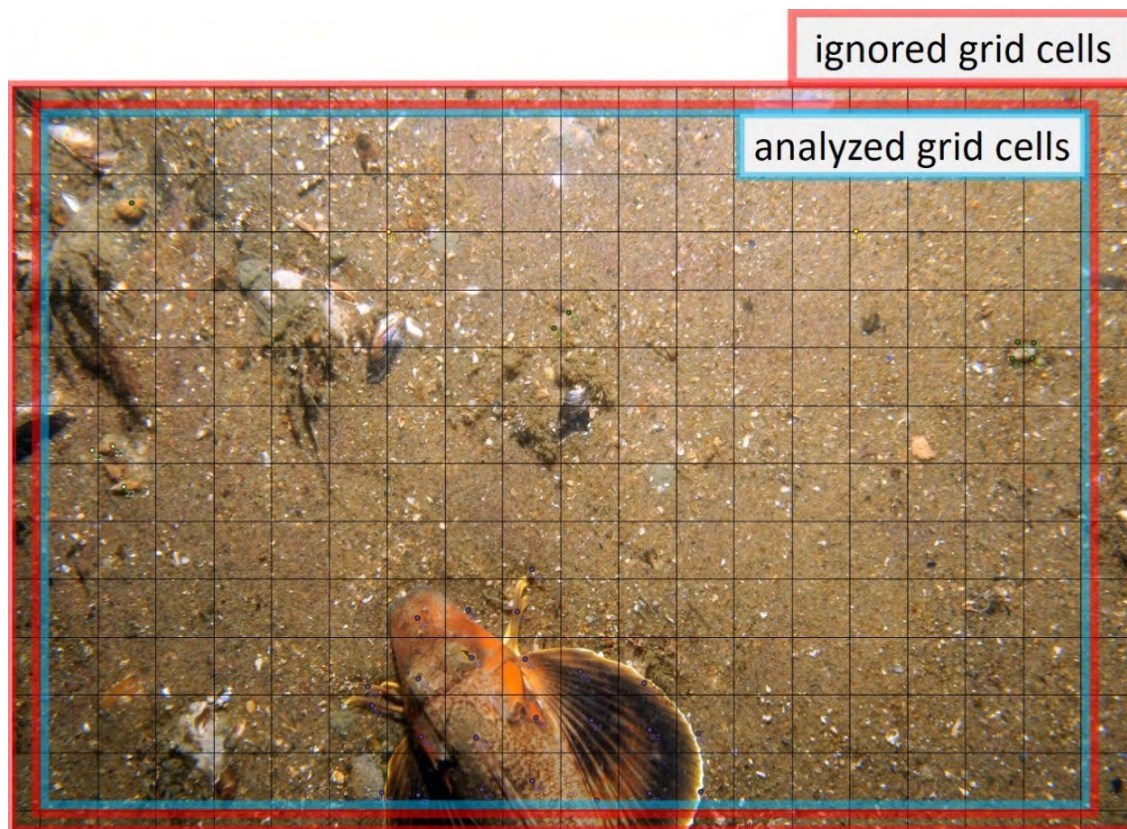
Figure 5.2-34. Screen capture of grid used for ImageJ analysis

Within each grid square, organisms and biogenic features were identified to lowest possible taxonomic level and marked using the "cell counter" tool in ImageJ. This function displays a mark

on each object as selected in the image and, in a separate window, displays counts of each object type. ImageJ only classifies objectives and related numerical counts as a series of undefined "Types" (e.g., Type 1, Type 2, etc.) and does not have a custom naming feature. Therefore, workflow processing of images required a separate record of the identity of "types" for each image and subsequently rectifying counts with actual taxonomic and feature classifications post-processing.

Several counting conventions (i.e., decision rules) were required to address variability in the cover of organisms and biogenic habitat features on the seafloor. Some colonial organisms (e.g., coral, sponge) and biogenic features occupied multiple grid squares. In addition, some solitary organisms (e.g., mussel, crab, gastropod) also were present in multiple squares. Such individuals were counted in each square to account for the area of coverage in each image. Conversely, more than one organism or biogenic feature could be in a single square and were each counted in order to account for all biological elements within an image. Therefore, the total grid count could be greater than the total number of squares in the grid (but then normalized across images by calculating percent cover, as described below).

Total counts for each taxa or type of biogenic feature from each image were entered into a spreadsheet. All taxa, excluding fish fauna captured in images, and biogenic features were counted from imagery. Taxa and features from the full matrix were parsed for analyses as taxa (i.e., both sessile and mobile invertebrates), taxa and biogenic features (i.e., those structures produced by biota such shell, worm tubes, burrows). Counts were saved and archived as .ROI files (format that saves their position within the image for future analysis). Using the scaling lasers in each image to calibrate length, the width and height of both the image and the grid was measured using the "measure" tool in ImageJ and area of coverage was calculated. Counts were converted to percent cover by dividing the count for each type of organism or feature by the total number of squares for the image. These data were subsequently used in multivariate and univariate analyses to address objectives regarding characterization of communities, variation in patterns of diversity, distribution of habitat features, and seasonality of patterns. Multivariate tests and diversity indices identified in results were implemented using PRIMER-e (v7.0.17, Clarke & Gorley, 2015). Maps, shapefiles, and layer files were created for the % cover of taxa and biogenic features, as well as diversity measures in ArcMap (v10.5).

5.2.3.4 Results

Epifaunal Diversity and Distribution of Communities

Broad scale sedimentary conditions are represented by acoustic patches classified using eCognition (see Section 5.1) and form the basis for delineating communities, patterns in biogenic features, and differential distribution of key taxa and features. Together, these results serve as a part of the foundation for the integrated habitat map (Section 5.2.4.4). Patch types A-E follow a general meso-scale gradient of increasing dominance of coarse sediment components. However, all patch types include a degree of coarse stable gravel, (from small patches and minimal representation to more spatially extensive and dominant) that is exposed at the sediment-water interface. These hard substratum surfaces facilitate settlement and survival of epifaunal structure-forming species. However, the composition of hard substratum and surrounding fine-grain sediment communities can be influenced by the interactions of species within and between patch types based on area and circumference mediating interactions such as predation and competition (Fagan et al., 1999; Zajac,

2008). It is noteworthy here that unlike the relatively distinct grain size composition and large spatial scale extent of eCognition acoustic patches in the Phase 1 Stratford Shoals area, exhibited distinct epi- and emergent-faunal dominants in each patch type, the Phase 2 ELIS-FIS region exhibits a high degree of spatial variability between as well as within eCognition acoustic patches.

A total of 119 taxa were identified to the lowest possible taxonomic unit and an additional 33 biogenic features, structures formed by organisms (e.g., shell, tubes, burrows) and used as habitat by vagile fauna were observed in the study region (Table 5-14). Multivariate analyses were implemented to test for differences in the composition of taxa and biogenic features based on eCognition patch assignments for image samples. ANOSIM routines identified statistically significant differences in Global R values for both taxa and biogenic features in fall and spring surveys as well as for live taxa only in the spring 2018 survey (Table 5-15). SIMPER comparisons of dissimilarity between eCognition patch types reveals variation in abundance (i.e., patterns of dominance based on cover values from image analysis) but not wholesale differences in composition between patch types (Table 5-16A). Dissimilarity analyses, as opposed to similarity, was used as a way to best present paired comparisons of taxa cover between acoustic patches. This is based on the aggregate of transect images, given the high degree of overlap in taxa presence across acoustic patches versus a smaller number of grab samples with more distinct compositions. This pattern in the composition of sedimentary habitats results in a corresponding pattern of gradients in the composition of structure-forming fauna and biogenic structures representative of each eCognition acoustic patch types (Table 5-16B). In summary, eCognition patches exhibit significant differences in both taxa and biogenic features such that each class has distinct characteristics useful to differentiate and map elements of habitats.

Table 5-14. List of taxa and biogenic features identified in survey imagery. Organisms were identified to the lowest taxon possible. SFT = Structure-forming taxa and denoted by row as "S"

Taxa	Common name - description	SFT	Major taxonomic group
Ahnfeltia plicata	landlady's wig	S	Rhodophyta
Amphipoda unidentified	unidentified amphipod		Crustacea
Andara spp.	unidentified cockle	S	Mollusca
Anomiidae	jingle shell	S	Mollusca
Anomura unidentified	unidentified crab		Anomura
Anthozoa anemone	unidentified anemone	S	Anthozoa
Arbacia punctulata	purple sea urchin	S	Echinodermata
Argopecten irradians	Bay scallop	S	Mollusca
Ascidacea colonial	Colonial ascidian	S	Tunicata
Ascidacea solitary	Solitary ascidian	S	Tunicata
Ascophyllum nodosum	rockweed, brown alga	S	Ochrophyta
Astarte undata	waved astarte	S	Mollusca
Asteroidea	unidentified seastar		Echinodermata
Astrangia poculata	northern star coral	S	Anthozoa
Astyris lunata	lunar dovesnail		Mollusca
Asterias forbesi	Forbes sea star		Echinodermata
bilvalve siphon	bivalve siphon	S	Mollusca
Bivalvia unidentified	bivalve	S	Mollusca
Botrylloides diegensis	chain sea squirt	S	Tunicata

Brachyura	unidentified brachyuran crab		Decapoda
Bryozoa encrusting	unidentified encrusting bryozoa		Bryozoa
Busyconidae	unidentified whelk		Mollusca
Cancer borealis	Jonah crab		Decapoda
Cancer irroratus	Rock crab		Decapoda
Cancer spp.	Cancrid crab		Decapoda
Caprellidae	skeleton shrimp		Amphipoda
Cardiidae	cockle		Mollusca
Cerastoderma pinnulatum	northern dwarf cockle	S	Mollusca
Cerantheopsis americana	North American tube anemone	S	Anthozoa
Cerripedia	unidentified barnacle	S	Crustacea
Cheliostomata	calcified bryozoan	S	Bryozoa
Chlorophyta	unidentified green macroalgae	S	Chlorophyta
Chondrus crispus	Irish moss	S	Rhodophyta
Chorda filum	sea lace	S	Ochrophyta
Ciona intestinalis	sea vase	S	Tunicata
Cliona spp.	boring sponge	S	Porifera
Coccotylus truncatus	leaf weed	S	Rhodophyta
Codium fragile	dead man's fingers	S	Chlorophyta
Corallina officinalis	coral weed	S	Rhodophyta
Corymorpha pendula	solitary pendula	S	Hydrozoa
Coryphella verrucosa	aeolid nudibranch		Nudibranchia
Costoanachis lafresnayi	well-ribbed dove snail		Mollusca
Crepidula fornicata	common slipper shell	S	Mollusca
Crucibulum striatum	striate cup-and-saucer	S	Mollusca
Cyclocardia borealis	northern cardida	S	Mollusca
Dendronotidea	dendronotid nudibranch		Mollusca
Desmarestia viridis	sour weed	S	Ochrophyta
Diadumene leucolena	ghost anemone	S	Anthozoa
Dichelopandalus leptocerus	bristled longbeak		Decapoda
Didemnum candidum	white colonial ascidian	S	Tunicata
Didemnum vexillum	sea vomit	S	Tunicata
Echinarachnius parma	common sand dollar		Echinodermata
Ectopleura crocea	pink-mouth hydroid	S	Hydrozoa
epifauna unidentified		S	
Euspira heros	northern moon snail		Mollusca
Fissurellidae	keyhole limpet	S	Mollusca
Fucus vesiculosus	bladder wrack	S	Ochrophyta
Gastropod nudibranch unidentified	unidentified nudibranch		Mollusca
Gastropod unidentified	unidentified snail		Mollusca
Grinellia americana	Grinnell's pink leaf	S	Rhodophyta
Halcampa duodecimcirrata	twelve-tentacle burrowing anemone	S	Anthozoa
Halichondria panicea	breadcrumb sponge	S	Porifera
Haliclona spp.	sponge	S	Porifera

Halisarca spp.	orange sponge	S	Porifera
Henricia sanguinolenta	blood star		Echinodermata
Hidenbrandia rubra	rusty rock	S	Rhodophyta
Holothroidea	sea cucumber		Echinodermata
Homarus americanus	American lobster		Decapoda
Hydroides dianthus	hard tube worm	S	Polychaeta
Hydrozoa-bryozoa erect	erect hydroid-bryozoan aggregate	S	Hydrozoa-Bryozoa
Ilyanassa spp.	mudsnail		Mollusca
Isopoda	Isopod		Crustacea
Laminariaceae	kelp	S	Ochrophyta
Libinia emarginata	spider crab		Crustacea
Libinia dubia	longnose spider crab		Crustacea
Doryteuthis pealeii	longfin squid		Mollusca
Euspira heros	northern moon snail		Mollusca
Macroalgae unidentified	macroalgae	S	Eukaryota
Majidae	crab		Decapoda
Melobesioideae	corallline algae		Rhodophyta
Mercenaria	quahog	S	Mollusca
Metridium senile	frilled anemone	S	Anthozoa
Microciona prolifera	red beard sponge	S	Porifera
Mogula spp.	sea grape	S	Tunicata
Mycale fibrexilis	flabby sponge	S	Porifera
Mysidea	mysid shrimp		Crustacea
Mytilus edulis	blue mussel	S	Mollusca
Nemertean	ribbon worm		Nemertea
Nucella lapillus	dog whelk		Mollusca
Encrusting macroalgae	unidentified encrusting macroalgae		Eukaryota
Paguridae	unidentified hermit crab		Decapoda
Palmaria palmata	dulse	S	Rhodophyta
Penaeidae	shrimp		Decapoda
Phaeophyceae	brown macroalgae	S	Ochrophyta
Placopecten magellancius	giant scallop	S	Mollusca
Polychaeta	polychaete worm	S	Polychaeta
Polyides rotundus	twig weed	S	Rhodophyta
Polymastia robusta	nipple sponge	S	Porifera
Polyplacophora	chiton	S	Mollusca
Polysiphonia spp.	polly	S	Rhodophyta
Porifera spp.	sponge	S	Porifera
Porphyra spp.	nori	S	Rhodophyta
Portunidae	swimming crab		Crustacea
Pycnogonida	sea spider		Arthropoda
Ralfsia verrucosa	tarspot		Ochrophyta
Rhodophyta	red macroalgae	S	Rhodophyta
Sabellid encrusting	featherduster worm	S	Polychaeta
Serpula spp.	tube building annelid	S	Polychaeta

Spirorbis spp.	coiled tube worm	S	Polychaeta
Spisula solidissima	Atlantic surf clam	S	Mollusca
Squilla empusa	mantis shrimp		Crustacea
Strongylocentrotus droebachiensis	green sea urchin		Echinodermata
Terebellida	bristle worm	S	Polychaeta
Tubularia indivisa	oaten pipes hydroid	S	Hydrozoa
Tubulariidae spp.	unidentified hydroid	S	Hydrozoa
Tunicata colonial	colonial tunicate	S	Tunicata
Ulva lactuca	sea lettuce	S	Chlorophyta
Unidentified siphon	emergent siphon	S	
Urosalpinx cinerea	Atlantic oyster drill		Mollusca
Worm-like organism unidentified	unidentified invertebrate		

Biogenic feature	Common name - description	Major taxonomic group
Astrangia poculata skeleton	skeleton of star coral	Anthozoa
biogenic depression	animal formed depression	
biogenic mound	animal formed mound	
biogenic tube unidentified	emergent animal produced tube	
Cirripedia test	attached barnacle test	Crustacea
Chondrichthyes egg case	egg case	Chondrichthyes
Crepidula spp. shell	shell	Mollusca
Crustacea exoskeleton	exoskeleton - molt or death	Crustacea
Diopatra tube	emergent tube	Polychaeta
Echinarachnius parma test	sand dollar test	Echinodermata
encrusting worm tube	encrusting tube	Polychaeta
Euspira spp. egg collar	egg collar	Mollusca
Euspira spp. shell	shell	Mollusca
Gastropod egg case	egg case	Mollusca
Gastropoda shell	shell	Mollusca
Hydroides dianthus tube	worm tube	Polychaeta
large burrow	animal produced burrow	
Macroalgal debris	unattached macroalgae	Eukaryota
medium burrow	animal produced burrow	
Mytilus edulis valve	shell	Mollusca
Nudibranch egg string	egg string	Mollusca
Shell hash	shell	Mollusca
Shell whole-partial	shell	Mollusca
siphon emergent unidentified	emergent bivalve siphon	Mollusca
small burrow	animal produced burrow	
Spirobis worm tube	attached worm tube	Polychaeta
Terrestrial vegetation debris	unattached terrestrial debris	
Urchin test	test	Echinodermata
Whelk shell	shell	Mollusca

Worm castings	coherent sediment in organic	Polychaeta
Worm tube flexible erect	emergent tube from sediment	Polychaeta
Worm tube debris	unanchored worm tube	Polychaeta
Zostera-seagrass debris	unattached seagrass debris	

Table 5-15. Results of ANOSIM procedure for comparisons of taxa and feature cover values based on assignment to eCognition acoustic patches as well as environmental factors (depth, TRI, tau max, longitude). Each cell includes the Global R value for each set of comparisons and significance level. Blocks-sites scale analyses, for aggregated image samples, are based on seasonal and total samples over time. Groups are based on results of hierarchical clustering of community composition (all significant clusters) and results of an iterative aggregation of cluster groups by geospatial adjacencies into four principle sub-areas with data from both seasons.

	2017	2017	2018	2018	2017-18	2017-18
Factors	Taxa/Features	Taxa	Taxa/Features	Taxa	Taxa/Features	Taxa
eCognition	0.077/0.1%	0.013/17.9%	0.077/0.1%	0.035/1.4%		
Depth	0.032/1.3%	0.075/0.1%	(0.037)/98.8%	0.06/0.2%		
TRI	0.075/0.1%	0.044/0.1%	(0.016)/92.7%	0.005/32.9%		
Tau max	0.248/0.1%	0.101/0.1%	0.07/0.1%	0.026/0.5%		
W-E Longitude	0.104/0.1%	0.119/0.1%	0.105/0.1%	0.195/0.1%		
Blocks & Sites						
All Clusters 1%	0.828/0.1%	0.784/0.1%	0.865/0.1%	0.811/0.1%	0.809/0.1%	0.665/0.1%
Cluster 1% 4 Grps					0.339/0.1%	0.364/0.1%

Table 5-16. A. Mean cover value, based on percent cover, for select biogenic habitat features and structure- forming taxa from fall 2017/spring 2018 surveys. These features and taxa were selected based on patterns of dominance and occurrence over the study region. Note that patch type A did not have any image samples collected in spring 2018, so cells contain "NA" as not available. (Column abbreviations as follows: SH = whole- partial shell, TB = terrestrial plant debris, ZD = Zostera debris, RH = Rhodophyta, LA = Laminariaceae, HB = hydrozoa/bryozoa, AP = Astrangia poculata, DL = Diadumene leucolena, CS = Crepidula sp., ME = Mytilus edulis, CL = Cliona spp., DS = Didemnum spp., CP = Corymorpha pendula.) B. Ranked order based on max value (from seasonal means). C. Mean, variance, and range of physical habitat characteristics.

A.

		Biogenic Features			Structure-forming Fauna									
eCog	Grain size	SH	TB	ZD	RH	LA	HB	AP	DL	CS	ME	CL	DS	CP
A	Sandy silt	24.7 NA	0 NA	0.5 NA	6.6 NA	0 NA	10.8 NA	0 NA	0 NA	31.7 NA	0 NA	6.4 NA	0 NA	0 NA
B	Silty sand	25.8 20.9	0.2 1.4	1 4.3	6.8 12.9	0.1 0.9	6.7 13.8	0.1 0.1	0.5 2.4	1.8 2.2	0.1 0	<0.1 1	0.1 0.1	0 0.1
C	Gravel- sand	32.4 33.4	0.5 1.6	2.1 2.4	4.4 3.8	0.1 0.8	11.7 26.6	0.4 0.9	5.4 2.6	6 5.7	<0.1 0.3	1.6 0.8	0.7 0.8	0 1.5
D	Gravelly sand	54.8 44.8	0.1 1	1.9 2.4	4.4 4	0 0.7	13 33	2.4 0.7	2.7 4.9	7.4 3.3	0.1 1.4	1.3 1.1	0.9 1.3	0 1.7
E	Gravelly sediment	77 50.3	0 0	0 0	0 0	0 0	22.9 53.4	0 1	0 0	0.5 1	0.3 0	0 0	1 0	0 4.4

B.

	Ranked order			Ranked order fauna									
eCog	SH	TB	ZD	R	LA	HB	AP	DL	CS	ME	CL	DS	CP

A	5	0	4	2	0	5	0	0	1	0	1	0	0
B	4	2	1	1	1	4	4	3	4	4	4	4	4
C	3	1	2	3	2	3	3	1	3	3	2	3	3
D	2	3	3	4	3	2	1	2	2	1	3	1	2
E	1	0	0	0	0	1	2	0	5	2	0	2	1

C.

eCog	Mean Depth	Depth SD	Depth Range	Mean TRI	Depth TRI	TRI Range	Mean Max Tau	Depth Max Tau	Max Tau Range
A	-9	0.1	-9.1 to -8.9	0.047	0.048	0.013 to 0.142	0.46	0.004	0.452 to 0.461
B	-21.4	17.8	-86.8 to -5	0.212	0.294	0.002 to 1.867	0.686	0.386	0.191 to 2.685
C	-27.6	18.9	-95 to -5.4	0.231	0.26	0.004 to 1.703	0.807	0.352	0.191 to 2.685
D	-34.2	18.6	-89.5 to -6.3	0.157	0.183	0.003 to 1.666	0.991	0.311	0.259 to 1.865
E	-34.4	7.1	-47.8 to -30.5	0.059	0.025	0.024 to 0.093	0.952	0.024	0.938 to 0.997

Additional factors, derived from geographically comprehensive data sets of observed and derived metrics within the study area were used to identify proxies to explain additional variation in distribution of taxa and biogenic features (Table 5-16C). These factors are depth (from multibeam bathymetry), TRI (derived from variation in bathymetry based on a moving window of surrounding each cell), tau max (value from the model of seafloor stress, see Section 6), and longitude (as an index of west to east variation in site characteristics). Each image sample was classified based on associated eCognition acoustic patch (i.e., A-E) and actual values for each of the environmental factors assigned.

PCA was used to assess the interactions of depth, TRI, tau max, and longitude values for each image sample in explaining variation in image location and coincident eCognition patch assignments. A PCA biplot (Figure 5.2-35) visualizes the PC scores of samples (points) and loadings of variables (vectors). The further away these vectors are from a PC origin, the more influence they have on that PC. Loading plots also provide some inference on which factors correlate with one another, with a small angle between factors indicating a positive correlation while a large angle indicates a negative correlation. A 90° angle indicates no correlation between two factors.
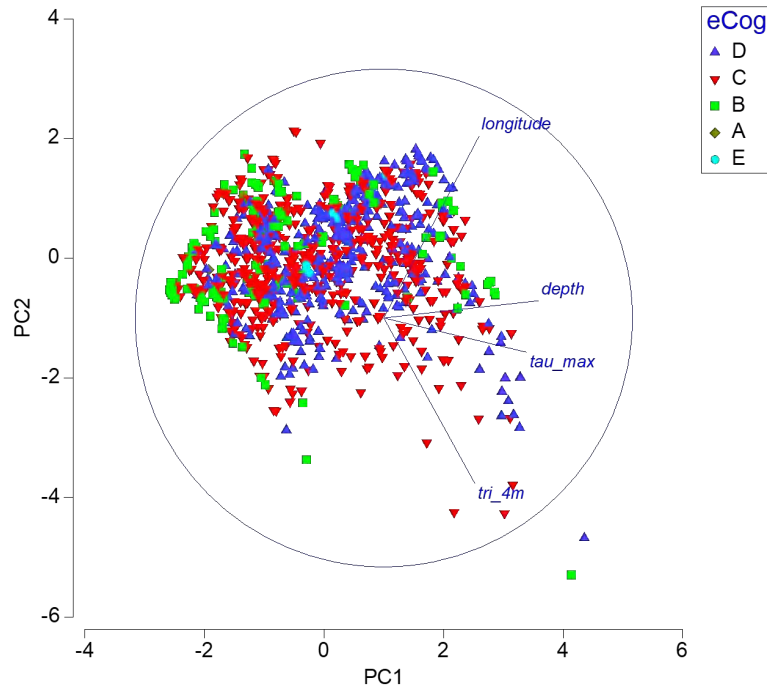
Figure 5.2-35. PCA biplot of environmental factors (see text for details). Factors are depth, TRI, tau max, and longitude. Factors were normalized for all locations

Here we find vectors for depth and tau max are separated by a small angle indicating a positive correlation, while TRI and longitude with opposing angles infer a negative correlation. TRI and depth as well as longitude and tau max are at nearly 90° separation indicating little correlation in these paired factors. The first two eigenvectors represent 65.1% of the variation in the data. The sample points in the PCA biplot show some separation and clustering of each eCognition class based on differences in the environmental factors attributed to each image, further indicating fundamental differences in habitat attributes.

An nMDS analysis validates this pattern with a low stress value (Figure 5.2-36). The global R for each environmental factor in results from ANOSIM for each survey (Table 5-15) are generally highly significant. The SIMPER results illustrate that each of the factors is important in quantifying the dissimilarities in pair-wise comparisons by patch type (Table 5-17).
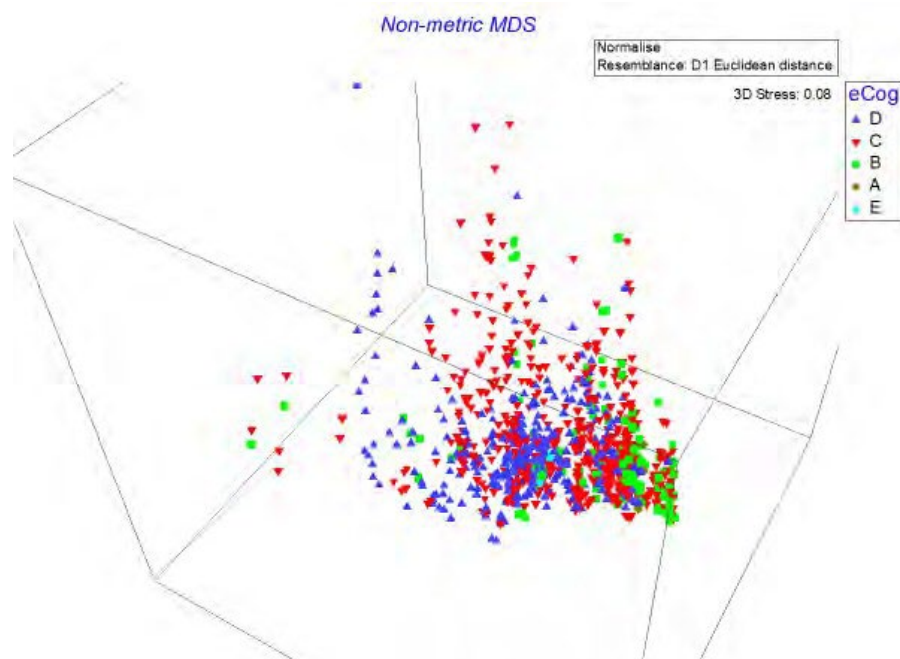
Figure 5.2-36. A 3-D nMDS plot of the four environmental factors analyzed in the PCA above, classified for each eCognition patch type. Note the low stress value, indicate this plot is realistic representation of differences and similarities between samples (images).

Table 5-17. Results pf SIMPER analyses of faunal and biogenic feature differences across eCognition patch types (A-E). Tables separate seasons (fall, spring) and live taxa only (no features) and taxa with biogenic features.

I. Fall 2017 Live taxa

Groups B & C

Average dissimilarity =87.43

eCog	Group B	Group C				
Species	Av.Abund	Av.Abund	Av.Diss	Diss/SD	Contrib%	Cum.%
Hydrozoa bryozoa erect	14.48	25.27	17.6	0.98	20.13	20.13
gastropod_unidentified	5.31	8.09	9.28	0.71	10.62	30.75
Crepidula fornicata	3.85	12.9	8.5	0.61	9.72	40.47
Rhodophyta	14.75	9.61	7.89	0.52	9.03	49.49
Paguridae	2.86	3.14	7.84	0.52	8.97	58.46
Cirripedia_unstalked	4.43	5.65	7.75	0.64	8.87	67.33
Diadumene leucolena	1.15	11.61	3.88	0.33	4.43	71.76

Groups B & D

Average dissimilarity =85.71

	Group B	Group D				
Species	Av.Abund	Av.Abund	Av.Diss	Diss/SD	Contrib%	Cum.%
Hydrozoa bryozoa erect	14.48	28.16	20.56	1.08	23.99	23.99
Crepidula fornicata	3.85	15.9	9.26	0.68	10.8	34.79
Cirripedia_unstalked	4.43	11.05	8.75	0.71	10.21	45
gastropod_unidentified	5.31	8.9	8.53	0.82	9.95	54.95
Rhodophyta	14.75	9.42	7.64	0.48	8.91	63.85
Paguridae	2.86	2.04	5.19	0.52	6.06	69.91

| *Chondrus crispus* | 10.29 | 4.31 | 3.63 | 0.37 | 4.24 | 74.15 |

Groups C & D
Average dissimilarity = 83.21

	Group C	Group D				
Species	Av.Abund	Av.Abund	Av.Diss	Diss/SD	Contrib%	Cum.%
Hydrozoa bryozoa erect	25.27	28.16	18.74	1.11	22.53	22.53
Crepidula fornicata	12.9	15.9	9.8	0.71	11.78	34.31
Cirripedia_unstalked	5.65	11.05	7.74	0.69	9.3	43.61
gastropod_unidentified	8.09	8.9	7.4	0.79	8.9	52.51
Rhodophyta	9.61	9.42	6.6	0.5	7.93	60.44
Diadumene leucolena	11.61	5.9	4.75	0.4	5.71	66.14
Paguridae	3.14	2.04	3.98	0.49	4.78	70.93

Groups B & E
Average dissimilarity = 81.13

	Group B	Group E				
Species	Av.Abund	Av.Abund	Av.Diss	Diss/SD	Contrib%	Cum.%
Hydrozoa_bryozoa_erect	14.48	49.5	36.79	1.97	45.35	45.35
Cirripedia_unstalked	4.43	11	9.71	1.25	11.97	57.31
gastropod_unidentified	5.31	10.5	8.08	1.3	9.96	67.28
Paguridae	2.86	9.33	6.8	0.85	8.38	75.66

Groups C & E
Average dissimilarity = 76.98

	Group C	Group E				
Species	Av.Abund	Av.Abund	Av.Diss	Diss/SD	Contrib%	Cum.%
Hydrozoa_bryozoa_erect	25.27	49.5	30.06	1.69	39.05	39.05
Cirripedia_unstalked	5.65	11	8.12	1.12	10.54	49.59
gastropod_unidentified	8.09	10.5	6.99	1.13	9.07	58.67
Paguridae	3.14	9.33	5.85	0.76	7.6	66.27
Crepidula fornicata	12.9	1	4.6	0.47	5.97	72.24

Groups D & E
Average dissimilarity = 8.40

	Group D	Group E				
Species	Av.Abund	Av.Abund	Av.Diss	Diss/SD	Contrib%	Cum.%
Hydrozoa_bryozoa_erect	28.16	49.5	23.85	1.43	34.87	34.87
Cirripedia_unstalked	11.05	11	8.28	1.12	12.11	46.98
Crepidula fornicata	15.9	1	5.79	0.58	8.46	55.44
gastropod_unidentified	8.9	10.5	5.59	1.11	8.17	63.61
Paguridae	2.04	9.33	4.95	0.79	7.24	70.85

Table 5-17 continued,

Groups B & A
Average dissimilarity =88.99

| | Group B | Group A | | | | |
Species	Av.Abund	Av.Abund	Av.Diss	Diss/SD	Contrib%	Cum.%
Crepidula fornicata	3.85	68.5	30.28	2.21	34.03	34.03
Hydrozoa_bryozoa_erect	14.48	22.33	10.99	1.26	12.35	46.38
Rhodophyta	14.75	14.33	10.63	0.82	11.95	58.32
Grinellia americana	0	18.83	5.74	0.66	6.45	64.78
Porphyra spp	3.49	8.17	5.55	0.66	6.23	71.01

Groups C & A
Average dissimilarity =85.12

| | Group C | Group A | | | | |
Species	Av.Abund	Av.Abund	Av.Diss	Diss/SD	Contrib%	Cum.%
Crepidula fornicata	12.9	68.5	27.02	1.98	31.74	31.74
Hydrozoa bryozoa erect	25.27	22.33	11.13	1.23	13.08	44.81
Rhodophyta	9.61	14.33	8.01	0.81	9.41	54.23
Grinellia americana	0.27	18.83	5.3	0.65	6.22	60.45
Cliona spp.	3.35	13.83	5.28	1.04	6.21	66.66
Porphyra spp.	1.28	8.17	4.51	0.63	5.3	71.96

Groups D & A
Average dissimilarity = 81.26

| | Group D | Group A | | | | |
Species	Av.Abund	Av.Abund	Av.Diss	Diss/SD	Contrib%	Cum.%
Crepidula fornicata	15.9	68.5	24.42	1.89	30.05	30.05
Hydrozoa bryozoa erect	28.16	22.33	11.59	1.09	14.26	44.31
Rhodophyta	9.42	14.33	7.53	0.79	9.26	53.58
Grinellia americana	0.03	18.83	5.05	0.66	6.22	59.8
Cliona spp.	2.73	13.83	4.79	1.16	5.9	65.7
Cirripedia_unstalked	11.05	2.17	4.24	0.58	5.22	70.91

Groups E & A
Average dissimilarity = 80.79

| | Group E | Group A | | | | |
Species	Av.Abund	Av.Abund	Av.Diss	Diss/SD	Contrib%	Cum.%
Crepidula fornicata	1	68.5	24.07	2.21	29.8	29.8
Hydrozoa bryozoa erect	49.5	22.33	18.03	1.3	22.32	52.12
Rhodophyta	0	14.33	5.08	0.98	6.29	58.41
Grinellia americana	0	18.83	5.04	0.68	6.23	64.64
Cirripedia_unstalked	11	2.17	4.9	1.09	6.07	70.71

Table 5-17 continued,

II. Fall 2017 Live taxa and biogenic features

Groups B & C
Average dissimilarity = 74.20

eCog Species	Group B Av.Abund	Group C Av.Abund	Av.Diss	Diss/SD	Contrib%	Cum.%
shell whole piece	55.74	77.03	16.15	1.21	21.77	21.77
shell hash	46.55	48.72	14.09	1.04	18.99	40.76
Hydrozoa bryozoa erect	14.48	25.27	5.93	0.76	7.99	48.75
Rhodophyta	14.75	9.61	3.94	0.47	5.31	54.07
worm castings	9.17	4.15	3.28	0.67	4.42	58.49
Crepidula_fornicata	3.85	12.9	2.7	0.45	3.64	62.13
Mytilus edulis valve	6.45	8.15	2.6	0.52	3.51	65.64
Chondrus crispus	10.29	6.33	2.4	0.39	3.24	68.87
worm tube flexible erect	5.02	4.43	2.2	0.57	2.96	71.83

Groups B & D
Average dissimilarity = 73.72

Species	Group B Av.Abund	Group D Av.Abund	Av.Diss	Diss/SD	Contrib%	Cum.%
shell whole piece	55.74	118.31	19.66	1.3	26.67	26.67
shell hash	46.55	38.44	11.65	0.99	15.8	42.47
Hydrozoa bryozoa erect	14.48	28.16	5.92	0.9	8.03	50.5
Mytilus edulis valve	6.45	18.61	4.31	0.61	5.85	56.35
Rhodophyta	14.75	9.42	3.61	0.44	4.89	61.24
Crepidula fornicata	3.85	15.9	2.97	0.52	4.02	65.26
worm castings	9.17	1.13	2.45	0.61	3.32	68.59
Cirripedia unstalked	4.43	11.05	2.32	0.63	3.14	71.73

Groups C & D
Average dissimilarity = 67.49

Species	Group C Av.Abund	Group D Av.Abund	Av.Diss	Diss/SD	Contrib%	Cum.%
shell whole piece	77.03	118.31	15.89	1.22	23.55	23.55
shell hash	48.72	38.44	10.89	0.99	16.13	39.68
Hydrozoa bryozoa erect	25.27	28.16	6.05	1	8.97	48.64
Mytilus edulis valve	8.15	18.61	4.14	0.62	6.13	54.77
Crepidula fornicata	12.9	15.9	3.72	0.58	5.51	60.29
Rhodophyta	9.61	9.42	2.73	0.47	4.04	64.33
Diadumene leucolena	11.61	5.9	2.41	0.39	3.57	67.9
Cirripedia unstalked	5.65	11.05	2.26	0.64	3.35	71.25

Table 5-17 continued,

Groups B & E
Average dissimilarity = 73.47

	Group B	Group E				
Species	Av.Abund	Av.Abund	Av.Diss	Diss/SD	Contrib%	Cum.%
shell whole piece	55.74	166.33	23.03	1.7	31.35	31.35
Hydrozoa bryozoa erect	14.48	49.5	8.52	1.8	11.59	42.95
shell hash	46.55	5.17	7.87	0.85	10.71	53.66
Mytilus edulis valve	6.45	41.83	7.78	1.29	10.59	64.25
Cirripedia test	1.8	34.67	6.5	2.01	8.84	73.09

Groups C & E
Average dissimilarity = 65.18

	Group C	Group E				
Species	Av.Abund	Av.Abund	Av.Diss	Diss/SD	Contrib%	Cum.%
shell whole piece	77.03	166.33	17.44	1.39	26.75	26.75
shell hash	48.72	5.17	7.81	0.86	11.98	38.74
Hydrozoa bryozoa erect	25.27	49.5	7.64	1.78	11.72	50.46
Mytilus edulis valve	8.15	41.83	7.15	1.29	10.97	61.43
Cirripedia test	3.34	34.67	5.71	1.88	8.76	70.19

Groups D & E
Average dissimilarity = 49.51

	Group D	Group E				
Species	Av.Abund	Av.Abund	Av.Diss	Diss/SD	Contrib%	Cum.%
shell whole piece	118.31	166.33	10.2	1.08	20.6	20.6
Mytilus edulis valve	18.61	41.83	6.43	1.26	12.99	33.59
Hydrozoa bryozoa erect	28.16	49.5	6.05	1.54	12.22	45.81
shell hash	38.44	5.17	5.73	0.74	11.58	57.39
Cirripedia test	10.74	34.67	4.93	1.73	9.96	67.35
Cirripedia unstalked	11.05	11	2.21	0.96	4.46	71.81

Groups B & A
Average dissimilarity = 82.39

	Group B	Group A				
Species	Av.Abund	Av.Abund	Av.Diss	Diss/SD	Contrib%	Cum.%
Crepidula fornicata shell	0.89	55.33	13.32	1.82	16.17	16.17
Crepidula_fornicata	3.85	68.5	12.99	1.69	15.76	31.93
shell whole piece	55.74	36.83	10.04	1.19	12.19	44.11
shell hash	46.55	10	9.34	0.9	11.34	55.45
Hydrozoa bryozoa erect	14.48	22.33	5.01	0.95	6.08	61.53
Rhodophyta	14.75	14.33	4.42	0.66	5.36	66.89
Grinellia americana	0	18.83	3.17	0.68	3.84	70.73

Table 5-17 continued,

Groups C & A
Average dissimilarity = 78.56

Species	Group C Av.Abund	Group A Av.Abund	Av.Diss	Diss/SD	Contrib%	Cum.%
Crepidula fornicata	12.9	68.5	11.93	1.62	15.18	15.18
Crepidula fornicata shell	3.21	55.33	11.69	1.78	14.88	30.07
shell whole piece	77.03	36.83	11.56	1.25	14.71	44.78
shell hash	48.72	10	8.99	0.87	11.44	56.22
Hydrozoa bryozoa erect	25.27	22.33	5.31	1.02	6.76	62.98
Rhodophyta	9.61	14.33	3.23	0.78	4.11	67.09
Grinellia americana	0.27	18.83	2.93	0.68	3.73	70.82

Groups D & A
Average dissimilarity = 77.03

Species	Group D Av.Abund	Group A Av.Abund	Av.Diss	Diss/SD	Contrib%	Cum.%
shell whole piece	118.31	36.83	16.53	1.58	21.46	21.46
Crepidula fornicata	15.9	68.5	10.61	1.57	13.77	35.23
Crepidula fornicata shell	3.37	55.33	10.3	1.85	13.37	48.59
shell hash	38.44	10	6.75	0.8	8.77	57.36
Hydrozoa bryozoa erect	28.16	22.33	4.85	1.09	6.3	63.66
Mytilus edulis valve	18.61	0	3.34	0.55	4.33	67.99
Rhodophyta	9.42	14.33	3.08	0.69	4	71.99

Groups E & A
Average dissimilarity = 78.95

Species	Group E Av.Abund	Group A Av.Abund	Av.Diss	Diss/SD	Contrib%	Cum.%
shell whole piece	166.33	36.83	22.07	3.26	27.95	27.95
Crepidula fornicata	1	68.5	9.89	1.69	12.53	40.49
Crepidula fornicata shell	0.67	55.33	9.41	2.49	11.92	52.4
Mytilus edulis valve	41.83	0	7.2	1.4	9.12	61.53
Hydrozoa bryozoa erect	49.5	22.33	6.01	1.59	7.62	69.14
Cirripedia test	34.67	3	5.43	2.09	6.87	76.02

III. 2018 Spring Live taxa
Groups B & D
Average dissimilarity = 86.45
eCog

Species	Group B Av.Abund	Group D Av.Abund	Av.Diss	Diss/SD	Contrib%	Cum.%
Hydrozoa bryozoa erect	29.84	71.28	22.99	1.16	26.59	26.59
Rhodophyta	27.77	8.73	10.02	0.68	11.59	38.18
Phaeophyceae	17.66	8.03	6.72	0.62	7.77	45.95

Species						
Paguroidea spp. unidentified	5.96	8.58	5.06	0.59	5.85	51.8
Chorda filum	11.81	6.76	5.04	0.55	5.83	57.63
Tubularia indivisa	6.3	13.78	4.27	0.38	4.94	62.57
Crepidula fornicata	4.76	7.19	3.45	0.43	3.99	66.56
Tubulariidae spp.	3.04	4.6	3.31	0.47	3.82	70.38

Groups B & C
Average dissimilarity = 86.94

	Group B	Group C				
Species	Av.Abund	Av.Abund	Av.Diss	Diss/SD	Contrib%	Cum.%
Hydrozoa bryozoa erect	29.84	57.39	21.82	1.1	25.09	25.09
Rhodophyta	27.77	8.27	10.83	0.68	12.46	37.55
Phaeophyceae	17.66	6.4	7	0.61	8.06	45.6
Paguroidea spp. unidentified	5.96	8.77	5.52	0.55	6.35	51.95
Chorda filum	11.81	5.69	5.38	0.52	6.19	58.14
Crepidula fornicata	4.76	12.27	4.56	0.48	5.24	63.39
Chondrus crispus	6.27	8.23	4.28	0.34	4.92	68.31
Tubulariidae spp.	3.04	4.41	3.81	0.45	4.38	72.68

Groups D & C
Average dissimilarity = 82.86

	Group D	Group C				
Species	Av.Abund	Av.Abund	Av.Diss	Diss/SD	Contrib%	Cum.%
Hydrozoa bryozoa erect	71.28	57.39	26.16	1.21	31.57	31.57
Paguroidea spp. unidentified	8.58	8.77	5.63	0.6	6.8	38.36
Rhodophyta	8.73	8.27	5.13	0.48	6.19	44.55
Crepidula fornicata	7.19	12.27	5.09	0.53	6.15	50.7
Tubularia indivisa	13.78	5.24	4.22	0.4	5.09	55.79
Phaeophyceae	8.03	6.4	3.68	0.52	4.44	60.24
Chorda filum	6.76	5.69	3.58	0.41	4.32	64.56
Tubulariidae spp.	4.6	4.41	3.24	0.44	3.91	68.47
Gastropoda unidentified	6.35	4.29	3.23	0.46	3.9	72.36

Groups B & E
Average dissimilarity = 83.47

	Group B	Group E				
Species	Av.Abund	Av.Abund	Av.Diss	Diss/SD	Contrib%	Cum.%
Hydrozoa bryozoa erect	29.84	115.25	35.08	1.63	42.03	42.03
Rhodophyta	27.77	0	8.06	0.62	9.65	51.68
Phaeophyceae	17.66	0	4.98	0.52	5.97	57.65
Tubularia indivisa	6.3	9.25	4.95	0.66	5.93	63.58
Paguroidea spp. unidentified	5.96	14	4.74	0.89	5.68	69.26
Chorda filum	11.81	0	3.3	0.49	3.96	73.22

Table 5-17 continued,

Groups D & E
Average dissimilarity = 72.28

Species	Group D Av.Abund	Group E Av.Abund	Av.Diss	Diss/SD	Contrib%	Cum.%
Hydrozoa bryozoa erect	71.28	115.25	32.59	1.47	45.09	45.09
Tubularia indivisa	13.78	9.25	5.63	0.67	7.79	52.88
Paguroidea spp. unidentified	8.58	14	4.74	0.97	6.56	59.44
Corymorpha pendula	3.77	9.5	3.02	0.7	4.17	63.61
Cerripedia	5.72	4.75	2.76	0.66	3.82	67.43
Tubulariidae spp.	4.6	3.5	2.56	0.62	3.55	70.98

Groups C & E
Average dissimilarity = 75.52

Species	Group C Av.Abund	Group E Av.Abund	Av.Diss	Diss/SD	Contrib%	Cum.%
Hydrozoa bryozoa erect	57.39	115.25	35.76	1.54	47.35	47.35
Paguroidea spp. unidentified	8.77	14	4.93	1.03	6.53	53.89
Tubularia indivisa	5.24	9.25	4.58	0.76	6.06	59.95
Crepidula fornicata	12.27	2.25	3.33	0.46	4.41	64.36
Corymorpha pendula	3.21	9.5	3.1	0.66	4.1	68.47
Tubulariidae spp.	4.41	3.5	2.77	0.59	3.66	72.13

Groups B & NA
Average dissimilarity = 88.91

Species	Group B Av.Abund	Group NA Av.Abund	Av.Diss	Diss/SD	Contrib%	Cum.%
Paguroidea spp. unidentified	5.96	20.75	16.9	0.94	19.01	19.01
Hydrozoa bryozoa erect	29.84	4.44	14.1	0.83	15.86	34.87
Rhodophyta	27.77	1.56	12.1	0.7	13.61	48.48
Phaeophyceae	17.66	0.13	7.39	0.57	8.31	56.79
Tubulariidae spp.	3.04	6.19	6.5	0.64	7.31	64.1
Chorda filum	11.81	0.94	5.49	0.55	6.18	70.27

Groups D & NA
Average dissimilarity = 88.78

Species	Group D Av.Abund	Group NA Av.Abund	Av.Diss	Diss/SD	Contrib%	Cum.%
Hydrozoa bryozoa erect	71.28	4.44	26.57	1.19	29.92	29.92
Paguroidea spp. unidentified	8.58	20.75	15.08	0.86	16.99	46.92
Tubulariidae spp.	4.6	6.19	6.12	0.61	6.89	53.81
Rhodophyta	8.73	1.56	4.18	0.45	4.71	58.52
Tubularia indivisa	13.78	0	3.79	0.34	4.27	62.79
Crepidula fornicata	7.19	1.31	3.59	0.47	4.04	66.83
Gastropoda unidentified	6.35	1	3.49	0.51	3.93	70.76

Table 5-17 continued,

Groups C & NA
Average dissimilarity = 89.26

Species	Group C Av.Abund	Group NA Av.Abund	Av.Diss	Diss/SD	Contrib%	Cum.%
Hydrozoa bryozoa erect	57.39	4.44	23.81	1.1	26.67	26.67
Paguroidea spp. unidentified	8.77	20.75	18.4	0.88	20.61	47.28
Tubulariidae spp.	4.41	6.19	7.18	0.6	8.05	55.33
Crepidula fornicata	12.27	1.31	4.97	0.51	5.57	60.9
Rhodophyta	8.27	1.56	4.61	0.45	5.16	66.06
Gastropoda unidentified	4.29	1	3.37	0.48	3.78	69.83
Chorda filum	5.69	0.94	3.3	0.35	3.69	73.53

Groups E & NA
Average dissimilarity = 87.77

Species	Group E Av.Abund	Group NA Av.Abund	Av.Diss	Diss/SD	Contrib%	Cum.%
Hydrozoa bryozoa erect	115.25	4.44	50.2	3.13	57.2	57.2
Paguroidea spp. unidentified	14	20.75	11.78	1.04	13.42	70.62

IV. Spring 2018 Live taxa and biogenic features

Groups B & D
Average dissimilarity = 72.69
eCog

Species	Group B Av.Abund	Group D Av.Abund	Av.Diss	Diss/SD	Contrib%	Cum.%
shell hash	81.68	97.71	12.99	1.14	17.87	17.87
Shell whole partial	45.04	96.87	11.47	1.32	15.79	33.66
Hydrozoa bryozoa erect	29.84	71.28	9.41	1.07	12.94	46.6
Rhodophyta	27.77	8.73	4.63	0.61	6.37	52.97
Phaeophyceae	17.66	8.03	3.07	0.55	4.22	57.19
Tubularia indivisa	6.3	13.78	2.49	0.35	3.43	60.62
Chorda filum	11.81	6.76	2.36	0.53	3.25	63.87
Diadumene leucolena	5.24	10.53	1.85	0.37	2.55	66.42
Mytilus edulis valve	0.5	16.3	1.84	0.43	2.53	68.95
terrestrial vegetation debris	11.05	0.2	1.81	0.26	2.5	71.45

Groups B & C
Average dissimilarity = 73.39

Species	Group B Av.Abund	Group C Av.Abund	Av.Diss	Diss/SD	Contrib%	Cum.%
shell hash	81.68	88.86	14.34	1.11	19.53	19.53
Shell whole partial	45.04	72.11	10.16	1.2	13.84	33.37
Hydrozoa bryozoa erect	29.84	57.39	8.87	0.99	12.08	45.46
Rhodophyta	27.77	8.27	4.94	0.61	6.72	52.18

Species	Av.Abund	Av.Abund	Av.Diss	Diss/SD	Contrib%	Cum.%
Phaeophyceae	17.66	6.4	3.17	0.56	4.32	56.5
Chorda filum	11.81	5.69	2.54	0.51	3.46	59.96
terrestrial vegetation debris	11.05	2.54	2.44	0.29	3.33	63.29
worm castings	9.27	9.28	2.16	0.77	2.94	66.22
Chondrus crispus	6.27	8.23	2.14	0.34	2.92	69.15
Crepidula fornicata	4.76	12.27	1.9	0.44	2.6	71.74

Groups D & C
Average dissimilarity = 65.29

	Group D	Group C				
Species	Av.Abund	Av.Abund	Av.Diss	Diss/SD	Contrib%	Cum.%
shell hash	97.71	88.86	12.13	1.14	18.58	18.58
Shell whole partial	96.87	72.11	10.87	1.29	16.65	35.22
Hydrozoa bryozoa erect	71.28	57.39	10.19	1.11	15.61	50.83
Mytilus edulis valve	16.3	7.04	2.33	0.52	3.56	54.39
Tubularia indivisa	13.78	5.24	2.23	0.37	3.41	57.8
Rhodophyta	8.73	8.27	2.16	0.43	3.3	61.1
Crepidula fornicata	7.19	12.27	1.98	0.5	3.03	64.14
Diadumene leucolena	10.53	5.52	1.85	0.38	2.84	66.97
worm castings	5.02	9.28	1.65	0.6	2.53	69.51
Paguroidea spp. unidentified	8.58	8.77	1.61	0.84	2.47	71.97

Groups B & E
Average dissimilarity = 71.25

	Group B	Group E				
Species	Av.Abund	Av.Abund	Av.Diss	Diss/SD	Contrib%	Cum.%
Hydrozoa bryozoa erect	29.84	115.25	13.93	1.68	19.55	19.55
Shell whole partial	45.04	108.75	12.41	1.79	17.42	36.96
shell hash	81.68	83.25	11.99	1.24	16.83	53.79
Rhodophyta	27.77	0	4.3	0.55	6.04	59.84
Phaeophyceae	17.66	0	2.65	0.46	3.72	63.55
Tubularia indivisa	6.3	9.25	2.22	0.47	3.12	66.67
Paguroidea spp. unidentified	5.96	14	2	0.93	2.8	69.47
terrestrial vegetation debris	11.05	0	1.9	0.27	2.67	72.14

Groups D & E
Average dissimilarity = 56.15

	Group D	Group E				
Species	Av.Abund	Av.Abund	Av.Diss	Diss/SD	Contrib%	Cum.%
Hydrozoa bryozoa erect	71.28	115.25	12.37	1.47	22.03	22.03
Shell whole partial	96.87	108.75	10.06	1.41	17.91	39.95
shell hash	97.71	83.25	9.98	1.2	17.77	57.72
Mytilus edulis valve	16.3	14	2.78	0.69	4.95	62.67
Tubularia indivisa	13.78	9.25	2.62	0.51	4.67	67.34
Paguroidea spp. unidentified	8.58	14	1.88	1.05	3.35	70.69

Table 5-17 continued,

Groups C & E
Average dissimilarity = 60.25

Species	Group C Av.Abund	Group E Av.Abund	Av.Diss	Diss/SD	Contrib%	Cum.%
Hydrozoa bryozoa erect	57.39	115.25	13.31	1.62	22.09	22.09
shell hash	88.86	83.25	11.44	1.2	18.98	41.07
Shell whole partial	72.11	108.75	10.8	1.55	17.92	58.99
	7.04	14	2.16	0.81	3.58	62.57
Paguroidea spp. unidentified						
	8.77	14	2.04	1.06	3.38	65.95
Tubularia indivisa	5.24	9.25	1.82	0.61	3.02	68.97
Crepidula fornicata	12.27	2.25	1.49	0.43	2.48	71.45

Groups B & NA
Average dissimilarity = 73.40

Species	Group B Av.Abund	Group NA Av.Abund	Av.Diss	Diss/SD	Contrib%	Cum.%
shell hash	81.68	87.81	13.84	1.2	18.86	18.86
terrestrial vegetation debris	11.05	77.25	12	0.92	16.35	35.21
Shell whole partial	45.04	48.19	8.02	1.21	10.92	46.13
Rhodophyta	27.77	1.56	4.5	0.58	6.13	52.26
Hydrozoa bryozoa erect	29.84	4.44	4.13	0.66	5.63	57.89
Zostera seagrass debris	9.26	23.81	3.83	0.87	5.22	63.11
Paguroidea spp. unidentified	5.96	20.75	3.21	1.27	4.38	67.48
Phaeophyceae	17.66	0.13	2.76	0.48	3.76	71.24

Groups D & NA
Average dissimilarity = 70.03

Species	Group D Av.Abund	Group NA Av.Abund	Av.Diss	Diss/SD	Contrib%	Cum.%
shell hash	97.71	87.81	11.17	1.19	15.95	15.95
terrestrial vegetation debris	0.2	77.25	10.41	0.87	14.87	30.82
Shell whole partial	96.87	48.19	10.3	1.38	14.71	45.53
Hydrozoa bryozoa erect	71.28	4.44	8.76	1.01	12.51	58.04
Zostera seagrass debris	5.21	23.81	3.19	0.76	4.55	62.6
Paguroidea spp. unidentified	8.58	20.75	2.73	1.21	3.9	66.5
worm tube flexible erect	1.74	11.88	2	0.7	2.85	69.35
Mytilus edulis valve	16.3	0.25	1.83	0.42	2.62	71.97

Groups C & NA
Average dissimilarity = 70.60

Species	Group C Av.Abund	Group NA Av.Abund	Av.Diss	Diss/SD	Contrib%	Cum.%
shell hash	88.86	87.81	12.78	1.21	18.1	18.1
terrestrial vegetation debris	2.54	77.25	11.32	0.89	16.03	34.13

Shell whole partial	72.11	48.19	9.14	1.28	12.95	47.08
Hydrozoa bryozoa erect	57.39	4.44	7.79	0.9	11.04	58.12
Zostera seagrass debris	5.27	23.81	3.37	0.78	4.78	62.9
Paguroidea spp. unidentified	8.77	20.75	3.03	1.27	4.3	67.2
worm castings	9.28	8.31	2.28	0.64	3.24	70.44

Groups E & NA
Average dissimilarity = 67.32

	Group E	Group NA				
Species	Av.Abund	Av.Abund	Av.Diss	Diss/SD	Contrib%	Cum.%
Hydrozoa bryozoa erect	115.25	4.44	14.81	2.05	22	22
terrestrial vegetation debris	0	77.25	11.04	0.87	16.4	38.4
shell hash	83.25	87.81	10.27	1.2	15.25	53.64
Shell whole partial	108.75	48.19	10.19	1.69	15.14	68.78
Zostera seagrass debris	0	23.81	3.07	0.7	4.57	73.35

Patterns of Diversity

SEABOSS and ROV still images were the principal samples for assessing variation in faunal components and biogenic features of habitats across the study area. Species accumulation curves were used for fall 2017 and spring 2018 sample sets to assess the adequacy of sample effort (Figure 5.2-37). Chao 1 and Michaelis-Menton diversity estimation indices were also calculated to estimate the total diversity of taxa in samples based on the accumulation of new taxa in successive samples. They both use different formulas for relationships that describe the number and abundance of species to estimate total species richness with the premise that the rate of new species occurrence is an indicator of total species within the community (see Morris et al., 2014). It is noteworthy that observed richness and estimated richness curves overlap indicating that sampling using this imaging platform and taxonomic classification approach adequately captured the diversity across the landscape. However, as studies in multiple aquatic and terrestrial settings have demonstrated, different sampling methods can yield different patterns. A comparison of SEABOSS and ROV results from 2018 (Table 5-18) illustrates differences in diversity between imaging platforms. Indeed, the richness estimates from Chao 1 illustrate that the ROV, with slower speed, greater resolution based on distance to surfaces, yielded greater species richness, although we interpret this to be based in part on ROV sampling in more heterogeneous habitats as well as greater resolution for identifying species to lower taxonomic levels.
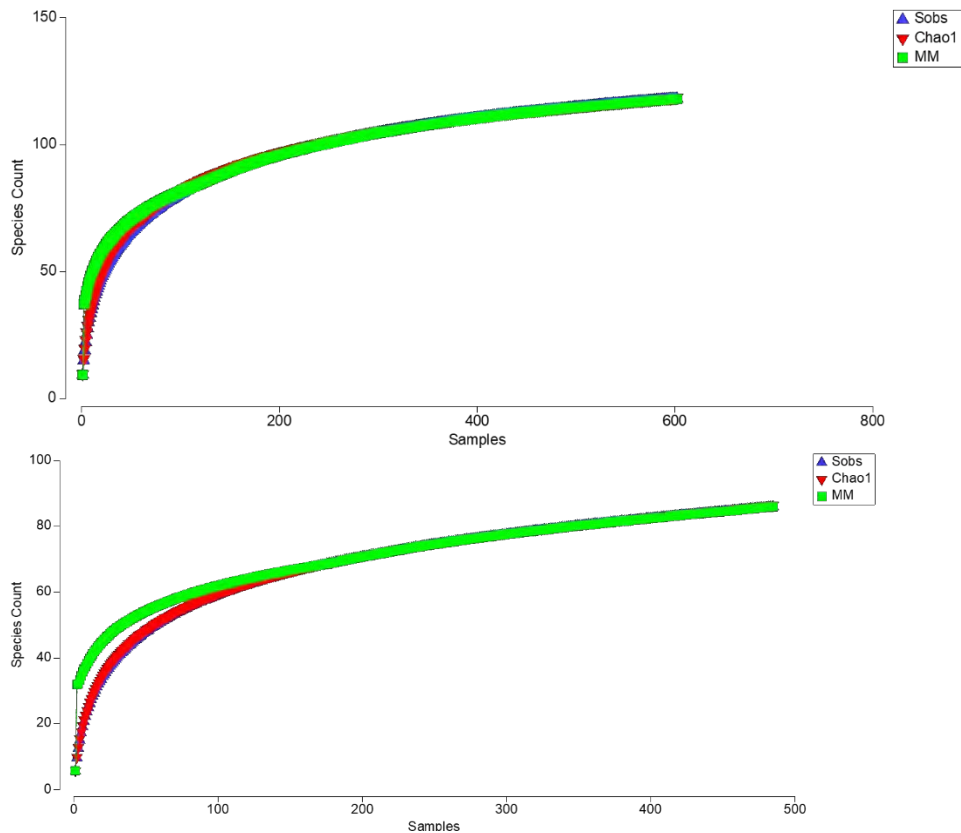
Figure 5.2-37. Species accumulations curves for 2017 (top) and 2018 (bottom) SEABOSS survey. Each graph includes Sobs (species richness based on observations) as well as Chao1 and Michaelis-Menton (MM) richness estimators based on the relationship between total species richness as samples accumulate (see REF xxxx for details). Each species richness estimator represents a unique approach to predict total richness. Lines are based on 999 (check this) randomizations of sample order.

Table 5-18. Comparison of observed and estimated richness of taxa from 2018 SeaBOSS and ROV surveys

Samples	S obs	MM	Chao 1
Seaboss	86	86	86.5
ROV	52	54.6	57.6
Combined	120	120	136.2

Image transects in some sample blocks and sites transcended one or more eCognition patch boundaries. This facilitated examination of the role that habitat variability played in enhancing the calculation of local diversity of fauna. Figure 5.2-38 illustrates patterns of accumulated taxon and biogenic feature richness based on linear accumulation of image samples along transects for both fall 2017 and spring 2018 surveys. The two time periods take into account seasonal patterns of recruitment and mortality of benthic fauna with short (annual) life histories. These results indicate that the number of patches and associated transitions have little effect on species richness at this spatial scale. Such patterns, in this ecological setting, can be attributed to the small-scale patchiness of coarse-grained sediments (sand to boulder) within eCognition patches. That is, while large scale patchiness in seafloor maps is attributed to overall patterns of grain size and acoustic reflectivity, small scale patchiness mediates the abundance, but not necessarily diversity, of epifaunal and emergent taxa. Correlating taxa and feature richness at the scale of each image with backscatter value (from multibeam), as a proxy for image scale habitat variation, revealed a similar lack of pattern (Figure 5.2-39).
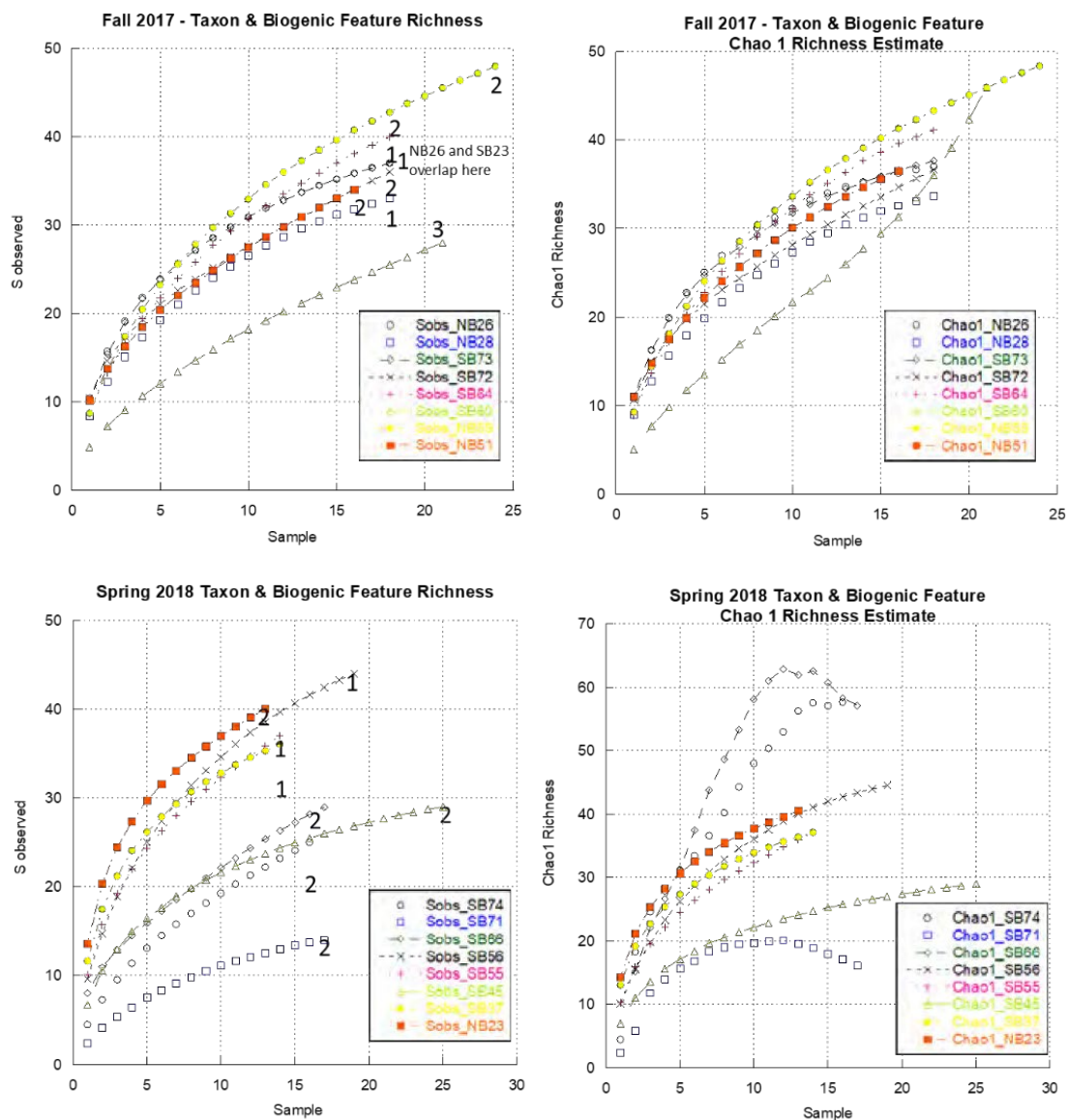
Figure 5.2-38. Number of eCog patches represented by data from each station with observed richness (left) and richness estimates (right) for 2017 (top) and 2018 (bottom) surveys. (Top) Noteworthy for the 2017 surveys is data from SB60 represents three eCog types and, if linear in arrangement, multiple transitions. In any case, a very different pattern with rising predicted S appears in the Chao1 analysis. Species accumulation curves are based on 999 permutations.
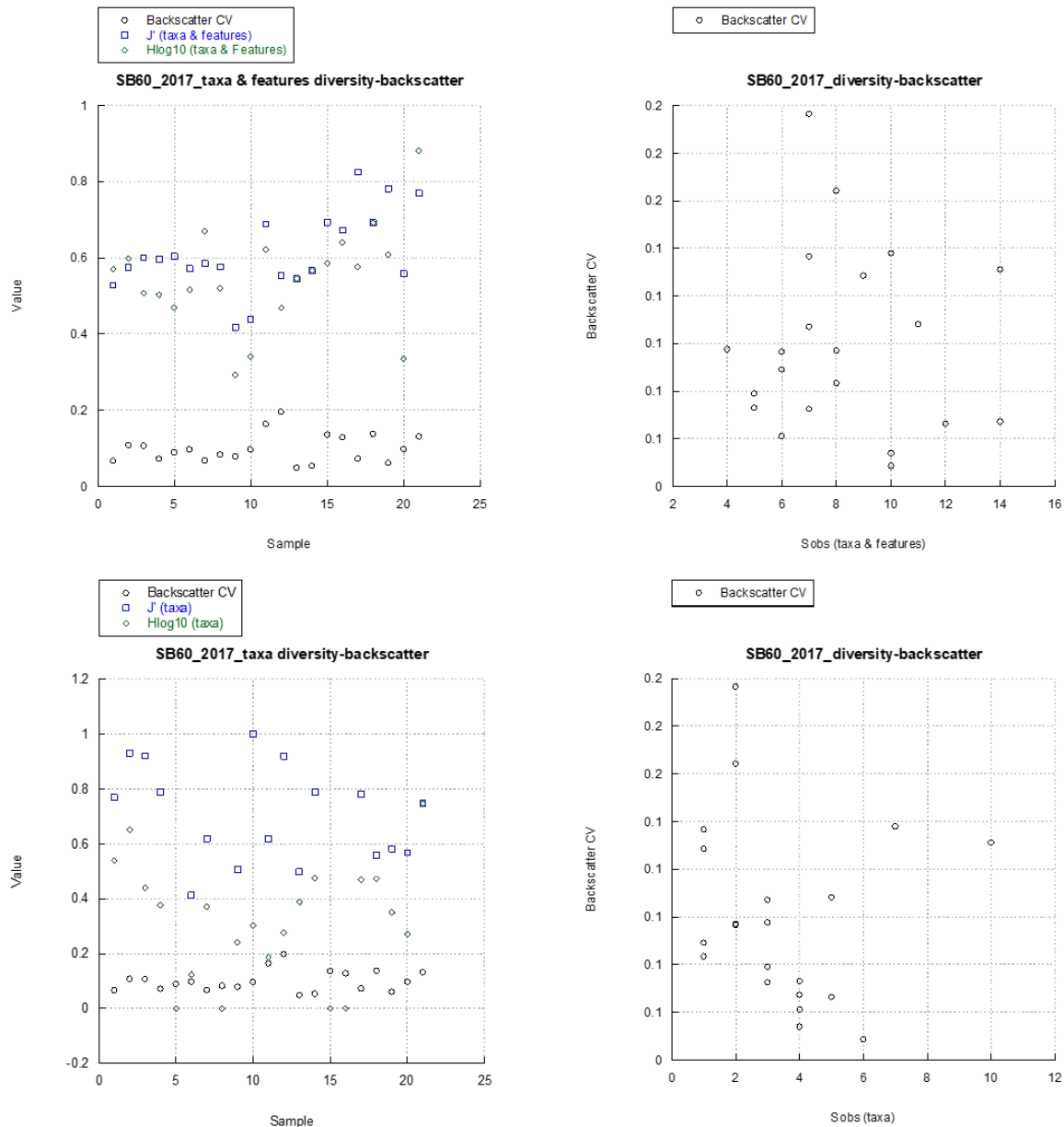
Figure 5.2-39. Relationship between taxa and features with backscatter for sample block SB60, crossing three eCognition classes. Little discernible relationship between sample-scale (i.e., image-specific) diversity and habitat complexity (as represented by acoustic backscatter).

Image sampling, while facilitating sampling across large areas with efficient use of time and ship resources, limits the ability to identify and assess cryptic species (i.e., those too small, transparent, camouflaged, or sheltered to be represented in images). To conduct an assessment of the degree that images under-sample components of diversity, a limited set of simultaneous image and airlift samples were collected via scuba diving in relatively shallow depths and at multiple sites with complex habitats. A 0.25 m^2 camera quadrapod and airlift were used (see Section 5.2.3.2) over the study period. Image and airlift samples were paired at sites but the entirety of sampling crossed seasons due to logistical constraints. Images identified 35 taxa using while airlift samples collected 130 taxa (Table 5-19, Figure 5.2-40). That the sampling was complementary with a total richness

of 157 taxa is Notable. Image samples were dominated by macroalgae and sponge taxa (Figure 5.2-41) while airlift samples were dominated by arthropods, mollusks, and annelids (Figure 5.2-42). Further, the arthropods were composed of amphipods, decapods, and isopods, all important prey taxa for secondary consumers, including fish of ecological and economic importance in LIS. An example of the diversity of organisms from a single airlift sample is illustrated with one from Latimer Reef (Table 5-20).

Table 5-19. Comparison of taxa richness from quadrapod image and suction samples.

Samples	S obs	MM	Chao 1
Suction	130	177.5	205
Quadrat photo	35	36.4	37
Combined	157	*	*
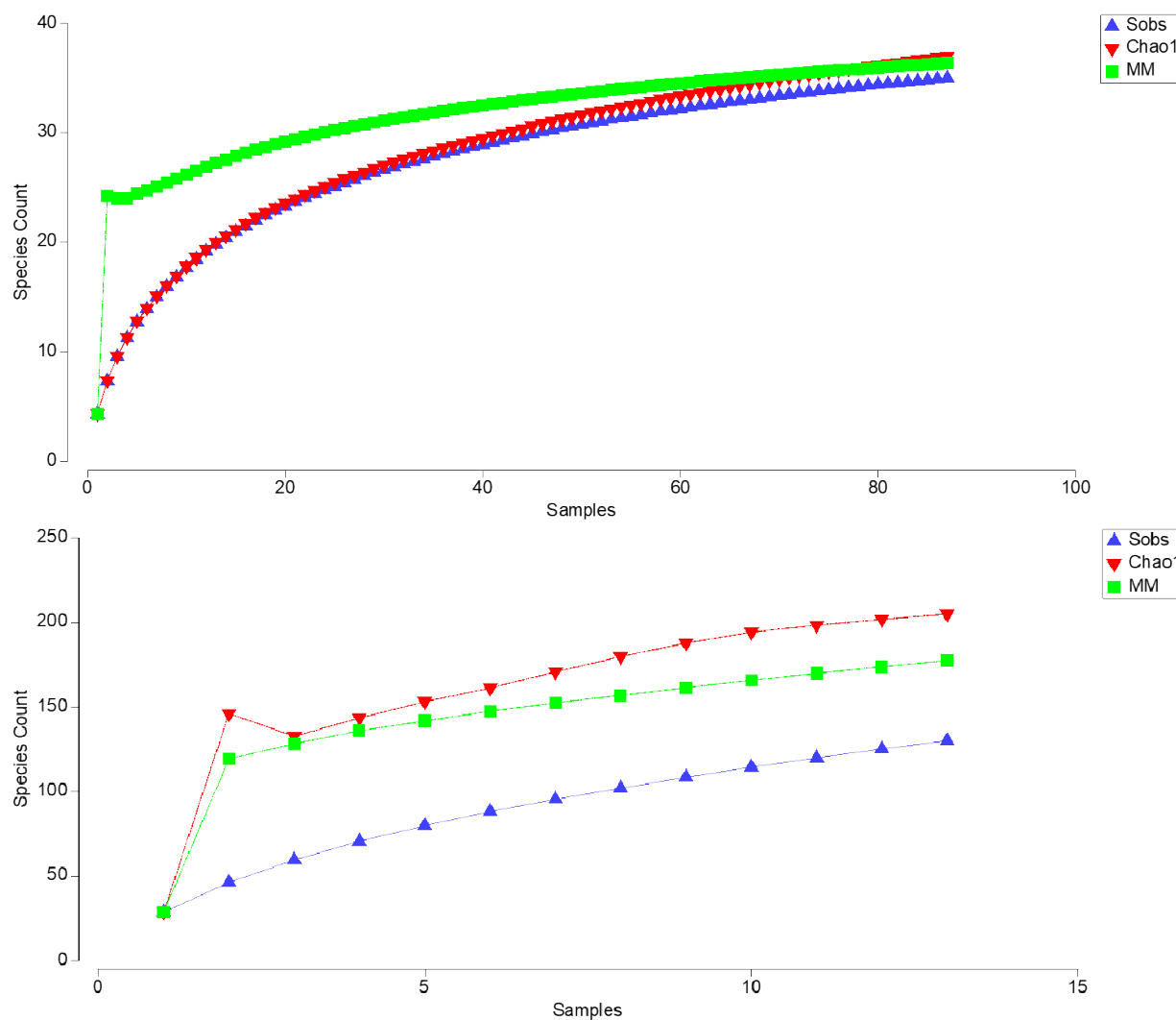
Figure 5.2-40. Taxa accumulation curves, based on observed richness and Chao1 and Michaelis-Menton richness estimators, for image (top) and airlift (bottom) samples

Figure 5.2-41. Results of quadrat images based on cover estimates
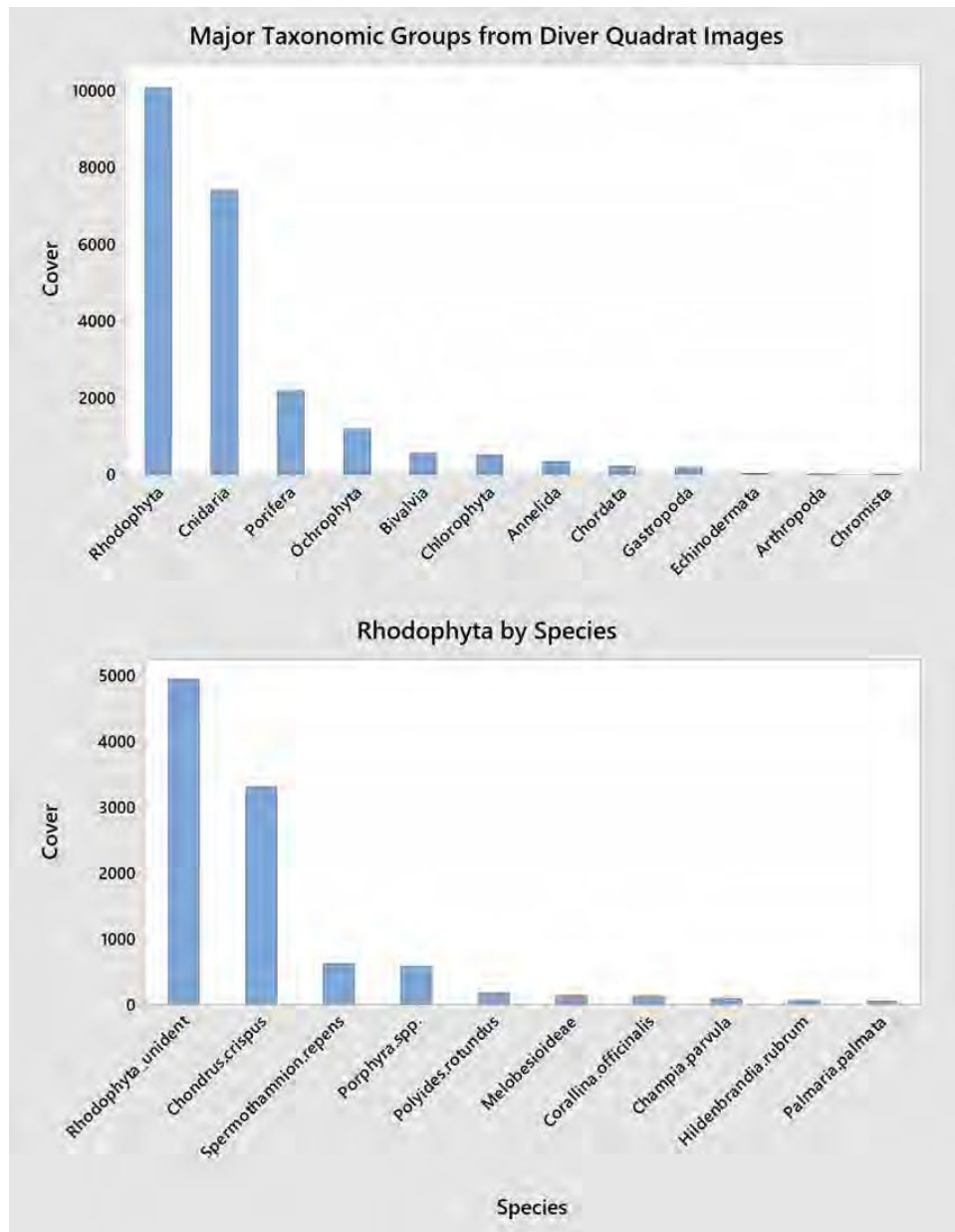
Taxa	Cover
Rhodophyta	10056
Cnidaria	7402
Porifera	2177
Ochrophyta	1179
Bivalvia	548
Chlorophyta	507
Annelida	342
Chordata	222
Gastropoda	189
Echinodermata	30
Arthropoda	19
Chromista	14

Major Taxonomic Groups in Suction Samples

Phylum (x-axis): Arthropoda, Gastropoda, Annelida, Bryozoa, Bivalvia, Cnidaria, Ochrophyta, Porifera, Rhodophyta, Echinodermata, Chlorophyta, Chordata, Sipuncula

Arthropods by Order

Order (x-axis): Amphipoda, Decapoda, Isopoda, Sessilia, Cyclopoida, Hexapoda, Mysida, Pycnogonida

Site	S
Latimer/2018	81
Ellis/2018	42
S of Seaside Pt/2017/S10	17
Black Ledge/2018	41
N of Plum Island/2018	37
Ram Island Reef/2017	37
Two Tree Island	21
S of Seaside Pt/2017/SD09	13
Latimer Reef/2017	12
NW of N Hill Point	7
N of Plum Island	19
Three Ft Rock	17
Ellis Reef	27

Figure 5.2-42. Results of analysis from airlift samples based on taxon richness

Table 5-20. Example from Latimer Reef on 15 June 2018 (sample site SD 11).

Site/Year:	Latimer/2018				
Taxonomy					**Total**
Mollusca	Bivalvia	Mytilida	Mytilidea	*Mytilus edulis*	16775
Arthropoda	Malacostraca	Amphipoda	Caprellidae	*Paracaprella tenuis*	643
Arthropoda	Malacostraca	Amphipoda	Caprellidae	Caprellidae	517
Mollusca	Gastropoda	Littorinimorpha	Littorinidae	*Littorina littorea*	473
Arthropoda	Malacostraca	Amphipoda	Caprellidae	*Aeginina longicornis*	397
Mollusca	Gastropoda	Littorinimorpha	Naticidae	*Euspira triseriata*	270
Arthropoda	Hexanauplia	Cyclopoida	Oncaeidae	Oncaeidae	269
Arthropoda	Malacostraca	Amphipoda	Caprellidae	*Caprella linearis*	214
Arthropoda	Malacostraca	Amphipoda	Corophiidae	Corophiidae	192
Arthropoda	Malacostraca	Amphipoda	Amphipoda	Amphipoda	122
Arthropoda	Hexanauplia	Sessilia	Balanidae	Balanus	97
Mollusca	Gastropoda	Neogastropoda	Columbellidae	*Astyris lunata*	93
Mollusca	Gastropoda	Neogastropoda	Columbellidae	*Cotonopsis lafresnayi*	81
Arthropoda	Malacostraca	Amphipoda	Aoridae	Aoridae	78
Annelida	Polychaeta	Sabellida	Serpulidae	*Hydroides dianthus*	63
Annelida	Polychaeta	Phyllodocida	Polynoidae	*Lepidonotus squamatus*	37
Arthropoda	Malacostraca	Amphipoda	Melitidae	Melitidae	35
Arthropoda	Malacostraca	Amphipoda	Stenothoidae	Stenothoidae	30
Arthropoda	Hexanauplia	Sessilia	Archaeobalanidae	*Semibalanus balanoides*	30
Arthropoda	Malacostraca	Amphipoda	Caprellidae	*Caprella penantis*	25
Arthropoda	Malacostraca	Amphipoda	Bateidae	Bateidae	22
Porifera	Calcarea	Leucosolenida	Leucosoleniidae	*Leucosolenia botryoides*	18
Arthropoda	Hexanauplia	Sessilia	Archaeobalanidae	*Chirona hameri*	17
Arthropoda	Malacostraca	Amphipoda	Liljeborgiidae	*Idunella clymenellae*	16
Arthropoda	Malacostraca	Amphipoda	Unciolidae	Unciolidae	15
Arthropoda	Malacostraca	Amphipoda	Gammarellidae	Gammarellidae	14
Echinodermata	Ophiuroidea	Amphilepidida	Amphiuridae	*Amphipholis squamata*	14
Cnidaria	Anthozoa	Actiniaria	Diadumenidae	*Diadumene leucolena*	13
Arthropoda	Malacostraca	Isopoda	Idoteidae	*Idotea balthica*	10

The distribution and abundance of particular taxa (epi- and emergent- fauna) and biogenic features did not follow uniform geographic trends, reflecting the varied seafloor habitats characterized by grain size, seafloor roughness, seafloor stress (from current flows), depth (temperature and light), and west-to-east variation in conditions within the estuary. While multiple spatial patterns were identified that provide important insights, multiple taxa and biogenic habitat features that represent larger gradients and general relationships between epifauna and physical characteristics of seafloor environments within the larger landscape were identified. It is noteworthy that the most diverse sites are to the east in the study area and offshore including eastern FIS, south of Fishers Island, and The Race (Figure 5.2-43).
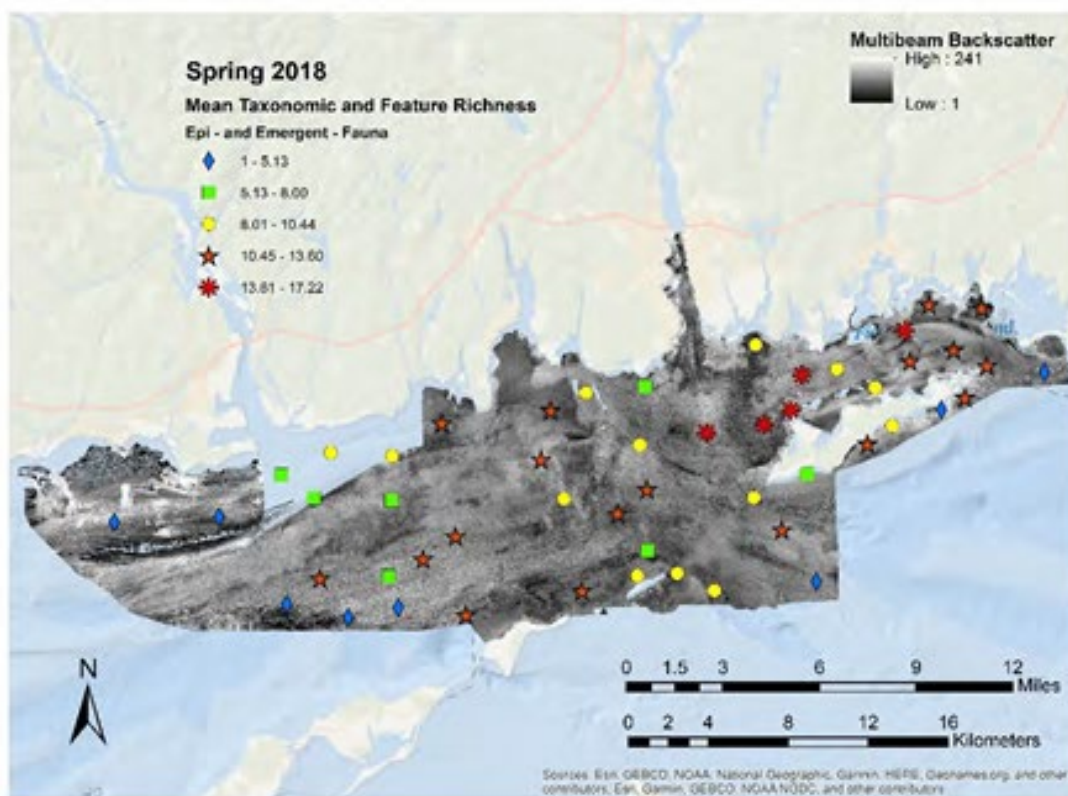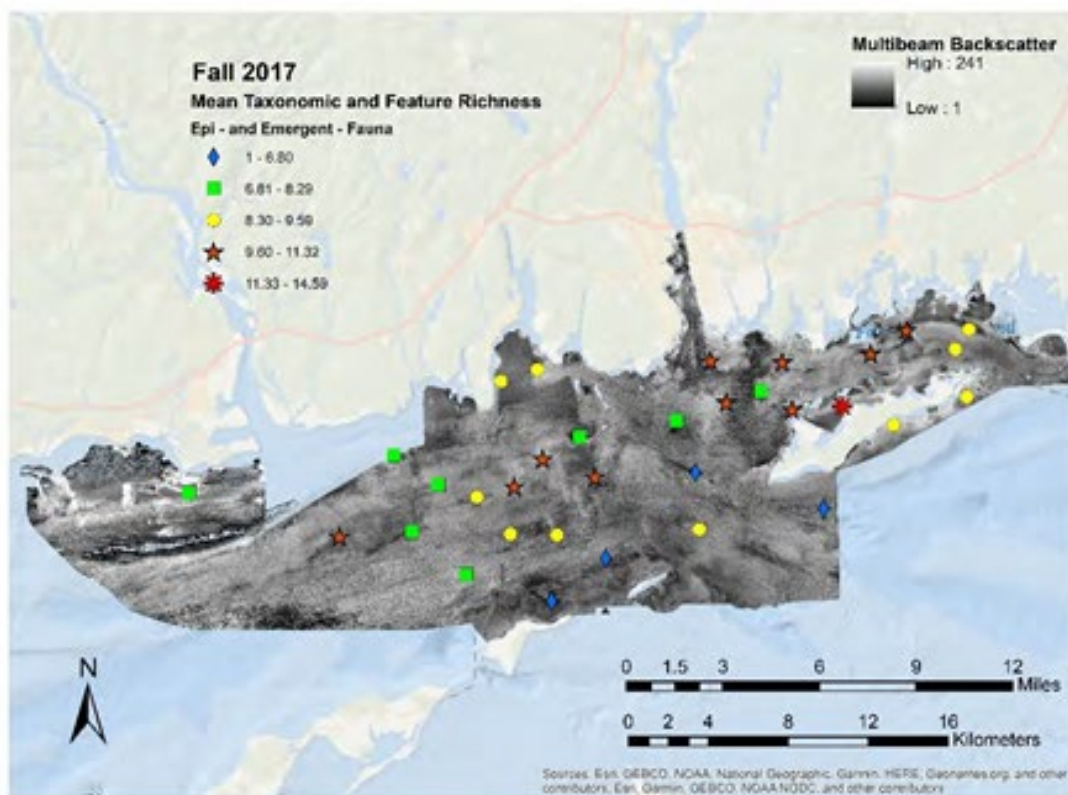
Figure 5.2-43. Block/site-scale taxonomic and biogenic feature richness as determined during fall (top) and spring (bottom) sampling. Note: the cluster of high richness in the eastern 1/3 of the Phase II study area.

Communities at Scale of Blocks and Sites

Image data from all SEABOSS surveys were aggregated to block and site designations and mean values calculated to identify large scale variation in community structure (i.e., images within sites treated as replicates versus samples). Multivariate analyses were implemented with live taxa and biogenic features as well as live taxa only. SIMPROF was used to identify similarities between sites at the 1% threshold level for hierarchical cluster analyses. These groupings were used as a factor for mMDS analysis, where 15 cluster groups were identified (Figure 5.2-45). Results of global ANOSIM, for both features and taxa, and taxa only, were highly significant (Table 5-15) as were multiple paired comparisons. SIMPER identified the features and taxa that contributed most to dissimilarity between sites. However, these results when visualized in a geospatial context provided little insight into general patterns of epifaunal and biogenic habitat features across the Phase II map area. A qualitative hierarchical approach for aggregating sites based on geographic proximity and similarity of ecological features was implemented. The most parsimonious was a set of four groupings representing coastal, west, central, and east regions within the map area (Figure 5.2-44). ANOSIM procedures demonstrated that post-hoc groupings were highly significant (Table 5-15). Results of SIMPER analyses (Table 5-17) demonstrated that the differential cover of biogenic features composed of shell and terrestrial debris as well as structure forming taxa including hydrozoan-bryozoan turfs, _Crepidula_, _Diadumene_, Rhodophyta, and _Chondrus_ separated groups of sites at this large scale. These results demonstrate there are differences in community structure across the study region and all similar patch types are not ecologically equivalent.
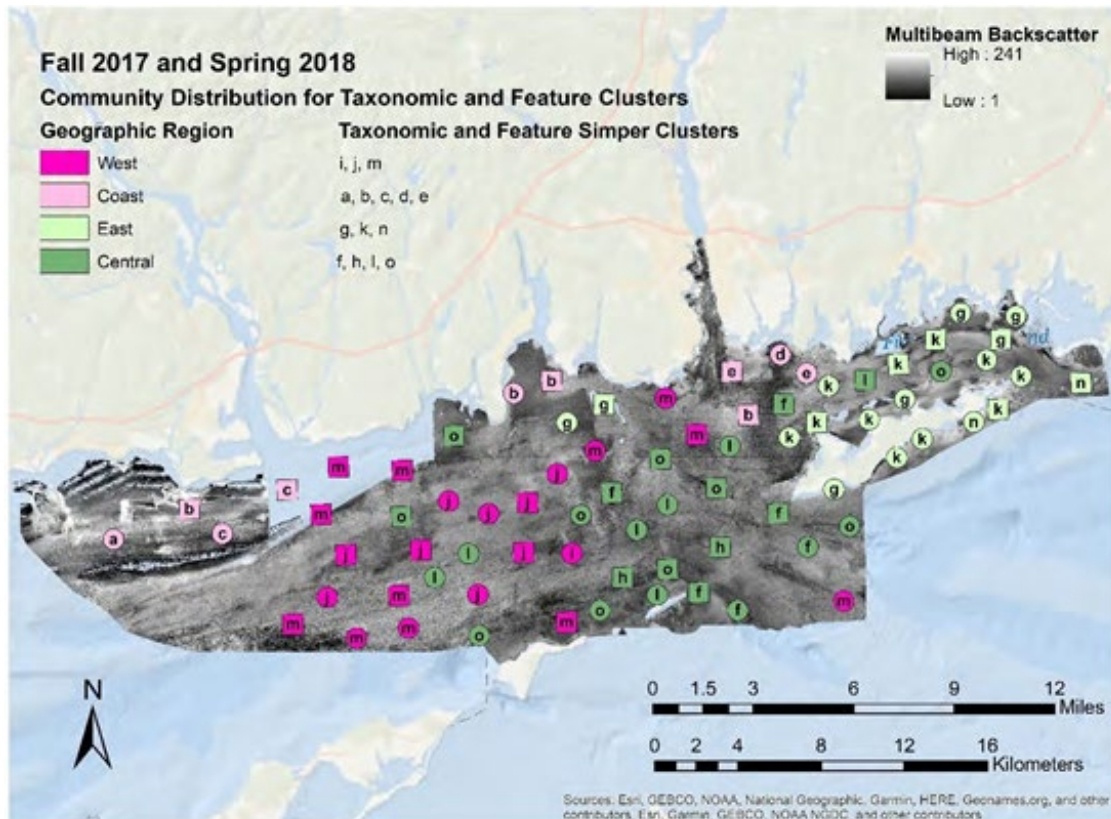
Figure 5.2-44. Four groupings of site-blocks yield an ecologically significant set of geographically aggregated community types parsing the Phase II landscape. Squares represent sample blocks, and ovals represent sample sites (Figure 5.2-27). See text for details on the determination of feature SIMPER clusters (hierarchical cluster analysis).
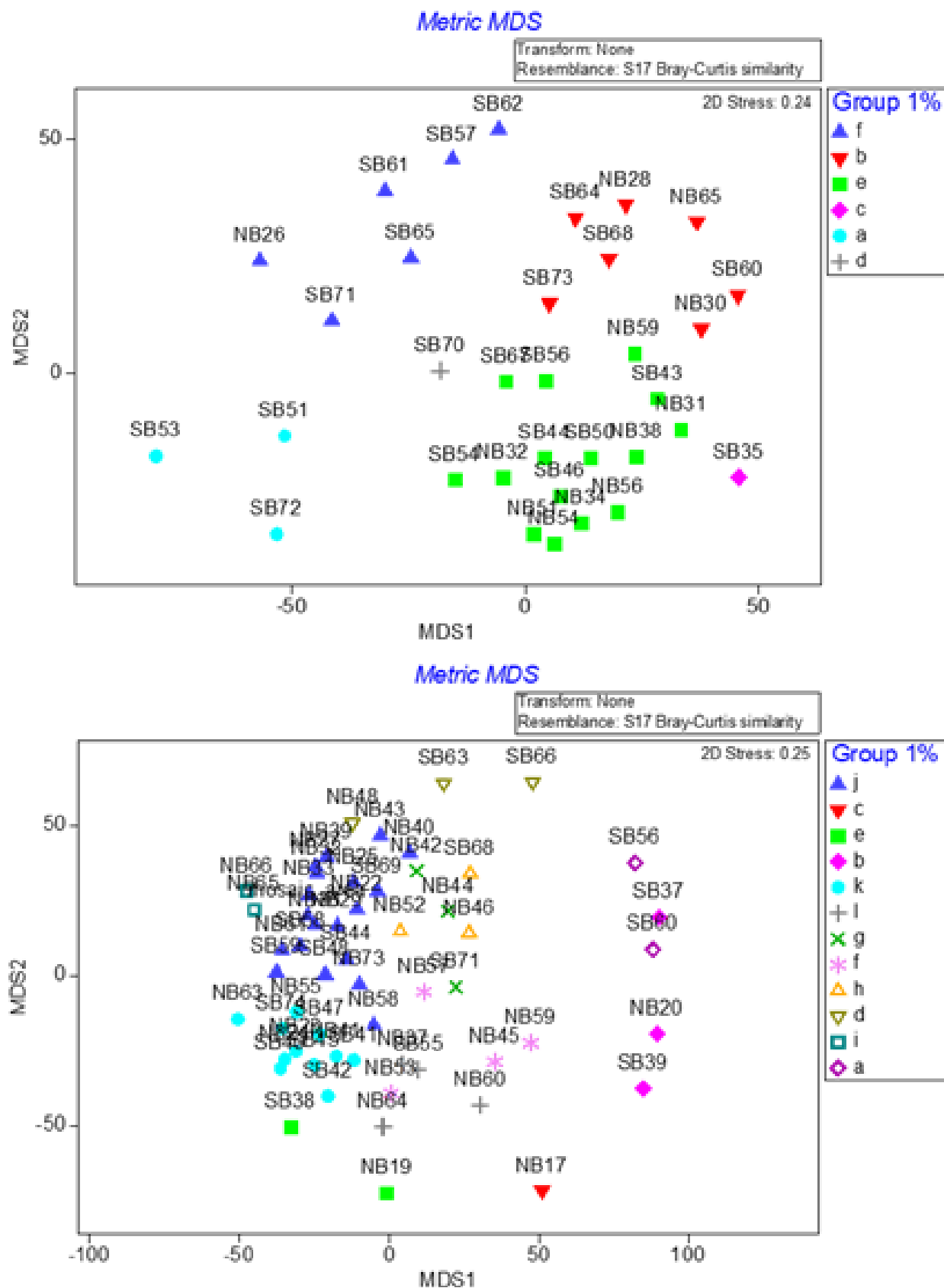
Figure 5.2-45. mMDS results from SIMPROF analyses based on groupings significant at 1%

The distribution and abundance of taxa and features did not follow uniform geographic trends, reflecting the varied seafloor habitats characterized by eCognition patches as described above. In any case, a number of spatial patterns were identified that provide important insights on this region of LIS. Multiple taxa and biogenic habitat features that represent larger gradients and general relationships with physical characteristics of seafloor environments were identified, as well as ecological responses to on-going changes in local and regional environmental conditions. Some taxa are worthy of specific consideration due to their role as an ecosystem engineer or biogenic habitat, or their vulnerability, conservation status, or dominance in the community. These taxa are: hydrozoan and bryozoan turfs, ghost anemone *Diadumene leucolena*, macroalgal taxa aggregated as Laminariaceae and Rhodopyhta, and the solitary hydroid *Corymorpha pendula*. These are identified in the analyses and GIS datasets as "Select Taxa" (Figure 5.2-46). Additional taxa are considered jointly as their spatial distributions and patterns of abundance may either represent fundamental changes in seafloor communities, as in blue mussel *Mytilus edulis* and Atlantic slipper shell *Crepidula fornicata*, or interactions between endemic and invasive taxa, as in yellow boring sponge *Cliona* spp., northern star coral *Astrangia poculata,* colonial tunicate *Didemnum vexillum.* Biogenic features that were widely distributed and known to serve as structural attributes of habitat were bivalve shell, seagrass debris, and terrestrial vegetation debris (Figure 5.2-47).
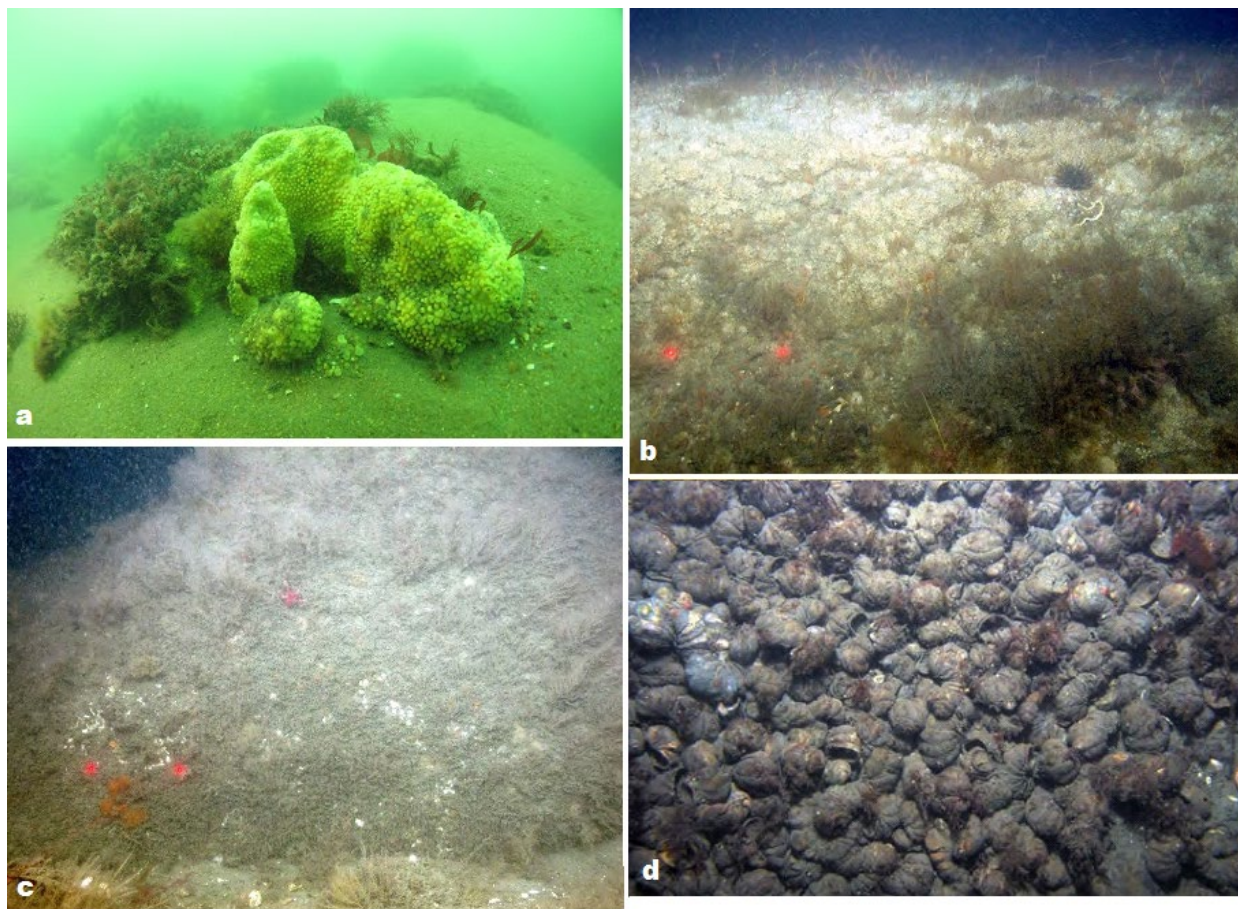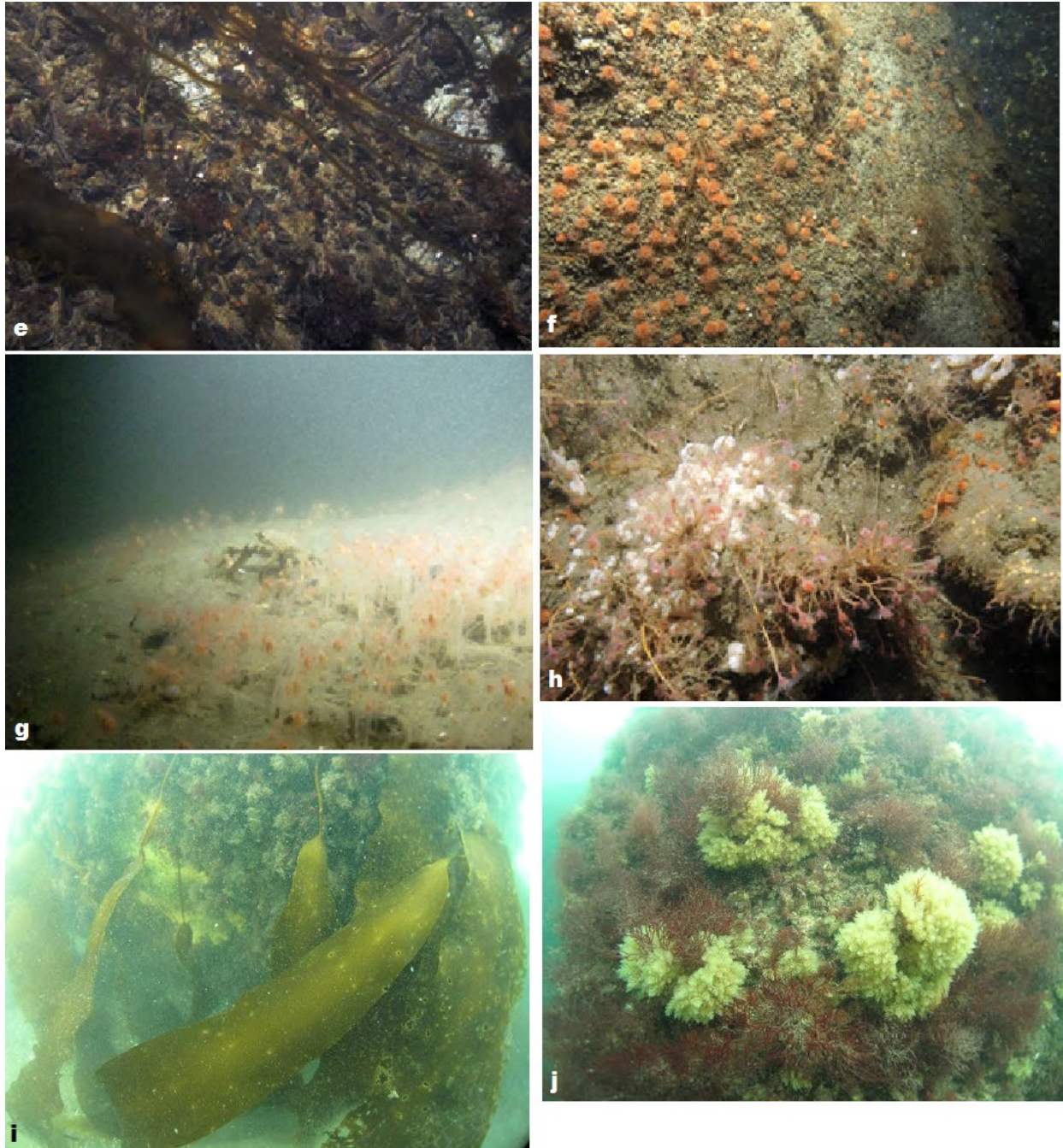
Figure 5.2-46. Examples of select taxa identified based on analyses for specific attention: (a) Cliona spp. towers at Ellis Reef; (b) massive aggregation of Astrangia poculata at 60m depth located midway between Goshen Point and Great Gull Island; (c) hydrozoan and bryozoan turf on the vertical face of a boulder at 21m depth south of the Thames River; (d) "stacks" of Atlantic slipper shell Credpula fornicata at 18m at the base of Ellis Reef; (e) blue mussel Mytilus edulis in sandy sediments at 11m depth east of Wicopesset Rock; (f) ghost anemones Diadumene leucolena on a vertical boulder face at 13m located midway between Noank and Clay Point in FIS; (g) dense aggregation of solitary hydroids Corymorpha pendula emerging from sand at 47m depth South of Old Saybrook; (h) invasive carpet tunicate Didemnum vexillum (bright white blobs) amongst tubularians at 82m depth in the Race; (i) kelp (Laminariaceae) at <3m depth located on Black Ledge; (j) red algae (Rhodophyta) at 5m depth located on Ramn Island Reef (Peter's photo). Examples of important taxa identified during sampling.
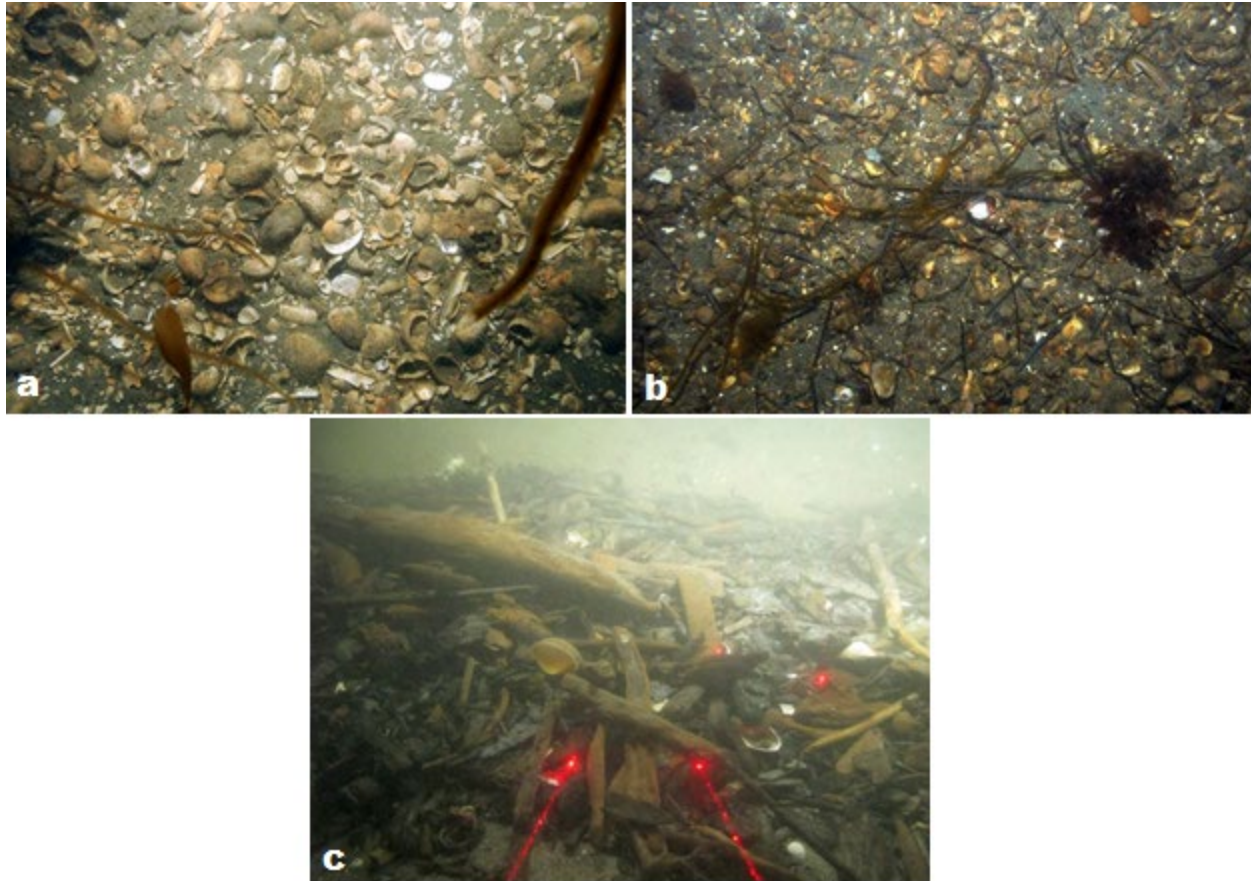
Figure 5.2-47. (a) Shell valves and pieces covering the seafloor at 24m depth South of Groton Long Point (99% cover); (b) drift seagrass at 22m depth located South of Ellis Reef and East of Ram Island Reef; (c) terrestrial debris at 45m depth located off Old Saybrook, CT.

Here we present a series of maps and brief descriptions that illustrate the distribution and abundance of epifaunal and emergent taxa with diverse life histories as well as biogenic features that fill important functional roles as seafloor habitat. Most of these taxa are structure forming, serving an "ecosystem engineering" role, while the biogenic features are themselves structure. These structures are utilized by vagile fauna for shelter from currents and predators (for physiological benefits and survivorship, respectively) as well as aggregating prey (e.g., amphipods, decapod shrimp) and used as foci for feeding (Cau et al., 2020). In addition, interactions between some benthic fauna and those organisms that influence other organisms and, in part, structure benthic communities are considered in more detail. These summaries are based on the observed distributions and occurrences of these organisms and features and, in the case of the more detailed section on interactions and structuring organisms, mixed effect hurdle models.

Taxa survey datasets often feature an excessive number of null records, or 0 counts where target organisms were not identified, making their analysis using simple linear models difficult (Potts & Elith, 2006). Hurdle modelling separates presence from abundance in distinct models, which both aids model fitting and implicitly acknowledges the unique ecological processes that influence presence and abundance (Ridout et al., 1998; Potts & Elith, 2006). The presence/absence of each taxa were modelled as Bernoulli trials using generalized linear mixed effects models (GLMM) with binomial link functions. When present, natural log transformed taxa abundance was modelled using

linear mixed effects models (LMM). Potential fixed effects for all analyses included eCognition patch type, maximum tau (τ), depth (m), TRI, longitude, and season; interactions were limited to two-way fixed effect crosses featuring eCognition patch type due to the difficulty of interpreting complex interactions. The intercept of sample block/site were included as random effects to account for non-target variation due to geographic heterogeneity. Best fit models were selected using corrected Akaike Information Criteria (AIC), while the contribution of individual model terms was assessed using likelihood ratio tests (LRT). Model effect size was assessed using marginal (fixed effects only) and conditional (fixed and random) effects (Nakagawa & Schielzeth, 2013). Best-fit models were used to predict mean probability of presence (GLMM) and abundance (LMM) as well as 95% confidence intervals across the range of explanatory variables to explore influences on observed patterns of taxa. Tukey's post-hoc pairwise comparisons were used to investigate relationships between taxa presence and abundance and eCognition patches.

Hydrozoan and bryozoan turfs

Hydrozoan and bryozoan turfs were very common throughout the Phase II study area, occurring in more than 70% of all images analyzed, albeit at varying densities. These turfs were especially dense east of the Connecticut River towards the Race and in western FIS (Figure 5.2-48). Dense turfs were most common in highly structured habitats across available depths, their abundance increasing with both sediment grain size (as represented by eCognition patch; Figure 5.2-49) and bottom complexity (as represented by the TRI; Riley et al., 1999; Figure 5.2-50). Dense turfs were often observed covering hard substrates, where they serve as cover for small sizes of many mobile species. Turfs were also associated with *C. pendula* aggregations. Hydroids exhibit seasonal recruitment due to short life-histories. These taxa also provide structure for small crustacea that are important prey items for vagile fauna like crustacean eating fishes (Cau et al., 2020).
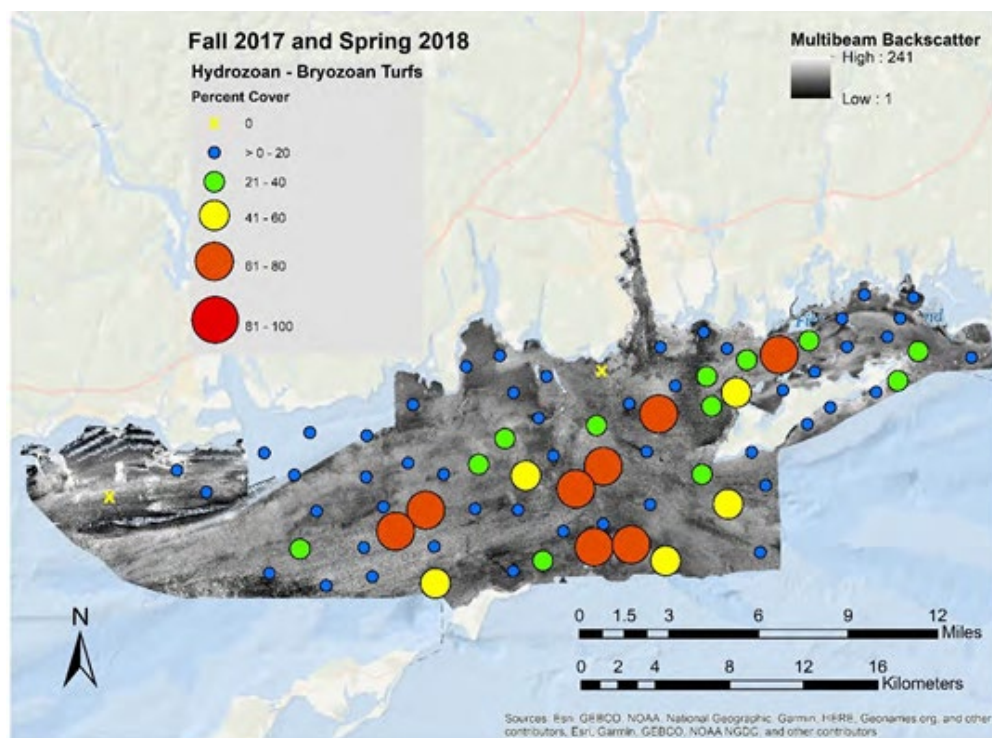
Figure 5.2-48. Mean percent cover of hydrozoan and bryozoan turfs per block/site sampled
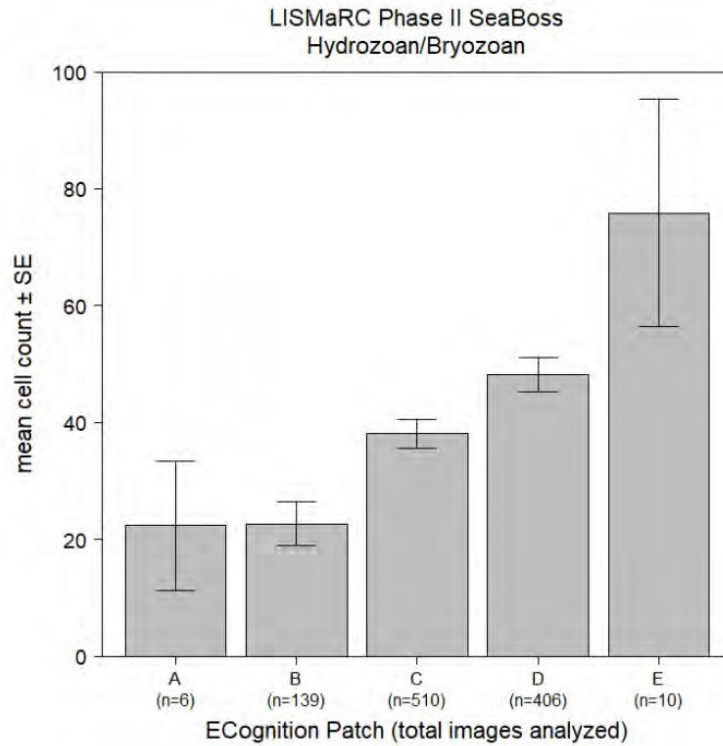
Figure 5.2-49. Hydrozoan and bryozoan mean abundance by eCognition acoustic patch. Whiskers in mean abundance plot report standard error.
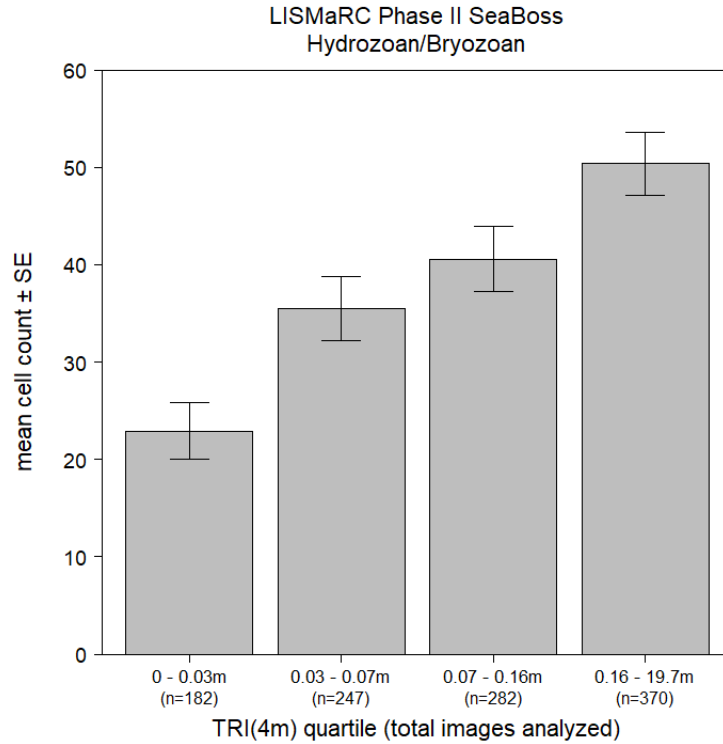
Figure 5.2-50. Hydrozoan and bryozoan mean abundance by TRI quartile. Whiskers in mean abundance plot report standard error.

Ghost anemone Diadumene leucolena

Ghost anemone *Diadumene leucolena* were scattered across the eastern 2/3 of the Phase II study area and were most densely concentrated at the Race and to the West of this feature (Figure 5.2-51). Largely limited to highly structured habitats in LIS (as represented by TRI; Figure 5.2-52), ghost anemones attach to hard substrates and are especially dense in areas that experience strong tidal currents (Figure 5.2-53). Despite having toxin-containing nematocysts, ghost anemones are preyed on by gastropods (this is mostly documented in areas where it is invasive; Goddard et al., 2020). Ghost anemones increase the structural complexity of the hard substrates where they attach.
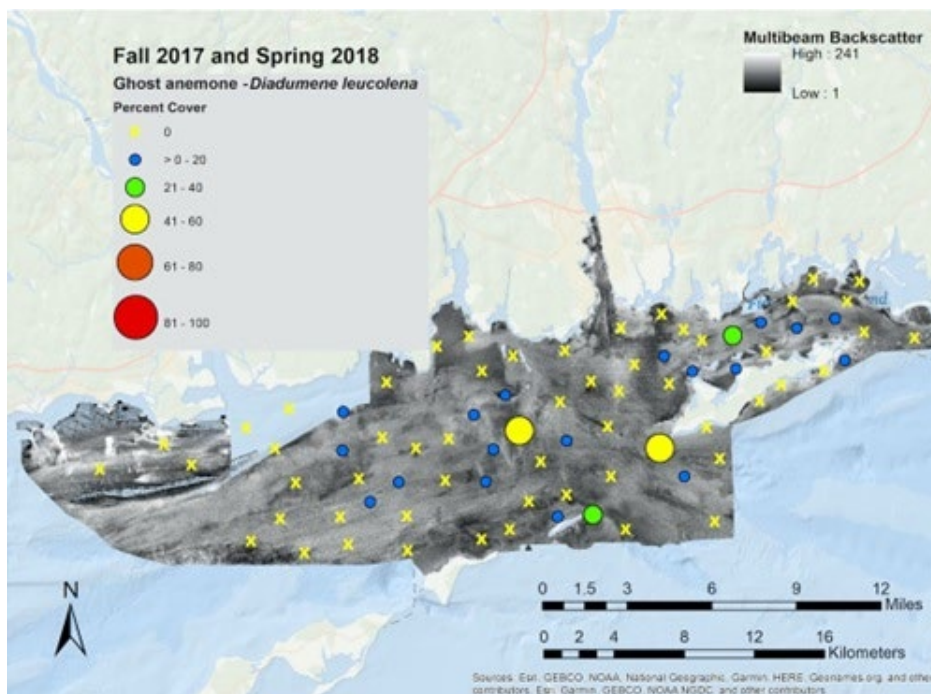
Figure 5.2-51. Mean percent cover of Diadumene leucolena per Block/site sampled
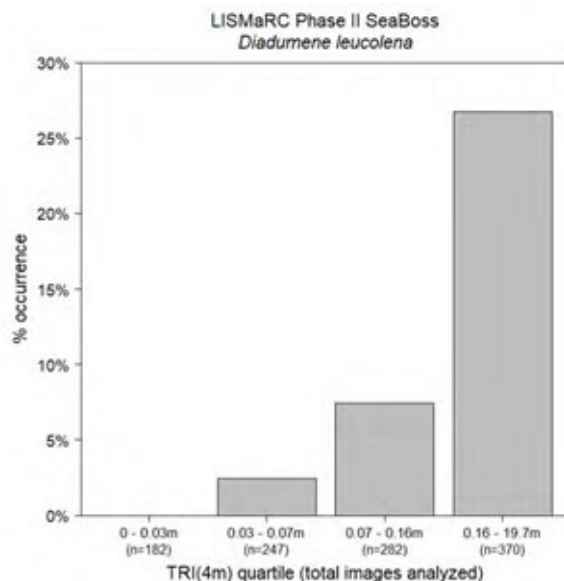
Figure 5.2-52. D. leucolena % occurrence by TRI quartile
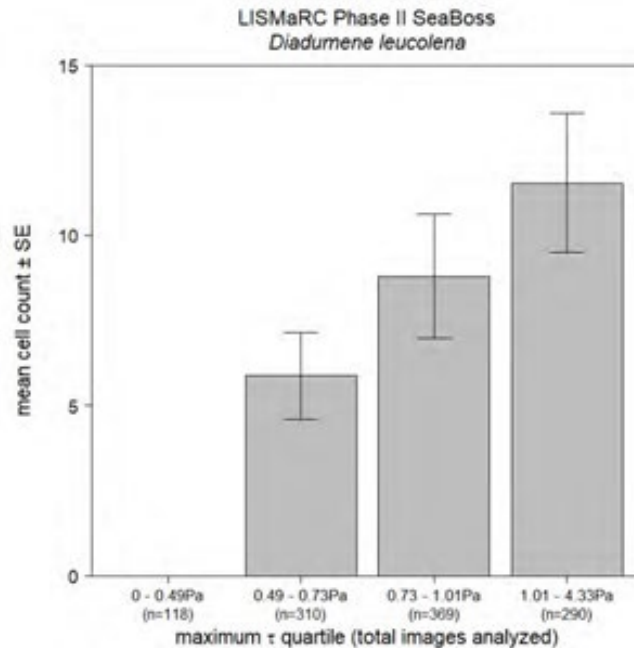
Figure 5.2-53. D. leucolena mean abundance by maximum monthly bottom stress quartile (maximum τ). Whiskers in mean abundance plot report standard error.

Kelps Laminariaceae

Kelps in the family Laminariaceae (*Laminaria* spp. and *Saccharina* spp.) were observed along the coast, across FIS, along the southern coast of Fishers Island, and at scattered nearshore locations between the Connecticut and Thames Rivers (Figure 5.2-54). Kelp were generally observed in complex hard substrata where they attach to the substrate via a holdfast. This taxon is limited in depth due to the specific characteristics of photosynthetic pigments (Figure 5.2-55). Kelp play important roles in the habitats they define- providing refuge and attachment surfaces for other organisms and promoting productivity and diversity (Steneck et al., 2002). Kelp also play a structuring role when present, limiting light availability to the seafloor and disturbing attached organisms via abrasion due to the movement of their fronds in tidal currents (Jacques et al., 1983; Grace, 2004). The cover provided by kelp species was low across occupied sites in the Phase 2 area. Limited sampling by divers revealed the highest density of kelp found at Black Ledge was <3 m^{-2} during August 2018 (mean cover 35%). Historically, kelp species occurred there at much higher densities, with maximum density of ~300 individuals per m^2 during the same month in 1986 (Egan & Yarish, 1990). These species are at the southern extent of their distributional ranges, but range shifts mediated by temperature trends are less clear due to limited monitoring (Merzouk & Johnson, 2011; Smale, 2020). Sugar kelp, *S. latissima*, has declined in abundance near the southern edge of its range (Witman & Lamb, 2018); Feehan et al., 2019), but partitioning the direct effects of temperature are complicated by indirect effects of elevated temperatures on grazing rates of herbivores, competition for space with turf algae, and settlement of invertebrates on kelp blades that are known to depress populations and impede recovery (Filbee-Dexter et al., 2016, 2018; Witman & Lamb, 2018; Feehan et al., 2019; Smale, 2020).
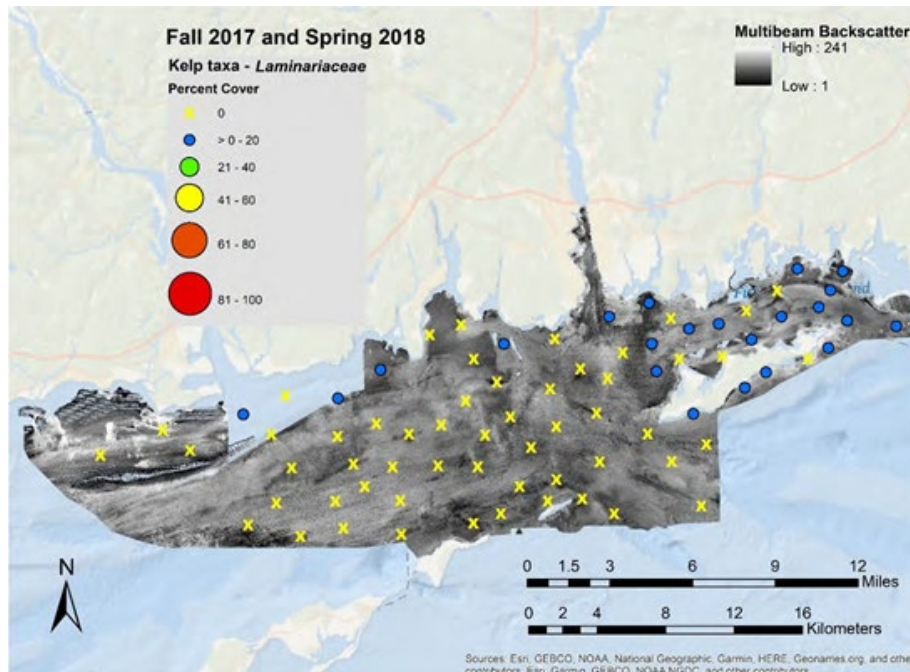
Figure 5.2-54. Mean percent cover of Laminariaceae per Block/site sampled
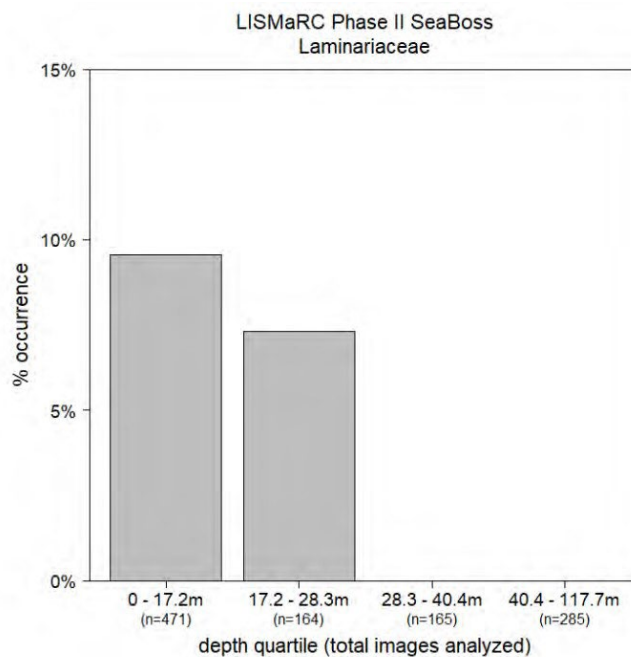
Figure 5.2-55. Laminariaceae % occurrence by depth quartile

Red Macroalgae Rhodophyta

Rhodopyta, red algae, were nearly ubiquitous in shallow nearshore areas across the eastern half of the Phase II study area- from the southern edge of Fishers Island, through FIS, continuing west along the coast to the Connecticut River, and north of Plum and the Gull Islands (Figure 5.2-56). A major characteristic of this taxon is the presence of a pigment that reflects red light and absorbs blue wavelength light, enabling species in this taxon to occur at depths deeper than green or brown

macroalgae due to the characteristics of spectral attenuation of light across depths (Figure 5.2-57 & Figure 5.2-58). The distribution of Rhodophyta species in the study area is more widespread than that of kelps, attaching to existing hard stratum materials and extending into deeper water. While more widespread based on this sampling approach, Rhodophyta were also more closely associated with hard, complex substrates than kelp (Figure 5.2-58). It is notable that Rhodophyta are generally smaller than kelp species and more resistant to effects of drag and dislodgement, so hydrodynamic forces can in part be responsible for some of the variability in distribution (Krumhansl et al., 2015; De Bettignies et al., 2013). Densities were particularly high in FIS and off of Fishers Island. Numerous taxa often co-occurred, including bushy *Polysophonia* spp., thin branching *Ahnfiletia picata* and *Polyides rotundes*, and fairly broad-leafed *Chondrus crispus*. These diverse forms provide refuge for small, mobile organisms.
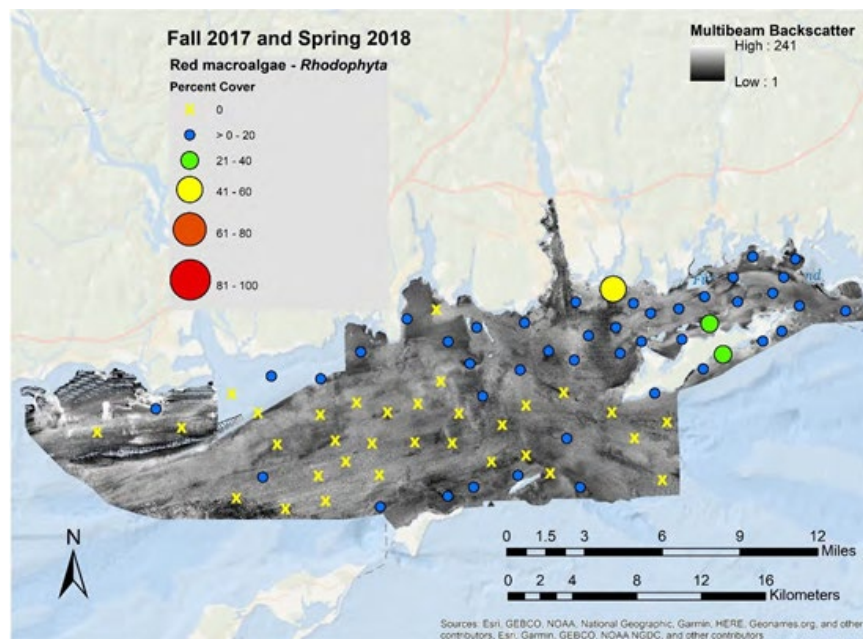
Figure 5.2-56. Mean percent cover of Rhodophyta per Block/site sampled
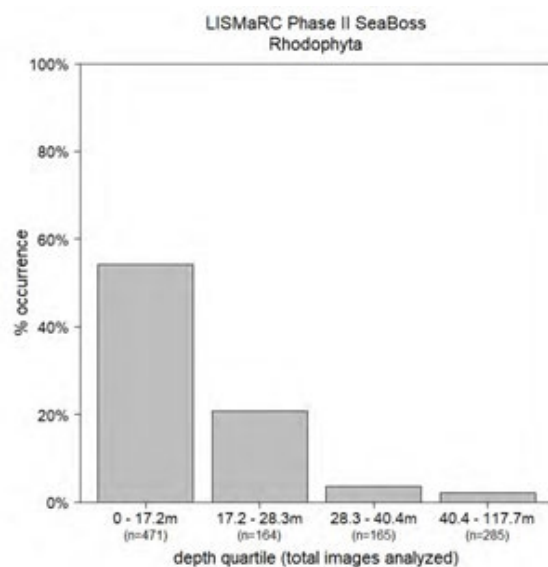
Figure 5.2-57. Rhodophyta % occurrence by depth quartile
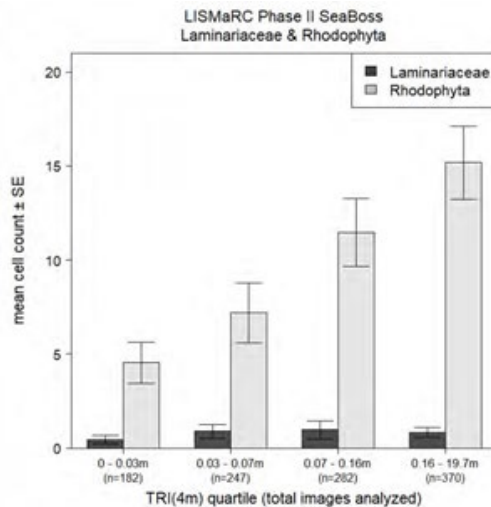
Figure 5.2-58. Rhodophyta (light gray bars) and Laminariaceae (dark gray bars) mean abundance by TRI quartile.

Solitary Hydroid *Corymorpha pendula: Diversity and Spatial Associations with other Fauna*

Solitary hydroid, *Corymorpha pendula*, is an ephemeral emergent hydroid found in fine sediment seafloor habitats. The benthic form of this species, the hydroid phase, is present in concentrated patches, but their distribution is dynamic and may change year to year. Following the dispersal of medusae the previously conspicuous hydroids are absent from the Sound by the transition of summer into fall. This species recruits on an annual basis to fine- grain sediment habitats.

When present, corymorphoid hydrozoans may be concentrated in moderately dense aggregations, which play similar ecological roles to those of terrestrial forests (Rossi et al., 2017). These aggregations contrast starkly with the mostly unstructured fine sediments that compose their preferred habitats. Dense aggregations of these erect hydroids can form important habitats for other sessile and mobile organisms (Cau et al., 2020; Byers & Grabowski, 2014; Di Camillo et al., 2017). Hydroids may form the basis of important and unique habitats, both altering the fine sediment environments where they proliferate seasonally (Cerrano et al., 2015) and providing refuge and surfaces that other benthic organisms utilize (Zintzen et al., 2008). During the hydroid phase, benthic biomass in these aggregations increases substantially likely fueled by a combination of factors, conversion of pelagic to benthic biomass via hydrozoan filter-feeding (Gili et al., 1998) and disruption of bottom currents (Hughes, 1978). Additionally, the release of medusae return concentrated biomass to pelagic waters (Gili et al., 1998). Although not as extensively studied as other marine animal forest phenomena, hydroid aggregations also host greater diversity than surrounding sediments (Zintzen et al., 2008).

The factors influencing ephemeral hydroid aggregations, or deciduous animal forests, are unclear and even unstudied for many taxa (Di Camillo et al., 2017), so identifying consistent patterns of conditions coinciding with *C. pendula* observations can provide important insights for their ecology in the LIS. As expected, the benthic hydroid stage of *C. pendula* was present in spring, but not Fall sampling. In spring, this solitary hydroid was found offshore, in deeper waters between the Connecticut and Thames Rivers (Figure 5.2-59). In fact, *C. pendula* was largely absent from the shallowest sampled habitats (< 17.2 m; Figure 5.2-60). *C. pendula* was completely absent from the eastern ¼ of the study area (Figure 5.2-61), which consists of FIS and nearshore BIS, and sites west of the Connecticut River. The western limit of their distribution is likely an artefact of sampling

locations at this end of the study area, which were fairly shallow and close to shore. Since sampling in FIS was extensive, *C. pendula*'s absence is unlikely to be an artefact. The FIS seafloor is variable and includes hard bottom, but much of the available habitat consists of sand or silt, so limitation due to inadequate fine sediments is unlikely. The eastern limit to the distribution of *C. pendula* may be due to competition in the shallow, higher salinity FIS, but at present this is speculative.
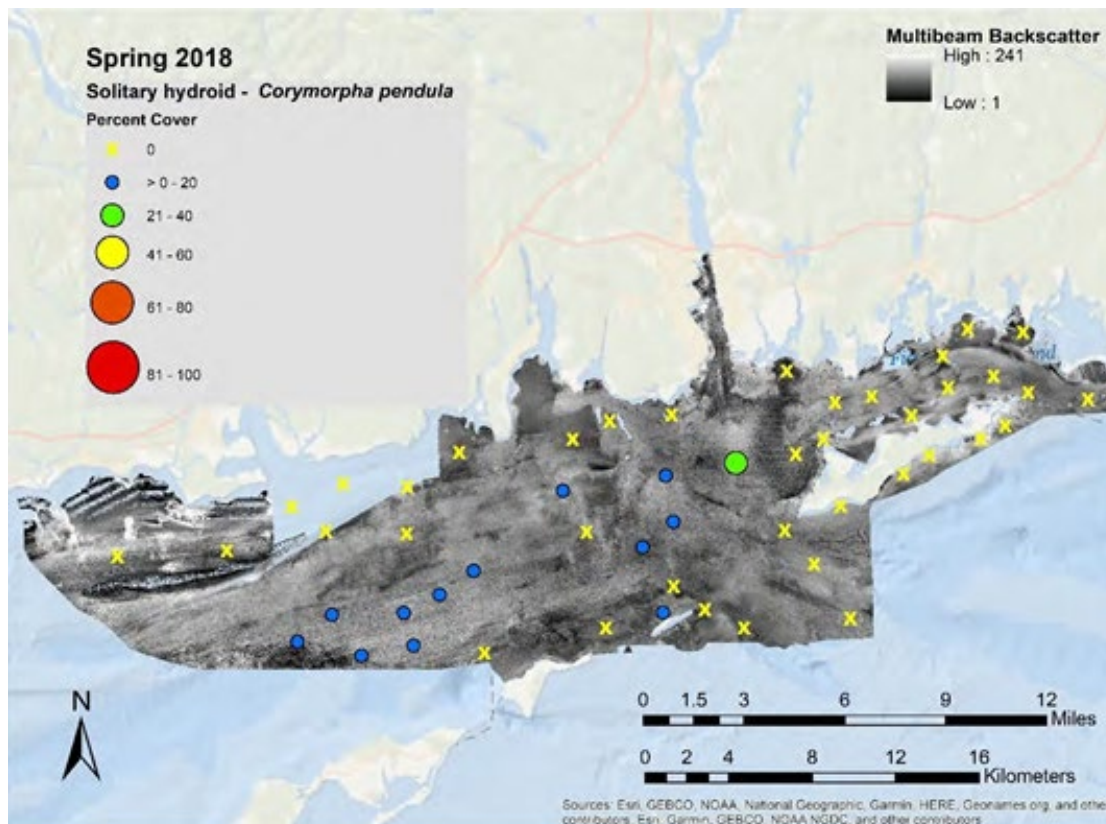
Figure 5.2-59. Distribution and block/site specific mean percent cover of C. pendula in spring 2018 sampling
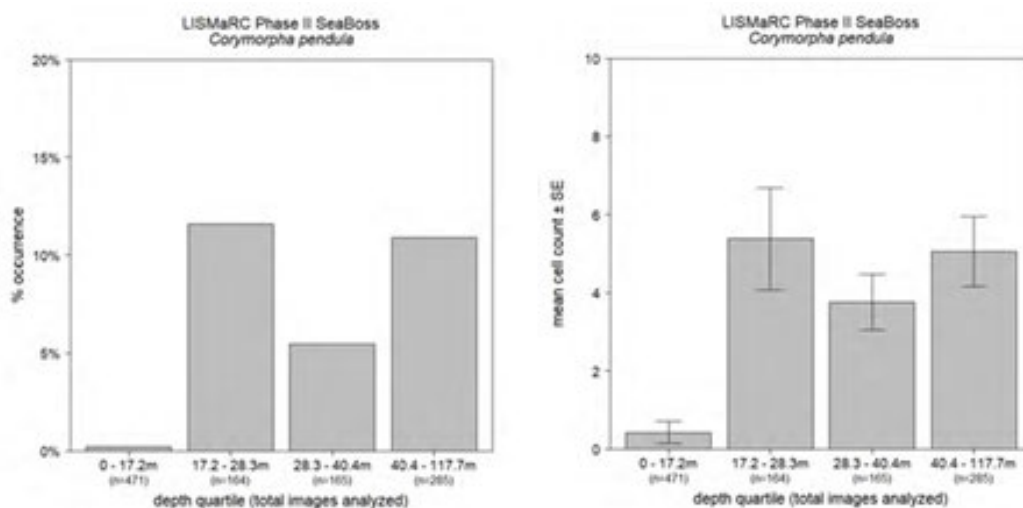
Figure 5.2-60. C. pendula % occurrence (left) and mean abundance (right) by depth quartile. Whiskers in mean abundance plot report standard error.
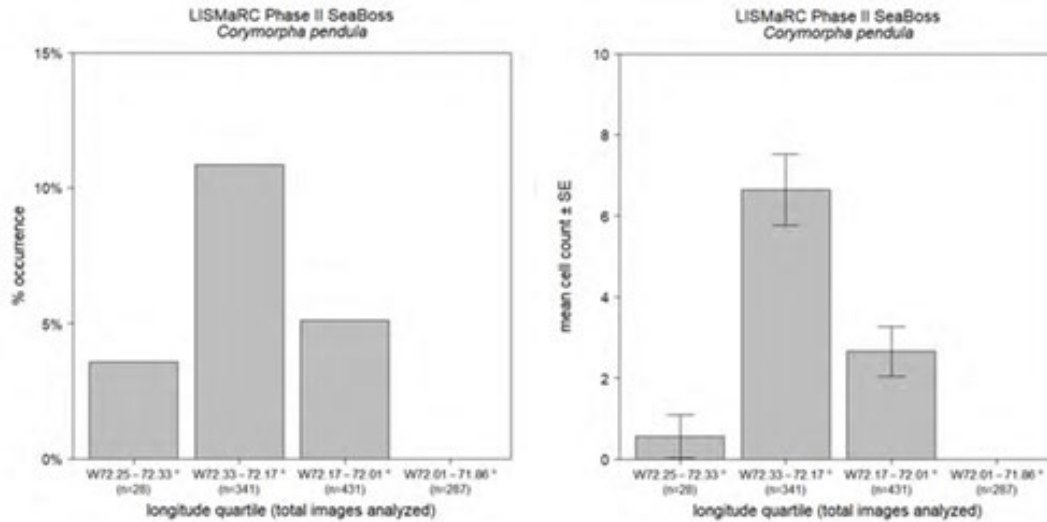
Figure 5.2-61. C. pendula % occurrence (left) and mean abundance (right) by longitudinal section. Whiskers in mean abundance plot report standard error.

Despite its association with fine sediments, *C. pendula* was increasingly common as sediment grain size increased (Figure 5.2-62). Although this appears to run counter to established genus preferences for finer sediments, it is important to note that *all* of the ECognition- defined habitat types were composed of primarily or substantially sand (Table 5-16C). *C. pendula* was also denser (i.e., greater percent cover) in coarser than in finer sediments, but for the most sampled habitat there was a clear separation between sediments featuring silt (patch B) and those that did not (patches C and D), which may belie a preference for sand over mud or silt. Another proxy for sedimentary environments is the complexity, or roughness, of the bottom as measured using derived products of acoustic bathymetry, such TRI (Riley et al., 1999). Courser seafloor tends to feature coarser sediments, including boulder and rock outcroppings. *C. pendula* was rarest in the most complex habitats (i.e., highest TRI quartile; Figure 5.2-63). Similarly, density decreased with increasing habitat complexity, as well. When present *C. pendula* usually covered a substantial proportion of available habitat, between 13.1% (least complex habitats) and 8.3% (most complex habitats) of sample images.
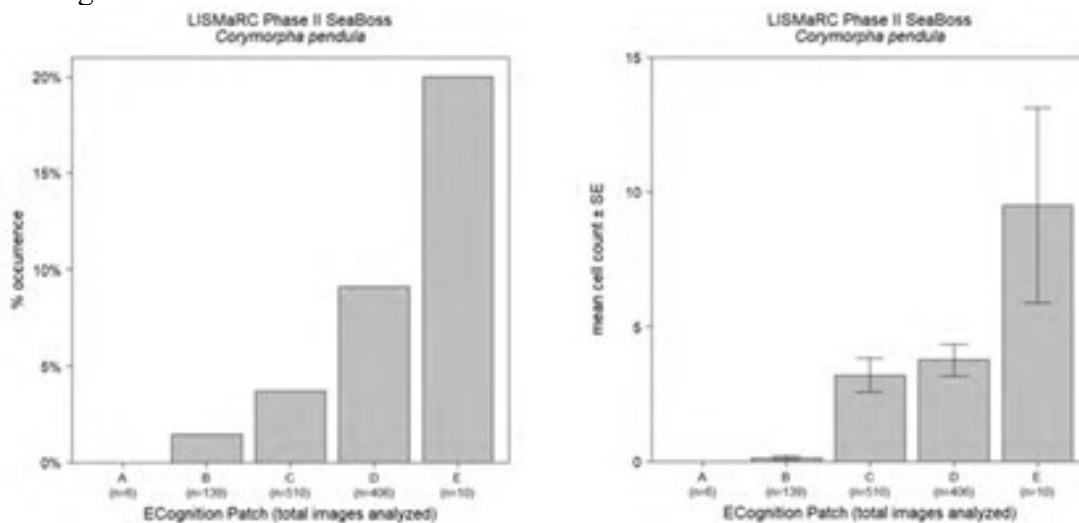
Figure 5.2-62. C. pendula % occurrence (left) and mean abundance (right) by eCognition acoustic patch. Whiskers in mean abundance plot report standard error.
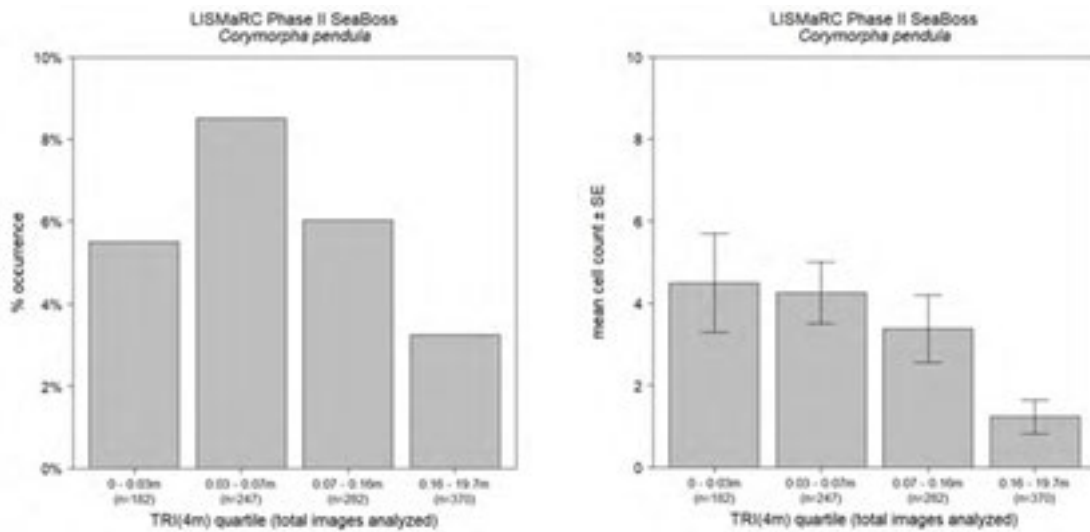
Figure 5.2-63. C. pendula % occurrence (left) and mean abundance (right) by TRI quartile

While *C. pendula* was observed in nearly 6% of samples collected in the highest energy habitats and completely absent from areas with the lowest bottom currents, disturbances can greatly impact this species over relatively short periods of time (i.e., < 1 year; Brooks, 1984; Auster et al., 1996). While seafloor experiencing stronger bottom currents would be more likely to feature more frequent disturbances, the feeding rates and efficiency of solitary hydroids may adapt to such conditions (Dutto et al., 2019). Under low flow conditions, *Corymorpha* hydroids have been observed with hydranths at the sediment surface with stalks bent (Parker, 1917), which may be a less efficient and more energetically costly feeding mode. While absent from habitats with very low bottom currents, *C. pendula* was densest under moderate current conditions (0.49 Pa > τ > 1.01 Pa; Figure 5.2-64). This may indicate a threshold flow rate below which filter feeding may be too costly to support established *C. pendula* aggregations.

Model results suggested depth was the most important factor in the occurrence of *C. pendula*, the hydroid became more common as depth increased. Depth alone explained 8% of the observed variance in the distribution (margin R^2 = 0.08), *C. pendula* occurrence increasing with depth. When present, a combination of location, bottom current strength, and seafloor complexity explained nearly 15% of the observed variance in hydroid densities (marginal R^2 = 0.15). From east to west, *C. pendula* percent cover increased, while the highest densities occurred in the least complex habitats (i.e., lowest TRI). Despite being absent from areas experiencing the lowest bottom currents, in areas where *C. pendula* did occur the best fit model predicted the densest aggregations in the least dynamic habitats (i.e., lowest maximum τ); it is important to note that since *C. pendula* was absent from seafloor habitats with the lowest flow conditions (τ < 0.49 Pa), so these conditions were excluded from density models.
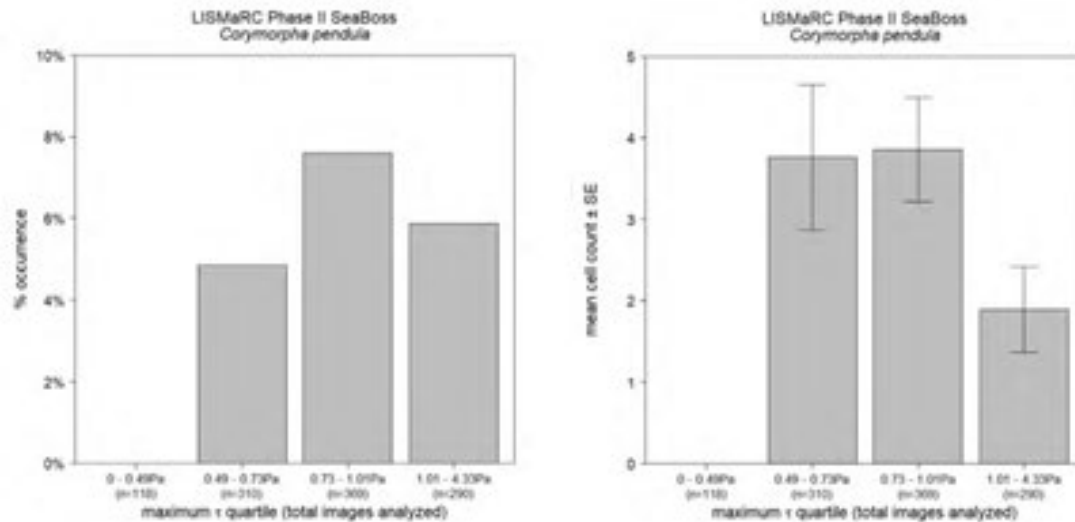
Figure 5.2-64. C. pendula % occurrence (left) and mean abundance (right) by maximum monthly bottom stress quartile (maximum τ). Whiskers in mean abundance plot report standard error.

As observed in some other habitat modifying fauna, *C. pendula* hydroid aggregations were associated with more diverse benthic habitats. There was a clear pattern of decreasing ep- and emergent taxa richness and diversity with distance from *C. pendula* aggregations. The mean number of taxa present reached a maximum in patches of hydroids, decreasing steadily to a distance of 400m, which consisted of relatively few taxa present per sample (Figure 5.2-65). Shannon diversity was high from aggregations to a distance of 200m, then dropped precipitously the further removed a sample was from *C. pendula* (Figure 5.2-66). There were also specific taxa closely associated with this solitary hydroid. Hydrozoan and bryozoan turfs were far more abundant in the presence of *C. pendula* than at other sampling locations (Figure 5.2-67). The association of *C. pendula* with greater epifaunal diversity and the distribution of specific taxa appears to support this species playing an important role as a habitat modifier and forming the basis of an important, ephemeral marine animal forest in sandy sediment environments throughout ELIS. Additional study is needed to assess the effects of *C. pendula* aggregations on local environmental conditions, local trophic dynamics, and overall productivity, as well as the conditions under which these aggregations form. This is especially important since *C. pendula* may be adversely impacted by physical disturbance, with unknown consequences for associated taxa and benthic diversity. This species may play an important and unrecognized role in fine sediment habitats within the Sound.
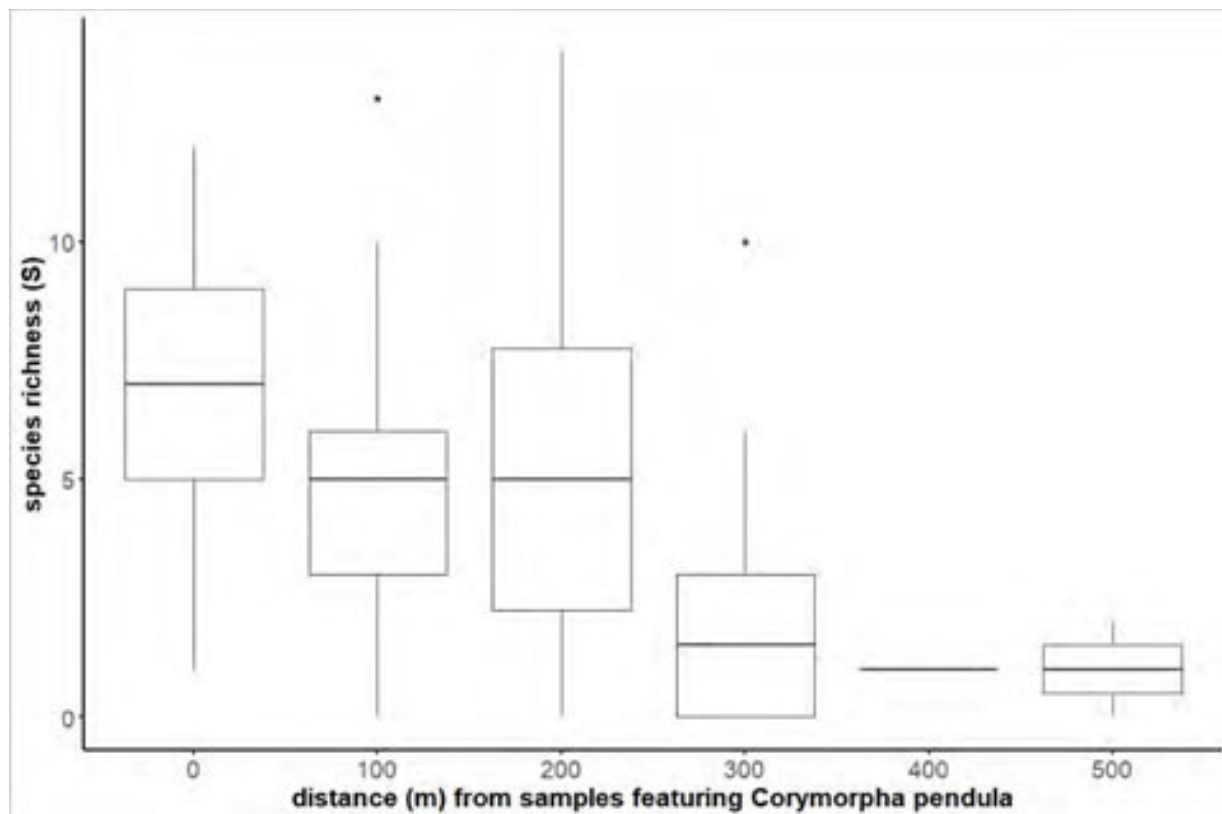
Figure 5.2-65. Species richness within (distance = 0) and at increasing distances from C. pendula occurrences
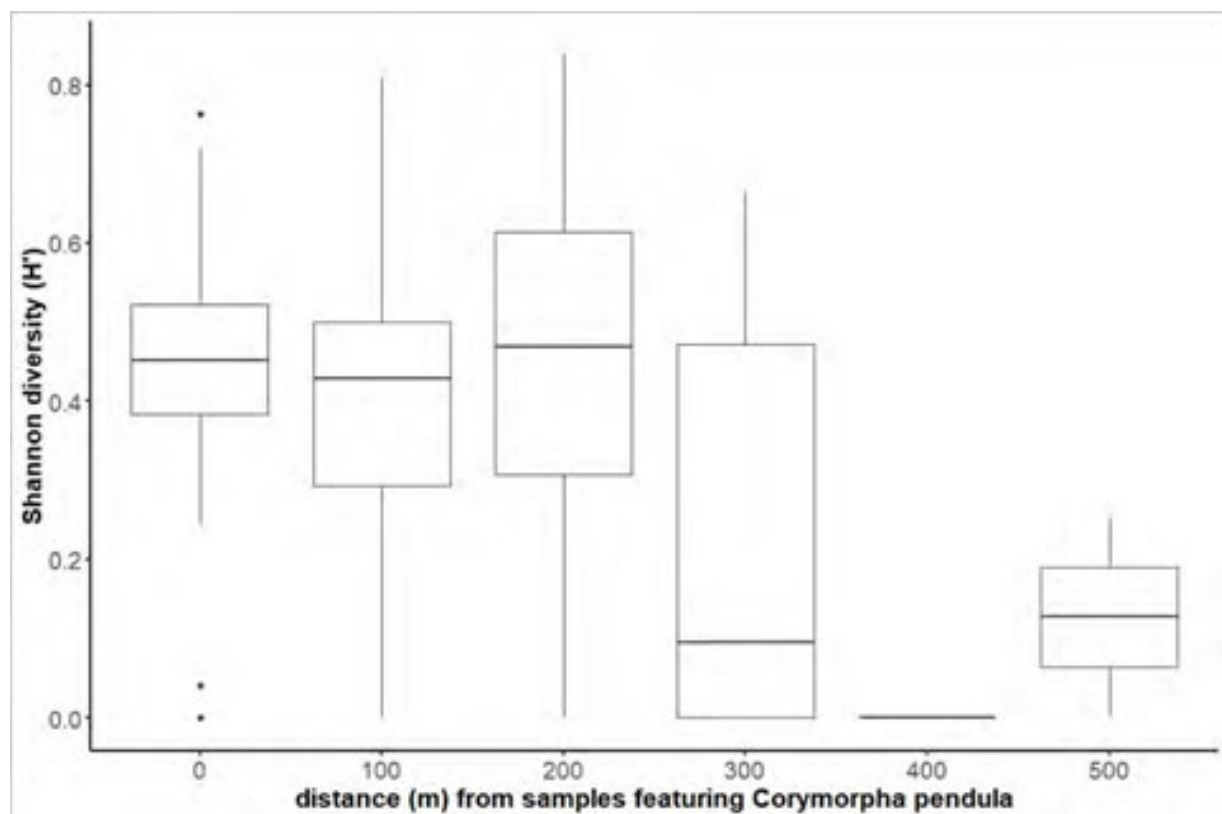
Figure 5.2-66. Shannon diversity index within (distance = 0) and at increasing distances from C. pendula occurrences
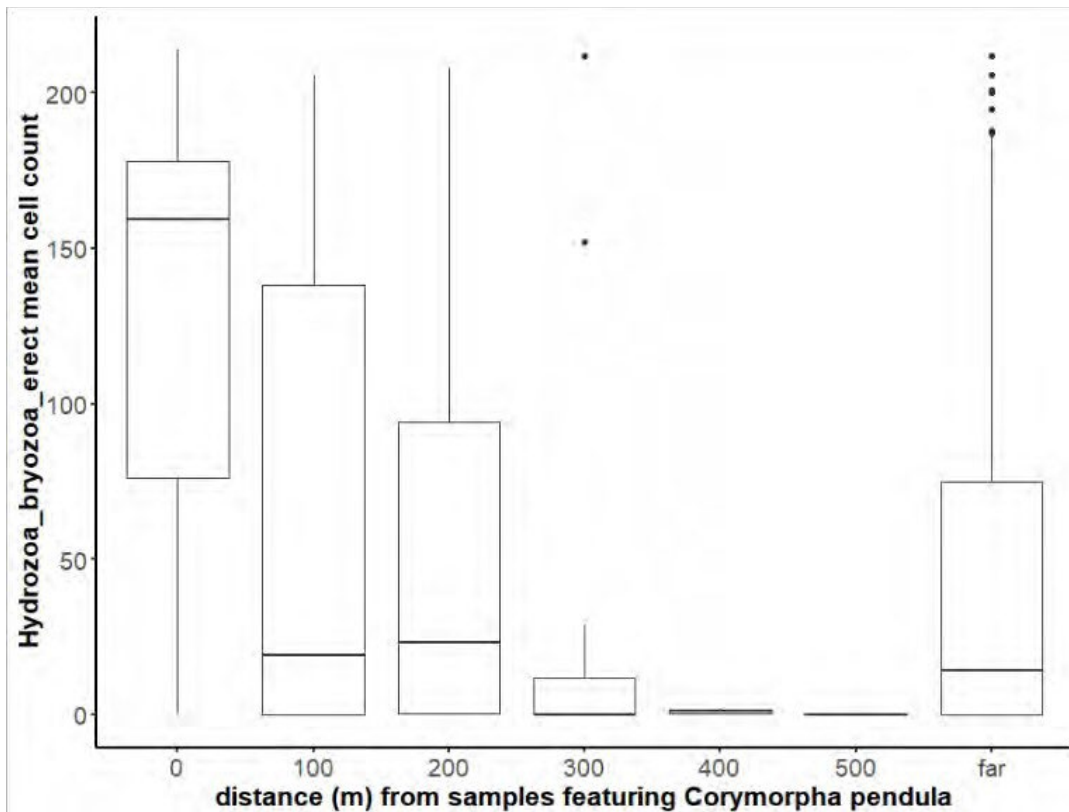
Figure 5.2-67. Hydrozoan and bryozoan turf abundance within (distance = 0) and at increasing distances from C. pendula occurrences

Mytilus edulis and Crepidula fornicata: A Filter Feeder Regime Shift

Mytilus edulis has long been recognized as an ecologically important species that, in part, structures benthic communities throughout ELIS and FIS (e.g., Langton et al., 1995). In his analysis of data collected over nearly 3 decades, Zajac (1998) identified this filter feeding bivalve as the dominant species in benthic communities between the Connecticut River and Goshen Point in ELIS, as well as throughout central and eastern FIS (Figure 5.2-68). *M. edulis* aggregations enhance complexity to hard substrate seafloor features (e.g., reefs, ledges, gravel pavements) and form connected mats on finer grain sediments (initially settled on shell fragments) forming communities that are more diverse and productive than those in the surrounding sediments (Langton et al., 1995; Norling & Kautsky, 2007; zu Ermgassen et al., 2020). Observed increases in diversity of epifauna and infauna is especially pronounced in fine sediments, where *M. edulis* reefs provides hard substrates for epifaunal recruitment, and alter the characteristics of local sediments through biodeposition (Hatcher et al., 1994; Norling & Kautsky, 2007; zu Ermgassen et al., 2020).
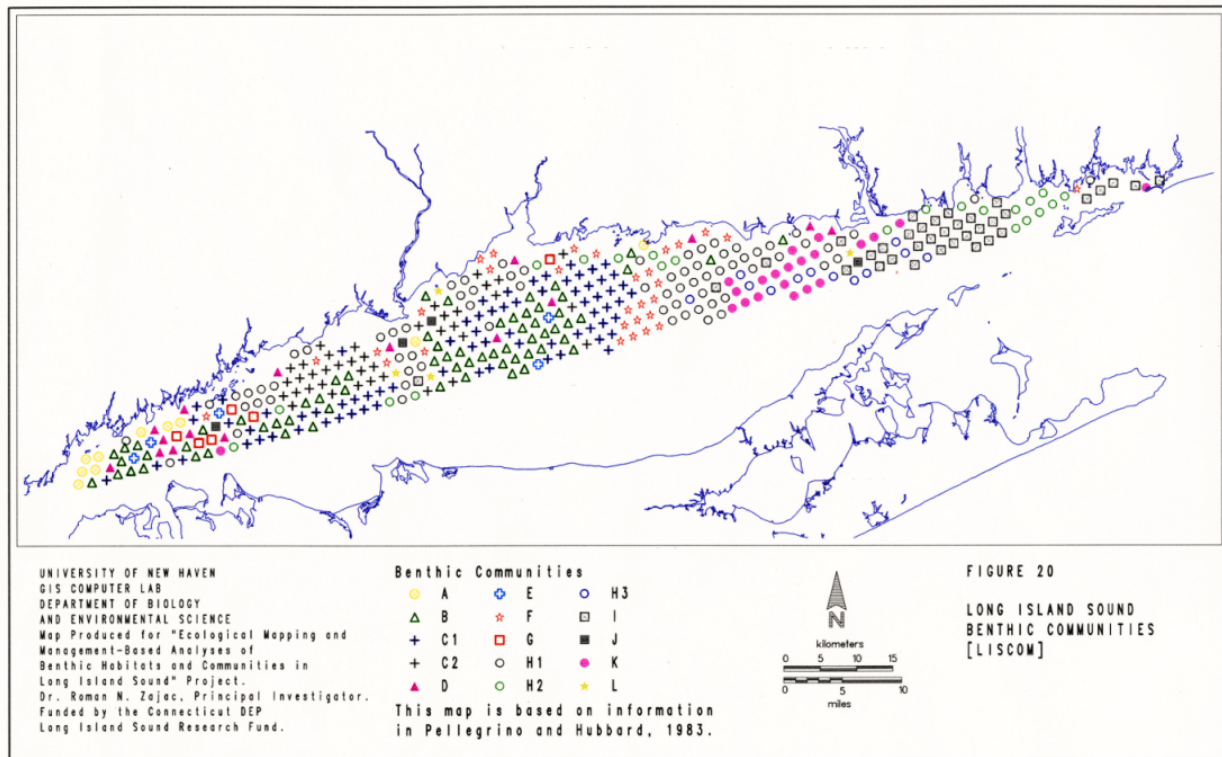
Figure 5.2-68. Figure 20 in Zajac (1998). Benthic community I, visualized using ⊠ in the map, was dominated by Mytilus edulis. See Zajac (1998) for analysis methods.

While *M. edulis* played a central role in diverse benthic communities of ELIS in these studies, the filter feeding gastropod *Crepidula fornicata* was not a dominant species in any of the more than dozen described benthic communities (Zajac, 1998). *C. fornicata* attach to hard substrates and form large stacks of conspecifics, which function in part as means of reproduction. In locations dominated by fine substrates, these stacks can form dense aggregations of *C. fornicata*, overlaying surficial sediments with a layer of irregular shell. When densities become very high, these aggregations can become reef-like structures with higher vertical profiles (Ackerman et al., 2015). Similar to *M. edulis* and other structure-forming suspension feeders, *C. fornicata* aggregations are associated with higher benthic diversity than surrounding sediments (de Montaudouin & Sauriau, 1999; de Montaudouin et al., 2018), but that increase in diversity may not match that of other benthic structure-forming suspension feeders (Preston et al., 2020).

Sampling using the SEABOSS platform revealed extensive changes in the distribution and abundance of these structure forming filter feeders. While *M. edulis* was still present from the Connecticut River through FIS, its distribution has decreased substantially since the 1980s (Figure 5.2-69a). Even when present, *M. edulis* was rarely the dominant benthic organism. The only sampling areas where *M. edulis* made substantial contributions to benthic communities (as determined by mean abundances of 5% cover or greater in SEABOSS images; Figure 5.2-70a) were limited to the eastern extent of FIS, where mean cover was 8.8% across all samples. In fact, these were the only sample areas in which *M. edulis* cover exceeded 5% in any single image.
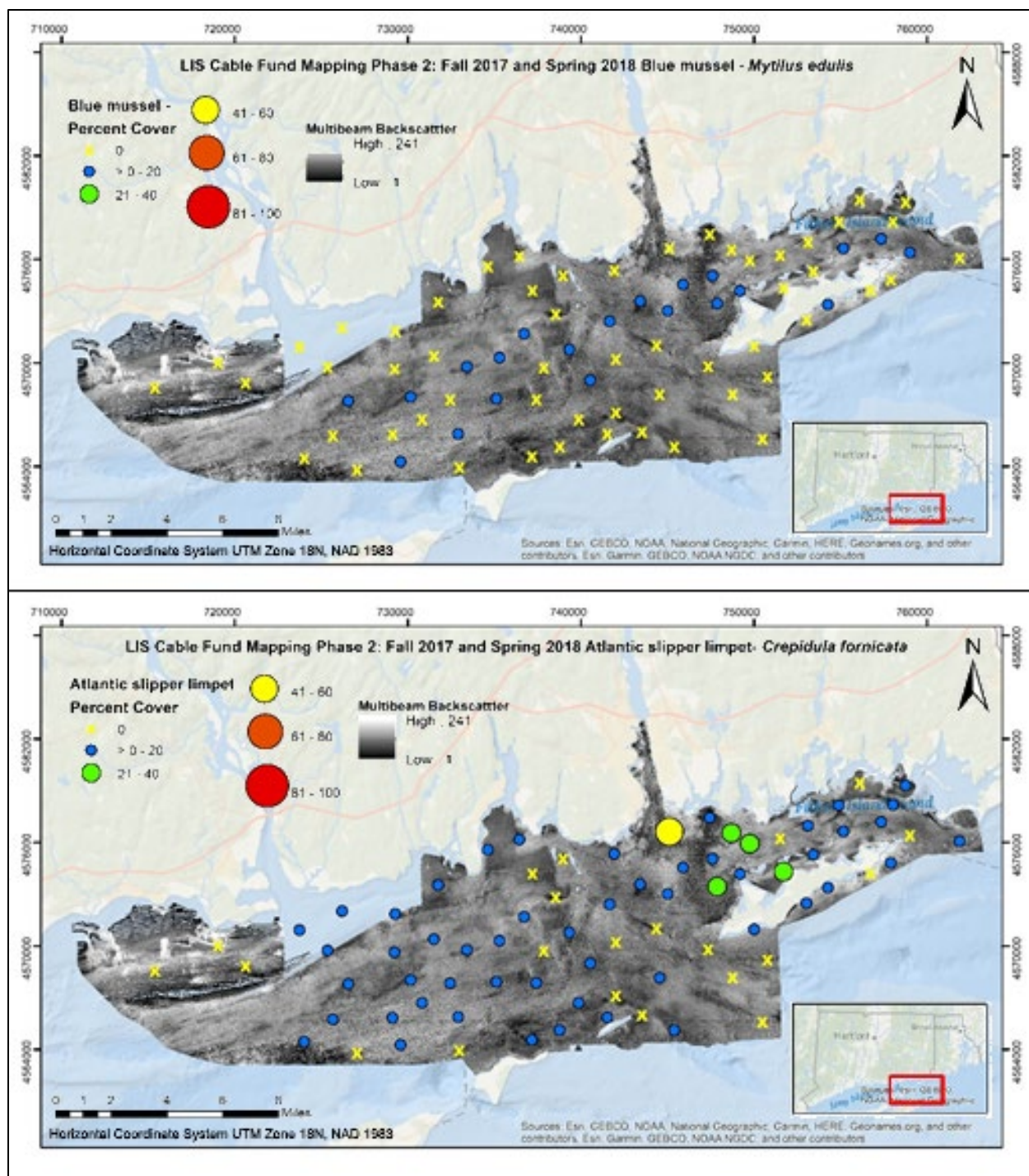
Figure 5.2-69. Mean percent cover of Mytilus edulis (a – top) and Crepidula fornicata (b – bottom)
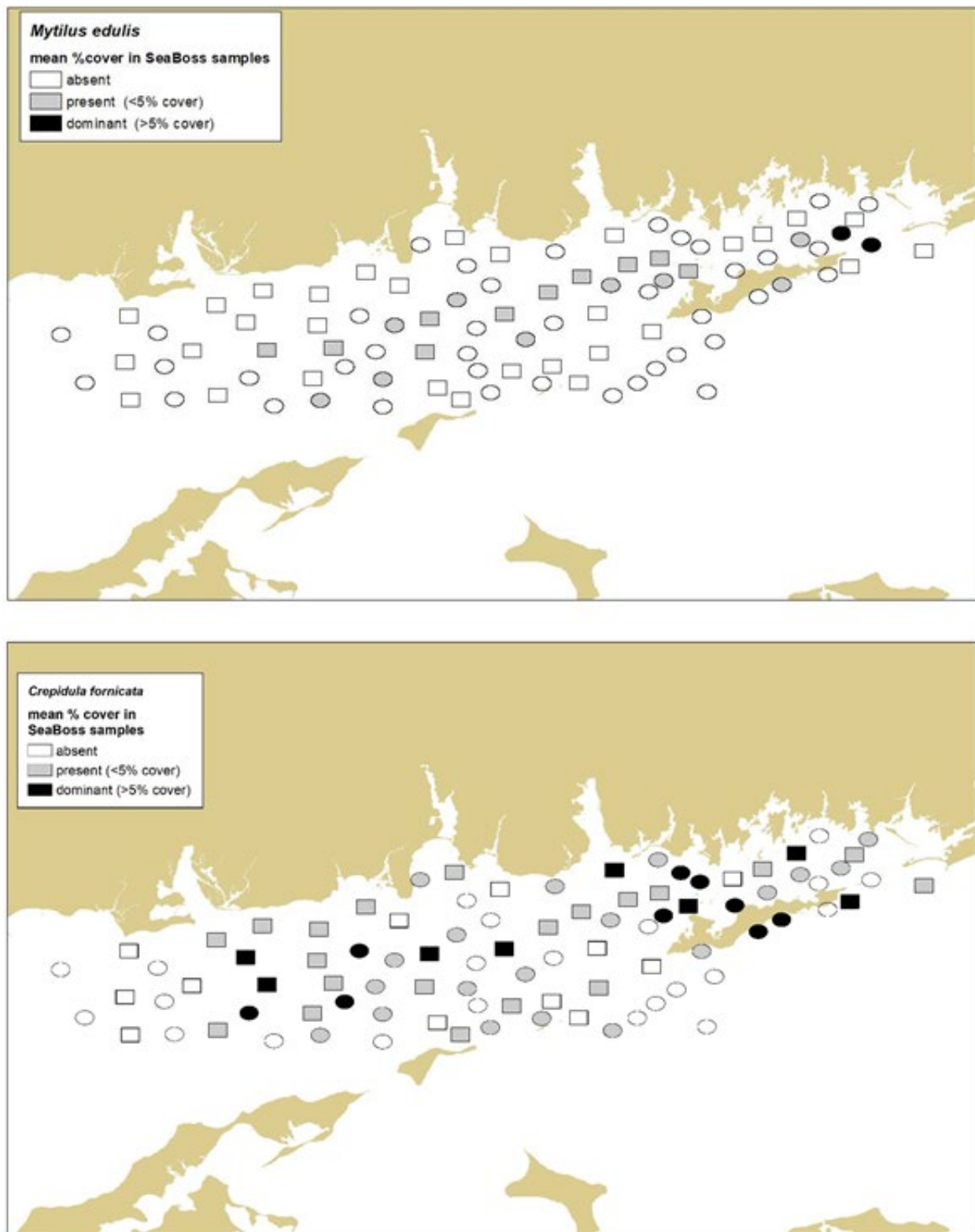
Figure 5.2-70. Sample areas where Mytilus edulis (a – top) and Crepidula fornicata (b – bottom) were present (gray box) or dominant (black box). Presence defined as mean % cover between 0% and 5%; dominant defined as mean % cover between 5% and 100%. Squares represent sample blocks, and ovals represent sample sites (Figure 5.2-27).

While *M. edulis* distribution has contracted and its abundance has decreased, *C. fornicata* has expanded substantially (Figure 5.2-69b). *C. fornicata* was distributed throughout the Phase II area, averaging at least 5% cover in more than 20% of sample areas (17 of 77 total sample areas; Figure 5.2-70b). While direct comparisons with the legacy datasets used in Zajac's (1998) analysis have not been determined (and are beyond the scope of this project), the areas of ELIS and FIS that were previously dominated by *M. edulis* approximately match those areas where *C. fornicata* is newly dominant apart from the eastern edge of FIS. In some locations, *C. fornicata* aggregations now form long, mostly continuous aggregations over fine sediments.

By dividing the Phase II area into 4 equal sections, not only can the wide longitudinal distributions of these species observed in the maps be seen, but also the center of those distributions (Figure 5.2-71). While *C. fornicata* is present throughout, *M. edulis* is completely absent from images in the far western extent of the study region. This includes areas where *M. edulis* had previously been found to be dominant. Additionally, although maximum abundance of *M. edulis* remains in eastern FIS, maximum occurrence (i.e., % of sample images in which *M. edulis* was observed) is much farther west, in the section of the study area extending from the mouth of the Connecticut River to Goshen Point where this species had previously been dominant. This is also the same region where occurrence of *C. fornicata* reaches its maximum, as nearly 50% of sample images contain this species.
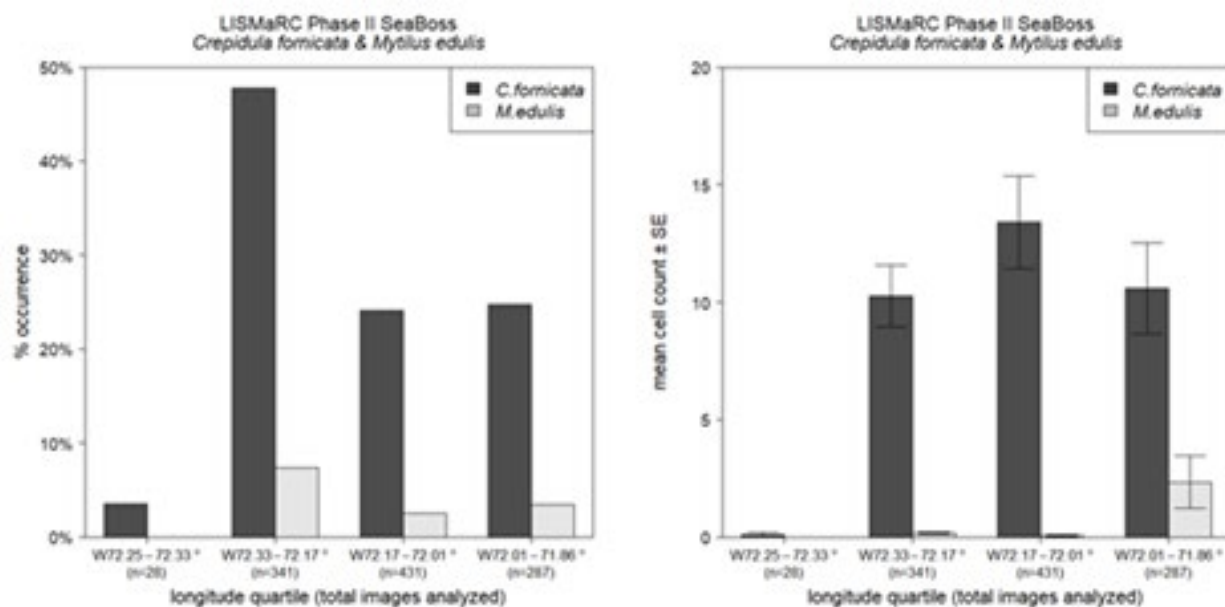
Figure 5.2-71. M. edulis (light gray bars) and C. fornicata (dark gray bars) % occurrence (left) and mean abundance (right) by longitudinal section. Whiskers in mean abundance plot report standard error.

Determining the drivers of this evident shift in benthic community composition using data collected during this project is not feasible, but by focusing on the relationships between both *M. edulis* and *C. fornicata* and available environmental parameters, some insights based on patterns of distribution and abundance can shed some light on these changes. Stark differences in in the abundance of these species were revealed in the context of bottom complexity. While both species were most common on level or near-level seafloor (TRI < 0.07m; Figure 5.2-72), the greatest densities of *M. edulis* were in the most complex habitats (mean TRI = 0.22 when *M. edulis* cover > 10%). Conversely, *C. fornicata* abundance dropped by nearly half in these same habitats

compared to flatter substrates (mean 3.5% cover versus mean 6.2% cover). And while *M. edulis* occurrence peaked in deeper waters, abundance was highest in the shallowest habitats sampled, which include the rocky and highly complex eastern end of FIS (Figure 5.2-73). Similar contrasts were apparent in these both species' apparent relationships with seafloor current strength (maximum monthly bottom stress, tau or τ), a measure of the physical forces exerted on bottom sediments and organisms by tidal currents (Figure 5.2-74). While *M. edulis* was most common and abundant under the most dynamic conditions (i.e., highest maximum bottom stress, $\tau > 1.01$ Pa), *C. fornicata* was relatively rare and in lower densities than in areas with less tidal current strength.
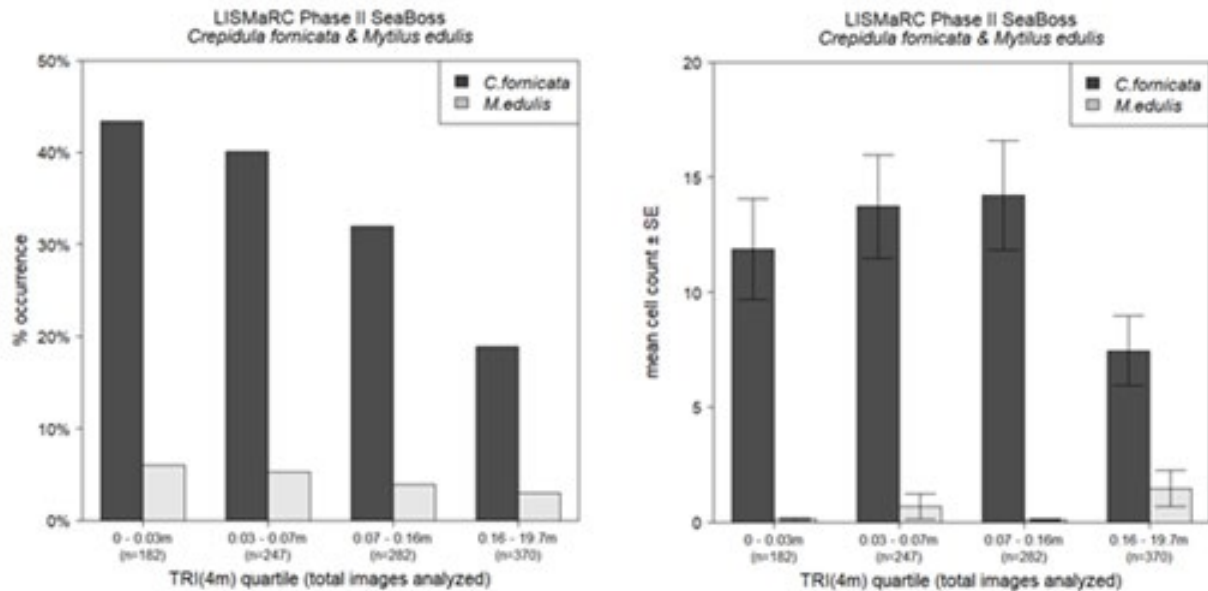
Figure 5.2-72. M. edulis (light gray bars) and C. fornicata (dark gray bars) % occurrence (left) and mean abundance (right) by TRI quartile. Whiskers in mean abundance plot report standard error.
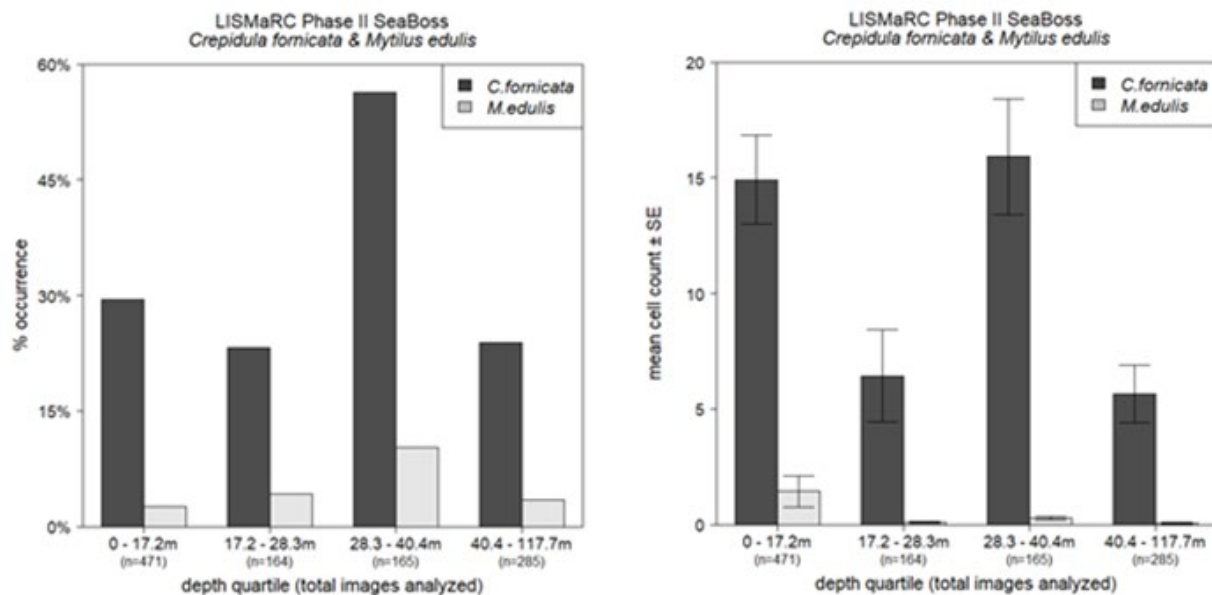
Figure 5.2-73. M. edulis (light gray bars) and C. fornicata (dark gray bars) % occurrence (left) and mean abundance (right) by depth quartile. Whiskers in mean abundance plot report standard error.
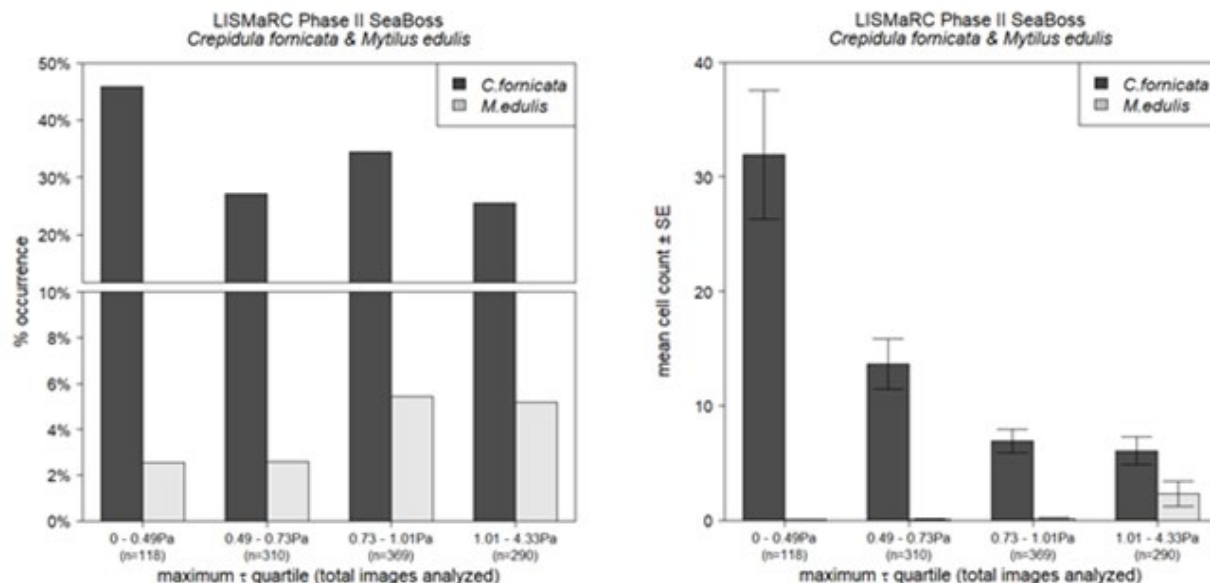
Figure 5.2-74. M. edulis (light gray bars) and C. fornicata (dark gray bars) % occurrence (left) and mean abundance (right) by maximum monthly bottom stress quartile (maximum τ). Whiskers in mean abundance plot report standard error.

While *C. fornicata* was common and abundant in all 5 eCognition patch types compared to other taxa, neither species was evenly distributed across patches (Figure 5.2-75). Of the three heavily sampled patch types, both *M. edulis* and *C. fornicata* were most common in patch D, which is characterized by coarser sediments than either patch B or C (Table 5-16A). *M. edulis* was also most abundant in patch D; *C. fornicata* % cover was greater in patch C than in patch D, but these differences were marginal and both substantially exceeded those in patch B. Despite observed differences between patches, *C. fornicata* was one of the most common and abundant organisms in each of the patches. In contrast to *C. fornicata*'s ubiquity, *M. edulis* did not exceed 8% occurrence and did not reach 1% mean cover in any patches.
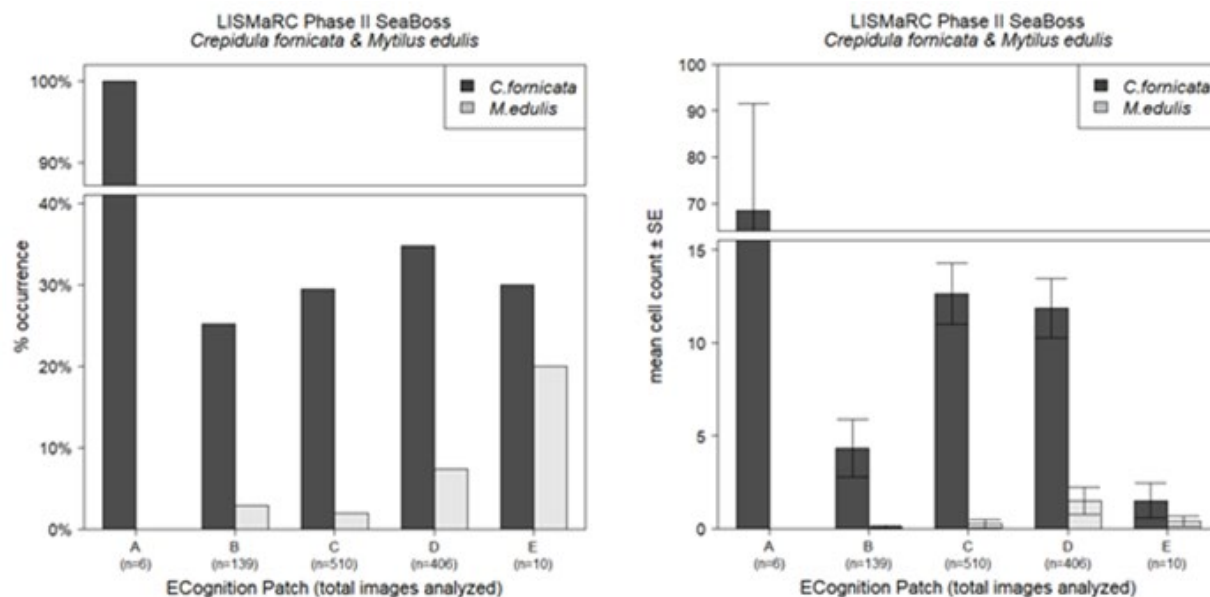
Figure 5.2-75. M. edulis (light gray bars) and C. fornicata (dark gray bars) % occurrence (left) and mean abundance (right) by eCognition acoustic patch. Whiskers in mean abundance plot report standard error.

Combined influences of some environmental, physical, and spatial factors were revealed in the results of GLMM of species occurrence. Bottom complexity (TRI) and depth provided the strongest influence on the observed distribution patterns of both *M. edulis* and *C. fornicata* (i.e., model parameters in the best-fit GLMM's for both species consisted of these factors), with similar effects on both species. Occurrence decreased by more than half for both *M. edulis* (from 6% to 3%) and *C. fornicata* (from 43% to 19%) between the least and most complex bottom habitats (Figure 5.2-72). Occurrences of both species peaked in depths between 28m and 41m, with *C. fornicata* present in more than half of samples (56%; Figure 5.2-73). When considered in total, these results indicate both *M. edulis* and *C. fornicata* were common in deeper, relatively flat seafloor locations. That the combined effects of TRI and depth did not explain a substantial portion of either *M. edulis*'s (marginal R^2 = 0.05) or *C. fornicata*'s (marginal R^2 = 0.07) occurrence suggests additional influences on these species' distributions.

Multiple factors also influenced the abundance of both species when they were present, as revealed by linear mixed models (LMM) of abundance. *M. edulis* density depended most on geographic location (longitude) and bottom current strength (maximum tau). While *M. edulis* was more than twice as likely to be observed between the Connecticut and Thames Rivers (present in 7.3% of images) than in eastern FIS (3.5% of images; Figure 5.2-71), abundance at the eastern extent of the Phase II area was nearly an order of magnitude greater (mean cover 1.1%) than further west to the mouth of the Connecticut River (mean cover 0.1%). Differences in the density of *M. edulis* at locations with the strongest bottom current conditions (mean cover 1.1%) were similarly much larger than in calmer areas of the seafloor (0.1%; Figure 5.2-74). The influence of longitude and maximum bottom stress explain most of the observed patterns in *M. edulis* abundances (margin R^2 = 0.58).

While the factors strongly affecting *M. edulis* abundances appeared to be clear, *C. fornicata* densities appeared to be the result of a complex mixture of influences including geography and bottom current conditions, as well as bottom complexity (TRI) and eCognition patch type. Where *M. edulis* abundance increased with bottom current strength, *C. fornicata* decreased in number. Under the calmest seafloor conditions *C. fornicata* was nearly 3 times more abundant (mean cover 14.8%) than in more dynamic areas (mean cover 5.2%; Figure 5.2-75). While the overall decrease in density with increasing bottom current strength is clear, *C. fornicata* meets the criterion for "dominance" discussed above in a number of sample areas where bottom currents are consistently strong. *C. fornicata* was most abundant at the eastern edge of LIS (Figure 5.2-71). Between the mouth of the Thames River (north) and the Race (south), *C. fornicata* densities for more than 1/3 greater (mean cover 6.2%) than in the remainder of the Phase II area (mean cover 4.6%). While densities on highly complex seafloor were less than those in flatter habitats (as described above), Tukey post-hoc comparisons of eCogntion-patch-specific *C. fornicata* abundances revealed significantly greater densities in patch C than in patch B (t = 2.97, df = 327; Figure 5.2-76). As might be expected when complex patterns are described by additive combinations of model parameters, the explanatory power of this model was limited (marginal R^2 = 0.08). What led to the observed shifts in dominant structure-forming suspension feeding organism in large parts of ELIS is not clear based on available sample data and the potentially contributing factors examined during this project. In regions where it is invasive (Northeast Atlantic) and coincident with *M. edulis*, *C. fornicata* attachment to *M. edulis* shells has been shown to reduce growth and survival (Thieltges, 2005). No cases of epibionty were observed with *M. edulis* as the basibiont, but when found in dense aggregations *C. fornicata* were attached to both conspecific and to non-specific shells, so this

process could have contributed to the observed changes. Another possible contributing factor could be a change in the quality of food resources. The dynamics of phytoplankton productivity, composition, dominance, and size spectra over recent decades in ELIS, while poorly resolved at this spatial scale (Lopez et al., 2014), could contribute to changes in survival, growth, and competitive interactions between these species. While phytoplankton is a predominant food resource, zooplankton also contributes to nutrition and growth in some ecological settings (Lehane & Davenport, 2006), and Rice et al. (2015) document a decrease in the size of zooplankton in LIS driven in part by temperature. While *M. edulis* feeding efficiency increases with particle size (Strohmeier et al., 2012), *C. fornicata* is not particularly size selective during suspension feeding and is highly efficient at consuming relatively small phytoplankton (Barillé et al., 2006); Beninger et al., 2007). Although not demonstrated in direct comparisons, the decreased size of available prey in LIS may have influenced competition for seafloor area in ELIS.
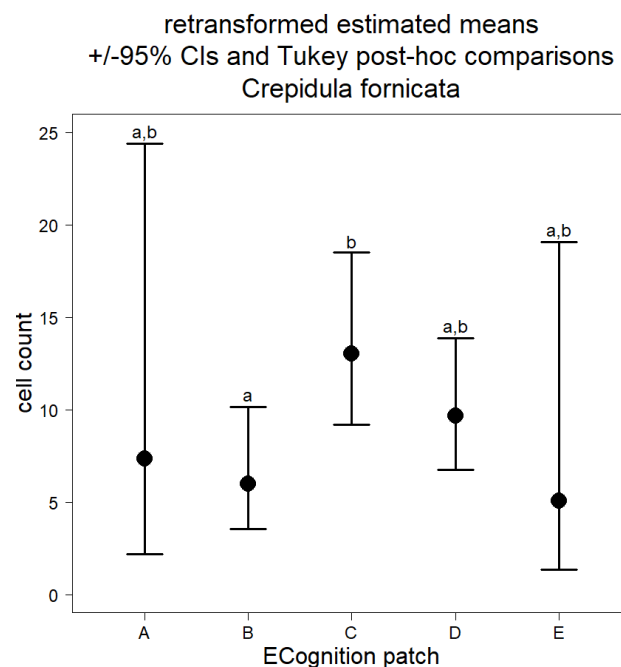
Figure 5.2-76. LMM-derived estimated marginal means of C. fornicata abundance. Whiskers report standard deviation. Different letters indicate significantly different abundance based on Tukey post-hoc comparisons.

While these species appear to occupy shared habitats, patterns of abundance revealed potentially important distinctions in their responses to specific environmental conditions, albeit at different scales of commonality and abundance. The distinct response of *M. edulis* to the strength of bottom currents, in contrast to *C. fornicata*'s apparent preference for less dynamic habitats, may explain part of the observed spatial patterns of abundance. Most importantly, the small "foot hold" in eastern FIS where *M. edulis* may be considered dominant could result, in part, from the strength of tidal currents flowing through the inlet from BIS. Swift currents may benefit *M. edulis*, providing conditions that lead to higher feeding efficiencies (Dolmer, 2000). Additionally, longitude is merely a proxy for other environmental conditions, including increasingly oceanic conditions in LIS from west to east and large-scale differences in food resources for suspension feeders (Lopez et al., 2014). The eastern end of FIS, where *M. edulis* densities were at their maximum, is heavily influenced by BIS and experiences near-marine conditions (Deignan-Schmidt & Whitney, 2018). This may result in greater availability of larger food, providing *M. edulis* with a food source in the size range allowing for more efficient feeding (see above; (Strohmeier et al., 2012).

As discussed previously, there are important differences in the influences of reef-forming suspension feeders (e.g., *C. fornicata* supports less diversity in surrounding benthic communities than *O. edulis*; Preston et al., 2020). With the spatial distributions of both species in ELIS and FIS mapped and characterized during this project, additional sampling and analysis would be warranted to assess other, possibly related changes in benthic communities.

Interactions between Hard Substrate and Ecosystem Engineers: Cliona spp.*, Astrangia poculata, and invasive Didemnum vexillum*

Shallow subtidal rocky habitats in LIS are also home to a range of attached and encrusting invertebrates. Among the characteristic species of these attached communities are a number of colonial organisms that can form large masses, including the stony coral *Astrangia poculata*, members of the boring sponge Genus *Cliona*, and the invasive colonial tunicate *Didemnum vexillum*. Each of these taxa are conspicuous when abundant and, to varying extents, form 3-dimensional structures that enhance habitat complexity (Schuhmacher & Zibrowius, 1985 Gittenberger, 2010; Schweitzer & Stevens, 2019). While competition between these taxa has been the focus of previous research in southern New England coastal waters (Grace, 2017), the ability to assess spatial distributions over such a large area that spans a range of habitat types provides the opportunity to gain new insights. This is especially pressing, considering the potential impacts of *D. vexillum*, a recently introduced invasive tunicate which can spread quickly via fragmentation and overgrow other benthic organisms (Daley & Scavia, 2008).

While early evidence of *D. vexillum* effects on benthic communities in LIS suggest either neutral or even positive influence on diversity (Mercer et al., 2009), its impacts on specific benthic taxa can be negative (Grace, 2017). Both coldwater corals and structure- forming sponges were identified as being worthy of special consideration and protection through the LIS Blue Plan, a marine spatial planning process developed under the direction of the State of Connecticut's legislature (CT DEEP, 2019). The Blue Plan identified "ecologically significant areas" (ESAs), locations that feature sensitive or rare habitats or biological communities, based in part on the distribution of key taxa, including *A. poculata* and *Cliona* spp. *D. vexillum* presence and high abundance in the Phase II study area, especially its co-occurrence with *A. poculata* or *Cliona* spp., could provide the groundwork for future targeted studies to resolve consequences of these interactions and ensure the persistence of these benthic organisms.

A. poculata, northern star coral, is a Scleractinian coral distributed along the North American continental shelf from the Gulf of Mexico to Cape Cod. Although ahermatypic (i.e., non-reef building), *A. poculata* is considered constructional (i.e., creates 3-dimensional carbonate structures; Schuhmacher & Zibrowius, 1985) due to the impacts on small-scale, localized complexity of its calcium carbonate "stony" skeleton. While *A. poculata* does host symbiont photosynthetic dinoflagellates, this relationship is facultative. Reliance on heterotrophy increases in conditions of low light availability and low winter temperatures (Dimond & Carrington, 2008; Dimond et al., 2013). Towards the northern limit of their range along the southern coast of New England, growth is limited to spring through fall, primarily relying on polyp feeding rather than endosymbiotic autotrophic sources (Dimond & Carrington, 2007). Although primarily heterotrophic, nearly ¼ of annual growth can be attributed to symbiont photosynthesis in New England waters, highlighting the importance of light availability to the persistence of *A. poculata* (Dimond & Carrington, 2007). Despite the availability of light for photosynthesis in shallow areas, competition for resources,

primarily access to light and hard substrates, limits *A. poculata* densities in very shallow waters. Macroalgae outcompete *A. poculata* in these habitats both reducing photosynthesis through consistent shading and even physical abrasion of soft tissue (Jacques et al., 1983; Grace, 2004). Direct competition for space with other epifauna also limits prevalence, as is the case for *A. poculata* with the invasive colonial tunicate *D. vexillum* and boring sponges of the Genus *Cliona* (Grace, 2017).

Members of the Genus *Cliona* are found in marine, estuarine, and freshwater habitats worldwide. Known as boring sponges, these demosponges excavate into calcium carbonate materials- including mollusk shell, coral, and limestone- using a combination of chemical and physical means (Rützler & Rieger, 1973). Clionaid boring sponges take various forms, even within the same species, making them difficult to define taxonomically without microscopic investigation of spicule composition and molecular analyses (Xavier et al., 2010). *Cliona* spp. can be found in boring form, with only oscula visible protruding from mollusk shells, as well as encrusting, as a thin sheet over boulder or bedrock, and massive, forming large masses or towers, forms (Figure 5.2-77); these forms are also referred to as alpha, beta, and gamma stages, respectively, in boring sponges (Rosell & Uriz, 2002). Gamma stage boring sponge can substantially increase substrate complexity, providing important habitat for mobile macrofauna including fish (Miller et al., 2010). Boring sponge infection of commercial aquaculture can result in reduced growth, high mortality, and visible damage precluding commercial value (Carver et al., 2010; Carroll et al., 2015). *Cliona* spp. boring extends beyond bivalves to gastropods (Stefaniak et al., 2005) and corals (Nava & Carballo, 2008).
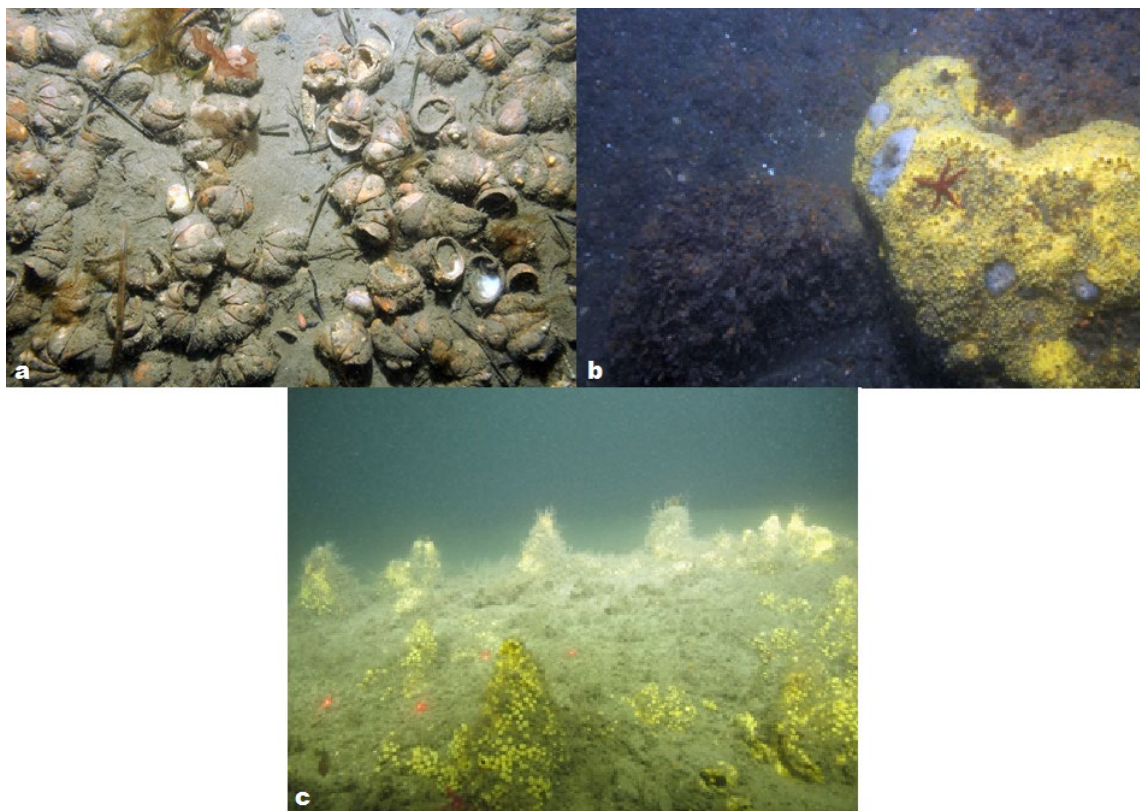
Figure 5.2-77. Forms of Cliona spp. *colonies: (a) alpha-stage visible as yellow oscules in C. fornicata shells (enlarged images below main image); (b) beta-stage colony covering a boulder; and (c) gamma-stage colonies forming towers.*

D. vexillum is a colonial ascidian that has reached nearly global distribution in the past 50 years (Lambert, 2009). First observed in LIS less than 2 decades ago, *D. vexillum* colonies form large contiguous masses, overgrowing substrates as well as epibenthos (Mercer et al., 2009). Following its appearance in US waters, the invasive tunicate garnered much attention due to its potential to harm native biological communities (Daley & Scavia, 2008), as well as to its conspicuousness (Auker, 2019).

All three taxa were relatively common occurrences during sampling. *Cliona* spp. were observed in 12.6% of all images, while *A. poculata* was observed in 9.29% and *D.* vexillum 3.56%. To put these values in context, all were in the top 20% of identified taxa based on occurrence. All were also widely distributed, present in 46% (*Cliona* spp.), 40% (*A. poculata*), and 24% (*D. vexillum*) of all sample areas (blocks or sites). *Cliona* spp. was very common in FIS and northern BIS, appearing in nearly ¾ of the sample areas to the east of the Thames River (20 of 27 sample areas; Figure 5.2-78). At the scale of each sample image, *Cliona* spp. became increasingly common moving east from the mouth of the Connecticut River into FIS, where boring sponges were observed in nearly 1/5 of all images (Figure 5.2-79). Mean abundance was highest in the eastern half of the Phase II area. *A. poculata* had 2 distinct spatial centers of their distribution- Fisher's Island Sound and west of the Race between Goshen Point/Niantic Bay and Plum Island (Figure 5.2-80). In this latter area *A. poculata* also reached its peak abundance, accounting for >12% of each sample image in which it was observed. While less common than *A. poculata*, *D. vexillum* was also observed more in this region than in any other and covered 13% of the substrate in sample images on average (Figure 5.2-81).
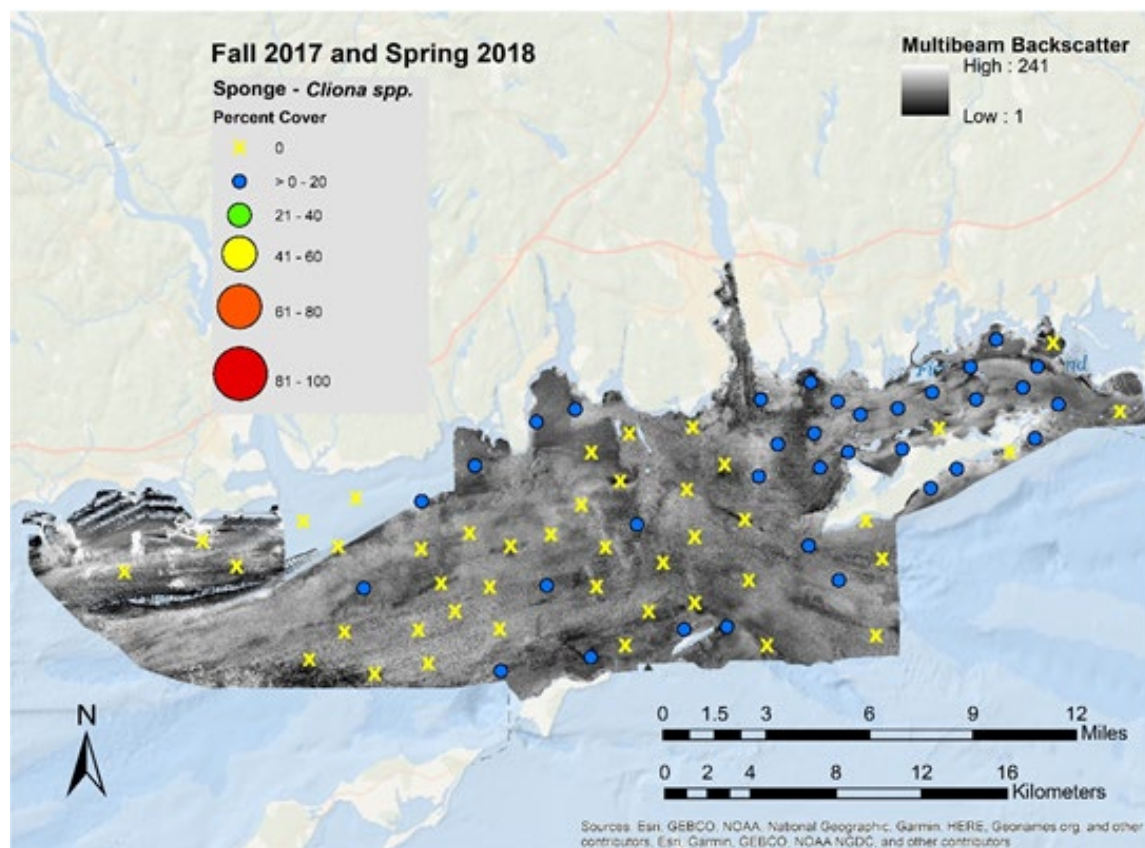
Figure 5.2-78. Mean percent cover of Cliona spp. *per Block/site sampled*

Figure 5.2-79. A. poculata (dark gray bars), Cliona spp. *(light gray bars), and D. vexillum (white bars) % occurrence (top) and mean abundance (bottom) by longitudinal section. Whiskers in mean abundance plot report standard error.*
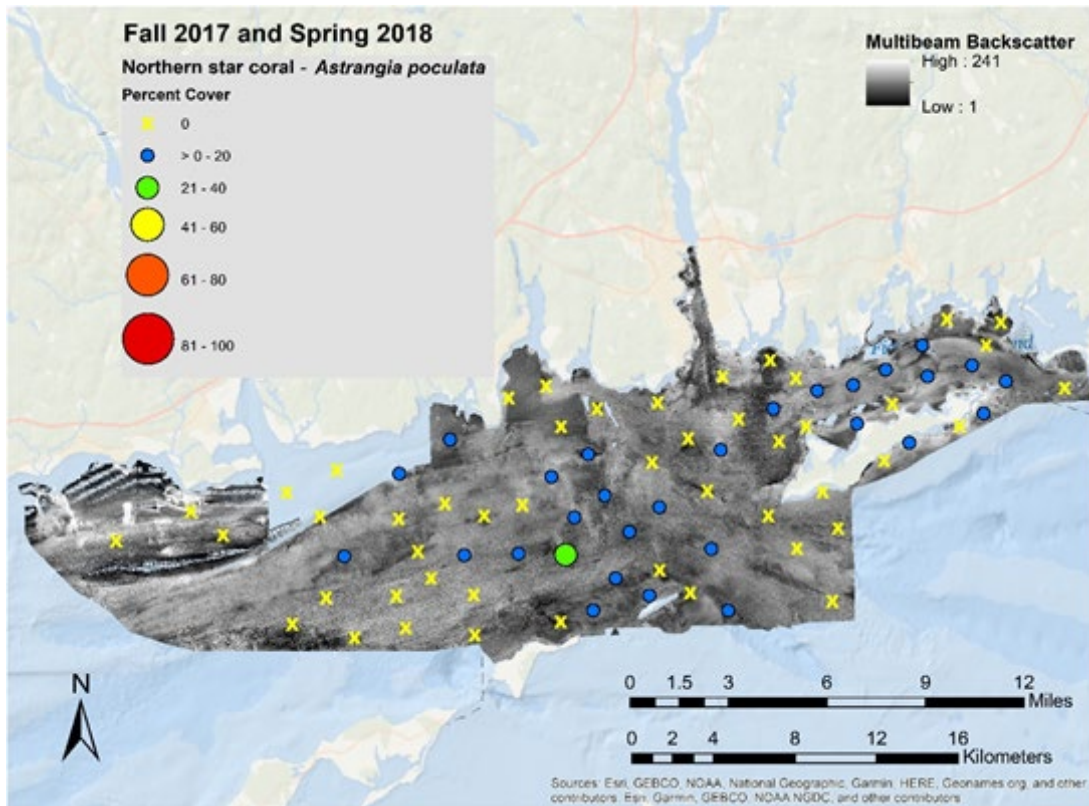
Figure 5.2-80. Mean percent cover of A. poculata per Block/site sampled
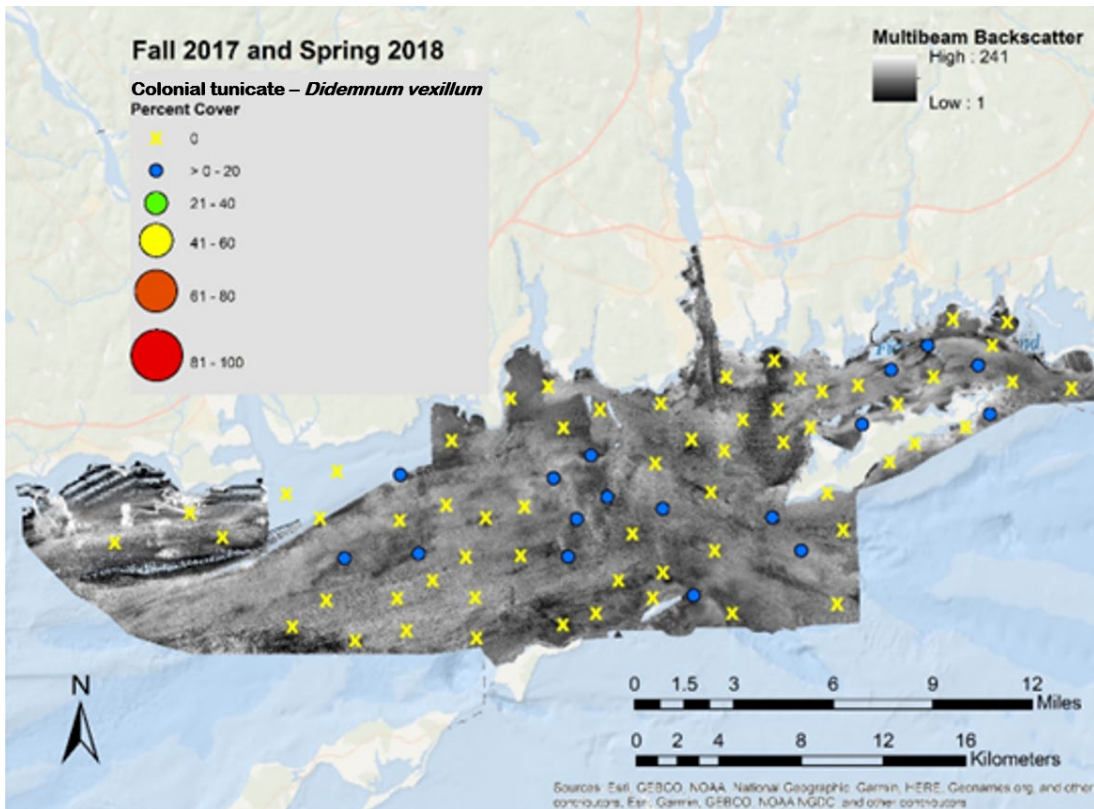
Figure 5.2-81. Mean percent cover of D. vexillum per Block/site sampled

A. poculata, *Cliona* spp., and *D. vexillum* share important characteristics, such as the need for solid surfaces for attachment and reliance on filter-feeding. These similarities likely drove some of the observed patterns in presence and abundance, such as the occurrences and abundances of all three taxa increasing with substrate complexity (i.e., TRI; Riley et al., 1999; Figure 5.2-82). Greater spatial complexity, as measured using derivatives of bathymetric data like TRI, are proxies for hard substrates. Another characteristic of these taxa was how often they were observed as large aggregations covering much of the visible substrate. When present, *A. poculata* exceeded 10% cover in 22% of sample images, *Cliona* spp. exceeded this threshold in 28% of occurrences, and *D. vexillum* did so in 1/3 of its observed occurrences. Although an imperfect measure, this 10% coverage value does serve as a useful threshold for instances where these organisms may strongly influence benthic communities (e.g., *Cliona* spp. impacts on mollusk communities; Coleman, 2014) and attract mobile macrofauna.
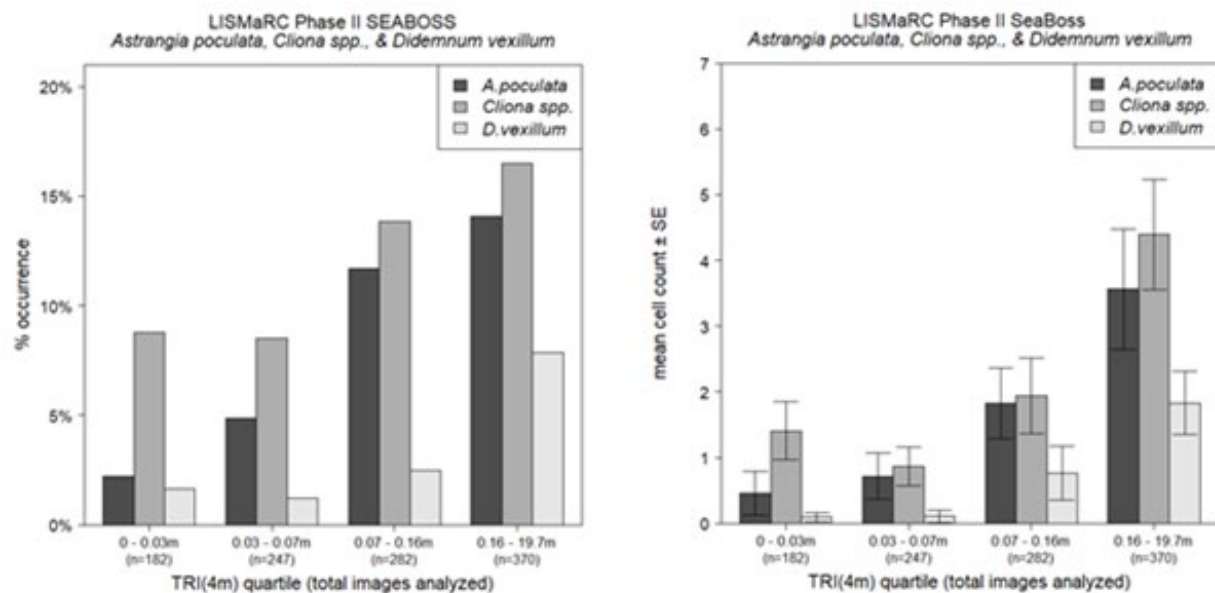
Figure 5.2-82. A. poculata (dark gray bars), Cliona spp. (light gray bars), and D. vexillum (white bars) % occurrence (left) and mean abundance (right) by TRI quartile. Whiskers in mean abundance plot report standard error.

Perhaps unsurprisingly, *Cliona* spp. and *A. poculata* were commonly observed in close proximity-boring sponge appears in 25% of the images where *A. poculata* was identified (15 of 60 images). Both of these organisms attach to hard substrates, so their co-occurrence could be expected. While *A. poculata* was mostly limited to hard geological substrates (i.e., mostly boulders), *Cliona* spp. was observed in finer substrates both as alpha stage sponges usually within large slipper shell beds and as gamma stage towers that likely began as alpha stage within bivalves. *D. vexillum* was less often found along the other two taxa, present in 8% and 9% of the images, respectively, featuring *A. poculata* and *Cliona* spp. Although *D. vexillum* was less widely distributed in comparison to *A. poculata* and *Cliona* spp., some tunicate colonies may have gone undetected in SEABOSS sampling. *D. vexillum* was observed on the lateral faces of boulders and rocky outcroppings during ROV and wet-diving sampling efforts (Figure 5.2-83) where they were far less likely to be capture by orthogonal imaging from the SEABOSS system.
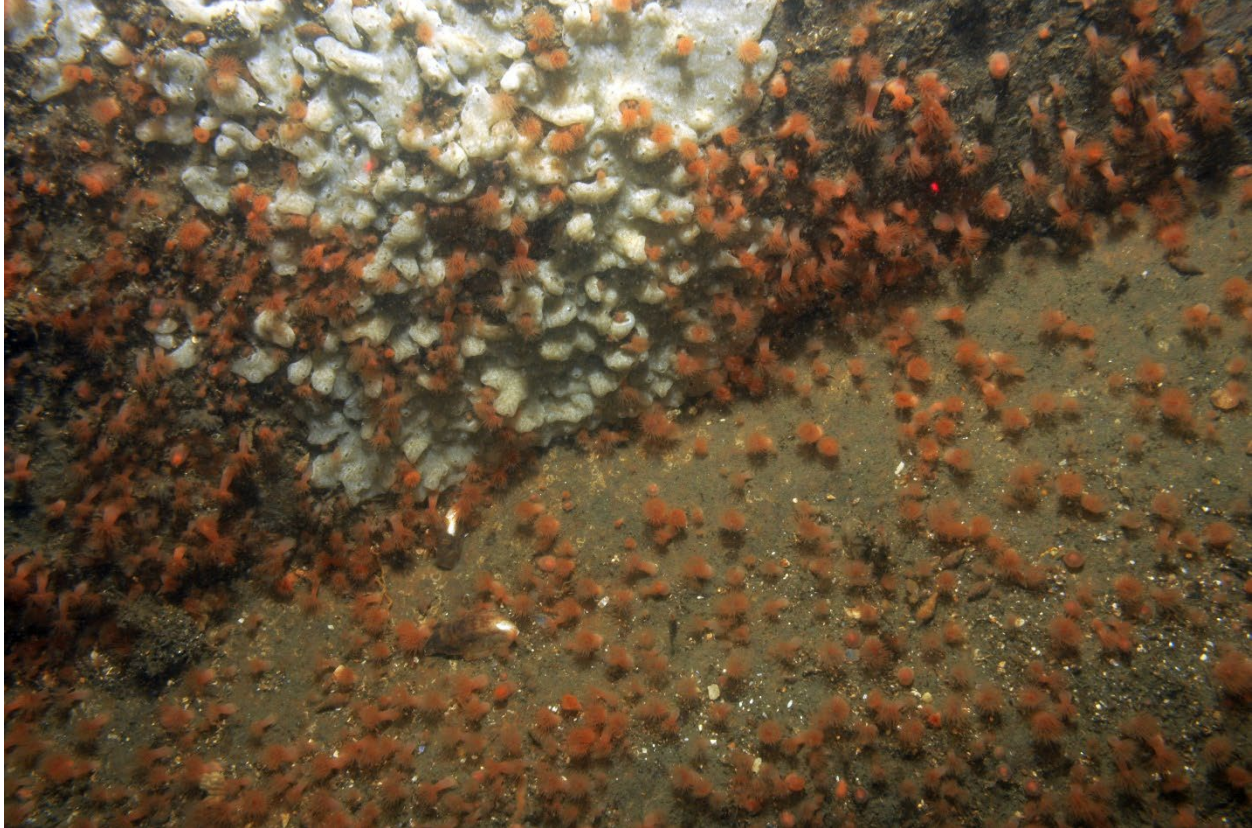
Figure 5.2-83. D. vexillum colony on a vertical rock face (LISMaRC_Fall2017_DSC_IrfColCor_3129)

While their similar ecology did lead to the above similarities, there were some interesting divergences in occurrence and abundance. The depths at which these organisms were most common differed, as *Cliona* spp. appeared in more than 1/5 of sample images taken in the shallowest areas sampled by SEABOSS (to 17m) and *A. poculata* was nearly as common in moderately deeper habitats (17m - 28m). *D. vexillum* was most common below 40m (Figure 5.2-84). Abundance peaked for these taxa in these same depths. *A. poculata*'s limited distribution on the shallowest hard substrates has been observed previously, and most likely is a consequence of competition for both substrate with other attached fauna and access to light with macroalgae (Jacques et al., 1983; Grace, 2004). While *D. vexillum* has been observed in shallow habitats during its worldwide expansion, there is some evidence of limits on its distribution induced by other fauna in places it has invaded, both in the form of direct competition with other epifauna for space (Grace, 2017) as well as predation (Forrest et al., 2013). While not documented in the LIS, similar interspecific interactions may control *D. vexillum* abundance and distribution.
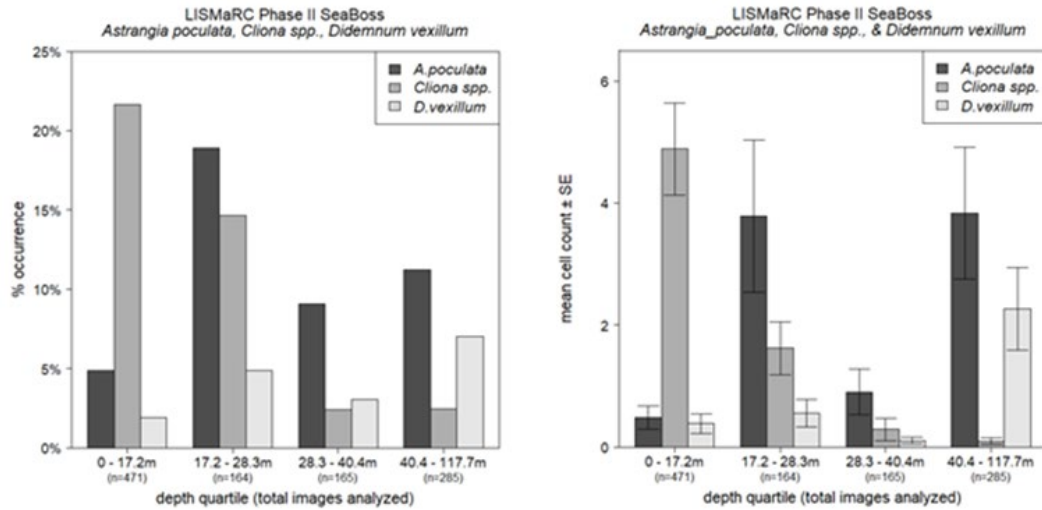
Figure 5.2-84. A. poculata (dark gray bars), Cliona spp. (light gray bars), and D. vexillum (white bars) % occurrence (left) and mean abundance (right) by depth quartile. Whiskers in mean abundance plot report standard error.

These three taxa also diverged in their apparent response to tidal currents (tau). While *A. poculata* was evenly distributed across areas experiencing a wide range of bottom current conditions, the coral was entirely absent from the lowest energy habitats (Figure 5.2-85). Boring sponges were observed more than four times as often in the less energetic half of the Phase II sample area as compared to the higher energy half (present in 23.3% and 5.6% of sample images, respectively). Although far less common overall, *D. vexillum* was nearly four times more common in areas that experience the strongest bottom currents (5.5%) than the remainder of the sample area (1.4%) and, like *A. poclulata*, was completely absent from areas with weak bottom current conditions. Slow currents are associated with higher sedimentation rates, which can negatively impact corals like *A. poculata* and may, in part, explain their absence from particularly low energy patches of seafloor (Baynes & Szmant, 1989). *D. vexillum* abundance in areas experiencing strong bottom currents is more surprising, as this colonial tunicate is associated with low energy areas in other locations where it is invasive (Vercaemer et al., 2015).
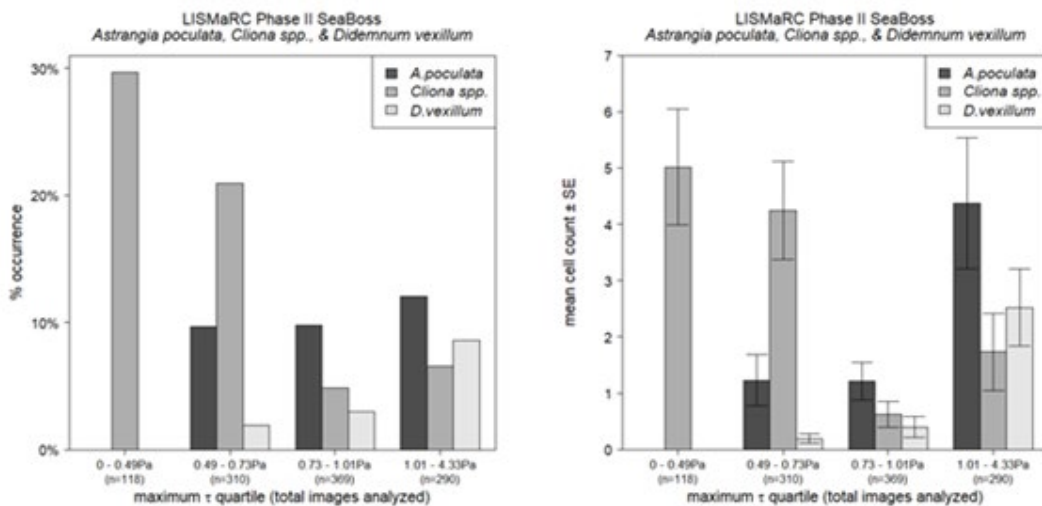
Figure 5.2-85. A. poculata (dark gray bars), Cliona spp. (light gray bars), and D. vexillum (white bars) % occurrence (left) and mean abundance (right) by maximum monthly bottom stress quartile (maximum τ). Whiskers in mean abundance plot report standard error.

Both *A. poculata* and *D. vexillum* were increasingly common in areas featuring coarser substrates (as represented by eCognition patches; Figure 5.2-86). Although no eCognition patch types were characterized as primarily consisting of hard substrates, neither organism would be expected in the fine sediments characterizing much of the Phase II area and represented by patch types A and B. While *Cliona* spp. similarly require hard substrates, boring sponges were most common and abundant in Patch Type C, which is primarily composed of gravelly sand. Interestingly, mean abundance of *C. fornicata* was also high in Patch Type C. Alpha-stage *Cliona* spp. were almost exclusively observed in *C. fornicata* beds, which may underlie the relatively high mean abundance of boring sponges in gravelly sand.
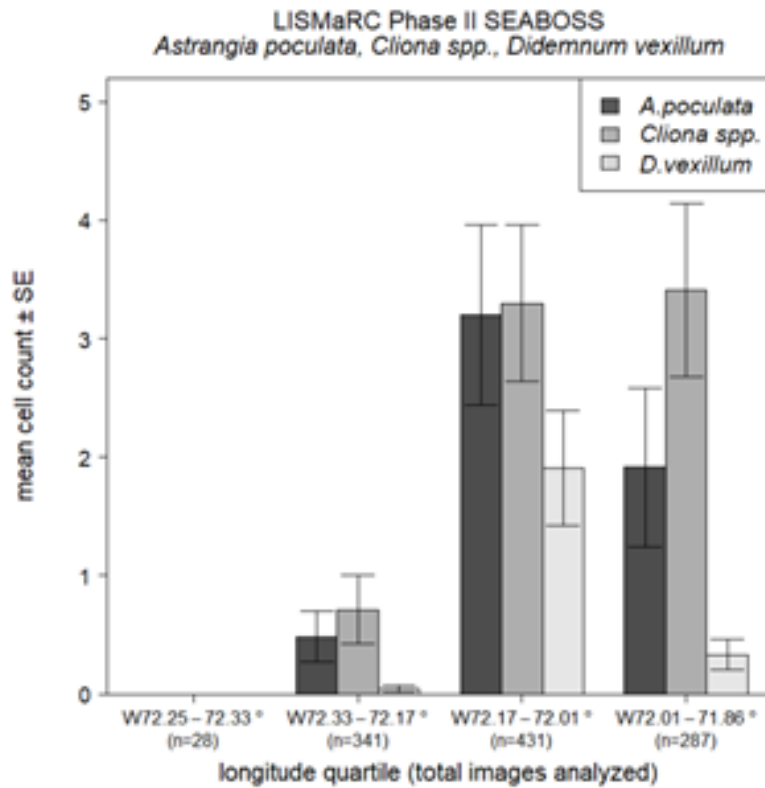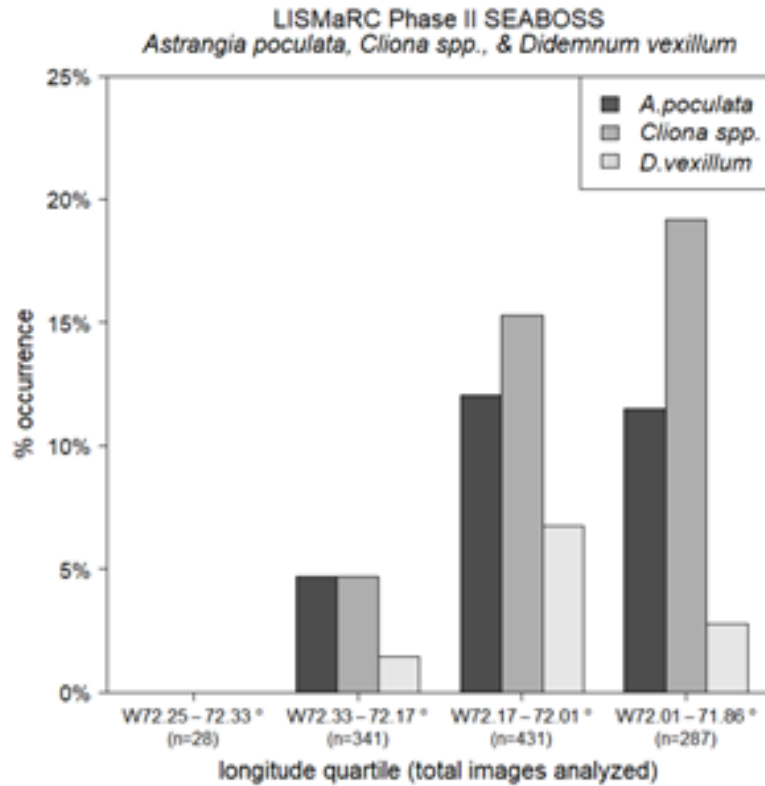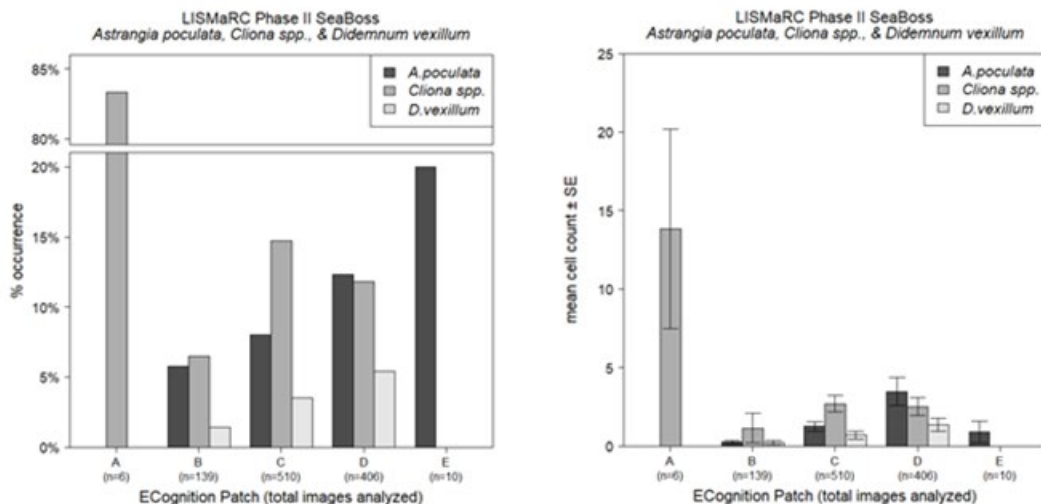

Figure 5.2-86. A. poculata (dark gray bars), Cliona spp. *(light gray bars), and D. vexillum (white bars) % occurrence (left) and mean abundance (right) by eCognition acoustic patch. Whiskers in mean abundance plot report standard error.*

Modeling results of occurrence confirmed the importance of substrate to *A. poculata*, as the best fit model was limited to TRI as the lone factor influencing occurrence. The combined influence of TRI and depth explained some of the observed distribution of *Cliona* spp. in the study area. While the best-fit model for *A.* poculata accounted for less than 1% of observed variance (marginal $R^2 < 0.01$), the combination of substrate complexity and depth explained 8% of *Cliona* spp. occurrences. Interestingly, no combination of explanatory factors exceeded the null model in describing *D. vexillum* occurrences. Both *A. poculata* abundance also varied with TRI and longitude, both more abundant as TRI increases but differing in longitudinal patterns, *A. poculata* increasing east to west and *Cliona* spp. west to east. Linear relationships with longitude proved to be fairly weak, explaining 3% of *A. poculata* and 1% of *Cliona* spp. abundance. *D. vexillum* abundance increased with both increasing current strength and from west to east, explaining 18% of variance in abundances.

Shell biogenic habitat

Biogenic shell debris, including both whole valves and pieces of shell, were almost ubiquitous, absent from only a single block/site (Figure 5.2-87). Present in more than 9 of 10 images analyzed (92.6%), shell cover varied throughout the sample area. In some places, shell consisted of several scattered valves over fine sediment habitats, while in others the seafloor was completely covered by shell debris. In limited areas, shell deposits were concentrated in troughs or depressions in finer sediments, which was also observed in Phase I area sampling (Stefaniak & Auster, 2015) as well as in other regions (Auster et al., 1996). Shell debris is present in areas featuring gastropods, but

can also aggregate shell at the base of steep slopes with fine grained sediments, in the roughs of sand waves, and in flow refuges when sorted by tidal currents and storm energy. Once deposited, shell may be further transported by currents, be covered by shifting sediments, or remain as an intact habitat for centuries. East of the Connecticut River mean shell cover was nearly 4 times greater than west of the river mouth (Figure 5.2-88). Shell covered more of the substrate in deeper areas, where it may have accumulated in deposits due to current-mediated transport. Shell cover did increase in areas with stronger bottom currents (as represented by maximum tau; Figure 5.2-89), and shell deposits in areas that experience strong bottom currents may either be covered by shifting sediments or undergo further transport. Shell density increased with sediment grain size (as represented by eCognition patch; Figure 5.2-90). Shell deposits increase the amount of hard substrate available for epifauna and flora (e.g., sponges, Nicol & Reisman, 1976), serve as refuge from predation (e.g., recently settled bivalves, Glaspie & Seitz, 2018; crustaceans, Auster, 1995; juvenile fish, Auster et al., 1995, Langton et al., 1995, and Scharf et al., 2006), and increase diversity across habitat mosaics (Thrush et al., 2006). The presence of shell can also limit emergent infaunal communities that prefer fine sediments (e.g., tube worms, Raineault et al., 2012).
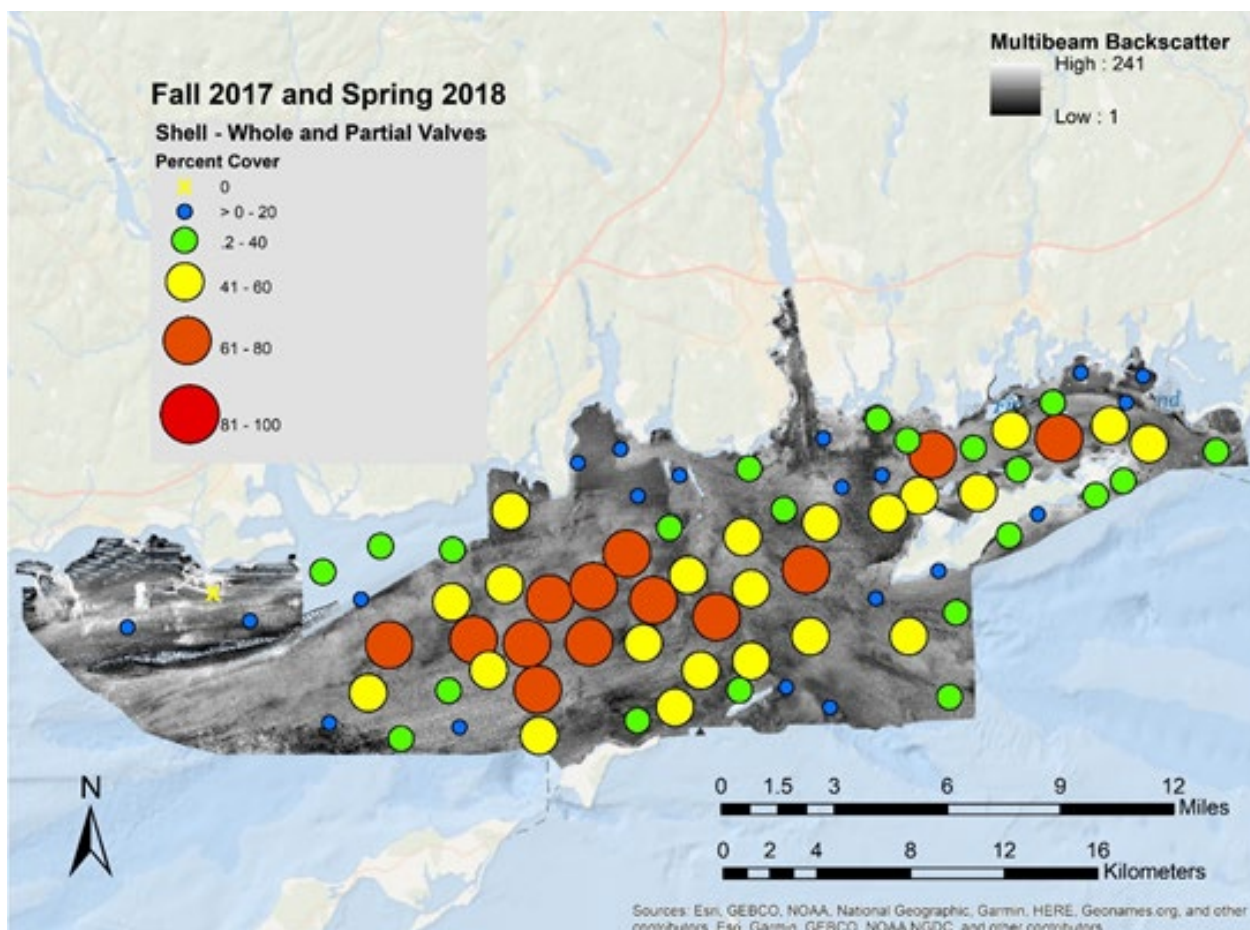
Figure 5.2-87. Mean percent cover of whole and partial shell
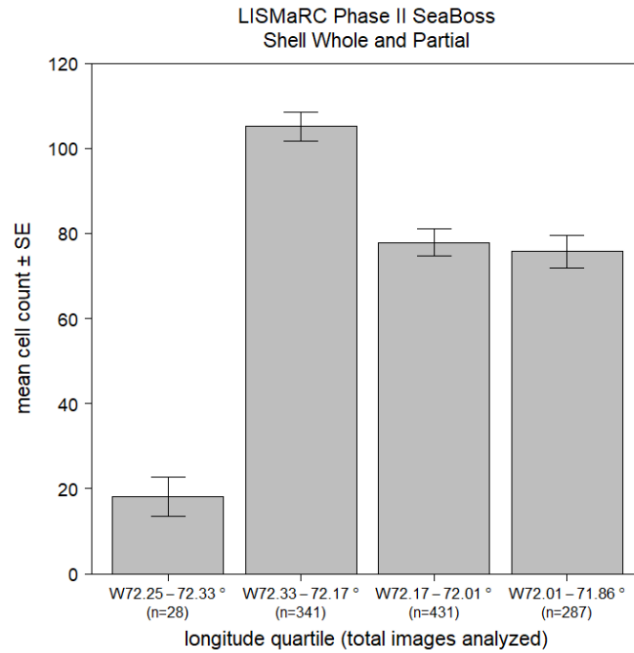
Figure 5.2-88. Shell mean abundance by longitudinal section. Whiskers in mean abundance plot report standard error.
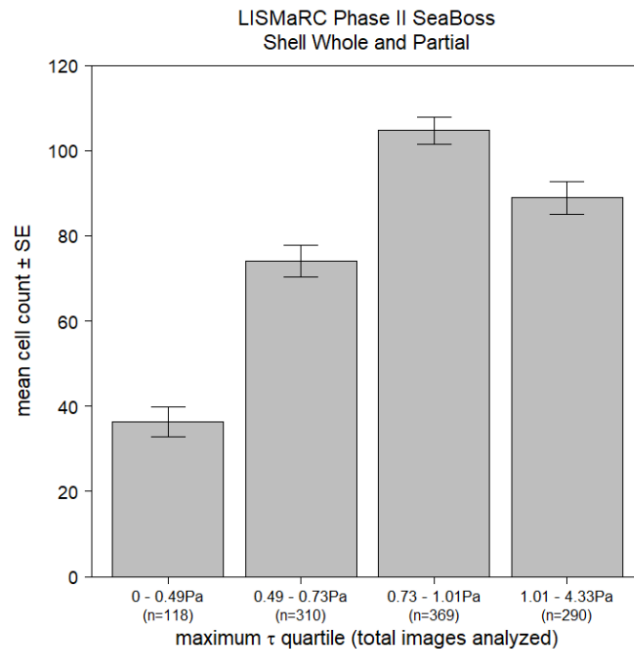
Figure 5.2-89. Shell mean abundance by maximum monthly bottom stress quartile (maximum τ). Whiskers in mean abundance plot report standard error.
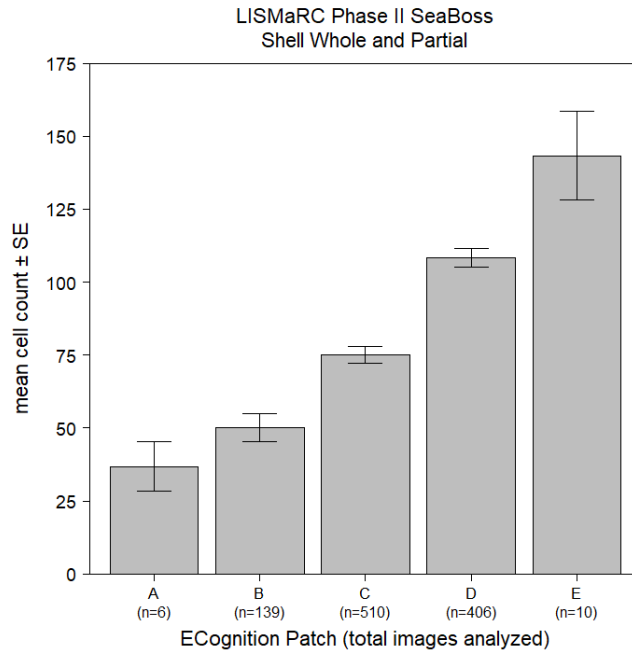
Figure 5.2-90. Shell mean abundance by eCognition acoustic patch. Whiskers in mean abundance plot report standard error.

Drift Seagrass (Zostera marina) and Terrestrial Debris

While shell valves was the most widespread and abundant biogenic debris present in the Phase II area, other organic material was available and abundant at sites specific sites. Drift seagrass (*Zostera marina*) was observed throughout the study in low quantities but was particularly concentrated in two areas–FIS and at the mouth of the Connecticut River (Figure 5.2-91). While persistent in the eastern portion of the study area (Figure 5.2-92), from the Connecticut River west drift seagrass increased dramatically from fall (mean cover 2%) to spring (mean cover 29%). Seagrass was most common and abundant in shallow (Figure 5.2-93), low energy (as represented by maximum bottom stress, tau; Figure 5.2-94) habitats.
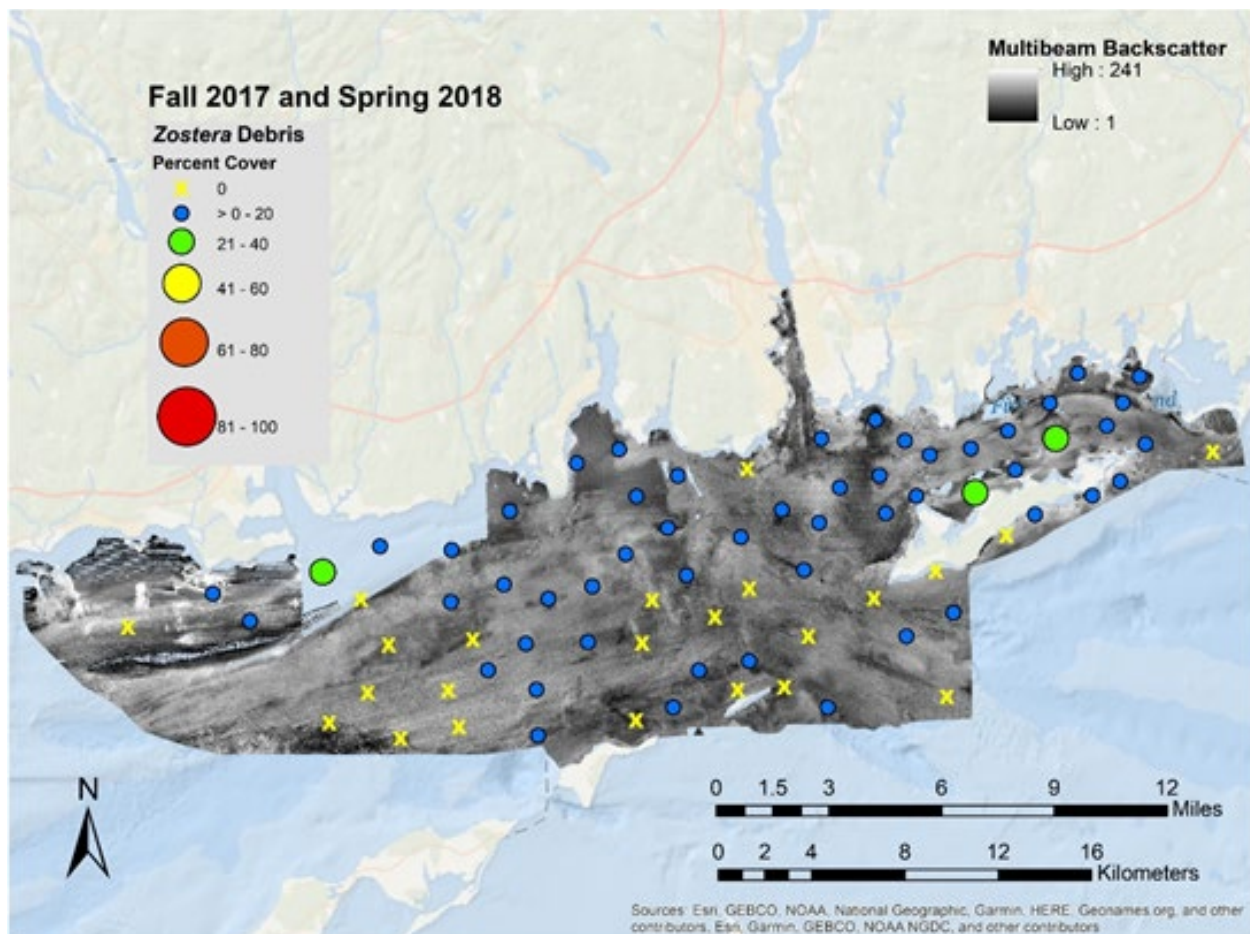
Figure 5.2-91. Mean percent cover of drift seagrass Zostera marina
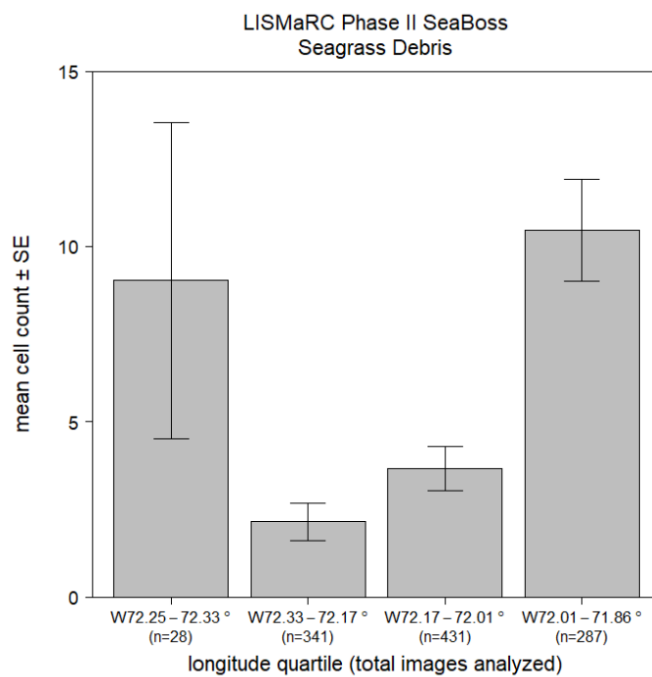
Figure 5.2-92. Drift seagrass mean abundance by longitudinal section. Whiskers in mean abundance plot report standard error.
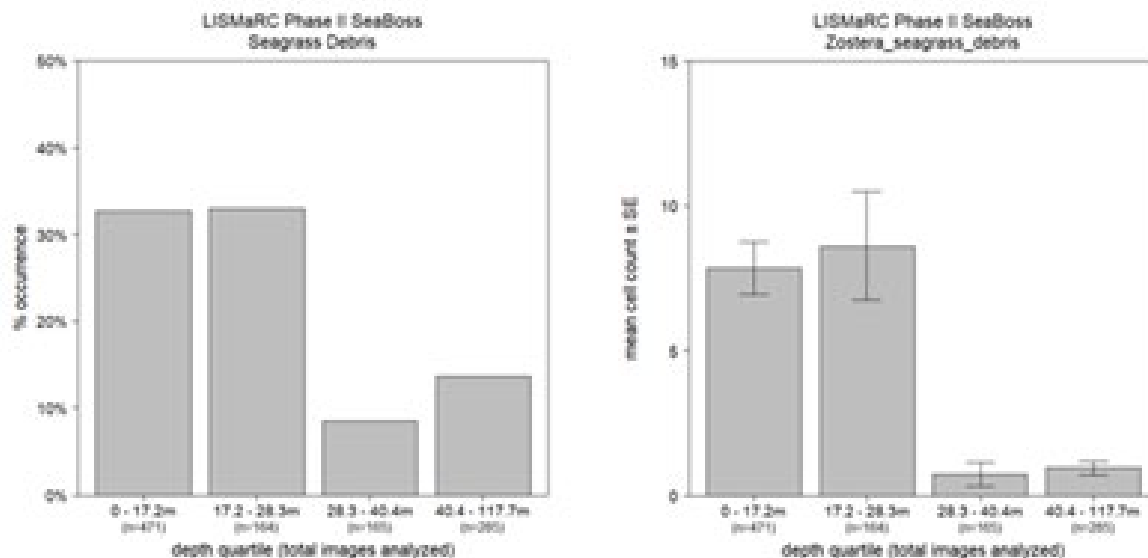
Figure 5.2-93. Drift seagrass % occurrence (left) and mean abundance (right) by depth quartile. Whiskers in mean abundance plot report standard error.
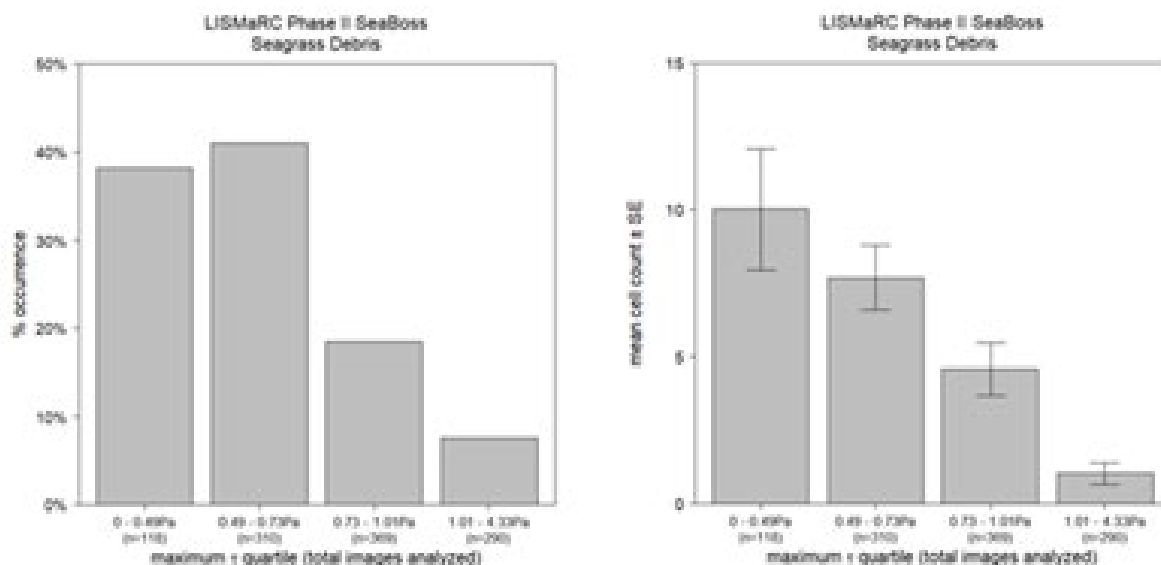
Figure 5.2-94. Drift seagrass % occurrence (left) and mean abundance (right) by maximum monthly bottom stress quartile (maximum τ). Whiskers in mean abundance plot report standard error.

Organic material from terrestrial sources was less widespread than seagrass but nearly ubiquitous near the Connecticut River during spring sampling (Figure 5.2-95). Organic terrestrial debris mostly consisted of leaf litter, branches, and other plant material that originated from the Connecticut River. More than ¾ of the nearly 30,000 km² Connecticut River watershed is forested (Clay et al., 2006), contributing seasonal inputs of plant material as the spring thaw, snow melt, and seasonal increases in precipitation greatly increase both river flow rates and terrestrial inputs.
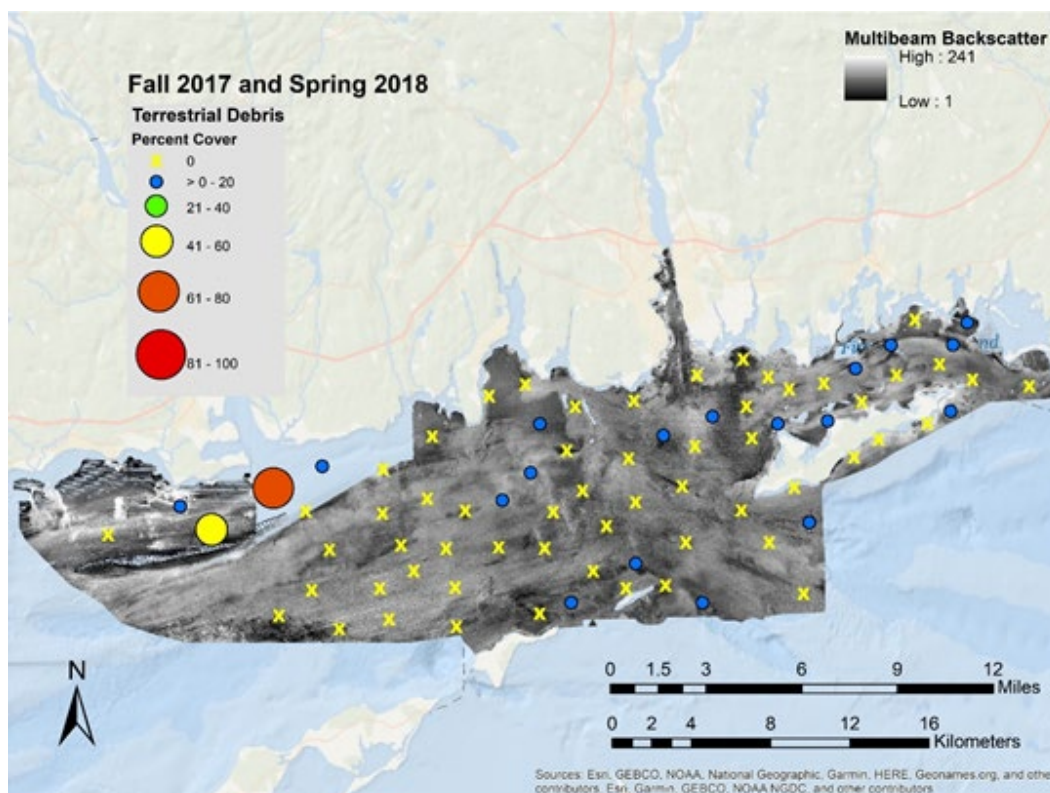
Figure 5.2-95. Mean percent cover of terrestrial debris

Where abundant in the study area, terrestrial debris covered much of the bottom and was easily disturbed, highlighting its ephemeral impacts to physical habitats. Terrestrial vegetation was most common and abundant in nearshore shallows (Figure 5.2-96) but, unlike seagrass litter, appeared to aggregate in higher energy habitats (Figure 5.2-97). Aggregation in areas with stronger bottom currents may have had different drivers depending on setting and conditions. Near the mouth of the Connecticut River where leaf litter and other terrestrial debris were often mobile during sampling, abundance was due to the continuous supply of new material from the river itself while in offshore areas troughs and depressions in the sediment experienced much lower flow rates than the surrounding area, limiting transport of light terrestrial vegetation.
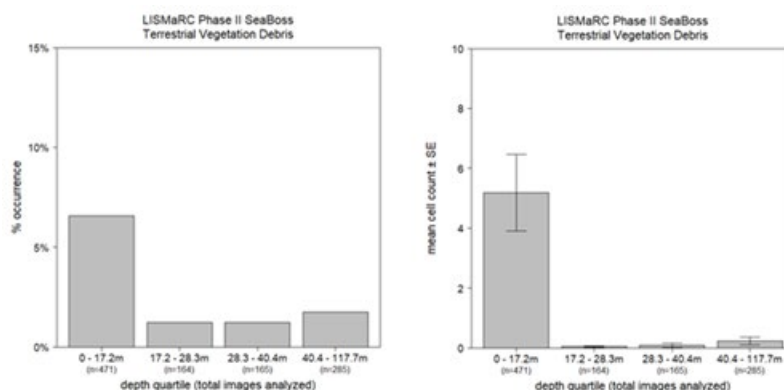
Figure 5.2-96. Terrestrial vegetation debris % occurrence (top) and mean abundance (bottom) by depth quartile. Whiskers in mean abundance plot report standard error.
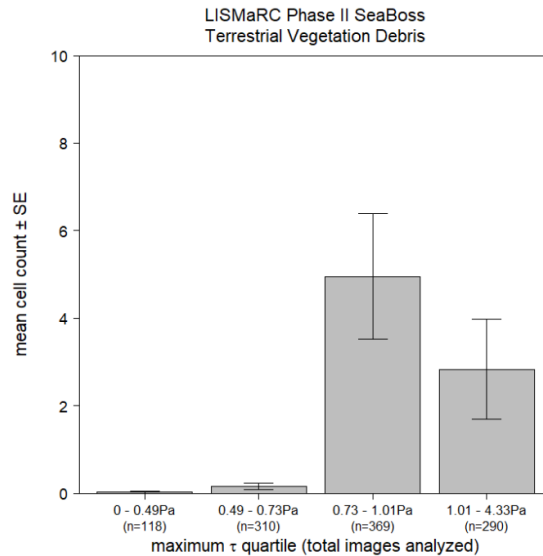
Figure 5.2-97. Terrestrial vegetation debris mean abundance by maximum monthly bottom stress quartile (maximum τ). Whiskers in mean abundance plot report standard error.

Despite the short duration of seagrass litter and terrestrial vegetation in marine habitats, this debris may have important impacts on local habitats over both the short and long term. Visibility was greatly decreased at the mouth of the Connecticut River when terrestrial vegetation was most abundant, likely influencing predation, and instances of organisms taking refuge in larger woody debris piles was observed as well. Seagrass litter also provided structure and surfaces to which organisms attached. Leaf litter and drift seagrass are also available as forage for benthic organisms; although, these materials are unlikely to form a major component of diet for most organisms (Beddingfield & McClintock, 1999). Beyond these apparent and temporary contributions to LIS habitats, seagrass litter and terrestrial debris also contribute both particulate and dissolved organic material and nutrients to the marine benthos. In addition to larger materials, rivers contribute substantial amounts of both natural and anthropogenic particulate and dissolved nutrients to coastal marine systems (Meybeck, 1982), impacting ecological processes. The residence time of both seagrass and terrestrial vegetation debris in the benthic habitats of LIS remains unclear, and may be highly variable.

5.2.3.5 Select Site Accounts

During this study multiple sites with notable biological and geological features were identified. Here each site location is briefly described and associated imagery is included to visualize local conditions.

Ellis Reef (SB-71)

Ellis Reef (Figure 5.2-98) is composed of a shallow platform and steep slope declining in depth westward to a deeper natural channel. Along the slope is a narrow rockfall with boulder-cobble substrate. Currents keep the hard substratum surfaces clear of fine sediments and facilitate extensive epifaunal cover that is dominated by *Cliona* spp. sponge and northern star coral, *Astrangia poculata*. Notable are sponge-coral tower or stack formations. Interstices of boulder piles and under boulder-sediment margins provide cover for shelter seeking vagile fauna (cunner *Tautogolabrus adspersus*), tautog (*Tautoga onitis*), black sea bass (*Centropristis striatus*), and

American lobster (*Homarus americanus*). Red and brown macroalgae are common in the shoaler portions of the formation. At the base of the steep slope is a coarse grain sediment step and then a deeper sloping mixed sand cobble sediment with an extensive cover of *Crepidula fornicata* with epibionts.
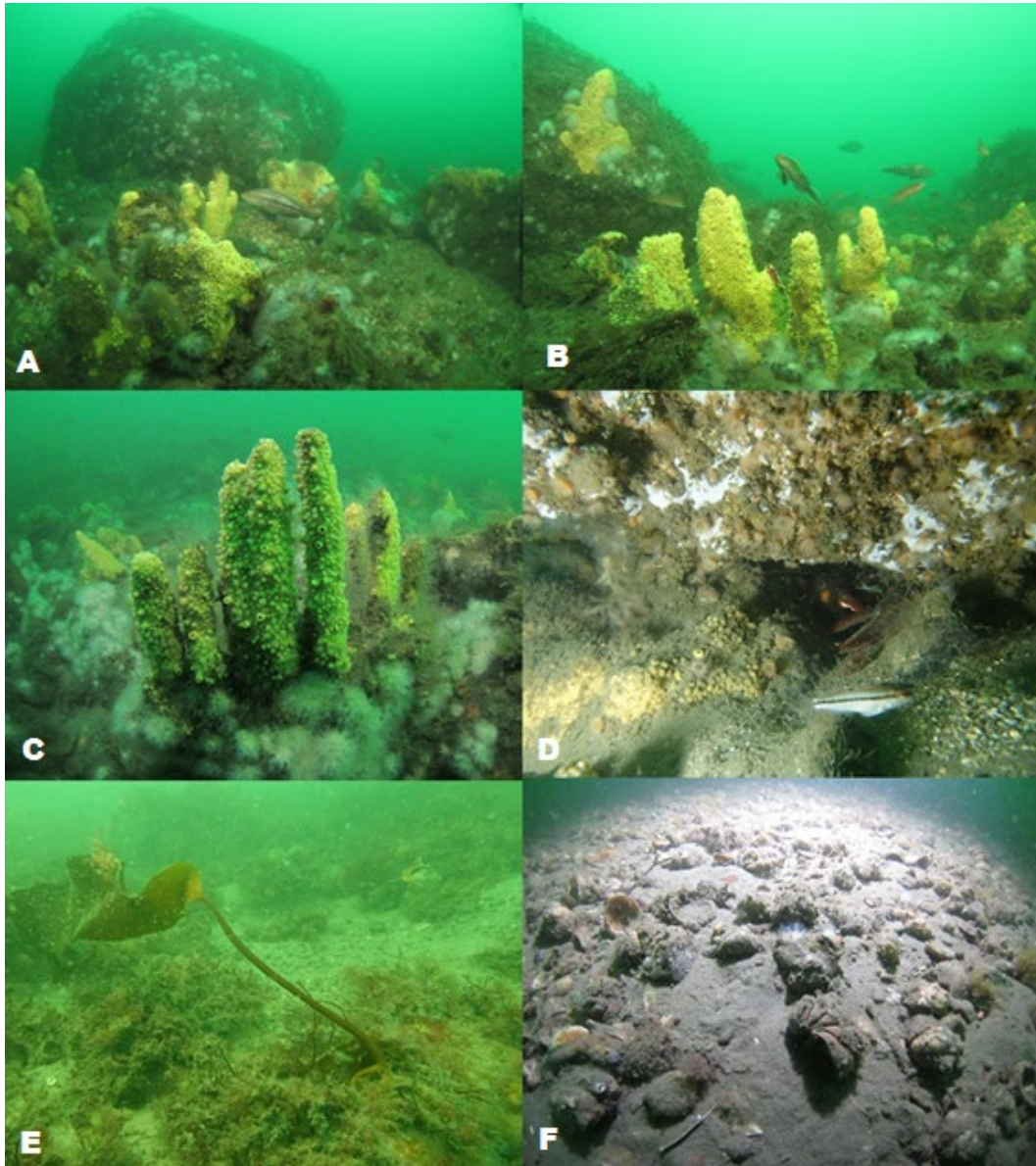
Figure 5.2-98. Ellis Reef (SB-71). A. Rock fall region along the slope of Ellis Reef with gravel-boulder substrate. Extensive epifaunal coverage is dominated by Cliona spp. sponge and star coral Astrangia poculata; B. The habitat formed by geologic and biologic elements are used by wide size classes of rock reef species, including black sea bass (Centropristis striata) and cunner (Tautogolabrus adspersus) as in image; C. Notable are sponge-coral towers or stack formations; D. Interstices of boulder piles and at boulder-sediment margin provide cover for shelter seeking vagile fauna; E. Red and brown macroalgae are common in the shallower portions of the upper slope and platform of the formation; F. At the base of the steep slope is a coarse grain sediment step and then a deeper shallow sloping mixed sand cobble sediment with an extensive cover of Crepidula with diverse epibionts including star coral.

Ram Island Reef (SB-70)

Ram Island Reef (Figure 5.2-99), to the south of Ram Island, is composed of a silt-coarse sand

substrate with scattered and piled boulders to approximately 2 m longest diameter. The area is characterized by a central channel bounded by dual boulder crests reaching less than 2 m depth at the peak. Boulder-cobble substrate slopes downward towards the center of the crests. Current velocity is enhanced due to topography and facilitates clearing of rock surfaces for settlement and growth of diverse macroalgae and attached invertebrates.
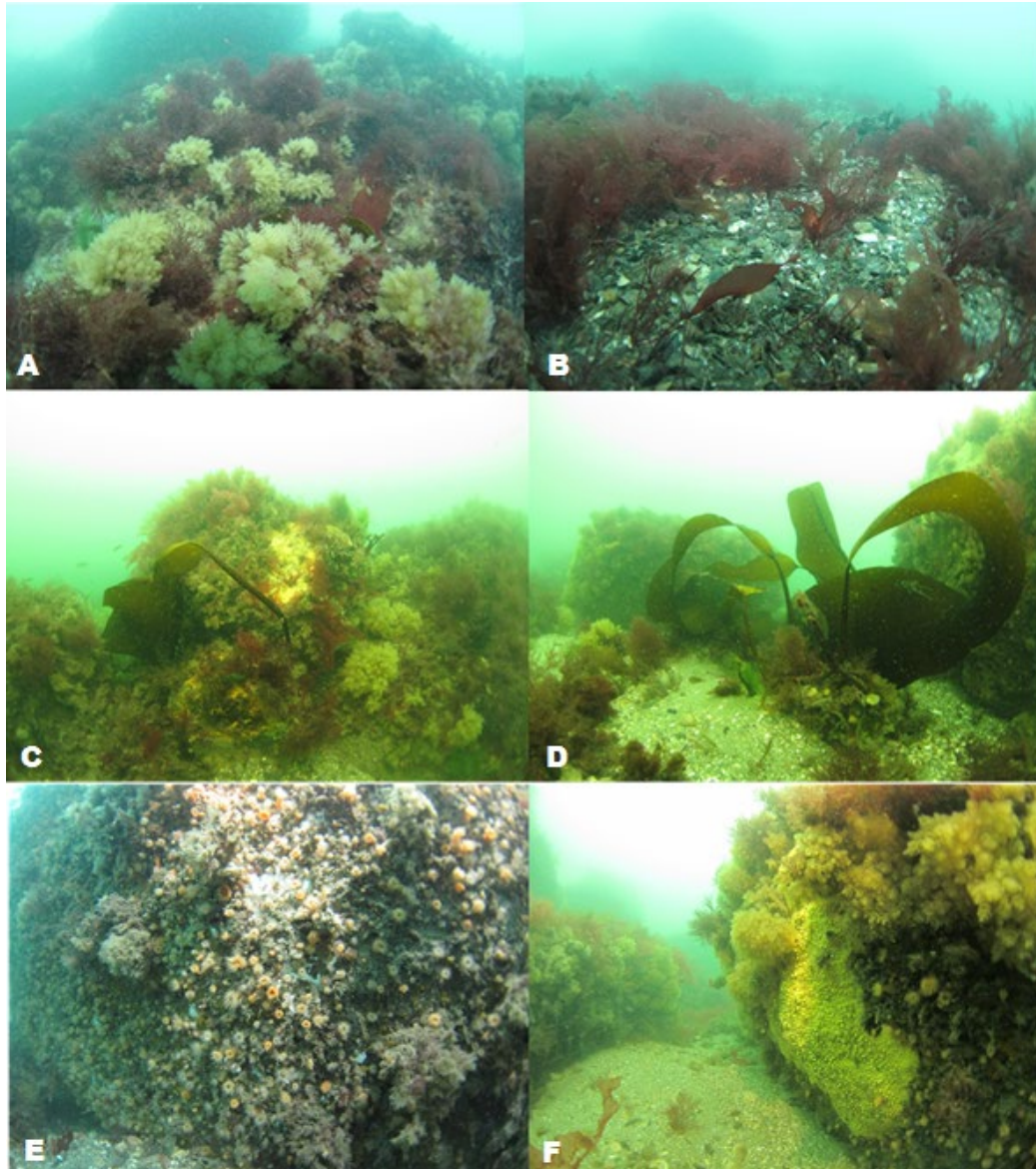
Figure 5.2-99. Ram Island Reef (SB-70). A. Mixed red macroalgae (Rhodophyta), tufted bryozoans (Bugula turrita), and other invertebrates beneath the algal-bryozoan canopy on boulder surfaces; B. Shell debris in a small sediment basin at the base of a boulder slope; C. Kelp (Saccahrina) attached to hydrozoan-bryozoan tufts on a boulder; D. Kelp attached to cobble-pebble in coarse sand; E. Anemones Diadumene leucolena and associated invertebrates on a boulder surface shaded from direct sunlight and canopy of macroalgae above the top of this image; F. Extensive Cliona spp. colony and associated invertebrates at an undercut location shielded from direct sunlight and free of macroalgae.

Black Ledge (Shallow water mapping site)

Black Ledge (Figure 5.2-100) is shallow coarse sediment and gravel-boulder platform located approximately 1 km offshore and to the southeast of the mouth of the Thames River. The shallow

peak, with a portion exposed at low water to approximately 4 m, covers an area of about 1 km^2 and is exposed to high current velocities (Egan & Yarish, 1990, this report). Nearly monthly observations of Atlantic kelp *Saccharina longicruis* density from 1985-1987 (Egan & Yarish, 1990) found seasonal variation based on recruitment and growth patterns. Observations during this study (August 2018) demonstrate density is significantly lower (mean density < 3 blades m^{-2}) compared to approximately 300 blades m^{-2} in the 1980s.

Figure 5.2-100. Black Ledge (Shallow water mapping site). Top: Dense but patchy stand of Saccharina longicruis, surrounded by algal tufts; Bottom: Single kelp blades attached to invertebrate tufts and not to underlying boulder surface. Such attachment increases susceptibility to dislodgement from high storm generated surge and current.

Varved Lake Clays and Deltaic Deposits (SB-39)

An area off the Connecticut River with varved lake clays and deltaic deposits exposed at the sediment surface (Figure 5.2-101; see Lewis & Stone, 1991 for an extensive treatment of seafloor structure due to post-glacial processes).
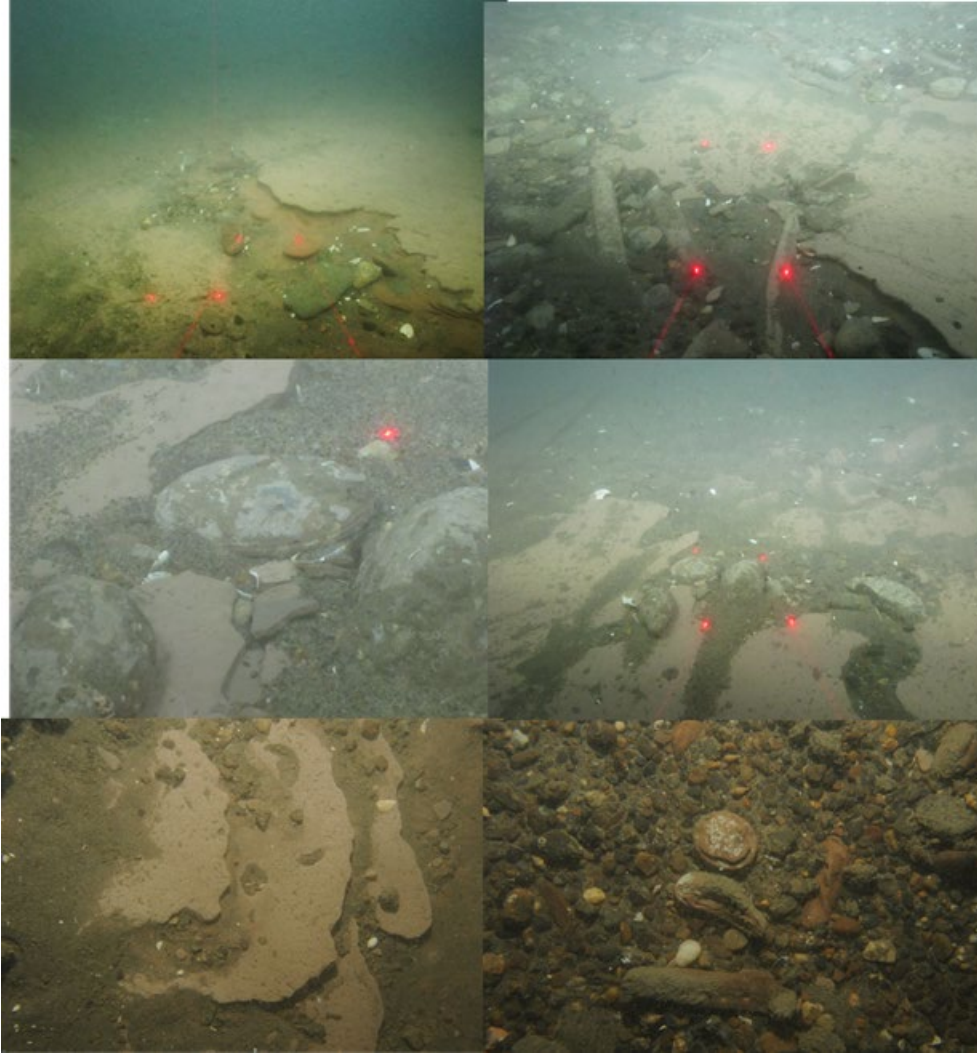
Figure 5.2-101. Varved clay and deltaic deposits off the mouth of the Connecticut River (SB-39). Exemplars of exposed deposits.

Deep Boulder Moraines (NB-42 and SB-56)

Boulder dominated habitats were formed by glacial transport processes and can be part of moraines from the last glaciation (Figure 5.2-102 & Figure 5.2-103; see Lewis & Stone, 1991). Boulder and more extensive gravel surfaces serve as sites for diverse epifaunal communities with composition influenced by angle to the seafloor (i.e., from horizontal to vertical) and angle to dominate currents.
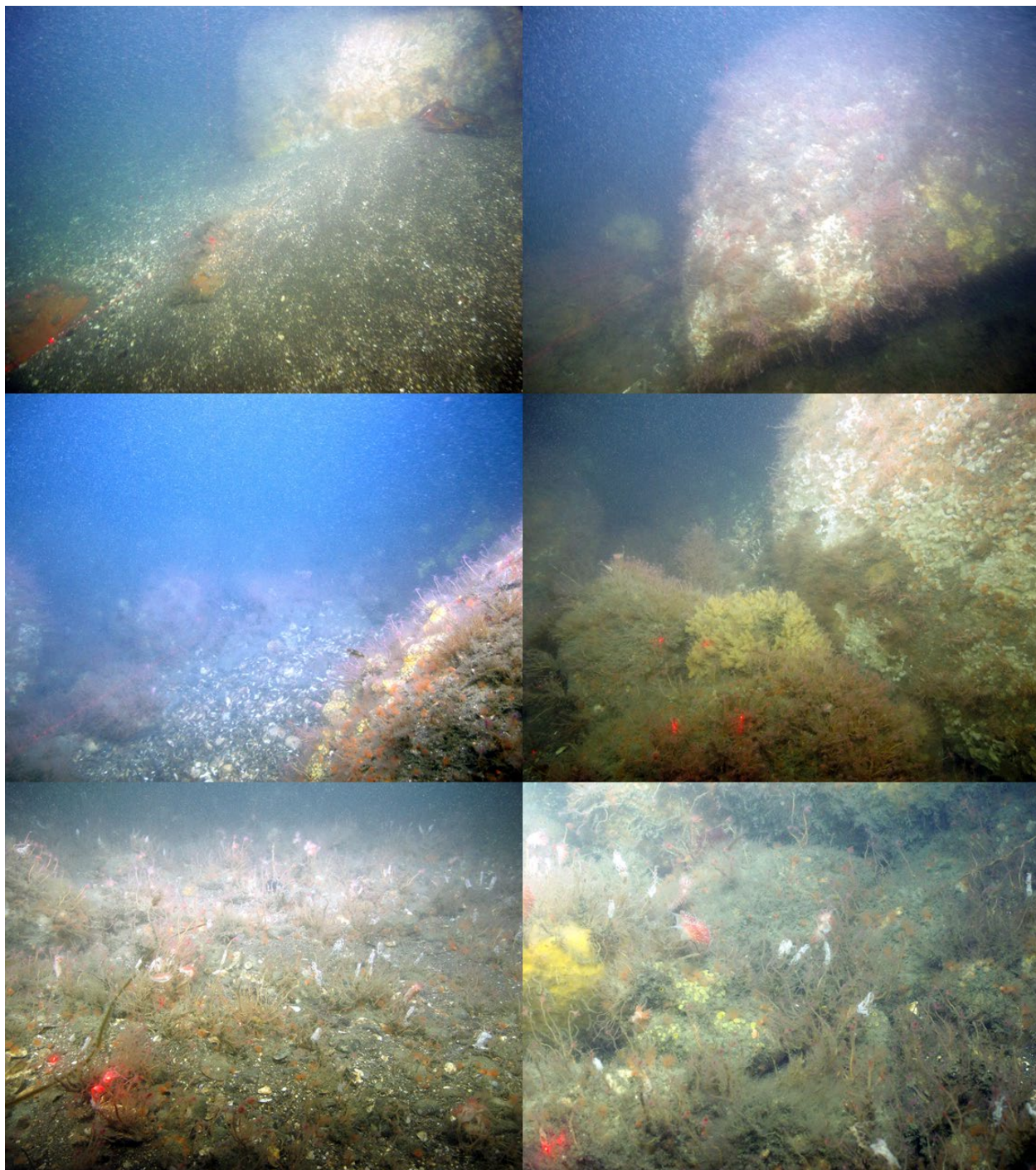
Figure 5.2-102. Images from NB-42 illustrating the glacial boulder-dominated landscape and associated fauna in deep mid-Sound region
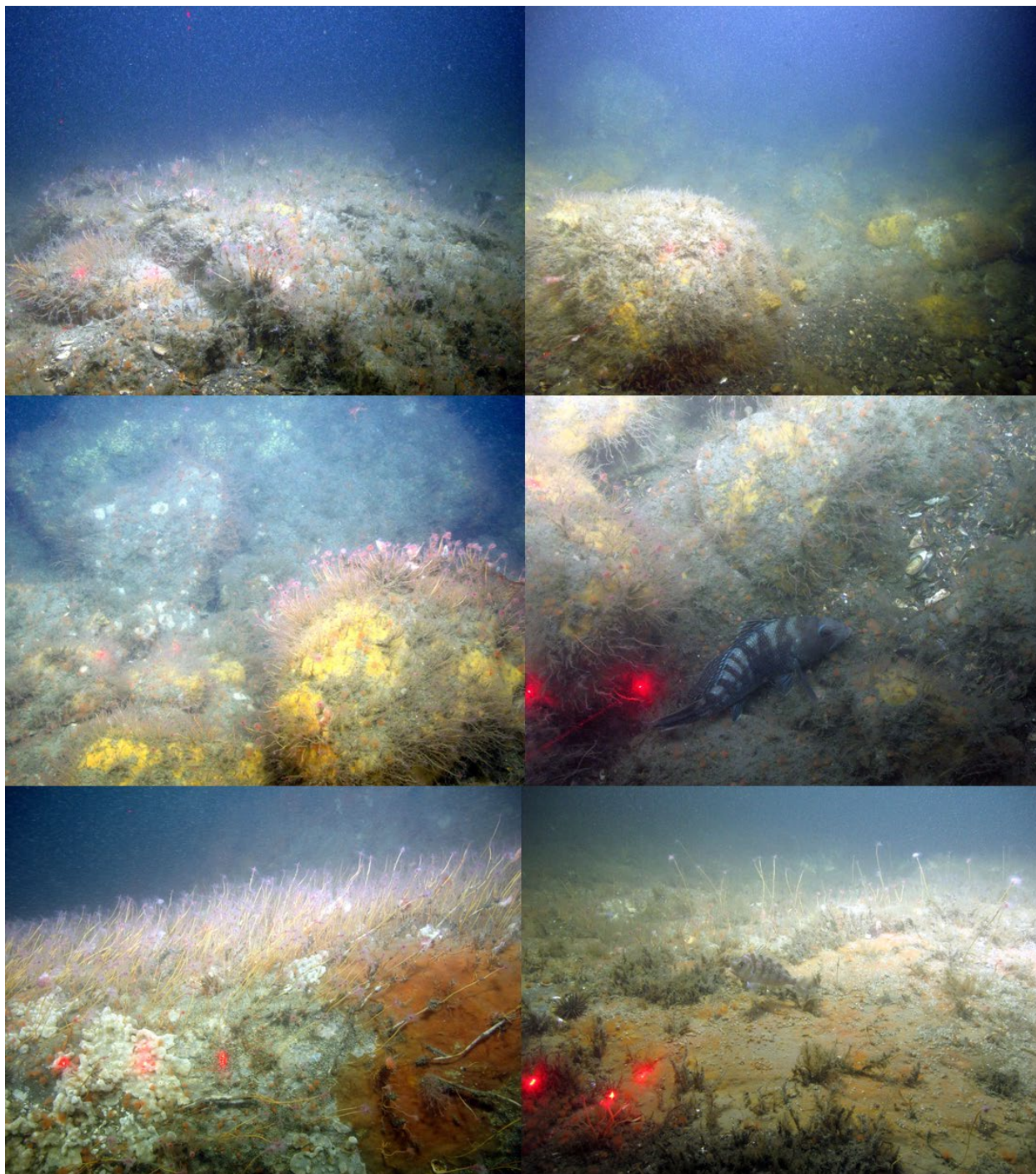
Figure 5.2-103. Images from SB-56 illustrating the glacial boulder-dominated landscape and associated fauna in deep mid-Sound region

South of The Race (SB-66)

The Race, a depression along a moraine segment that stretches from Orient Point to Fishers Island, is inferred to be the extant form of the spillway for glacial Lake Connecticut and is the eastern opening to LIS (Figure 5.2-104; see Poppe et al., 2006 and references therein). The area has been described as a complex habitat of steep sedimentary habitats with boulder-gravel deposits and

extreme current velocities. The circulation through The Race, in part influenced by the rapid changes in depth and constriction of west and east walls of the sloping seafloor and between landforms, produces a tidal forcing. This forcing produces larger scale gyres that transport offshore water from BIS westward through the Race and along the north shore of LIS and brackish estuarine water from the western sound eastward along the southern shoreline. These conditions transport propagules from communities over a wide region and deliver them to a diversity of seafloor habitats based on sediment and outcrop characteristics and orientations. Hard rock surfaces were densely colonized along the transect site on the east slope.
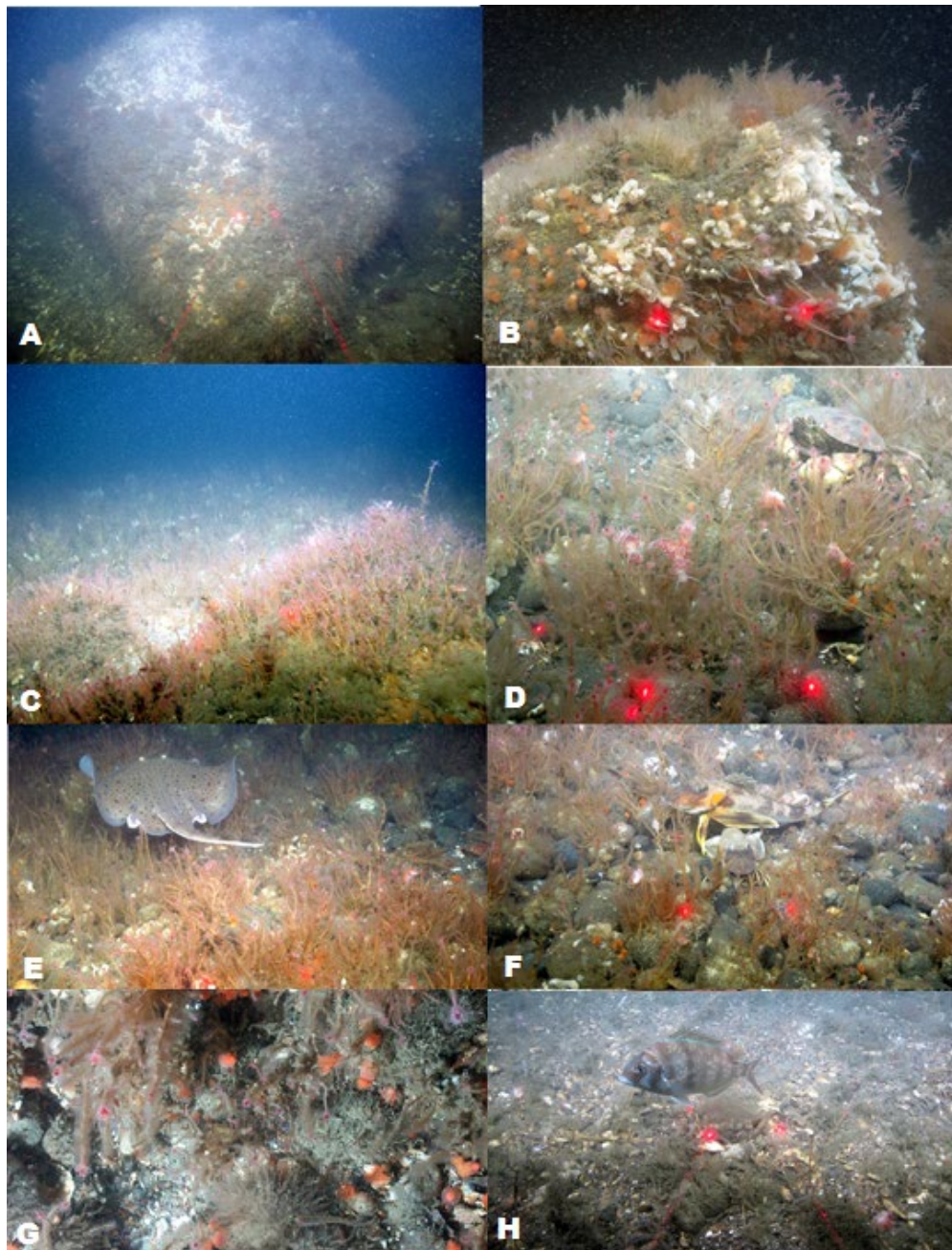
Figure 5.2-104. South of Race Rock (SB-66). A-C. Boulders and coarse gravel with high cover of hydroids and bryozoans characteristic of this area; D-G. Diverse vagile species utilize this habitat for shelter and to forage for prey; H. A young-of-year fish typically using the gavel-biogenic habitat for shelter from currents and predators.

Boulder deposits on the south side of Fishers Island are the southern extent of a glacial moraine. The hard rock surfaces are within depths to sustain photosynthesis and support extensive macroalgal and invertebrate communities (Figure 5.2-105).
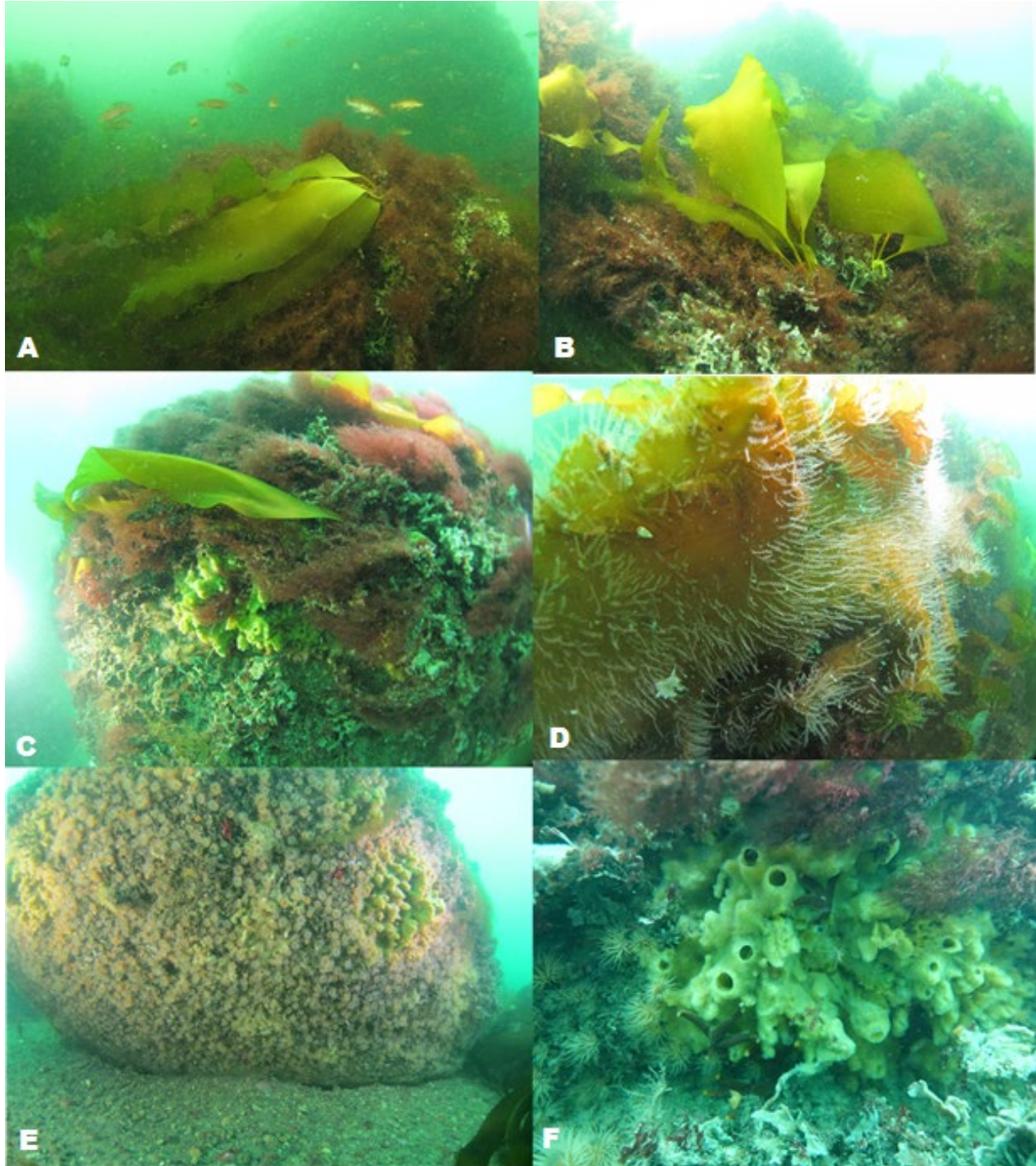
Figure 5.2-105. South of Fishers Island (SB-39). A-C. Kelp blades streaming in the direction of current, shading understory macroalgae and invertebrates; D. Epifaunal hydroids attached to kelp blade; E-F. Understory and shaded epifauna.

5.2.4 Integrated Ecological Characterization

5.2.4.1 Overview and approach

The ecosystem dynamics of the seafloor and bottom waters are shaped by both the infaunal and epifaunal communities that are found in any particular habitat/bottom type. Both sets of organisms are critical in seafloor and demersal food webs, and are often key ecosystem engineers generating a variety of habitats, both when live and dead (e.g., shell hash from bivalves) that are critical to different life stages of the full biotic diversity of the seafloor. Thus, being able to determine patterns of joint infaunal and epifaunal community structure can provide insights into ecosystem function and also assessments for conservation and management.

In order to show the joint trends in several community characteristics for both infauna and epifauna in the Phase II study area, mean taxonomic richness and mean diversity were calculated at the sampling block (SB) and single sample site (NB) levels and plotted those together in GIS. For the epifaunal data, the mean from all the image data taken along the transect at a particular SB and NB was calculated. For infauna, at the SB sites means were calculated based on the three samples taken within the SB; for the NB sites the value for the one sample taken at that site was used. Abundances were not jointly assessed due to the difference in how the number of total individuals within a sample was measured for the infauna (number per sample area) and epifauna (percent occurrence).

5.2.4.2 Taxonomic Richness

Up to 47 different taxa were found in the infaunal samples compared to approximately 11 for epifauna in the images analyzed. These differences reflect how data was collected from either the sediment or image samples (see Section 5.2.2 & Section 5.2.3 for detailed methodologies). As such, these integrated characterizations reflect the relative values given the sampling differences. There were several sections of the Phase II study area where both infaunal and epifaunal taxonomic richness was high; these included areas around Fishers Island, just south of the Thames River, within and south of Niantic Bay and an area just north of Plum Island (Figure 5.2-106). Areas that had high epifaunal taxonomic richness and relatively low infaunal richness included an area in the eastern portion of Fishers Island Sound, and in the central – southern portion of the study area. Areas that had low taxonomic richness for both community types were located within the Race in the southeast corner of the study area, and also south of the Connecticut shore between the Connecticut River and Niantic Bay extending into the central portions of the Phase II area. There were also several single locations with both low epifaunal and infaunal taxonomic richness such as in the sand wave fields along the southwest border of the study area.
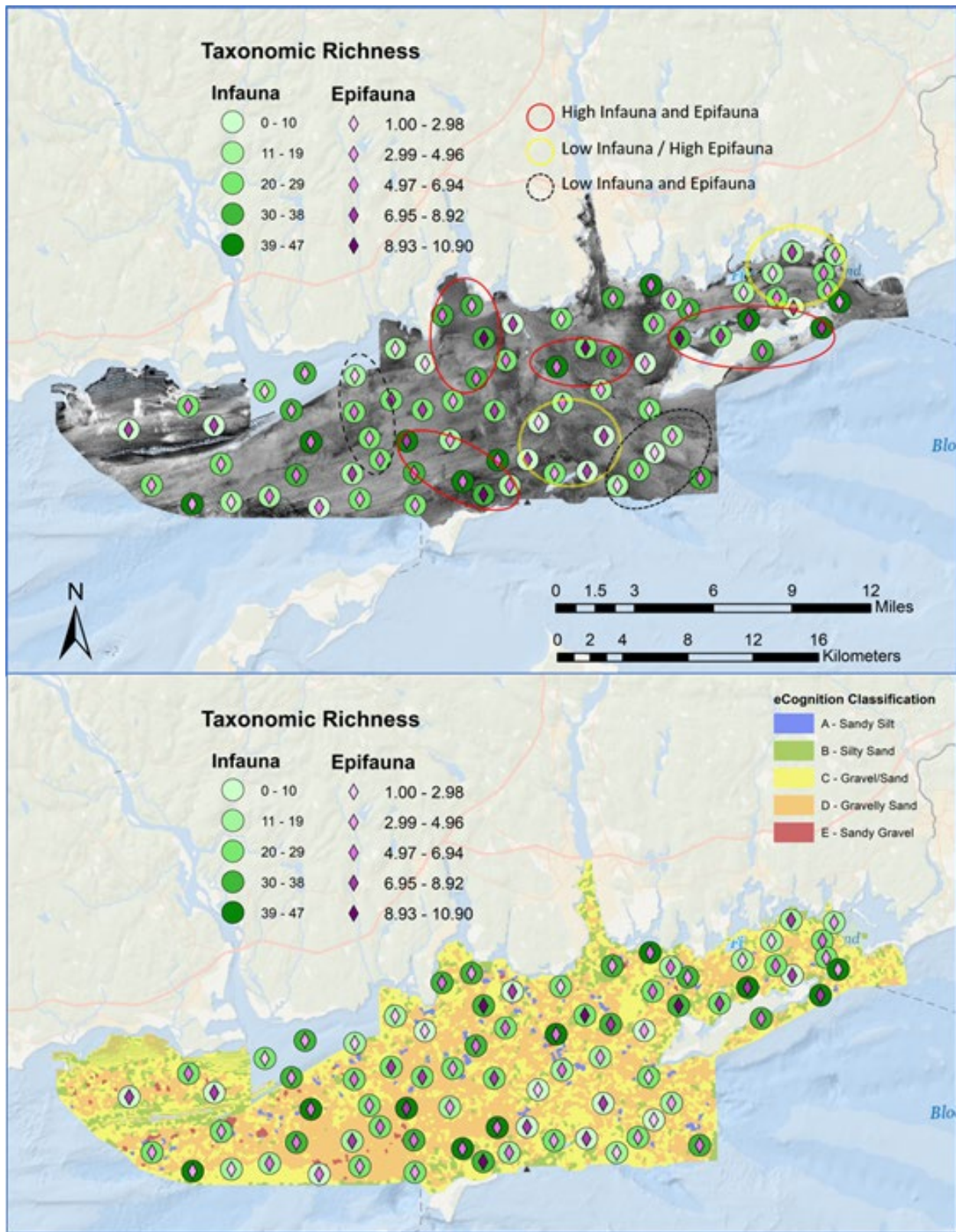
Figure 5.2-106. Comparisons of infaunal and epifaunal taxonomic richness in the Phase II study area in ELIS. Both figures show the same data with the top using the backscatter mosaic as a background and the lower using the distribution of acoustic patch types. Encircled areas (top) indicate general trends in taxonomic richness; these trend polygons were removed from the bottom figure for clarity. See text for details.

5.2.4.3 Diversity

The Shannon diversity index, H', which was calculated for both communities is a metric that assesses both species richness and relative abundance of the taxa found within the sample. The values generally range from <1 in less diverse communities to ~3 in highly diverse communities. As such, diversity values for infauna and epifauna are relatively more comparable than the taxonomic richness values assessed above. Overall, diversity values were relatively low for both the infauna and epifauna (Figure 5.2-107). There were several portions of the study area that had both relatively high infaunal and epifaunal diversity, which were similar to that for taxonomic richness (Figure 5.2-106) but generally covered a larger area–for example, that around Fishers Island and south of the Thames River. There is also a large area in the central portion of the study area. Epifaunal diversity was relatively high compared to infaunal diversity generally in the southeast portion of the Phase II study area. Locations where diversity was low for both infauna and epifauna included the eastern portion of FIS, and several areas in the western most portion of the study area, where large sand wave fields are located.
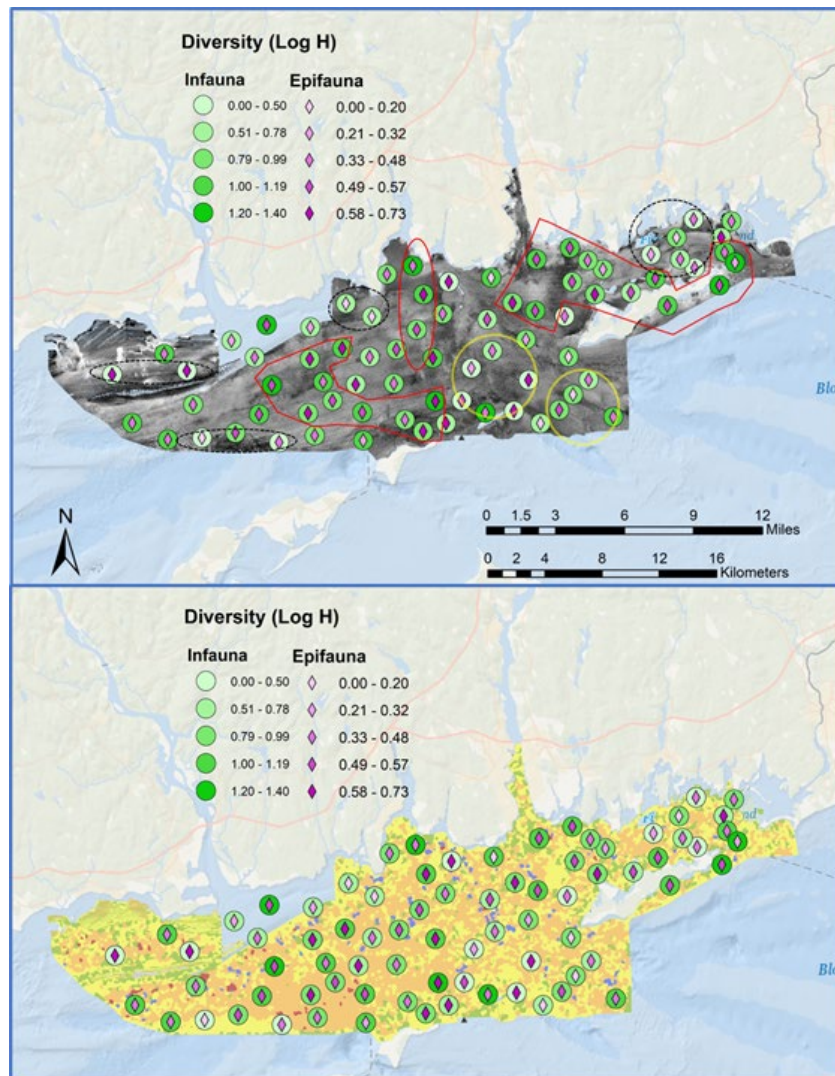
Figure 5.2-107. Comparisons of infaunal and epifaunal taxonomic richness in the Phase II study area in ELIS. Enclosed areas indicate general trends in taxonomic richness; symbology as in Figure 5.2-106. Both figures show the same data with the top using the backscatter mosaic as a background and the lower the distribution of acoustic patch types.

5.2.4.4 Integrated Habitat Map

An integrated habitat map (Figure 5.2-108) links acoustic patch types to the defining ecological and generalized physical characteristics of biogenic features, infauna, and epi- and emergent fauna. It is notable that patterns of faunal composition and abundance (cover) follow the general grain size composition that is evident in the acoustic patch types (i.e., finer to coarser sediments) along with the concomitant physical attributes. The ecological pattern in this area comports with the similarity of sediment composition (a gradient of sand-gravel) such that patterns of diversity and dominance shift across patches but are drawn from a similar species pool. Depth, tidal stress, and related measures are correlated with such changes (e.g., acute versus chronic stresses and small versus large spatial scales; (Auster & Langton, 1999; Grabowski et al., 2014).

Patch type A - *Physical:* Generally shallow, low complexity, low energy. *Biogenic:* Lowest coverage of shell, low *Zostera* debris; *Infaunal taxa:* Tube building and burrowing fauna, molluscs, *Ampelisca*, bamboo worms, burrowing anemones; *Epi- emergent- taxa:* Low hydrozoan-bryozoan turf, high *Crepidula*, high *Cliona*, high Rhodophyta (some shallow sites).

Patch type B - *Physical:* Moderate depths, moderate to high complexity, low to moderate energy. *Biogenic:* Low-mod shell coverage, moderate *Zostera* and terrestrial debris; *Infaunal taxa:* Tube building and burrowing fauna, hermit crabs, amphipods, bamboo worms, burrowing worms, sand dollars; *Epi-emergent- taxa:* Low-mod hydrozoan-bryozoan turf, low *Astrangia*, low *Crepidula*, low *Mytilus*, *Diadumene*, *Corymorpha* (winter-spring), *Cliona*, high Rhodophyta cover at some shallow sites.

Patch type C - *Physical:* Deepest, highest complexity, moderate to high energy; *Biogenic:* Moderate shell coverage, moderate *Zostera* and terrestrial debris; *Infaunal Taxa:* Tube building and burrowing Fauna, molluscs, *Astarte* spp., amphipods. bamboo worms, burrowing worms, sand dollars; *Epi- emergent- taxa:* Moderate hydrozoan-bryozoan turf, moderate *Astrangia*, moderate *Crepidula*, moderate *Mytilus*, *Diadumene*, moderate *Corymorpha* (winter-spring), *Cliona*, moderate *Rhodophyta* (some shallow sites).

Patch type D - *Physical:* Deep, moderate complexity, highest energy; *Biogenic:* Mod-high shell coverage, low *Zostera* and terrestrial debris; Infaunal Taxa: Molluscs, *Astarte* spp., tube building and burrowing fauna, amphipods, bamboo worms, sand dollars. *Epi- emergent- taxa:* Moderate-high to highest *Astrangia*, moderate *Crepidula*, high *Mytilus*, high *Diadumene*, moderate *Corymorpha* (winter-spring), *Cliona*, moderate *Rhodophyta* (some shallow sites).

Patch type E - *Physical:* Shallow to moderate depths, low complexity, high energy; *Biogenic:* Highest coverage of shell; *Infaunal taxa:* Molluscs, *Astarte* spp. tube building and burrowing fauna, ophiuroids, sand dollars; *Epi- emergent- taxa:* Highest hydrozoan-bryozoan turf, high *Astrangia*, low *Crepidula*, moderate *Mytilus*, high *Corymorpha* (winter-spring).

Figure 5.2-108. Integrated Habitat Map for the Phase II study area. Descriptors below summarize the main habitat and ecological characteristics of each acoustic patch type

5.2.5 Seafloor/Habitat Classification

5.2.5.1 Overview and Classification Approach for the Phase II Area

Over the past decade there have been considerable efforts to integrate information from seafloor mapping and associated geological and ecological studies to develop and apply habitat/ecological classification systems (Greene et al., 1999; Mumby & Harborne, 1999; Allee et al., 2000; Auster et al., 2009; Verfaillie et al., 2009; Guarinello et al., 2010; FGDC, 2012). The overarching goal of such systems is to provide a common, hierarchical typology that classifies seafloor habitats and ecological systems across a broad spectrum of spatial scales, from 1000's of km^2 to the spatial extent of a single sample, and in turn provide a consistent framework for assessment and management of seafloor environments.

In 2012, CMECS was adopted by the Federal Geographic Data Committee (FGDC). This system is comprised of multiple classification components within the context of Biogeographic and Aquatic Settings (Figure 5.2-109). These include Water Column, Geoform, Substrate, and Biotic components, each of which can have a number of modifiers (Figure 5.2-110 & Figure 5.2-111) providing specific descriptors. Together these form a biotope for the specific setting.
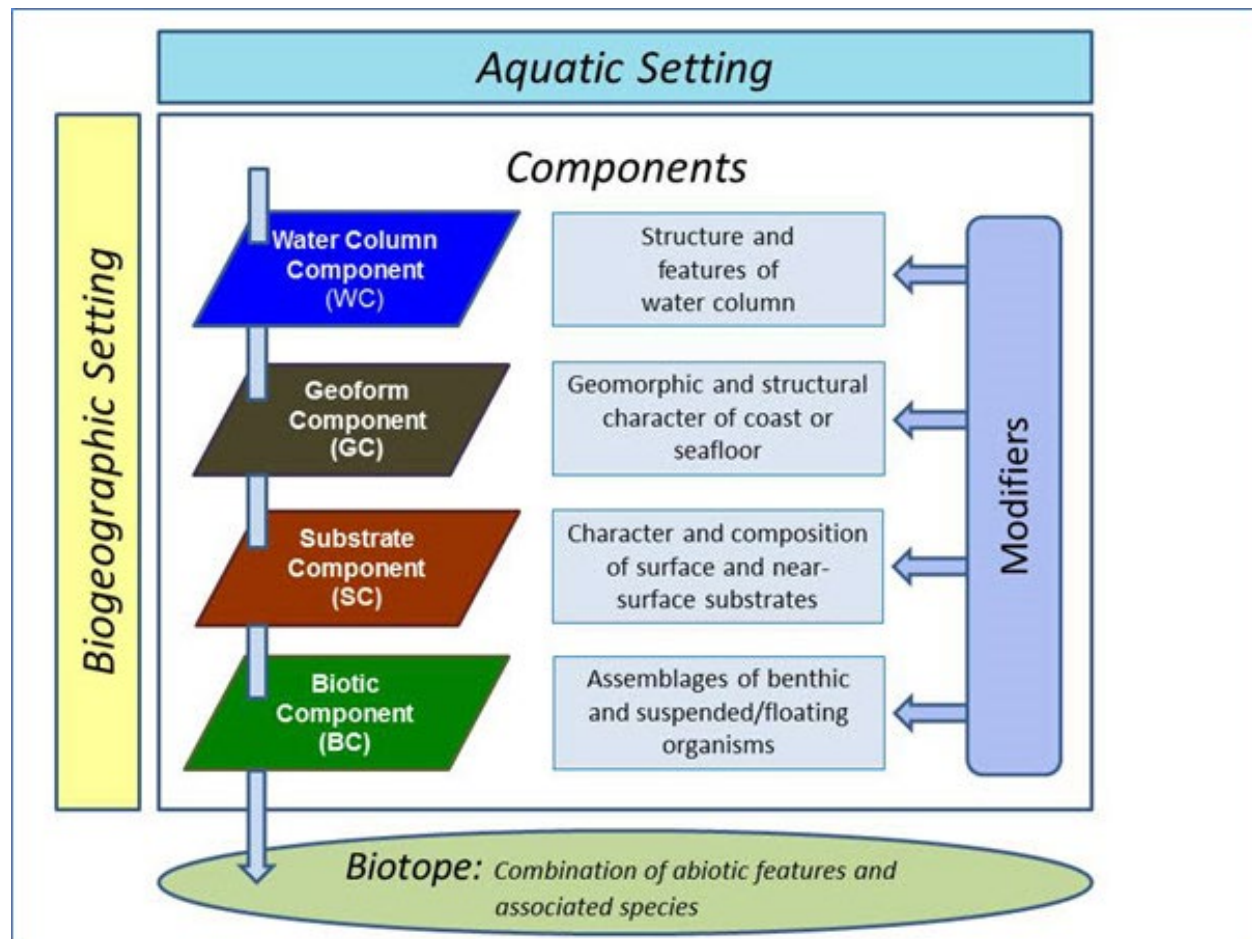
Figure 5.2-109. Overall organization of CMECS including hierarchical components and their modifiers
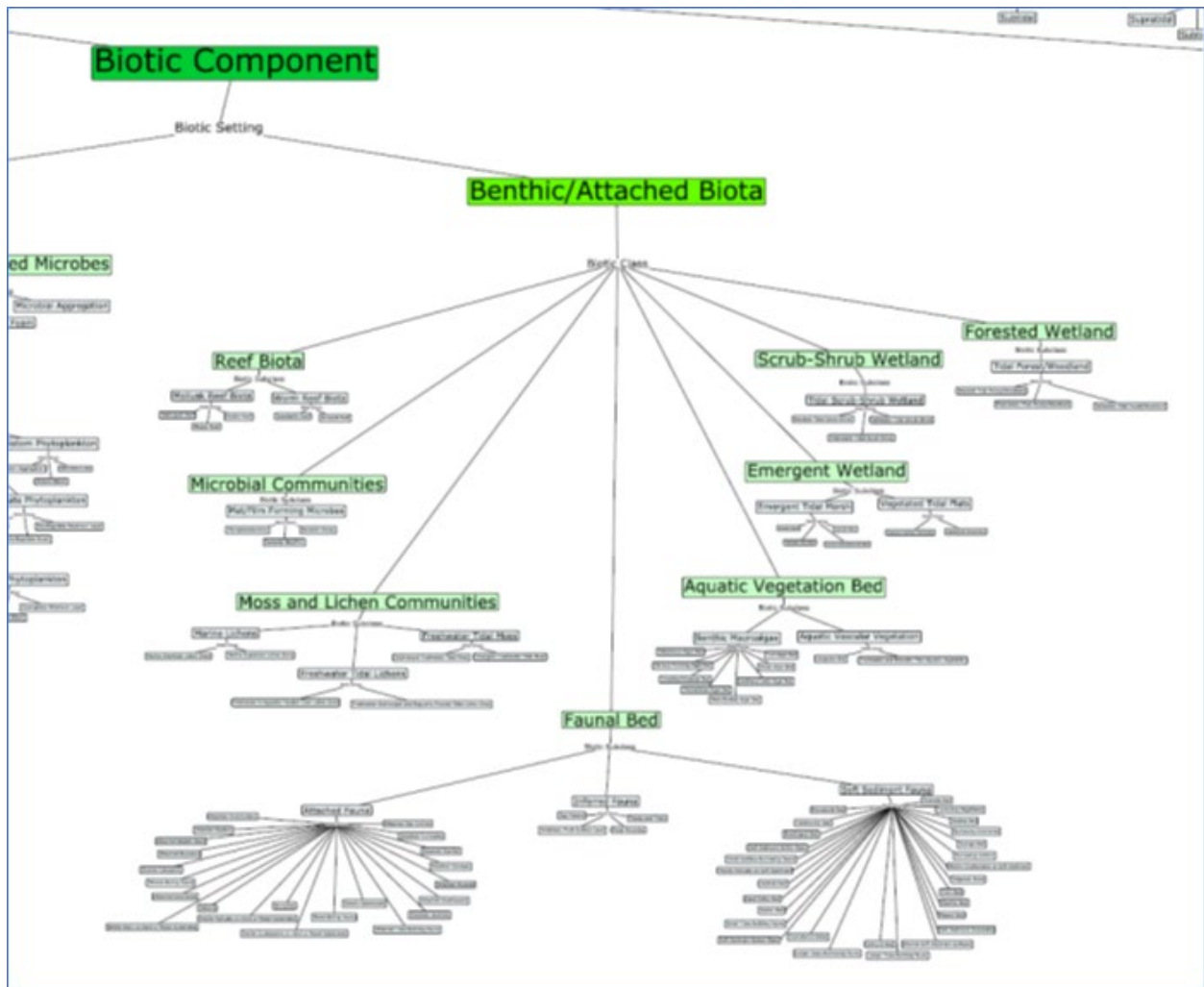
Figure 5.2-110. Biotic component modifiers in the CMECS classification system for the Benthic/Attached Biota biotic setting
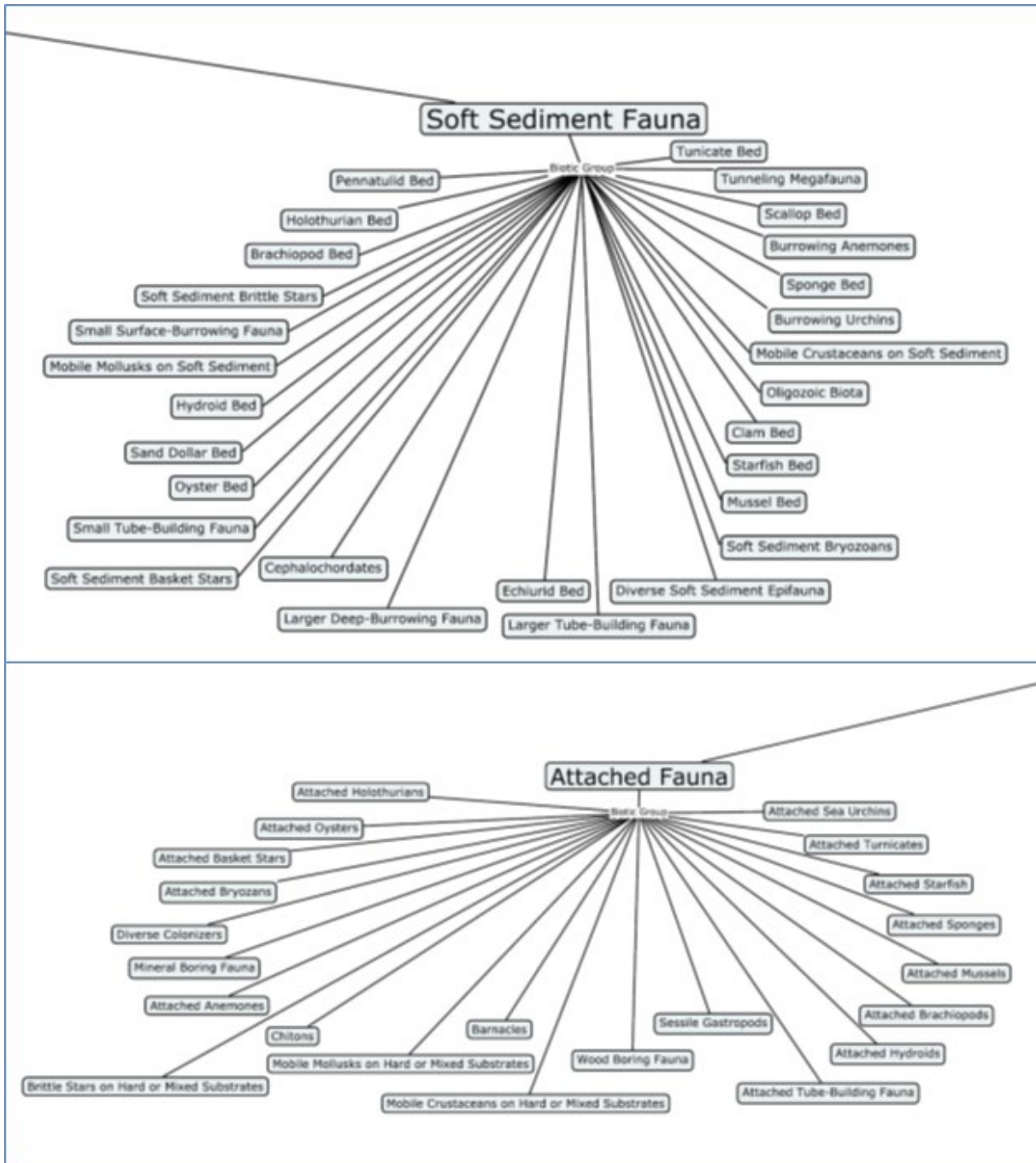
Figure 5.2-111. Detailed view of Biotic Sub-classes for the Attached Fauna and Soft Sediment Fauna for the Faunal Bed Biotic Class in the CMECS Classification system showing suggested modifiers

CMECS has been applied and assessed for a variety of marine environments (e.g. Keefer et al., 2008; Ackerman et al., 2015; Bassett et al., 2017; Mittermayr et al., 2020). These studies demonstrate the utility of CMECS, and collectively add to the catalogue of seafloor environments that have been classified using this standard. They also provide suggestions on how to improve CMECS and recognize that the component subgroups and modifiers need to be flexible so that the environmental and ecological characteristics of a specific area can be effectively portrayed at different spatial scales and be relevant to management efforts.

Sub-components and modifiers included in the CMECS documentation do not necessarily apply in all seafloor environments, which was recognized by its developers, so our approach was to adhere to the extent possible to CMECS modifiers but also to define our own as necessary to accurately describe biotic components specific to the Phase II area. Our selections of sub-components and modifiers for the classification are based on the in-depth analyses conducted of the infaunal (Section 5.2.2.2) and epifaunal (Section 5.2.3.2) communities, as well as the analyses of the sediment and environmental data associated with characterization of the seafloor patch structure (Section 5.1).

We developed CMECS classifications at two levels of resolution, at the sample level and at the acoustic patch level. At the sample level this included CMECS classifications for both infauna (based on analyses of grab samples; see Section 5.2.5.2) and epifauna (based on analyses of digital images; see Section 5.2.5.3). Having classifications for both groups of biota provides for more detailed information at the scale of a sample site (infauna) and image transect location (epifauna). At the acoustic patch level (see Section 5.2.5.4), we integrated these two sets of data to provide an overall CMECS class at this greater spatial resolution.

5.2.5.2 Infauna

The CMECS classification for each infaunal sample site includes several standard CMECS component modifiers and study-specific, Biotic Group modifiers for the Biotic Sub-class (Table 5-21 & Table 5-22). The Biotic Group modifiers (types) in Table 5-22 were based on data for each of the samples and were developed by assessing the dominant taxa and their general functional characteristics. Also included are two additional components, Biotic Community and Other Elements. The Biotic Community component lists the specific and or common names of the dominant taxa making up the community at that sample location. These are given in decreasing relative abundance. The Other Elements component provides some additional information regarding taxa of interest, such as deep burrowing crustaceans, and other information such as low overall abundance in the sample.

Table 5-21. CMECS classification components for infaunal communities in the Phase II study area in ELIS

Physical Setting	Sound: Long Island Sound is a sound
Geoform	Basin: The system-scale geologic form of LIS is a basin
Substrate	Varied sediment classes: Types is based on general sediment classification acoustic within which the sample was found[#]
Biotic Setting	Benthic / Attached Biota: CMECS based
Biotic Class	Faunal Bed: CMECS based
Biotic Sub-class	Soft Sediment Fauna: CMECS based
Biotic Group	Varied: Based on dominant taxa in the sample and their functional characteristics; See Table 5-22 for specific descriptions
Biotic Community	Dominant Taxa found given in order of decreasing abundance*
Other Elements	Other taxa of note found in samples / relevant other information

In the Infaunal Communities Phase II GIS shapefile detailed data on sediment composition at each infaunal sample site is also provided including percent composition by weight of general sediment classes (gravel, sand, silt, clay) as well as detailed sediment composition by Wentworth scale phi values

* In the Infaunal Communities Phase II GIS shapefile, there is a column (field) that provides the community type designation (a-m) based on multivariate analyses of the infaunal data; see Section 5.2.2.2 of this report for details.

Table 5-22. Modifiers for the biotic group component of the CMECS classification for infaunal sample sites in the Phase II study area in ELIS. Modifiers were developed based on the data for each infaunal sample location.

Biotic Groups

Clam Bed	Sample dominated by bivalves
Clam Bed / Burrowing Fauna	Sample dominated by bivalves and burrowing fauna, generally polychaetes
Clam Bed / Small Tube Building Fauna	Sample dominated by bivalves and small tube builders, generally spionid polychaetes
Clam Bed / Tube Building and Burrowing Fauna	Sample dominated by bivalves with tube building and burrowing polychaetes of varied sizes
Faunal Bed	No evident dominant taxa
Large Tube Building Fauna	Mostly large tube building fauna such as bamboo worms
Mollusk Bed	Sample dominated by both bivalves and other mollusks
Mollusk Bed / Burrowing Fauna	Sample dominated by both bivalves and other mollusks and burrowing polychetes
Mollusk Bed / Burrowing Fauna /Motile Fauna	as above but with surface motile taxa
Mollusk Bed / Tube Building and Burrowing Fauna	Sample dominated by bivalves and other mollusk with tube building and burrowing polychaetes of varied sizes
Mollusk Bed / Tube Building Fauna	Sample dominated by bivalves and other mollusk with tube building polychaetes
Motile Crustaceans	Sample dominated by surficial motile crustaceans
Motile Gastropods and Crustacea	Sample dominated by gastropods and crustaceans
Motile Surface Fauna	sample with surface motile fauna but no dominant taxa
Ophiuroids / Clam Bed	Brittle stars and bivalves
Sand Dollar Bed	Sample with large numbers of sand dollars
Sessile and Mobile Mollusks	Sample with gastropods and mix of sessile mollusks
Small & Large Tube Building Fauna	Sample dominated by large and small builders such as spionids and bamboo worms
Small Surface-Burrowing Fauna	Sample dominated by small polychaetes usually living just below the surface of the sediment
Small Tube Building Fauna	Sample dominated by tube building polychaete such as spionids
Tube Building Fauna	Sample dominated by a variety of tube building polychaetes
Tube Building and Burrowing Fauna	Sample dominated by a variety of tube building and burrowing fauna
Tube Building and Burrowing Fauna / Clam Bed	Sample dominated by a variety of tube building and burrowing fauna and bivalves
Tube Building and Burrowing Fauna / Mollusk Bed	Sample dominated by a variety of tube building and burrowing fauna and mollusks

Examples of the CMECS classification for several infaunal sample sections are shown in Figure 5.2-112 and Figure 5.2-113. These CMECS classifications are included in the Infaunal Communities Phase II GIS shapefile, which also contains data for total abundance, taxonomic richness, and Shannon Diversity, as well as community type designations. Environmental data (e.g., sediment grain size distributions, depth) are also included in that GIS shapefile.
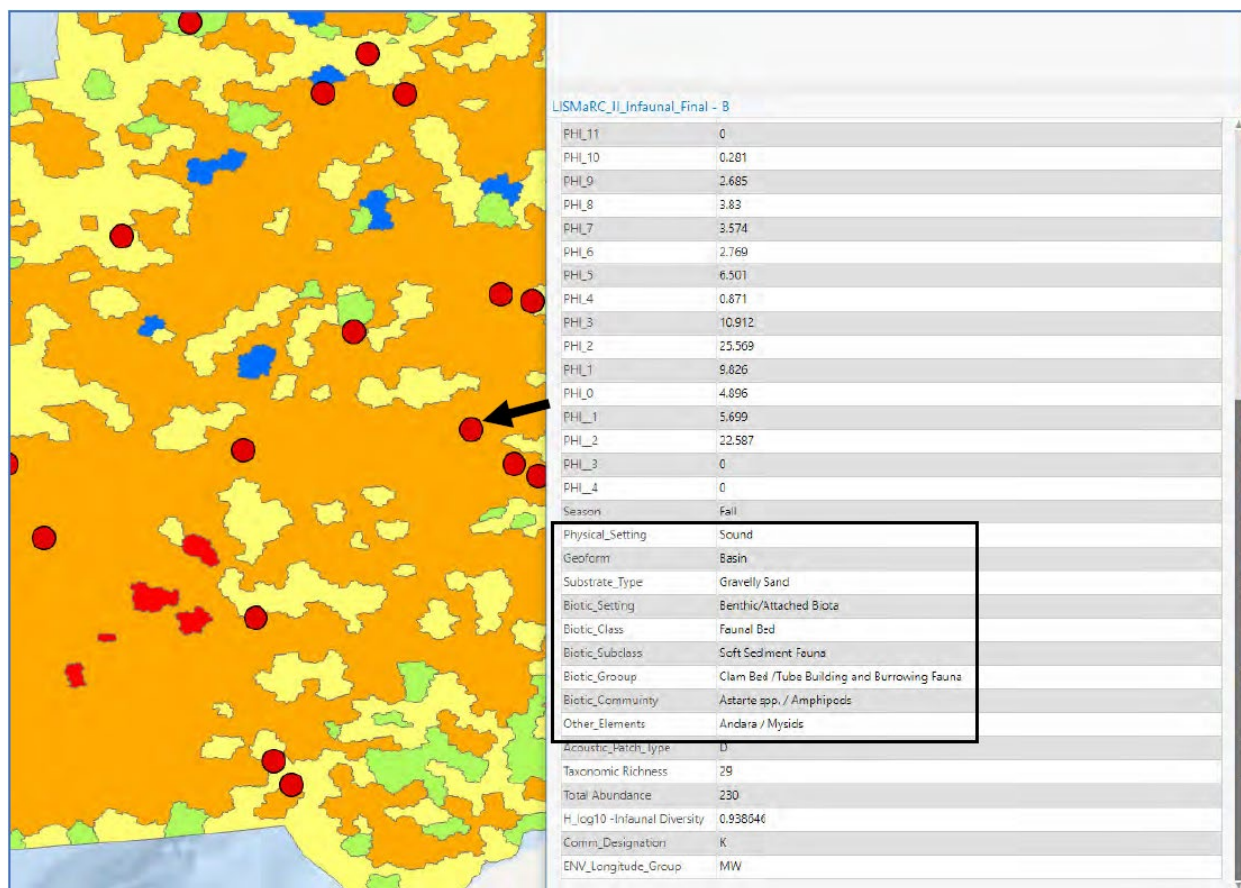
Figure 5.2-112. Example of GIS query of database associated with the Infaunal Community Phase II shapefile showing CMECS classification (in black box) for sample SB51-1. Arrow points to sample location in the middle of the Phase II study area.
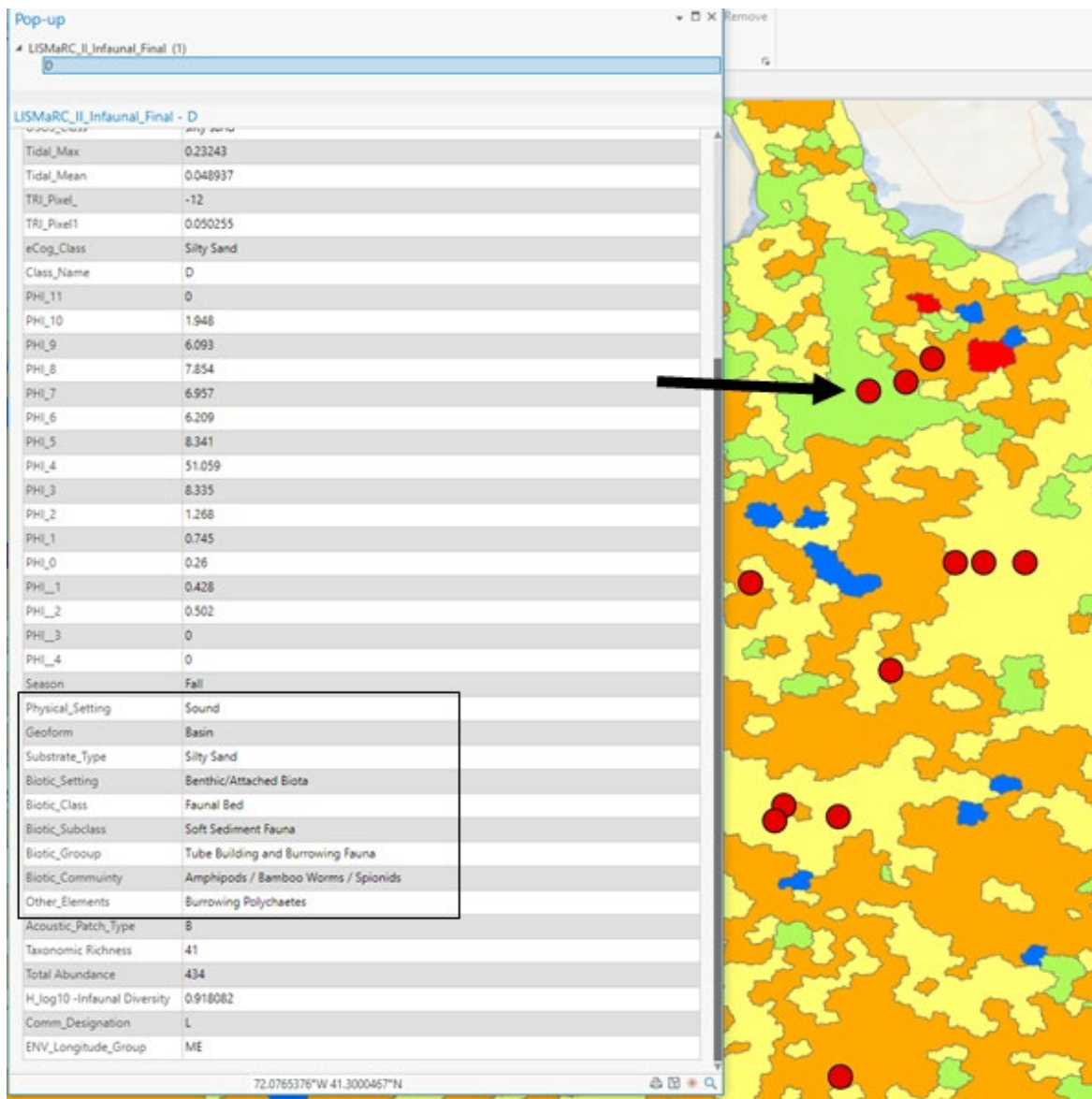
Figure 5.2-113. Example of GIS query of database associated with the Infaunal Community Phase II shapefile showing CMECS classification (in black box) for sample SB64-3. Arrow points to location of sample just south of the mouth of the Thames River.

5.2.5.3 *Epifauna*

The CMECS classification for emergent and epifaunal images includes several standard CMEC component modifiers and study-specific, Biotic Group modifiers for the Biotic Sub-class (Table 5-23 & Table 5-24). The Biotic Group modifiers (types) in Table 5-24 were based on data for each of the image sets for each acoustic patch type and were developed by assessing the dominant taxa, features, and the physical setting in which they occur and their general functional characteristics. These classes were then assigned to each image and the associated acoustic type. The taxa and feature composition for each image sample are associated with the CMECS hierarchical classes.

Examples of the CMECS classification for several image sample sections are shown in Figure 5.2-114 and Figure 5.2-115.

Table 5-23. CMECS classification components for epifaunal communities in the Phase II study area in ELIS

Physical Setting	Sound: Long Island Sound is a sound
Geoform	Basin: The system-scale geologic form of LIS is a basin
Substrate	Varied sediment classes: Types is based on general sediment classification acoustic within which the sample was found[#]
Biotic Setting	Benthic / Attached Biota: CMECS based
Biotic Class	Faunal bed/aquatic vegetation bed (some shallow patches): CMECS based
Biotic Sub-class	Attached fauna/soft sediment fauna/benthic macroalgae (some shallow patches): CMECS based
Biotic Group	Varied: Based on dominant taxa across sample site and their functional characteristics; See Table 5-24 for specific descriptions

Table 5-24. Modifiers for the biotic group component of the CMECS classification for infaunal sample sites in the Phase II study area in ELIS. Modifiers were developed based on the data for each infaunal sample location.

Biotic Groups

Clam Bed	Sample dominated by bivalves
Clam Bed / Burrowing Fauna	Sample dominated by bivalves and burrowing fauna, generally polychaetes
Clam Bed / Small Tube Building Fauna	Sample dominated by bivalves and small tube builders, generally spionid polychaetes
Clam Bed / Tube Building and Burrowing Fauna	Sample dominated by bivalves with tube building and burrowing polychaetes of varied sizes
Faunal Bed	No evident dominant taxa
Large Tube Building Fauna	Mostly large tube building fauna such as bamboo worms
Mollusk Bed	Sample dominated by both bivalves and other mollusks
Mollusk Bed / Burrowing Fauna	Sample dominated by both bivalves and other mollusks and burrowing polychetes
Mollusk Bed / Burrowing Fauna /Motile Fauna	as above but with surface motile taxa
Mollusk Bed / Tube Building and Burrowing Fauna	Sample dominated by bivalves and other mollusk with tube building and burrowing polychaetes of varied sizes
Mollusk Bed / Tube Building Fauna	Sample dominated by bivalves and other mollusk with tube building polychaetes
Motile Crustaceans	Sample dominated by surficial motile crustaceans
Motile Gastropods and Crustacea	Sample dominated by gastropods and crustaceans
Motile Surface Fauna	sample with surface motile fauna but no dominant taxa
Ophiuroids / Clam Bed	Brittle stars and bivalves
Sand Dollar Bed	Sample with large numbers of sand dollars
Sessile and Mobile Mollusks	Sample with gastropods and mix of sessile mollusks
Small & Large Tube Building Fauna	Sample dominated by large and small builders such as spionids and bamboo worms
Small Surface-Burrowing Fauna	Sample dominated by small polychaetes usually living just below the surface of the sediment
Small Tube Building Fauna	Sample dominated by tube building polychaete such as spionids
Tube Building Fauna	Sample dominated by a variety of tube building polychaetes
Tube Building and Burrowing Fauna	Sample dominated by a variety of tube building and burrowing fauna
Tube Building and Burrowing Fauna / Clam Bed	Sample dominated by a variety of tube building and burrowing fauna and bivalves
Tube Building and Burrowing Fauna / Mollusk Bed	Sample dominated by a variety of tube building and burrowing fauna and mollusks

Figure 5.2-114. Example of GIS query of database associated with the Epifaunal Community Phase II shapefile showing CMECS classification (in black box) for sample SB64-3. Arrow points to locations of images.
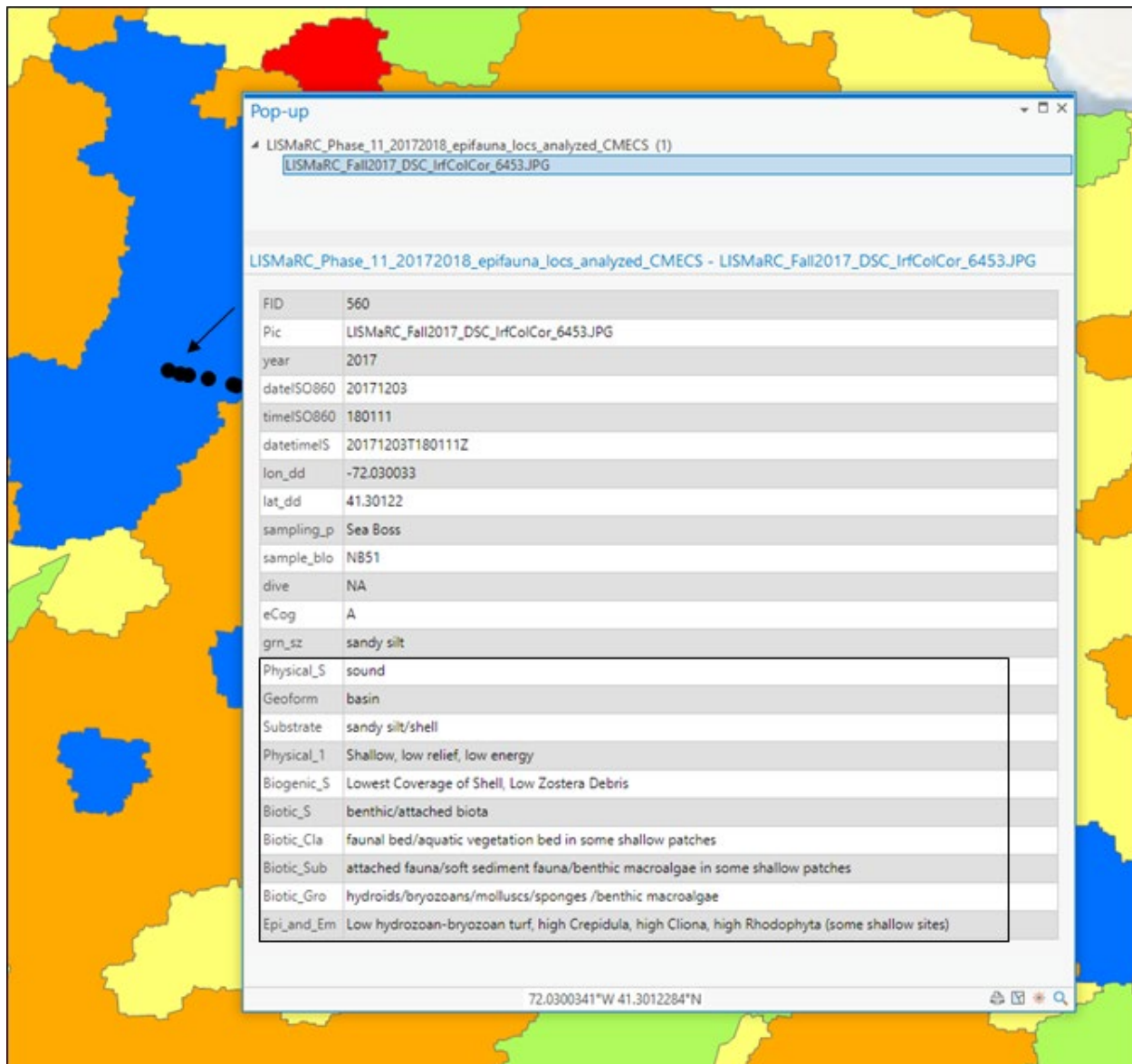
Figure 5.2-115. Example of GIS query of database associated with the Epifaunal Community Phase II shapefile showing CMECS classification (in black box) for sample NB51. Arrow points to locations of images within the acoustic patch.

5.2.5.4 *Acoustic Patch Level CMECS Classification*

The CMECS classifications of the acoustic patch types summarize the results from the analyses of both the infaunal and epifaunal communities and associated environmental characteristics, such as surficial features that are ecologically relevant (see Section 5.2.2.3 & Section 5.2.3.4). Several classification levels were added to provide details about the habitat and ecological characteristics in the acoustic patch types (Table 5-25). To provide more in-depth environmental information about each acoustic patch type two additional classes were added including Physical Setting Notes and Biogenic Surface Features. The Biotic Group class was split into Epi- and Emergent Fauna and Infauna, with both classes having a Notes class to provide information on specific taxa that were dominant in each acoustic patch type. The modifiers in each of these classification levels attempt to encompass both the primary characteristics of biotic communities in the acoustic patch types and, to the extent possible, their variability.

An example of a query showing the CMECS classification for an acoustic patch type is shown in Figure 5.2-116. In some sense the acoustic patch types may be considered as Biotopes as they are classified across all the CMECS components and indeed cover areas larger than that of a grab or photographic sample location. It is important to note that although each patch of a particular acoustic patch type has the same CMECS classification, there is variation in the specific community types and other ecological characteristics found across the Phase II study area. The CMECS classification for the acoustic patch types attempts to capture their general attributes across the Phase II study area. As such, it should be used as a starting point for a more detailed consideration of ecological characteristics in any specific portion of the area using the more in-depth analyses presented in Section 5.2.2.2 and Section 5.2.3.2, and their associated GIS databases.

Table 5-25. CMECS classification components for acoustic patch types in the Phase II study area in ELIS

| Physical Setting	Sound: Long Island Sound is a sound
Geoform	Basin: The system-scale geologic form of LIS is a basin
Substrate	Varied sediment classes: Types are based on general sediment classification of the acoustic patch types but also includes information on surficial features found in photographs, such as the presence of shell
Physical Setting Notes	General characteristics in terms of depth, topographic complexity, and bottom stress energy
Biogenic Surface Features	General incidence of surface features created or deposited by biota and other features that occur in some of the patches of this acoustic patch type
Biotic Setting	Benthic / Attached Biota: CMECS based
Biotic Class	Faunal Bed: CMECS based, noting variations, such as vegetation beds in some shallow areas
Biotic Sub-class fauna	CMECS based: combination of attached fauna / soft sediment/benthic macroalgae depending on patch type and how these may vary by depth
Biotic Group Epi-Emergent Fauna	Varied: General types of dominant taxa in the specific acoustic patch types as determined by analyses (see Section 5.2.3.4)
Epi- and Emergent Fauna Notes	General abundance levels of specific epifaunal taxa, noting any seasonality
Biotic Group Infauna	Varied: General types of dominant taxa in the specific acoustic patch types as determined by analyses (see Section 5.2.2.3)
Infauna Notes	General abundance levels of specific taxa
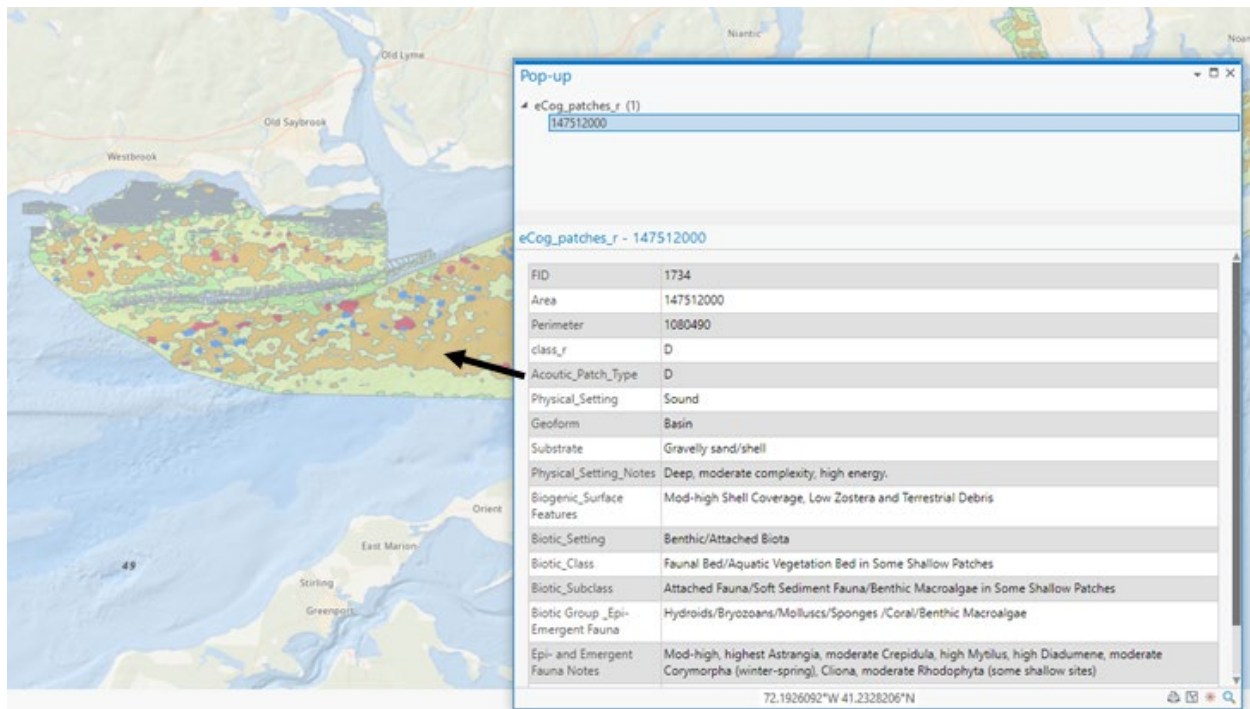
Figure 5.2-116. Example of GIS query of database associated with the Infaunal Community Phase II shapefile showing CMECS classification for acoustic patch D in the central portion of the study area. Arrow points to the acoustic patch being queried.

5.2.6 Overall Discussion and Conclusions

5.2.6.1 Habitat Mapping

The seafloor environment in the Phase II study area is spatially complex, reflecting the mix of large-scale hydrodynamic and geomorphological features that influence its features. In the eastern portion of the study area the major flux of water occurs through the Race, creating strong currents throughout much of the Phase II area and overall erosional/non-depositional and coarse-grained bedload transport sedimentary environments (Knebel & Poppe, 2000). Along the Connecticut shore, outflow from the Connecticut River carries sediment and organic matter into the western portion of the Phase II area and adds complexity to this area's hydrodynamics. The Thames River also is a source of sediment and affects the hydrodynamics of the area south of its mouth and the western portion of FIS, which is also affected by fluxes of water that occur at its eastern end. The influence of these features leads to the sand and coarse sediments that comprise most of the Phase II area (see Section 5.1), and also geomorphological features such as extensive sand waves of various spatial scales in some locations and areas dominated by large rocks and boulders. Areas with finer sediments are generally confined to just south of the mouths of the Connecticut and Thames rivers and in embayments such as Niantic Bay.

The dominance of sands and coarser sediments in the Phase II study area is evident in the backscatter mosaic that was used for the characterization of seafloor habitat structure. Much of the mosaic has a complex pattern of image characteristics that are primarily associated with sandy/harder sediments than that of muddy/finer sediments. This is in contrast to the Pilot project area where there are large areas of muddy sediments that were distinct features in the backscatter mosaic. Seafloor characterization, which can be used as a basis for habitat mapping, can be difficult in an area such as eastern LIS. Difficulties stem from the subtle differences in backscatter returns

in an environment that is primarily comprised of sands/coarse sediments and their varied geomorphologies such as flat beds, sand waves, cobble/ boulder fields, and mixtures of these. Montereale-Gavazzi et al. (2019) found that water column conditions (e.g., complex current patterns) and shifting geomorphology could cause significant backscatter variability, particularly in dynamic sandy and muddy areas. Testing of several supervised classification approaches for backscatter mosaics indicated overall accuracies of around 50% and limitations in discriminating subtle differences between sediment types with only fractional differences in sediment composition at small spatial scales (Diesing et al., 2020). Acknowledging these and other possible image collection, processing and analysis issues that can affect the interpretation of backscatter mosaics, the acoustic patch types identified in this study represent a set of seafloor conditions that have relatively distinct attributes in terms of ecological habitats. Each acoustic patch type has a different overall distribution of sediment grain-sizes and other environmental characteristics (Figure 5.1-8, Figure 5.1-10 & Figure 5.1-11), despite being comprised primarily of sandy / coarse sediments. Although there was overlap in their characteristics, there is a trend of acoustic patch types A to E, respectively, being comprised of progressively coarser sediments, and higher maximum bed stress (Figure 5.1-13) and other features such as shell hash, and certain other surficial features (Table 5-16A). While there was some variation in sediment composition within each acoustic patch type, analyses indicated relatively consistent sediment grain-size composition in acoustic patch types B, C, and D when separated into groups spanning the west to east gradient in the study area.

The acoustic patch types can be designated as habitat types, and their mapped distribution forms the basis of an overall habitat map for the Phase II study area (Figure 5.1-6 and see below). This also forms the framework for subsequent research and surveys that can assess the accuracy of the characteristics of these habitat types as determined in this study, and also the extent of the distribution of seafloor habitats in this portion of LIS. Based on the analyses and resultant habitat map (Figure 5.2-108) produced in this study, there are several areas that should be studied in additional detail. More samples should be taken in acoustic patch types A and E, as only one grab sample was collected in these two patch types. The sediment data collected by the LDEO group in this study could be used to provide more detail as to sediment composition in the acoustic patch types, and as a test of the characterization presented in Section 5.1. Unfortunately, these data were not available in a final form in time to be used in our analyses within the period of project completion.

5.2.6.2 Infaunal Communities

Infaunal community characteristics vary across the Phase II study area, but there are some general trends, notably higher total abundance and taxonomic richness from west to east. There are several areas of relatively high diversity throughout the study area. Infaunal community composition for each acoustic patch type, is relatively distinct, but variable within acoustic patch types, predominantly due to changes in taxonomic dominance. The relative mix of sediment grain-sizes within each acoustic patch type, particularly the dominant sand fractions, are not different to the extent that they support distinct sets of communities. Analysis of community structure without grouping by acoustic patch type revealed that differences were most notable between the south/central, and north coastal portions of the Phase II area. The eastern central portion of the study area is comprised of a variable mix of community types but their similarity is relatively high (Figure 5.2-22). Each acoustic patch type was found to support a variety of these community types,

although there was generally one dominant type (Table 5-10). As such, the determinants of infaunal community composition across the Phase II study area include the habitat characteristics of the acoustic patch types and specific seafloor characteristics that may be found in a particular area, such as bottom stress conditions and/or differences in geomorphology (e.g., sand dunes or featureless bottom areas).

Due to sequence of designing the field surveys relative to availability of information and related analyses, only one sample was collected in acoustic patch types A (sandy silts) and E (gravelly sand). Any future surveys should collect more samples in these areas to fully characterize the community types that they may support. Also, there was a set of samples taken in areas where there was no backscatter available at the time the sampling design was being developed. These are designated as ND and were located along the Connecticut shore. These have sedimentary characteristics that are intermediate to patch types A and B, and had relatively distinct communities from the other acoustic patch types. Future surveys of infauna community structure should also include more detailed sampling of these nearshore areas and also classification of the seafloor based on approaches used in this study.

In addition to clearly defined communities and dominant species, rare infauna (i.e., infaunal organisms present in low numbers) fill important ecological roles in benthic habitats. The presence of these rare organisms, including ophiuroids, deep burrowing shrimp, sand dollars, and large polychaetes, also indicate less disturbed seafloor areas. The presence of these at each of the infaunal sampling locations are noted in the CMECS classifications generated in the study.

5.2.6.3 Epifaunal Communities

The communities of attached and emergent taxa associated with each acoustic patch type were distinct principally based on changes in dominance and not wholesale differences in composition. As with infaunal community characteristics linked to sediment size fractions, epi- and emergent taxa were associated with multiple grain-sizes differentially represented within each acoustic patch type. That is, epifaunal taxa that require stable sites for attachment (i.e., cobble to boulder size rocks) occurred in all patch types, but the frequency of occurrence of these size fractions of gravel differed along a gradient (i.e., patch types A-E). Indeed, the spatial variation of taxa occurred at much finer spatial scales than could be resolved in the map products, although larger scale patterns were clearly identified based on acoustic patches and regions within the study area (i.e., communities at sample site scale, Section 5.2.3.4).

5.2.6.4 Management Considerations and Implications

The habitat and ecological characterization of the Phase II study area can inform managers, stakeholders, and policymakers about several important issues related to assessing risk and benefits of human activities in this region.

1. Our results indicate complexity in the distribution of taxa at multiple spatial scales. That is, distributions of specific taxa varied within acoustic patches, between acoustic patches and between regions with multiple acoustic patch types. This infers complexity across the landscape of the ecological drivers that mediate recruitment and survival of multiple taxa. Such drivers can have direct (e.g., depth, grain size, bottom stress) and indirect roles (e.g., predation, competition) in mediating distribution. Put simply, and despite similarity in grain size distribution (sands-gravels) across the study region, all areas are not ecologically equal and

assessing risks and benefits of particular projects that result in disturbance should address impacts at multiple scales.

2. The maps and data products represent a snapshot in time. Results for both infauna and epifauna have identified particular differences in composition and functional roles of taxa, and based on the two sampling periods, some temporal changes were found. However, while the general spatial differences in ecological characteristics determined in this study may be relatively consistent over time, they do not incorporate the full extent of the temporal changes that occur within the study area. The benthic fauna in Long Island Sound can exhibit significant seasonal fluctuation (e.g., Zajac, 1998), and such potential fluctuations should be considered within the scope of management activities.

3. In addition to the seasonal differences in benthic communities observed over the duration of Phase II, comparing results to past studies and sampling efforts reveal longer-term changes in seafloor ecology. Previously documented benthic communities and dominant taxa were found to have changed on the scale of decades, likely responding to larger regional disturbances such as changing seafloor conditions and the influence of non-native species. While the differences in community structure found across the study area can be used to gauge their relative susceptibility and resilience to disturbances and their abilities to recover to a previous state, these community characteristics remain uncertain. Due to the nature of the habitats and communities in this portion of LIS, models of benthic response to and patterns of recovery after disturbances developed in other portions of the Sound (e.g., Rhoads et al., 1978) where there are different sedimentary environments and benthic communities, may not be applicable, and alternative recovery pathways and scenarios may occur (Zajac, 2001). Additionally, community responses within eastern LIS will likely change over time, as longer term shifts in community composition continue, necessitating periodic sampling in order to characterize recovery.

4. The integrated habitat map, diversity, community, and taxon-specific maps, and the aggregate of supporting analyses, can inform decisions related to the spatial and temporal extent of potential impacts from human activities. The spatial extent of habitats, associated communities, and particular taxa can be used to assess the localized uniqueness of the natural resources and, along with the life histories of the taxa, can be used to estimate potential for recovery and resilience from disturbances.

5.2.7 References

Abramoff, M. D., Magalhães, P. J., & Ram, S. J. (2004). Image Processing with ImageJ. *Biophotonics international, 11*(7), 36-42.

AECOM. (2009). *Monitoring Survey at the New London Disposal Site, July/August 2007.* DAMOS Contribution No. 180, U.S. Army Corps of Engineers, New England District, Concord, MA, 80 pp.

Ackerman, S. D., Huntley, E. C., Blackwood, D. S., Babb, I. G., Zajac, R. N., Conroy, C. W., . . . Walton, O. L. (2020). *Sea-floor sediment and imagery data collected in Long Island Sound, Connecticut and New York, 2017 and 2018.* (U.S. Geological Survey data release) Retrieved from USGS ScienceBase: https://doi.org/10.5066/P9GK29NM

Ackerman, S. D., Pappal, A. L., Huntley, E. C., Blackwood, D. S., & Schwab, W. C. (2015). *Geological sampling data and benthic biota classification: Buzzards Bay and Vineyard Sound, Massachusetts.* Open File Report 2014-1221, U.S. Geological Survey. Retrieved from https://pubs.er.usgs.gov/publication/ofr20141221

Allee, R. J., Dethier, M., Brown, D., Deegan, L., Ford, R. G., Hourigan, T. F., . . . Yoklavich, M. (2000). *Marine and estuarine ecosystem and habitat classification.* NOAA Technical Memorandum NMFS-F/SPO-43, U.S. Department of Commerce, National Oceanic and Atmospheric Administration, National Marine Fisheries Service.

Auker, L. (2019). A decade of invasion: changes in the distribution of *Didemnum vexillum* (Kott, 2002) in Narragansett Bay, Rhode Island, USA, between 2005 and 2015. *BioInvasions Records, 8*(2), 230-241.

Auster, P. J., & Langton, R. W. (1999, August). The effects of fishing on fish habitat. *American Fisheries Society Symposium*, *22. No. 150-187.*

Auster, P. J., Heinonen, K. B., Witharana, C., & McKee, M. (2009). *A habitat classification for the Long Island Sound region. Long Island Sound Study Technical Report.* Stamford, CT: EPA Long Island Sound Office.

Auster, P. J., Malatesta, R. J., & Donaldson, C. L. (1997). Distributional responses to small-scale habitat variability by early juvenile silver hake, *Merluccius bilinearis*. *nvironmental Biology of Fishes, 50*(2), 195-200.

Auster, P. J., Malatesta, R. J., & LaRosa, S. C. (1995). Patterns of microhabitat utilization by mobile megafauna on the southern New England (USA) continental shelf and slope. *Marine Ecology Progress Series, 127*, 77-85.

Auster, P. J., Malatesta, R. J., Langton, R. W., Watting, L., Valentine, P. C., Donaldson, C. S., . . . Babb, I. G. (1996). The impacts of mobile fishing gear on seafloor habitats in the gulf of Maine (Northwest Atlantic): Implications for conservation of fish populations. *Reviews in fisheries Science, 4* (2), 185-202.

Auster, P. J., Michalopoulos, C., Page, C. V., & Malatesta, R. J. (1997). Delineating and monitoring habitat management units in a temperate deep-water marine protected area. In N. P. Munro, & J. H. Martin Willison (Ed.), *Linking Protected Areas with Working Landscapes, Conserving Biodiversity: Proceedings of the Third International Conference on Science and Management of Protected Areas* (pp. 169-185). Wolfville, Nova Scotia: Science and Management of Protected Areas Association.

Barillé, L., Cognie, B., Beninger, P., Decottignies, P., & Rincé, Y. (2006). Feeding responses of the gastropod *Crepidula fornicata* to changes in seston concentration. *Marine Ecology Progress Series, 322*, 169-178.

Bassett, R. D., Finkbeiner, M. A., & Etnoyer, P. J. (2017). *Application of the Coastal and Marine Ecological Classification Standard (CMECS) to Deep-Sea Benthic Surveys in the Northeast Pacific: Lessons from Field Tests in 2015.* NOAA Technical Memorandum NOS NCCOS

228, U.S. Department of Commerce, National Oceanic and Atmospheric Administration, Charleston, SC. Retrieved from https://doi.org/10.7289/V5/TM-NOS-NCCOS-228

Baynes, T. W., & Szmant, A. M. (1989). Effect of current on the sessile benthic community structure of an artificial reef. *Bulletin of Marine Science, 44*(2), 545-566.

Beddingfield, S. D., & McClintock, J. B. (1999). Food Resource Utilization in the Sea Urchin *Lytechinus variegatus* in Contrasting Shallow-Water Microhabits of Saint Joseph Bay, Florida. *Gulf of Mexico Science, 17*(1), 3.

Beninger, P. G., Decottignies, P., Guiheneuf, F., Barillé, L., & Rincé, Y. (2007). Comparison of particle processing by two introduced suspension feeders: selection in *Crepidula fornicata* and *Crassostrea gigas*. *Marine Ecology Progress Series, 334*, 165-177.

Bokuniewicz, H. J., Gordon, R. B., & Kastens, K. A. (1977). Form and migration of sand waves in a large estuary, Long Island Sound. *Marine Geology, 24*(3), 185-199.

Brooks, A. L. (1984). *A Study of the Benthic Macrofauna at the Central Long Island Sound Disposal Site.* Naval Underwater Systems Center, New London Lab, New London, CT.

Brown, C. J., Sameoto, J. A., & Smith, S. J. (2012). Multiple methods, maps, and management applications: Purpose made seafloor maps in support of ocean management. *Journal of Sea Research, 72*, 1-13.

Byers, J. E., & Grabowski, J. H. (2014). Soft-sediment communities. In M. D. Bertness, J. F. Bruno, B. R. Silliman, & J. J. Stachowicz (Eds.), *Marine Community Ecology and Conservation* (pp. 227-249). Sunderland, MA: Sinauer.

Carroll, J. M., O'Shaughnessy, K. A., Diedrich, G. A., & Finelli, C. M. (2015). Are oysters being bored to death? Influence of Cliona celata on Crassostrea virginica condition, growth and survival. *Diseases of Aquatic Organisms, 117*(1), 31-44.

Carver, C. E., Thériault, I., & Mallet, A. L. (2010). Infection of cultured eastern oysters *Crassostrea virginica* by the boring sponge Cliona celata, with emphasis on sponge life history and mitigation strategies. *Journal of Shellfish Research, 29*(4), 905-915.

Cau, A., Mercier, A., Moccia, D., & Auster, P. J. (2020). The nursery role of marine animal forests. In S. Rossi, & L. Bramanti (Eds.), *Perspectives on the Marine Animal Forests of the World* (pp. 309-331). Switzerland AG: Springer Nature. Retrieved from https://doi.org/10.1007/978-3-030-57054-5_10#DOI

Cerrano, C., Bianchelli, S., Di Camillo, C. G., Torsani, F., & Pusceddu, A. (2015). Do colonies of *Lytocarpia myriophyllum, L.* 1758 (Cnidaria, Hydrozoa) affect the biochemical composition and the meiofaunal diversity of surrounding sediments? *Chemistry and Ecology, 31*(1), 1-21.

Clarke, K. R., & Gorley, R. N. (2006). PRIMER v6: User Manual/Tutorial. *(Plymouth Routines in Multivariate Ecological Research)*. Plymouth: PRIMER-E.

Clay, C., Deininger, M., & Hafner, J. (2006). *The Connecticut River Watershed: Conserving the Heart of New England.* The Trust for Public Land.

Coleman, S. E. (2014). *The effects of boring sponge on oyster soft tissue, shell integrity, and predator-related mortality.* M.Sc. Thesis, University of North Carolina at Chapel Hill.

Connecticut Department of Energy and Environmental Protection. (2019). *Long Island Sound Blue Plan.* Hartford, CT.

Daley, B. A., & Scavia, D. (2008). *An Integrated Assessment of the Continued Spread and Potential Impacts of the Colonial Ascidian, Didemnum sp. A, in U.S. Waters.* Technical Memorandum NOS NCCOS 78, NOAA, National Centers for Coastal Ocean Science.

De Bettignies, T., Wernberg, T., & Lavery, P. S. (2013). Size, not morphology, determines hydrodynamic performance of a kelp during peak flow. *Marine Biology, 160*(4), 843-851.

de Montaudouin, X., & Sauriau, P.-G. (1999). The proliferating Gastropoda *Crepidula fornicata* may stimulate macrozoobenthic diversity. *Journal of the Marine Biological Association of the United Kingdom, 79*(6), 1069-1077.

de Montaudouin, X., Blanchet, H., & Hippert, B. (2018). Relationship between the invasive slipper limpet *Crepidula fornicata* and benthic megafauna structure and diversity, in Arcachon Bay. *ournal of the Marine Biological Association of the United Kingdom, 98*(8), 2017-2028.

Deignan-Schmidt, S. R., & Whitney, M. M. (2018). A model study on the summertime distribution of river waters in Long Island Sound. *Estuaries and Coasts, 41* (4), 1002-1020.

Di Camillo, C. G., Bavestrello, G., Cerrano, C., Gravili, C., Piraino, S., Puce, S., & Boero, F. (2017). Hydroids (Cnidaria, Hydrozoa): a neglected component of animal forests. *Marine Animal Forests*, 397–427.

Diesing, M., Mitchell, P. J., O'Keeffe, E., Montereale-Gavazzi, G. O., & Le Bas, T. (2020). Limitations of predicting substrate classes on a sedimentary complex but morphologically simple seabed. *Remote Sensing, 12*(20), 3398.

Dimond, J. L., Kerwin, A. H., Rotjan, R., Sharp, K., Stewart, F. J., & Thornhill, D. J. (2013). A simple temperature-based model predicts the upper latitudinal limit of the temperate coral Astrangia poculata. *Coral Reefs, 32*(2), 401-409.

Dimond, J., & Carrington, E. (2007). Temporal variation in the symbiosis and growth of the temperate scleractinian coral *Astrangia poculata*. *Marine Ecology Progress Series, 348*, 161-172.

Dimond, J., & Carrington, E. (2008). Symbiosis regulation in a facultatively symbiotic temperate coral: zooxanthellae division and expulsion. *Coral Reefs, 27*(3), 601–604.

Dolmer, P. (2000). Feeding activity of mussels *Mytilus edulis* related to near-bed currents and phytoplankton biomass. *Journal of Sea Research, 44*(3-4), 221-231.

Dutto, M. S., Carcedo, M. C., Nahuelhual, E. G., Conte, A. F., Berasategui, A. A., Garcia, M. D., . . . Hoffmeyer, M. S. (2019). Trophic ecology of a corymorphid hydroid population in the Bahía Blanca Estuary, Southwestern Atlantic. *Regional Studies in Marine Science, 31*, 100746.

Egan, B., & Yarish, C. (1990). Productivity and life history of *Laminaria longicruris* at its southern limit in the Western Atlantic Ocean. *Marine Ecology Progress Series, 67*(3), 263-273.

Etter, R. J., & Grassle, J. F. (1992). Patterns of species diversity in the deep sea as a function of sediment particle size diversity. *Nature, 360*(6404), 576-578.

Fagan, W. F., Cantrell, R. S., & Cosner, C. (1999). How habitat edges change species interactions. *American Naturalist, 153*(2), 165-182.

Federal Geographic Data Committee (FGDC). (2012). *Coastal and Marine Ecological Classification Standard.* Publication# FGDC-STD-018-2012.

Feehan, C. J., Grace, S. P., & Narvaez, C. A. (2019). Ecological feedbacks stabilize a turf-dominated ecosystem at the southern extent of kelp forests in the Northwest Atlantic. *Scientific Reports, 9*(1), 1-10.

Fenster, M. S., Fitzgerald, D. M., Bohlen, W. F., Lewis, R. S., & Baldwin, C. T. (1990). Stability of giant sand waves in eastern Long Island Sound, USA. *Marine Geology, 91*(3), 207-225.

Filbee-Dexter, K., & Wernberg, T. (2018). Rise of turfs: a new battlefront for globally declining kelp forests. *Bioscience, 68*(2), 64-76.

Filbee-Dexter, K., Feehan, C. J., & Scheibling, R. E. (2016). Large-scale degradation of a kelp ecosystem in an ocean warming hotspot. *Marine Ecology Progress Series, 543*, 141-152.

Forrest, B. M., Fletcher, L. M., Atalah, J., Piola, R. F., & Hopkins, G. A. (2013). Predation limits spread of *Didemnum vexillum* into natural habitats from refuges on anthropogenic structures. *PLoS One, 8*(12), e82229.

Fuchs, H. L., Chant, R. J., Hunter, E. J., Curchitser, E. N., Gerbi, G. P., & Chen, E. Y. (2020). Wrong-way migrations of benthic species driven by ocean warming and larval transport. *Nature Climate Change, 10*(11), 1052-1056.

Gili, J. M., Alvà, V., Coma, R., Orejas, C., Ribes, M., Zabala, M., . . . Hughes, R. G. (1998). The impact of small benthic passive suspension feeders in shallow marine ecosystems: the hydroids as an example. *Zoologische verhandelingen, 323*(8), 99-105.

Gittenberger, A. (2010). *Risk analysis of the colonial sea-squirt Didemnum vexillum Kott, 2002 in the Dutch Wadden Sea, a UNESCO World Heritage Site.* GiMaRIS.

Glaspie, C. N., & Seitz, R. D. (2018). Habitat complexity and benthic predator-prey interactions in Chesapeake Bay. *PloS One, 13*(10), e0205162.

Goddard, J. H., Goddard, W. M., & Goddard, Z. E. (2020). Benthic Heterobranch Sea Slugs (Gastropoda: Heterobranchia) from Santa Barbara County, California. *Proceedings of the California Academy of Sciences*, *Series 4, Volume 66(10)*, pp. 275-298.

Gottschall, K. F., Johnson, M. W., & Simpson, D. G. (2000). *The distribution and size composition of finfish, American lobster, and long-finned squid in Long Island Sound based on the Connecticut Fisheries Division Bottom Trawl Survey, 1984–1994.* Technical Report, National Oceanic and Atmospheric Administration, National Marine Fisheries Service.

Grabowski, J. H., Bachman, M., Demarest, C., Eayrs, S., Harris, B. P., Malkoski, V., . . . Stevenson, D. (2014). Assessing the Vulnerability of Marine Benthos to Fishing Gear Impacts. *Reviews in Fisheries Science & Aquaculture, 22*(2), 142-155.

Grace, S. (2017). Winter quiescence, growth rate, and the release from competition in the temperate scleractinian coral *Astrangia poculata* (Ellis & Solander 1786). *Northeastern Naturalist, 24*, B119-B134.

Grace, S. P. (2004). *Ecomorphology of the temperate scleractinian Astrangia poculata: coralmacroalgal interactions in Narragansett Bay.* Doctoral Dissertation, University of Rhode Island.

Gray, J. S. (2002). Species richness of marine soft sediment. *Marine Ecology Progress Series, 244*, 285-297.

Greene, H. G., Yoklavich, M. M., Starr, R. M., O'Connell, V. M., Wakefield, W. W., Sullivan, D. E., . . . Cailliet, G. M. (1999). A classification scheme for deep seafloor habitats. *Oceanologica acta, 22*(6), 663-678.

Guarinello, M. L., Shumchenia, E. J., & King, J. W. (2010). Marine habitat classification for ecosystem-based management: a proposed hierarchical framework. *Environmental Management, 45*(4), 793-806.

Hatcher, A. G., Grant, J., & Schofield, B. (1994). Effects of suspended mussel culture (*Mytilus* spp.) on sedimentation, benthic respiration and sediment nutrient dynamics in a coastal bay. *Marine Ecology-Progress Series, 115*, 219-219.

Holcomb, M., Cohen, A. L., & McCorkle, D. C. (2012). An investigation of the calcification response of the scleractinian coral *Astrangia poculata* to elevated pCO_2 and the effects of nutrients, zooxanthellae and gender. *Biogeosciences, 9*(1), 29-39.

Howell, P. T., Pereira, J. J., Schultz, E. T., & Auster, P. J. (2016). Habitat Use in a Depleted Population of Winter Flounder: Insights into Impediments to Population Recovery. *Transactions of the American Fisheries Society, 145*(6), 1208-1222.

Hughes, R. G. (1978). Life-histories and abundance of epizoites of the hydroid *Nemertesia antennina (L.)*. *Journal of the Marine Biological association of the United Kingdom, 58*(2), 313-332.

Jacques, T. G., Marshall, N., & Pilson, M. Q. (1983). Experimental ecology of the temperate scleractinian coral *Astrangia danae*. *Marine Biology, 76*, 135-148.

Keefer, M. L., Peery, C. A., Wright, N., Daigle, W. R., Caudill, C. C., Clabough, T. S., . . . Zacharias, M. A. (2008). Evaluating the NOAA coastal and marine ecological classification standard in estuarine systems: a Columbia River estuary case study. *Estuarine, Coastal and Shelf Science, 78*(1), 89-106.

Knebel, H. J., & Poppe, L. J. (2000). Sea-Floor Environments within Long Island Sound: A Regional Overview. *Journal of Coastal Research, 16*(3), 533-550.

Kostylev, V. E., Todd, B. J., Fader, G. B., Courtney, R. C., Cameron, G. D., & Pickrill, R. A. (2001). Benthic habitat mapping on the Scotian Shelf based on multibeam bathymetry, surficial geology and seafloor photographs. *Marine Ecology Progress Series, 219*, 121-137.

Krumhansl, K. A., Demes, K. W., Carrington, E., & Harley, C. D. (2015). Divergent growth strategies between red algae and kelps influence biomechanical properties. *American journal of botany, 102*(11), 1938-1944.

Lambert, G. (2009). Adventures of a sea squirt sleuth: unraveling the identity of *Didemnum vexillum*, a global ascidian invader. *Aquatic Invasions, 4*(1), 5-28.

Langton, R. W., Auster, P. J., & Schneider, D. C. (1995). A spatial and temporal perspective on research and management of groundfish in the northwest Atlantic. *Reviews in Fisheries Science, 3*(3), 201-229.

Lehane, C., & Davenport, J. (2006). A 15-month study of zooplankton ingestion by farmed mussels (*Mytilus edulis*) in Bantry Bay, Southwest Ireland. *Estuarine, Coastal and Shelf Science, 67*(4), 645-652.

Lewis, R. S., & Stone, J. R. (1991). Late Quaternary stratigraphy and depositional history of the Long Island Sound basin: Connecticut and New York. *Journal of Coastal Research*, 1-23.

Lindholm, J. B., Auster, P. J., & Kaufman, L. S. (1999). Habitat-mediated survivorship of juvenile (0-year) Atlantic cod Gadus morhua. *Marine Ecology Progress Series, 180*, 247-255.

Lopez, G., Carey, D., Carlton, J. T., Cerrato, R., Dam, H., DiGiovanni, R., . . . Zajac, R. (2014). Biology and Ecology of Long Island Sound. In J. S. Latimer, M. A. Tedesco, R. L. Swanson, C. Yarish, P. E. Stacey, & C. Garza (Eds.), *Long Island Sound: prospects for the urban sea* (pp. 285-479). New York, NY: Springer.

Lund, W. A., Stewart, L. L., & Weiss, H. M. (1971). *Investigation on the Lobster Homarus americanus.* Commerical Fisheries Research and Development Act -- Final Report, Project No. 3-130-R, Department of Commerce, National Oceanic and Atmospheric Administration, National Marine Fisheries Service.

Malatesta, R. J., & Auster, P. J. (1999). The importance of habitat features in low-relief continental shelf environments. *Oceanologica Acta, 22*(6), 623-626.

Mercer, J. M., Whitlatch, R. B., & Osman, R. W. (2009). Potential effects of the invasive colonial ascidian (Didemnum vexillum Kott, 2002) on pebble-cobble bottom habitats in Long Island Sound, USA. *Aquatic Invasions, 4*(1), 133-142.

Merzouk, A., & Johnson, L. E. (2011). Kelp distribution in the northwest Atlantic Ocean under a changing climate. *Journal of Experimental Marine Biology and Ecology, 400*(1-2), 90-98.

Meybeck, M. (1982). Carbon, nitrogen, and phosphorus transport by world rivers. *American Journal of Science, 282*(4), 401-450.

Miller, A. N., Strychar, K. B., Shirley, T. C., & Rützler, K. (2010). Effects of heat and salinity stress on the sponge Cliona celata. *International Journal of Biology, 2*(2), 3-16.

Mittermayr, A., Legare, B., & Borrelli, M. (2020). Applications of the coastal and marine ecological classification standard (CMECS) in a partially restored New England salt marsh lagoon. *Estuaries and Coasts*, 1-12.

Montereale-Gavazzi, G., Marc Roche, Degrendele, K., Lurton, X., Terseleer, N., Baeye, M., . . . Van Lancker, V. (2019). Insights into the short-term tidal variability of multibeam backscatter from field experiments on different seafloor types. *Geosciences, 9*(1), 34.

Morris, K. E., Caruso, T., Buscot, F., Fischer, M., Hancock, C., Maier, T. S., . . . Rillig, M. C. (2014). Choosing and using diversity indices: insights for ecological applications from the German Biodiversity Exploratories. *Ecology and evolution, 4*(18), 3514-3524.

Mumby, P. J., & Harborne, A. R. (1999). Development of a systematic classification scheme of marine habitats to facilitate regional management and mapping of Caribbean coral reefs. *Biological Conservation, 88*(2), 155-163.

Nakagawa, S., & Schielzeth, H. (2013). A general and simple method for obtaining R² from generalized linear mixed-effects models. *Methods in ecology and evolution, 4*(2), 133-142.

Nava, H., & Carballo, J. L. (2008). Chemical and mechanical bioerosion of boring sponges from Mexican Pacific coral reefs. *Journal of Experimental Biology, 211*(17), 2827-2831.

NCSS, LLC. (2012). *Statistical Software*. Kaysville, Utah, USA. Retrieved from www.ncss.com

Nicol, W. L., & Reisman, H. M. (1976). Ecology of the boring sponge (Cliona celata) at Gardiner's Island, New York. *Chesapeake Science, 17*(1), 1-7.

Norling, P., & Kautsky, N. (2007). Structural and functional effects of *Mytilus edulis* on diversity of associated species and ecosystem functioning. *Marine Ecology Progress Series, 351*, 163-175.

Parker, G. H. (1917). The activities of Corymorpha. *Journal of Experimental Zoology, 24* (2), 303-331.

Parker, J. H., & Revelas, E. C. (1989). *1985 monitoring surveys at the central Long Island Sound disposal site: an assessment of impacts from disposal and Hurricane Gloria.* DAMOS Contribution #57, U.S. Army Corps of Engineers, New England Division, Waltham, MA.

Parry, E. H. (1981). *Ecology of sponges of lower Mystic estuary and Fisheries Island Sound, with emphasis on Cliona celata: distribution, reproduction and winter condition.* M.A. Thesis, Connecticut College, New London.

Pellegrino, P. E., & Hubbard, W. A. (1983). *Baseline shellfish data for the assessment of potential environmental impacts associated with energy activities in Connecticut's coastal zone.* State of Connecticut Department of Agriculture, Bureau of Aquaculture. Connecticut Coastal Energy Impact Program.

Poppe, L. J., Ackerman, S. D., Doran, E. F., Beaver, A. L., Crocker, J. M., & Schattgen, P. T. (2006). *Interpolation of reconnaissance multibeam bathymetry from north-central Long Island Sound.* Open-File Report 2005-1145, U.S. Geological Survey.

Poppe, L. J., DiGiacomo-Cohen, M. L., Smith, S. M., Stewart, H. F., & Forfinski, N. A. (2006). Seafloor character and sedimentary processes in eastern Long Island Sound and western Block Island Sound. *Geo-Marine Letters, 26*, 59. Retrieved from https://doi.org/10.1007/s00367-006-0016-4

Poppe, L. J., Knebel, H. J., Mlodzinska, Z. J., Hastings, M. E., & Seekins, B. A. (2000). Distribution of surficial sediment in Long Island Sound and adjacent waters: texture and total organic carbon. *Journal of Coastal Research*, 567-574.

Poppe, L. J., Lewis, R. S., Denny, J. F., Parolski, K. F., & DiGiacomo-Cohen, M. L. (1998). *Sidescan sonar image, surficial geologic interpretation, and bathymetry of the Fishers Island Sound seafloor. Connecticut, New York, and Rhode Island.* Geologic Investigations Series Map Survey Number 5, U.S. Geological Survey.

Poppe, L. J., McMullen, K. Y., Ackerman, S. D., Guberski, M. R., & Wood, D. A. (2013). *Seafloor character and geology off the entrance to the Connecticut River, northeastern Long Island Sound.* (No. 2012-1103). U.S. Geological Survey. Retrieved from https://doi.org/10.3133/ofr20121103

Poppe, L. J., Paskevich, V. F., Moser, M. S., DiGiacomo-Cohen, M. L., & Christman, E. B. (2004). *Sidescan sonar imagery and surficial geologic interpretation of the seafloor off Branford, Conneticut.* Open-File Report 2004-1003. U.S. Geological Survey.

Potts, J. M., & Elith, J. (2006). Comparing species abundance models. Ecological modelling. *Ecological modelling, 199*(2), 153-163.

Preston, J., Fabra, M., Helmer, L., Johnson, E., Harris-Scott, E., & Hendy, I. W. (2020). Interactions of larval dynamics and substrate preference have ecological significance for benthic biodiversity and Ostrea edulis Linnaeus, 1758 in the presence of Crepidula fornicata. *Aquatic Conservation: Marine and Freshwater Ecosystems, 30*(11), 2133-21.

Raineault, N. A., Trembanis, A. C., & Miller, D. C. (2012). Mapping benthic habitats in Delaware Bay and the coastal Atlantic: acoustic techniques provide greater coverage and high resolution in complex, shallow-water environments. *Estuaries and Coasts, 35*(2), 682-699.

Rhoads, D. C., McCall, P. L., & Yingst, J. Y. (1978). Disturbance and Production on the Estuarine Seafloor: Dredge-spoil disposal in estuaries such as Long Island Sound can be managed in ways that enhance productivity rather than diminish it. *American Scientist, 66*(5), 577-586.

Rice, E., Dam, H. G., & Stewart, G. (2015). Impact of climate change on estuarine zooplankton: surface water warming in Long Island Sound is associated with changes in copepod size and community structure. *Estuaries and coasts, 38*(1), 13-23.

Ridout, M., Demétrio, C. G., & Hinde, J. (1998, December). Models for count data with many zeros. *Proceedings of the XIXth international biometric conference. 19*, pp. 179-192. Cape Town, South Africa: International Biometric Society Invited Papers.

Riley, S. J., DeGloria, S. D., & Elliot, R. (1999). Index that quantifies topographic. *Intermountain Journal of sciences, 5*(1-4), 23-27.

Rosell, D., & Uriz, M. J. (2002). Excavating and endolithic sponge species (Porifera) from the Mediterranean: species descriptions and identification key. *Organisms Diversity & Evolution, 2*(1), 55-86.

Rossi, S., Bramanti, L., Gori, A., & Orejas, C. (Eds.). (2017). *Marine Animal Forests: The Ecology of Benthic Biodiversity Hotspots.* Cham: Springer International Publishing.

Rützler, K., & Rieger, G. (1973). Sponge burrowing: fine structure of Cliona lampa penetrating calcareous substrata. *Marine Biology, 21*(2), 144-162.

Scharf, F. S., Manderson, J. P., & Fabrizio, M. C. (2006). The effects of seafloor habitat complexity on survival of juvenile fishes: species-specific interactions with structural refuge. *Journal of Experimental Marine Biology and Ecology, 335*(2), 167-176.

Schuhmacher, H., & Zibrowius, H. (1985). What is hermatypic? *Coral reefs, 4*(1), 1-9.

Schweitzer, C. C., & Stevens, B. G. (2019). The relationship between fish abundance and benthic community structure on artificial reefs in the Mid-Atlantic Bight, and the importance of sea whip corals Leptogorgia virgulata. *PeerJ, 7*, e7277.

Smale, D. A. (2020). Impacts of ocean warming on kelp forest ecosystems. *New Phytologist, 225*(4), 1447-1454.

Snyder, J., Whitney, M. M., Dam, H., Jacobs, M. W., & Baumann, H. (2019). Citizen science observations reveal rapid, multi-decadal ecosystem changes in eastern Long Island Sound. *Marine environmental research, , 146*, 80-88.

Stefaniak, L. M., & Auster, P. J. (2015). Emergent and epi-fauna Characterization. Section 5.5. In *Seafloor Mapping of Long Island Sound – Final Report: Phase I Pilot project* (pp. 268-375).

Stamford, CT: (Unpublished project report). U. S. Environmental Protection Agency, Long Island Sound Study.

Stefaniak, L. M., Auster, P. J., & Babb, I. G. (2014). Loss of an erect sponge on a rock reef in Long Island Sound (north-west Atlantic). *Marine Biodiversity Records, 7*, 1-6.

Stefaniak, L. M., McAtee, J., & Shulman, M. J. (2005). The costs of being bored: effects of a clionid sponge on the gastropod Littorina littorea (L). *Journal of Experimental Marine Biology and Ecology, 327*(1), 103-114.

Steneck, R. S., Graham, M. H., Bourque, B. J., Corbett, D., Erlandson, J. M., Estes, J. A., & Tegner, M. J. (2002). Kelp forest ecosystems: biodiversity, stability, resilience and future. *Environmental Conservation, 29*(4), 436-459.

Stewart, L. L. (1980). Chronological records of in-situ physical and biological conditions obtained by diver survey at the Central Long Island Sound and New London Disposal Sites. *Second International Ocean Dumping Symposium. DAMOS Contribution No. 9.* Woods Hole, MA: U.S. Army Corps of Engineers, New England District.

Strohmeier, T., Strand, Ø., Alunno-Bruscia, M., Duinker, A., & Cranford, P. J. (2012). Variability in particle retention efficiency by the mussel *Mytilus edulis*. *Journal of Experimental Marine Biology and Ecology, 412*, 96-102.

Thieltges, D. W. (2005). Impact of an invader: epizootic American slipper limpet Crepidula fornicata reduces survival and growth in European mussels. *Marine Ecology Progress Series, 286*, 13-19.

Thrush, S. F., Gray, J. S., Hewitt, J. E., & Ugland, K. I. (2006). Predicting the effects of habitat homogenization on marine biodiversity. *Ecological Applications, 16*(5), 1636-1642.

Thrush, S. F., Hewitt, J. E., Norkko, A., Nicholls, P. E., Funnell, G. A., & Ellis, J. I. (2003). Habitat change in estuaries: predicting broad-scale responses of intertidal macrofauna to sediment mud content. *Marine Ecology Progress Series, 263*, 101-112.

Tiner, R. H., Bergquist, H., Halavik, T., & MacLachlan, A. (2003). *Eelgrass Survey for Eastern Long Island Sound, Connecticut and New York.* National Wetlands Inventory report, U.S. Fish and Wildlife Service, National Wetlands Inventory Program, Northeast Region., Hadley, MA.

Valentine, P. C., Blackwood, D. S., & Parolski, K. F. (2000). *Seabed observation and sampling system.* (No. 142-00), U.S. Geological Survey.

Vercaemer, B., Dawn, S., Clément, P., Harman, A., Stewart-Clark, S., & DiBacco, C. (2015). Distribution of the non-indigenous colonial ascidian Didemnum vexillum (Kott, 2002) in the Bay of Fundy and on offshore banks, eastern Canada. *Management of Biological Invasions, 6*(4), 385.

Verfaillie, E., Degraer, S., Schelfaut, K., Willems, W., & Van Lancker, V. (2009). A protocol for classifying ecologically relevant marine zones, a statistical approach. *Estuarine, Coastal and Shelf Science, 83*(2), 175-185.

Welsh, B. L., & Stewart, L. (1984). *The effects of energy-related transport activities on benthic marine plants, fish, shellfish, and lobsters in the Thames River estuary.* Hartford: Connecticut Office of Policy and Management.

Whitlatch, R. B. (1981). Animal-sediment relationships in intertidal marine benthic habitats: Some determinants of deposit-feeding species diversity. *Journal of Experimental Marine Biology and Ecology, 53*(1), 31-35.

Witman , J. D., & Lamb, R. W. (2018). Persistent differences between coastal and offshore kelp forest communities in a warming Gulf of Maine. *PLoS ONE, 13*(1), e0189388. Retrieved from https://doi.org/10.1371/journal.pone.0189388

Xavier, J. R., Rachello-Dolmen, P. G., Parra-Velandia, F., Schönberg, C. L., Breeuwer, J. J., & Van Soest, R. M. (2010). Molecular evidence of cryptic speciation in the "cosmopolitan" excavating sponge Cliona celata (Porifera, Clionaidae). *Molecular phylogenetics and evolution, 56*(1), 13-20.

Zajac, R. (2001). Organism–sediment relations at multiple spatial scales: implications for community structure and successional dynamics. In J. Y. Aller, S. A. Woodin, & R. C. Aller, *Organism-sediment interactions* (Belle W. Baruch Library in Marine Science Series No. 21 ed., pp. 119-140). University of South Carolina Press.

Zajac, R. N. (1998). A review of research on benthic communities conducted in Long Island Sound and an assessment of structure and dynamics. In L. J. Poppe, & C. Polloni (Eds.), *Long Island Sound Environmental Studies.* Retrieved from https://pubs.usgs.gov/of/1998/of98-502/chapt4/rz1cont.htm

Zajac, R. N. (2008). Challenges in marine, soft-sediment benthoscape ecology. *Landscape Ecology, 23*(1), 7-18.

Zajac, R. N., Lewis, R. S., Poppe, L. J., Twichell, D. C., Vozarik, J., & DiGiacomo-Cohen, M. L. (2000). Relationships among sea-floor structure and benthic communities in Long Island Sound at regional and benthoscape scales. *Journal of Coastal Research*, 627-640.

Zajac, R. N., Lewis, R. S., Poppe, L. J., Twichell, D. C., Vozarik, J., & DiGiacomo-Cohen, M. L. (2003). Responses of infaunal populations to benthoscape structure and the potential importance of transition zones. *Limnology and Oceanography, 48*, 829-842.

Zajac, R. N., Stefaniak, L. M., Babb, I. G., Conroy, C. W., Penna, S., Chadi, D., & Auster, P. J. (2020). Chapter 10: An integrated seafloor habitat map to inform marine spatial planning and management: A case study from Long Island Sound (Northwest Atlantic). In P. Harris, & E. Baker (Eds.), *Seafloor Geomorphology as Benthic Habitat* (Second ed., pp. 199-217). Cambridge, MA: Elsevier.

Zintzen, V., Norro, A., Massin, C., & Mallefet, J. (2008). Temporal variation of Tubularia indivisa (Cnidaria, Tubulariidae) and associated epizoites on artificial habitat communities in the North Sea. *Marine Biology, 153*(3), 405-420.

zu Ermgassen, P. S., Thurstan, R. H., Corrales, J., Alleway, H., Carranza, A., Dankers, N., . . . Sanderson, W. G. (2020). The benefits of bivalve reef restoration: A global synthesis of underrepresented species. *Aquatic Conservation: Marine and Freshwater Ecosystems, 30*(11), 2050-2065.

6   Physical Characterization

Recommended Citations:

O'Donnell, J., McCardell, G., & Fake, T. (2023). Objective. Section 6.1, p. 294 in: "Seafloor Mapping of Long Island Sound – Final Report: Phase II Project." (Unpublished project report). U. S. Environmental Protection Agency, Long Island Sound Study, Stamford, CT.

O'Donnell, J., McCardell, G., & Fake, T. (2023). Historical Context. Section 6.2, p. 294-295 in: "Seafloor Mapping of Long Island Sound – Final Report: Phase II Project." (Unpublished project report). U. S. Environmental Protection Agency, Long Island Sound Study, Stamford, CT.

O'Donnell, J., McCardell, G., & Howard-Strobel, M.M. (2023). New Data Acquisition. Section 6.3, p. 295-302 in "Seafloor Mapping of Long Island Sound – Final Report: Phase II Project." (Unpublished project report). U. S. Environmental Protection Agency, Long Island Sound Study, Stamford, CT.

O'Donnell, J., McCardell, G., & Howard-Strobel, M.M. (2023). Model Implementation. Section 6.4, p. 302-304 in "Seafloor Mapping of Long Island Sound – Final Report: Phase II Project." (Unpublished project report). U. S. Environmental Protection Agency, Long Island Sound Study, Stamford, CT.

O'Donnell, J., McCardell, G., & Howard-Strobel, M.M. (2023). Model Skill Assessment. Section 6.5, p. 304-307 in "Seafloor Mapping of Long Island Sound – Final Report: Phase II Project." (Unpublished project report). U. S. Environmental Protection Agency, Long Island Sound Study, Stamford, CT.

O'Donnell, J., McCardell, G., & Howard-Strobel, M.M. (2023). FIS Comparisons. Section 6.6, p. 307-308 in "Seafloor Mapping of Long Island Sound – Final Report: Phase II Project." (Unpublished project report). U. S. Environmental Protection Agency, Long Island Sound Study, Stamford, CT.

O'Donnell, J., McCardell, G., & Howard-Strobel, M.M. (2023). Along-track MSL reference heights. Section 6.7, p. 309-312 in "Seafloor Mapping of Long Island Sound – Final Report: Phase II Project." (Unpublished project report). U. S. Environmental Protection Agency, Long Island Sound Study, Stamford, CT.

O'Donnell, J., McCardell, G., & Howard-Strobel, M.M. (2023). Physical Oceanographic Products. Section 6.8, p. 312 in "Seafloor Mapping of Long Island Sound – Final Report: Phase II Project." (Unpublished project report). U. S. Environmental Protection Agency, Long Island Sound Study, Stamford, CT.

O'Donnell, J., McCardell, G., & Howard-Strobel, M.M. (2023). Summary and Conclusions. Section 6.9, p. 313 in "Seafloor Mapping of Long Island Sound – Final Report: Phase II Project." (Unpublished project report). U. S. Environmental Protection Agency, Long Island Sound Study, Stamford, CT.

6.1   Objective

LIS is an estuary with complex bathymetry formed by the tectonic and glacial history of the region. The water of LIS moves continuously as a consequence of winds, tidal forcing from the adjacent shelf waters, and the density field created by fresh water delivered from rivers and uneven distributions of surface heating and vertical mixing. The primary freshwater sources are the Connecticut River and the East River. These rivers situated at nearly opposite ends of the Sound create a complicated circulation pattern within its waters.

The distribution and variability of salinity, temperature, dissolved oxygen, currents, and bottom stresses created by the complex interaction of geometry and forcing affects the biological communities on the seafloor. Characterization of the seasonal evolution of these fields with limited resources requires the combination of observations and a model that interpolates in space and time between the measurements in a manner that is consistent with our understanding of the physical processes that determine and constrain changes. This section describes the field work and the model employed to develop maps of bottom stress, temperature, and salinity in the Phase II study area.

6.2   Historical Context

The eastern end of LIS is freshened by several rivers emptying into the Sound from the Pawcatuck River at the Rhode Island border to the Connecticut River. This region of the Sound is responsive to significant weather changes, so it experiences seasonal variance in current magnitudes and wave parameters (O'Donnell, 2015). An enduring survey program collects extensive data across LIS that provides a comprehensive view of the seasonal variation including the vertical structure of salinity (S), temperature (T) and density fields (σ_T), which is described in Kaputa & Olsen (2000) and summarized in O'Donnell et al. (2014). The physical oceanography of eastern LIS has been further reviewed in the literature by O'Donnell (2015), which recognized that while the seasonal variations in salinity and temperature are well characterized along the axis of LIS, the north-south structure and variability within the study area were much less resolved and are much better defined as a result of this effort that identified the north-south, as well as east-west, patterns in salinity and temperature in the generated map products. O'Donnell (2015) also found there are few existing, direct observations of bottom stress in ELIS. While several model studies developed estimates of the bottom stress distributions (e.g., Signell et al., 2000), none have reported direct measurements (O'Donnell, 2015).

Observations acquired and analyzed by Bennett et al. (2010) confirmed that the principal tidal constituent in sea level variations in LIS is the semidiurnal lunar, or M_2, signal first described by Swanson (1976). Practical demands for predictions of the transport and fate of materials in the

Sound prompted the development of three-dimensional circulation models beyond the two-dimensional numerical models developed by Murphy (1979) and Kenefick (1985); see Valle-Levinson & Wilson (1994a,b), Valle-Levinson et al. (1995), Schmalz et al. (1994), Blumberg et al. (1999), and Signell et al. (2000). Later, Hao (2008) extended the study of Crowley (2005) and Wilson & Swanson (2005), implementing the Regional Ocean Model System (ROMS) for LIS (see Shchepetkin & McWilliams, 2005), and reported the results of a comprehensive study on the dynamics of the tidal circulation in LIS.

The non-tidal currents in the Sound are also difficult to measure and the data archive is limited. The three-dimensional models of Blumberg & Pritchard (1997), Crowley (2005), and Hao (2008) have provided estimates of the along-Sound volume fluxes at several sections across LIS, and recent ship survey programs by O'Donnell & Bohlen (2003), Bennett et al. (2010), and Fribance et al. (2013) have provided measurements that are generally consistent with the volume flux estimate of the models. However, detailed comparisons remain to be conducted.

By examining the time series of wind stress and wave parameters during large events, and the dependence of the differences in the observations of significant wave height buoys in the eastern and western ends of the Sound, O'Donnell et al. (2014) showed the significant wave heights were sensitive to the direction of the winds. When the wind blows from the east, waves in the western Sound are similar to those in the east. But when winds blow from the west, the waves in the eastern Sound are significantly larger than those in the west. This asymmetry is consistent with the idea that waves in LIS are fetch limited as proposed by Bokuniewicz & Gordon (1980), Signell et al. (2000), and Lemus (2008).

Wind velocity and wave height and period observations in the Sound have been measured at several buoys and locations on the shoreline for over a decade. O'Donnell et al. (2014) report that the coastal site measurements of the daily mean stress magnitude are 1 to 1/2 of that measured at buoys. The buoy observations also demonstrate that at frequencies higher than approximately 1/day, the winds at the two sites have low coherence at frequencies higher than approximately one per day, but at lower frequencies the coherence is high. This suggests that dense local observations will be required in applications where short time-scale meteorological events are important. Model calculations that don't have realistic wind forcing should, therefore, only be expected to represent larger scale changes. O'Donnell (2015) further concluded that bottom stress, wave field, and circulation measurements from different wind and river flow conditions in ELIS are necessary to adequately evaluate model predictions so they can be reliably used in site assessment applications.

6.3 New Data Acquisition

Springtime and wintertime deployments of bottom tripods with an array of instruments measuring temperature, salinity, currents, and stresses were executed, and two ship surveys were executed, in which salinity, temperature, density structure and current patterns were measured. Tripod-style bottom-frames were deployed in and near FIS to collect measurements for determining bottom stresses, current structure, wave characteristics, salinity, and temperature. Three frames were deployed in spring 2017 and five during winter 2018. Table 6-1 and Table 6-2 summarize the frame deployments for fall 2017 and winter 2018, respectively; Figure 6.3-1 and Figure 6.3-2 show the frame deployment locations for fall 2017 and winter 2018, respectively. These observations supplement previous data from ELIS.

Table 6-1. Spring 2017 Moored Frames - Station Location and Deployment Summary

Station ID	Latitude	Longitude	Sensors	Deploy Date (2017)	Recovery Date (2017)	Water Depth (m)	Deployment Length (days)
SOW1	41.303300°	-71.903817°	-AQD 2 kHz HR -SBE37 CT/P -ADCP 600 kHz	30 MAR	7 JUN	22.6	70
EID2	41.325933°	-71.927667°	-AQD 2 kHz HR -SBE37 CT/P -ADCP 1200 kHz	28 MAR	7 JUN	4.6	72
WID3	41.310900°	-71.968917°	-AQD 2 kHz HR -SBE37 CT/P -ADCP 1200 kHz	28 MAR	8 JUN	5.5	73

Table 6-2. Winter 2017-2018 Moored Frames - Station Location and Deployment Summary

Station ID	Latitude	Longitude	Station Depth (meters)	RDI ADCP SN/Freq	SBE 37 SN	AQD SN
SOW1	41 18.1977	-71 54.2284	21.5	1094/600	9695	8445
EID2	41 19.5557	-71 55.6593	3.9	10463/1200	9673	8455
WID3	41 18.6537	-71 58.1355	4.8	10462/1200	9696	8432
WFW4	41 17.4727	-72 02.2383	10.3	6615/600	9694	8438
SFW5	41 16.2218	-71 58.3172	6.3	11708/1200	9674	8554
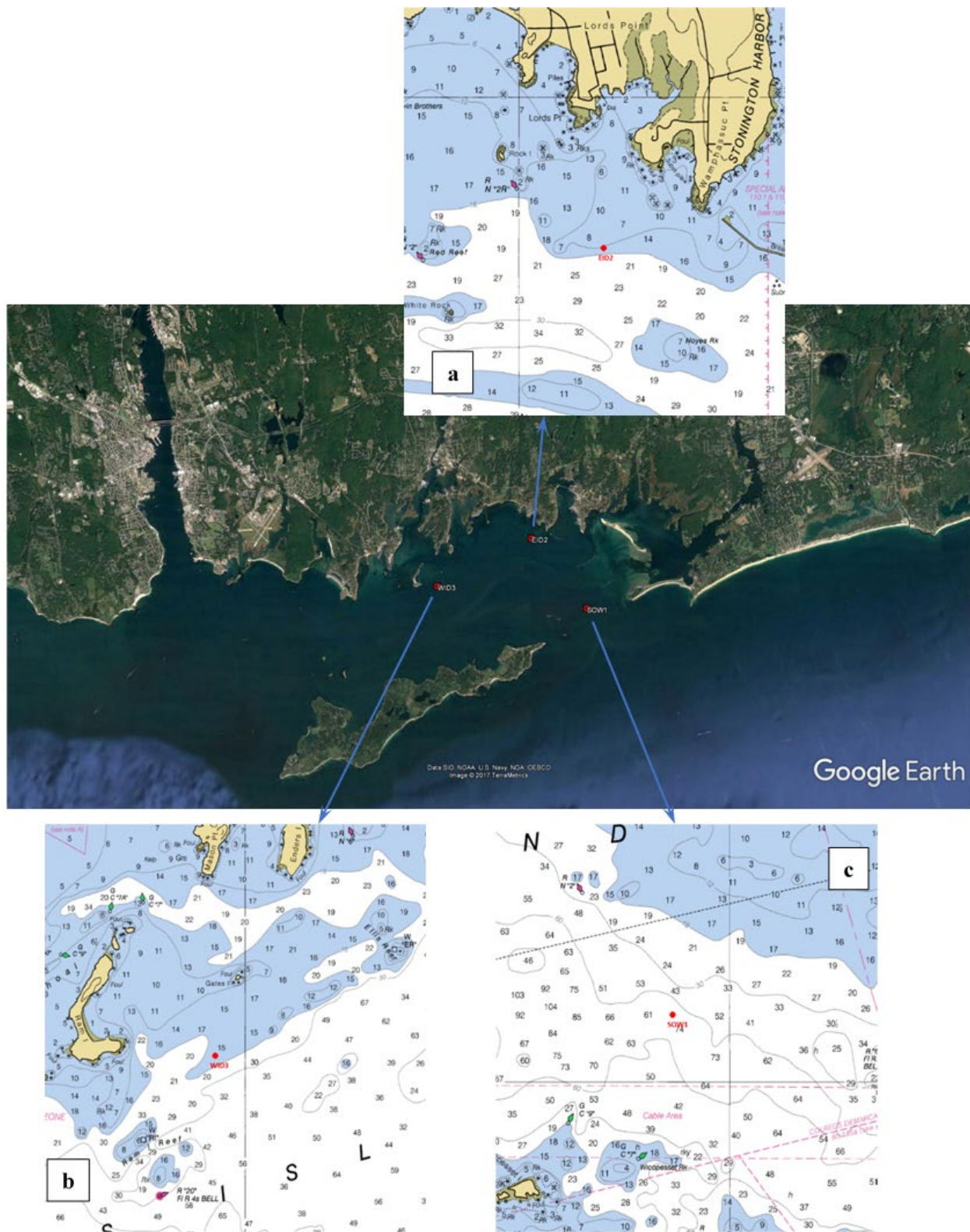
Figure 6.3-1. Location of the three frames deployed in FIS during spring of 2017, a) detail of bathymetry (in feet) near EID2 – the Eastern Inside Dissipative station, b) bathymetry (in feet) at WID3 - Western Inside Dissipative station, c) bathymetry (in feet) at SOW1 - Southern Outside Wave station.

Figure 6.3-2. Location of the five bottom moored frames in FIS for the winter 2017-2018 data collection campaign. Yellow stations were occupied during the spring 2017 campaign, the two red stations are new locations.

The moored instrument array configuration for the frames is shown in Figure 6.3-3. Each frame was equipped with an RDI acoustic Doppler current profiler (ADCP) with wave sampling enabled located 1.5 meters above bottom, a Nortek Aquadopp 2 kHz High-Resolution phase coherent profiler looking downward at 0.75 meters above the bottom, and a Sea-Bird Model 37 SMP measuring salinity, temperature, and pressure also at 0.75 meters above bottom. The RDI ADCP sampled currents every 15 minutes and waves once per hour. The Nortek Aquadopp sampled every hour, and the Sea-Bird CT/P sensor sampled every 15 minutes.
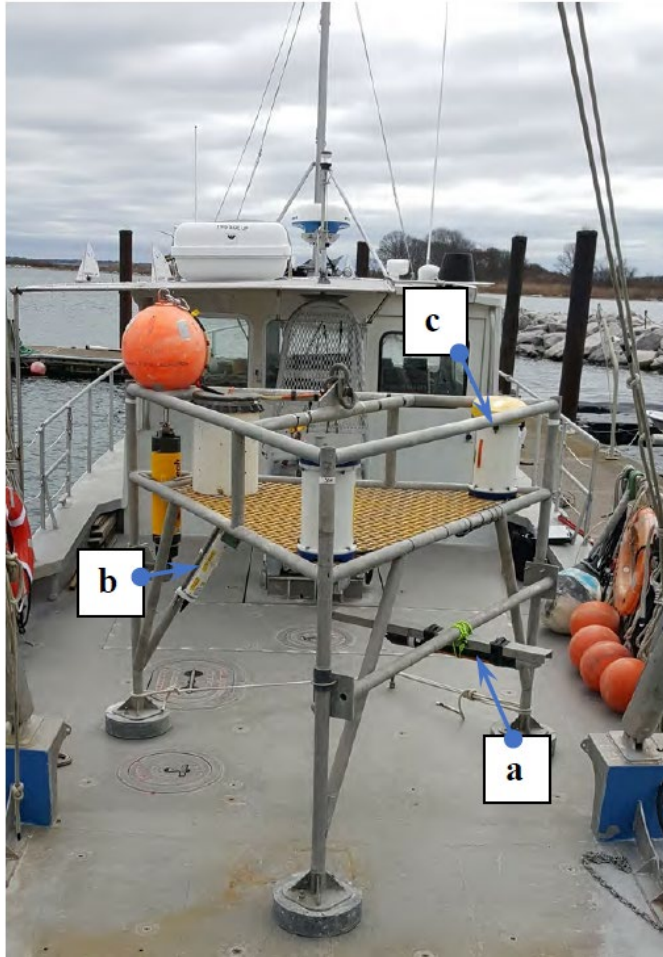
Figure 6.3-3. Frame deployed at SOW1 – all frames were equipped similarly, with a) Nortek High Resolution downward looking Aquadopp profiler, b) Sea-Bird Instruments Model 37 SMP Conductivity/Temperature/Pressure sensor, and c) RD Instruments acoustic Doppler current profiler with wave array firmware.

Transect and station data were collected during fall 2017 and spring 2018 cruises. During both cruises, a single transect was continually and repeatedly sampled during a 12-hour period with a ship-mounted ADCP. Stations along the transect were also repeatedly sampled with a Sea-Bird Model 19+ CTD (conductivity, temperature, depth). During the fall 2017 cruise, four stations were sampled. During the spring 2018 cruise, additional stations were added to look at cross-bathymetric contours in the eastern half and the eastern entrance to FIS, and near the western limit of the study area south of Clinton Harbor. Cruise data collection summaries are presented in Table 6-3 and Table 6-4. Location details of the cruise sampling stations are shown in Appendix 3. Table 6-5 shows the timeline of the data collection effort.

Table 6-3. CTD 12 Hour Survey – Winter 2017 - Station Locations

Station ID	Latitude	Longitude	Station Depth (meters)	N Casts
N1-1	41 17.9177	72 05.0212	6.1	5
N1-2	41 17.1696	72 05.4720	10.9	10
N1-3	41 16.4313	72 05.9873	20.1	10
N1-4	41 15.5349	72 06.5856	33.5	6
N2-1	41 18.1732	72 10.7515	9.8	6
N2-2	41 17.3729	72 10.7154	14.0	12
N2-3	41 16.5301	72 10.6272	17.7	12
N2-4	41 15.5604	72 10.5426	32.6	7
N3-1	41 17.1089	72 14.6969	16.5	6
N3-2	14 16.1559	72 14.6969	17.4	11
N3-3	41 15.2662	72 14.6969	28.0	11
N3-4	41 14.3049	72 14.6969	33.8	6
N4-1	41 15.5647	72 20.4353	5.8	6
N4-2	41 15.0995	72 19.6817	8.5	11
N4-3	41 14.5568	72 18.7853	32.3	11
N4-4	41 13.9125	72 17.7541	36.6	6
N5-1	41 17.7994	72 02.5349	9.1	8
N5-2	41 16.8567	72 02.5349	12.5	8
N5-3	41 17.3042	72 00.0604	14.0	8
N5-4	41 18.1633	72 00.0604	9.8	9

Table 6-4. CTD 12 Hour Survey - Spring 2018 - Station Locations

Station ID	Latitude	Longitude	Station Depth (meters)	N Casts
N0-1	41 17.6108	71 51.4745	21.1	7
N0-2	41 17.0093	71 53.4086	22.0	7
N0-3	41 16.3598	71 53.0402	42.9	7
N0-4	41 17.0412	71 51.0424	36.7	8
N1-1	41 18.8733	71 55.3366	9.5	8
N1-2	41 18.8733	71 57.3814	16.4	8
N1-3	41 18.0035	71 57.3814	19.4	8
N1-4	41 18.0035	71 55.3366	20.0	8
N21-1	41 17.9177	72 05.0212	6.1	7
N21-2	41 17.1696	72 05.4720	10.9	12
N21-3	41 16.4313	72 05.9873	20.1	13
N21-4	41 15.5349	72 06.5856	33.5	7
N22-1	41 18.1732	72 10.7515	9.8	6
N22-2	41 17.3729	72 10.7154	14.0	11
N22-3	41 16.5301	72 10.6272	17.7	12
N22-4	41 15.5604	72 10.5426	32.6	6
N23-1	41 17.1089	72 14.6969	16.5	6
N23-2	14 16.1559	72 14.6969	17.4	12
N23-3	41 15.2662	72 14.6969	28.0	12
N23-4	41 14.3049	72 14.6969	33.8	7
N24-1	41 15.5647	72 20.4353	5.8	6
N24-2	41 15.0995	72 19.6817	8.5	12
N24-3	41 14.5568	72 18.7853	32.3	12
N24-4	41 13.9125	72 17.7541	36.6	7
N6-1	41 14.7994	72 31.4255	9.8	7
N6-2	41 13.8567	72 31.4255	26.1	13
N6-3	41 13.3042	72 31.4255	32.5	13
N6-4	41 12.1633	72 31.4255	17.2	7

Table 6-5. Data Collection Timeline

2017

28 March	Deploy WID3, EID2 in Fishers Island Sound
30 March	Deploy SOW1 east entrance FIS
07 June	Recover SOW1, EID2
08 June	Recover WID3
28 Nov-3 Dec	SEABOSS cruise -> underway ADCP
28-29 Nov	12 hour CTD survey stations N1-1, N1-2, N1-3, N1-4
29-30 Nov	12 hour CTD survey stations N2-1, N2-2, N2-3, N2-4
30 Nov-1 Dec	12 hour CTD survey stations N3-1, N3-2, N3-3, N3-4
01-02 Dec	12 hour CTD survey stations N4-1, N4-2, N4-3, N4-4
02-03 Dec	12 hour CTD survey stations N5-1, N5-2, N5-3, N5-4
21 Dec	Deploy WID3, EID2, SOW1, SFW5, WFW4

2018

19 March	Recover WID3, EID2, SOW1, SFW5, WFW4
08-15 May	SEABOSS cruise -> underway ADCP and mTSG
08-09 May	12 hour CTD survey stations N1-1, N1-2, N1-3, N1-4
09-10 May	12 hour CTD survey stations N21-1, N21-2, N21-3, N21-4
10-11 May	12 hour CTD survey stations N22-1, N22-2, N22-3, N22-4
11-12 May	12 hour CTD survey stations N23-1, N23-2, N23-3, N23-4
12-13 May	12 hour CTD survey stations N24-1, N24-2, N24-3, N24-4
13-14 May	12 hour CTD survey stations N6-1, N6-2, N6-3, N6-4
14-15 May	12 hour CTD survey stations N0-1, N0-2, N0-3, N0-4

6.4   Model Implementation

The LIS Finite Volume Coastal Ocean Model (FVCOM) was initially developed with support from the Connecticut Sea Grant College Program and the collaboration of Professor C. Chen of the University of Massachusetts (UMass), Dartmouth. The domain of the model and the resolution are shown in Figure 6.4-1. We developed an implementation of FVCOM (Chen et al., 2007) at UConn and designed it to use the results of the operational northwest Atlantic regional model, operated as the Northeast Coastal Forecast System (NECOFS), to provide ocean boundary conditions. This 'nesting' approach is computationally efficient since it allows the effect of the larger-scale processes to be simulated at coarse resolution through NECOFS and allows UConn computing resources to focus on the smaller-scale structures in LIS and BIS. The FVCOM implementation uses the General Ocean Turbulence Model (GOTM; Burchard et al., 1999) to model vertical turbulent mixing. O'Donnell et al. (2015) found that a bottom roughness value of z_0=1 cm provided the best representation of bed stresses within LIS in the FVCOM model and this value was used throughout the domain.
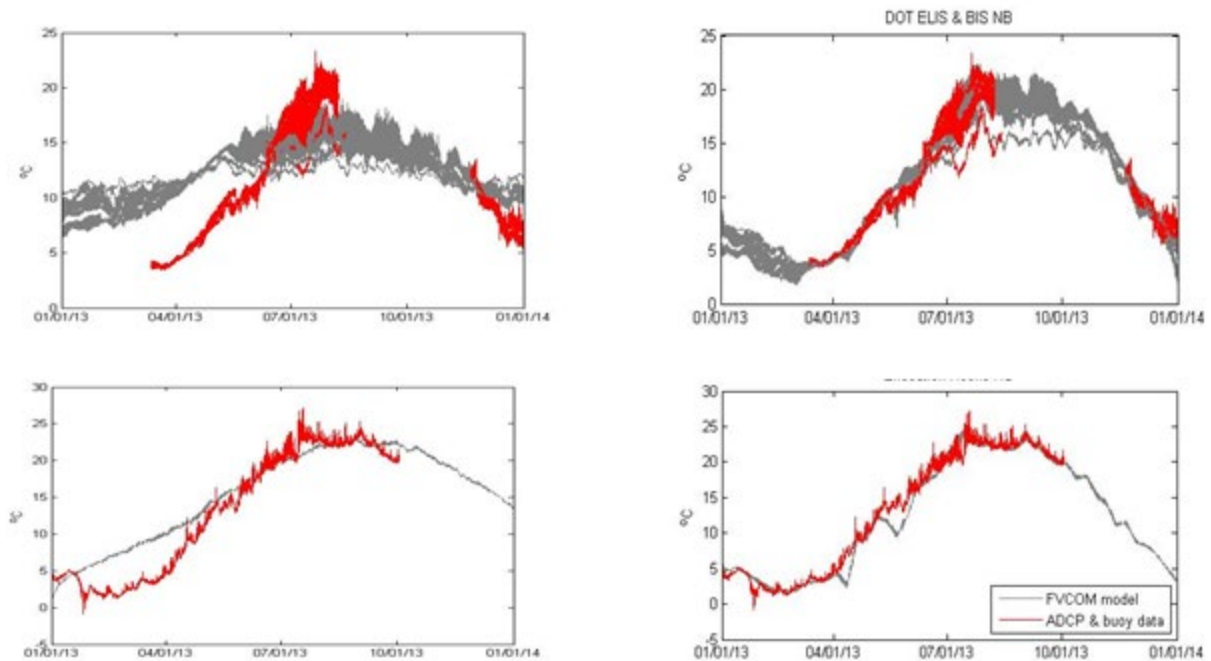
Figure 6.4-1. Comparison of model temperature predictions (gray) with observations (red) in LIS during 2013 with and without SST data assimilation. (a,c) show comparisons when the model is forced using only WRF heat fluxes; (b,d) show the comparisons when MODIS-a SST is also assimilated into the model. (a,b) show comparisons of near-bottom temperatures at seven locations in the ELIS and BIS during 2013 (See O'Donnell et al., 2015); (c,d) show comparisons of near-surface temperatures at the LISICOS Execution Rocks buoy.

LIS-FVCOM was initialized using a temperature and salinity climatology data set derived via objective interpolation of CT DEEP station data as described by O'Donnell et al. (2015) and the data in the NOAA archive described by Codiga & Ullman (2010). In order to be input into the FVCOM model, these OI fields were linearly interpolated to a set of standard depths. The 2018 model runs were initialized using end-of-year conditions from 2017.

LIS-FVCOM is forced at the seaward boundaries by sea level variations and salinity and temperature. The sea level is initially prescribed using tidal constituents derived from the global tidal model (Egbert et al., 1994). The amplitudes and phases of the major constituents were then iteratively adjusted to achieve an optimal representation of the amplitude and phase at each tidal frequency using NOAA tidal height observations at Montauk and King's Point (NY) and at New London, New Haven, and Bridgeport (CT). Subtidal fluctuations at the open boundary are incorporated from the NECOFS system by de-tiding and low-pass filtering the NECOFS solution at the open boundary locations using t-tide (Pawlowicz et al., 2002) and a 25-hour raised cosine low-pass filter. The model's subtidal performance was further optimized by removing the low-passed error in the NECOFS subtidal forcing as determined by comparing the NECOFS solution with NOAA sea-surface height (SSH) gauges at Newport, RI and Atlantic City, NJ. These stations are near the open boundary of the LIS model. The de-tided and adjusted NECOFS subtidal solution was then combined with the time series of tidal heights generated using the optimized tidal constituents as described above.

Freshwater enters the LIS FVCOM domain through seven model cells corresponding to the locations of the Thames, Connecticut, Niantic, Quinnipiac, Housatonic, and Hudson rivers and

New York City wastewater treatment plants (WWTP). These fluxes are based on gauged flows measured by the USGS at Thompsonville, CT, and lagged by one day to account for the distance between the head of the Connecticut River in our model and Thompsonville. Each river, R_i, is adjusted using the USGS Thompsonville data as $R_i = 1.20 \frac{R_{CT}}{\overline{R_{CT}}} \overline{R_i}$ where R_{CT} is the day-specific Connecticut River flow, $\overline{R_{CT}}$ is the mean Connecticut River flow, and $\overline{R_i}$ is the mean flow for river i. The factor of 1.20 follows from the salt budget of Gay et al. (2004) and accounts for the portion of the watersheds of the rivers below the USGS gauges. A fixed input of 40 $m^3 s^{-1}$ was added to the East River to represent the freshwater discharged from the New York WWTPs.

Domain-variable winds derived from the Weather Research and Forecasting model (WRF) run as hindcasts at UMass, Dartmouth are used for the LIS-FVCOM surface wind forcing. The LIS-FVCOM model originally used heat fluxes also obtained from the UMass WRF model. However, the UMass WRF heat fluxes substantially underestimate the wintertime cooling at LIS locations. To correct this issue, sea surface temperatures (SSTs) were assimilated into the model using NASA Moderate Resolution Imaging Spectroradiometer (MODIS) Aqua 8-day composited and de-clouded (level 3) satellite data. Because the NASA SST product has poor coverage in cells that are close to the coast, the entire dataset was pre-screened to keep only data from cells that had at least 86.7% coverage for the entire year (i.e., all data was removed from those cells with 7 or more missing 8-day SSTs out of the total of 45 8-day products for the 2017 year). The remaining SST data was then linearly interpolated in time to fill any temporal gaps and then spatially interpolated to 100% coverage using the nearest spatial neighbor with good coverage. The net effect of this pre-screening and interpolation methodology is that values in cells at the coast where coverage is poor are replaced with the values from the nearest offshore cell.

Figure 6.4-1 shows time-series of the model to data temperature comparisons both with and without SST temperature assimilation. Note that the improvement in the bottom temperatures (panels a, b) is similar to the improvement in the surface temperatures (panel c, d), indicating that the model is capturing the downward heat fluxes within the water column adequately.

6.5 Model Skill Assessment

To evaluate the model performance, we use the 'skill', s, statistic defined as:

Equation 7

$$s = 1 - \frac{\left\langle \left(f_m - f_d \right)^2 \right\rangle}{\left\langle \left(f_d - \left\langle f_d \right\rangle \right)^2 \right\rangle}$$

where f_m and f_d represent the model and data values (e.g. f represents sea level (η) or temperature (T), etc.) and the $\langle \rangle$ notation represents the mean of the argument over the simulation interval (i.e. $<f_d>$ is the mean of the data) (von Storch & Zwiers, 1999). The LIS model skill assessment using this metric is described in O'Donnell et al. (2015). Since the time of that report, the model has been improved by Dr. McCardell. Most notably, the model now assimilates SSTs from the NASA MODIS Aqua satellite.

6.5.1 Sea Surface Height Skills

Table 6-6 shows the model SSH skill (Equation 7) from the 2017 simulation compared to hourly measurements at the four NOAA tidal gauges in LIS: New London, New Haven, Bridgeport, and King's Point. The first row shows the skills when simulated sea surface heights (relative to MSL) are compared to the raw observations. The second and third rows shows the skills when the model and data series are divided into tidal and weather components using harmonic analysis (Pawlowicz et al., 2002). The errors in the simulation of tides are small - the skills all exceed 93%. The errors in the simulation of the total water level (SSH) mainly arise from the errors in the simulation of the meteorologically driven motions and are to some extent due to inadequacies in the atmospheric model used to prescribe winds.

Table 6-6. Model skills (Equation 7) when model elevations are compared to NOAA gage data at New London, New Haven, Bridgeport, and Kings Point. The first row (Total SSH skill) shows the skills when sea-surface heights (relative to MSL) are compared, the second row shows the skills at tidal frequencies, the third row shows the skills for the subtidal residuals.

	New London	New Haven	Bridgeport	King's Point
Total SSH skill	91%	92%	93%	93%
Tidal skill	94%	93%	94%	94%
Subtidal skill	77%	75%	77%	54%

Figure 6.5-1 shows a comparison of the spectral power density obtained from the NOAA record at the four LIS gauges with that from the LIS-FVCOM model at these locations. Note that although the model does a good job at capturing the M2 amplitudes and M4 harmonics, it significantly underestimates the M6 harmonics.
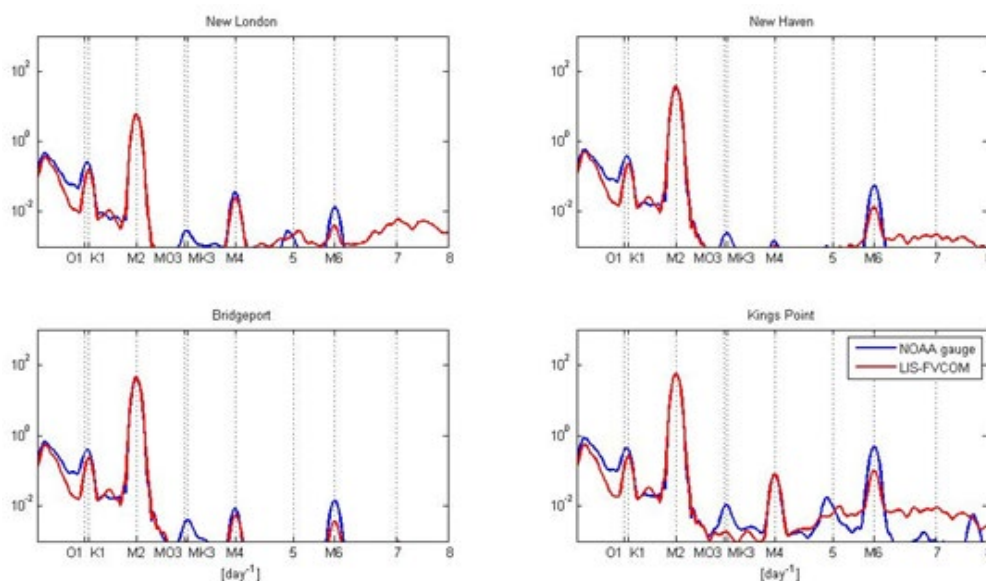
Figure 6.5-1. Comparison of the power spectral density (PSD) of the SSH records from the NOAA gauges (blue) at New London (a),

6.5.2 Temperature and Salinity Skills

Figure 6.5-2 shows a comparison of surface and bottom model temperatures with monthly climatologies derived from 1993-2015 CT DEEP surveys and the 2017 CT DEEP surveys. These data are described by Kaputa & Olsen (2000) and O'Donnell et al. (2014). The skills listed in the panels were calculated by combining the individual station scores using the mean square methodology described in Ganju et al. (2016).

For comparison, the surface and bottom traditional skills from runs that only used the WRF heat flux forcing (did not use the SST assimilation) were in the 0.70-0.90 range. Note that the CT DEEP dataset used to evaluate the temperature skills shown in Figure 6.5-2 was not what was assimilated into the model. The high skill scores are thus indicative of both the success of the data assimilation itself and of excellent agreement between the screened remote sensing temperature data and the in situ temperature measurements made by the CT DEEP.

As shown in Figure 6.5-3, the near-surface and near-bottom traditional salinity skills are 0.15, and 0.19, respectively. Figure 6.5-3 indicates that much of the salinity error is due to a bias error. This was removed prior to creating the interpolated map products.
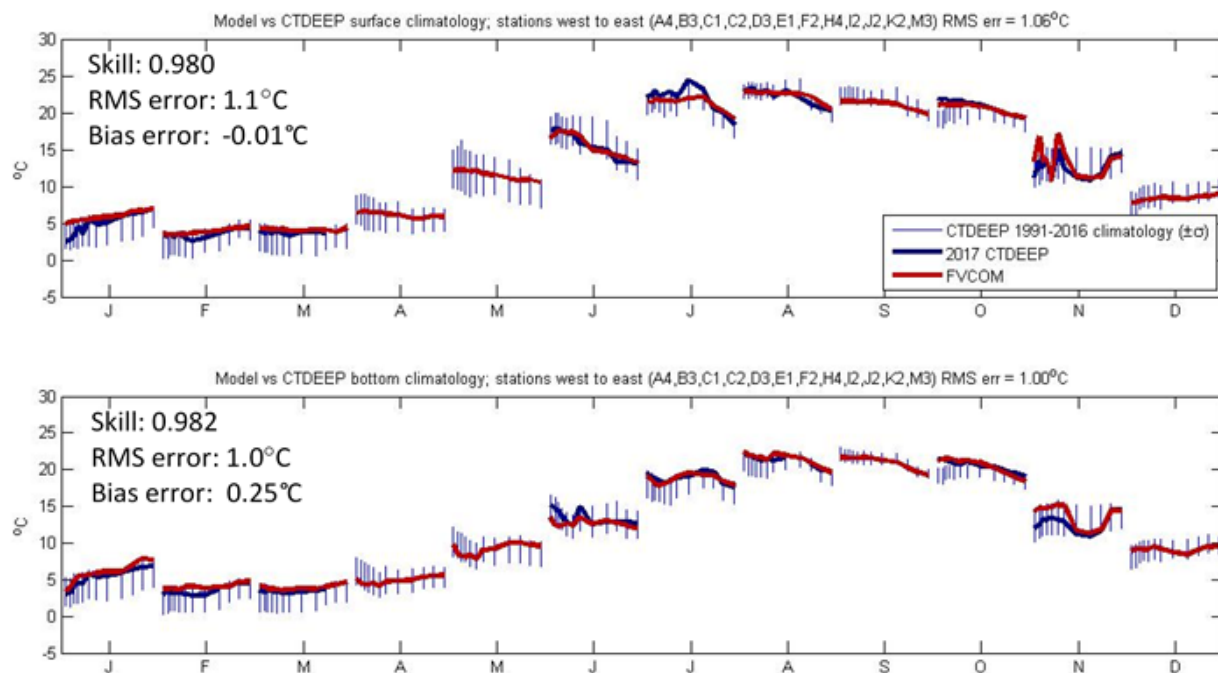
Figure 6.5-2. Plots by month showing surface (top panel) and bottom (bottom panel) temperature comparisons between model predictions (red lines) and monthly climatologies from 1993-2016 CT DEEP survey data (thin vertical blue bars, ±σ) and the 2017 CT DEEP surveys (thick blue lines). Within each month, the CT DEEP stations are plotted by longitude from west to east.
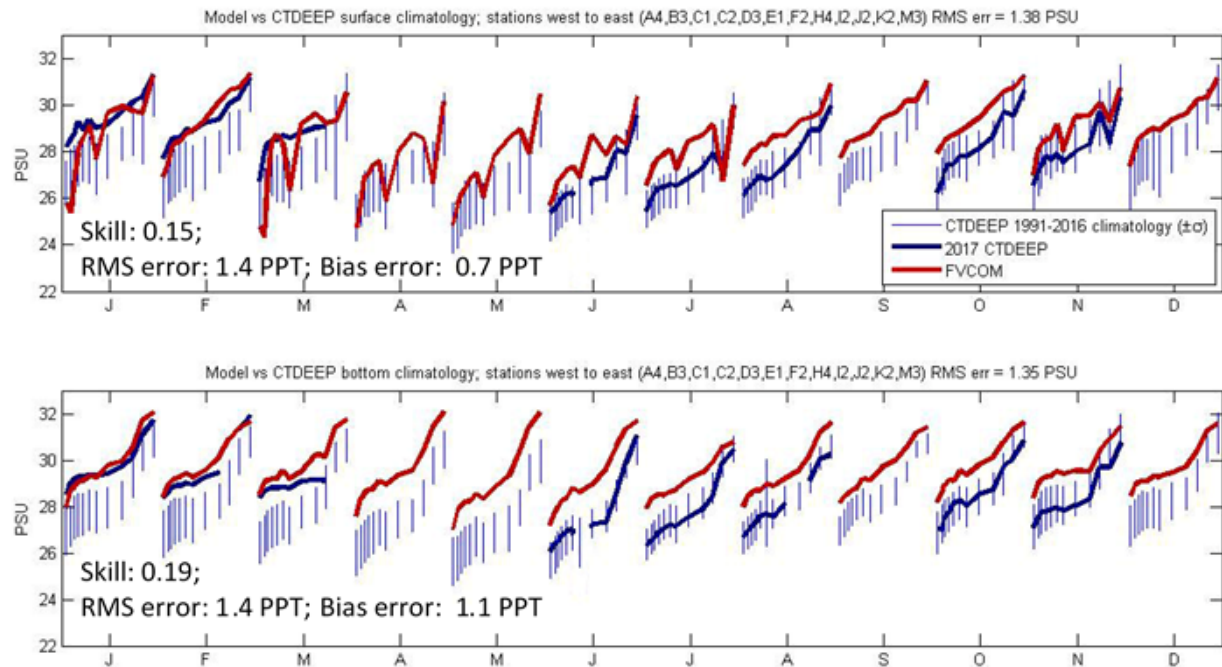
Figure 6.5-3. Plots by month showing surface (top panel) and bottom (bottom panel) salinity comparisons between model predictions (red lines) and monthly climatologies from 1993-2016 CT DEEP survey data (thin vertical blue bars, ±σ) and the 2017 CT DEEP surveys (thick blue lines). Within each month, the CT DEEP stations are plotted by longitude from west to east.

6.6   FIS comparisons
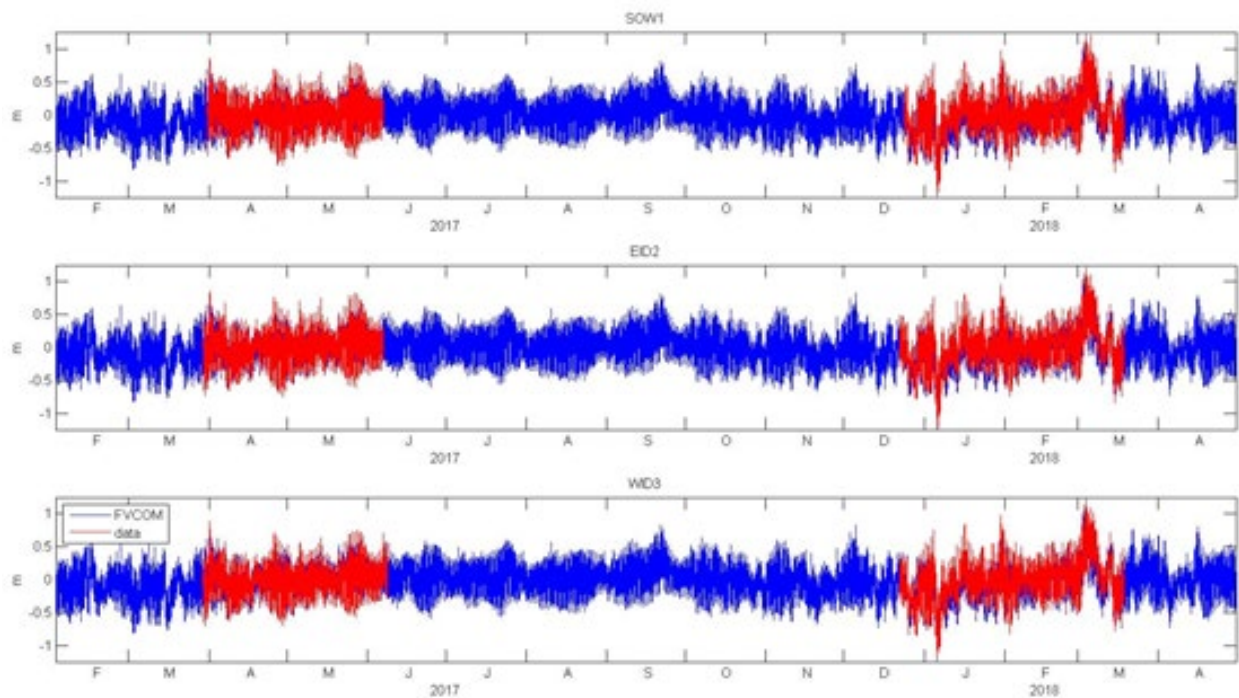
Figure 6.6-1. Time-series plots of SSH at the three FIS bottom-mooring deployment locations comparing the FVCOM predictions (blue) with measurements from the moored instruments (red).
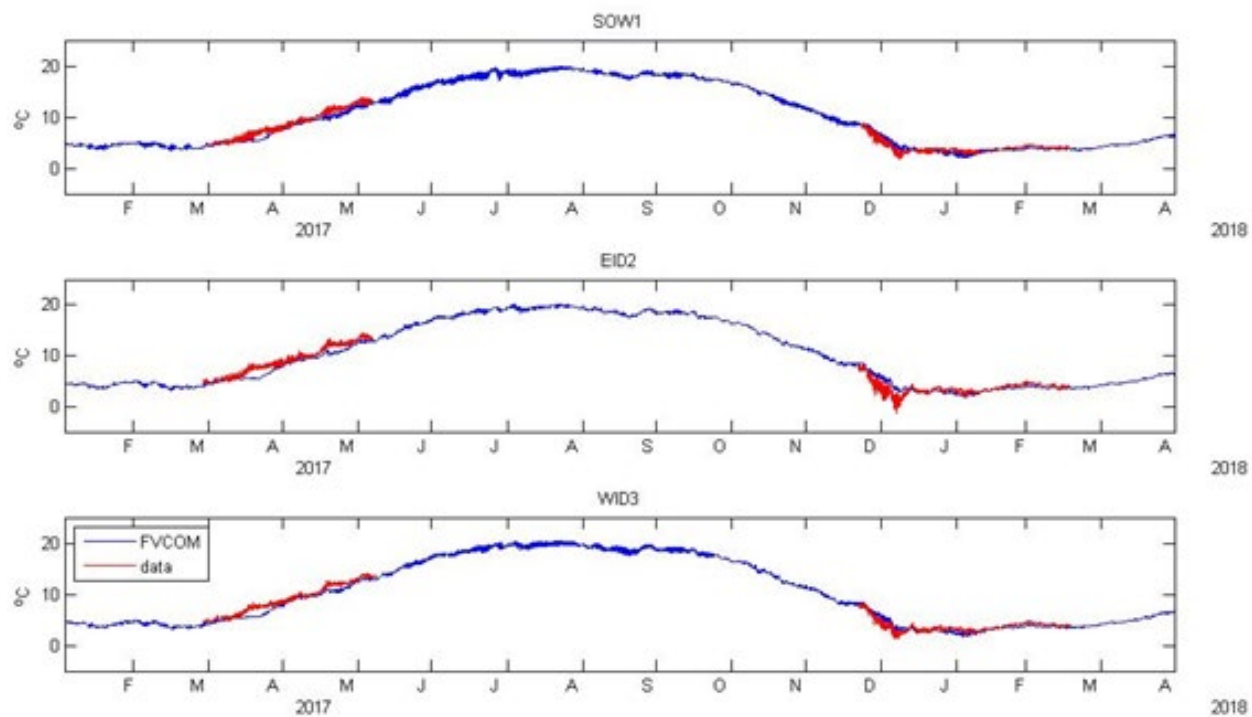
Figure 6.6-2. Time-series plots of near-bottom temperatures at the three FIS bottom mooring deployment locations comparing the FVCOM predictions (blue) with measurements from the moored instruments.
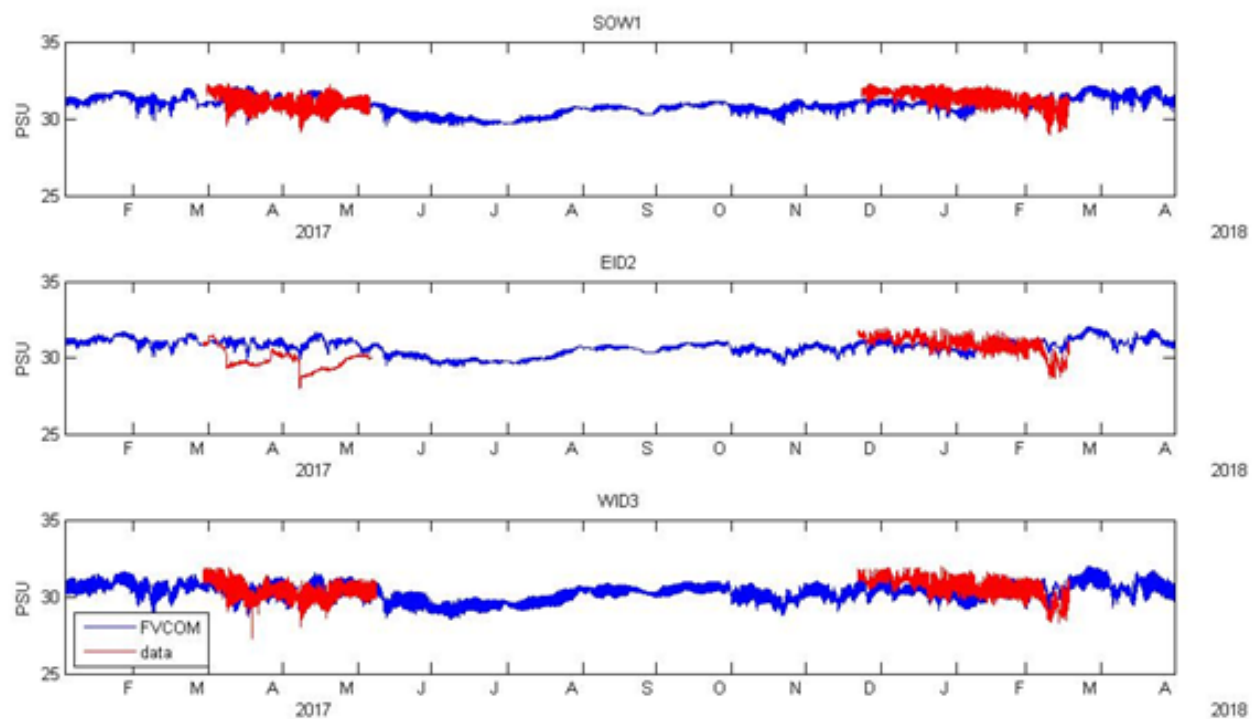
Figure 6.6-3. Plots of near-bottom salinities at the three FIS bottom mooring deployment locations comparing the FVCOM predictions (blue) with measurements from the moored instruments.

6.7 Along-track MSL reference heights

The model was used to produce estimates of along-track MSL and water heights to support the acoustic surveys conducted by Dr. Roger Flood, Stony Brook University, as well as provide further validation of the model results. These surveys took place in Dec 2017, January 2018, and March 2018. Soundings were made at approximately 60k locations and times. Figure 6.7-1 shows the location of these surveys. Figure 6.7-2 and Figure 6.7-3 show the times of the surveys in dark grey at the bottom of the top panel.
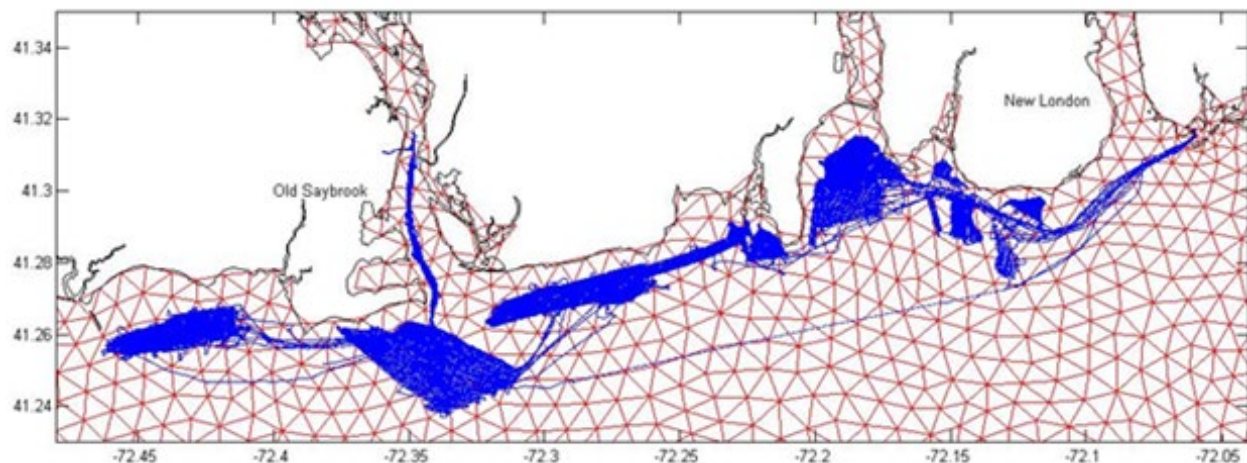
Figure 6.7-1. Acoustic survey tracks (blue) for Dec 2017 through Mar 208 surveys, the FVCOM LIS model grid (red), and the CT coastline (black)
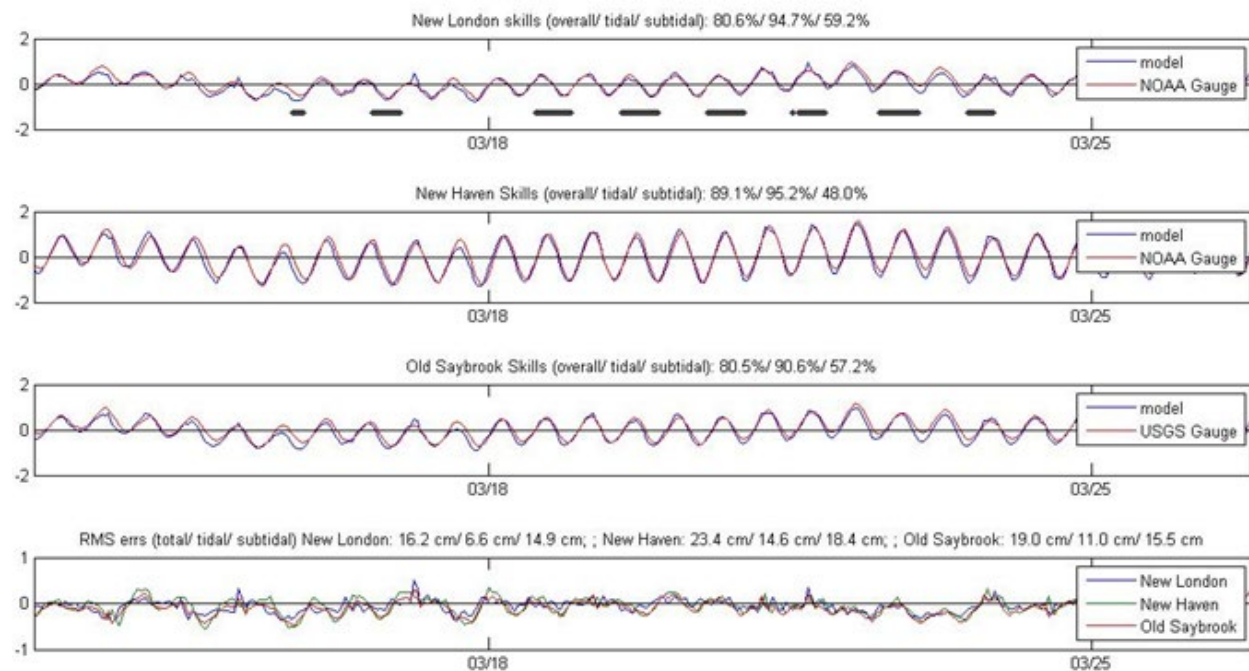
Figure 6.7-2. Comparison of uncorrected model results (blue) with NOAA gauged observations at New London (top panel) and New Haven (second panel) and with USGS gauged observations at Old Saybrook (3rd panel). The grey dots/ bars in the top panel show the acoustic survey times. The bottom panel shows the differences between the model predictions and the observations for all three stations. Note that these errors are highly correlated.
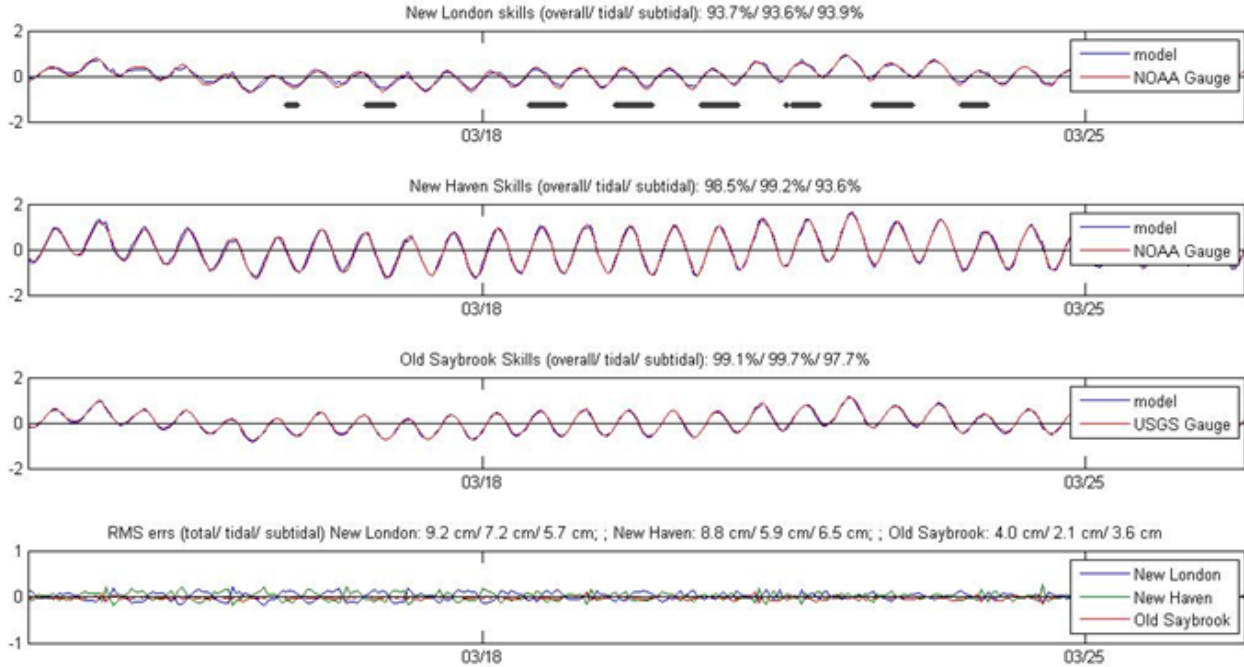
Figure 6.7-3. Comparison of corrected model results (blue) with NOAA gauged observations at New London (top panel) and New Haven (second panel) and with USGS gauged observations at Old Saybrook (3ʳᵈ panel). The grey dots/ bars in the top panel show the acoustic survey times. The bottom panel shows the differences between the model predictions and the observations for all three stations. Note that these errors are no longer highly correlated since the correlated error has been removed.

In order to remove known errors from the model predictions, the hourly FVCOM LIS SSH solution was compared to the NOAA hourly observations at New London and New Haven and the USGS observations at Old Saybrook. Prior to these comparisons, both the model results and the observations were de-tided using t_tide (Pawlowicz et al., 2002). The subtidal and tidal model results were then corrected using the 3-station mean model-observational discrepancy as shown in Equation 8.

Equation 8

$$\eta_{corrected_i}^{j} = \eta_{pred_i}^{j} + \frac{1}{3} \sum_{i=[\,i_{NLN}, i_{HVN}, i_{OS}]} \left(\eta_{obs_i}^{j} - \eta_{pred_i}^{j} \right)$$

where $\eta_{pred_i}^{j}$ are the model SSH predictions at locations $i = [1, ..., N]$ and hourly times $j = [1, ..., M]$ and $\eta_{obs_i}^{j}$ are the SSH observations at the three gauge locations $i = [i_{NLN}, i_{HVN}, i_{OS}]$ and hourly times $j = [1, ..., M]$.

The corrected hourly model results were then temporally interpolated to the 60k unique acoustic survey times using t_tide for the tidal portion and a linear interpolation for the subtidal portion. These time-interpolated results (at the acoustic survey times) were then spatially interpolated from the 200-500 m FVCOM grid to the 60k unique acoustic survey locations. The observations at the three tidal gauges significantly corrects the subtidal model error (which is highly spatially correlated) and, to a lesser extent, the tidal model error while preserving the spatial gradients in the model. Table 6-7 shows the tidal and subtidal skills and RMS errors for both uncorrected and corrected model results.

Table 6-7. Skills $(1 - [model - obs]^2/var[obs])$ and RMS errors (cm) at the three tidal stations for uncorrected model, corrected model, and corrected null model for the period from 1 Dec 2017 through 31 Mar 2018.

			New London	New Haven	Old Saybrook
Tidal	Skill	uncorrected	94.7%	95.2%	90.6%
		corrected	93.6%	99.2%	99.7%
		corrected null	33.0%	81.4%	97.4%
	RMS error (cm)	uncorrected	6.5	14.6	11.0
		corrected	7.2	5.9	2.1
		corrected null	23.3	28.5	5.8
Subtidal	Skill	uncorrected	59.2%	48.0%	57.2%
		corrected	94.0%	93.6%	97.7%
		corrected null	93.9%	95.0%	99.0%
	RMS error (cm)	uncorrected	14.9	18.4	15.5
		corrected	5.7	6.5	3.6
		corrected null	6.1	5.7	2.4
Overall	Skill	uncorrected	80.6%	89.1%	80.5%
		corrected	93.7%	98.5%	99.1%
		corrected null	57.5%	83.0%	98.1%
	RMS error (cm)	uncorrected	16.2	23.4	19.0
		corrected	9.2	8.8	4.0
		corrected null	24.0	29.3	5.9

Also included in table are the skills and errors for a corrected null model. A null model that is corrected by the mean error at the three stations is the mean SSH of the three stations. Because of the high correlation in subtidal SSH in the local region of the three gauges, the corrected null model performs well for subtidal SSHs, particularly at Old Saybrook which is located midway between New London and New Haven. The corrected null model does a poor job with the tides, however.

The results were referenced to NAVD88 by looking at the long-term bias differences between the subtidal model results and the subtidal observations at New London and Old Saybrook, both of which were referenced to NAVD88. Because the model is expected to be able to capture the long-term mean SSH gradients, this also provides a means of comparing the NAVD88 reference for the New London NOAA record with the NAVD88 reference for the USGS Old Saybrook record. There appears to be about a 5 cm difference between these two references. Because the model predicts only a 2 mm difference in the long-term wintertime mean between Old Saybrook and New London, we chose the mean of the NAVS references at these two locations as the "zero" reference and adjusted the model results by a fixed offset accordingly.

Figure 6.7-2 shows a comparison of the uncorrected model results with the observations for the period of the March acoustic surveys, while Figure 6.7-3 shows the comparison with the corrected model results. Also shown in the bottom panels of Figure 6.7-2 and Figure 6.7-3 are the model-

observation residuals (i.e., the model error). Figure 6.7-2 indicates that this error is highly correlated between the three stations. Since the model is corrected by removing the mean of this error, the remaining error in the corrected model (Figure 6.7-3) is no longer positively correlated.

6.8   Physical Oceanographic products

The model was used to produce maps of:

1. the bottom temperature distributions throughout the study area for each month
2. the bottom salinity distributions throughout the study area for each month
3. the spatial structure of the maximum bottom stress magnitude due to (mainly) tidal currents
4. the spatial structure of the mean bottom stress magnitude due to (mainly) tidal currents

These fields were rasterized into GIS format and transferred to the map server to distribute the results. Products are best viewed through that interface. As examples, Figure 6.8-1 shows estimates of mean near-bottom temperatures in the study area during July of 2017 while Figure 6.8-2 shows estimates of the maximum bottom stresses due to tidal currents. Note that the magnitude of the spatial gradients predicted by the model far exceeds the estimates of the model error.
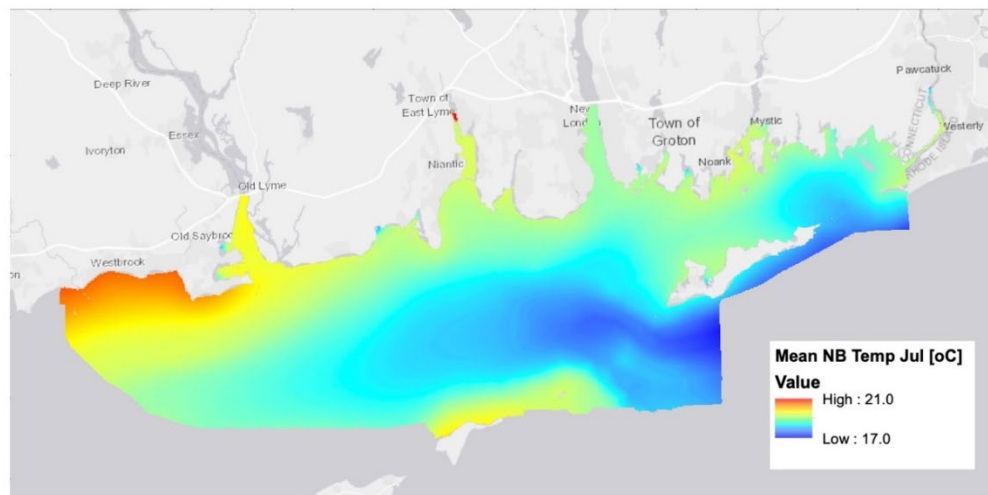

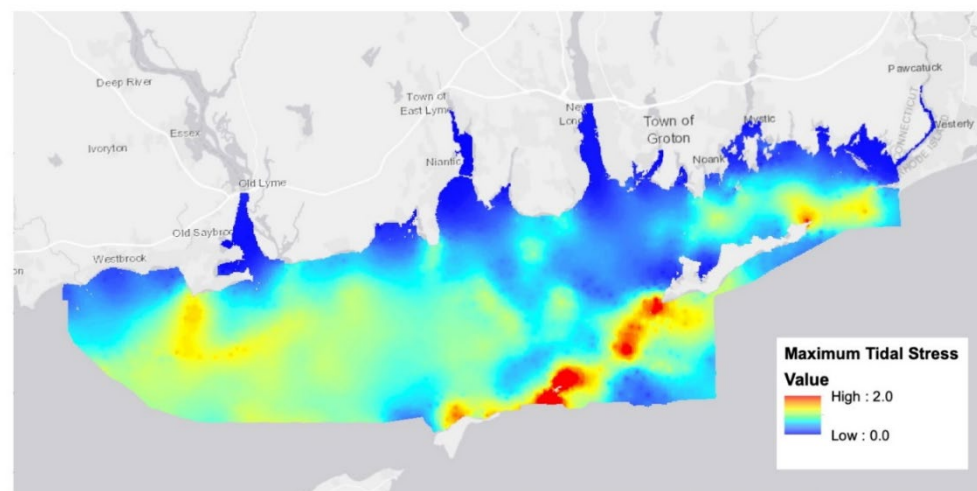*Figure 6.8-1. Example map product showing mean bottom temperatures during July, 2017*

Figure 6.8-2. Example map product showing maximum bottom stresses due to tides

6.9 Summary and Conclusions

We report the results of a numerical model to estimate the distributions of ecologically relevant characteristics of the near bottom environment. Using the model, we developed GIS-format map products with information that span the domain. Figure 6.8-1 shows an example. Others are included in Appendix 1.

A limited measurement program was executed to acquire salinity, temperature, and current distributions so that the performance of the model in describing the small-scale spatial variations and the seasonal scale evolution of the variables could be critically assessed. The comparison of the model simulations to observed temperatures is excellent. In the study region, model temperatures were generally well within ±1°C of measured values (See Figure 6.5-2 & Figure 6.6-2). Salinities are generally within ±1 ppt (Figure 6.5-3 & Figure 6.6-3).

That the spatial and temporal structures of the temperature, salinity, and velocity fields captured by the model show excellent agreement with the field studies clearly supports the model's use as a tool to interpolate spatially between the observations for the purpose of making maps of the ecologically important characteristics of the bottom environment. Each of these parameters are significant determinants of the distributions of benthic fauna within the Phase II study area.

The mean temperature and salinity maps were generated for each month and provide insights into the temporal and spatial variability of these measures within the Phase II area. It is well known that LIS experiences some of the largest seasonal variation in water temperature, which is supported by the model results, with a mean low of 3.5° C occurring particularly in the western regions of the area in the months of February and March. The same western area experiences high water temperature (23° C) in August. Salinity was not surprisingly more stable over the course of the year, with higher salinities occurring in the eastern end of the area and lower salinities near the mouth of the Connecticut during the spring and summer months.

Water currents directly affect benthic organisms through bottom stress, which is a measure of the force the current creates over the bottom. Bottom stress maps were generated for tidal mean, maximum tidal, and overall maximum and in each case illustrated similar patterns, with highest values in and around the Race, eastern Fishers Island Sound, and to some degree west of the mouth of the Connecticut River. Bottom stress is a key factor in the distribution of sediment types through scouring in high current areas and deposition in lower current regimes. Additionally, bottom stress influences rates of recruitment and feeding by benthic taxa, can impact attachment to the substrates, and survivorship during storm events. For these reasons the bottom stress map products were utilized by the Ecological Characterization team as a critical element in the development of the Integrated Habitat Map product.

6.10 References

Bennett, D. C., O'Donnell, J., Bohlen, W. F., & Houk, A. (2010). Tides and Overtides in Long Island Sound. *Journal of Marine Research, 68*(1), 1-35.

Blumberg, A. F., & Pritchard, D. W. (1997). Estimates of the transport through the East River, New York. *Journal of Geophysical Research: Oceans, 102*(C3), 5685-5703.

Blumberg, A. F., Khan, L. A., & St. John, J. P. (1999). Three-Dimensional Hydrodynamic Simulations of the New York Harbor, Long Island Sound and the New York Bight. *Journal of Hydraulic Engineering, 125*(8), 799-816.

Bokuniewicz, H. J., & Gordon, R. B. (1980). Sediment transport and deposition in Long Island Sound. *Advances in Geophysics, 22*, 69-106.

Burchard, H., Bolding, K., & Ruiz-Villarreal, M. (1999). *GOTM, a general ocean turbulence model: theory, implementation and test cases.* Report EUR 18745, European Commission.

Chen, C., Huang, H., Beardsley, R. C., Liu, H., Xu, Q., & Cowles, G. (2007). A finite-volume numerical approach for coastal ocean circulation studies: comparisons with finite difference models. *Journal of Geophysical Research: Oceans, 112*(C3).

Codiga, D. L., & Ullman, D. S. (2010). *Characterizing the physical oceanography of coastal waters off Rhode Island, Part 1: Literature review, available observations, and a representative model simulation.* Appendix to Rhode Island Ocean Special Area Management Plan.

Crowley, H. A. (2005). *The seasonal evolution of thermohaline circulation in Long Island Sound.* Doctoral dissertation, State University of New York at Stony Brook. ProQuest Dissertations Publishing.

Egbert, G. D., Bennett, A. F., & Foreman, M. G. (1994). TOPEX/POSEIDON tides estimated using a global inverse model. *Journal of Geophysical Research: Oceans, 99*(C12), 24821-24852.

Fribance, D. B., O'Donnell, J., & Houk, A. (2013). Residual circulation in western Long Island Sound. *Journal of Geophysical Research: Oceans, 118*(9), 4727-4745.

Ganju, N. K., Brush, M. J., Rashleigh, B., Aretxabaleta, A. L., del Barrio, P., Grear, J. S., . . . Vaudrey, J. M. (2016). Progress and Challenges in Coupled Hydrodynamic-Ecological Estuarine Modeling. *Estuaries and Coasts, 39*(2), 311-32.

Gay, P. S., O'Donnell, J., & Edwards, C. A. (2004). Exchange between Long Island Sound and adjacent waters. *Journal of Geophysical Research: Oceans, 109*(C6).

Hao, Y. (2008). *Tidal and residual circulation in Long Island Sound.* Doctoral dissertation, Stony Brook University, Marine Sciences Research Center, Stony Brook, NY.

Kaputa, N. P., & Olsen, C. B. (2000). *Summer Hypoxia Monitoring Survey 1991-1998 Data Review.* State of Connecticut Department of Environmental Protection, Long Island Sound Ambient Water Quality Monitoring Program, Hartford.

Kenefick, A. M. (1985). Barotropic M2 tides and tidal currents in Long Island Sound: a numerical model. *Journal of Coastal Research, 1*(2), 117-128.

Lemus, E. R. R. (2008). *Wind waves in central Long Island Sound : a comparison of observations to an analytical expression.* Doctoral dissertation, University of Connecticut, Department of Marine Sciences, Avery Point.

Murphy, D. L. (1980). *A numerical investigation into the physical parameters which determine residual drift in Long Island Sound.* Doctoral dissertation, University of Connecticut, Department of Marine Sciences. ProQuest Dissertations Publishing.

O'Donnell, J., Wilson, R. E., Lwiza, K., Whitney, M., Bohlen, W. F., Codiga, D., . . . Varekamp, J. (2014). The Physical Oceanography of Long Island Sound. In J. S. Latimer, M. A. Tedesco, R. L. Swanson, C. Yarish, P. E. Stacey, & C. Garza (Eds.), *Long Island sound: prospects for the urban sea* (pp. 79-158). New York, NY: Springer. doi:10.1007/978-1-4614-6126-5_3

O'Donnell, J. (2015). *Physical Oceanography of Eastern Long Island Sound: Literature Review.* Technical Report, United States Environmental Protection Agency. doi:10.13140/RG.2.2.25683.99365

O'Donnell, J., & Bohlen, W. F. (2003). *The Structure and Variability of the Residual Circulation in Long Island Sound.* Final Project Report, Connecticut Department of Environmental Protection, Long Island Sound Research Fund Grant CWF, Hartford, CT.

O'Donnell, J., McCardell, G., Fake, T., Cifuentes-Lorenzen, A., & Horwitz, R. (2015). *Physical Oceanography of Eastern Long Island Sound Region: Appendix C-2, Modeling.* Technical Report, United States Environmental Protection Agency.

Pawlowicz, R., Beardsley, B., & Lentz, S. (2002). Classical tidal harmonic analysis including error estimates in MATLAB using T_TIDE. *Computers & Geosciences, 28*(8), 929-937.

Schmalz, R. A., Devine, M. F., & Richardson, P. H. (1994). *Residual circulation and thermohaline structure, Long Island Sound Oceanography Project Summary Report, Volume 2.* NOAA Technical Report NOS-OES-003, U.S. Department of Commerce, National Oceanic and Atmospheric Administration, Rockville, MD.

Shchepetkin, A. F., & McWilliams, J. C. (2005). The regional oceanic modeling system (ROMS): a split-explicit, free-surface, topography-following-coordinate oceanic model. *Ocean Modelling, 9*(4), 347–404.

Signell, R. P., List, J. H., & Farris, A. S. (2000). Bottom Currents and Sediment Transport in Long Island Sound: A Modeling Study. *Journal of Coastal Research, 16*(3), 551-566.

Swanson, R. L. (1976). *Tides (MESA New York Bight Atlas Monograph #4).* New York: New York Sea Grant Institute.

Valle-Levinson, A., & Wilson, R. E. (1994a). Effects of Sill Bathymetry, oscillating barotropic forcing and vertical mixing on estuary ocean exchange. *Journal of Geophysical Research: Oceans, 99*(C3), 5149-5169.

Valle-Levinson, A., & Wilson, R. E. (1994b). Effects of sill processes and tidal forcing on exchange in eastern Long Island Sound. *Journal of Geophysical Research: Oceans, 99*(C6), 12667-12681.

Valle-Levinson, A., Wilson, R. E., & Swanson, R. L. (1995). Physical mechanisms leading to hypoxia and anoxia in western Long Island Sound. *Environment International, 21*(5), 657-666.

von Storch, H., & Zwiers, F. W. (1999). *Statistical Analysis in Climate Research.* Cambridge University Press.

Wilson, R. E., & Swanson, R. L. (2005). A perspective on bottom water temperature anomalies in Long Island Sound during the 1999 Lobster Mortality event. *Journal of Shellfish Research, 24*(3), 825-830.

7   Data Management

Recommended Citations:

Fake, T. and Ferrini, V. (2023). Objective. Section 7.1, p. 317-318 in: "Seafloor Mapping of Long Island Sound – Final Report: Phase II Project." (Unpublished project report). U. S. Environmental Protection Agency, Long Island Sound Study, Stamford, CT.

Ferrini, V. and Nitsche, F. (2023). MGDS Data System Design and Infrastructure. Section 7.2, p. 318-319 in: "Seafloor Mapping of Long Island Sound – Final Report: Phase II Project." (Unpublished project report). U. S. Environmental Protection Agency, Long Island Sound Study, Stamford, CT.

Ferrini, V. and Nitsche, F. (2023). Technical Overview. Section 7.3, p. 319 in: "Seafloor Mapping of Long Island Sound – Final Report: Phase II Project." (Unpublished project report). U. S. Environmental Protection Agency, Long Island Sound Study, Stamford, CT.

Ferrini, V. and Nitsche, F. (2023). Hardware and interface improvements. Section 7.4, p. 319 in: "Seafloor Mapping of Long Island Sound – Final Report: Phase II Project." (Unpublished project report). U. S. Environmental Protection Agency, Long Island Sound Study, Stamford, CT.

Ferrini, V. and Nitsche, F. (2023). Archived data. Section 7.5, p. 320-322 in: "Seafloor Mapping of Long Island Sound – Final Report: Phase II Project." (Unpublished project report). U. S. Environmental Protection Agency, Long Island Sound Study, Stamford, CT.

Ferrini, V. and Nitsche, F. (2023). Summary/Recommendations. Section 7.6, p. 322-323 in: "Seafloor Mapping of Long Island Sound – Final Report: Phase II Project." (Unpublished project report). U. S. Environmental Protection Agency, Long Island Sound Study, Stamford, CT.

7.1   Objective

The data management efforts of the Phase II Project are intended to (1) ensure that the collaborative teams have access to data during the project to facilitate the creation of final data products, (2) ensure long-term preservation and open access to data generated during the Project, and (3) establish and refine procedures and protocols for documenting, sharing, and archiving data that may be acquired during subsequent efforts. To meet the specific needs of the Phase II Project the 2016 SOW defined the following data system design requirements:

- well-coordinated data management throughout the full life cycle of the project;
- data are collected such that they can be broadly used for all aspects of the multi-disciplinary effort and are consistent enough to support interoperability (Table 7-1);
- data and metadata are made available to members of the LIS Consortia to meet the goals of the project and produce the necessary products;
- the long-term archiving plan ensures that data are sufficiently documented to enable scientific discovery and facilitate management of natural resources within LIS well beyond the completion of the project;
- data can be accessed and downloaded though various user-interfaces and OGC-compliant

web services (e.g., Web Feature Services, Web Map Services);

- data are discoverable and easily accessible to a wide range of stakeholders (managers, scientists, educators, public);
- data management components that include:
  - data sharing policies;
  - comprehensive inventory and metadata;
  - data system that enables download and visualization of data and metadata;
  - tools/workflows for contributing data and metadata to the data system; and
  - long-term access and archiving of data/metadata

Table 7-1. Summary of diverse anticipated data products, types and file formats

Category	Product	Data Type	Preferred Format
Cruise Info	Cruise Tracks	GIS layer(s)	ESRI Geodatabase Feature Class (point/line)
	Cruise Reports/Logs	Digital Documents	PDF
Acoustic	Acoustic Intensity mosaics (composition/roughness/texture)	Rasters	ESRI Grid, GeoTIFF
	Topographic mosaics (bathymetry)	Rasters	ESRI Grid, GeoTIFF
	Sub-Bottom images	GIS layer(s) & images subbottom data	ESRI Geodatabase Feature Class (line), JPEG, SEGY
Sampling	Station Data (Biology/Geology/Chemical/Physical)	GIS layer(s)	ESRI Geodatabase Feature Class (point/line/poly)
	Video	Digital Movies	MOV
	Photos	Digital Photos	JPEG
Geospatial Interpretations	Ecological/Habitat Data	GIS layer(s)	ESRI Geodatabase Feature Class (point/line/poly)
	Sediment Texture/Grain Size	GIS layer(s)	ESRI Geodatabase Feature Class (point/poly)
	Sedimentary Environments (Chem/Organic/Inorganic)	GIS layer(s)	ESRI Geodatabase Feature Class (poly)
Maps/Reports	Analysis Reports/Summaries	Digital Documents	PDF
	Cartographic Maps	Digital Documents	GeoPDF

In order to meet the needs of all partners with respect to access to data, the LIS Data Portal at the LDEO MGDS (Section 7.2) was utilized to provide a comprehensive metadata catalog and long-term data stewardship solution focused on open access and preservation of all data products (raw and derived) and metadata. The LIS Data Portal ensures compliance with metadata standards and includes links to related content in distributed data systems. The data management operations of the Phase II Project are described in detail in the following sections.

7.2   MGDS Data System Design and Infrastructure

The LIS Data Portal deployed at LDEO leverages the technical infrastructure of the MGDS, which is supported primarily by the NSF. MGDS is a trusted data repository that provides free public access to a curated collection of marine geophysical data products and complementary data that support the needs of a diverse community of marine scientists, policy makers, educators, and the general public. The MGDS team curates a metadata catalog and digital data repository that serves over 103 TB of data files, and provides links to data at over 30 external data systems and institutions. Investigator-focused data stewardship offered by MGDS supports through the entire data life cycle – from planning through acquisition to long-term data archiving, dissemination, and

publication. The LIS Data Portal hosted within the MGDS provides a solution for long-term archiving of metadata and data, as well as full access to the suite of MGDS services.

7.3 Technical Overview

MGDS is supported by enterprise-level IT infrastructure ensuring that data are replicated and systems are monitored to safeguard the integrity and security of data holdings. All data files curated by MGDS are stored locally on their servers, with the data system backed up in triplicate, and long-term (100-year) preservation of data handled through agreements with the National Data Centers operated by NOAA for appropriate data types and formats, and through Columbia University Libraries for long-tail data that is not handled by NOAA Data Centers.

MGDS data cataloging, archiving, and discovery services are driven by a geospatially-enabled PostgreSQL relational database backend, which is a rich metadata catalog that describes and provides access to data files and complementary descriptive metadata and related documents. Data can be discovered and access through user interfaces and through web services. In addition to PostgreSQL, the data system makes use of PostGIS, MapServer, Google Maps API, GDAL, MB-System, GMT, and OpenLayers, as well as a suite of software tools developed in-house.

7.4 Hardware and interface improvements

Dedicated hardware for hosting LIS content has been fully integrated into the MGDS infrastructure to accommodate data submissions. Recent complementary work undertaken within MGDS that benefits the LIS project include hardware refresh and optimization of processes for data redundancy, as well new optimized workflows and tools for data validation and integration into the system. Enhancements have also been made to web services and interfaces that allow viewing of some data types (such as bottom photographs) within maps interfaces (Figure 7.4-1).
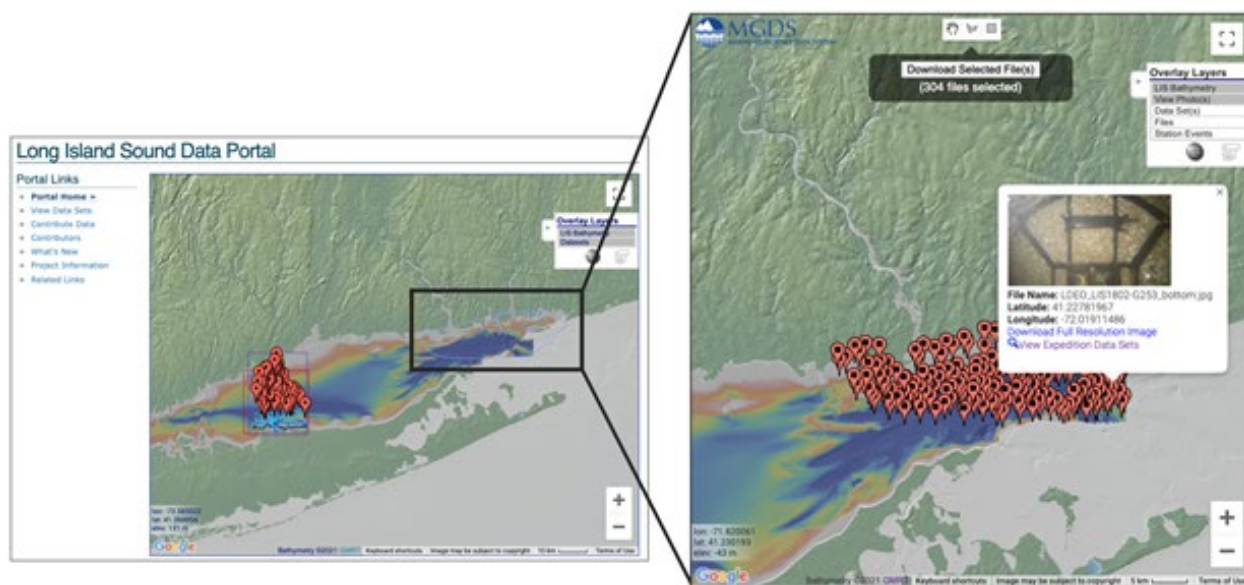

Figure 7.4-1. Snapshot of the LIS Data Portal showing the geospatial extent of data (left); Interactive access to geo-located bottom photos acquired during Phase II (right).

7.5 Archived data

As of Nov 9, 2022, more than 29,000 total data files (~2.1TB) have been contributed to the LIS Data Portal at LDEO from several of the categories described in the SOW, including cruise data, sampling data, and maps/reports. For the Phase II project, this represents more than 22,000 files totaling 1.9 TB (Table 7-2). Geospatial metadata were extracted from data files where possible and were otherwise assembled manually. Geospatial metadata were manually associated with individual seafloor images so each image could be ingested, enabling the creation of simple image galleries and geo-located exploratory map interfaces.

Table 7-2. Summary of Phase II Data Holdings in the LIS Data Portal at LDEO as of January 5, 2023. Data include direct contributions from investigators as well as most of the content contained within the LISMARC data portal. Additional CARIS-formatted data files (contributed by R. Flood) were sent directly to NOAA for inclusion in the final integrated data products generated by the NOAA team and are not included in this list. Those data files are available upon request (see the google sheet for reference).

Entry ID	Category	Data Type(s)	Link	File format	File count	File size
LIS2:BenthicEcology	Sampling	Photograph	https://www.marine-geo.org/tools/files/30889	JPEG	9166	16.8GB
LIS2:BenthicEcology	Sampling	Photograph:Video	https://www.marine-geo.org/tools/files/30899	MOV	38	1.8TB
LIS2:BenthicEcology	Sampling	Photograph	https://www.marine-geo.org/tools/files/30890	JPEG	2050	4.8GB
LIS2:BenthicEcology	Sampling	Photograph	https://www.marine-geo.org/tools/files/30891	JPEG	702	2.8GB
LIS2:BenthicEcology	Geospatial Interp	Biology:Species:Abundance, Biology:Species:Distribution, Sediment:Description	http://www.marine-geo.org/tools/files/30893	SHP	7	6.7MB
LIS2:BenthicEcology	Geospatial Interp	Biology:Species:Abundance, Biology:Species:Distribution, S ediment:Description	https://www.marine-geo.org/tools/files/30892	PDF	2	14.5MB
LIS2:BenthicEcology	Geospatial Interp	Biology:Species:Abundance, Biology:Species:Distribution, Sediment:Description	https://www.marine-geo.org/tools/files/30894	XLS	6	1.1MB
LIS2:BenthicGeology	Sampling	Photograph	https://www.marine-geo.org/tools/files/30906	JPEG	8670	40.1GB
LIS2:BenthicGeology	Sampling	Sediment:Description	http://www.marine-geo.org/tools/files/30914	SHP	1	21.3kB
LIS2:BenthicGeology	Sampling	Photograph:Video	https://www.marine-geo.org/tools/files/30907	MP4	218	50.5GB
LIS2:BenthicGeology	Sampling	Sediment:Description	https://www.marine-geo.org/tools/files/30915	ASCII	1	76.8kB
LIS2:BenthicGeology	Sampling	Sediment:Description	https://www.marine-geo.org/tools/files/30916	ASCII	1	114.0kB
LIS2:BenthicGeology	Sampling	Photograph	https://www.marine-geo.org/tools/files/30923	ASCII	1	2.1MB
LIS2:BenthicGeology	Sampling	Photograph	http://www.marine-geo.org/tools/files/30917	SHP	2	1000.0kB
LIS2:BenthicGeology	Sampling	Photograph:Video	http://www.marine-geo.org/tools/files/30919	SHP	1	639.5kB
LIS2:NOAA_Acoustics	Acoustic	Backscatter:Acoustic	http://www.marine-geo.org/tools/files/27506	GEOTIFF	1	381.9MB

Entry ID	Category	Data Type(s)	Link	File format	File count	File size
LIS2:NOAA_Acoustics	Acoustic	Bathymetry:Swath	http://www.marine-geo.org/tools/files/27504	GEOTIFF	5	4.7GB
LIS2:NOAA_Acoustics	Acoustic	Backscatter:Optical	http://www.marine-geo.org/tools/files/27507	GEOTIFF	1	240.5MB
LIS2:PhysEnv	Sampling	Documentation	http://www.marine-geo.org/tools/files/30896	SHP	2	5.6kB
LIS2:PhysEnv	Sampling	Conductivity, Pressure, Temperature	https://www.marine-geo.org/tools/files/30897	NetCDF	103	6.6MB
LIS2:PhysEnv	Sampling	BottomStress,Salinity, Temperature	https://www.marine-geo.org/tools/files/30895	PDF	1	2.9MB
LIS2:PhysEnv	Sampling	Conductivity,Pressure, Temperature	https://www.marine-geo.org/tools/files/30898	NetCDF	247	57.5MB
LIS2:Sediments	Sampling	Photograph:Video	http://www.marine-geo.org/tools/files/29813	MP4	313	4.8GB
LIS2:Sediments	Sampling	Photograph: Video: Frame Grab	http://www.marine-geo.org/tools/files/29812	JPEG	304	37.9MB
LIS2:Sediments	Sampling	Photograph	http://www.marine-geo.org/tools/files/31156	JPEG	28	5.3MB
LIS2:Sediments	Sampling	SampleInfo:Sediment	http://www.marine-geo.org/tools/files/31160	SHP	1	6.1kB
LIS2:Sediments	Sampling	Sediment:Description	https://www.marine-geo.org/tools/files/31157	PDF	1	1.9MB
LIS2:Sediments	Sampling	SampleInfo:Sediment	https://www.marine-geo.org/tools/files/31161	XLS	1	11.8kB
LIS2:Sediments	Sampling	PhysicalProperties: Sediment	https://www.marine-geo.org/tools/files/31158	XLS	1	431.4kB
LIS2:Sediments	Sampling	Chemistry:Sediment	https://www.marine-geo.org/tools/files/31159	XLS	1	331.1kB
LIS2:Sediments	Sampling	SampleInfo:Sediment	https://www.marine-geo.org/tools/files/31226	XLS	1	146kB
LIS2:Sediments	Sampling	SampleInfo:Sediment, Sediment:Description	https://www.marine-geo.org/tools/files/31227	SHP	1	76kB
LIS2:Sediments	Sampling	SampleInfo:Sediment, Sediment:Description	https://www.marine-geo.org/tools/files/31228	GEOTIFF	6	5.5MB
LIS2:Sediments	Sampling	Chemistry:Sediment	https://www.marine-geo.org/tools/files/31229	XLS	1	50kB
LIS2:Sediments	Sampling	Chemistry:Sediment	https://www.marine-geo.org/tools/files/31230	SHP	1	44kB
LIS2:Sediments	Sampling	Chemistry:Sediment	https://www.marine-geo.org/tools/files/31231	GEOTIFF	5	4.4MB
LIS2:Sediments	Sampling	Chemistry:Sediment	https://www.marine-geo.org/tools/files/31232	XLS	1	166kB
LIS2:Sediments	Sampling	Chemistry:Sediment	https://www.marine-geo.org/tools/files/31233	SHP	1	111kB
LIS2:Sediments	Sampling	Chemistry:Sediment	https://www.marine-geo.org/tools/files/31234	GEOTIFF	15	13.7MB
LIS2:Sediments	Interpretation	Interpretation:Geologic: SedimentaryEnvironments	https://www.marine-geo.org/tools/files/31235	SHP	1	739kB
LIS2:Sediments	Interpretation	Interpretation:Geologic: SedimentaryEnvironments	https://www.marine-geo.org/tools/files/31236	SHP	1	494kB

Entry ID	Category	Data Type(s)	Link	File format	File count	File size
LIS2:Sediments	Interpretation	Interpretation:Geologic: SedimentaryEnvironments	https://www.marine-geo.org/tools/files/31237	SHP	1	507kB
LIS2:Subbottom	Cruise Info	Seismic:Active:Subbottom	http://www.marine-geo.org/tools/files/26477	SHP	1	775.2kB
LIS2:Subbottom	Acoustic	Seismic:Active:Subbottom	http://www.marine-geo.org/tools/files/26476	SEGY	69	7.9GB
LIS2:Subbottom	Acoustic	Seismic:Active:Subbottom	http://www.marine-geo.org/tools/files/26478	JPEG	69	404.9MB
LIS2:UConn_Acoustics	Acoustic	Sidescan	http://www.marine-geo.org/tools/files/29908	GEOTIFF	2	104.9MB
LIS2:UConn_Acoustics	Acoustic	Bathymetry, Sidescan, Tide:Height, Velocity:Sound	http://www.marine-geo.org/tools/files/29913	RFF	16	37.2GB
LIS2:UConn_Acoustics	Acoustic	Bathymetry	http://www.marine-geo.org/tools/files/29907	GEOTIFF	2	52.6MB
LIS2:UConn_Acoustics	Acoustic	Bathymetry	http://www.marine-geo.org/tools/files/30882	GEOTIFF	2	30.4MB

Data contributions to the LIS Data Portal at LDEO were received in a variety of ways. The most efficient mechanism for transfer and integration was when specific data files intended for ingestion were contributed directly (by FTP, email, or DropBox) from the primary investigator following the suggested naming conventions and guidelines. Some large data sets were transferred by sending a portable hard drive.

Web pages that present datasets contributed for the Phase II Project are:
- https://www.marine-geo.org/tools/search/entry.php?id=LIS2:NOAA_Acoustics
- https://www.marine-geo.org/tools/search/entry.php?id=LIS2:UConn_Acoustics
- http://www.marine-geo.org/tools/search/entry.php?id=LIS2:BenthicEcology
- http://www.marine-geo.org/tools/search/entry.php?id=LIS2:BenthicGeology
- http://www.marine-geo.org/tools/search/entry.php?id=LIS2:PhysEnv
- https://www.marine-geo.org/tools/search/entry.php?id=LIS2:Sediments
- https://www.marine-geo.org/tools/search/entry.php?id=LIS2:Subbottom

7.6 Summary/Recommendations

Data Management infrastructure has been updated as part of the LIS Data Portal at LDEO to receive the data from the Phase II project. Guidelines and workflows have been developed to facilitate data management and integration into the LIS Data Portal at LDEO, which is responsible for ensuring long-term data curation. The Data Management efforts undertaken as part of this project demonstrate that existing infrastructure can be used to manage data acquired through this effort. Data contribution and ingestion workflows for the Phase II project demonstrate increased adoption of processes and more completeness of metadata. Feedback on improvements, updates to the data portal, and data submission flow are welcome and will be used for potential improvements as part of future phases.

7.6.1 Recommendations

- Aspire to contemporaneous documentation and timely contribution of data and metadata for long-term archiving to facilitate data management efforts;
- Clearly establish and commit to a policy that optimizes data flow and meets the needs of all partners; and
- Submit data products early in the project, whenever a product is ready for submission to avoid backlog at the end of the project.